FLUTTER ANALYSIS AND PREVENTION FOR WINGS WITH LARGE CONCENTRATED INERTIAS

by

V. T. NAGARAJ

Thesis submitted in fulfilment of the requirements
for the award of the Degree
of Doctor of Philosophy
of Loughborough University of Technology

Department of Transport Technology
December 1968

Supervisor: Prof. D.J. Johns

ACKNOWLEDGEMENTS

I would like to express my sincere thanks to Professor D.J. Johns for his encouragement and guidance throughout this project.

Thanks are also due to Dr. H. Gollnitz of the Max-Planck Institut fur Physik und Astrophysik for the computer programme for solving the characteristic value problem of complex eigenvalues.

Appreciation is extended to Professor K.L.C. Legg, the Director of Research for his encouragement throughout the project.

SUMMARY

The influence of concentrated inertias on the flutter characteristics of a uniform cantilever wing were investigated both by experimental and by theoretical methods.

The experimental work consisted of wind tunnel tests on a segmented wing model on which concentrated masses in the shape of large pods could be mounted at a number of spanwise and chordwise positions. The weight of these pods was comparable to the weight of the bare wing, and their pitching moment of inertia was varied to values upto ten times the pitching moment of inertia of the bare wing.

The influence of the spanwise and chordwise position of these pods on the flutter speed was investigated. In order to assess the influence of the aerodynamic shape of the pods, four different pods were tested, each having a different aerodynamic shape. The effect of adding horizontal fins to the trailing edge of the pods was also investigated as a means of increasing the aerodynamic damping and hence the flutter stability.

The flutter speeds and frequencies were also obtained by theoretical methods. Assumed mode methods were used to predict the flutter speeds of some of the wing-inertia combinations tested and these gave good agreement with the measured flutter speeds. In all these analyses, the fundamental bending and torsion modes of the appropriate wing-inertia combinations were used.

The main attention was devoted to the use of a 'Direct Matrix' method in which it is not necessary to

specify in advance the modes of the oscillating wing (as in the case of the assumed mode method). This method makes use of the inertial and aerodynamic properties of the wing-inertia combination in terms of matrices of influence coefficients. It can be used for both vibration and flutter analyses. If desired, the in-vacuo vibration modes may also be obtained. This method was applied to obtain the flutter speeds of a large number of wing-inertia combinations to assess the influence of some of the concentrated mass parameters (such as the inertia ratio, the spanwise and chordwise positions of the centre of gravity, etc.) on the flutter speed. It was also used to obtain the flutter characteristics of some wing-inertia combinations examined by other investigators. The results obtained in all these cases showed good agreement with the experimentally measured values.

TABLE OF CONTENTS

APPENDICES

LIST OF TABLES

LIST OF FIGURES

NOTATION

$[a]$	Element of flexibility Matrix, in./lb
A.R	Aspect Ratio (Eq.3.13)
AR	Element of the real part of AIC Matrix
AI	Element of the imaginary part of the AIC Matrix
q_R	Generalized amplitude of rigid body modal series in or rad.
$[a_{rs}]$	Matrix of (inertia + aerodynamic) forces, Eq. 4.55
b	Semi-chord of wing ft
b_r	Reference semi-chord, ft
$[b_{rs}]$	Matrix of elastic forces, Eq. 4.55
c	Wing chord = $2b$, ft
C_n	Element of AIC Matrix
$C(k)$	Theoderesen's Function
$[D]$	Diagonal Matrix of the eigenvalues, Eq. 5.113
EI	Bending stiffness, lb.ft^2
e_1, e_2	Distance of the control stations from the elastic axis, ft
E_{ae}	Aerodynamic "stiffness" matrix, Eq. 4.68
F	Element of force matrix, lb
$F(\eta)$	Torsion mode shape, Eq.6.4
$f(\eta)$	Bending mode shape, Eq. 6.4
$f(\lambda)$ $f_1(\lambda)$	Eq. 4.51
GJ	Torsional stiffness, lb.ft^2
g	coefficient of "artificial structural damping"
h	Deflection, in
h_o	Control point deflection due to rigid body motion, in
	control point deflection, in
h_R	Element in rigid-body modal matrix, in or dimension

$\bar{I}$	Pitching Inertia Ratio
$[I_{mn}]$	Co-ordinate transformation Matrix, Eq. 5.20
$[I_{as}]$	Interpolation Matrix, Eq. 5.36
$[k]$	Eq. 5.77
K_1, K_3, K_M	Eq. 5.65
K_2	Pitching radius of gyration of concentrated mass, ft^2
L_h, L_α	Aerodynamic Derivatives, Eq. 3.10
$L_{\dot{h}}, L_{\dot{\alpha}}, L_{h_{etc}}$	Aerodynamic Derivatives, Eq. 3.3
$[M]$	Mass Matrix, lb
$\bar{M}$	Mass Ratio
$M_h, M_\alpha \ldots$	Aerodynamic Derivatives, Eq. 3.10
$m_{\dot{h}}, m_{\dot{\alpha}}$ etc	Aerodynamic Derivatives, Eq. 3.3
$\bar{m}_{RF}, \bar{m}_{FF}$	See Eqs. 5.72, 5.73, 5.79, 5.80
n	Number of degrees of freedom
p	variable in the Laplace Transform
q	Generalized co-ordinate
r	Criterion in the Aitken δ^2 procedure, Eq. 5.153
S	Body cross sectional area (Eq.5.56) ft^2
s	Wing semispan, ft
T	Kinetic Energy
U	Strain Energy
$[U]$	Dynamic Matrix $(= U_R + iU_I)$: Eq. 5.102
V	Velocity, ft/sec
V_F	Flutter speed, ft/sec
$\bar{V}$	Flutter speed ratio
$\bar{V}_T$	Tail volume coefficient, Fig. 2.40
W	Weight of concentrated mass (Eq. 4.2), lb
$[W]$	Weighting matrix, Eq. 5.4

W_a Local velocity, (Eq. 5.61), ft/sec

$[X]$ A 2 x 2 matrix with unit elements, Eq. 5.45

x Co-ordinate along body axis, Eq. 5.54

x_i Eigenvectors Eq. 5.134

$\bar{x}_p$ Distance of concentrated mass c.g. from wing elastic axis, nondimensionalized with respect to the wing chord. Positive for c.g. aft of the elastic axis

y spanwise co-ordinate

Z $(1+\lambda g)/\omega^2$ Eq. 4.53

α Angle of attack, rad

ϵ Error in series solution, Eq. 5.75

η Non-dimensional span

θ Angular displacement in pitch, rad.

Λ Wing sweepback angle, deg.

μ concentrated mass ratio in Fig. 2.37

ν Reduced Frequency $(b\omega/V)$

ρ Air density, slugs/ft^3

Ω Complex frequency parameter, Eq. 5.69

ω Frequency of oscillation, rad/sec

Subscripts

r Reference value

R Real Part

I Imaginary Part

Superscripts

$\dot{}$ Represents differentiation with respect to time

$'$ Represents differentiation with respect to y

Represents transpose of a matrix

Abbreviations

AIC	Aerodynamic Influence Coefficient
c.g.	centre of gravity
e.a.	elastic axis
SIC	Structural Influence Coefficient

Notes

1. Other symbols are explained in the text.

2. Some of the above symbols have been used in other contexts when there is no scope for confusion. These symbols are explained in the sections where they appear.

3. The notation for the Appendices are explained in the Appendices.

CHAPTER 1

INTRODUCTION

It is well known that the aeroelastic characteristics of a wing can be radically altered by the addition of concentrated masses such as fuel tanks,weapons, podded engines, etc. This problem could become more serious when the concentrated inertia assumes large values. For example, a Design Project Study was made at the College of Aeronautics, Cranfield of a freighter aircraft which was given VTOL capability by means of podded lift engines attached to each wing (Ref. 1). This aircraft is shown in Figure 1.1. The large lift engine pods (each containing 22 lift engines) were mounted at 65% semispan of the wing. (The pod had a mass ratio $\bar{M}$ of 1.5 and an inertia ratio $\bar{I}$ of 10.0) Assuming the same stiffness distributions for both the conventional and the VTOL designs, Momirsky (Ref. 2) calculated the effect of the pods on the natural frequencies of the wing:-

MODE	FREQUENCY (CPS)	
	Conventional	VTOL
Fundamental Bending	3.74	2.89
Fundamental Torsion	22.20	6.05

The effect of the pod on the calculated flutter speed (Refs. 2, 3) is even more revealing. For the conventional wing the flutter speed was 658 knots while the corresponding flutter speed for the VTOL wing was only 164 knots.

This study shows the importance of a knowledge of the effect of adding large concentrated inertias on the flutter speeds of wings. For wings of conventional design, it is now possible to predict, with reasonable accuracy, the values of the flutter speed and frequency. It is also possible to obtain fairly accurate estimates of the effects of changing certain parameters (e.g. wing mass, moment of inertia,

chordwise position of the centre of gravity, etc.,) on the wing flutter speed. This is no longer true for the case of wings with added masses, in spite of the fact that this topic has received a great deal of attention from various investigators. The problem of formulating a set of rules for the prediction of flutter speeds of a wing with added masses is complicated by the number and range of parameters which can be varied both independently and simultaneously.

AIMS AND OBJECTIVES

It is the purpose of the present research programme:

(a) to obtain a better physical understanding of the effect of added inertias on wing flutter,

(b) to observe the effect of varying each of the added inertia parameters independently,

(c) to investigate methods of improving the flutter characteristics of a given configuration of wing and added mass,

(d) to compare the effectiveness of the various methods of analysis when applied to this problem.

Both theoretical and experimental investigations were conducted with the above objectives in mind. In the experimental investigations an aeroelastic model of a uniform wing capable of having a large pod attached to it at various points along the span was used. Several parameters of the pod (mass, moment of inertia, position of the centre of gravity, aerodynamic shape, etc.) were varied independently. The theoretical calculations consisted of flutter analyses of this model wing under various conditions of added mass.

Several different methods were used, but the main interest was in the use of a "Direct Matrix Method" which makes use of the structural, inertial and aerodynamic data in the form of matrices of the respective influence coefficients.

CHAPTER 2

A REVIEW OF PREVIOUS RELEVANT STUDIES OF THE PHYSICAL PROBLEM

The flutter of wings with concentrated inertias has been studied by several investigators both by theoretical and by experimental methods. Most of these are concerned with fixed root wings and almost all the published results are confined to incompressible flow.

When a concentrated inertia is added to a wing, there is a change in the flutter speed and the flutter frequency. If one of the concentrated inertia parameters, e.g. the mass, is increased from zero, there is in general, a gradual change in the flutter speed for low values of the parameter. However, at a certain critical value of the parameter there is an abrupt change in the flutter speed, this change being due to the change in the modes participating in the flutter.

Molyneux (Ref. 4 and 5) has analysed some of the published data with a view to identifying these modes and has recommended a set of modes to be included in an energy-type flutter analysis of a wing-inertia system.

In the following, a slightly different approach is used. The influence of each of the parameters of a concentrated inertia on the flutter characteristics is examined with a view to obtaining some trend in the behaviour of the flutter speed with changes in the parameters.

The influence of the added concentrated inertia on the flutter speed can be felt through the following parameters:

(a) The Mass Ratio (concentrated mass/bare wing mass)

(b) The Inertia Ratio (concentrated mass inertia/bare wing pitching inertia)

(c) The chordwise position of the centre of gravity of the concentrated inertia.

(d) The spanwise position of the concentrated inertia

(e) The flexibility of the attachment of the added concentrated inertia to the wing

(f) The aerodynamic shape of the added concentrated inertia

(g) The effect of adding more than one inertia at the same time to the wing

(h) The influence of the root degrees of freedom (both Symmetric and Anti-Symmetric)

(i) The influence of fuel sloshing

(j) The sweepback angle of the wing

(k) The effect of compressibility and Reynolds Number.

In experiemntal analyses, it is difficult to vary each of these parameters separately without varying many of the other parameters. In theoretical analyses, this type of independent variation is possible to a certain extent. The published literature from which the data for the comparisons are extracted contains a large amount of data. Of these, only a limited amount has been extracted and sometimes redrawn, in terms of non-dimensional graphs in order to study the effect of varying a particular parameter.

In Appendix I, as much data as could be obtained from the literature about the geometric, inertial and structural properties of the wing-inertia systems analysed therein is given. It is unfortunate that for some wings, not all the important information is presented. For example, some of the authors do not include data about the frequencies of vibration of the wings or details of the mass and moment of inertia distributions.

2.1. THE INFLUENCE OF MASS RATIO

Figs. 2.1 to 2.6 illustrate the effect of variation of the mass ratio on the flutter speed of the wing-inertia combination. In all these figures $\bar{V}$ denotes the ratio of the flutter speed of the wing-inertia combination to the bare wing flutter speed. $\bar{M}$ denotes the ratio of the mass of the concentrated inertia to the bare wing mass.

In examining these figures, it is instructive to compare the bare wing bending and torsional frequencies of the different wings examined. Due to lack of data, it has not been possible to obtain this information for all the wings, and the following table gives the values of these frequencies for some of the wings:

Fig.	Ref.	Wing Cg aft of LE	Wing ea aft LE	Frequencies Fundamental Bending cps	Frequencies Fundamental Torsion cps
2.1	6	0.40C	0.32C	--	--
2.2	7	0.43C	0.30C	3.9	15.3
2.3	8	0.43C	0.32C	20.1	66.1
2.4	9	0.35C	0.25C	3.6	14.5
2.5	10	0.40C	0.40C	--	--
2.6	5	0.45C	0.25C	16.0	50.0

All the frequencies quoted above refer to the bare wing. When a concentrated inertia is added to the wing, both the fundamental bending and fundamental torsional frequencies decrease. For all these wings, the bare wing flutter involved a coupling of the fundamental bending and the fundamental torsion modes.

The influence of the mass ratio of the concentrated inertia on the flutter speed seems to depend primarily on the chordwise position of its centre of gravity with respect to the elastic axis (at any given spanwise location).

2.1.1 When the centre of gravity is ahead of the elastic axis, the curve of $\bar{V}$ vs $\bar{M}$ displays a characteristic trend. At most of the spanwise locations, the flutter speed ratio increases at first as the mass ratio is increased from very low values. After a critical value of $\bar{M}$ is reached, the value of $\bar{V}$ decreases. Further increases in $\bar{M}$ bring about a decrease in $\bar{V}$ until an asymptotic value is reached. In general, for all values of $\bar{M}$, the flutter speeds of the wing-inertia combination are higher than the bare wing flutter speed. By a judicious placing of the concentrated inertia, fairly large increases in the flutter speed can be obtained, thus suggesting a method of eliminating any flutter problems of the bare wing.

For all the wings, the critical modes at the flutter, for values of $\bar{M}$ less than the critical, are the fundamental bending and fundamental torsional modes. For values of $\bar{M}$ greater than the critical, the modes participating in the flutter are the overtone bending mode and the fundamental torsion mode.

Fig. (2.7) shows the value of M_{crit}, (the critical value of the mass ratio), plotted against the span of the wing for the wings of Figs. (2.1) to (2.6).

As the concentrated inertia is moved outboard from the wing root, the value of $\bar{M}_{crit}$ shows a gradual decrease.

The ratio of the fundamental bending to the fundamental torsion frequency is approximately of the same order for the four wings for which this data is available.

Fig. (2.4) also shows the effect of wing sweepback on $\bar{V}$. For concentrated masses located at the two-thirds span position, three values of the wing sweep, 15°, 30° and 45° were considered. For all these conditions,

the structural and inertial properties were not altered. It is seen that there is only a slight change in the value of the maximum value of $\bar{V}$. The value of the critical mass ratio, $\bar{M}$ crit, increases with increase in sweepback. (It should be noted that the bare wing flutter speed is not the same for all these wings as this is approximately proportional to $\text{Sec}(\Lambda - \frac{\pi}{10})$ where Λ is the sweepback angle.)

From a study of Figs. (2.1) to (2.7), the following conclusions can be drawn:

(a) For all values of the concentrated mass, the flutter speed of the wing-inertia combination is, in general, higher than the bare wing flutter speed.

(b) At a given spanwise position, as the value of the concentrated mass is increased from zero, the flutter speed increases from the bare wing value to a maximum value at a certain critical mass ratio. Any further increases in the concentrated mass brings about a decrease in the flutter speed until an asymptotic value is reached for $\bar{V}$.

(c) The actual value of $\bar{V}$ depends on the configuration.

(d) Keeping the structural and inertial properties the same, if the wing is sweptback, the maximum value of $\bar{V}$ is not much affected. The value of $\bar{M}$ crit increases with increasing sweepback angle.

(e) For wings with the same ratio of fundamental bending to fundamental torsion frequency (for the bare wing), the value of $\bar{M}$ crit seems to have the same order of magnitude.

2.1.2 When the concentrated mass is located on the elastic axis the curve of $\bar{V}$ vs $\bar{M}$ does not seem to follow any well defined pattern.

For the wings of Ref. (6) (Fig. 2.1) and of Ref. (5) (Fig.2.6), the $\bar{V}$ - $\bar{M}$ curve is similar to the curve obtained when a concentrated mass is located ahead of the elastic axis. For both these wings, the flutter speed is higher than the bare wing flutter speed for values of $\bar{M} < 2.0$. This holds true for all the spanwise positions.

The wing of Ref. (7) (Fig. 2.2) shows a different pattern of behaviour and is influenced by the spanwise location of the concentrated mass. For position near the root, there is no change in the flutter speed, this being equal to the bare wing flutter speed for all values of the concentrated mass.

For masses placed at the mid span and the three-quarter position, the flutter speed decreases with increasing values of the concentrated mass. A mass located at the tip shows a different behaviour. As the concentrated mass value is increased, the flutter speed falls rapidly at first and then increases to give value of $\bar{V} = 1.2$ at $\bar{M} = 0.9$.

It may not be possible to compare the values for the wing of Ref (5) (Fig. 2.6), since these refer to a wing with symmetric body freedom.

It is difficult to draw any general conclusions from the evidence available. The reason for this apparently inconsistent influence of the concentrated mass may be due to the fact that a mass placed on the elastic axis does not have any inertia coupling and each wing mass combination has to be analysed individually.

2.1.3 Concentrated mass positions aft of the elastic axis show a more consistent influence on the flutter speeds. (Figs. 2.1, 2.3, 2.4, 2.5). For all these wings there is a decrease in the flutter speed with increases in the value of the concentrated mass.

2.1.4

In general, for concentrated mass positions forward of the elastic axis the flutter speed of the wing-mass combination is higher than the bare wing flutter speed. For masses positioned aft of the elastic axis, the flutter speed is lower than the bare wing flutter speed.

For concentrated mass positions ahead of the elastic axis, the modes participating in the flutter abruptly change (at a critical value of the mass ratio), from the fundamental to one containing the overtone modes. For masses located aft of the elastic axis, usually there is no apparent change in the modes participating in the flutter.

2.2 EFFECT OF THE INERTIA RATIO

The influence of the value of the pitching moment of inertia of the concentrated mass is shown in Figs. (2.8) to (2.11). In each of these figures, the effect on the flutter speed of an increase in the pitching moment of inertia is shown, the following quantities being held constant. (a) the mass of the concentrated inertia and (b) the position of its centre of gravity (both spanwise and chordwise positions.) Due to the difficulties in keeping all these quantities constant while varying only the moment of inertia, not much information is available on the effect of the moment of inertia on the flutter speed.

As in the previous case, the effect of the moment of inertia will be considered with reference to the position of its centre of gravity.

The flutter speeds are again plotted as ratios of the bare wing flutter speed. In all the figures $\bar{I}$ represents the ratio of the pitching inertia of the concentrated mass to the pitching moment of inertia of the bare wing, both values being measured with respect to a given reference axis. When the values of $\bar{M}$ and the pod centre of gravity are fixed, variation in $\bar{I}$ can be attributed to a corresponding variation in the pitching radius of gyration of the concentrated mass.

Fig. (2.8) (Ref.9) shows the effect of varying the inertia ratio on the flutter speed when the centre of gravity of the concentrated mass is located 0.1c ahead of the elastic axis. Four spanwise locations of the inertia and three values of $\bar{M}$ are considered.

For values of $\bar{M}$ equal to 0.25 and 0.5, the curves show a similar behaviour in that for all the spanwise positions, except at the tip, the flutter speed generally decreases with increase in inertia ratio.

For the mass located at the tip, the flutter speed at first increases with small increases in the inertia ratio, but after reaching a maximum value, decreases with further increases in the inertia ratio.

For values of $\bar{M} = 1.0$, the curves show a similar behaviour for spanwise locations of two-thirds and $\frac{3}{4}$ span respectively. For masses located at the mid-span and at the tip, the flutter speed again shows a similar behaviour. The flutter speed increases first and then decreases, with increases in the pitching moment of inertia.

For the same wing, Fig. (2.9) shows the effect of $\bar{I}$ on $\bar{V}$ for different angle of sweepback (obtained by a rotation about the root). For all these curves, the mass was placed at the 2/3 span position and the centre of gravity was 0.1c ahead of the elastic axis. Three values of the mass ratio, $\bar{M}$ = 0.25, 0.5 and 1.0 are considered. (It should be noted that for the bare wing, the flutter speed varies with the angle of sweepback Λ, approximately as Sec $(\Lambda - \frac{\pi}{16})$. Since all the curves presented in this figure are normalised with respect to the flutter speed of the swept wing, they have not been normalised with respect to the same speed).

For $\bar{M}$ = 0.25, the curve of $\bar{V}$ against $\bar{M}$ shows approximately the same trend as for the unswept wing. For $\bar{M}$ = 0.5, the flutter speed shows a larger decrease than for the unswept wing. For $\bar{M}$ = 1.0, the flutter speed shows approximately the same trend as for the bare wing only for sweepback angles of 15° and 30°. For a sweepback angle of 45°, the flutter speed decreases first with increase in $\bar{I}$ and then increases with increases in $\bar{I}$.

Fig. (2.10) refers to the wing of Ref (10). This wing was allowed the root degree of freedom of body pitching.

The effect of $\bar{I}$ is considered for four spanwise stations with the centre of gravity of the concentrated mass located at three chordwise positions for each spanwise location. Two sweepangles $\Lambda = 0^{\circ}$ and 45° are considered.

In Fig. (2.11) (Ref. 7) the concentrated mass is located at the tip and at the midspan and three (chordwise) centre of gravity locations and four sweepback angles are considered.

For all the wings considered, the general trend seems to be for the flutter speed to decrease with increase in the inertia ratio. The actual behaviour is influenced mainly by the value of the mass ratio and the spanwise location.of the concentrated mass.

At a given spanwise location and for a given centre of gravity location of the concentrated mass, there is no change in the modes involved in the flutter with increases in the value of $\bar{I}$.

(Note: In Figs. (2.8) to (2.11), the value of $\bar{V}$ at $\bar{I} = 0$ need not be equal to unity since the flutter speed for this condition will be equal to that of a wing carrying a point mass).

2.3 EFFECT OF THE CHORDWISE C.G. LOCATION

In general, the chordwise position of the centre of gravity of the concentrated mass has the strongest influence on the flutter speed of the wing-mass combination. Mass positions ahead of the elastic axis have a stabilising influence on the flutter speed while positions aft of the elastic axis tend to have a destabilising effect.

Figs (2.12) to (2.19) show the influence of the chordwise location of the concentrated mass centre of gravity.

Fig. (2.12) refers to the wing of Ref. (9). Four spanwise positions and two values of the inertia

ratio, $\bar{I}$, are considered. For all these, the mass ratio was kept constant at $\bar{M} = 0.5$. All the curves (except for $\bar{I} = 1.0$ and $\bar{I} = 0$) show a similar behaviour. As the location of the centre of gravity is moved forward from a position aft of the elastic axis, the flutter speed increases to a maximum value just ahead of the elastic axis and then decreases as the centre of gravity is moved further ahead of the elastic axis. This decrease is associated with a change in the modes participating in the flutter, when the flutter involves one of the overtone modes.

Fig (2.13) also refers to the wing of Ref (9). For masses located at the two-thirds span location, two values of $\bar{I}$ (0 and 0.84) and three values of the sweepback angle (15°, 30° and 45°) are considered. The behaviour of the $\bar{V}$ vs $\bar{X}_p$ curve is essentially the same as for the unswept case. The values for the sweepback angle of 45° follow a different trend, the flutter speed showing a continuous increase as the mass centre of gravity is moved progressively from a location aft of the elastic axis to a location forward of the elastic axis. The chordwise position at which the transition from fundamental to overtone flutter occurs moves further ahead of the elastic axis as the sweepback angle is increased. (It should be noted that all the chords are measured in the streamwise direction. So, with an increase in the sweepback angle, the value of the streamwise chord also increases).

The values in Figs. (2.14, 2.15, 2.16a and 2.16b) refer to the wing of Ref. (10). All these wings were allowed the root symmetric degrees of freedom (pitch and normal translation).

The flutter speed for all these wings is very sensitive to the chordwise position of the centre of gravity,

especially for positions near the elastic axis. Again, in general, locations forward of the elastic axis tend to have a stabilising influence on the flutter speed.

Fig. (2.18) also refers to a wing with the symmetric degrees of root freedom (Ref. 8). For this wing also, the flutter speed is very sensitive to movements of the location of the centre of gravity in the neighbourhood of the elastic axis.

Figs (2.17a and 2.17b) refer to the wing of Ref. (16). In Fig.(2.17a) the variation of $\bar{V}$ with respect to $\bar{X}_p$ is shown for four different spanwise locations of the concentrated mass. For most spanwise locations, the flutter speed is not very sensitive to the chordwise position of the centre of gravity, provided that this is forward of the ~~ealstic~~ elastic axis. In Fig. (2.17b) the behaviour of the $\bar{V}_p - \bar{X}_p$ curve is examined for (a) three different sweepback angles while the value of $\bar{M}$ is held constant and (b) for three values of $\bar{M}$ for a given value of Λ (= 13°). The concentrated mass is located at the wing tip. The behaviour of these curves is similar to the corresponding curve in Fig. (2.17a). The flutter speed has its maximum value for centre of gravity locations in the neighbourhood of the elastic axis.

In Fig. (2.19), which refers to the wing of Ref (6), the variation of $\bar{V}$ with $\bar{X}_p$ is more gradual. Three different spanwise locations (η = 0.1, 0.3 and 0.5) and for each spanwise location, three different ~~chordwise~~ mass ratios ~~locations~~ are considered.

For all the wings considered here, the general pattern seems to be for the flutter speed to increase as the c.g. of the concentrated mass is moved forward from a location aft of the elastic axis.

At a certain centre of gravity location in the neighbourhood of the elastic axis, a maximum value for the flutter speed is attained, and any further movements of the c.g. forward of this location tend to to decrease the flutter speed. This decrease is generally due to the flutter being one of the overtone type.

2.4 EFFECT OF THE SPANWISE LOCATION

The behaviour of the curve of the flutter speed when plotted against the span depends primarily on the chordwise location of the c.g. of the concentrated mass and to a lesser extent on the value of the mass ratio,(M).

Figs.(2.20) to (2.26) show the effect of moving the concentrated mass along the span for a constant position of the chordwise c.g. location.

For most of the wings, two basic patterns can be seen, which are determined mainly by the chordwise location of the centre of gravity with respect to the elastic axis. For locations forward of the elastic axis, the flutter speeds aregenerally higher than the vare wing flutter speed at all the spanwise locations. As the concentrated mass is moved outboard from the wing root, the flutterspeed increases at first, and reaches a maximum value at a point along the the span, generally between the midspan location and the tip. After this, the flutter speed decreases as the concentrated mass is moved towards the tip.

For the concentrated mass c.g. located aft of the elastic axis, the flutter speeds are, in general, lower than the bare wing flutter speeds. As the concentrated mass is moved outboard from the root, the flutter speed decreases gradually to have a minimum value at around the mid-span position. If the concentrated mass is moved further outboard the

flutter speed again increases and a maximum value is obtained at the tip. This maximum value is generally lower than the bare wing flutter speed.

As the figures show, the most critical parameter in determining the behaviour of the $\bar{V}-\eta$ curve is the chordwise location of the centre of gravity of the concentrated mass with respect to the elastic axis. For the concentrated mass c.g. located on the elastic axis itself the behaviour of this curve seems to depend on the value of the mass ratio and probably on the location of the elastic axis with respect to the wing leading edge, (e.g. Figs. 2.24, 2.25 and 2.26).

An examination of Figs (2.20) to (2.26) suggests that by properly locating a concentrated mass (both in the spanwise and the chordwise locations), it is possible to obtain large increases in the flutter speed. This can be used as a cure for the flutter of the basic wing i.e., to obtain a mass balancing effect.

2.5 EFFECT OF FLEXIBILITY OF ATTACHMENT

The flutter characteristics considered so far have been concerned with the cases when the concentrated mass is rigidly attached to the wing. Considerable changes can occur in the flutter speed when the concentrated mass is not rigidly attached to the wing. This depends on the value of the natural frequency of the mass system compared to the natural frequencies of the basic wing.

Young and Ruhlin (Ref. 11) investigated the effect of the pitching frequency of the concentrated mass on its attachment on the flutter speed (Fig. 2.27). For the concentrated mass centre

of gravity located aft of the elastic axis, they found that a large effect of the pitching frequency was felt when the ratio of the pitch frequency to the fundamental torsion frequency of the wing (ω_N/ω_T) was about 0.16. At the value, the flutter speed reached its lowest value and either a decrease or an increase in the value of (ω_N/ω_T) gave a relatively large increase in the flutter speed. A similar, but opposite effect was observed when the c.g. of the concentrated mass was moved to a location very near the elastic axis, but still aft of it. Around the value $\omega_N/\omega_T = 0.16$, a very large increase of the flutter speed was obtained. They suggest that at this value of the ratio of the frequencies the mass system acts as a vibration absorber and that specially designed attachments could be used as flutter suppressors.

Gaukroger (Ref 12) has made an extensive study of the effects of allowing the attachment flexibilities in pitch, roll, yaw and normal translation on the flutter characteristics of a uniform wing. The wing was a cantilever uniform wing and varying sweepback angles, between 0° and 45° were considered. All the masses were mounted on the elastic axis.

Fig. (2.28) shows the effect of the pitching frequency on the flutter speed. Two values of the mass ratios ($\bar{M}$ = 0.5 and 1.0) and two values of the sweepback angle ($\Lambda = 0^\circ$ and 30°) are considered. For both these the behaviour of the $\bar{V}$ - ω_N/ω_T curve is similar to that in Fig. (2.27). When the pitching rigidity of the attachment is reduced from an infinite value, two critical regions can be

observed, where the flutter speed drops to a value of less than half the flutter speed with the rigidly mounted mass. For the rigidly mounted mass, the flutter was of the overtone type. As the rigidity of the attachment is decreased, a transition to the fundamental type of flutter was obtained. From his calculations, Gaukroger found no simple rules for determining the critical values of ω_N except that these values lie between the fundamental bending and torsion frequencies of the bare wing.

Fig. (2.29) shows the effect of the roll flexibility on the flutter speed. For both values of the mass ratio ($\bar{M}$ = 0.5 and 1.0) considered, there is no coupling between the wing torsion and mass roll modes. As the sweepback angle is increased, the coupling between these two modes increases and the coupling between the wing bending and mass roll modes decreases. For the unswept wing, increases in the mass roll frequency leads to a slight decrease in the flutter speed which is associated with a slight rise in the flutter frequency. For the swept wing, there is a pronounced drop in the flutter speed at a critical value of the roll frequency.

Gaukroger also investigated the effect of varying the mass ratio in this case. He found that the effect of roll flexibility with mass variation was negligible for large values of $\bar{M}$, but that this can be considerable for small values of $\bar{M}$.

The effects of allowing yaw flexibility are shown in Fig. (2.30). The effects are similar to those of the roll flexibility case (Fig. 2.29), except that the U-shaped branch (for N_χ = 0) does not appear in the roll flexibility case. For a mass

ratio, $\bar{M} = \frac{1.0}{0.5}$, the effects of allowing yaw flexibility do not appear to be significant.

Fig. (2.31) shows the effect of allowing the normal translation flexibility in the attachment. At a certain critical value of the frequency ratio (ω_{NT}/ω_T) a minimum value of the flutter speed is obtained. The flutter frequency of the second branch (for values of ω_{NT}/ω_T greater than the critical) is lower than the flutter frequency for the first branch.

For all these figures (2.28 to $\frac{2.31}{2.30}$) the concentrated mass was located at the tip, and the wing was cantilevered from the root.

Fig. (2.32) shows the effect of allowing both the normal translation and pitching of mass for a wing which also had root frequencies in pitch, normal translation and yaw (Ref. 10). The symmetric and anti-symmetric flutter speeds are shown separately Two different spanwise locations were considered ($\bar{\eta}$ = 0.5 and 1.0). For both these locations, the results are very similar to Gaukroger's cantilever wing results.

The above results indicate that flexibilities in the attachment of the concentrated mass can lead to very low flutter speeds under certain conditions, thus nullifying any advantages gained by a judicious placing of the concentrated mass.

2.6 EFFECT OF THE AERODYNAMIC SHAPE OF THE CONCENTRATED MASS

The effect of the aerodynamic shape of the concentrated mass on the flutter speed of the wing have been investigated by several authors (Refs. 7, 13, 14, 15 and 16).

All the flutter speeds investigated were at subsonic Mach Numbers. Some of the results are shown in Figs. (2.33, 2.34 and 2.35).

Sewall and Woolston (Ref. 16) studied the effect of the aerodynamic shape of concentrated weights rigidly attached to a cantilever wing. Two types of weights were used, a streamlined body resembling an external fuel tank and a blunt body. Both were weighted to have similar inertial properties.

Fig. (2.33) shows the effect of the spanwise position of the two masses on the flutter speed. For all the span positions the two flutter speeds are very close and the flutter speeds for the non-streamlined body are slightly higher than those for the streamlined body. The difference is at the most about 3% between the two speeds. For both these weights the centres of gravity were slightly aft of the elastic axis.

Two more sets of weights, one with the centres of gravity on the leading edge and other with the centres of gravity aft of the elastic axis were also tested. For these weights also, the flutter speeds were very close, the non-streamlined body giving a slightly higher flutter speed.

A theoretical study of the effects of the aerodynamic loads due to an external fuel tank on the flutter of the Fokkier F.27 wing was made by Yff (Ref. 13). He found that by taking the pod aerodynamic loads into account a flutter speed was obtained which was approximately 3% lower than the flutter speed obtained by neglecting the pod aerodynamic loads.

Gaukroger (Ref. 7) tested the effect of different aerodynamic shapes resembling aircraft fuel tanks. Two spanwise locations for these aerodynamic ~~shpaes~~ Shapes were chosen. Two types of tanks were tested. Both had the same geometrical shpae, but one of them was attached (at the mid span position) so that about a third of its length was exposed in front of the wing. For the second pod, only a fifth of the length was exposed. At the tip location, about a third and a half of the wing were exposed respectively.

At both the spanwise locations and for both the aerodynamic shapes the flutter speeds were very similar and differed very little compared to the bare wing flutter speed. This influence was not consistent when the centre of gravity of the store was moved chordwise, one shape giving slightly higher flutter speed at one position of the centre of gravity and these results being reversed at another chordwise position.

Fig. 2.34 shows the effect of the position of the centre of gravity of a tip tank on the Mach Number for symmetric flutter (Ref. 14). Two tip tanks of the same inertial characteristics were used, but one was smaller than the other. The smaller tank was a scaled-down model of a 230 gallon capacity and the larger tank corresponded to a tank with a 700 gallon capacity.

The trends in the flutter curves are very similar for both the tanks. In the region covered by the tests the larger tank causes a reduction in the flutter speed of about 15%. All these tests were made with the fins as in Fig. (2.34).

In another interesting experiment, when the centre of gravity of the tip tank was approximately 1 to 2 ins. aft of the elastic axis, removing the fin was found to reduce the flutter speed of the small tank by about 7%, while removing the fin on the large tank had only a slight effect, "perhaps tending to increase the flutter speed by a small amount".

Two tip pods of different sizes, but having approximately the same inertial characteristics and centre of gravity positions were tested (for the anti-symmetric flutter of a model of the Northrop F.89 - Scorpion wing) by Gayman (Ref. 15). These tests showed that the changes in the pod shape had small effects on the flutter characteristics, the largest differences being only slightly greater than the limits of accuracy.

In an interesting approach, an attempt was made to define an "aerodynamic equivalent" tip-pod. This was defined as a rectangular extension of the wing, which had a semi chord, span and quarter-chord location relative to the wing elastic axis and which gave the same aerodynamic effect under analysis (by the assumed mode method), as does the actual pod under test conditions. The aerodynamic equivalent was arrived at by a process of iteration: assuming a number of different span extensions and calculating the flutter speed by the assumed mode method. The additonal "wing" which gave the closest agreement with the test results was taken as the "aerodynamic equivalent" of the tip pod.

Fig. (2.35) shows the results of one such analysis in the form of a conventional V - g plot.

All the results were obtained by assuming three modes - roll, fundamental bending and fundamental torsion. The line (1a) represents the results of a four degree of freedom analysis in which the overtone torsion mode was also included in addition to the above modes.

From a series of similar analyses, it was concluded for this wing that an accurate tip pod representation was more important than the number of degrees of freedom included in the analysis. The "aerodynamic equivalent" of the tip pods considered had smaller plan form areas compared to the plan form areas of the pods.

From these results it can be concluded that at subsonic speeds, even radical changes in the aerodynamic shape of the concentrated mass have very little effect on the flutter speed. In general, a streamlining of the external (added) mass tends to be destabilising, this resulting in a lower flutter speed. The aerodynamic shape of the added mass may become more important at supersonic speeds.

2.7 THE EFFECT OF ADDING MORE THAN ONE INERTIA AT THE SAME TIME

Lambourne and Weston (Ref 6) tested the influence of adding more than one mass at the same time on the flutter speeds. Figs. (2.36) and (2.37), show the results of their investigations for two cases. In Fig. (2.36) the centres of gravity of both the masses is on the wing elastic axis. The mass at the midspan position was kept constant at a chosen value and the variation of the flutter speed with changes in the tip mass were observed. Three values

for M (0, 0.155 and 0.312 slugs)are shown. In Fig. (2.37) the effect of varying two concentrated masses palced at the span positions of η = 0.3 and 0.5 is shown for two locations of the chordwise c.g. Also shown is the effect of varying three masses located at η = 0.1, 0.38 and 0.3.

These figures show a behaviour which is similar to those of Fig. (2.1) which also refers to the same wing.

An important conclusion which can be deduced by comparing the flutter speeds for the simultaneous loading of the masses with the cases when they are individually varied. The effect on the flutter speed of the masses are not additive. The value of the flutter speed due to a simultaneous loading cannot, in general, be predicted from a knowledge of the flutter speeds due to an individual loading of the masses.

2.8 THE INFLUENCE OF THE ROOT DEGREES OF FREEDOM

The influence of body freedom on wing flutter has been examined both theoretically (Refs. 8, 10, 13, 15 and 17) and experimentally (Refs. 8, 14, 15, 18 and 19).

In examining the effects of the root degrees of freedom, it is convenient to consider the symmetric (pitch and normal translation) degrees of freedom and the anti-symmetric (roll) degree of freedom separately since these are uncoupled.

Figs. 2.38(a), 2.38(b), 2.38(c) are taken from Ref. (10). The effects of a concentrated mass on the flutter speeds (symmetric and anti-symmetric) of four different wings are shown in the form of contours of constant flutter speed. From these figures, it can be seen that the overall effects of a concentrated mass are very similar to the case with a fixed root, though the actual values of the flutter speeds may be different.

Fig. (2.39) refers to tests carried out by means of ground launched rocket vehicles (Ref. 8). This figure illustrates the effects of the body centre of gravity on the body freedom flutter speed for a uniform wing carrying tip masses. Two different values of the tip mass and two different values of the tip mass pitching inertia are considered. For all these values, the position of the body mass centroid has an appreciable influence on the flutter speed. From separate tests it was shown that the body freedom flutter speed was increased when the body mass was increased. Fitting the vehicle with different sizes of horizontal tails had practically no effect on the flutter speed. This may be due to the fact that for this particular configuration, the tail plane effectiveness was very low as it was fairly close to the main wings.

When the symmetric root degrees of freedom are allowed, in general, two different types of flutter occur under proper conditions: (a) Body Freedom Flutter in which the principal modes participating in the flutter are the regid body modes and the primary wing modes, and (b) Disturbed Root Flutter which involves mainly the modes of fundamental bending and fundamental torsion of the wing.

Both types of flutter were encountered in the investigations of Ref (8).

Gaukroger (Ref. 18) conducted tests on wings which were allowed root freedoms in pitch and in roll separately. For the symmetric degree of freedom he found that both body freedom and disturbed root types of flutter may be obtained. He also found that for the symmetric degree of freedom, the effect of the body mass was small. Unlike Ref (8) he found that (a) the effect of the centre of gravity position of the body was small and (b) the effect of adding a

horizontal tail was to reduce the value of the fuselage pitching moment of inertia at which the change from body freedom flutter to disturbed root flutter occurred.

Fig. (2.40) (Ref. 18) shows the effect of increasing the fusalage moment of inertia on a wing with a sweepback angle (of the spar) of 9°. Two values of $\bar{V}_T$ - the horizontal tail volume coefficient are considered. The two types of flutter - body freedom flutter and disturbed root flutter - can be distinguished. The body freedom flutter involves the modes of fuselage pitching and wing bending and has a lower flutter speed than the fixed root flutter speed. Disturbed root flutter is similar to the fixed root flutter and has comparable values for the flutter speed and frequency.

From his tests Gaukroger concluded that the most important parameters affecting symmetric flutter were the fuselage pitching moment of inertia and the horizontal tail volume coefficient. The addition of the tailplane stabilises body freedom flutter. From separate tests he found that sweepback of the wing also has a stabilising effect on the body freedom type of flutter.

Molyneux (Ref. 5) has investigated theoretically the effect of allowing root freedoms - symmetric and anti-symmetric on wings carrying concentrated masses. His results indicate the possibility that on a wing, initially free from flutter involving body motions, addition of concentrated masses may induce this type of flutter. Fig (2.41) (Ref. 5) shows the effect of allowing the root degrees of freedom in pitch and normal translation on the flutter speed.

When there is a central mass only (and no outboard masses), (Fig. 2.41.a), the flutter speed with root freedom in pitch is lower than the fixed root flutter speed for low values of the central mass pitching inertia. The

modes involved in this flutter include a large pitching oscillation of the central mass. After a certain value of the central mass pitching inertia is reached, the flutter resembles fixed root flutter and, the flutter speeds are higher than the fixed root flutter speeds.

The effect of adding a concentrated mass at the tip to the above configuration is shown in Figs. (2.41.b) and (2.41.c) when the centre of gravity of the tip mass is on the wing leading edge (Fig. 2.41.b) the fixed root flutter involves the modes of large motions in pitch and translation of the tip mass for low values of $\bar{M}_T$. ($\bar{M}_T$ = Tip mass/wing mass). When the root freedoms (pitch and normal translation) are allowed three different types of flutter can occur. The first branch involves translation and pitch of the outboard mass but no motion of the central mass. The second branch involves translation and pitch of the outboard mass, but only pitch of the central mass. For large values of the tip mass the flutter involves zero translation and zero pitch of the tip mass. When the tip mass centre of gravity is located on the elastic axis, only the first two branches of the previous curve were obtained (Fig. 2.41.c).

From Figs. (2.41.b) and (2.42.c) it can be seen that under certain conditions, values of the flutter speed far less than the fixed root case can be obtained by allowing root degrees of freedom.

When the wing is allowed the anti-symmetric degree of freedom (i.e. in roll) and when there are no outboard masses, the flutter mode initially involves large roll motions of the central mass (Fig. 2.42.a). The second branch involves very little roll motion of the mass. For this branch, the flutter speeds are less than the fixed root flutter speeds.

For the case when an outboard mass is present at the tip (Fig. 2.42.b, 2.42.c) introduction of the roll degree of freedom does not seem to have an adverse effect as severe as that obtained when the symmetric degrees of freedom are allowed. The results of Molyneux (Ref. 5) and Gaukroger (Ref. 18) suggest that for a conventional aircraft, it is unlikely that antisymmetric flutter would occur at speeds appreciably less than the corresponding fixed root flutter.

The above results show that the root degrees of freedom can be important parameters in the flutter of wings with concentrated masses, under certain circumstances, flutter speeds which are considerably lower than the corresponding fixed root flutter speeds can be obtained.

2.9 EFFECT OF FUEL SLOSHING

An important class of concentrated masses - the fuel content in integral wing tanks or in external fuel tanks - possesses some properties which can adversely affect the flutter speeds. The fuel can move inside the tank and its quantity is variable.

Yff (Ref. 13) found that for a pylon tank without internal baffles the attitude of the tank can have large detrimental effects on the flutter speed. (Fig 2.43). When the fuel tank was in a nose-up attitude, flutter speeds considerably lower than the bare wing flutter speed were obtained for partially filled tanks. It was also found that for a given fuel tank content the flutter speed decreased with increasing nose-up attitude. These results would be somewhat modified if the contribution of the moving fuel to the torsional damping is taken into account.

For an external fuel tank without internal baffles, the fuel can move freely inside the tank. One method of taking this factor into account is to use the "frozen fuel"

method. The fuel is treated as a rigid body for purposes of taking the moment of inertia into account. Gayman (Ref. 15) found from experiments on a model tank, that for a partially filled tank the measured moment of inertia can be very much lower than the values obtained by using a 'frozen fuel' model.

Sewall (Ref. 20) made some analytical and experimental studies on two dimensional fuel-loaded wing models. The wing models had two degrees of freedom only, these being controlled by two springs which allowed only the rigid vertical translation and rigid body pitching respectively. In the analytical studies, Sewall used "effective" values for the mass and moment of inertia of the fuel tank with fuel.

From his experiments on internal (baffled) fuel tanks Sewall found that there was one particular sequence of emptying the fuel tank which gave the optimum (i.e. consistently the highest possible) flutter speeds. Even from this limited survey it can be appreciated that correct analytical representation of fuel in an externally mounted tanks (or in integral wing tanks) can be important.

2.10 EFFECT OF WING SWEEPBACK

For a bare cantilever wing, when the wing sweepback is increased from zero, the flutter speed falls initially until, in general, a sweepback angle of 10° and 15° is reached. A further increase in the sweepback brings a about an increase in the flutter speed. From a study of experimental results, Molyneux (Ref. 21) suggested the following approximate relationship:

$$(V_F)_{\Lambda} = (V_F)_{\Lambda=0} \cdot \sec^{3/2}\left(\Lambda - \frac{\pi}{16}\right) \qquad (2.10.1)$$

where $(V_F)_\Lambda$ = Flutter speed of the swept-back wing

$(V_F)_{\Lambda=0}$ = Flutter speed of the unswept wing

and Λ = Sweepback angle of the span

Sanford et al (Ref. 22) tested wings of different aspect ratios for the effect of sweepback. They found that the variation of the flutter speed was close to the variation of $(\text{Sec}^{\frac{1}{2}}\Lambda)$ with variation in the sweepback angle.

In the above tests the flutter was of the fixed root type. Wilts (Ref. 10) obtained some interesting results from his analogue computer analyses on the effect of the sweepback angle in the presence of the root degrees of freedom. Fig. (2.44) shows some of the results for four different wings. For the range of sweepback angles investigated, the increases in flutter speed that would be expected from Eqn. (2.10.1) are not obtained. In general for the bare wings, the symmetric fluttter speed seems to show a slight decrease as the sweepback angle is increased.

Fig. (2.45) shows the effect of sweepback on a cantilever wing. On the same graph is plotted the variation of the flutter speed with sweepback when the symmetric degrees of freedom are allowed (Ref. 18). Both the curves show that the flutter speed increases with increasing sweepback angles, but the actual rates of increase are different.

Addition of concentrated inertias also modifies the behaviour of the flutter speed to increases in the sweepback angle. For example, Figs (2.11) and (2.13) show that it is not possible to predict a regular trend for the $\bar{V}$ - Λ curve and that each wing has to be treated separately.

2.11 INFLUENCE OF COMPRESSIBILITY AND REYNOLDS NUMBER

Most of the experimental results surveyed so far have been obtained from ~~wing~~ Wind tunnel tests on flexible models. It is important to know how these results can be used to predict the behaviour of the full-scale aeroplane. In the wind tunnel models, it is possible to represent the structural and inertial properties of the full-scale aeroplane, but not the aerodynamic forces and moments which act on the aeroplane. It is usual to test models having a symmetrical cross section in order to avoid trimming problems. No measurements seem to have been made to ascertain the effects of aerodynamic scale effects on flutter. Bisplinghoff et al (Ref. 33, p. 710) suggest that provided the Reynolds Number in the wind tunnel is above about 4×10^5 the effects of changes in Reynolds Number are small and the flutter speed and frequency are relatively insensitive to changes in the Reynolds Number. Molyneux (Ref. 24) suggests that wind tunnel models should be built ith a mean chord of at least 8 ins for tests on main surface flutter.

Martin and Sewall (Ref. 14) give an interesting qualitative comparison between a flight flutter test result and the flutter speeds predicted by wind tunnel tests (Fig. 2.46).

The shaded area shows the flutter speeds expected from wind tunnel tests and the flight flutter point is shown as an elongated line because of uncertainties in the amount of fuel present in the tanks at the time of flutter. From this and from other results, they conclude that the model flutter characteristics may be close to those of the full scale aeroplane.

The effect of compressibility can be allowed for

in one of two ways. The model can be constructed so that flutter occurs at the same speed as on the prototype ("True Speed" model"). Use of a variable density tunnel in which the working medium is a mixture of air and another gas, results in some simplification of the model. By varying the amount of the added gas, it is possible to vary the mass ratio, Reynolds Number and the Mach Number independently. A great deal of work has been carried out to assess the effect of Mach Number on the flutter speed. Fig. (2.47) from Ref. (22) is a typical illustration and it refers to a wing with an aspect ratio of 9 and two values of the sweep angle, 16° and 39°, are considered. The effect of the Mach Number is most critical at the transonic speeds.

Very little is known about the effect of Reynolds Number on the flutter speed at supersonic speeds.

2.12 SUMMARY OF THE REVIEW

A review of the available information on the flutter of wings with concentrated inertias has shown that there are a number of parameters which control the flutter characteristics and that these can be varied over a wide range. For cantilever wings of conventional planforms (and having no discontinuities), it is possible to derive criteria (e.g. Ref. 21) from which the effect of varying a certain parameter on the flutter speed can be ascertained. In addition to the geometric, inertial and structural properties (of an unswept cantilever wing) the effects of sweepback and of compressibility can also be taken into account as these confirm to fairly well defined patterns. However, when a concentrated mass is added to the wing, it is not possible to predict with any degree of certainty, the changes in the flutter speed. It is possible to isolate the concentrated mass

parameters which have the most significant effect on the flutter speed. These are (a) the mass, (b) the pitching moment of inertia and (c) the centre of gravity location of the mass (both chordwise and spanwise).

In general, locations of the centre of gravity forward of the elastic axis give increases in the flutter speed. These speeds are generally higher than the flutter speed of the bare wing. For a given wing by a judicious placing of the concentrated mass, it is possible to obtain a large increase in the flutter speed (compared ~~to~~ with the bare wing flutter speed).

These remarks apply to wings with a fixed root. When root degrees of freedom in ~~putch~~ pitch and normal translation are allowed, the flutter speed can be adversely affected. Any flexibility in the attachment of the concentrated mass to the wing can also have an adverse effect on the flutter speed.

Thus, for a given wing mass system, it is difficult to obtain any criteria which would predict the flutter speed and frequency. The particular system has to be analysed either by theoretical means or by experiments in order to estimate the flutter speeds.

CHAPTER 3.

A BRIEF REVIEW OF THE METHODS OF REPRESENTATION OF THE AERODYNAMIC LOADS

3.1. REPRESENTATION OF THE AERODYNAMIC LOADS

The amount of time and effort involved in setting up and solving the equations of motion of a fluttering wing is largely determined by the method used for representing the aerodynamic loads. It is very difficult to take into account the exact airloads acting on a wing which is oscillating in an arbitrary mode. It is usual to make a number of approximations to obtain relatively simple expressions for the lift and moment on an oscillating wing. These are:-

(i) The aerofoil is assumed to have vanishing but finite thickness and very little camber.

(ii) Potential flow is assumed. (The satisfaction of the Kutta condition tacitly assumes the existence of viscosity).

(iii) The aerofoil is assumed to be oscillating harmonically.

(iv) The oscillations are assumed to have small amplitudes (so that linearity of the forces and moments with the deflections is assumed.

3.1.1 Quasi - Steady Approximations

A simple, if very approximate estimate of the lift and moment can be obtained by regarding the loads on the oscillating wing as having the same values as in the case of steady motion, but with the angle of attack being given by the instantaneous inclination between the resultant velocity vector and the wing chord line. If we assume that the downward displacement of the elastic axis is given by h and the instantaneous angle of attack is given by α (Fig. 3.1),

the lift and moment per unit span are given by (Ref. 23, p.279)

$$L = -\pi \rho b^3 \omega^2 \left(i \frac{2}{\nu} \frac{h_0}{b} + i \frac{2}{\nu^2} \alpha_0 \right)$$

$$M_y = L \left(b \bar{a} + \frac{1}{2} \right) \qquad 3.1$$

Where,

$\nu = \frac{b\omega}{V}$ = Reduced Frequency

$h = h_0 \exp(i\omega t)$

$\alpha = \alpha_0 \exp(i\omega t)$

and ω = Frequency of Oscillation

In deriving Eq. (3.1) it has been assumed that the lift curve slope is given by 2π per radian, and that the value of ν is very small.

A more sophisticated approximation is the quasi-steady approximation where only the effect of the wake vortices is neglected. This is equivalent of replacing the Theodoresen function by its limiting value as ν tends to zero. The lift and moment are then given by:-

$$L = \pi \rho b^3 \omega^2 \left[\left(-1 + i\frac{2}{\nu}\right) \frac{h_0}{b} + \left\{ a + \frac{2}{\nu^2} + i\frac{1}{\nu} + i\left(\frac{1}{2}+a\right)\frac{2}{\nu} \right\} \alpha_0 \right]$$

$$M = \pi \rho b^4 \omega^2 \left[\left\{ -a + i\frac{2}{\nu}\left(\frac{1}{2}+a\right) \right\} \frac{h_0}{b} + \left\{ \left(\frac{1}{8}+a^2\right) + \left(\frac{1}{2}+a\right)\frac{2}{\nu^2} - i\left(\frac{1}{2}-a\right)\frac{1}{\nu} + i\left(\frac{1}{4}-a^2\right)\frac{2}{\nu} \right\} \alpha_0 \right] \qquad (3.2)$$

one attraction of using the quasi-steady approximation is that the expressions for the lift and the moment are considerably simpler than the complete expressions obtained from two dimensional strip theory as they do not contain any transcendental functions of the reduced frequency, ν.

3.1.2 Two Dimensional Strip Theory Derivatives

Instead of using the quasi-steady derivatives, a more accurate approximation to the lift and moment is obtained if we divide the wing into a number of spanwise strips and treat

each strip as if it were part of a two dimensional wing. The derivatives are functions of the reduced frequency ($\nu = \frac{b\omega}{V}$) and these as defined in the same sense as in differential calculus and are the differential coefficients of a non-dimensional aerodynamic force with respect to a non-dimensional amplitude of motion.

There are two main notations in use for defining the aerodynamic derivatives. For a two-dimensional wing, they are defined in the British Notation as:-

$$L = \rho V^2 C \left[\left(-\bar{\nu}^2 L_{\ddot{h}} + i\bar{\nu} L_{\dot{h}} + L_h \right) \frac{h_o}{C} + \left(-\bar{\nu}^2 L_{\ddot{\alpha}} + i\bar{\nu} L_{\dot{\alpha}} + L_\alpha \right) \alpha \right]$$

$$M = \rho V^2 C^2 \left[\left(-\bar{\nu}^2 m_{\ddot{h}} + i\bar{\nu} m_{\dot{h}} + m_h \right) \frac{h_o}{C} + \left(-\bar{\nu}^2 m_{\ddot{\alpha}} + i\bar{\nu} m_{\dot{\alpha}} + m_\alpha \right) \alpha \right] \qquad (3.3)$$

where L and M are the lift and moment per unit span and act at the wing leading edge it should be noted that the reduced frequency $\bar{\nu}$ is based on the wing chord and is given by

$$\bar{\nu} = \frac{C\omega}{V} = 2\nu \qquad (3.4)$$

The values of the derivatives are given by (Eg. Ref. 25)

(a) Inertia Derivatives:

$$L_{\ddot{h}} = \pi/4 \quad L_{\ddot{\alpha}} = +\frac{\pi}{8} \quad m_{\ddot{h}} = -\frac{\pi}{8}, \quad m_{\ddot{\alpha}} = -\frac{9\pi}{128} \qquad (3.5)$$

(b) Damping Derivatives:

$$L_{\dot{h}} = \pi F \qquad L_{\dot{\alpha}} = \frac{\pi}{4}\left(1 + 3F + 4G/\bar{\nu}\right)$$

$$m_{\dot{h}} = -\frac{\pi}{4}F \qquad m_{\dot{\alpha}} = -\frac{\pi}{16}\left(3 + 3F + 4G/\bar{\nu}\right) \qquad (3.6)$$

(c) Stiffness Derivatives:

$$L_h = -\pi\bar{\nu}G \qquad L_\alpha = \frac{\pi}{4}\left(4F - 3\bar{\nu}G\right)$$

$$m_h = -\pi\bar{\nu}G \qquad m_\alpha = \frac{\pi}{16}\left(4F - 3\bar{\nu}G\right) \qquad (3.7)$$

In Eqs. 3.6 and ~~3.6~~ 3.7, F and G are the real and imaginary parts of the Theoderesen function,

$$C(\bar{\nu}) = F(\bar{\nu}) + i\,G(\bar{\nu})$$

The values of F and G are tabulated in, for example, Refs. (27), (28).

Van de Vooren (Ref. 26) gives approximate formulae for the evaluation of F and G:

$$F(\bar{\nu}) = \frac{0.021573 + 0.2104\,\bar{\nu} + 0.512607\,\bar{\nu}^2 + 0.500502\,\bar{\nu}^3}{0.021508 + 0.2512395\,\bar{\nu} + 1.035378\,\bar{\nu}^2 + \bar{\nu}^3}$$

$$G(\bar{\nu}) = \frac{0.001995 + 0.32724\,\bar{\nu} + 0.122397\,\bar{\nu}^2 + 0.000146\,\bar{\nu}^3}{0.089318 + 0.93453\,\bar{\nu} + 2.481481\,\bar{\nu}^2 + \bar{\nu}^3} \qquad (3.8)$$

These are valid for values of $\bar{\nu}$ between $\bar{\nu} = 0.1$ and $\bar{\nu} = 3.0$ and the percentage error in this region is less than 4×10^{-4}

The derivatives in the Eqs. (3.5) to (3.7) refer to the lift and moment acting at the wing leading edge. The derivatives with respect to any other axis can be obtained by applying proper transformation formulae (Eg. Ref. 27). If the reference axis is situated at a distance ec aft of the leading edge and if the derivatives with respect to this axis are denoted by $\bar{l}_{\ddot{h}}$, $\bar{l}_{\dot{\alpha}}$, etc, we have

$$\bar{l}_{\ddot{h}} = l_{\ddot{h}} \qquad \bar{l}_{\dot{h}} = l_{\dot{h}} \qquad \bar{l}_{h} = l_{h}$$

$$\bar{l}_{\ddot{\alpha}} = l_{\ddot{\alpha}} - e\,l_{\ddot{h}} \quad \text{etc}$$

$$\bar{m}_{\ddot{h}} = m_{\ddot{h}} + e\,l_{\ddot{h}} \quad \text{etc.}$$

$$\bar{m}_{\ddot{\alpha}} = m_{\ddot{\alpha}} - e\,m_{\ddot{h}} + e\,l_{\dot{\alpha}} - e^2 l_{\ddot{h}} \quad \text{etc.} \qquad (3.9)$$

In the American Notation, the inertia, damping and stiffness derivatives are combined into one unit and the lift and moment per unit span are defined as:

$$L = -\pi\rho b^2\omega^2 \left(L_h \cdot \frac{h_o}{b} + L_\alpha\,\alpha \right)$$

$$M = -\pi\rho b^3\omega^2 \left(M_h \frac{h_o}{b} + M_\alpha\,\alpha \right) \qquad (3.10)$$

If the reference axis is taken as the midchord line of the wing, the derivatives are given by (e.g.Ref. 28)

$$L_h = 1 - \frac{2\lambda}{\nu}(F + \lambda G)$$

$$L_\alpha = \frac{1}{2} - \lambda\left(\frac{1}{\nu}\right)\left\{1 + 2(F + \lambda G)\right\} - \frac{2}{\nu^2}(F + \lambda G)$$

$$M_h = \frac{1}{2}$$

$$M_\alpha = \frac{3}{8} - \frac{\lambda}{\nu} \qquad (3.11)$$

For obtaining the lift and moment about a reference axis situated at a distance (ba) aft of the midchord (Fig.3.1) the following transformation formulae are used:-

$$\bar{L}_h = L_h$$

$$\bar{L}_\alpha = L_\alpha - \left(\frac{1}{2} + a\right) L_h$$

$$\bar{M}_h = M_h - \left(\frac{1}{2} + a\right) L_h$$

$$\bar{M}_\alpha = M_\alpha - \left(\frac{1}{2} + a\right)(L_\alpha + M_h) + \left(\frac{1}{2} + a^2\right) L_h \qquad (3.12)$$

Similar, appropriate derivatives can be defined when the wing has control surfaces and tabs (Eg. Refs. 25, 29).

3.2.3 Empirical Values of the Derivatives

For wings of moderate to large aspect ratio, the use of two dimensional strip theory derivatives in assumed mode analyses gives values of the flutter speed which are generally about 10 to 15% lower than the experimentally measured flutter speeds (Ref. 30, 31).

When the derivatives are defined as in Eqn. (3.3) empirical and semi-empirical corrections can be applied to the derivatives in order to take into account the effect of the tip. One method is to define equivalent constant strip derivatives. These derivatives do not give the correct forces on each strip of the wing but are defined in such a way that they are independent of the spanwise position and after appropriate integration over the span, give the correct generalized forces on the wing.

Another method is to use overall strip derivatives, i.e. derivatives related to the forces on the complete wing. For a wing oscillating in a set of deformation modes, these derivatives are related to the generalized forces and vary with the mode shapes.

Reissner (Ref. 32) has developed a finite span theory for wings of high aspect ratio, but its application to routine flutter calculations is somewhat laborious. In this method the finite span effect is obtained, for a given mode ~~shape~~ shape, by applying corrections to the two dimensional values of the derivatives. Reissner and Stevens (Ref. 30) have prepared tables which simplify the calculations. They also discuss the systematic modifications of the flutter calculations when Reissner's Theory is used to modify a strip theory analysis.

The values of the Equivalent Constant Strip derivatives can be calculated by using an approximate three dimensional theory. Guyett (Ref. 33) gives a comparison between the values of the derivatives obtained from three different theories and the values obtained from two dimensional theory (Fig. 3.2, 3.3, 3.4). These apply to rigid wings oscillating in the modes of pitch and translation. It can be seen that significant finite span effects can occur even for wings of large aspect ratio.

Molyneux and Hall (Ref. 34) tested a number of rigid wings which had freedoms in uniform pitch and linear flexure. The wings had aspect ratios from 2 to 6 and sweepback angles from zero to 60°. It was found for these wings that the calculated and the measured values of the derivatives agreed fairly well if the two dimensional theoretical derivatives were modified in the following way:

(a) Multiply the damping derivatives (l_k, $l_{\dot{\alpha}}$ etc) by $1/f(A)$

(b) Multiply the stiffness derivatives (l_h, l_α etc) by $(1/f(A))^2$

where $$f(A) = \left\{1 + \frac{0.8}{A.R.}\right\} \qquad (3.13)$$

It is not possible to obtain such simple corrections for the derivatives defined as in Eqn. (3.10) since each of the derivatives contains the influence of the inertia, damping and stiffness derivatives.

CHAPTER 4

A REVIEW OF METHODS OF FLUTTER ANALYSIS APPROPRIATE TO WINGS WITH LARGE CONCENTRATED INERTIAS

A number of analytical methods have been used to obtain the flutter speeds of wings with concentrated masses. The methods differ from each other in three important respects:

(a) The mathematical model used to represent the wing and the method used to obtain the equations of motion,

(b) The method used for describing the aerodynamic loading on the wing,

(c) The method employed to solve the equations of motion to obtain the flutter speed and flutter frequency.

The behaviour of the physical system can be expressed in terms of one of the following: the basic differential equations, the basic integral equation or by using an energy approach.

In general, for an arbitrary wing, the inertial and structural properties are known at a set of points on the wing and are not easily definable in terms of simple mathematical functions. It will not therefore be possible to obtain an exact solution for the flutter speed. However, there exists a class of simple wings for which it is possible to obtain exact solutions. These solutions can be regarded as standards of comparison for estimating the accuracy of other analytical methods.

It should be noted that these solutions are 'exact' only in so far as the aerodynamic terms used in the analysis are 'exact'.

4.1 'EXACT' SOLUTION - DIFFERENTIAL EQUATION AND OPERATIONAL APPROACH

Subject to the above limitation, the first exact solution was obtained by Goland (Ref. 35) who treated the bending-torsion flutter of a bare, uniform cantilever wing with uniformly distributed inertial and elastic properties. Starting from the partial differential equations of motion and using the boundary conditions at the root and at the tip of the wing, he was able to obtain the solution of the flutter problem by straightforward methods.

Goland and Luke (Ref. 36) used a differential equation approach to solve the flutter problem of a uniform wing with tip weights. They also included the fuselage degrees of freedom (both symmetric and anti-symmetric) in the analysis and the differential equations of motions were solved by an operational method. The results from both Ref. (35) and from Ref(36) showed good agreement with the results obtained by energy methods.

An important extension to the method of Ref.(36) was made by Runyan and Watkins (Ref. 37) to consider the flutter of a uniform wing with an arbitrarily placed concentrated mass.

Consider a uniform cantilever wing, whose stiffnesses EI, GJ and the quantities m (mass per unit length), S_α (static unbalance per unit length) and I_α (pitching moment of inertia per unit length) are all constant along the span (Fig. 4.1) The differential equations of motion can be written as:

$$\begin{aligned} m\ddot{h} + S_\alpha \ddot{\alpha} + EI \frac{d^4 h}{dy^4} &= L(y,t) \\ S_\alpha \ddot{h} + I_\alpha \ddot{\alpha} - GJ \frac{d^2\theta}{dy^2} &= M(y,t) \end{aligned} \qquad (4.1)$$

The appropriate boundary conditions are

$$h(0) = \left.\frac{dh}{dy}\right|_{y=0} = \alpha(0) = 0$$

$$\left.\frac{d^2h}{dy^2}\right|_{y=s} = \left.\frac{d^3h}{dy^3}\right|_{y=s} = \left.\frac{d\alpha}{dy}\right|_{y=s} = 0$$

$$\left\{\left.\frac{d^2h}{dy^2}\right|_{L_1^-} - \left.\frac{d^2h}{dy^2}\right|_{L_1^+}\right\} = -\frac{W}{g}\frac{\omega^2}{EI}\left\{h(L_1) + e_2\alpha(L_1)\right\}$$

$$\left\{\left.\frac{d\theta}{dy}\right|_{L_1^-} - \left.\frac{d\theta}{dy}\right|_{L_1^+}\right\} = \frac{W}{g}\frac{\omega^2}{GJ}\left\{e_2 h(L_1) + K_2^2\alpha(L_1)\right\} \quad (4.2)$$

In Eqs. (4.1) and (4.2)

L = Lift per unit span

M = Moment per unit span

W = Weight of concentrated mass

e_2 = Distance of the concentrated mass c.g. from the wing elastic axis

K_2 = Radius of gyration of the concentrated mass about the elastic axis

and the subscripts 1_1^- and 1_1^+ represent the values of the derivatives as 1_1 is approached from the side $y < L_1$ and from $y > L_1$ respectively.

Runyan and Watkins solved Eqs. (4.1) by first taking the Laplace transform of the two equations and solving for $\bar{h}$ and $\bar{\alpha}$, the transforms of h and α respectively. After using the boundary conditions at the root these can be written as:

$$\bar{h}(p) = \frac{1}{\Delta p}\left[(p^3+p\delta)H_2 + (p^2+\delta)H_3 + \beta\theta_1 - \beta e^{-pL_1}\left(\left.\frac{d\alpha}{dy}\right|_{L_1^-} - \left.\frac{d\alpha}{dy}\right|_{L_1^+}\right)\right\}$$
$$- (p^2+\delta)\left(\left.\frac{d^3h}{dy^3}\right|_{L_1^-} - \left.\frac{d^3h}{dy^3}\right|_{L_1^+}\right)\Big]$$

$$\bar{\alpha}(p) = \frac{1}{\Delta p}\Big[p^4\theta_1 - \gamma p H_2 - \gamma H_3 - \alpha\theta_1 + \gamma e^{-pL_1}\left(\left.\frac{d^3h}{dy^3}\right|_{L_1^-}\right.$$
$$\left. - \left.\frac{d^3h}{dy^3}\right|_{L_1^+}\right) + (\alpha - p^4)\, e^{-pL_1}\left(\left.\frac{d\alpha}{dy}\right|_{L_1^-} - \left.\frac{d\alpha}{dy}\right|_{L_1^+}\right)\Big] \quad (4.3)$$

where

$$\Delta p = p^6 + \delta p^4 - \alpha p^2 + \gamma\beta - \alpha\delta$$

$$\alpha = \frac{1}{EI}\left(m + L_h + \lambda L_h'\right)\omega^2$$

$$\beta = \frac{1}{EI}\left(me_1 + L_\theta + \lambda L_\theta'\right)\omega^2$$

$$\gamma = \frac{1}{GJ}\left(me_1 + M_h + \lambda M_h'\right)\omega^2$$

$$\delta = \frac{1}{GJ}\left(I + M_\theta + \lambda M_\theta'\right)\omega^2$$

and the lift and moment are defined by

$$L\,dy = \left(\omega^2 L_h h + \omega L'_h \frac{dh}{dt} + \omega^2 L_\alpha \alpha + \omega L'_\alpha \frac{d\alpha}{dt}\right) dy$$

$$M\,dy = \left(\omega^2 M_h h + \omega M'_h \frac{dh}{dt} + \omega^2 M_\alpha \alpha + \omega M'_\alpha \frac{d\alpha}{dt}\right) dy$$

In general it is not possible to factorize Δp and so obtain the inverse of $\bar{h}(p)$ and $\bar{\alpha}(p)$. Runyan and Watkins expanded the function $(1/\Delta(p))$ in the form of a power series:

$$\frac{1}{\Delta p} = \frac{1}{p^6} \sum_{n=0}^{\infty} \frac{T_n}{p^{2n}} \qquad (4.4)$$

where the T_n are functions of α, β, γ and δ. The series converges rapidly and in calculations, only a few terms of the series need be used.

After obtaining the mode shapes $h(y)$ and $\alpha(y)$ by inverting Eq. (4.3), the flutter determinant can be derived by using the boundary conditions at the tip as:

$$\begin{vmatrix} h''_1(l) & h''_2(l) & h''_3(l) \\ h'''_1(l) & h'''_2(l) & h'''_3(l) \\ g'_1(l) & g'_2(l) & g'_3(l) \end{vmatrix} = 0 \qquad (4.5)$$

where the terms in the flutter determinant are functions of the inertial and structural properties of the wing, the aerodynamic loads and the concentrated mass parameters.

To obtain the flutter speed, flutter frequency and the flutter mode shapes, a trial and error procedure has to be followed. For a given wing-mass configuration, the coefficients in Eq. (4.5) are functions of the flutter frequency ω and the corresponding reduced frequency ν $(= b\omega/v)$, and the problem is one of finding values of ω and ν which cause the flutter determinant to vanish.

Runyan and Watkins applied this method to obtain the flutter speeds of a uniform cantilever wing carrying a large concentrated mass placed ahead of the elastic axis (weight 7a of Ref. 38). The flutter speeds obtained were within 7% of the experimental values. On the other hand, a Rayleigh type analysis for the same wing gave highly unconservative values.

In this formulation the order of the flutter determinant depends only upon the order of the system of differential equations to be solved and not upon the number of modes involved. It is not limited to the case of a uniform cantilever wing with a single concentrated mass. By proper attention to the boundary conditions the theory can be extended to cover the case of a wing carrying a number of masses. One of these could be the fuselage and both symmetric and anti-symmetric types of flutter can be analysed. The same type of analysis, with the air loads equated to zero, can be used to obtain the coupled modes and frequencies of the wing-mass system.

4.2 EXACT SOLUTION - DIFFERENTIAL EQUATIONS AND LYAPUNOV'S DIRECT METHOD

Lyapunov's second (or direct) method has been used in control system analysis, but so far has found very little application in aeroelasticity. The advantages of this method - the ability to deal directly with the distributed system in the form of partial differential equations or integral equations without having to resort to approximations and its ability to handle system non-linearities seem to be more than offset by the difficulties in choosing a proper 'functional' which is an essential part of the analysis.

In Ref. (39), Parks used Lyapunov's method to obtain the stability boundaries for the problem of fluttering panel.

Wang (Ref. 40) obtained the stability boundaries of a horizontal tail mounted on a flexible fuselage by using this method.

In Ref 41, Wang discusses the formulation of stability problems of both elastic and aeroelastic systems in the framework of the Lyapunov stability theory. Among other problems, he considers the flutter problem of a cantilever wing and that of a cantilever wing carrying two concentrated masses at the tip, one of which is attached to the other by means of a spring.

In using the second method of Lyapunov, we attempt to obtain information on the stability of the equilibrium states of the system without actually solving the system equations for the roots. This method is based on a generalisation of the idea that if a system has an asymptotically stable equilibrium state, then the stored energy of the system decays with increasing time until it reaches its minimum value at the equilibrium state. In the second method of Lyapunov, a fictitious 'energy' function or a Lyapunov function is determined first.

The equations of motion of a cantilever wing can be written as:

$$m(\eta) V^2 s^2 \frac{\partial^2 h}{\partial t^2} + S_\alpha(y)\, V^2 s \frac{\partial^2 \alpha}{\partial t^2} + \frac{\partial^2 [EI(\eta)]}{\partial \eta^2} \frac{\partial^2 h}{\partial \eta^2} = s^3 \left[L\left(h, \frac{\partial h}{\partial t}, \alpha, \frac{\partial \alpha}{\partial t}\right) + D_h\left(h, \frac{\partial h}{\partial t}\right) \right]$$

$$S_\alpha(\eta) V^2 s \frac{\partial^2 h}{\partial t^2} + \lambda(\eta) V^2 \frac{\partial^2 \alpha}{\partial t^2} - \frac{\partial [GJ(\eta)]}{\partial \eta} \frac{\partial \alpha}{\partial \eta} = s^2 \left[M_y\left(h, \frac{\partial h}{\partial t}, \alpha, \frac{\partial \alpha}{\partial t}\right) + D_\alpha\left(\alpha, \frac{\partial \alpha}{\partial t}\right) \right] \qquad 4.6$$

Where,

$$L + D_h = K_{h_1} h + K_{\dot{h}_1} \frac{\partial h}{\partial t} + K_{\alpha_1} \alpha + K_{\dot{\alpha}_1} \frac{\partial \alpha}{\partial t}$$

$$M + D_\alpha = K_{h_2} h + K_{\dot{h}_2} \frac{\partial h}{\partial t} + K_{\alpha_2} \alpha + K_{\dot{\alpha}_2} \frac{\partial \alpha}{\partial t} \qquad (4.7)$$

and $\eta\ (=y/s)$ is the non dimensional span. Consider the case when two concentrated masses M and $\bar{M}$ are attached to each other by a non-linear spring and damper.

Let the mass $\bar{M}$ be attached rigidly to the wing tip. Let $\hat{z}$ denote the displacement, normalized with respect to s, of M with respect to the (x, y) plane. The equation of motion for M can be described by

$$M V^2 s \frac{d^2\hat{z}}{dt^2} + V^2 s^2 f_d\left(\hat{z}+h(1,t)\right)\left(\frac{d\hat{z}}{dt}+\frac{dh(1,t)}{dt}\right) + \rho^2 K\left(\hat{z}+h(1,t)\right) = 0 \qquad (4.8)$$

where time t is normalized with respect to s/V, and f_d and K are specified functions, corresponding to the damping coefficient and the spring force, respectively.

The boundary conditions at the root and at the tip are now given by:

Root: $h = \frac{\partial h}{\partial \eta} = \alpha = 0$

Tip:

$$\frac{\partial}{\partial \eta} EI(\eta)\frac{\partial^2 h}{\partial \eta^2} = \bar{M} V^2 s \frac{\partial^2 h}{\partial t^2} + V s^2 f_d\left(\hat{z}+h(1,t)\right) \times \left(\frac{d\hat{z}}{dt}+\frac{dh}{dt}\right) + \rho^2 K\left(\hat{z}+h(1,t)\right)$$

$$EI(\eta)\frac{\partial^2 h}{\partial \eta^2}\Big|_{\eta=1} = 0 \qquad GJ\frac{\partial \alpha}{\partial \eta}\Big|_{\eta=1} = \frac{I_1 V^2}{s}\frac{d^2\alpha}{dt^2}\Big|_{\eta=1} \qquad (4.9)$$

where I_1 is the moment of inertia of M and $\bar{M}$ about the wing elastic axis.

To obtain sufficient conditions for the stability of the system, Wang considers a functional of the form:

$$V = V_1 + V_2 + V_3 \qquad (4.10)$$

where:

$$V_1 = \frac{1}{2}\int_0^1 \left\{ m(\eta) V^2 s^2 \left(\frac{\partial h}{\partial t}\right)^2 + EI(\eta)\left(\frac{\partial^2 h}{\partial \eta^2}\right)^2 - 2 S_\alpha(\eta) V^2 s \frac{\partial h}{\partial t}\frac{\partial \alpha}{\partial t} + GJ(\eta)\left(\frac{\partial \alpha}{\partial \eta}\right)^2 + \lambda(\eta) V^2 \left(\frac{\partial \alpha}{\partial t}\right)^2 \right\} d\eta$$

$$V_2 = \int_0^1 \left\{ c_1 h \left[m(\eta) V^2 s^2 \frac{\partial h}{\partial t} - S_\alpha(\eta) V^2 s \frac{\partial \alpha}{\partial t}\right) + c_2 \alpha \lambda(\eta) V^2 \frac{\partial \alpha}{\partial t} - S_\alpha(\eta) V^2 \frac{\partial h}{\partial t}\right) d\eta$$

$$V_3 = \frac{1}{2} V^2 s \left\{ M\left(\frac{d\hat{z}}{dt}\right)^2 + \bar{M}\left(\frac{dh(1,t)}{dt}\right)^2 + I_1 s^{-2}\left(\frac{d\alpha(1,t)}{dt}\right)^2 + \int_0^{\hat{z}+h(1,t)} s^2 K(\xi)\, d\xi \right.$$

To ensure the asymptotic stability of the system with respect to four metrics ρ_1, ρ_2, ρ_3 and ρ_4 the following conditions have to be satisfied:

i) The symmetric matrix Q_1 be positive definite for all $\eta \in [0,1]$ The elements of Q_1 are given by:

$$q_{11} = \tfrac{1}{2} \min_{\eta \in [0,1]} EI(\eta) \qquad q_{12} = q_{21} = c_1 m(\eta)\, V^2 S^2$$
$$q_{22} = m(\eta)\, V^2 S^2 \qquad q_{23} = q_{32} = -c_2 S_\alpha(\eta)\, V^2 S^2$$
$$q_{13} = q_{31} = 0 \qquad q_{24} = q_{42} = -S_\alpha(\eta)\, V^2 S$$
$$q_{14} = q_{41} = -c_1 S_\alpha(\eta) V^2 S \qquad q_{34} = q_{43} = c_2 i(\eta)\, V^2$$
$$q_{33} = \min_{\eta \in [0,1]} GJ(\eta) \qquad q_{44} = i(\eta)\, V^2 \qquad (4.11)$$

ii) The symmetric matrix Q_2 be negative definite. The elements of Q_2 are given by:

$$q_{11} = 2c_1 S^3 K_{h1} - \min_{\eta \in [0,1]} EI(\eta)$$
$$q_{12} = q_{21} = S^3 (c_1 K_{\dot{h}_1} + K_{h_1})$$
$$q_{13} = q_{31} = S^2 (c_1 S K_{\alpha_1} + c_2 K_{h_2})$$
$$q_{14} = q_{41} = S^2 (c_1 S K_{\dot{\alpha}_1} + K_{h_2})$$
$$q_{22} = 2 S^2 (c_1 m(\eta) V^2 + K_{\dot{h}_1} S)$$
$$q_{23} = q_{32} = S^2 (c_2 K_{\dot{h}_2} + S K_{\alpha_1})$$
$$q_{33} = 2 c_2 (1^2 K_{\alpha_2} - \min_{\eta \in [0,1]} GJ(\eta))$$
$$q_{34} = q_{43} = S^2 (c_2 K_{\dot{\alpha}_2} + K_{\alpha_2})$$
$$q_{44} = 2 (c_2 i(\eta) V^2 + S^2 K_{\dot{\alpha}_2}) \qquad (4.12)$$

and, iii) the following conditions also be satisfied:

$$f_d(\hat{z} + h(t,1)) > 0$$
$$(\hat{z} + h(t,1)) \cdot K(\hat{z} + h(t,1)) > 0 \quad \text{for } (\hat{z} + h(t,1)) \neq 0 \qquad (4.13)$$

The stability boundaries in a given parameter space can be obtained with the help of a digital computer.

No numerical results are given by Wang. From the short description given above it can be seen that the stability boundaries can be obtained without having to make any assumptions about the behaviour of the system. There is no need to find ~~out~~ the roots of the equations of motion. This type of formulation is very helpful in studying the influence of the variation of certain parameters on the flutter speeds. One disadvantage of the method is that no information about the frequencies and modes of the system can be obtained.

Another difficulty is in the correct representation of the aerodynamic forces. The usual form of the aerodynamic forces and moments obtained by assuming simple harmonic motion are applicable to divergent oscillations but not for convergent oscillations (Ref. 23, pp. 281 - 2).

4.3 INTEGRAL EQUATION APPROACH

Van de Vooren (Ref. 42) has given a procedure in which the normal modes calculated by using a matrix procedure are used in obtaining the flutter speed, frequency and also the flutter mode. His procedure considers a system with a large number of degrees of freedom, and is applicable to an aeroplane with concentrated masses, controls, etc. The fuselage degrees of freedom can be included in the analysis.

Consider an aeroplane carrying some concentrated masses on the wings. For symmetric vibrations the displacements in bending and torsion of the wing can be represented by the equations

$$z(y) - z(0) = \int_0^S K_{11}(y,\eta)\, F(\eta)\, d\eta$$

$$\Phi(y) - \Phi(0) = \int_0^S K_{22}(y,\eta)\, M(\eta)\, d\eta + \sum_{i=1}^{n} \int_0^S K_{22}(y,\eta)\, P(\eta)\, \delta(\eta-\eta_i)\, d\eta$$

$$\Theta(y_i) - \Phi(y_i) \quad (i = 1, \ldots n) = \int_0^S K_{44}(y_i,\eta)\, P(\eta)\, \delta(\eta-\eta_i)\, d\eta, \qquad (4.12)$$

where

$z(\eta)$ = wing deflection measured (at the elastic axis)

$\Phi(y)$ = twist angle at y about elastic axis

$\Theta(y_i)$ = twist angle of the conc. mass concentrated at y_i, $i = 1, \ldots n$

$F(\eta)$ = mass of (wing + conc. mass) at station η per unit span

$m(\eta)$ = moment of inertia of wing + moment of inertia of the concentrated mass (assumed as concentrated at the attachment) All moments of inertia are about the elastic axis/unit span

$P(y_i)$ = moment of inertia of the concentrated mass about the attachment point at y_i

$k_{11}(y,\eta)$ = influence function of wing deflection

$k_{22}(y,\eta)$ = influence function of wing torsion

$k_{44}(y,\eta)$ = influence function of the torsion of the concentrated mass

$z(0)$, $\Phi(0)$ = fuselage deflections

$\delta(\eta-\eta_i) = 0$ for $\eta \neq \eta_i$ (Dirac delta)

The forces and moments are completely determined by the mass distribution and by the vibration amplitudes $z(y)$, $\Phi(y)$ and $\Theta(y_i)$ as:

$$F(y) = \{ m_{11} z + m_{12} \Phi + m_{14} \Theta \cdot \delta(y-y_i) \} \nu^2$$

$$m(y) = \{ m_{12} z + m_{22} \Phi + m_{24} \Theta \, \delta(y-y_i) \} \nu^2$$

$$P(y_i)\,\delta(y-y_i) = [m_{14} z + m_{24} \Phi + m_{44} \Theta \cdot \delta(y-y_i)] \nu^2 \qquad (4.14)$$

Substituting (4.14) in (4.13) we have the equation for the displacements as

$$\underline{f_d} = \nu^2 \int_0^s \underline{K}(y,\eta)\, \underline{m}(\eta)\, \underline{f}(\eta)\, d\eta \qquad (4.15)$$

where

$$\underline{f_d} = \text{col}\{ (z(y)-z(0)),\ (\Phi(y)-\Phi(0)),\ (\Theta(y_i)-\Theta(0)) \}$$

$$\underline{f}(y) = \text{col}\{ z(y),\ \Phi(y),\ \Theta(y_i) \}$$

$$\underline{m}(y,\eta) = \begin{bmatrix} m_{11}(\eta) & m_{12}(\eta) & m_{14}(\eta)\,\delta(\eta-\eta_i) \\ m_{12}(\eta) & m_{22}(\eta) & m_{24}(\eta)\,\delta(\eta-\eta_i) \\ m_{14}(\eta)\,\delta(\eta-\eta_i) & m_{24}(\eta)\,\delta(\eta-\eta_i) & m_{44}(\eta)\,\delta(\eta-\eta_i) \end{bmatrix}$$

and

$$\underline{K}(y,\eta) = \begin{bmatrix} K_{11}(y,\eta) & 0 & 0 \\ 0 & K_{22}(y,\eta) & K_{22}(y,\eta_i) \\ 0 & K_{22}(y,\eta) & K_{22}(y,\eta_i) + K_{44}(y_i,\eta_i) \end{bmatrix}$$

To eliminate the fuselage motions we equate the sum of all the vertical forces and the sum of all the moments about the ea separately to zero, i.e.

$$\left.\begin{aligned} \int_0^S F(\eta)\, d\eta &= 0 \\ \int_0^S \{ M(\eta) + P(\eta)\, \delta(\eta-\eta_i) \}\, d\eta &= 0 \end{aligned}\right\} \quad 4.16$$

Using these two conditions we have

$$\underline{f}_d = \nu^2\, \underline{D}\, \underline{f}_d \qquad 4.17$$

where

$$\underline{D} = \underline{K}\cdot \underline{m}^* \qquad 4.18$$

$\underline{K}$ and $\underline{m}^*$ are both symmetrical Matrices and $\underline{m}^*$ represents the mass matrix after the elimination of the fuselage motions.

The frequencies ν and the modes $\underline{f}_d$ can be obtained from Eqn 4.17 using the standard procedures of Matrix iteration. It should be noted that though $\underline{K}$ and $\underline{m}^*$ are Symmetrical Matrices, $\underline{D}$ will not, in general, be symmetrical ~~$\underline{D}$ need not be Symmetrical~~.

The integral equations (4.17) are also valid for flutter, but now the elements of $\underline{D}$ will be defined as

$$\underline{D} = \underline{K}\ (\underline{m} + \underline{A}^*) \qquad (4.18)$$

where $\underline{A}^*$ is the matrix of aerodynamic coefficients.

The iteration procedures can be simplified if we know the matrix $\underline{D}$ as the product of symmetric matrices (as in equations 4.17). In the case of flutter, introduction of the aerodynamic matrix $\underline{A}^*$ removes this possibility since the element of $\underline{A}^*$ are in general complex and A^* itself is non-Hermitian.

To simplify the task of solving Equation (4.17) with $\underline{D}$ expressed as in Eq. (4.18), Van de Vooren introduces the normal co-ordinates, thereby effectively restricting the number of degrees of freedom. The normal

co-ordinates are given by:

$$\underline{f}_d = \underline{F} \cdot \underline{q} \qquad (4.19)$$

where $\underline{F}$ is a rectangular matrix whose p- columns are eigenvectors $\underline{f}_1, \underline{f}_2, \ldots, \underline{f}_p$ (which are the eigenvectors of $\underline{D}$ in Eqn. (4.17)).

Substituting (4.19) in (4.17) we get

$$\underline{F}\,\underline{q} = \nu^2\, \underline{D}\,\underline{F}\,\underline{q} \qquad (4.20)$$

This equation could be put into the standard characteristic value problem format by premultiplying both sides by $\underline{G}^T$. (The p rows of $\underline{G}^T$ are $\underline{g}_1^T, \underline{g}_2^T, \ldots, \underline{g}_p^T$ the eigenvectors of the transpose of $\underline{D}$, i.e, $\underline{D}^T$). By invoking the condition of orthogonality $\underline{G}^T\underline{F}$ becomes a unit matrix and Eq. (4.20) can be written as

$$\underline{q} = \nu^2\, \underline{G}^T\, \underline{D}\, \underline{F}\, \underline{q} \qquad (4.21)$$

This equation can be solved for the eigenvalues ν and the eigenvectors q, the flutter speed and frequency are obtained by the V-g method.

4.4 INTEGRAL EQUATION - WIELANDT'S ITERATIVE TRANSFORMATION PROCEDURE

Gossard (Ref. 43) illustrated the use of Wielandt's iterative transformation procedure for the vibration and flutter problem of wings. He obtained the flutter speed, frequency and mode shapes for a particular case of the wing of Ref. (38)

For the solution of the equations of the vibrating system Wielandt's procedure is similar in form to the standard iteration procedure. The lower order eigenvalues and eigenvectors are obtained first and these are swept out to obtain the higher order eigenvalues and eigenvectors. In the standard iteration procedure, sweeping is carried out

by invoking the orthogonality relationship between the modes. In the Wielandt procedure, a forcing function is used which greatly simplifies the numerical work. The true value of the nth eigenvalue is found directly in the iterative transformation procedure, but the true nth mode is computed from quantities within the iteration cycle after the transformed nth mode has been found. This transformed nth mode is a particular combination of all the modes from the fundamental to the nth mode.

Consider the problem of the coupled vibrations of a wing mass system. The equation for the mode shape components in bending and in torsion for a cantilever wing is:

$$h = \omega^2 \int_0^y \int_0^y \frac{1}{EI} \int_y^L \int_y^L (P_h h + P_\alpha \alpha)\,(dy)^4$$

$$\alpha = \omega^2 \int_0^y \frac{1}{GJ} \int_y^L (Q_h h + Q_\alpha \alpha)\,(dy)^2 \qquad 4.22$$

These relations have been obtained by integration of the basic differential equation using the proper boundary conditions at the root and at the tip.

In Eqn (4.22) the expressions $(P_h h + P_\alpha \alpha)$ and $(Q_h h + Q_\alpha \alpha)$ are the intensities of applied force and torque respectively. The P and Q coefficients are given by

$$\begin{aligned} P_h &= m \\ P_\alpha &= m\,b\,e = Q_h \\ Q_\alpha &= m b^2 r^2 \end{aligned} \qquad (4.23)$$

and m = mass/unit length

be = distance of the c.g. from the elastic axis

br = radius of the gyration of the wing about the elastic axis

The inertia forces and torques due to a concentrated mass are:

$$(P_h h + P_\alpha \alpha) = \lim_{dy \to 0} \frac{\bar{P}_h h + \bar{P}_\alpha \alpha}{dy}$$

$$(Q_h h + Q_\alpha \alpha) = \lim_{dy \to 0} \frac{\bar{Q}_h h + \bar{Q}_\alpha \alpha}{dy} \qquad 4.24$$

In Eqns (4.24)

$$\bar{P}_h = M$$

$$\bar{P}_\alpha = \bar{Q}_h = M\, b\, \bar{e}$$

$$\bar{Q}_\alpha = M \cdot b^2 \bar{r}^2 \qquad 4.25$$

Each coupled mode is a solution of the simultaneous relations given by (4.22). Each mode contains both the flexural and torsional components which always appear together in a fixed relation to each other.

In most cases the integrations must be performed numerically and this is best done by dividing the wing into a number of segments. The number and disposition of the stations have a great influence on the amount of labour involved and the accuracy of the results. In general, a station must be placed at each discontinuity such as concentrated masses, discontinuities in the structural stiffness distribution, etc.

The flexural and torsional components of the first mode are obtained by using the standard procedure for iteration: (a) assuming a plausible mode shape, (b) performing the integrations indicated in equations (4.22) (c) comparing the derived and assumed mode shape and (d) if necessary repeating the process until reasonable agreement is obtained between the assumed mode shape and the derived mode shape. From the results of two successive iterations, the fundamental coupled frequency can be obtained.

To obtain the sweeping function which would 'sweep out' the fundamental mode from the integral relations (4.22), the standard iteration procedures invoke the orthogonality requirement between the first mode and the second mode.

In the iterative transformation procedure, the immediate aim is to find a linear combination of the first and second modes which is called the transformed second mode.

The iteration process can be illustrated diagramatically as in Fig. (4.A).

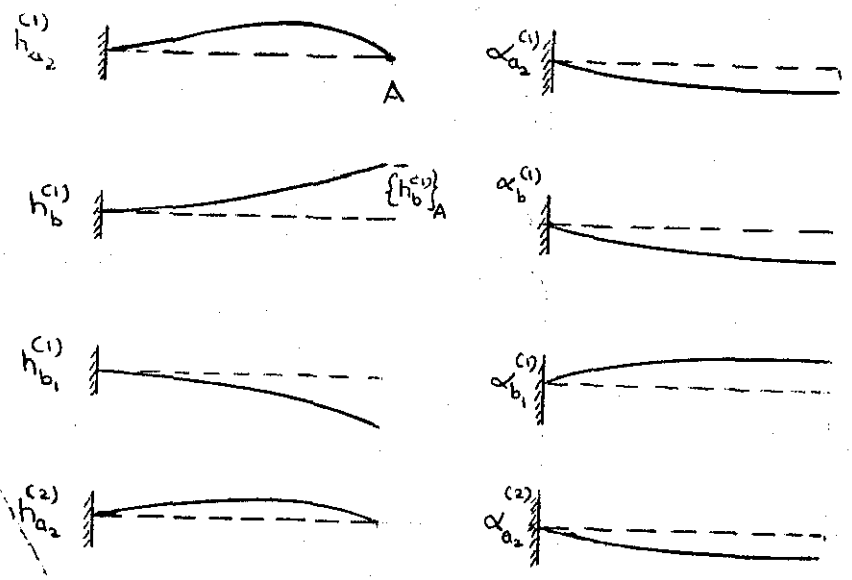

FIG. 4.A

In the first step a plausible form for the transformed second mode is assumed (for greatest accuracy, the transformed second mode should have a nodal point in the component and at the station where the first coupled mode has the greatest amplitude). In Fig. 4.A(a), these assumed forms are designated as $h_{a_2}^{(1)}$ and $\alpha_{a_2}^{(1)}$ respectively for the bending and torsional components.

The second step is to obtain intermediate derived modes $h_b^{(1)}$ and $\alpha_b^{(1)}$ which are the results of carrying out the integrations indicated in Eq. (4.22) using the mode shapes $h_{a_2}^{(1)}$ and $\alpha_{a_2}^{(1)}$ respectively.

The sweeping function can now be derived. This is found such that it has the shape of the (previously determined) first coupled mode. Its magnitude is found from the condition that the sum of the intermediate derived mode and the sweeping function equals zero at station A, i.e. at any given station:

$$h_{b_1}^{(1)} = -\left(\frac{h_b^{(1)}}{h_1}\right)_A h_1 \qquad \alpha_{b_1}^{(1)} = -\left(\frac{h_b^{(1)}}{h_1}\right)_A \alpha_1 \qquad 4.26$$

The first iteration to the transformed second mode is given by

$$h_{a_2}^{(2)} = h_b^{(1)} - \left(\frac{h_b^{(1)}}{h_1}\right)_A \cdot h_1$$

$$\alpha_{a_2}^{(2)} = \alpha_b^{(1)} - \left(\frac{h_b^{(1)}}{h_1}\right)_A \alpha \qquad (4.27)$$

These values of $h_{a_2}^{(2)}$ and $\alpha_{a_2}^{(2)}$ are taken as the starting point for the next iteration cycle, and the iterations are repeated until the values of the ratios $\left\{h_{a_2}^{(2)}/h_{a_2}^{(1)}\right\}$ and $\left\{\alpha_{a_2}^{(2)}/\alpha_{a_2}^{(1)}\right\}$ are reasonably the same at all stations. If the assumed mode shape is exactly equal to the transformed second mode shape, all these ratios are equal to each other and contain the single unknown ω_2^2. The value of ω_2^2 is that which makes these ratios equal to unity.

A physical interpretation of the transformed second mode is that the vibration in this mode is the response of the beam to an oscillatory load having the shape of the first mode shape and a frequency equal to the second natural frequency, superimposed on the free vibration modeform of the beam in the second natural mode. The procedure can be extended in a similar manner to determine the higher order frequencies. The free mode shapes can be derived from the transformed mode shape.

The equations of a fluttering wing are similar to equations (4.22) except that the P and Q components are now complex and depend on the value of the reduced frequency, ν. The solution to the problem would include complex values of the frequency ω. Since the velocities should be real quantities and flutter occurs for only real values of it is necessary to introduce an artificial damping factor g so that the complex eigenvalue is now given by $(\omega^2/1+ig)$. Gossard calls this transformed problem the pseudo-flutter problem. With this notation and neglecting structural damping the equation of the fluttering cantilever wing can be

$$h = \frac{(1+ig)}{\omega^2} \int_0^y \int_0^y \frac{1}{EI} \int_y^L \int_y^L (P_h h + P_\alpha \alpha)\,(dy)^4$$

$$\alpha = \frac{(1+ig)}{\omega^2} \int_0^y \frac{1}{GJ} \int_y^L (Q_h h + Q_\alpha \alpha)\,(dy)^2 \qquad 4.28$$

In Eqs.(4.28),

$$P_h = P_{Rh} - i\,P_{Ih} \qquad 4.29$$

where:

$$P_{Rh} = \pi \rho\, b_o^2 \left(\frac{b}{b_o}\right)^2 \left(2G/\nu + 1 + m/\pi \rho b_o^2\right)$$

$$P_{Ih} = \pi \rho\, b_o^2 \cdot \left(\frac{b}{b_o}\right)^2 2F/\nu$$

$$P_\alpha = P_{R\alpha} - P_{I\alpha} \qquad 4.30$$

$$P_{R\alpha} = \left(\frac{b}{b_o}\right)^3 \left[\left(\tfrac{1}{2}-a\right) 2G/\nu - 2F/\nu^2 - a + m.e/\pi \rho b_o^2\right] \cdot \pi \rho b_o^3$$

$$P_{I\alpha} = \left(\frac{b}{b_o}\right)^3 \left[1/\nu + 2G/\nu^2 + \left(\tfrac{1}{2}-a\right) 2F/\nu\right] \cdot \pi \rho b_o^3$$

$$Q_h = Q_{Rh} - i\,Q_{Ih} \qquad 4.31$$

$$Q_{Rh} = \pi \rho b_o^3 \cdot \left(\frac{b}{b_o}\right)^3 \left[-\left(\tfrac{1}{2}+a\right) 2G/\nu - a - m.e/\pi \rho b_o^2\right]$$

$$Q_{Ih} = \pi \rho b_o^3 \left(\frac{b}{b_o}\right)^3 \left[-\left(\tfrac{1}{2}+a\right) 2F/\nu\right]$$

$$Q_\alpha = Q_{R\alpha} - Q_{I\alpha} \qquad 4.32$$

$$Q_{R\alpha} = \pi \rho b_o^4 \left(\frac{b}{b_o}\right)^4 \left[-(1/4 - a^2) 2G/\nu + \left(\tfrac{1}{2}+a\right) 2F/\nu^2 + 1/8 + a^2 + mr^2/\pi \rho b_o^2\right]$$

$$Q_{I\alpha} = \pi \rho b_o^4 \left(\frac{b}{b_o}\right)^4 \left[\left(\tfrac{1}{2}-a\right)/\nu - \left(\tfrac{1}{2}+a\right) 2G/\nu^2 - (1/4-a^2)\, 2F/\nu\right]$$

Equations (4.28) can be solved in a way analoguous to the solution of Eqns. (4.23). The main differences in the case of Eqn (4.28) are that (a) the coefficients P and Q are complex and depend on the reduced frequency and (b) all the calculations involve complex numbers and the modes now involve complex numbers, reflecting the phase difference in each of the modes along the span.

The actual mechanics of solving Eqns (4.28) involves first of all the assumption of a value for the reduced frequency parameter. From this the values of the P and Q coefficients are evaluated. For this system of equations the iteration processes are applied and the values of the frequency, velocity and the damping appropriate to each mode are calculated. This process is repeated for several values of the reduced frequency parameter. A plot on the V-g plane gives the flutter speed when g, the artificial damping coefficient is zero.

Gossard applied the above procedure for a uniform cantilever wing carrying a large concentrated mass (weight 7a of Ref.38). Using four spanwise stations he obtained values for the flutter speed which gave closer agreement with the experimental result than even the 'exact' solution of Runyan & Watkins. A Rayleigh analysis using 4 modes (Ref. 44) predicted a flutter speed which was 22% higher than the experimental value. This may be due to the eight degrees of freedom used in the iterative transformation procedure. The mode shape at flutter obtained by application of the iterative transformation method also showed agreement with the 'exact' mode shape obtained by Runyan & Watkins (Ref. 37).

Of the methods examined so far, the iterative transformation procedure seems to be best suited to analyse an arbitrary wing. It is well suited for solving the flutter

problem using a digital computer, especially if the computer has the capability of handling arithmetic involving complex numbers. Theoretically any amount of desired accuracy can be achieved using repeated iterations. A number of discontinuities can be taken into account and the flutter modes and frequencies can also be obtained from the analysis.

4.5 ASSUMED MODE ANALYSES

A vibrating wing in an airstream can be considered as an elastic structure supporting certain masses and subject to oscillatory aerodynamic forces. For practical computations, this system with an infinite number of degrees of freedom has to be replaced by an equivalent system which has as few dgrees of freedom as is possible and which still retains all the essential characteristics of the original wing. For representing the elastic-inertia characteristics of the wing, the free vibration modes in vacuo can be used. For all but the simplest structures it is generally impossible to obtain exact solutions for the mode shapes and it is common practice to prescribe arbitrary modes in the belief that the true mode is a linear combination of these modes. The wing is then termed 'semi-rigid' in the sense that it is allowed only a limited number of degrees of freedom.

In deciding the number and types of modes to be selected (or the degrees of freedom to be allowed), it is necessary to approximate as closely as possible the true mode shape of the wing in the flutter condition. Usually it is only a few of the modes which participate in any one type of flutter and all the other modes will be damped out. It is thus possible to exclude many of the degrees of freedom from the calculations. For the 'classical' type of flutter, at least two degrees of freedom must be used.

The structural and inertial contributions can be obtained by applying Lagrange's equations of motion.

To obtain the contribution of the aerodynamic forces, the forces are expressed in the form of derivatives which are mainly based on the following assumptions:

(i) Thin aerofoil theory

(ii) Perfect fluid with two dimensional irrotational flow

(iii) Harmonic motion of the surfaces

There are mainly two distinct methods of presenting aerodynamic derivatives and in main these govern the form of the equations of the fluttering wing. One is the Classical British technique in which the aerodynamic derivatives are presented as the amount of the particular force concerned with a unit displacement, velocity or acceleration of the particular motion concerned, the motion being relative to the equilibrium position (Refs. 25, 29). In the Classical American technique, the aerodynamic derivatives are presented as the amount of the particular forces concerned with a unit displacement of the particular motion from an equilibrium position (eg. Refs. 23, 28). In the British presentation, the derivatives are all real numbers while in the American method they are, in general, complex numbers. Because of this difference, the methods of accounting for the finite span effects are also different in the two methods.

In the treatment of the flutter problem also, two methods can be distinguished. These will be called the 'Classical British Method' and the 'Classical American Method' respectively.

4.5.1 The Classical British Method

The derivation of the flutter determinant for a uniform wing with a concentrated mass attached to it is presented in Appendix V. Briefly, this consists in obtaining the values of the kinetic energy, the strain energy and the work done by the aerodynamic forces when the wing is

oscillating in the prescribed modes. (Instead of determining the stability boundaries of the system directly it is assumed in advance that the system is oscillating harmonically and then the roots of the flutter determinant are examined for stability). Using the values of the kinetic energy, strain energy and the work done by the aerodynamic forces in Lagrange's equations yield the equations of motion of the system in the form:

$$\left[\lambda^2(A+\bar{A}) + \lambda(B+D) + \left(C + \frac{E}{V^2}\right)\right] \cdot q = 0 \qquad 4.33$$

where

A = matrix of inertia coefficients

$\bar{A}$ = matrix of aerodynamic inertia coefficients

B = matrix of aerodynamic damping coefficients

D = matrix of structural damping coefficients

C = matrix of aerodynamic stiffness coefficients

E = matrix of structural stiffness coefficients

V = velocity

$\lambda = 2ik = i\,\omega c/V$

Some methods of solving eq. (4.33) for the flutter speed and flutter frequency are discussed in Section (4.5.3).

4.5.2 The Classical American Method

Due to the difference in representing the aerodynamic forces, the equations of motion of the fluttering system are obtained in the form:

where
$$\left[A + P - \left(\frac{1+ig}{\omega^2}\right)E\right] q = 0 \qquad 4.34$$

A = structural inertia matrix

P = aerodynamic matrix (function of k)

g = fictitious damping (assumed to be of the structural damping type

ω = flutter frequency

$k = b\omega/V$

The deaivation of these equations is presented in Appendix V.

4.5.3 Methods of Solution of the Flutter Determinant

There exist several methods of solving the flutter determinant. Only a few of these are discussed here, as they are considered to be of greater practical utility, especially for problems with a large number of degrees of freedom.

4.5.3.1. Solutions to Equations of the type of Eq. (4.33)

The flutter determinant obtained by the classical British Method has the form:

$$\Delta = \left| \lambda^2 (A + \bar{A}) + \lambda (B + D) + (C + F/V^2) \right| = 0 \qquad 4.35$$

The main object of the solution is to find the values of the flutter speed V_F and the flutter frequency ω_F which make the above set of linear equations compatible.

The elements of the matrices $\bar{A}$, B and C depend on the frequency parameter , and the elements of the other matrices are determined by the inertia and stiffness distributions.

For a particular value of , all the elements of Eqn (4.35) are known quantities and the equation can be axpanded into the characteristic polynomial equation:

$$f(\lambda) = \sum_{r=0}^{2n} p_r (i\omega)^r = \sum_{r=0}^{2n} p_r \lambda^r = 0 \qquad 4.36$$

In Eq (4.36) all the p_r's have positive values. Since the complex roots λ can have values which are other than the purely imaginary values $\lambda = i\omega$, Eq. (4.36) represents motions which are other than harmonic and allows for the existence of oscillating and non-oscillating convergent and divergent motions.

The methods of obtaining the flutter speed V_F and the flutter frequency ω_F (through the reduced frequency $2\nu = \frac{\omega b}{V}$) will now be discussed:

(a) The orthodox method of solution

(a.i) The Direct Iterative Method.

If we separate the real and imaginary parts of the polynomial(4.36) we get two real equations, one containing the even powers of ν and the other containing only the odd pwers of ν. These can be written as

$$f_1(\lambda) = 0$$
$$f_2(\lambda) = 0 \qquad (4.37)$$

The result of eliminating λ from these equations yields

$$T_{n-1}(1/V^2) = 0 \qquad (4.38)$$

where T_{n-1} is the penultimate Routhian test function (Ref. 45). Equation (4.38) is a polynomial for $(1/V^2)$ and the roots of this polynomial give the values of the flutter speeds from this, the corresponding flutter frequency and the complex modal ratios can be found. This method is systematic and yields all the desired information. Its drawback is that it becomes very laborious when the number of degrees of freedom is greater than three.

Templeton (Ref. 27) calls this the "direct iterative" method, since (a) the flutter speed and frequency are calculated directly and (b) since in principle, it involves iteration in respect of the value of the frequency parameter. In practice, however, if the assumed value of the frequency parameter agrees even reasonably well with the value obtained from the solutions, no further iterations need be carried out. This is particularly true for values of 2ν around 0.6 (since the aerodynamic coefficients are not very sensitive to changes in 2ν in the neighbourhood of this value).

(a, ii) The Indirect Noniterative Solution

In this method, the determinant (4.34) is expanded as a function of (e_{ii}/ν^2) where the e_{ii} are elements of the structural stiffness matrix, E. For a determinant involving only two modes, this equation takes the form (after making the substitution $\bar{e}_{ii} = \frac{e_{ii}}{\nu^2}$)

$$\delta_1 + \delta_2 \bar{e}_{11} + \delta_3 \bar{e}_{22} + \bar{e}_{11}\bar{e}_{22} = 0 \qquad (4.39)$$

when the real and imaginary parts are equated to zero this yields

$$\begin{aligned} a_1 + a_2 \bar{e}_{11} + a_3 \bar{e}_{22} + a_4 \bar{e}_{11}\bar{e}_{22} &= 0 \\ b_1 + b_2 \bar{e}_{11} + b_3 \bar{e}_{22} + b_4 \bar{e}_{11}\bar{e}_{22} &= 0 \end{aligned} \qquad (4.40)$$

On eliminating $\bar{e}_{11}$ a quadratic equation in $\bar{e}_{22}$ is obtained from this, the values of $\bar{e}_{22}$ and hence $\bar{e}_{11}$ can be obtained. The whole process is repeated for several values of ν and a plot of $(\bar{e}_{11}/\bar{e}_{22})$ is made against, say, $\bar{e}_{22}$. From this curve, the value of $\bar{e}_{22}$ corresponding to the actual value of $(e_{22}/\bar{e}_{11})$ is obtained and hence the flutter speed.

Compared to the direct iterative method, this method involves a greater amount of work and for binary systems the former method is much simpler to use.

(b) Frazer's Method

Instead of expanding the determinant Δ (eqn 4.34) as a polynomial (4.6.31), Frazer (Ref. 46) expands it in the form of

$$\Delta(\lambda, y) = f(x, y) + \sqrt{x}\, g(x, y) \qquad (4.41)$$

where, $\sqrt{x} = \lambda$ and $y = 1/\nu^2$ (4.42)

$f(x,y)$ and $g(x,y)$ have the following forms (for an nth order determinant):

$$f(x, y) = c_0 x^n + c_2 x^{n-2} + \ldots + c_{2n-2} x + c_{2n}$$

$$g(x, y) = c_1 x^{n-1} + c_3 x^{n-3} + \ldots + c_{2n-1}$$

When the order, n, of the determinant is large, direct expansion of Δ into $f(x,y)$ and $g(x,y)$ presents a computational problem of considerable difficulty. Frazer overcomes this difficulty by making use of the methods of bivariate interpolation. He shows that the full expression for the function f and g can be calculated directly from expression in partial fraction form containing values of $\Delta(\lambda,\nu)$ corresponding to a special set of points (ξ,η). These are intersections of a standard set of straight lines satisfying the conditons:

(a) no two are parallel, (b) no three are concurrent.

The cnnditions at flutter require that $f(x,y)=0$ and $g(x,y)=0$ with $x\ (=-\nu^2)$ real and negative and y real and positive. Hence the possible critical pairs of values of x and y are given by the ~~real~~ intersections of the curves $f(x,y)=0$ and $g(x,y)=0$ which lie in the second quadrant of the (x,y) plane (i.e., $x<0$, $y>0$).

This method can be used to advantage when the number of degrees of freedom is large. It has also the advantage of being amenable to solution by means of digital computers for the expansion and solution of differential equations of the type whichoccur in the investigations of aeroplane stability.

(c) Method Using Matrices

Frazer, Duncan and Collar (Ref. 45, p. 148) suggest a method whereby the determination of the roots of the characteristic polynomial, Δ, is converted into one of finding the eigenvalues of a certain matrix.

The equation:

$$\lambda^n + p_1\lambda^{n-1} + \cdots + p_{n-1}\lambda + p_n = 0 \qquad (4.44)$$

is the characteristic equation of the matrix $[U] - [I]\lambda = 0$.

where

$$[U] = \begin{bmatrix} 0 & 1 & 0 & \cdots & 0 & 0 \\ 0 & 0 & 1 & \cdots & 0 & 0 \\ 0 & 0 & 0 & \cdots & & \\ \vdots & & & & 0 & 1 \\ -p_n & -p_{n-1} & -p_{n-2} & & -p_2 & -p_1 \end{bmatrix} \qquad (4.45)$$

Hence, the roots of Eq. (4.45) are the same as those of Eq. (4.44). There exist several methods of obtaining the eigenvalues of an equation of the type of Eq. (4.45). For large systems, a digital computer can be used with advantage.

(d) Crisp's Method

In Ref (47), Crisp has outlined a method of flutter analysis which can lead to a simplification and reduction of the numerical effort for systems with up to say, four degrees of freedom.

From an analysis of the behaviour of the roots of the real and imaginary parts of the characteristic equation on the Nyquist plot (Eg. Ref 48) he derives a criterion which the roots must satisfy if stability should exist. He also shows how a quantitative measure of the damping present in the modes at a given air speed can be obtained.

The application of this method to numerical calculations can be summarised as follows:

(i) the real and imaginary parts of the characteristic polynomial are separated and written as

$$f_1(\lambda) = \sum_{r=0}^{n} p_{2r} \cdot (i\omega)^{2r}$$
$$f_2(\lambda) = \frac{1}{i} \sum_{r=1}^{n} p_{2r-1} (i\omega)^{2r-1} \qquad (4.46)$$

(ii) for a given value of the velocity V, all the coefficients of two polynomials $f_1(\lambda)$ and $f_2(\lambda)$ are evaluated. The polynomial $f_2(\lambda)$ (the imaginary part) is equated to zero and its real positive roots $\lambda_1^2, \lambda_2^2, \ldots$ etc.

are found. For each of these roots, the values of the real part $f_1(\lambda)$ are evaluated. The system is stable when the signs of the different f_1's, arranged in a sequence corresponding to increasing magnitudes of the roots of $f_2(\lambda)$, $(\lambda_1^2, \lambda_2^2, \ldots \text{etc})$ are alternately positive and negative.

(iii) This process is carried out for several choices of the air speed V until instability is shown by this criterion.

Consider a ternary system. The real and imaginary parts of the characteristic polynomial are:

$$\begin{aligned} f_1(\lambda) &= p_0 - p_2 v^2 + p_4 v^4 + p_6 v^6 \\ f_2(\lambda) &= v(p_1 - p_3 v^2 + p_5 v^4) \end{aligned} \tag{4.47}$$

The positive real roots of $f_2(\lambda)$ are given by

$$v_1 = 0$$

$$v_2^2, v_3^2 = \frac{p_3}{2p_5} \pm \sqrt{\left\{\left(\frac{p_3}{2p_5}\right)^2 - \left(\frac{p_1}{p_3}\right)\right\}} \tag{4.48}$$

in ascending order of magnitude.

Then stability exists if

$$\begin{aligned} f_1(v_1) &= p_0 > 0 \\ f_1(v_2) &< 0 \\ f_1(v_3) &> 0 \end{aligned} \tag{4.49}$$

Four types of instability can be visualised. $p_0 < 0$ indicates a non-oscillatory divergence. Other kinds of instability exist when

(i) $f_1(v_2) > 0$
$f_1(v_3) > 0$

(ii) $f_1(v_2) > 0$
$f_1(v_3) < 0$

(iii) $f_1(v_2) < 0$, $f_1(v_3) < 0$

This type of solution is well suited for solution on analogue or digital computers, especially for higher order systems. It is in fact necessary only to find the roots of the imaginary part of the characteristic polynomial and to evaluate the values of the real part of the polynomial. Many convenient methods exist for the evaluation of the roots of a polynomial and the calculations are comparatively easy since the coefficients of the polynomial are all real numbers.

(e) Theodoresen's Method

The characteristic polynomial is separated into two polynomials - the real and imaginary parts, as:

$$f_r(\lambda) = 0 \quad , \quad f_i(\lambda) = 0 \qquad (4.51)$$

The coefficients of the two polynomials depend on the frequency parameter, $\nu = b\omega/V$. For different values of ν, the two polynomials are evaluated and the roots λ plotted against ν. The intersections of these two curves give the desired value of λ. From this the flutter speed and frequency can be obtained.

(f) Assessment of the different methods of solution(of equations of the type of Eqn. 4.33)

The starting point for most of the methods is the expansion of the flutter determinant into the characteristic polynomial. For systems with a large number of degrees of freedom, this can involve a great deal of labour. Frazer's method overcomes this difficulty by making use of the methods of bivariate interpolation. This method can be of considerable help when a system with a large number of degrees of freedom is being investigated.

Another, possibly more popular, approach is the use of analogue computers. Analogue computers which can solve

equations up to 12 degrees of freedom are in use. The main problem in using analogue computers is the setting up of the equations of motion in a proper form, so that they are not 'ill-conditioned'. Once this is done the effect of any changes in the system parameters can be easily investigated.

For binary and ternary systems, one of the methods illustrated by Templeton can be used. Crisp's method also finds application for these systems, especially if more information is needed regarding the subcritical behaviour of the system.

For larger systems a combination of Frazer's method of expanding the flutter determinant and another method of solving for the flutter speed and frequency e.g. Crisp's method could be used for advantage. Use could be made of a digital computer both for expanding the determinant and for solving the characteristic equation.

4.5.3.2 Solutions of Equations of the type of Eqn 4.34
(The classical American technique)

For non trivial solutions of the Eqn (4.34) we must have

$$\Delta = \left|A + P - \left(\frac{1+ig}{\omega^2}\right)E\right| = 0 \qquad (4.52)$$

The coefficients of all these matrices depend on the frequency parameter, ν ($= b\omega/V$). For a fixed value of ν, equation (4.52) can be solved for the complex eigenvalue $\left(\frac{1+ig}{\omega^2}\right)$. From this, the values of V, g and w can be obtained. This process is repeated for a number of values of ν until the flutter condition is obtained as given by the vanishing of g for a particular mode.

In principle all the methods which are useful in solving equations of the type of Eqn (4.33) are also useful in solving Eqn. (4.34).

If we put

$$Z = (1+ig)/\omega^2 \qquad 4.53$$

Equation (4.34) can be written in the form

$$[\bar{A}]\{q\} = Z\{q\} \qquad 4.54$$

which is a typical eigenvalue problem. In general the elements of $\bar{A}$ are complex and $\bar{A}$ itself is non symmetric. The eigenvalues Z can be determined by the methods of iteration applied to complex non Hermitian matrices.

4.5.3 Selection of Modes

In setting up the flutter equations by using Lagrange's equation, the number of generalized coordinates chosen and the mode shapes corresponding to these play an important part. This needs a balance between two factors, on the one hand the number of modes to be chosen is governed by the amount of time and the type of computing equipment available. Increasing the number of modes increases the amount of labour involved in setting up the equations and also in solving the equations. On the other hand, selecting an insufficient number of or of unrepresentative modes can give highly unreliable estimates of the flutter speed, especially if the wing is of unconventional design or has concentrated masses attached to it. This of course is a problem common to all analyses of this type where estimates of the mode shape have to be made in advance (e.g. Ref. 44 and Appendix VIII).

In vibration analyses by energy methods, since the wing is constrained to vibrate in a certain number of artificial modes which may not correspond to the exact modes, the estimates of the natural frequencies will be higher than the exact values. If the same argument is carried to the flutter analysis, it may be argued that estimates of the reduced frequency parameter $V/b\omega$ will be on the low side.

Thus a conservative estimate of the flutter speed will be obtained. This argument seems to hold for simple wings without any added masses. But when the wing carries concentrated masses, this argument does not hold, and sometimes estimates of the flutter speed can be obtained which are too high compared to the actual flutter speed. (Ref. 44).

Ideally, the modes chosen should be the actual modes of the wing at flutter. Then, an analysis involving only the critical modes would give the true flutter speed and frequency.

However, this is not possible in practice, especially if the wing is carrying added masses. Apart from the difficulty of knowing the critical flutter modes in advance, another difficulty comes in. Fig. (4.2) shows the bending and torsion components of the flutter mode for a uniform wing carrying a concentrated mass at about the quarter span point (from the root). (Ref. 37). There is a considerable phase difference between the bending oscillations at the tip and for points near the root. Prescribing modes which incorporate this phase difference (if the values are known in advance) would make the analysis more difficult.

From these considerations, the best policy seems to be to choose the mode shapes in such a way that a linear combination of them will give a reasonable approximation to the true flutter mode.

One such selection may prescribe the normal modes of the structure. These are an idealised concept since they are the modes obtained when the structure is oscillating in still air and in the absence of any damping forces. These have the advantage that they are othogonal to each other both in respect of the inertia distribution and the

stiffness distributions. Since these modes represent the structural and inertial properties accurately, any discontinuities in the structure are automatically taken into account and the boundary conditions are also satisfied. Since any mode can be built up as a linear combination of the normal modes, these are more likely to represent the true flutter mode with fewer degrees of freedom than an arbitrary combination of simple modes.

When normal modes are used, the evaluation of the inertia and stiffness coefficients in the flutter equations becomes simpler since the cross inertias are zero and the stiffness terms can be obtained directly from the frequencies of each of the modes. For solutions of the equations on the analogue computer normal modes have the added attraction that the equations are well-conditioned and the coefficients do not have to be evaluated to great accuracy.

Since normal modes are an idealised concept, the nearest approach is to use the resonance modes obtained by ground resonance testing of the structure. These have the disadvantage that they are not known until after the aeroplane has been built and may not be truly orthogonal. Hence one of the attractions of the normal modes is lost.

The ideal or normal modes can of course be calculated theoretically. In this case the advantage that the elastic coefficients in the flutter equation can be calculated is lost, since these have got to be evaluated first in order to obtain the normal modes. The use of normal modes also makes tedious the investigation of the effect, on the flutter spped, of changes in the structure or of added masses. Any change in the structure or in the inertia distribution will change the normal modes and these will have to be evaluated all over again for each change.

Thus, in some cases, it is more advantageous to select arbitrary modes for inclusion in the flutter analysis. These have the advantage that if simple algebraic expressions are prescribed for the modes, the evaluation of the coefficients of the structural, inertial and aerodynamic terms by integration becomes a straightforward task. It is not always possible to select modes which satisfy the end conditions at both the root and tip of the wing. The satisfactory representation of zero shear zero torque at the tip is not very important, as the error in strain energy due to this will be small. Use of Duncan functions or of Rauscher's station functions eliminates this discrepancy.

Flutter equations set up using normal modes can be used directly for simulation on an analogue computer. If arbitrary modes are used they may have to be transformed into a proper form for avoiding problems arising from ill conditioned equations.

For wings which have no structural discontinuities and do not carry concentrated masses, it is well established that the use of a few arbitrary modes gives acceptable approximations to the flutter speed. However, as has already been pointed out, this is no longer true when the wing is carrying concentrated masses.

Woolston & Runyan analysed the flutter of a uniform cantilever wing carrying concentrated masses (Ref. 44), using the calculated values of the uncoupled normal modes. For a mass located ahead of the elastic axis, they obtained highly unconservative estimates for the flutter speed.

Molyneaux (Ref. 5) observed that for wings carrying concentrated masses (on or ahead of the elastic axis) one

feature was common. When the value of the concentrated mass is gradually increased from zero, there is a more or less abrupt change in the type of flutter that occurs. This is associated with the change in the motion of the mass. Flutter involving large motions of the mass changes abruptly to a type of flutter where the motion of the mass is small. The initial motion may be a large translation (or a large pitch) and this becomes a flutter which is associated with a small translation (or small pitch) of the mass. He approximates this by assuming that the transition is from a large movement of the mass to zero movement of the mass. Using artificial constraints to represent this, he recommends that the following (uncoupled) modes be included in a flutter analysis to give good approximations to the flutter speed.

(a) Bending with root fixed (of the bare wing)

(b) Bending with root and concentrated mass section fixed

(c) Torsion with root fixed (of the bare wing)

(d) Torsion of the inner wing with the root and the mass section fixed.

(e) Torsion of the outer wing with the mass section fixed.

Modes (a), (b), and (c) are continuous over the wing span. However for modes (d) and (e) there are two distinct torsion modes at different frequencies for the inboard and outboard parts of the wing.

Gaukroger and others have used these modes extensively for analysing the flutter speeds of various wing mass combinations (e.g. Refs. 4, 9, etc.) The trends for the flutter speed (with variations in the different parameters) obtained from these analyses show good agreement with the experimentally established trends.

From the above, it can be seen that the success of the flutter analysis depends very much on the proper selection of the modes. For wings with concentrated masses the modes suggested by Molyneux seem to give the most reasonable results for the flutter speed. However, because of the number of the modes that must be included in the analysis, the calculations have to be done either using a digital or an analogue computer.

4.6 METHOD USING RESPONSE FUNCTIONS (Ref. 49)

The equations of motion of a fluttering wing can be expressed in the form:

$$\omega^2 [A]\{x\} - \omega_r^2 [B]\{x\} + \{q_f\} = 0 \qquad (4.55)$$

where $\omega^2 [a_{rs}]$ represents the matrix of the aerodynamic - plus - inertia forces, ω_r is a reference frequency, $\omega_r^2 [b_{rs}]$ is the matrix of elastic forces and $\{q_f\}$ represents the generalized forces.

Equation (4.55) can be written in the form

(with $\lambda = (\omega_r/\omega)^2$, $W_r = -q_r/\omega^2$),

$$[A]\{x\} - \lambda [B]\{x\} = \{W\} \qquad (4.56)$$

When the external forces are absent, $W_r = 0$, and we obtain a set of homogeneous equations. These can be solved for the vibration frequencies and the modes. With each characteristic value λ, there are associated two characteristic vectors. One is called the 'direct characteristic mode' and the other is called the 'conjugate characteristic mode'. The direct characteristic mode is the solution of the equations:

$$[A]\{x\}^{\nu} - \lambda [B]\{x\}^{\nu} = 0 \qquad (4.57)$$

The conjugate characteristic mode is the solution of the set of equations:

$$[A]^T\{y\}^\nu - \lambda [B]^T\{y\}^\mu = 0 \qquad (4.58)$$

For a conservative system, $a_{rs} = a_{sr}$ and $b_{rs} = b_{sr}$ and the two vectors (x^ν) and (y^ν) are identical (if $B^{-1}A$ had an orthogonal modal matrix).
Aerodynamic systems are in general, non conservative, the difference between the vectors (x^ν) and (y^ν), when the two vectors are made compatible by normalising on the same component, is associated with the energy-absorbing or energy-producing characteristic of the system.

The 'harmonic response function' is defined as the deflection of the system under the action of harmonic external forces represented by $W_1, W_2, \ldots, W_n$

A physical interpretation of the conjugate characteristic mode and the harmonic response function would be as follows. The conjugate characteristic mode can be regarded as the direct characteristic mode of a hypothetical system with with coefficient matrices a'_{rs} and b'_{rs} which are the adjoints of a_{rs} and b_{rs}. The harmonic response function can be regarded as the deflection of the aeroplane wing in flight under the action of vibrators.

In Ref. (49) Serbin and Castilow illustrate the use of the harmonic-response-function and the conjugate characteristic mode in the calculation of the change of flutter characteristics of a wing due to the addition of a concentrated mass.

It is assumed that a flutter analysis has been made for the wing and that the following data are available: The characteristic numbers λ_ν, the direct modes (x^ν) and the conjugate modes (y^ν).

If now a concentrated, harmonic force $F \exp(i\omega t)$ is applied at a point P, and if the displacement of P in the direction of F is given by x, then we can write

$$x = \beta_1 x_1 + \beta_2 x_2 + \cdots + \beta_n x_n \qquad (4.59)$$

where the β_i represent suitable geometric constraints and the x_j are the characteristic modes.

The harmonic response is given by

$$x = -\frac{F}{\omega^2} \sum_{\nu=1}^{\ell} \frac{(y^\nu, \beta)(\beta, x^\nu)}{(\lambda_\nu - \lambda) B(y^\nu, x^\nu)} - \frac{F}{\omega^2} (\beta, x^{(+)}) \qquad (4.60)$$

where, for example, (y^ν, β) represents the inner product of the vectors y^ν and β

$$(y^\nu, \beta) = \sum_{r=1}^{n} y_r, \beta_r \qquad (4.61)$$

and $$B(y^\nu x^\nu) = \sum_{r,s} y_r^\nu \, b_{rs} \, x_s^\nu \qquad (4.62)$$

If there are no rigid body modes and if the mass is rigidly attached to the wing,

$$x = -F/m\omega^2 \qquad (4.63)$$

Substituting this in Eq. (4.60):

$$-\frac{1}{m} = \sum_{\nu=1}^{n} \frac{(y^\nu, \beta)(\beta, x^\nu)}{(\lambda_\nu - \lambda) B(y^\nu, x^\nu)} \qquad (4.64)$$

The right hand side of this equation are functions only of $b\omega/V$ and of ω/ω_1. In principle, Eqn (4.64) can be solved for the value of m and ω for each value of $b\omega/V$. In practice, it appears desirable to use a graphical technique. In the procedure given by Serbin and Castilow, one regards the right hand side of Eqn (4.64), for each value of $b\omega/V$, as a function of the real parameter $\lambda = \omega_1^2/\omega^2$. The function is plotted in the complex plane and the abscissa of the intersection of the resulting plot on the real axis is equal to $(-1/m)$ for which flutter will occur. The parameter λ defines the flutter frequency and the corresponding value of m is the mass

required to maintain flutter. The flutter speed is obtained from the assumed value of the parameter $(b\omega/V)$.

4.7 MATRIX METHODS

The methods of matrix calculus have been used with advantage both in the setting up of and in solving of the flutter equations (eg. Ref. 45). Loring (Ref. 50, 51) shows how the matrix notation simplifies and systematizes the derivation and solving of the flutter equations by the assumed mode method.

There have been some approaches in which an attempt is made to avoid some of the disadvantages of the assumed mode methods.

4.7.1 One of these approaches is outlined by Lancaster (Ref. 52).

The deflections at a set of points on the wing can be related to the corresponding forces by means of a matrix of flexibility influence coefficients, consider a net of 'structural' collocation points. The displacements h at these points are related to the concentrated force F at the collocation by means of a flexibility matrix $[a]$ such that

$$\{h\} = [a]\{F\} \tag{4.65}$$

If $[K] = [a]^{-1}$ represents the stiffness matrix, the strain energy U is given by

$$U = \frac{1}{2} h' K h \tag{4.66}$$

where h' denotes the transpose of h.

The kinetic energy T is given by

$$T = \frac{1}{2} \dot{h}' M \dot{h} \tag{4.67}$$

where M is the diagonal matrix of lumped masses at the collocation points.

Assuming that it is possible to represent the aerodynamic forces by a "stiffness" influence coefficient matrix, by a suitable integration we can write the forces F as:

$$F = E_{ae}\, h \tag{4.68}$$

If the displacements h_i are chosen as the generalized co-ordinates, then we can derive the equations of motion using Lagranges equations as

$$M\ddot{h} + K h = E_{ae}\, h \tag{4.69}$$

To obtain the aerodynamic matrix E_{ae} Lancaster uses the Multhopp-Garner Theory. This gives the downwash at a set of prescribed collocation stations in terms of the aerodynamic loads, so that an inversion of a set of linear equations given a relation of the form of Eq. (4.69)

In general, E_{ae} is a complex matrix and has the form

$$E_{ae} = -(\nu^2 C + i\nu\omega B) \tag{4.70}$$

where the matrices C and B are proportional to the air density. Thus eqn. (4.68) becomes

$$F = -\nu^2 C h - \nu B \dot{h} \tag{4.71}$$

and the flutter equation (4.69) becomes

$$M\ddot{h} + \nu B h + (\nu^2 C + E) h = 0 \tag{4.72}$$

In setting up the equations, it was not assumed that the collocation points selected for the structural, inertial and aerodynamic forces are the same. It is necessary that these should be the same if Eqn. (4.72) is to be meaningful. The location of the collocation points is usually decided by the method used for defining the aerodynamic forces. In the Multhopp theory the points tend to cluster towards the wing tip. If only two or three chordwise points are chosen

it may be difficult to represent all the inertial properties. Lancaster points out two ways of overcoming these difficulties. One of these is to obtain the aerodynamic forces for a set of collocation stations and then, by applying a co-ordinate transformation to correct these to apply for the set of points dictated by the inertial collocation.

The second method is to include additional mass points in addition to those already used to define the external (aerodynamic) forces. These mass points can be situated anywhere on the wing but they will have zero aerodynamic forces associated with them.

To solve the flutter equation (4.72) the flutter determinant is written as:

$$\left| I\lambda^2 + (\nu^2 A^{-1}B + A^{-1}D)\lambda + (\nu^2 A^{-1}C + A^{-1}E) \right| = 0 \qquad (4.73)$$

where I is the unit matrix.

If this equation is expanded for a specific value of ν, a polynomial in λ results. This polynomial can be solved by using the Newton-Raphson method.

The method has the inherent advantage that no assumptions are made about the mode ~~shapes~~ Shapes and is applicable to wings of small aspect ratio and those carrying concentrated masses, etc. The type of method used to specify the aerodynamic loading can be flexible and the analysis can be simplified by using strip theory aerodynamics.

The choice of the collocation points is determined mainly by the method used to integrate the aerodynamic loads both in the chordwise and the spanwise directions. The location of these points depends on the method used and the scheme recommended by Multhopp is the one in common use. These stations may not be the ideal ones for obtaining the structural

or inertial influence coefficients. For the chordwise integration at least two points are necessary. A minimum of three points is necessary, however, to take into account the mass, inertia and static unbalance of any particular spanwise strip. Assuming that the structural influence coefficients can be obtained for any given set of points on the wing it will be necessary to have a transformation matrix which will transform the inertia influence coefficients worked out for a given set of points to those corresponding to the aerodynamic (A.I.C.) set.

In using lifting surface theory aerodynamics, the task of working out the A.I.C. s increases rapidly with the increase of number of points chosen for collocation. This imposes a practical limitation on the number of points chosen for collocation.

The coefficients in the flutter determinant are, in general, complex numbers. The method of solutions involves the expansion of a complex determinant and the solution of a complex polynomial by a method such as the Newton – Raphson method. For most cases, this would involve the use of a digital computer. Even when the computer has the capability of handling complex arithmetic, the above prodecures involve relatively long computer time and it may be of advantage ot set up the flutter problem as a complex eigenvalue problem.

4.7.2 Another application of matrix methods to the solution of the flutter problem was given by Hereshoff (Ref. 53). He used steady state aerodynamic loads with the magnitude of the lift curve slope corrected by the magnitude of the Theodoresen log function.

If $[a]$ represents the flexibility matrix, $[M]$ the diagonal mass matrix, and $\{h\}$ the column matrix of deflections at the collocation points, by assuming simple harmonic motion

the equation of the fluttering wing can be written as

$$\{h\} = (\omega^2 [D] + q [A])\{h\} \qquad (4.74)$$

where

$[A]$ = the matrix of 'aerodynamic influence' coefficients

and q = Dynamic Pressure = $\frac{1}{2}\rho V^2$

Eqn (4.74) can be written as

$$[\bar{D}]\{h\} = \omega^2 \{h\} \qquad (4.75)$$

where $[\bar{D}] = ([I] - q[A]).D^{-1}$

This equation can be solved for assumed values of For a number of value of q (i.e. the velocity) the eigenvalues of Eqn (4.75) which are the corresponding frequencies are obtained. If these frequencies are plotted against the velocity they tend to merge at the value of the flutter speed.

Herreshoff used this method to obtain the flutter speed of the uniform wing analysed by Goland (Ref. 35) and obtained very good agreement with Goland's results.

4.7.3 Mazelsky and O'Connell (Ref. 54) have given a

for the flutter analysis (of a straight cantilever wing) where no assumptions are made on the mode shapes of the wing to be included in the analysis. This formulation is suitable for solution or digital computers.

According this method, the formulation of the bending torsion flutter equations proceeds as follows:

Consider a cantilever wing as shown in Fig. 4.1.

Let the properties EI, GJ position the elastic axis, c.g., etc. be specified at a certain number of spanwise stations. The relation between the torsional deflection α and the running torque, t, can be written in integral form as

$$\alpha = \int_0^\eta \frac{t}{GJ}\, d\eta \qquad (4.76)$$

If M is the bending moment at a particular station, the relation between the bending deflection h and M can be written as:

$$\frac{dh}{d\eta} = S^2 \int_0^{\eta} \frac{M}{EI}\, d\eta \tag{4.77}$$

and therefore

$$h = S^2 \int_0^{\eta}\int_0^{\eta} \frac{M}{EI}\, d\eta\, d\eta \tag{4.78}$$

The accumulated torque T can be expressed in terms of the running torque t as

$$T = S \int_{\eta}^{1.0} t\, d\eta \tag{4.79}$$

Similarly the bending moment M can be expressed in terms of the running load l:

$$M = S^2 \int_{\eta}^{1.0} (\eta_0 - \eta)\cdot l\, d\eta \tag{4.80}$$

where η_0 is a dummy variable.

Both the running load l and the running torque t contain contributions from the inertial and the aerodynamic forces of the oscillating wing.

Assuming simple harmonic motion, l and t can be expresses as follows:

$$\begin{aligned} l &= l_{aero} + l_{inertia} \\ &= \tfrac{1}{2}\rho V^2 c \left(P_h \frac{h}{c} + P_\alpha \alpha\right) + \mu \omega_h^2 h + \mu e c \omega^2 \alpha \end{aligned} \tag{4.81}$$

$$\begin{aligned} t &= t_{aero} + t_{inertia} \\ &= \tfrac{1}{2}\rho V^2 c^2 \left(T_h \frac{h}{c} + T_\alpha \alpha\right) + \mu e c \omega_h^2 h \\ &\quad + \mu \left\{ (ec)^2 + r^2 \right\} \omega_\alpha^2 \alpha \end{aligned} \tag{4.82}$$

Using equations (4.81) and (4.82) the values of T and M can be evaluated from equations (4.79) and (4.80) by numerical integration. Substituting these values in equations (4.76) and (4.77) the relations for α and h can be obtained as:

$$\begin{Bmatrix} \{\alpha\} \\ \{\frac{h}{c}\} \end{Bmatrix} = \frac{1}{\lambda} \begin{bmatrix} [A_{\alpha\alpha}] & [A_{h\alpha}] \\ [A_{\alpha h}] & [A_{hh}] \end{bmatrix} \begin{Bmatrix} \{\alpha\} \\ \{\frac{h}{c}\} \end{Bmatrix} \tag{4.83}$$

The square matrices $A_{\alpha\alpha}$, A_{hh}, etc, are complex matrices due to the presence of the aerodynamic forces and moments. Since these are functions of the reduced frequency parameter Eq. (4.83) has to be solved for several values of this parameter to give values of λ . These values will, in general be complex. The flutter speed is obtained by the usual $V-g$ method.

The order of the characteristic matrix in (4.83) will be twice the number of bays considered for analysis. If 5 bays are specified for the analysis, the order of the matrix will be 10 and this will have complex elements. To overcome the difficulty involved in solving these large matrices, Bernard and Mazelsky point out that by assuming only two or three arbitrary modes, the order of the characteristic matrix can be drastically reduced (Cp Van de Vooren Ref. 42)

To include the effects of concentrated masses, etc. special interpolating matrices would be needed which would account for the discontinuities in the inertial distribution. A similar formulation can be used to solve the flutter problem using an analogue computer.

4.7.4 A unified approach to vibration and flutter analysis which makes use of the inertial, structural and aerodynamic forces in the form of influence coefficients was given by Rodden in Ref. 55

Briefly, this consists in writing the deflection integral equation of a cantilevered surface in the form

$$\{h\} = [a]\{F\} \tag{4.65}$$

where the h, a and F correspond to a chosen set of control points, the column matrix of forces F includes both the inertial and aerodynamic forces:

$$\begin{aligned}\{F\} &= \{F_{inertia}\} + \{F_{aero}\} \\ &= \omega^2[M]\{h\} + \rho\omega^2 b_r^2 s[C_h]\{h\}\end{aligned} \tag{4.84}$$

It should be noted that the inertial, structural and aerodynamic influence coefficients are derived at a common set of points.

Substituting eqn (4.84) in eqn. (4.65) we obtain the equation for flutter

$$\frac{1}{\omega^2}\{h\} = [a]\left([M] + \rho b_r^2 s [c_h]\right)\{h\} \qquad (4.85)$$

This equation can be solved for the eigenvalues ω_λ and the corresponding eigenvectors $\{h_\lambda\}$. In general the eigenvalues will be complex numbers since the characteristic matrix will be complex due to the presence of the aerodynamic terms. Flutter occurs only for real values of ω_λ It is necessary to assume a number of values for ν, the reduced frequency and to solve the equation (4.85) to obtain the frequencies ω_λ and hence the flutter speed for these values of To interpret the complex values of ω, it is customary to define a fictitious eigenvalue

$$\lambda = \frac{1+ig}{\omega^2} = \lambda_R + i\lambda_I \qquad (4.86)$$

and to write equation (4.86) as

$$\lambda\{h\} = [a]\left([M] + \rho b_r^2 s [c_h]\right)\{h\} \qquad (4.87)$$

From this, the frequency is obtained as $\omega = \frac{1}{\sqrt{\lambda_R}}$ The ratio of the imaginary part to the real part of λ gives a fictitious 'structural damping' necessary to maintain harmonic motion:

$$g = \lambda_I / \lambda_R \qquad (4.88)$$

The corresponding flutter speed is obtained from the assumed value of ν as

$$V_F = b_r \omega / \nu \qquad (4.89)$$

This analysis can be modified to include the effects of body freedom - both symmetric and anti-symmetric-and control surfaces, etc.

The main difference between Rodden's method and the method proposed by Mazelsky and O'Connell (Ref. 54) is in the treatment of the deflections. Mazelsky and O'Connell treat the bending and torsional deflections separately as for a moderate to high aspect ratio wing. In Rodden's formulation only a single variable is used and the procedure is more flexible and is applicable to most configurations including low aspect ratio wings and novel configurations.

As in the case of Mazelsky and O'Connell's procedure the number of degrees of freedom in the analysis can be reduced by the introduction of assumed modes.

4.8 COMPARATIVE EVALUATION OF THE METHODS OF ANALYSIS

From the foregoing descriptions it can be seen that the various methods of flutter analysis (for wings with added masses) differ from each other mainly in the following respects:

(i) The method of handling the structural and inertial properties.

(ii) The representation of the aerodynamic forces acting on the oscillating wing.

(iii) The method of taking into account of the energy balance in the system.

(iv) The mathematical approach used in deriving the characteristic equation of the fluttering system.

and, (v) The mechanics of obtaining the flutter speed and frequency of the wing mass combination.

For uniform cantilever wings Goland and Luke (Ref. 35) and Runyan and Watkins (Ref. 37) obtained a solution for the flutter speed using the differential equation approach. Since the inertial and structural properties were constant along the span for these wings, the partial differential equations for the bending and torsional oscillations had constant coefficients. A strip theory aerodynamics was used so that the system behaviour

could be described, (after assuming harmonic motion), by a pair of simultaneous ordinary differential equations with constant coefficients. The amount of labour involved in obtaining the flutter speed of a uniform wing with an attached mass using this method is very large. Though this method could be modified to obtain the flutter speed of a non-uniform wing with uniformly varying inertial and structural properties the work involved would be prohibitive and is not to be preferred over some of the other methods.

Another class of "exact" solutions using an integral formulation were given by (a) Mazelsky and O'Connell (Ref. 54) (b) by Herreshoff (Ref. 53) and (c) Van de Vooren (Ref. 42). Mazelsky and O'Connell gave the analysis for a uniform cantilever wing, though the effects of concentrated masses could be taken into account by means of special interpolation matrices.

Herreshoff's solution has not been used to obtain the flutter speed of wings with concentrated masses and doubts may exist about the use of steady state aerodynamics to represent the oscillatory aerodynamic forces. However, he has shown that the method gives good results when applied to a uniform cantilever wing.

Of the three methods, Van de Vooren's method is the only one which is of general applicability to wings having an arbitrary plan form and carrying concentrated masses. If need be, a large number of degrees of freedom can be included in the analysis. Van de Vooren recommends the determination of the normal modes of vibration of the wing as a first step. If these modes are used in flutter analysis, a large decrease in a number of degrees of freedom can be accomplished.

The use of Lyapunov's second method to obtain the stability boundaries of a wing-mass system has not been so far formalized. Wang (Ref. 41) has outlined how this method

could be used to obtain the flutter stability boundaries of complex combinations of wing and concentrated masses. There are, however, some reservations about the functional used by Wang (See Parks Ref. 56). As there do not exist any numerical results for flutter speeds predicted by this method, it is difficult to assess its utility.

Gossard (Ref. 43) has shown how the flutter problem of wings with concentrated masses could be solved by using Wielandt's iterative transformation procedure. This procedure can be applied to a non-uniform wing carrying concentrated masses.

One advantage of this method is that the normal modes of the wing are obtained as part of the solution. The operations can be performed on a desk calculator and, with degital computers, solutions can be obtained in a short space of time.

Rayleigh-Ritz type solutions have been used widely to obtain the flutter speeds of wings with concentrated masses. Comparisons with measured values of flutter speeds have shown that the assumed mode type of methods can give highly unconservative results, (Ref. 44). This is especially so when the concentrated masses are placed ahead of the elastic axis. The modes used in Ref. 44 were the uncoupled normal modes of the wing with the mass. Using four of these modes gave values for the flutter speed which were too high when compared with the measured speeds. But these showed the correct trend for the flutter speed when the concentrated mass was moved outboard from the root. Gaukroger has analysed various combinations of wings and concentrated masses using the mode shapes suggested by Molyneux. For example, in Ref. (5) he has investigated the effects of varying some of the concentrated mass parameters on the flutter speed of uniform wings - both swept and unswept. No experimental confirmation was obtained for this particular wing, though the calculated values exhibited a trend similar to

those obtained in tests on a comparable wing.

In Refs. (55, 57, 58) Rodden et al have applied the direct matrix method to obtain the flutter speed of the hypothetical jet transport wing example of Bisplinghoff, Ashley and Halfman (Ref. 23). He obtained very good agreement with the flutter speed obtained in Ref. 23 by a Rayleigh Ritz procedure.

CHAPTER 5

THE DIRECT MATRIX METHOD

In this formulation, the equations of the fluttering system are set up using an integral equation approach. The integral equations consist of two basic relationships: The first is the relation between the structural deformation and the loads (due to the inertial and aerodynamic forces), expressed through the structural influence coefficients. The second is the relation between aerodynamic disturbance (the downwash) and the aerodynamic pressure, expressed through the aerodynamic influence coefficients.

To solve the integral equation, a collocation approach is considered most feasible because of the ease of obtaining the solution from the corresponding matrix form. The deformation integral equation is written in matrix form by requiring that the integral equation be satisfied at a discrete set of control points.

A novelty of this method is that all the deformations are represented by one type of co-ordinate viz, the deflection h (Fig. 5.1) This results in simplifying the matrix equations and has an added advantage that it is more meaningful on a cambered vehicle. Also, deflection influence coefficients are usually more directly obtainable from a structural analysis than slope (or twist) influence coefficients.

5.1. DERIVATION OF EQUATIONS

Consider the wing shown in Fig. 5.1. If $[a]$ represents the matrix of structural influence coefficients (the flexibility matrix), the relation between the control station deflections and the applied forces F is given by

$$\{h_i\} - \{h_o\} = [a]\{F\} \tag{5.1}$$

where

$\{h_i\}$ = column matrix representing the abosulute deflections of the control points

$\{h_o\}$ = column matrix representing the deflections of the control points due to rigid body motion of some reference point.

and $[a]$ is the matrix of flexibility influence coefficients for the wing cantilevered from (or otherwise restrained at) the reference point.

The column matrix $\{F\}$ of the forces consists of contribution from (a) the set of inertial forces integrated throughout the region adjacent to the control point and (b) of the set of aerodynamic force components integrated over the vehicle surface adjacent to each control point, i.e.

$$\{F\} = \{F_i\} + \{F_a\} \tag{5.2}$$

The inertial forces may be written in terms of a mass matrix $[M]$ and the control point accelerations as

$$\{F_i\} = -[M]\{\ddot{h}_i\} \tag{5.3}$$

If we express the aerodynamic control point forces in terms of the control point deflections as:

$$\{F_a\} = \rho\omega^2 b_r^2 s[W][C_h]\{h\} \tag{5.4}$$

and use equations (5.3) and (5.4) in equation (5.2) we have

$$\begin{aligned}\{F\} &= \omega^2\left([M] + \rho b_r^2 S[W][C_h]\right)\{h_i\} \\ &= \omega^2[\bar{M}]\{h_i\}\end{aligned} \tag{5.5}$$

In equation (5.1) it is possible to include the rigid body degrees of freedom. (These could take the form of rigid body pitch, roll, yaw, etc.). This is done in the following way:- Each component of the control point deflections

is related linearly to the rigid body translations and rotations, provided the rotations are small. We may therefore define a rigid body modal matrix $[h_R]$ as the transformation.

$$\{h_o\} = [h_R]\{a_R\} \tag{5.6}$$

where a_R is the set of rigid body translations and rotations of the reference point. If we select a_R to have two elements: z_s the plunging displacement and θ the pitching angular displacement, then $[h_R]$ will consist of two columns. The first column will be a unit column corresponding to the plunging mode and the second will consist of the x - co-ordinate of each control point, corresponding to the pitching mode.

The rigid body modal matrix provides the basis for a statement of the free-free boundary conditions. As an example consider the symmetric flutter analysis of an aircraft whose wing, aft fuselage and tail are flexible but whose forward fuselage may be assumed as rigid. If we choose the reference point (the cantilever point) along the intersection of the wing and fuselage then the wing is independent of the aft fuselage tail combination, but the tail and aft fuselage must be considered together. The motion of the forward fuselage is determined by the motion of the reference point. If it is assumed that there is no dynamic coupling between the rigid and the flexible components, the free-free boundary conditions for harmonic motion may be written as:-

$$[h_R]^T [\bar{M}]\{h_i\} + [\Delta\bar{m}]\{a_R\} = 0 \tag{5.7}$$

where $[\Delta\bar{m}]$ is an incremental generalized mass matrix, including aerodynamic effects and is not considered in the formulation of the flexible component mass and aerodynamic matrices.

Substituting equations (5.6) and (5.5) in (5.1) we have

$$\{h_L\} - [h_R]\{a_R\} = \omega^2 [a][\bar{M}]\{h_L\} = \omega^2 [U]\{h_L\} \tag{5.8}$$

where $$[U] = [a][\bar{M}] \tag{5.9}$$

Premultiplying equation (5.8) by $[h_R]^T[\bar{M}]$ and subtracting it from equation (5.7), permits solution for the amplitudes of the rigid body motion:

$$\{a_R\} = -\omega^2 [\bar{m}]^{-1}[h_R]^T[\bar{M}][U]\{h_L\} \tag{5.10}$$

where $$[\bar{m}] = [\Delta\bar{m}] + [h_R]^T[\bar{M}][h_R] \tag{5.11}$$

Substituting equation (5.10) in equation (5.8) yields the equation for free-free flutter:

$$\{h_L\} = \omega^2 \left([I] - [h_R][\bar{m}]^{-1}[h_R]^T[\bar{M}]\right) \times [U]\{h_L\}. \tag{5.12}$$

The solutions to the matrix equations yield values for the frequencies ω^2 and the amplitudes $\{h_L\}$. Because of the presence of the oscillatory aerodynamic forces the matrix $[U]$ is complex and hence the solutions for ω^2 are in general complex numbers.

Since we have assumed simple harmonic motion, we have stipulated that the values of ω^2 be real. To interpret the complex values for the roots, it is common to define the eigenvalues $\bar{\lambda}$ as

$$\bar{\lambda} = \omega^2/(1+ig) \tag{5.13}$$

and to write equation (5.12) in the canonical form as

$$\lambda\{h_i\} = \left([I] - [h_R][\bar{m}]^{-1}[h_R]^T[\bar{m}]\right)[U]\{h_i\} \qquad (5.14)$$

where

$$\lambda = \lambda_R + i\lambda_I = (1+ig)/\omega^2 \qquad (5.15)$$

The value g represents the amount of damping which should be added to the structure in order to sustain the assumed harmonic motions, (the artificial structural damping).

For flutter to exist, the artificial structural damping must be equal to the actual structural damping in the system. Values of g higher than this indicate that the oscillations are unstable since extra damping would have to be added to attain neutral stability.

In equation (5.14) the characteristic matrix is usually complex and non-Hermitian. From a solution of this equation for the complex eigenvalues, we obtain the free-free frequency and the required structural damping as:

$$\omega = \frac{1}{2\pi}\sqrt{1/\lambda_R} \quad (c.p.s) \qquad (5.16)$$

$$g = \lambda_I/\lambda_R \qquad (5.17)$$

Since the formulation of the aerodynamic influence coefficients requires the assumption of a reduced frequency $\nu_r \left(= \frac{b_r\omega}{V}\right)$ the velocity is obtained as

$$V = \omega b_r/\nu_r \quad (ft/sec) \qquad (5.18)$$

From a series of solutions of equation (5.14) for various values of ν_r the flutter speed at a specific altitude can be obtained by constructing the usual V-g diagram.

Equation (5.14) is seen to be completely general being applicable from the cantilever case $([h_R]=0)$, to the case of six rigid body degrees of freedom. The vibration characteristics can

also be obtained from equation (5.14) by deleting the aerodynamic terms and the artificial structural damping.

The format of the various constituent matrices of equation (5.14) will now be discussed.

5.2 THE MASS MATRIX

It is desirable to have a common set of control points among the structural, inertial and aerodynamic influence coefficients. However, the choice of control point locations is usually governed by aerodynamic considerations. (For example specific spanwise spacing and chordwise locations). The inertial data are usually given as the total weight, c.g. moment and product of inertia at a set of points in the structure. It is necessary to transform these data into an equivalent system of lumped masses. The six inertial properties in each region can be matched by a system of three non-collinear masses having arbitrary co-ordinates; however, since the choice of co-ordinates is limited by aerodynamic considerations, a more useful representation is by six concentrated masses having fixed co-ordinates. In this case there are more lumped masses to be determined than the inertial conditions available and a least squares condition has to be imposed to obtain the lumped mass distribution.

Consider the wing of figure (5.1). Let control points be located along the quarter chord line, aileron hinge line and the trailing edge. For a spanwise location such as at Section XX, the inertial properties can be represented by lumped masses as shown in Figure 5.2. It is necessary to find a dynamically equivalent system of concentrated masses $\bar{M}_1$, $\bar{M}_2$, $\bar{M}_3$ corresponding to the lumped masses, $M_1 \ldots M_6$.

In terms of the masses $M_1 \ldots\ldots M_6$ and the deflections $z_1 \ldots\ldots z_6$ the kinetic energy is given by:

$$T = \frac{1}{2} \{\dot{z}\}^T [M] \{\dot{z}\} \qquad (5.19)$$

The deflections z can be expressed in terms of the three control point deflections h by means of a transformation matrix I_{mn} as

$$\{z\} = [I_{mn}]\{h\} \tag{5.20}$$

Substituting equation (5.20) into (5.19)

$$T = \frac{1}{2}\{\dot{h}\}^T [I_{mn}]^T [M][I_{mn}]\{\dot{h}\} \tag{5.21}$$

The inertial forces $\{F_\lambda\}$ are obtained from Eq. (5.19) by using Lagrange's equation

$$\{F_\lambda\} = -\frac{d}{dt}\left\{\frac{\partial T}{\partial \dot{h}}\right\} = -[M^*]\{\ddot{h}\} \tag{5.22}$$

Hence

$$[M^*] = [I_{mn}]^T [M][I_{mn}] \tag{5.23}$$

If the above procedure had not been adopted, it would have been necessary to consider a very large number of degrees of freedom.

As an illustration, consider the wing shown in Fig.(5.3) The wing is assumed to have six degrees of freedom.

The inertial properties of the wing both in the spanwise and the chordwise directions have been approximated by point masses at the control points and by a system of masses connected together by rigid massless bars. Assuming that linear interpolation is valid for the displacements, the total kinetic energy can be expressed as:

$$T = \frac{1}{2}\sum_{\lambda=1}^{6} M_\lambda \dot{h}_\lambda^2 + \frac{M_{12}}{2}\left(\frac{\dot{h}_1+\dot{h}_2}{2}\right)^2 + \frac{M_{13}}{2}\left(\frac{\dot{h}_1+\dot{h}_3}{2}\right)^2 + \frac{M_{24}}{2}\left(\frac{\dot{h}_2+\dot{h}_4}{2}\right)^2$$
$$+ \frac{M_{34}}{2}\left(\frac{\dot{h}_3+\dot{h}_4}{2}\right)^2 + \cdots + \frac{M_{56}}{2}\left(\frac{\dot{h}_5+\dot{h}_6}{2}\right)^2 \tag{5.24}$$

The inertia force at the first control point is given by:

$$F_1 = -\frac{d}{dt}\left(\frac{\partial T}{\partial \dot{h}_1}\right) = -\left(M_1 + \frac{M_{12}}{4} + \frac{M_{13}}{4}\right)\ddot{h}_1 - \frac{M_{12}}{4}\ddot{h}_2 \tag{5.25}$$
$$- \frac{M_{13}}{4}\ddot{h}_3$$

By proceeding in a similar manner, we obtain the mass matrix as

$$[M^*] = \begin{bmatrix} M_{11} & \frac{M_{12}}{4} & \frac{M_{13}}{4} & 0 & 0 & 0 \\ \frac{M_{12}}{4} & M_{22} & 0 & \frac{M_{24}}{4} & 0 & 0 \\ \frac{M_{13}}{4} & 0 & M_{33} & \frac{M_{34}}{4} & \frac{M_{35}}{4} & 0 \\ 0 & \frac{M_{24}}{4} & \frac{M_{34}}{4} & M_{44} & 0 & \frac{M_{46}}{4} \\ 0 & 0 & \frac{M_{35}}{4} & 0 & M_{55} & \frac{M_{56}}{4} \\ 0 & 0 & 0 & \frac{M_{46}}{4} & \frac{M_{56}}{4} & M_{66} \end{bmatrix} \tag{5.26}$$

where

$$\begin{aligned} M_{11} &= M_1 + \frac{M_{12}}{4} + \frac{M_{13}}{4} \\ M_{22} &= M_2 + \frac{M_{12}}{4} + \frac{M_{24}}{4} \\ M_{33} &= M_3 + \frac{M_{34}}{4} + \frac{M_{35}}{4} \\ M_{44} &= M_4 + \frac{M_{34}}{4} + \frac{M_{46}}{4} \\ M_{55} &= M_5 + \frac{M_{35}}{4} + \frac{M_{56}}{4} \\ M_{66} &= M_6 + \frac{M_{46}}{4} + \frac{M_{56}}{4} \end{aligned} \tag{5.27}$$

The dynamically similar mass matrix is symmetric, but not necessarily diagonal.

5.3 THE STRUCTURAL INFLUENCE COEFFICIENT MATRIX

In most cases, the structural information is available as a stiffness on flexibility matrix with respect to a certain set of points. If these do not coincide with the set of control stations used for the aerodynamic influence coefficients, a transformation matrix has to be found. Denoting by the subscript 'a' the aerodynamic net and by 's' the structural net, we are given a structural (flexibility) matrix $[a]_s$ such that

$$\{h_s\} = [a]_s \{F_s\} \tag{5.28}$$

We want to find an equivalent matrix $[a]_a$ such that

$$\{h_a\} = [a]_a \{F_a\} \tag{5.29}$$

If we relate the column matrices $\{F_a\}$ and $\{F_s\}$ such that the set of forces $\{F_a\}$ produce the same deflection mode $\{h_s\}$ as does the set $\{F_s\}$ we can define the structural equivalence as

$$\{h_s\} = [C_{sa}] \{F_a\} \tag{5.30}$$

By Maxwell's law of reciprocity

$$\{h_a\} = [C_{sa}]^T \{F_s\} \tag{5.31}$$

From equations (5.28) and (5.30)

$$\{h_a\} = [C_{sa}]^T [a]_s^{-1} \{h_s\} \tag{5.32}$$

and from equations (5.30) and (5.32)

$$\{h_a\} = [C_{sa}]^T [a]_s^{-1} [C_{sa}] \{F_a\} \tag{5.33}$$

By identifying equations (5.29) and (5.33) we find

$$[a]_a = [C_{sa}]^T [a]_s^{-1} [C_{sa}] \tag{5.34}$$

To determine $[C_{sa}]$ we assume a deflection interpolation matrix:

$$\{h_a\} = [I_{as}] \{h_s\} \tag{5.35}$$

By identifying equations (5.32) and (5.35) we find

$$[I_{as}] = [C_{sa}]^T [a]_s^{-1} \tag{5.36}$$

from which

$$[C_{sa}] = [a]_s [I_{as}]^T \tag{5.37}$$

Substituting equation (5.37) into (5.34) yields the desired transformation:

$$[a]_a = [I_{as}] [a]_s [I_{as}]^T \tag{5.38}$$

(The following derivation is due to Dr. A. Simpson)

The derivation of the $[a]_a$ matrix can be simplified by the use of contravariant variables. In the following the stiffnesses and the deflections are taken as contravariant variables.

Eq.(5.28) gives: $\{F\}_s = [a]_s^{-1} \{h_s\}$ .. (5.28)'

It is desired to find a matrix $[a]_a$ such that

$$\{F\}_a = [a]_a^{-1} \{h_a\} \qquad (5.29)'$$

We now define a deflection interpolation matrix $[I_{as}]$ such that

$$\{h_s\} = [I_{as}]^{-1} \{h_a\} \qquad (a)$$

Then, by using the principle of contragradience, we get, from (a),

$$\{F\}_a = \left([I_{as}]^{-1} \right)^T \{F\}_s \qquad (b)$$

Substituting for $\{F\}_s$ from Eq.(5.28)', and for $\{h_s\}$ from Eq.(a), we get :

$$\{F\}_a = \left(\left([I_{as}]^{-1} \right)^T [a]_s^{-1} [I_{as}]^{-1} \right) \{h_a\} \qquad (c)$$

Comparing Eq.(5.29)' with Eq.(c), we get

$$[a]_a^{-1} = \left([I_{as}]^{-1} \right)^T [a]_s^{-1} [I_{as}]^{-1}$$

Hence $$[a]_a = [I_{as}] [a]_s [I_{as}]^T \qquad (5.38)$$

which is the requered transformation matrix.

Thus the determination of the structurally equivalent transformation is dependent on the determination of the interpolation matrix. Schmitt (Ref. 59) suggested a least squares interpolation. Rodden (Refs. 57 and 58) recommends the use of interpolation-in-the-small, although its use requires a considerable amount of judgement.

When the wing has an elastic axis, and the structural information is given as separate sets of influence coefficients for the bending and torsion components (and for the control surfaces), the determination of the structurally equivalent transformation is fairly straightforward.

As an illustration, consider the wing shown in figure (5.4) Let the bending flexibility coefficients be defined by

$$\{z\} = [C^z_{ij}]\{F_z\} \tag{5.39}$$

and the torsional flexibility coefficients by

$$\{\alpha\} = [C^\alpha_{ij}]\{F_\alpha\} \tag{5.40}$$

Here z and α are the bending deflection and the twist angle measured at the elastic axis.

The geometric equivalence between the system of deflections $\{h\}$ and $\{z\}$ is given by

$$\begin{Bmatrix} h_1 \\ h_2 \\ \vdots \\ h_9 \\ h_{10} \end{Bmatrix} = \begin{bmatrix} 1 & -e_1 & & & 0 \\ 1 & e_2 & & & \\ \vdots & \vdots & & & \\ & & & 1 & -e_9 \\ 0 & & & 1 & e_{10} \end{bmatrix} \begin{Bmatrix} z_a \\ \alpha_a \\ \vdots \\ z_e \\ \alpha_e \end{Bmatrix} \tag{5.41}$$

The deflections z and α can be expressed in terms of the forces $\{F\}$ as

$$\begin{Bmatrix} z_a \\ \alpha_a \\ \vdots \\ z_e \\ \alpha_e \end{Bmatrix} = \begin{bmatrix} C^z_{aa} & C^z_{aa} & \cdots & C^z_{ae} & C^z_{ae} \\ -e_1 C^\alpha_{aa} & e_2 C^\alpha_{aa} & & -e_1 C^\alpha_{ae} & e_2 C^\alpha_{ae} \\ \vdots & \vdots & & \vdots & \vdots \\ C^z_{ea} & C^z_{ea} & & C^z_{ee} & C^z_{ee} \\ -e_1 C^\alpha_{ea} & e_2 C^\alpha_{ea} & & -e_1 C^\alpha_{ee} & e_2 C^\alpha_{ee} \end{bmatrix} \begin{Bmatrix} F_1 \\ F_2 \\ \vdots \\ F_9 \\ F_{10} \end{Bmatrix} \tag{5.42}$$

Substituting equation (5.42) into equation (5.41) the required flexibility matrix can be derived in the form:

$$\{h\} = [a]\{F\} \tag{5.43}$$

where

$$[a] = \begin{bmatrix} C^z_{aa}X & C^z_{ab}X & \cdots & C^z_{ae}X \\ \vdots & & & \vdots \\ C^z_{ea}X & C^z_{eb}X & \cdots & C^z_{ee}X \end{bmatrix} + \begin{bmatrix} e_1 & & & 0 \\ & -e_2 & & \\ & & \ddots & \\ 0 & & & -e_{10} \end{bmatrix} \times \begin{bmatrix} C^\alpha_{aa}X & C^\alpha_{ab}X & \cdots & C^\alpha_{ae}X \\ \vdots & & & \vdots \\ C^\alpha_{ea}X & C^\alpha_{eb}X & \cdots & C^\alpha_{ee}X \end{bmatrix} \times \begin{bmatrix} e_1 & & & 0 \\ & -e_2 & & \\ & & \ddots & \\ 0 & & & -e_{10} \end{bmatrix} \tag{5.44}$$

In Eq. (5.44), X represents the (2 x 2) matrix containing unit elements

$$X = \begin{bmatrix} 1 & 1 \\ 1 & 1 \end{bmatrix} \tag{5.45}$$

It should be noted that in Eqs. (5.44) and (5.45) X is defined in the sense of matrix algebra.

By a similar reasoning, the structural influence coefficient matrix for wingswith controls can also be obtained.

5.4 THE AERODYNAMIC INFLUENCE COEFFICIENT MATRIX FOR WINGS

The aerodynamic influence coefficient matrix relates the aerodynamic force at any control point to the motion of all the control points. For use in the direct matrix method the aerodynamic influence coefficient matrix is defined as:

$$F = \rho \omega^2 b_r^2 s [C_h] \{h\} \tag{5.46}$$

The form of the aerodynamic influence coefficient matrix $[C_h]$ depends on the particular theory being employed. This could be either (a) strip theory or (b) lifting surface theory. The latter could further be divided according to the method of solving the aerodynamic integral equation: (a) assumed mode methods and (b) collocation methods.

The strip theory formulation of the aerodynamic influence coefficients will be considered first as it is applicable to a variety of wing planforms from large aspect ratio wings at subsonic speeds to ~~wings of~~ all wings at high ~~supersonic~~ supersonic speeds. The two dimensional oscillatory derivatives are generally tabulated as the lift and moment coefficients referred to the wing quarter chord (e.g. Tables of Ref. 25 Tables of Ref. 26, 28 and 29)

Fig. (5.5) shows the given system of deformations and the forces acting at the quarter chord and also the corresponding equivalent configuration required in the matrix formulation. Since the main surface lift and moment are given as derivatives referred to the wing quarter chord, it is convenient to take this point as the forward control point in the matrix formulation. Similarly it is convenient to choose the aileron hinge line for the middle control point. The rear control point location can still be arbitrary and in the present case, this is taken to be on the wing TE.

In terms of tabulated quantities (e.g. Ref. 28) the oscillatory aerodynamic lift and moments are given by:

$$\begin{Bmatrix} L \\ M \\ T \end{Bmatrix} = \pi \rho \omega^2 b^2 \Delta y \begin{bmatrix} 1 & 0 & 0 \\ 0 & b & 0 \\ 0 & 0 & b \end{bmatrix} \begin{bmatrix} L_z & L_\alpha & L_\beta \\ M_z & M_\alpha & M_\beta \\ T_z & T_\alpha & T_\beta \end{bmatrix} \begin{Bmatrix} z \\ b\alpha \\ b\beta \end{Bmatrix} \tag{5.47}$$

where Δy is the width of the strip.

The load equivalence between the forces F_1, F_2, F_3 and the forces L, M, T is given by

$$\begin{Bmatrix} L \\ M \\ T \end{Bmatrix} = \begin{bmatrix} 1 & 1 & 1 \\ 0 & d & (d+c_a) \\ 0 & 0 & c_a \end{bmatrix} \begin{Bmatrix} F_1 \\ F_2 \\ F_3 \end{Bmatrix} \tag{5.48}$$

The relation between the two sets of deformations is given by

$$\begin{Bmatrix} z \\ b\alpha \\ b\beta \end{Bmatrix} = \begin{bmatrix} 1 & 0 & 0 \\ -b/d & b/d & 0 \\ b/d & -(b/d + b/c_a) & b/c_a \end{bmatrix} \begin{Bmatrix} h_1 \\ h_2 \\ h_3 \end{Bmatrix} \tag{5.49}$$

Using equations (5.47), (5.48) and (5.49) and identifying with equation (5.46) yields the strip aerodynamic influence coefficient matrix

$$[C_h] = \pi \left(\frac{b}{b_r}\right)^2 \left(\frac{\Delta y}{S}\right) \begin{bmatrix} 1 & -b/d & b/d \\ 0 & b/d & -(b/d + b/c_a) \\ 0 & 0 & b/c_a \end{bmatrix} \times \begin{bmatrix} L_z & L_\alpha & L_\beta \\ M_z & M_\alpha & M_\beta \\ T_z & T_\alpha & T_\beta \end{bmatrix} \times \begin{bmatrix} 1 & 0 & 0 \\ -b/d & b/d & 0 \\ b/d & -(b/d + b/c_a) & b/c_a \end{bmatrix} \tag{5.50}$$

When there is no control surface, we need to consider only two chordwise control stations, one at the quarter chord and the other can be arbitrary. In this case, the aerodynamic influence coefficients for each strip take the form

$$[C_h] = \pi \left(\frac{b}{b_r}\right)^2 \left(\frac{\Delta y}{S}\right) \begin{bmatrix} 1 & -b/d \\ 0 & b/d \end{bmatrix} \begin{bmatrix} L_z & L_\alpha \\ M_z & M_\alpha \end{bmatrix} \begin{bmatrix} 1 & 0 \\ -b/d & b/d \end{bmatrix} \tag{5.51}$$

When assembled for the complete wing the aerodynamic influence coefficients for the entire wing take the form

$$[C_h] = \begin{bmatrix} \left(\frac{b_1}{b_r}\right)^2 \left(\frac{\Delta y_1}{S}\right) [C_h]_1 & & 0 \\ & \left(\frac{b_2}{b_r}\right)^2 \left(\frac{\Delta y_2}{S}\right) [C_h]_2 & \\ 0 & & \left(\frac{b_n}{b_r}\right)^2 \left(\frac{\Delta y_n}{S}\right) [C_h]_n \end{bmatrix} \tag{5.52}$$

In addition to the two dimensional subsonic theories referred to earlier, solutions are available for the other Mach Number regimes.

The aerodynamic influence coefficients can also be derived using one of the unsteady lifting surface theories. Rodden and Revell (Ref 60) give a comprehensive review for some of the theories and illustrate the derivation of the aerodynamic influence coefficient matrices using a collocation approach to the solution of the downwash integral equation.

For wings of arbitrary planform oscillating in subsonic flow, Rodden and Revell show that the influence coefficients can be represented by:-

$$[C_k^j] = K \nu^2 [B_{nm}^j][A_{nm}^\lambda][W_{ij}] \qquad (5.53)$$

where $[B_{nm}^j]$ is a pressure integration matrix, $[A_{nm}^\lambda]$ is a matrix relating pressure loading coefficients to down wash and $[W_{ij}]$ relates the down wash to the deflections of the collocation points.

5.6. AERODYNAMIC INFLUENCE COEFFICIENTS FOR OSCILLATING BODIES

In most flutter analyses of wing-body combinations, it has been the usual practice to neglect the aerodynamic forces due to the oscillating body. The limited experimental data available seems to support this practice as the effect of the aerodynamic forces seems to be relatively unimportant compared to the inertial forces of the bodies. (as was seen in Section 2.6) (This holds only for subsonic speeds. There is no data available at supersonic speeds on the importance of the aerodynamic forces due to the body). Another reason for neglecting the body aerodynamic forces could be that presently available knowledge does not permit accurate theoretical calculations of

the forces without the imposition of rather severe restrictions. There is very limited knowledge of wing-body interference effects and this is confined to particular combinations.

A theoretical analysis of the wing-body interference problem in unsteady flow presents formidable problems which have been overcome only in a few specialized cases (e.g. Ref.61).

The forces acting on an isolated body of revolution in unsteady flow can be obtained by one of the following methods:

(a) Exact solution of the differential equation satisfying all the boundary conditions. Lamb (Ref. 62) has applied this method to arbitrary ellipsoids in incompressible flow.

(b) Linearization of the problem, under the assumption that the lateral dimensions are small compared to the length in the flight direction. (Refs. 63, 64, 65 and 66).

(c) Using the momentum theory of Munk (Ref. 23, p.414, Ref. 60).

Bond and Packard (Ref. 66) show that for low values of the reduced frequency and supersonic M Nos, application of the momentum theory gives satisfactory results and that there is no special advantage in using the linearized slender body theory. Miles (Refs. 63, 64) has shown that so long as the lateral flow velocities are small compared to the flight speed the first order forces and moments are independent on the Mach number in compressible flow.

(This holds when $M\delta << 1$, $\omega M\delta <<$ where

$\delta =$ slenderness ratio, $\omega = \omega l/V$, $M = V/a$)

The mementum theory seems to be most suitable for obtaining the aerodynamic influence coefficients for slender bodies. By analogy with steady flow practice it is reasonable to assume that the shape of the cross section of the slender body does not influence the lift and moment (e.g. Ref. 67).

Consider the slender body shown in Fig. (5.9). For small values of the local incidence, the z - velocity at any cross section is

$$w_a = -V\frac{\partial h}{\partial x} + \frac{\partial h}{\partial t} \tag{5.54}$$

If S is the local cross sectional area, the momentum of the virtual mass per unit length is

$$\frac{dI}{dx} = \rho S w_a = \rho S\left(-V\frac{\partial h}{\partial x} + \frac{\partial h}{\partial t}\right) \tag{5.55}$$

The z-force acting per unit length of the body is the reaction to the substantive rate of charge of dI/dx i.e.,

$$\frac{dF}{dx} = -\frac{D}{Dt}\left(\frac{dI}{dx}\right) \tag{5.56}$$

$$= -\left(V\frac{\partial}{\partial x} + \frac{\partial}{\partial t}\right)\left\{\rho S\left(-V\frac{\partial h}{\partial x} + \frac{\partial h}{\partial t}\right)\right\} \tag{5.57}$$

If we assume harmonic motion this equation can be written as:-

$$\frac{dF}{dx} = \rho V\frac{d}{dx}\left\{S\left(-V\frac{dh}{dx} + i\omega h\right)\right\} - i\omega\rho S\left(-V\frac{dh}{dx} + i\omega h\right) \tag{5.58}$$

To obtain the force on a specified length of the body, it is necessary to integrate equation (5.58) over that length. Rodden & Revell (Ref. 60) give expressions for the aerodynamic influence coefficients of a slender body with an arbitrary deformation of the centre line. In what follows the body will be considered rigid, with a undeformed straight centre line (Fig. 5.7)

If the body length L is divided into N sections, the force on the ith section is given by

$$F_i = \int_{x_{i-1/2}}^{x_{i+\frac{1}{2}}} \frac{dF}{dx}\,dx \tag{5.59}$$

where

$$x_{i-1/2} = x_i - \frac{\Delta h}{2}$$

$$x_{i+\frac{1}{2}} = x_i + \frac{\Delta h}{2} \tag{5.60}$$

From (5.59) and (5.58),

$$F_i = \rho V \left[S \left(-V \frac{dh}{dx} + i\omega h \right) \right]_{x_{i-\frac{1}{2}}}^{x_{i+\frac{1}{2}}} - i\omega\rho \int_{x_{i-\frac{1}{2}}}^{x_{i+\frac{1}{2}}} S \left(-V \frac{dh}{dx} + i\omega h \right) dx \qquad (5.61)$$

Since no deformations have been assumed for the body it is reasonable to use linear interpolation for the evaluation of the terms in Eq. (5.61):-

$$h = h_i + h'(x - x_i)$$
$$S = \frac{1}{\Delta_i} \left[S_{i-\frac{1}{2}} (x_{i+\frac{1}{2}} - x) + S_{i+\frac{1}{2}} (x - x_{i-\frac{1}{2}}) \right] \qquad (5.62)$$

Where the quantities with the subscript $(i-\frac{1}{2})$ refer to the forward end of the section and those with $(i+\frac{1}{2})$ to the rear end of the section.

Using this, eqn. (5.61) can be expressed as

$$F_i = -\rho V^2 h' (S_{i+\frac{1}{2}} - S_{i-\frac{1}{2}}) + i\omega\rho V \left[S_{i+\frac{1}{2}} \{ h_i + h'(x_{i+\frac{1}{2}} - x_i) \} - S_{i-\frac{1}{2}} \{ h_i - h'(x_i - x_{i-\frac{1}{2}}) \} \right] - i\omega\rho h' \left[S_{n-\frac{1}{2}} x_{n+\frac{1}{2}} + S_{n+\frac{1}{2}} x_{n-\frac{1}{2}} \right] \qquad (5.63)$$

Since linear interpolation has been used, there will be two nonzero elements in each row of the aerodynamic influence coefficient matrix. Therefore,

$$F_i = \rho \omega^2 b_r^3 S \left(C_{h_i, i-1} h_{i-1} + C_{h_i, i} h_i \right) \qquad (5.64)$$

In equation (5.64) the terms in the brackets can be obtained from Eq. (5.63) as

$$\left(C_{h_i, i-1} h_{i-1} + C_{h_i, i} h_i \right) = \frac{1}{\nu_r^2 S} \left\{ -\left(S_{i+\frac{1}{2}} h' - S_{i-\frac{1}{2}} h' \right) + \frac{\nu_r^2}{b_r^2} \left[h_i \Delta V_i + \frac{\Delta_i^2}{12} \left(S_{i+\frac{1}{2}} - S_{i-\frac{1}{2}} \right) h' \right] + i \frac{\nu_r}{b_r} \left(S_{i+\frac{1}{2}} h_{i+\frac{1}{2}} - S_{i-\frac{1}{2}} h_{i-\frac{1}{2}} + h' \Delta V_h \right) \right\} \qquad (5.64)$$

The deflections $h_{i+\frac{1}{2}}$ and $h_{i-\frac{1}{2}}$ can be obtained in terms of h_i and h_{i-1}. For $i=1$ and N, the deflections can be obtained in terms of the deflections at $i=1,2$ and $i=N-1,N$, respectively.

If the body is attached to a wing, the forces due to the body could be directly added on to the wing control point forces. In this case, a more direct method would be to obtain the total forces and moment acting on the body. These are given by (eg. Ref. 23)

$$L = \rho \cdot K_V (V\dot{\alpha} + \ddot{h}) + \rho K_M \ddot{\alpha}$$
$$M = \rho V K_V (V\alpha + \ddot{h}) - \rho K_M \ddot{h} - \rho K_J \ddot{\alpha} \qquad (5.65)$$

where

$$K_V = \int_{body} S\, dx$$
$$K_M = \int_{body} S(x - x_{REF})\, dx$$
$$K_J = \int_{body} S(x - x_{REF})^2\, dx$$
$$\alpha = (h_2 - h_1)/(x_2 - x_1)$$

5.6 THE USE OF ASSUMED MODES IN THE DIRECT MATRIX METHOD

By specifying arbitrary modes, the number of degrees of freedom included in the flutter analysis can be reduced drastically. To include the arbitrary modes, it is convenient to consider cantilever modes and free-free modes separately.

(a) Cantilever Modes

Let N be the number of modes to be included in the analysis, F the number of control points at which the modes are specified and R the number of rigid body degrees of freedom.

After introducing the coefficient of artificial structural damping, g, equation (5.8) can be written in the form

$$\{h_i\} - \{h_0\} = \frac{\omega^2}{(1+ig)} [a][\bar{m}]\{h_i\} \qquad (5.66)$$

For the purpose of seeking series solutions of Eq. (5.66) it is convenient to introduce the (cantilever) stiffness matrix

$$[K] = [a]^{-1} \tag{5.67}$$

Using this definition, the flutter equation can be written as

$$\Omega [K](\{h_L\} - \{h_0\}) = [\bar{M}]\{h_L\} \tag{5.68}$$

where $$\Omega = (1+ig)/\omega^2 \tag{5.69}$$

The series solution to Eq. (5.68) can be written in terms of the assumed modes as

$$\{h_L\} - \{h_0\} = [h_F]\{a_F\} \tag{5.70}$$

here $[h_F]$ is the matrix of assumed modes and $\{a_F\}$ are the modal amplitudes.

Introducing Eqs. (5.6) and (5.70), (5.7) yields the boundary conditions for ~~the~~ free-flutter as

$$[\bar{m}_{RF}]\{a_F\} + [\bar{m}_{RR}]\{a_R\} = 0 \tag{5.71}$$

where

$$\begin{aligned}[\bar{m}_{RF}] &= [m_{RF}] + [Q_{RF}] \\ &= [h_R]^T [M][h_F] + [h_R]^T [A][h_F]\end{aligned} \tag{5.72}$$

$$\begin{aligned}[\bar{m}_{RR}] &= [m_{RR}] + [Q_{RR}] \\ &= \left([h_R]^T [M][h_R] + [\Delta m]\right) \\ &\quad + \left([h_R]^T [A][h_R] + [\Delta Q]\right)\end{aligned} \tag{5.73}$$

From Eq. (5.71)

$$\{a_R\} = -[\bar{m}_{RR}]^{-1}[\bar{m}_{RF}]\{a_F\} \tag{5.74}$$

The flutter equation, Eq. (5.68) now becomes

$$\Omega [K][h_F]\{a_F\} = [\bar{M}]\left([h_F]\{a_F\} + [h_R]\{a_R\}\right) + \{\epsilon\} \tag{5.75}$$

where $\{\epsilon\}$ is the error in the series solution. Applying Galerkin's principle $\left([h_F]^T\{\epsilon\} = 0\right)$ yields

$$\Omega [K_F] \{a_F\} = \left([\bar{m}_{FF}] \{a_F\} + [\bar{m}_{FR}] \{a_R\} \right) \tag{5.76}$$

where

$$[K_F] = [h_F]^T [K] [h_F] \tag{5.77}$$

$$[\bar{m}_{FF}] = [m_{FF}] + [Q_{FF}] = [h_F]^T [M] [h_F] + [h_F]^T [A] [h_F] \tag{5.78}$$

$$[\bar{m}_{FR}] = [m_{FR}] + [Q_{FR}] = [m_{RF}]^T + [h_F]^T [A] [h_R] \tag{5.79}$$

If we eliminate the rigid body degrees of freedom by substituting eq. (5.74) into eq (5.76) the flutter equation becomes

$$\Omega [K_F] \{a_F\} = \left([\bar{m}_{FF}] - [\bar{m}_{FR}] [\bar{m}_{RR}]^{-1} [\bar{m}_{RF}] \right) \{a_F\} \tag{5.80}$$

or in the canonical form, with (5.81)

$$\Omega \{a_F\} = [K]^{-1} \left([\bar{m}_{FF}] - [\bar{m}_{FR}] [\bar{m}_{RR}]^{-1} [\bar{m}_{RF}] \right) \{a_F\} \tag{5.82}$$

The flutter equation can be solved to yield the eigenvalues $\Omega = \Omega_R + i\Omega_I$, from which we find the frequency

$$\omega = 1/\sqrt{\Omega_R} \tag{5.83}$$

the required structural damping

$$g = \Omega_I / \Omega_R \tag{5.84}$$

and form the assumed value of the reduced frequency ν_r,

$$V = \frac{b_r \omega}{\nu_r} \tag{5.85}$$

(b) Free-Free Modes

When free-free vibration data are available for flutter analysis, it is necessary to write two series expressions that provide the basis for the modal solution:

$$\{h_L\} = [h'_F] \{a'_F\} + [h_R] \{a_g\} \tag{5.86}$$

$$\{a_R\} = [a_{RF}] \{a'_F\} + \{a_g\} \tag{5.87}$$

where the prime denotes the free-free condition, $\{a_g\}$ is the matrix of centroidal generalized co-ordinates, and is the rigid component modal matrix.

Substituting eqns. (5.87) and(5.86) into the boundary conditions, Eq. (5.7) yields

$$[h_R]^T[\bar{M}]\left([h'_F]\{a'_F\}+[h_R]\{a_g\}\right) + [\Delta\bar{m}]\left([a_{RF}]\{a'_F\}+\{a_g\}\right)=0 \tag{5.88}$$

From Eq.(5.88), $\{a_g\}$ is obtained as

$$\{a_g\} = -[\bar{m}_{RR}]^{-1}[\bar{m}_{RF}]\{a'_F\} \tag{5.89}$$

where

$$[\bar{m}_{RF}] = [h_R]^T[\bar{M}][h'_F]+[\Delta\bar{m}][a_{RF}] \tag{5.90}$$

In order to apply the Galerkin principle when free-free modes are used in the series solution, it is necessary to obtain the equation of motion of the rigid component. This equation can be obtained by eliminating the flexible system between Eqs. (5.7) and (5.68)

$$-\Omega[h_R]^T[K]\left(\{h_1\}-\{h_0\}\right)=[\Delta\bar{m}]\{a_R\} \tag{5.91}$$

Substituting the series solutions, eq (5.86) and (5.87) the above equation becomes:

$$\Omega[h_R]^T[K][h''_F]\{a'_F\}=[\Delta\bar{m}]\left([a_{RF}]\{a'_F\}+\{a_g\}\right)+\{\epsilon_R\} \tag{5.92}$$

where $\{\epsilon_R\}$ is the error in equation (5.91) due to the series solution, and

$$[h''_F]=[h'_F]-[h_R][a_{RF}] \tag{5.93}$$

Substituting the series solutions into the flexible system equation of motion, equation (5.68) yields

$$\Omega^2[K][h'_F]\{q'_F\} = [\bar{M}]\left([h'_F]\{q'_F\} + [h_R]\{q_R\}\right) + \{\epsilon_F\} \quad (5.94)$$

where $\{\epsilon_F\}$ is the error in (5.68) due to the series solution. Application of Galerkin's principle,

$$\left([q_{RE}]^T\{\epsilon_R\} + [h'_F]^T\{\epsilon_F\} = 0\right),$$

yields the generalized equation of motion:

$$\Omega^2[K'_F]\{q'_F\} = \left([\bar{m}'_{FF}]\{q'_F\} + [\bar{m}'_{FR}]\{q_R\}\right) \quad (5.95)$$

where

$$[K'_F] = [h''_F]^T[K][h''_F] \quad (5.96)$$

$$[\bar{m}_{FF}] = [m'_{FF}] + [Q'_{FF}]$$
$$= \left([h'_F]^T[M][h'_F] + [q_{RF}]^T[\Delta m][q_{RF}]\right)$$
$$+ \left([h'_F]^T[A][K_F] + [q_{RF}]^T[\Delta Q][q_{RF}]\right) \quad (5.97)$$

$$[\bar{m}'_{FR}] = [h'_F]^T[\bar{M}][h_R] + [q_{RF}]^T[\Delta\bar{m}] \quad (5.98)$$

By substituting Eq. (5.89) into Eq. (5.95) the centroidal degrees of freedom can be eliminated to give the free-free modal equations:

$$\Omega^2[K'_F]\{q'_F\} = \left([\bar{m}'_{FF}] - [\bar{m}'_{FR}][\bar{m}_{RR}]^{-1}[\bar{m}_{RF}]\right)\{q_F\} \quad (5.99)$$

or, in the canonical form:

$$\Omega^2\{q'_F\} = [K'_F]^{-1}\left([\bar{m}'_{FF}] - [\bar{m}'_{FR}][\bar{m}_{RR}]^{-1}[\bar{m}_{RF}]\right)\{q_F\} \quad (5.100)$$

The flutter equation can be solved as before for a number of values of the reduced frequency ν to obtain the flutter speed and frequency by the V-g method.

5.7 METHODS OF SOLUTION OF THE CHARACTERISTIC MATRIX

The characteristic equation of the fluttering system has the form

$$\lambda\{h\} = [U]\{h\} \tag{5.101}$$

The matrix U is an $(N \times N)$ square matrix, where N is the number of degrees of freedom allowed. For the flutter problem the elements of U are in general complex and the elements are real for vibration problems. It is very rarely that U is ~~symmetrical~~ hermitian.

Thus the problem is one of determining the eigenvalues and eigenvectors of a non-Hermitian matrix. In most cases we are interested only in a few roots starting from the eigenvalue with the largest modulus.

There are two basic approaches ~~of~~ to solving this problem: (a) All the methods applicable to similar real matrices are also applicable to the case when elements are complex or, (b) the computations can be confined to the domain of realnumbers by adopting the following method. Let the matrix U be written as:

$$[U] = [UR] + \lambda[UI] \tag{5.102}$$

where UR represents the real part and UI the imaginary part. Then the eigenvalues of U are the same as those of the real matrix

$$\begin{bmatrix} UR & -UI \\ UI & UR \end{bmatrix} \tag{5.103}$$

(This can be proved as follows:

The equation $[U]\{h\} = \lambda\{h\}$ can be written as

$$[U_R + iU_I]\{h\} = \lambda\{h\}$$

Multiplying by $(-i)$ gives $[U_I - iU_R]\{h\} = -i\lambda\{h\}$

Now,

$$\begin{bmatrix} U_R & -U_I \\ U_I & U_R \end{bmatrix} \begin{Bmatrix} h \\ -ih \end{Bmatrix} = \begin{bmatrix} [U_R + iU_I]\{h\} \\ [U_I - iU_R]\{h\} \end{bmatrix} = \lambda \begin{Bmatrix} h \\ -ih \end{Bmatrix}$$

Thus, by definition, λ is also an eigenvalue of the modified system).

By using this method the methods applicable to a real unsymmetric matrix can be used for obtaining the eigenvalues of the matrix $[U]$. One disadvantage of this method is that it is wasteful of computer storage space.

Basically, the methods of solution can be classified into three broad groups:-

(a) Methods in which the characteristic determinant is expanded into a polynomial equation involving λ. This equation is then solved for the eigenvalues λ.

(b) Methods in which the characteristic determinant is transformed into a standard form (e.g tri-diagonal form, the Hessenberg forms, etc). The eigenvalues are obtained by making use of the properties of these special matrices.

(c) Iterative Methods.

5.7.1 Direct Methods

When the characteristic determinant is expanded into a polynomial in λ, the methods discussed in Section (4.5.3) can be used.

In addition to these methods, a modification by Frazer et al to a method of Krylov (Ref. 45) can be used for small matrices. This method makes use of

the Cayley-Hamilton Theorem which states that the characteristic equation of

$$|A - \lambda I| = 0$$

(i.e., $\lambda^N + \sum_{\lambda=0}^{N-1} b_\lambda \lambda^\lambda = 0$)

is also satisfied by the matrix A

i.e., $$A^N + \sum_{\lambda=0}^{N-1} b_\lambda A^\lambda = 0 \qquad (5.104)$$

If y represents an arbitrary vector, then operation on it by Eqn (5.104) must satisfy the equation

$$A^N y + \sum_{\lambda=0}^{N-1} b_\lambda A^\lambda y = 0 \qquad (5.105)$$

This amounts to N linear equations in the unknowns b_λ, $(\lambda = 0, \ldots N-1)$. The method is to calculate, for any vector y, the N iterates Ay .....$A^N y$ from the linear expressions represented by Eqn (5.105) and to solve these equations by a linear equation solving scheme.

For small matrices the Souriau-Frame Method (Ref. 68 p. 225) is very useful to obtain the coefficients of the polynomial.

Another procedure would be to evaluate the determinant $p(\lambda) = |A - \lambda I|$ for a number of values of λ. These values are plotted and the eigenvalues λ are obtained as those which cause the determinant to vanish. When only a few roots (of the lowest magnitude) are required, this is a very useful method even for large matrices. For a (21 x 21) real, unsymmetric matrix this method gave very consistent results (Ref. 69). This method would probably be impractible for use with complex matrices in view of the labour involved.

5.7.2 Methods involving transformations

If the characteristic matrix is transformed into a standard form, the determination of the eigenvalues and the eigenvectors becomes somewhat easier.

Lanczos (Ref. 70) gives a method which reduces the given matrix into a tridiagonal form. In this method, two bi-orthogonal vectors $x_\lambda (\lambda = 1, \ldots N)$ and $y_\lambda (\lambda = 1, \ldots N)$ are the first assumed. The vector x_λ is a column vector and the vector y_λ is a row vector and it is assumed that $y_i^* x_j = 0 (i \neq j)$ where y_λ^* represents the complex conjugate of y_λ. the next two vectors are defined as follows:

$$x_{k+1} = A x_k - a_k x_k - b_{k-1} x_{k-1}$$
$$y_{k+1} = y_k A^* - a_k^* y_k - b_{k-1}^* y_{k-1} \qquad (5.106)$$

where

$$a_k = y_k^* A x_k / y_k^* x_k$$
$$b_{k-1} = y_{k-1}^* A x_k / y_{k-1}^* x_{k-1}$$

and $b_0 = 0$

The recursion formulae for x can be written as

$$A x_1 = x_2 + a_1 x_1$$
$$A x_2 = x_3 + a_2 x_2 + b_1 x_1$$
$$\vdots$$
$$A x_k = x_{k+1} + a_k x_k + b_{k-1} x_{k-1} \qquad (5.107)$$

In matrix form, this can be written as

$$A \cdot S = S \begin{bmatrix} a_1 & b_1 & 0 & \cdots & 0 \\ 1 & a_2 & b_2 & & \\ 0 & a_1 & a_3 & b_3 & \\ & & & & \\ 0 & & & 1 & a_{N-1} \; b_{N-1} \\ & & & & 1 \quad a_N \end{bmatrix}$$
$$= S T \qquad (5.108)$$

Equation (5.108) can also be written as $S^{-1} A S = T$ and shows that T is obtained from A by a similarity transformation. Hence the eigenvalues of T are the same as those of A.

This method does not give accurate results for large matrices due to the difficulties in maintaining the bi-orthogonality condition with sufficient accuracy. However, the method is accurate for small matrices.

Gregory (Ref. 71) has given a modification to the Lanczos method. In this method, the matrix A is transformed into an upper-triangular form. He considers the recursive relations to have the form

$$x_{k+1} = A x_k - a_{kk} x_k - a_{k-1,k-1} x_{k-1} - \cdots - a_{k1} x_1$$

$$y_{k+1} = y_k A^* - a^*_{kk} x_k - a^*_{k-1,k-1} x_{k-1} - \cdots - a^*_{k1} x_1 \quad (5.109)$$

where

If the vectors $(x_1 \cdots x_k)$ and $(y_1 \cdots y_k)$ are bi-orthoganal, the recursion relations can be written:

$$A S = S \begin{bmatrix} a_{11} & a_{21} & \cdots & a_{N1} \\ 1 & a_{22} & \cdots & a_{N2} \\ 0 & 1 & a_{33} & a_{N3} \\ 0 & \cdots & 1 & a_{NN} \end{bmatrix}$$

$$= S T' \quad (5.110)$$

Gregory found that the terms above the first principal diagonal were small compared to the other terms, and considered T' to be a triangular matrix. Even so, this method gave improved accuracy over the Lanczos method.

In some cases, it is possible to apply the methods available to solve the eigenvalue problem of symmetric matrices to the solution of unsymmetric matrices. For example, this is possible in vibration problems where the equation can be written as

$$[K]\{h\} = \omega^2 [M]\{h\} \quad (5.111)$$

Where the stiffness matrix K and the mass matrix M are both real and symmetric.

Since $[M]$ is symmetric, there exists an orthogonal matrix such that

$$[U]^{-1} = [U]^T$$

and

$$[U][M][U]^{-1} = [D] \quad (5.112)$$

Where D is a diagonal matrix containing the eigenvalues of M (which are all real and positive).

$$[D] = \begin{bmatrix} \lambda_1 & & & \\ & \lambda_2 & & \\ & & \ddots & \\ & & & \lambda_N \end{bmatrix} \tag{5.113}$$

The matrix U has for its elements the eigenfunctions V_N of $[M]$

$$[U] = [\{V_N^{(1)}\} \{V_N^{(2)}\} \cdots \{V_N^{(M)}\}] \tag{5.114}$$

From equation (5.112)

$$[M] = [U][D][U]^T \tag{5.115}$$

Since the diagonal elements of D are all positive, it is possible to write:

$$[D] = [D]^{1/2}[D]^{1/2} \tag{5.116}$$

Using the relations (5.115) and (5.116), Eqn. (5.111) becomes

$$[K]\{h\} = \omega^2 [U][D]^{1/2}[D]^{1/2}[U]^T\{h\} \tag{5.117}$$

Defining the two matrices

$$\begin{aligned} \{y\} &= [U]^T\{h\} \\ \{x\} &= [D]^{1/2}\{y\} \end{aligned} \tag{5.118}$$

Eqn (5.117) can be written as

$$\begin{aligned} &[D]^{-1/2}[U]^T[K][U][D]^{-1/2}\{x\} = \omega^2\{x\} \\ &\text{or} \quad [C]\{x\} = \omega^2\{x\} \end{aligned} \tag{5.119}$$

Since K is Symmetric, $K^T = K$.
Hence, $C = D^{-\frac{1}{2}} U K U D^{-\frac{1}{2}}$ is
also Symmetric

(5.120)

Thus the original problem has been reduced to one of finding the eigenvalues and vectors of two symmetric matrices. The steps in the calculations will be:

(i) Solve the eigenvalue problem $[M]\{y\} = \mu\{y\}$

(ii) Form the matrix U whose columns are the eigenvectors of M and the diagonal matrix $[D]^{-1/2}$ whose elements are $1/\sqrt{\mu_\lambda}$ where μ_λ is the eigenvalue of M

(iii) Form the matrix $[C] = [D]^{-1/2}[U]^T[K][U][D]^{-1/2}$

(iv) The eigenvalues of the equation $[C]\{x\} = \lambda\{x\}$ are the eigenvalues of the original problem and the eigenvector $\{q\}$ is given by

$$\{q\} = [U]^{-1}[D]^{-1/2}\{x\}$$

This method has been used to solve the vibration frequencies and modes of beams by Young and McCallum in Ref. (72).

One major advantage of this method is that the methods available for the relatively simple problem of finding the eigenvalues of a symmetric matrix can be used directly.

5.7.3. Iterative Methods

These are the most powerful methods for obtaining the eigenvalues of arbitrary matrices. Most matrix iterative methods are based on the Power Method of Von Mises.

5.7.2.1 The Basic Power Method

This is based on a theorem of Von Misses (e.g. Ref 73) which states that if $x_1 \ldots\ldots x_n$ are a linearly independent set of eigenvectors of an N x N matrix $[A]$ and if the dominant eigenvalue λ_1 is real, then the sequence converges to the eigenvector corresponding to λ_1, where $\{h\}$ is an arbitrary vector not orthogonal to x_1. This result follows from the following argument:

Assuming that the eigenvalues of $[A]$, $\lambda_1, \lambda_2, \ldots, \lambda_N$ are different and that

$$|\lambda_1| \geq |\lambda_2| \geq \cdots \geq |\lambda_N| \qquad (5.121)$$

Consider an arbitrary vector $\{h_0\}$ with N components. This can be conceived as a linear combination of the N eigenvectors $x_1 \ldots\ldots x$ of $[A]$ i.e.

$$\{h_0\} = c_1 x_1 + c_2 x_2 + \cdots + c_N x_N \qquad (5.122)$$

Applying the matrix $[A]$ to (5.122) we obtain

$$[A]\{h_0\} = c_1 \lambda_1 x_1 + c_2 \lambda_2 x_2 + \cdots + c_N \lambda_N x_N \qquad (5.123)$$

If this process is continued, say, m times we have

$$[A]^m \{h_0\} = c_1 \lambda_1^m x_1 + c_2 \lambda_2^m x_2 + \cdots + c_N \lambda_N^m x_N \qquad (5.124)$$

Assuming that all the roots are different and that λ_1 is the dominant eigenvalue, the first term on the right hand side of Eq. (5.124) will dominate and $[A]^m \{h_0\}$ will converge to $c_1 \lambda_1^m x_1$

i.e.,

$$\{h_m\} = [A]^m \{h_0\} \simeq c_1 \lambda_1^m x_1 \qquad (5.125)$$

Applying the matrix [A] once more to (5.125) we got

$$\{h_{m+1}\} = [A]^{m+1}\{h_0\} \simeq c_1 \lambda_1^{m+1} x_1 \qquad (5.126)$$

From (5.124) and (5.126) we obtain

$$\lambda_1 = h_{m+1} / h_m \qquad (5.127)$$

where h_{m+1} and h_m are corresponding components in the vectors $\{h_{m+1}\}$ and $\{h_m\}$

This method can also be used in the case of multiple eigenvalues (Ref. 73, p. 247 or Ref. 74 p. 277). Consider the case when $|\lambda_1| \simeq |\lambda_2|$. In this case the mth iteration will converge to $(c_1 \lambda_1^m \{x_1\} + c_2 \lambda_2^m \{x_2\})$.

Introducing the notation

$$\{x_k\} = c_k \lambda_k^m \{x_k\} \qquad (5.128)$$

The mth iterate can be written as

$$\begin{aligned} \{h_m\} &= \{x_1\} + \{x_2\} \\ \{h_{m+1}\} &= \lambda_1 \{x_1\} + \lambda_2 \{x_2\} \\ \{h_{m+2}\} &= \lambda_1^2 \{x_1\} + \lambda_2^2 \{x_2\} \end{aligned} \qquad (5.129)$$

neglecting terms of higher order.

The vectors $\{h_m\}$, $\{h_{m+1}\}$ and $\{h_{m+2}\}$ are situated in approximately the same plane.

Hence,

$$\{h_{m+2}\} + a_1 \{h_{m+1}\} + a_0 \{h_m\} = 0 \qquad (5.130)$$

Since the vectors have at least two components, the values of a_0 and a_1 can be determined from two simultaneous equations. Inserting (5.130) into (5.128) we obtain

$$(\lambda_1^2 + a_1\lambda_1 + a_0)\{X_1\} + (\lambda_2^2 + a_1\lambda_2 + a_0)\{X_2\} = 0 \qquad (5.131)$$

Since X_1 and X_2 are linearly independent λ_1 and λ_2 must satisfy the equation

$$\lambda^2 + a_1\lambda + a_0 = 0 \qquad (5.132)$$

The corresponding eigenvectors $\{h\}$ are obtained from (5.129) as

$$\{h_1\} = \frac{\{X_{m+1}\} - \lambda_2\{X_m\}}{\lambda_1 - \lambda_2}$$

$$\{h_2\} = \frac{\{X_{m+1}\} - \lambda_1\{X_m\}}{\lambda_1 - \lambda_2} \qquad (5.133)$$

Basically, the power method consists of choosing a vector $\{X\}$ from which $\{x_1\} = [A]\{x\}$ is computed. Usually $\{x_1\}$ is then normalized by dividing all the elements by the element with the largest modulus, thus obtaining a new vector $\{y_1\}$ whose largest element has a modulus of unity. The vector $\{x_2\} = [A]\{y_1\}$ is computed and normalized as before to $\{y_2\}$. Repeated application of this process leads to the computation of $\{x_k\} = [A]\{x_{k-1}\}$ which is then normalized to $\{y_k\}$. If the vectors converge, then the vector to which they converge will be the principal eigenvector. The maximum component of $\{x_k\}$, because of the normalization will converge to λ_1. Usually, if the iteration does not converge after a specified number of iterations a pair of close magnitude or equal roots is suspected and an alternative procedure

is adopted. Once the dominant eigenvalue (or dominant pair of eigenvalues) has been found, the matrix $[A]$ is reduced to one containing all the other undetermined eigenvalues, but which does not contain the eigenvalues already determined.

This method is very accurate since the successive vectors $\{x_k\}$ and $\{y_k\}$ are always generated using the original matrix $[A]$ and the errors created in $\{y_k\}$ for some value of k tend to correct themselves in the later steps.

There are some modifications to the basic power method which improve the method.

5.7.3.2. Wilkinson's Method

If the matrix $[A]$ has N linearly independent eigenvectors $x_1, x_2 \ldots\ldots x_n$, then any vector V can be written as

$$V = x_1 + x_2 + \cdots + x_N \tag{5.134}$$

where the x_i have been suitably scaled. Similarly after K iterations,

$$(A-pI)^K V = (\lambda_1-p)^K x_1 + (\lambda_2-p)^K x_2 + \cdots + (\lambda_N-p)^K x_N \tag{5.135}$$

Thus, as in the basic power method, if $|\lambda_1-p| \geq |\lambda_2-p| \geq \cdots \geq |\lambda_N-p|$, then the term $(\lambda_1-p)^K x_1$ eventually dominates. All the restrictions and limitations of the basic power method remain, but the freedom to choose p gives scope for improvement. By choosing a proper value for p the convergence of the iteration process can be speeded up. The method also permits the calculation of the lowest eigenvalue

without having to calculate all the other values.

5.7.3.3 Aitken's δ^2 Acceleration

If the matrix has closely spaced eigenvalues the convergence of the basic power method will be too slow. In this case, the δ^2- process (e.g. Ref: 73, p. 243) can be applied to speed-up the convergence.

Let $\{x_\lambda\}$ converge to α such that

$$e_{\lambda+1} = K e_\lambda \quad , \quad |K|<1 \tag{5.136}$$

where $e_\lambda = x_\lambda - \alpha$ and K is a constant. . This is called 'geometric convergence' to distinguish it from linear convergence which is

$$(e_{\lambda+1}) = (K+\sigma_\lambda) e_\lambda \qquad \begin{matrix} |K|<1 \\ \sigma_\lambda \to 0 \end{matrix} \tag{5.137}$$

If we eliminate K between successive relations of (5.136) and solve for

$$\alpha = \frac{x_{\lambda+2}x_\lambda - x_{\lambda+1}^2}{x_{\lambda+2} - 2x_{\lambda+1} + x_\lambda} \tag{5.138}$$

For a sequence which converges linearly rather than geometrically the expression on the right hand side of (5.138) does not yield the limit in one step. For this we define a new sequence by

$$z_\lambda = (x_{\lambda+2}x_\lambda - x_{\lambda+1}^2) / (x_{\lambda+2} - 2x_{\lambda+1} + x_\lambda) \tag{5.139}$$

This may also be written in the forms

$$\begin{aligned} z_\lambda &= x_\lambda - \{(x_{\lambda+1}-x_\lambda)^2 / (x_{\lambda+2} - 2x_{\lambda+1} + x_\lambda)\} \\ &= x_{\lambda+1} - \{(x_{\lambda+1}-x_\lambda)(x_{\lambda+1}+x_\lambda) / (x_{\lambda+2} - 2x_{\lambda+1} + x_\lambda)\} \\ &= x_{\lambda+2} - \{(x_{\lambda+2}-x_{\lambda+1})^2 / (x_{\lambda+2} - 2x_{\lambda+1} + x_\lambda)\} \end{aligned} \tag{5.140}$$

5.7.3.4. Bodewig's Method for Nearly Equal Roots

Bodewig's method (Ref. 73, p. 249) can be applied in cases where the eigenvalues have nearly equal roots and consequently the iteration by the power method is proceeding slowly.

If the first two dominant eigenvalues are nearly equal, then the convergence will reach a stage where the first two terms will dominate and the iterates $V_k = A^k V$ will be approximately equal to $(\lambda_1^k x_1 + \lambda_2^k x_2)$

Considering the two previous steps of iteration, we can write (after proper scaling of the vectors x_1 and x_2),

$$\begin{aligned} V^{(k-2)} &= A^{k-2} V = x_1 + x_2 \\ V^{(k-1)} &= \lambda_1 x_1 + \lambda_2 x_2 \\ V^{(k)} &= \lambda_1^2 x_1 + \lambda_2^2 x_2 \end{aligned} \tag{5.141}$$

From the first two equations:

$$\begin{aligned} x_1 &= \frac{V^{(k-2)} - V^{(k-1)}/\lambda_2}{(1 - \frac{\lambda_1}{\lambda_2})} \\ x_2 &= \frac{V^{(k-2)} - V^{(k-1)}/\lambda_1}{(1 - \lambda_1/\lambda_2)} \end{aligned} \tag{5.142}$$

From the last two equations of (5.142)

$$\begin{aligned} x_1 &= \frac{V^{(k-1)} - V^{(k)}/\lambda_2}{\lambda_1 (1 - \lambda_1/\lambda_2)} \\ x_2 &= \frac{V^{(k-1)} - V^{(k)}/\lambda_1}{\lambda_2 (1 - \lambda_2/\lambda_1)} \end{aligned} \tag{5.143}$$

If we now equate the two expressions for x_1 (or x_2) we obtain:

$$V^{(k-2)} - \left(\frac{1}{\lambda_1} + \frac{1}{\lambda_2}\right) V^{(k-1)} + \frac{1}{\lambda_1 \lambda_2} V^{(k)} = 0 \qquad (5.144)$$

This is a vector equation which is valid for every element of the vectors. If V_l and V_m represent two different elements, we have

$$\begin{aligned} V_l^{(k-2)} - \left(\frac{1}{\lambda_1} + \frac{1}{\lambda_2}\right) V_l^{(k-1)} - \frac{1}{\lambda_1 \lambda_2} V_l^{(k)} &= 0 \\ V_m^{(k-2)} - \left(\frac{1}{\lambda_1} + \frac{1}{\lambda_2}\right) V_m^{(k-1)} - \frac{1}{\lambda_1 \lambda_2} V_m^{(k)} &= 0 \end{aligned} \qquad (5.145)$$

From these two equations

$$\begin{aligned} \left(\frac{1}{\lambda_1} + \frac{1}{\lambda_2}\right) &= \left\{ V_l^{(k-2)} V_m^{(k)} - V_l^{(k)} V_m^{(k-2)} \right\} / \Delta \\ \frac{1}{\lambda_1 \lambda_2} &= \left\{ V_l^{(k-2)} V_m^{(k-1)} - V_l^{(k-1)} V_m^{(k-2)} \right\} / \Delta \end{aligned}$$

w.m

$$\Delta = V_l^{(k-1)} V_m^{(k)} - V_l^{(k)} V_m^{(k-1)}$$

(5.146)

This means that $1/\lambda_1$ and $1/\lambda_2$ are roots of the quadratic equation

$$\left\{ V_l^{(k-1)} V_m^{(k)} - V_l^{(k)} V_m^{(k-1)} \right\} \left(\frac{1}{\lambda}\right)^2 - \left\{ V_l^{(k-2)} V_m^{(k)} - V_l^{(k)} V_m^{(k-2)} \right\} \frac{1}{\lambda} + \left\{ V_l^{(k-2)} V_m^{(k-1)} - V_l^{(k-1)} V_m^{(k-2)} \right\} = 0 \qquad (5.147)$$

5.7.3.5 Deflation

In all the iteration processes described above, after one eigenvalue and its associated eigenvector have been found, it is necessary to reduce the given matrix to one in which the known value and its vector are no longer present. This ~~is known as~~ can be done by 'sweeping' or 'deflation'.

For arbitrary matrices, the most popular method seems to be Wielandt's method.

This is based on Wielandt's theorem that the matrix

$$[B] = [A] - \lambda_1 \{x_1\}[z_1] \tag{5.148}$$

where $\{x_1\}$ is a column eigenvector and $[z_1]$ is an arbitrary row vector with $z_1 x_1 = 1$, has the same eigenvalues as $[A]$ except that $\lambda_1 = 0$. Also the eigenvectors $\{W_\lambda\}$ of $[B]$ satisfy the relations

$$\{x_\lambda\} = \left([A] - \lambda_\lambda [I]\right)\{W_\lambda\}$$
$$x_1 = W_1 \tag{5.149}$$

Since $\{z\}$ is arbitrary, it may chosen so as to make one row of $[B]$ equal to zero, and thus $[B]$ is effectively reduced in rank to order $(N - 1)$.

5.8 METHODS SUITABLE FOR THE FLUTTER DETERMINANT

The characteristic matrix of the fluttering system has complex elements and is non-Hermitian. One method of solving this matrix for its eigenvalues and the eigenvectors would be to use the methods applicable to real matrices, but using complex arithmetic. The ICL 1905 digital computer has facilities for handling complex numbers in single precision arithmetic. Since some of the eigenvalues of the characteristic matrix can have close or equal magnitude roots, the calculations have to be carried out in double-precision arithmetic to determine these values accurately. The double precision calculations can be carried out only with real numbers. Hence, in the two methods to be described, all the calculations are confined to the realm of real numbers,

but with proper regard to the rules of complex algebra. The calculations are carried out in double-precision arithmetic where necessary.

5.8.1 Method of Rodden et al (Ref. 58)

This method has been formulated so that the eigenvalues and eigenvectors of a real or complex non-Hermitian matrix can be obtained by the Power Method. Convergence to the dominant eigenvalue is accelerated by using Aitken's δ^2 method. The convergence difficulties due to a dominant pair of close or equal magnitude roots is overcome by using Bodewig's Method. (This includes as special cases complex conjugate roots and equal but opposite roots). The deflation method of Wielandt is used to permit the iteration to converge to the next most dominant root.

5.8.1.1 Iteration and Acceleration

Consider the matrix $[A]$. The application of the power method for the dominant root yields, after $(n+1)$ iterations

$$\lambda_{n+1}\{h_{n+1}\} = [A]\{h_n\} \tag{5.150}$$

where $\{h_{n+1}\}$ and $\{h_n\}$ are normalized on the largest element and λ_{n+1} is the normalizing factor and the $(n+1)$ estimate for the eigenvalue the iteration may be started either by assuming a unit vector or with any arbitrary vector, convergence is obtained, in the real case, when all the elements of $\{h\}$ satisfy the condition

$$|h_n - h_{n-1}| < \epsilon_1 \tag{5.151}$$

where ϵ_1 is a small positive number (taken as 0.5×10^{-6}). In the complex case, the condition is

$$|Re(h_n - h_{n-1})| + \lambda |Im(h_n - h_{n-1})| < (1+\lambda)\epsilon_1 \tag{5.152}$$

The convergence test is made as a difference rather than as a ratio since all the vectors have been normalized.

If the iteration process is converging, the convergence is accelerated by using Aitken's δ^2 process (Section 5.7.3.3) which permits extrapolation to a better approximation of each element of the vector. The extrapolation is made only if all the elements satisfy the condition

$$\left|\frac{(h_n - h_{n-1})}{(h_{n-1} - h_{n-2})}\right| < \eta < 1 \qquad (5.153)$$

(Real case)

or

$$\left|\frac{(h_n - h_{n-1})}{(h_{n-1} - h_{n-2})}\right|^2 < \eta^2 < 1 \qquad (5.154)$$

(Complex case)

The value of η must be less than, but not too close to, unity. Rodden and Farkas (Ref. 103) noted that when $\eta = 0.9$ optimum convergence was obtained.

The extrapolation formula for each element of the (n + 1)th eigenvector is

$$h_{n+1} = h_{n-2} - \frac{(h_{n-1} - h_{n-2})^2}{(h_n - 2h_{n-1} + h_{n-2})} \qquad (5.155)$$

In the single precision calculations, the extrapolation is attempted as often as possible, i.e, following an extrapolation, the test is attempted every iteration past the third iteration. In the double precision calculation, the test is attempted every iteration past the fifth iteration following an extrapolation.

5.8.1.2 Close or Equal Magnitude Roots

If convergence is not obtained in 40 iterations, the presence of close or equal magnitude roots is suspected and the calculation is continued in double precision, anticipating convergence to the quadratic form

$$\lambda^2 + p\lambda + q = 0 \tag{5.156}$$

whose roots are the two close eigenvalues

$$|\lambda^{(1)}| > |\lambda^{(2)}| \tag{5.157}$$

The coefficients p and q are found from

$$p_n = \frac{\lambda_{n-1}(\lambda_{n-2} h_{n-1} h_{n-2} - \lambda_n h_n h_{n-3})}{(\lambda_{n-1} h_{n-1} h_{n-3} - \lambda_{n-2} h_{n-2}^2)} \tag{5.158}$$

$$q_n = \frac{\lambda_{n-1}\lambda_{n-2}(\lambda_n h_n h_{n-2} - \lambda_{n-1} h_{n-1}^2)}{(\lambda_{n-1} h_{n-1} h_{n-3} - \lambda_{n-2} h_{n-2}^2)} \tag{5.159}$$

where λ_i denotes the i-th estimate of the eigenvalue and represents a particular element from the i-th vector (usually this is the normalized element, i.e. $h_i = 1$, but more general expressions for p_n and q_n are necessary in the case that the same element has not been normalized in successive iterations.)

The convergence conditions are:

$$\left| \left(|p_n - p_{n-1}| \right) / \sqrt{|q_n|} \right| < \epsilon_2 \tag{5.160}$$

$$\left| \left(|q_n / q_{n-1}| \right) - 1 \right| < \epsilon_2 \tag{5.161}$$

where ϵ_2 is a small positive number taken as (0.5×10^{-7}) here. The two eigenvectors are found from

$$\{h^{(1)}\} = \lambda^{(2)} \{h_{n-1}\} - \lambda_n \{h_n\} \tag{5.162}$$

$$\{h^{(2)}\} = \lambda_n \{h_n\} - \lambda^{(1)} \{h_{n-1}\} \tag{5.163}$$

The following tests are also made in the programme for testing the possibility of convergence to a single root or to a pair of close roots.

Convergence to a single root has been observed when

$$\left|\lambda^{(2)}/\lambda^{(1)}\right| < \left|\lambda^{(3)}/\lambda^{(2)}\right| \tag{5.164}$$

and to a pair of close roots when

$$\left|\lambda^{(2)}/\lambda^{(1)}\right| < \left|\lambda^{(3)}/\lambda^{(2)}\right| \tag{5.165}$$

5.8.1.3 Deflation

When convergence to a dominant eigenvalue has been obtained, its effect is swept out using Wielandt's method so that the succeeding iterations will converge to the next most dominant eigenvalue.

Let $\left[A^{(r)}_{S_\lambda}\right]$ denote a matrix in which r represents the number of eigenvalues absent from $[A]$ and S_λ denotes the number of the row in $\left[A^{(r)}\right]$ which corresponds to the row containing the normalized element in the vector. The iteration will converge to the next dominant eigenvalue such that

$$\left[A^{(\lambda-1)}\right]\left\{h^{(\lambda)}\right\}_{\lambda-1} = \lambda^{(\lambda)}\left\{h^{(\lambda)}\right\}_{\lambda-1} \tag{5.166}$$

where $\left\{h^{(\lambda)}\right\}_{\lambda-1}$ denotes the vector number $\mathrm{cond}(\lambda-1)$ is a modification number.

The true vector is recovered by successive applications of the recurrence relation:

$$\left\{h^{(\lambda)}\right\}_{\lambda-j-1} = \left\{h^{(\lambda-j)}\right\}_{\lambda-j-1} - \left(\frac{\lambda^{(\lambda-j)} - \lambda^{(\lambda)}}{\left[A^{(\lambda-j-1)}_{S_{\lambda-j}}\right]\left\{h^{(\lambda)}\right\}_{\lambda-j}}\right)\left\{h^{(\lambda)}\right\}_{\lambda-j}$$

$$(j = 1, 2, \ldots, \lambda-1) \tag{5.167}$$

In the case of multiple repeated roots the coefficient $\left(\lambda^{(\lambda-j)} - \lambda^{(\lambda)}\right) / \left[A^{(\lambda-j-1)}_{s_{\lambda-j}}\right] \{h^{(\lambda)}\}_{\lambda-j}$ becomes indeterminate and is arbitrarily assigned the value 1.0, whenever $\left|\left(\lambda^{(\lambda-j)}/\lambda^{(\lambda)}\right)-1\right| < \epsilon_1$, (or $\left|Re\left(\lambda^{(\lambda-j)}/\lambda^{(\lambda)}\right)-1\right| + i\left|Im\left(\lambda^{(\lambda-j)}/\lambda^{(\lambda)}\right)-1\right| < (1+i)\epsilon_1$ in the complex case), since the vectors correpsonding to repeated roots cannot be determined uniquely but only to the extent that they are linearly independent.

The eigenvalue is then swept out of the matrix by

$$\left[A^{(\lambda)}\right] = \left[A^{(\lambda-1)}\right] - \{h^{(\lambda)}\}_{i-1} \left[A^{(\lambda-1)}_{s_i}\right] \qquad (5.168)$$

5.8.2. Method of Gollnitz et al (Ref. 77)

In this method an initial estimate of the eigenvalues is made by the power method and by sweeping the known eigenvalues out of the matrix. Wielandt's reciprocal iteration (Section 5.8.3.e) is used to improve the accuracy of the eigenvalues which have already been obtained.

5.8.2.1 First Estimate of the Eigenvalues

As in the previous method, the application of the power method leads to the first dominant eigenvalue. In case of two equal or close valued roots, Bodewig's method is used.

If we assume that the m roots λ of the equation

$$(A - \lambda I) = 0 \qquad (5.169)$$

are such that

$$|\lambda_1| \geq |\lambda_2| \geq \cdots \geq |\lambda_m| \qquad (5.170)$$

To determine the eigenvalue with the largest modulus, λ_1, we assume an arbitrary vector Z_o with n components. This may be considered as a linear combination of the n eigenvectors $h_1, h_2 \ldots\ldots h_n$ belonging to the eigenvalues $\lambda_1, \lambda_2, \ldots, \lambda_n$.

$$Z_o = c_1 h_1 + c_2 h_2 + \cdots + c_n h_n \qquad (5.171)$$

where the c_i are constants.

After m applications for the matrix A to the basic vector Z_o we have

$$Z_m = A^m Z_o = c_1 \lambda_1^m h_1 + c_2 \lambda_2^m h_2 + \cdots + c_n \lambda_n^m h_n \qquad (5.172)$$

First we consider the case when $|\lambda_1| > |\lambda_2| > \cdots > |\lambda_n|$. In this case the first term of equation (5.172) will dominate and after a further application of the matrix A to the vector Z_m, we can obtain the first dominant eigenvalue as

$$\lambda_1 = Z_{m+1} / Z_m \qquad (5.173)$$

Considering now the case when $|\lambda_1| \simeq |\lambda_2|$ we introduce a column vector X given by

$$X_k = c_k \lambda_k h_k \qquad (5.174)$$

By Bodewig's method the two eigenvalues λ_1 and λ_2 are obtained as solutions of the quadratic equation

$$\lambda^2 + p\lambda + q = 0 \qquad (5.175)$$

The eigenvectors corresponding to λ_1 and λ_2 are obtained as

$$X_1 = \frac{h_{m+1} - \lambda_2 h_m}{\lambda_1 - \lambda_2} \quad ; \quad X_2 = \frac{h_{m+1} - \lambda_1 h_m}{\lambda_1 - \lambda_2} \tag{5.176}$$

Having obtained the eigenvalue λ_1 and the corresponding eigenvector X_1 these values have to be eliminated from the matrix A before proceeding with the iteration.

The determinental form of Eq. (5.169) is

$$\det | A - \lambda I | = 0 \tag{5.177}$$

we replace the first column of this determinant by

$(A - \lambda I) X_1$, yielding,

$$\begin{bmatrix} (a_{11}-\lambda)x_1 + a_{12}x_2 + \cdots + a_{1n}x_n & a_{12} & \cdots & a_{1n} \\ \vdots & & & \\ (a_{n1}x_1 + a_{n2}x_2 + \cdots + (a_{nn}-\lambda)x_n & a_{n2} & \cdots & a_{nn} \end{bmatrix} = 0 \tag{5.178}$$

Further, we have

$$a_{j1}x_1 + \cdots + a_{jn}x_n = \lambda_1 x_j, \quad j = 1, 2, \cdots n \tag{5.179}$$

Substituting Eq. (5.179) into Eq (5.178) we have

$$(\lambda_1 - \lambda) \begin{vmatrix} x_1 & a_{12} & \cdots & a_{1n} \\ x_2 & a_{22}-\lambda & \cdots & a_{2n} \\ & & & \\ x_n & a_{n2} & \cdots & a_{nn}-\lambda \end{vmatrix} = 0 \tag{5.180}$$

We multiply the first row by (x_k/x_1) and subtract it from the k th row $(k = 2, 3, \ldots, n)$ to obtain

$$(\lambda_1 - \lambda)\begin{vmatrix} x_1 & a_{12} & \cdots & a_{1n} \\ 0 & a_{22}-\lambda-\frac{x_2}{x_1}a_{12} & & a_{2n}-\frac{x_2}{x_1}a_{1n} \\ \vdots & \vdots & & \vdots \\ 0 & a_{n2}-\frac{x_n}{x_1}a_{12} & \cdots & a_{nn}-\lambda-\frac{x_n}{x_1}a_{1n} \end{vmatrix} = 0 \qquad (5.181)$$

For $\lambda = \lambda_2, \lambda_3, \ldots \lambda_n$ the bordered sub-determinant becomes zero and hence the reduced matrix

$$A_1 = \begin{vmatrix} a_{22}-\frac{x_2}{x_1}a_2 & & a_{2n}-\frac{x_2}{x_1}a_{1n} \\ \vdots & & \vdots \\ a_{n2}-\frac{x_n}{x_1}a_{12} & \cdots & a_{nn}-\frac{x_n}{x_1}a_{1n} \end{vmatrix} \qquad (5.182)$$

has the eigenvalues $\lambda_2, \lambda_3 \ldots \lambda_n$. Using the power method on A_1 we obtain the eigenvalue λ_2. The matrix A_1 is then reduced as above to determine the eigenvalue and so on to λ_n.

5.8.2.2 Reciprocal iteration by Wielandt's Method

Let λ'_k represent the approximate values (of the true eigenvalues λ_k) determined by application of the power method, i.e.

$$|\lambda'_k - \lambda_k| < |\lambda'_k - \lambda_j|, \quad j \neq k \qquad (5.183)$$

Then

$$\epsilon = \lambda_k - \lambda'_k \qquad (5.184)$$

will be the eigenvalue with the smallest modulus of the matrix

$$[B] = [A] - \lambda'_K [I] \tag{5.185}$$

To calculate ϵ we introduce the basic vector

$$X_0 = c_1 Q'_1 + c_2 Q'_2 + \cdots + c_n Q'_n, \quad (c_1 \neq 0,\ c_2 \neq 0) \tag{5.186}$$

where the Q'_λ are the eigenvectors of the matrix $[B]$

After m iterations we have

$$(A - \lambda'_K E)\ X_{m+1} = \epsilon_{m+1}\ X_m\ ;\quad m = 0, 1, 2, \ldots \tag{5.187}$$

It is convenient to normalize the last component of X_{m+1},

$$x_n^{(m+1)} = 1.0 \tag{5.188}$$

If we exchange the last component on the right hand side of Eq. (5.187) with the right hand side, we obtain a system of linear, non homogeneous equations, whose unknowns are the remaining (n - 1) components of $x_i^{(m+1)}$ and the eigenvalues ϵ_{m+1}. Using the Gaussian algorithm we transform this modified equation into a triangular form:

$$\begin{aligned} a'_{11} x_1^{(m+1)} + a'_{12} x_2^{(m+1)} + \cdots - \epsilon_{m+1} \bar{x}_1^{(m)} &= -a'_{1n} \\ a'_{22} x_2^{(m+1)} + \cdots - \epsilon_{m+1} \bar{x}_2^{(m)} &= -a'_{2n} \\ \cdots \\ - \epsilon_{m+1} \bar{x}_n^{(m)} &= -a'_{nn} \end{aligned} \tag{5.189}$$

In eq. (5.189) $x_i^{(m)}$ represent the components of the iteration vector after m iteration teps

After a sufficiently large number of steps, the eigenvalue is calculated as

$$\epsilon \simeq \epsilon_{m+1} = \frac{a'_{nn}}{x_n^{(m)}} \qquad (5.190)$$

Hence the true eigenvalue is

$$\lambda_k = \lambda'_k + \epsilon \qquad (5.191)$$

If the matrix B possesses two close-valued eigenvalues ϵ_1, ϵ_2, the two root procedure described before is applied to determine this as roots of the quadratic

$$a_0 \epsilon^2 + a_1 \epsilon + 1 = 0 \qquad (5.192)$$

In the actual computations, after M = 26 steps of iteration by the power method the two-root procedure is applied to the two vector sets

$$(Z_m, Z_{m+1}, Z_{m+2})$$

and $(Z_{m+1}, Z_{m+2}, Z_{m+3})$

From both sets the approximate eigenvalues λ_1, λ_2 and λ'_1, λ'_2 are calculated and compared with each other. If λ_1 agrees with λ'_1 and λ_2 with λ'_2 upto three figures, the matrix is reduced by using the eigenvector X_1 corresponding to λ'_1 and the power method is applied to the reduced matrixc and so on until all the roots have been obtained. If no agreement has been obtained after 26 steps, ten further steps of the power method are applied and the above procedure is repeated with M = 36. If still no agreement has been obtained, ten more steps are applied (M = 46) and so on until the postulated

agreement has been obtained.

After the approximate values of all the eigenvalues have been found, Wielandt's inverse iteration is applied to obtain more accurate estimates of the eigenvalue.

The flow chart and the computer programme are given in Appendix VII.

CHAPTER 6

THEORETICAL ANALYSIS OF THE FLUTTER OF THE MODEL WING WITH LARGE CONCENTRATED INERTIAS

6.1 DESCRIPTION OF THE PROBLEM

In order to assess their relative merits some of the analytical methods discussed Chapters 4 and 5 were used to predict the flutter speeds and frequencies of the model wing used in the wind tunnel tests (Fig. 6.1) under various combinations of added inertias.

Three different sets of wings were used in the experimental analyses. All the wings had similar geometric properties, but had different values for the bending and the torsional stiffnesses. The details of these wings are given in Appendix II. Briefly, the wings had a span of 24 ins., a chord of 6 ins, and were cantilevered from the root. (The wings were tested in a vertical position in the wind tunnel). For all the wings, the elastic axis was at the 35% chord position and the inertia axis at the 45% chord position.

In all the theoretical calculations the structural damping has been assumed to be zero. Also, except where they have been specifically introduced into the calculations, the aerodynamic loads due to the pods have been assumed to be negligible in comparison to the other forces acting on the wing-pod combination.

6.2. Vibration Analysis

As a starting point to the flutter analysis it was necessary to have a knowledge of the frequencies and modes of vibration of the model wing-pod combinations.
It was felt that the flutter mode could be considered as a linear combination of the uncoupled bending and torsional modes of a uniform wing carrying an added inertia.

To obtain the frequencies and modes of a uniform beam (or shaft) carrying a concentrated mass or moment of inertia an operational method (Ref. 37) was used. By using this method the frequencies and modes of a uniform beam (or shaft) with an arbitrarily placed concentrated mass (or moment of inertia) can beobtained. This method permits exact, closed form solutions to be obtained for the frequencies and modes of the system under consideration. The analysis and some results obtained from it are given in Appendix III.

For a given wing-pod configuration, the uncoupled modes and frequencies in bending and in torsion can be obtained using this method. To simplify the numerical calculations (in the flutter analysis), the mode shapes were approximated by a polynomial function for the bending modes and by a function containing the power of sines for the torsion modes. The coefficients of the approximating function were obtained by using a least squares technique. A computer programme which enables a given function (eg ,

$$y = a f_1(x) + b f_2(x) + c f_3(x) + \cdots)$$

to be fitted to a given curve was written and is given in Appendix IV.

6.3. "Exact"Solution by the Method of Ref. (37)

Because of the lengthy calculations involved, only two cases were analysed using this method. Two different span positions of the pod were investigated, the details of which are given on the following page.

Wing A3:

Pod: $M = 0.83$; $I = 10.0$; $x_p = 0.1$

Span Locations: $\eta = 0.5$ and 0.75

The flutter speeds and frequencies were calculated by the procedure described in Section 4.1. Two dimensional airloads were used in all the calculations.

Table 6.1 gives the values of the flutter speeds and frequncies obtained by using this method for the two span locations considered. In the same table are also given the measured speeds for Pod A.

It is seen that the calculated speeds showgood agreement with the measured flutter speeds. A similar trend was also noted in Ref(37)

6.4 Solution of the Flutter Problem by the Assumed Mode Method:

6.4.1 Bare Wing (No pod)

For bare wings, the use of the assumed mode method is fairly well established, the details being available in several text-books and in an extensive report(Refs 27, 23). For a wing with concentrated masses, the analysis is outlined in Appendix V where both the British and the American techniques are illustrated. For bare wings, the terms containing the concentrated mass parameters are omitted.

For all the wings, the aerodynamic forces and moments were calculated using the two-dimensional strip

theory derivatives. Since the elastic axis position was the same for all the wings, it was found convenient to tabulate the aerodynamic forces and moments (referred to the elastic axis) as functions of the reduced frequency $\left(\nu = \frac{b\omega}{V}\right)$. These values are given in Table V.1 of Appendix V.

British Method In applying the British Method only one value of the reduced frequency, $\nu = \frac{b\omega}{V} = 0.24$ was used.

All the integrals appearing in the equations were evaluated by integrating the mode shape functions, the mass, static unbalance and moment of inertia being assumed to be uniformly distributed along the span.

In evaluating the structural stiffness coefficients a number of definitions are possible, each giving a slightly different value for these coefficients.

(a) "Static" Stiffnesses: These are obtained by measuring the deflections at the reference section due to the appropriate loads applied at that section.

The direct flexural stiffness and the direct torsional stiffness are defined by

$$l_\phi = W l^2 / \delta_R$$
$$m_\theta = T / \theta_R \qquad (6.1)$$

Where W and T are the load and moment respectively, applied at the reference section. δ_R and θ_R are the resulting flexural and the torsional displacements respectively l is the distance from the wing root to the reference section. (Usually l = 0.7 span).

For a uniform cantilever wing these become

$$l_\phi = 3EI / l^3$$
$$m_\theta = GJ / l \qquad (6.2)$$

(b) The "Strain Energy' Stiffnesses

It is felt by some investigators that since the assumed mode method is based on arbitrary modes, it is more logical to use the strain energy of the wing deformed in these modes in order to define the stiffnesses.

If W denotes the bending displacement and α the torsional displacement, the strain energy is given by

$$V = \frac{1}{2}\int_0^S EI\left(\frac{d^2W}{dy^2}\right)^2 dy + \frac{1}{2}\int_0^S GJ\left(\frac{d\alpha}{dy}\right)^2 dy \tag{6.3}$$

If the modes assumed for the bending and the torsional displacements are:

$$W = l\,\Phi_R \cdot f(\eta)$$
$$\alpha = \Theta_R \cdot F(\eta) \tag{6.4}$$

the'strain energy'stiffnesses are given by

$$C_{11} = \frac{EI}{l}\int_0^{S/l} (f'')^2 d\eta$$
$$C_{22} = \frac{GJ}{l}\int_0^{S/l} (F')^2 d\eta \tag{6.5}$$

The calculation of these stiffness coefficients is made easier by defining artificial vibration frequencies ω_W and ω_Θ for these assumed modes:

$$C_{11} = \omega_W^2 \int_0^{S/l} m \cdot f^2 d\eta$$
$$C_{22} = \omega_\Theta^2 \int_0^{S/l} I F^2 d\eta \tag{6.6}$$

Where m and I are the mass and moment of inertia per unit length respectively. These frequencies are the same as those which would be obtained by artificially decoupling the modes.

(c) "Dynamic" Stiffnesses

If the normal modes of vibration or the uncoupled modes of vibration are used as the assumed modes, the definition of the stiffnesses becomes simpler:

$$c_{11} = \omega_1^2 \int_0^{S/L} m f^2 \, d\eta$$

$$c_{22} = \omega_2^2 \int_0^{S/L} I F^2 \, d\eta \qquad (6.7)$$

where ω_1 and ω_2 are the frequencies of free vibration.

The values of the stiffness coefficients obtained form the three definitions generally differ from each other. These differences are due to the differences in the mode shapes involved in the three definitions. The 'Static' stiffnesses (Eq. 6.2) are the easiest of the three to determine. These have been used in deriving approximate formulae for flutter and for flutter criteria.

The 'dynamic' stiffnesses can be obtained only after the normal modes or the uncoupled modes have been obtained. These are the values used in the calculations described in Appendix V. In this way, these stiffnesses will be the same as the 'strain energy' stiffnesses as defined in Eq. (6.5).

For all the wings without any added massss the flutter speeds obtained from the assumed mode method are given below:

WING	Assumed Mode Method					
	British		American		Experimental	
	V_F	ω_F	V_F	ω_F	V_F	ω_F
A1	81.0	12.35	80.0	13.2	80.0	14.5
A2	140.0	21.5	146.0	22.0	-	-
A3	153.0	23.6	152.5	21.2	-	-
B4	172.0	26.2	167.0	19.5	-	-
B5	225.0	34.4	227.0		-	-

(V_F = ft/sec, ω_F = c.p.s)

For the wing A1, it is seen that the Energy Method using both the British and American techniques, gives results which are in very good agreement with the experimentally measured value. The result obtained by use of the approximate formula of Molyneaux (Ref. 39) also shows good agreement with the other values. (In this formula, the stiffness coefficients used are the 'static' stiffnesses.)

For the other wings, no experimental results are available since for wings A2 and A3, the flutter speed is greater than the maximum wind tunnel speed and wings B4 and B5 are hypothetical wings.

These results demonstrate once again the adequacy to the energy method to predict values of the flutter speed and frequency for wings without concentrated masses.

In applying the energy method by the British technique, the results could be refined by further iteration, since only one value of the reduced frequency was used here.

6.4.2 Wings with Pod

For the wings with pods, the energy analyses were based on the U.S. technique. This method was used mainly because comparisons could be made with the results from the Direct Matrix Method.

Since the experimental results and some of the Direct Matrix Method results indicated that for the wings A2 and A3 (with pods), flutter always occurred mainly as a result of coupling between the fundamental bending and the fundamental torsion modes, it was decided to use these two modes in the analyses. These were prescribed as the (uncoupled) fundamental bending and

fundamental torsion modes for the relevant wing-pod configuration.

6.4.2.1 Wing A1

Preliminary calculations for a pod ($\bar{M}$ = 1.0, $\bar{I}$ = 10.0, $\bar{x}p$ = +0.1) showed that the flutter speeds would be very low. Tests with this pod in the wind tunnel confirmed that for some spanwise locations, the flutter speed was below the minimum wind tunnel speed. No further calculations were made for this wing with added inertias.

6.4.2.2 Wings A2 and A3

For the Wing A2 the influence on the flutter speed of the following pods was investigated.

(a) $\bar{M}$ = 1.0 $\bar{I}$ = 10.0 $\bar{x}p$ = 0.0

(b) $\bar{M}$ = 1.0 $\bar{I}$ = 10.0 $\bar{x}p$ = +0.1

(c) $\bar{M}$ = 1.0 $\bar{I}$ = 8.5 $\bar{x}p$ = 0.0

(d) $\bar{M}$ = 1.0 $\bar{I}$ = 8.5 $\bar{x}p$ = +0.1

For all these cases, four spanwise positions, η = 0.33, 0.5, 0.67 and 0.875 were investigated. The results are shown in Table 6.2 and in Fig. 6.2.

For the Wing A3, the influence on the flutter speed of the following pods was investigated:

(a) $\bar{M}$ = 0.83 $\bar{I}$ = 10 $\bar{x}_p$ = 0

(b) $\bar{M}$ = 0.83 $\bar{I}$ = 10 $\bar{x}_p$ = +0.1

In these cases also, four spanwise locations η = 0.33, 0.5, 0.67 and 0.875 were used.

The results are given in Table 6.2 and in Fig.6.3.

6.4.3 A comparison of these results with the experimentally measured values is given in Section 9.4.

6.5 Direct Matrix Method

For the model wing, all the properties (geometric, structural and inertial) are uniform along the span. This brings about a number of simplifications in the calculations of the various matrices involved in the direct matrix method (Chapter 5).

The fact that the wing is cantilevered from the root brings about considerable simplifications in the flutter equations. The flutter equation (Eq. 5.14) now becomes

$$\lambda\{h_i\} = [U]\{h_i\} \tag{6.8}$$

In the calculations, this equation is further simplified by seperating the aerodynamic matrix into its real and imaginary parts.

The matrix $[U]$ is given by Eqs. (5.9) and (5.5)

$$[U] = [a]([M] + \rho b^2 s [W][C_h]) \tag{6.9}$$

By defining the aerodynamic matrix as

$$[A] = [AR] + \lambda[AI] \quad (= \rho b^2 s [W][C_h]) \tag{6.10}$$

and

$$[U] = [UR] + \lambda[UI], \tag{6.11}$$

we have

$$[UR] = [a]([M] + [AR]) \tag{6.12}$$

$$[UI] = [a][AI] \tag{6.13}$$

For all the calculations, the wing was divided into five segments, so that there are ten control points (Fig 6.4) The forward control stations are located on the $\frac{1}{4}$ chord line and the rear control stations are on the $\frac{3}{4}$ chord line.

Since no chordwise deformations are allowed the deflections of the intermediate control stations (located on the mid chord line) can be expressed in terms of the deflections of the forward and rearward control point deflections. This limits the number of degrees of freedom to ten.

The details of the matrices of the inertia, structural and aerodynamic influence coefficients are given in Appendix VI.

To check the accuracy of the structural and inertial matrices, the coupled frequencies were calculated for the bare wings. These are compared with the experimentally measured values and with the uncoupled theoretical bending and torsional frequencies in the following table.

WING	DMM		EXPERIMENT	
	ω_b c.p.s	ω_t c.p.s	ω_b c.p.s	ω_t c.p.s
A1	9.6	19.2	9.5	21.5
A2	9.06	34.24		
A3	9.06	37.50		
B4	5.80	36.37	-	-
B5	5.80	48.97	-	-

(ω_b = Fundamental Bending Frequency

ω_t = Fundamental Torsion Frequency)

From the above table, it can be seen that the assumed ten degree of freedom system adequately represents the vibrational characteristics of the model wings.

In Table VI.1 the coupled frequencies of fundamental bending and fundamental torsion are compared with the uncoupled frequencies predicted by the method of

Appendix III. There is reasonable agreement between the two frequencies.

The values of the two bending frequencies agree reasonably well with each other. The torsional frequencies calculated from the direct matrix method are generally lower than the uncoupled values.

Flutter Speeds

6.5.1 Wing A.1

For this wing, the flutter speed and frequency were calculated only for the bare wing condition. The following table gives the results of the Direct Matrix analysis and also the results obtained by two other methods.

Method	Frequencies		Flutter Speed
Experiment	9.5	21.5	80.0
Direct Matrix Method	9.6	19.2	80.0
Molyneux's Approximate formula (Ref. 39)	-	-	81.0
Assumed Mode Method			81.0 and 80.0

It is seen that for the bare wing, all the methods show very close agreement. The fundamental bending frequency calculated by the direct matrix method is in close agreement with the measured value, while the fundamental torsion frequency is lower than the measured value.

6.5.2. Wing A2

For this wing, the bare wing and a number of wing-mass configurations were analysed. For all the

concentrated masses, the mass ratio, $\bar{M}$ was kept at unity. Three values of inertia ratio, $\bar{I}$ = 0, 5 and 10 were considered.

For each inertia ratio, the chordwise position of the concentrated mass c.g. was set successively at 0.25C, 0.3C, 0.35C, 0.45C, and 0.5C, measured from the wing leading edge. For each of these combinations, the concentrated mass was located successively at the five spanwise positions of the control stations. For each of the resulting configurations. both vibration and flutter analyses were conducted. The results are given in Table 6.3. In Figs (6.5) to (6.19).

In obtaining the flutter speeds, the structural damping was assumed to be zero and the aerodynamic loads due to the pods not considered. In most cases, the curve of the artificial damping, g, against the speed V gave a well defined intersection with the g = 0 line. In certain cases (Figs. 6.9, Fig. 6.10, Fig. 6.12 and Fig. 6.13) the intersection was not so well defined. Fig. 6.20 shows two cases. It is seen that a value of g = 0.01 in the torsion mode increases the flutter speed from 60 ft/sec to 66ft/sec in one case and from 51.0 ft/sec to 61.0 ft/sec in the second. However, all the flutter speeds quoted in Table ~~6.4~~ 6.3 and Figs (6.5) to (6.19.) are for a value of g = 0.

6.5.3 Wing A3

For this wing, the following values of the pod inertial parameters were cnnsidered:

Mass Ratio $\bar{M}$ = 0.833, 1.0

Inertia Ratio $\bar{I}$ = 5.0, 10.0

c.g. Position $\bar{x}$ = 0.35C, 0.45C, and 0.5C aft of the leading edge.

The results are shown in Table 6.4 and Figs. 6.21 to 6.25.

As in the case of Wing A2, in all the results quoted here the structural damping has been neglected and pod aerodynamic loads are not included. In some cases, the intersection of the V - g curve with the g = 0 axis was not well defined, as in some cases of the wing A2.

6.5.5 Wings B4 and B5

For the wings A2 and A3, the modes involved in the flutter, for all the wing-mass combinations investigated, were the fundamental bending and the fundamental torsion modes. For all these combinations the maximum flutter speeds were obtained for a mass centre of gravity location forward of the elastic axis and a mass located at the tip gave the greatest increase in the flutter speed.

An inspection of the results of previous investigations (Chapter 2, Section 2.1.1 and Figs. 2.1 to 2.6) showed that for most of these wings, the best spanwise location for maximum flutter speed was at a location between the midspan position and the wing tip.

It was felt that this was due to the relative values of the fundamental bending and fundamental torsional frequencies of these wings being of such a value that the likelihood of the overtone bending mode coupling with the fundamental torsion mode was more favourable.

To check this hypothesis, it was decided to investigate the effects of varying the stiffnesses of wing A3 on the flutter speeds.

First only the bending stiffness was changed. A value of EI = 3000 lb in^2 was considered, all the other parameters being the same as for wing A3. This hypothetical wing was termed 'wing B4'. The results of the Direct Matrix analysis

for thin wing are given in Table 6.5 and in Fig.6.26. Since for thin wing also the flutter was due to a combination of the fundamental modes, it was decided to change the value of the torsional stiffness to GJ = 3000 lb.in^2. All the other characteristics were the same as for wing B4. This wing was investigated for flutter by the Direct Matrix Method. The results are given in Table 6.6 and in Fig.6.27. In this case, the flutter was of the overtone type for some spanwise stations. For this case, the inertial characteristics of the concentrated mass were:

Mass ration $M = 0.83$

Inertia ratio $I = 0.0$

Location of c.g. $x_p = -0.1$

For wing B5, the maximum flutter speed was obtained when the mass was located at about the midspan position, thus suggesting that by a suitable modification of EI and GJ the optimum location of the concentrated mass can be altered.

6.5.6 Inclusion of the Pod Aerodynamic Loads.

Some of the wing-pod combinations were analysed by the Direct Matrix Method in order to investigate the effect of including the aerodynamic loads due to the pods in the analysis. The pod aerodynamic loads were calculated by using the momentum theory(Section 3.6) For all the cases investigated, the difference between the flutter speeds with and without the inclusion of the pod aerodynamics was small. In general, t the inclusion of the pod aerodynamic loads in the analysis gave a value of the flutter speed which was lower than the flutter speed without the pod aerodynamics. A typical result is given in Table 6.7.

Since the wind tunnel results showed that large increases in the flutter speed could be obtained by adding horizontal fins to the pods, the effect of including these loads in

the analysis was also investigated. To obtain the aerodynamic loads of the finned-pod by the momentum theory the length of pod containing the fin was replaced by an equivalent body of revolution. This had a radius of $\left(S^2 - R^4 \frac{R^4}{S^2}\right)^{\frac{1}{2}}$ where R is the radius of the pod and S is the span of the fin, measured the pod centre line to the tip of the fin.

Table (6.8) shows the results for two spanwise positions, η = 0.5 and 0.67. The inertial details of the pod are $\bar{M}$ = 0.83, $\bar{I}$ = 10 and $\bar{x}_p$ = +0.1. In the same table are also given the measured values of the flutter speed. For both the spanwise locations, the results of the Direct Matrix Method do not predict the correct increases in the flutter speed as obtained in the tests.

A comparison of these results with the flutter characteristics obtained from the wind tunnel tests is given in Sec.9.4.

5.6 Effect of the Inclusion of the Aileron Degrees of Freedom

A preliminary investigation was made to assess the influence of the aileron degrees of freedom on the flutter of the wing-mass combinations.

The calculations were made by the assumed-mode method. Only one wing-mass combination was considered. The relevant details are:

Wing	Wing A3
Pod	$\bar{M} = 0.83$
	$\bar{I} = 10.0$
	$\bar{x}_p = +0.1$
	$\eta = 0.67$

The aileron was assumed to have a span of 0.67 ft., extending from the two-thirds span position to the wing-tip. The aileron had a constant chord of 0.15 ft. The other details of the aileron are:

Leading Edge : 0.7c aft of wing leading edge

Hinge Line : 0.8c aft of wing leading edge

Aileron c.g. : 0.1c aft of the hinge line

Aileron mass : 0.01 slug ft.

Aileron Pitching radius of gyration: 0.33c

(where c is the wing chord).

For this wing-aileron combination, the following flutter speeds were obtained. In the case of a free aileron, the flexure-aileron flutter speed was 66.9 ft/sec, but the torsion-aileron flutter speed was 45.3 ft/sec. In the case of an infinitely-rigid aileron, the flexure-aileron flutter speed was 65.7 ft/sec and the torsion-aileron flutter speed was 63.2 ft/sec.

These results indicate that the control surface degrees of freedom can have an unfavourable influence on the flutter

speed under certain conditions. A similar trend was noticed by Bisplinghoff et al (Ref. 23) for a wing carrying a concentrated mass (with aileron degrees of freedom). From this, it is expected that the model wing will also show similar trends.

CHAPTER 7

WIND TUNNEL TESTS ON THE FLUTTER OF WINGS WITH LARGE CONCENTRATED INERTIAS

7.1 Selection of the Geometric Inertial and Structural Properties of the Model

In designing the wind tunnel model, it was decided to keep the wing as simple as possible, since the main interest was in the influence of concentrated inertias on the flutter of wings. With this in view, a uniform cantilever wing with constant properties along the span and of segmented construction was chosen. The wing was to be mounted in a vertical position in the wind tunnel to avoid the large static deflections which might occur when the concentrated masses were attached to the wing. The geometric and other properties were derived as follows:

(a) Geometric: A span of 2 ft was chosen for the model since a preliminary survey of the wind tunnel working section showed that this would be the optimum span for a vertically mounted model. To keep the aspect ratio as large as possible a wing chord of 6" was chosen. A symmetrical profile, the NACA 0018, was chosen for the wing cross section. It was decided to locate the ealstic axis at the 0.35c position.

A comparison with the wing-pod configuration of the VTOL aircraft described in Ref. 1. showed that a pod length of 20" and a pod span of 2" would be representative of the pod of Ref. 1. In order to enable the pod to be attached at a number of spanwise positions along the span, the span of the wing sections was also fixed at 2". This resulted in the wing having eleven segments of 2" each and two segments (at the root and at the tip) of 1" each.

Thus the pod could be attached at eleven points along the span.

(b) Inertial:

For all the wings described in Appendix II, the inertia axis was located at the 0.45 chord position. The details of the mass, moment of inertia and static unbalance are given in Appendix II.

(c) Structural:

It was first thought that a bare wing flutter speed of 80 ft/sec would allow the testing of the effect of the pods, allowing any decreases or increases due to the pod to be kept within the speed range of the wind tunnel. Using the approximate formula for the flutter speed given by Molyneux (Ref. 39) a value for the torsional stiffness was obtained.

A single spar construction was chosen in order to keep the wing design as simple as possible. A number of different shapes of cross section can be used to give a desired value of the stiffness. Of these, it was decided that the channel section offered the best possibility. The dimensions of the channel sections are given in Appendix II.

Fig. 7.1 shows the general arrangement of the wings tested in the wind tunnel. To test the influence of the aerodynamic shape of the pods on the flutter speeds, four different pods were tested. These are shown in Figs. 7.2, 7.3, 7.4, 7.5 and 7.6. Two of the pods had approximately the same cross-sectional area distribution, but different shapes of cross section - rectangular and circular respectively. The third pod was similar to the pod with the circular cross section, but only in the portion ahead of the wing leading edge. Aft of the wing trailing edge, the pod was cut off and lead weights mounted on a $\frac{1}{8}$" steel rod were

used to obtain the necessary inertial properties. The fourth 'pod' was made of metal and had the same shape as the other wing segments. Load weights mounted on 1/8 in. dia. rods provided the necessary inertial properties.

7.2 Instrumentation

For wing A1, the frequencies were measured by means of strain-gauges mounted on the spar near the wing root. As these proved unsatisfactory, the frequencies of vibration were obtained for the wings A2 and A3 by means of two piezo-electric accelerometers, one of which was attached to the spar and was mainly sensitive to the bending oscillations. The second was attached was attached to the pod as shown in Fig. (7.6). This was mainly sensitive to the torsional oscillations. The signals from the accelerometers were amplified through two charge amplifiers. As the frequencies of interest (for flutter testing) were mainly in the region below about 30 c.ps., a filter was constructed with a cut-off frequency of about 30 c.p.s. The resulting signals were well defined and were recorded by means of a pen recorder. (Fig. 7.7).

7.3 Determination of the Stiffnesses of the Spars

Since the spar has uniform properties along the span, the values of EI and GJ are also constant and can be most conveniently obtained by applying a load at one station and measuring the deflection at another station.

(a) Static Testing: To obtain the 'static' values of EI and GJ simultaneously, the loading rig shown in Fig 7.9 was used.

If δ_A and δ_B represent the deflections at A and B, the torsional displacement at this section is given by

$$\theta = (\delta_A - \delta_B)/d$$

If the load is moved from x to $(x+dx)$ the increase in the torsional displacement is given by:

$$d\theta = \{(\delta_A-\delta_B)_x - (\delta_A-\delta_B)_{x+dx}\}/d$$

Using this, we get the torsional rigidity as

$$GJ = W\,l\,\frac{dx}{d\theta}$$

In practice is obtained from the graph of θ vs x

When the load is applied at the elastic axis, $(\delta_A-\delta_B)$ the flexural stiffness is given by

$$EI = Wl^3/3\delta_A$$

The value of EI and GJ for the spars were also obtained by obtaining the free vibration frequencies of the cantilevered spar and also the frequencies when either a concentrated mass or a moment of inertia was attached at the tip. The values of the stiffnesses thus obtained are given in Appendix II.

7.4 Description of the Wind Tunnel

The wind tunnel used in the tests was of the return circuit type with an open working section. The speed control is by means of two biased switches.

By using the biased switches an increase or a decrease of within about 1 ft / sec can be obtained after some practice.

The working section has a cross section of 2½ft x 3½ft. Due to the rectangular shape of the entry section, the flow was not uniform in some parts of the wind tunnel. It was established by a survey of the velocity distribution in the cross-section that a model span of 2ft would be optimum. In the early stages of the investigations a

maximum speed of approximately 100 ft/sec could be obtained. However, the turbulence-screen at one of the corners had to be replaced and this reduced the maximum speed attainable to about 96 ft/sec.

7.5 Test Technique

The model was mounted in a vertical position in the wind tunnel. The technique of testing was as follows. The wind tunnel speed was increased from rest by regular increments of about 1 ft/sec. At each stabilized speed, the wing would be disturbed and the rate of decay of the oscillations noted both visually and on the pen recorder. The pen recorder traces provided a clue of the damping in the system. The flutter speed as recorded in these tests is the speed at which the disturbed wing continues to oscillate at a constant amplitude.

After each test, the bending and torsional frequencies of the wing were measured in order to assess ~~if~~ whether the wing had been damaged by the flutter oscillations.

7.6 Results

7.6.1 Bare Wings a) Wing A1

For this wing, flutter could be obtained only for the wing without pods. Two wings, which had the same characteristics were built and were tested to destruction. The flutter was due to a coupling of the fundamental bending and fundamental torsion modes and was of an extremely violent nature. The flutter occurred without any need for disturbing the wing. The flutter frequencies were obtained by means of strain gauges and also from analysis of high speed motion pictures taken of the fluttering wing. The flutter speed for both the wings was approximately 80 ft/sec.

(b) Wings A2 and A3

For these two wings, no flutter could be obtained within the speed range of the wind tunnel (for the bare wings)

7.6.2 Wing A2 with Pods

For tests with the wing A2, pods of two different cross sections were used. One had a circular cross section (Pod A) and the other a rectangular cross section (Pod B). The geometric details of these pods are given in Appendix II.

By a proper adjustment of lead weights mounted inside the pods, the following combinations of $\bar{M}$, $\bar{I}$ and $\bar{x}_p$ were obtained:

$\bar{M}$ = 1.0

$\bar{I}$ = 8.5 and 10.0

$\bar{x}_p$ = 0.0c and 0.10c aft of the elastic axis

The pods were fixed regidly to the spar at a number of spanwise stations and the flutter speed and frequency were measured. The results are shown in Table 7.1 and Figs (7.9) to (7.14) show the effect on the flutter speed of attaching a pod at different positions along the wing span.

For all the cases, the principal modes participating in the flutter were the fundamental bending and the fundamental torsion modes. For the pods located around the midspan position, the flutter was of the "mild" type and the wing pod configuration could be set to flutter for a number of cycles at moderate amplitudes. For most of these cases, divergent amplitudes built up only very slowly. For outboard positions, the flutter was closer to the "explosive" type of flutter large divergent amplitudes tending to build up in a rapid fashion.

To check the repeatability of the results, the flutter speeds for both the pods were measured more than once at some spanwise locations. It was found that all the flutter speeds could be reproduced to within about ± 2ft/sec and the flutter frequencies to within about ± 0.5 c.p.s. The results presented here are the mean values.

7.6.3. Wing A3 with Pods

For this wing, four different pods were tested. These were - Pod A (circular cross section), Pod B (rectangular cross section) Pod C (Pod A with the section aft of the wing trailing edge removed) and Pod D (Metallic pod having the same cross section as the wing itself).

The flutter speeds and frequencies are presented as variations with the spanwise locationof the pods in Table 7.2 and in Figures 7.15 to 7.19. For these pods the values of $\bar{M}$, $\bar{I}$ and $\bar{x}_p$ were:

$\bar{M}$ = 0.83

$\bar{I}$ = 10 and 8.5

$\bar{x}_p$ = 0.0 and 0.1 aft of the elastic axis.

For all the cases shown in these figures, the principal modes involved in the flutter were the fundamental bending and the fundamental torsion modes.

For all the pods, some checks were made on the repeatability of the results. These tests were conducted at different times and the agreement in the flutter speeds were poorer for the pods located between the mid span and the two-thirds span region. For these locations, the maximum variations in the flutter speed were about ±5 ft/sec and the flutter frequencies showed good agreement, the deviations being about ± 0.5 c.p.s. The agreement for the inboard and

outboard regions were good, the flutter speeds varying between ± 2 ft /sec and the frequencies showing variations of about ± 0.5 c.p.s. The values quoted are the average values of the flutter speed.

For pod B, tests with the centre of gravity 0.1c ahead of the elastic axis indicated that flutter would probably occur at speeds higher than the maximum wind tunnel speed (at all span positions).

7.6.4. Effect of attaching fins to the Pods

Some preliminary tests showed that by attaching fins to the trailing edge of the pods, it was possible to increase the flutter speed.

The different fins tested on the pods are shown in Fig. 7.5 . The fins were constructed from 1/32 in sheet balsa and were attached to the pods by balsa cement.

The influence of the pods on the flutter speed was investigated for both the Pods A and B. The results are shown in Table 7.3. Fig. 7.20 shows the damping-velocity curve for two fins on pod B. The values of the damping coefficient were calculated from the pen recorder traces at different wind tunnel speeds.

7.7. Accuracy of the Results

As a guide to the accuracy of the results, the expected errors in the measurement of the various parameters involved are discussed in the following:

7.7.1 Mass In order to obtain the required mass characteristics for each of the wing segments, the following procedure was adopted: A 2in. length of the spar section was attached to each of the wing segments in the same manner as in the completed wing. This, together with the required lead weights

and the 22 gauge aluminium strip (used for attaching the weights to the wing) was weighed in a chemical balance. The weight of the lead was varied until the required value for the total weight was obtained. All the masses were obtained in grammes and the accuracy of these measurements was $\pm$ 0.005 gm. The wing segments were weighed again with the weights attached to the wing by means of the aluminium strip and this was used as the final value of the wing weight.

7.7.2 Chordwise Position of the Centre of Gravity

Two methods were used to locate the position of the centre of gravity of the wing segments and the pods. In the first, an approximate idea of the centre of gravity location was obtained by balancing the wing section (complete with the 2 in spar section and the lead weights) on a knife edge. This was used for obtaining the approximate locations of the lead weights to obtain the necessary centre of gravity location. The weights would then be secured to the wing section (or pod) by adhesive tape and the pitching moment of inertia determined. Usually it proved necessary to relocate the lead weights to obtain the desired moment of inertia. This trial and error process was repeated until the desired values of the centre of gravity location and the pitching moment of inertia were obtained.

After this, a more accurate method of determining the centre of gravity location was used. In this, the wing section (or pod) was suspended successively from a number of points. The positions of a weighted string

would be marked on a paper attached to the wing section (or pod). The intersection of a number of these lines gave the location of the centre of gravity.

The positions of the centre of gravity were determined by the intersection of at least three different lines, and the maximum error tolerated was 0.05 in ($\pm$0.01c)

7.7.3 Moment of Inertia

Two methods were used to measure the moment of inertia of the wing sections (or the pod). In the first, the section was oscillated as a compound pendulum and the moment of inertia deduced from the frequency of oscillation and the distance of the support point to the centre of gravity. (Ref. 76). The results from this method are sensitive to the accuracy in measuring this distance. Also, the accuracy decreases as this distance becomes large. This method was used to obtain a preliminary estimate of the moment of inertia.

In the final stages of the trial-and-error process, a more accurate method was used. In this method (Ref. 76) a trifilar pendulum was used and the moment of inertia calculated from the frequency of oscillations of the pendulum with the section in it and from the characteristics of the pendulum. Tests with a number of bodies having regular shapes and with moments of inertia having values comparable to the pod moments of inertia showed that the errors in the measurements could be upto 6% of the theoretical values.

7.7.4 Frequency

The frequencies of vibration were obtained from pen recorder traces. The accuracy with which the frequencies can be determined is a function of the speed at which the paper used for the traces is made to move. A paper speed

of 20cm/sec was used in most cases. At this speed, the accuracy with which the frequencies could be determined was about 0.25 c.p.s.

7.7.5 Speed

The speed of the air flow in the wind tunnel was obtained from readings of a differential manometer which registered the dynamic pressure in the working section in inches of water S everal calibrations were made to translate this reading into the air speed in the test section. The calibrations were made without any model in the test section and also with a rigid model of the wing in the test section. The final calibration chart was obtained as a mean curve through these points. The maximum deviation in the calibrations was about $\pm$ 5%.

7.7.6

By attaching wool tufts to the bare wing A3 it was found that the flow remained attached throughout the speed range. With the pods A and B attached to the wing A3, similar tests were made for some of the spanwise locations. These showedthat the flow remained attached to the pods when the model was held rigidly.

7.7.7

In order to prevent variations in the weight of the wing sections due to changes in the humidity of the atmosphere, they were coated with varnish. By weighing the sections over a period of time, it was found that the weights of the wing sections remained almost constant throughout all the tests. Pod A was also coated with varnish and Pod B was coated with paint. These also showed very little variation

in their respective weights during the test programmes.

7.7.8

At the end of each flutter test, the fundamental bending and torsion frequencies of the wing-pod combination were obtained in order to check if the spar had weakened due to the flutter oscillations. Within the accuracy of measurement, the spar for all the tests showed very little deterioration in strength. Even so, for the wing A3, two spars were used (both with identical properties).

7.7.9

To determine whether the effect of attaching the balsa wing sections had any appreciable effect on the flexibilities of the spar, the following experiment was conducted (for the spar of wing A1). On an identical spar, weights were attached to simulate the mass, moment of inertia and chordwise centre of gravity position of the wing A1. The weights were attached by means of $\frac{1}{4}$" wide aluminium bars at appropriate spanwise stations. The differences in the fundamental bending and fundamental torsion frequencies of this system and the wing itself agreed to within the experimental accuracy.

This showed that the method by which the wing segments were attached to the pod has very little influence on the flexibilities of the spar (within the accuracy of measurement) and that all the structural properties can be considered to be contributed solely by the spar.

CHAPTER 8

APPLICATION OF THE DIRECT MATRIX METHOD TO WINGS OF REF (38) and REF(9)

The flutter of the model wing (Chapters 6 and 7) was due to a combination of the fundamental modes of bending and torsion for all the cases investigated. In order to assess the accuracy of the results obtained by using the Direct Matrix Method when applied to cases when the flutter is due to a combination of one or more overtone modes, the wings analysed in Ref. (38) and Ref (9) were also analysed by this method.

8.1 Wing of Ref 9

Gaukroger (Ref. 9) investigated the effects of localised masses on the flutter speeds of a uniform cantilever wing. Four values of the sweepback angle (0°, 15°, 30° and 45°) were considered by him, but only the unswept case is considered here.

Gaukroger solved the flutter equations on the R A E flutter simulator. The equations were set up using two or more of the following modes:

(a) Fundamental flexure of the bare wing.

(b) Fundamental torsion of the bare wing.

(c) Flexure of the wing with a restraint to prevent displacement at the localised mass position.

(d) Torsion of the wing between the root and the localised mass section when restrained in twist at the localised mass section.

(e) Torsion of the wing between the tip and the localised mass section when retrained in twist at the localised mass section.

The details of this wing are given in Appendix I.

Gaukroger has quoted the flutter speeds of the various wing - mass configurations considered by him as the ratios of these flutter speeds to the bare wing flutter speed. But the actual flutter speed of the bare wing itself is not given. Hence it is necessary to establish the flutter speed of the bare wing.

Using the values of the fundamental bending and fundamental torsional frequencies and the values of the mass, inertia and the inertia axis position given by Gaukroger, the values of the bending and torsional stiffnesses were calculated as:

$$\left.\begin{aligned} EI &= 56920 \text{ lb in}^2 \\ GI &= 15{,}520 \text{ lb in}^2 \end{aligned}\right\} \quad (8.1)$$

(The frequencies given by Gaukroger were assumed to be the uncoupled bending and torsion frequencies.)

The flutter speed of the bare wing were calculated by three methods:

$$\left.\begin{aligned} &\text{(a) Molyneux's Approximate formula (Ref. 39):} && 143.0 \text{ fps} \\ &\text{(b) Assumed mode method} && 140.0 \text{ fps} \\ &\text{(c) Direct matrix method (Ten control stations)} && 139.0 \text{ fps} \end{aligned}\right\} \quad (8.2)$$

In the assumed mode method, the modes used were the uncoupled bending and torsion modes of the bare wing.

In view of the above results (8.2), the flutter speed of the bare wing was taken as 140.0 fps.

To check the accuracy of the inertial and structural matrices used in the Direct Matrix Method, a vibration analysis was made. The coupled fundamental bending and torsional frequencies were obtained as 3.59 cps and 14.40 cps respectively. (The fundamental bending and fundamental torsion frequencies given by

Gaukroger for this wing are 3.6 cps and 14.50 cps respectively.

Three sets of concentrated masses were investigated by the Direct Matrix Method for their influence on the flutter speed. These were:

$\bar{M}$	$\bar{I}$	$\bar{x}_p$		
0.5	0	0.15	)	
			)	
0.5	3.8	0.15	)	(8.3)
			)	
1.0	0	0.15	)	
			)	

Where $\bar{M}$, $\bar{I}$ and $\bar{x}_p$ represent the mass ratio, the inertia ratio and the position of the centre of gravity of the concentrated inertia aft of the elastic axis respectively.

The results are shown in Table 8.1 and Figure 8.1.

These results show very good agreement with the values obtained by Gaukroger. The flutter conditions for all the wing mass combinations involved mainly the modes of fundamental bending and fundamental torsion.

8.2 Wing of Ref.38

The wing mass systems investigated in Ref 38 have been the analysed by anumber of methods (Refs. 10,37,43 and 44). An estimate of the relative accuracy of the Direct Matrix Method could be obtained by analysing these wing-mass systems by this method.

The details of the bare wing are given in Appendix II.

Using ten collocation stations (as for the model wing, Fig. 6.4) the matrices of the inertial, structural and aerodynamic coefficients were set up.

To check the accuracy of the inertial and structural matrices, a vibration analysis was carried out. The results

of this are given below:

Fundamental Bending	6.69 cps	(6.44)
Fundamental Torsion	32.86 cps	(39.2)
First overtone Bending	45.66 cps	(47.44)

The values given in the brackets are the average values of the coupled frequencies measured ~~on~~ the bare wing.

Both the fundamental and first overtone bending frequencies agree well with the measured values, but the fundamental torsion frequency is under estimated by about 16% by the Direct Matrix Method.

The flutter speed and frequency calculated by the Direct Matrix Method are compared with the values obtained by other methods in the following Table:

	Method	Flutter Speed (f.p.s.)
1.	Direct Matrix Method	332.0
2.	Measured (Ref 38)	334.0
3.	Analogue Solution (Ref.10)	334.0
4.	Exact Analysis (Ref. 37)	333.0
5.	Assumed Mode Method (Ref44)	
	(a) Two Modes	321.0
	(b) Three Modes	340.0
6.	Iterative Transformation Procedure (Ref. 43)	334.0

It is seen that for the uniform wing, the flutter speed obtained by the Direct Matrix Method is in very good agreement with the measured speed. All the other methods, except the assumed mode method (Ref. 44), show very good agreement with the measured speed.

A particular wing-mass combination (Weight 7a) tested in Ref. 38 has received considerable attention as the flutter speed is very sensitive to the spanwise location

of the concentrated mass (Fig. 8.2). The values of the flutter speed for different spanwise locations of the mass are shown in Table 8.2.

For positions of the concentrated mass between about 36% of the span and 95% of the span, the flutter speed was higher than the divergence speed of the wing. However, for these stations, the flutter speeds can be obtained by theoretical methods.

Since the collocation stations were located at the 0.25, 0.33, 0.5, 0.67 and 0.875 of the span positions, the values from the Direct Matrix Method cannotgive a direct comparison with the results of Table (8.2). These can, however, be used to check the accuracy of the method.

The results from the Direct Matrix method are also shown in Fig. 8.2

For positions of the concentrated mass from the wing root to the 1/3 span location, the results from the Direct Matrix Method show very good agreement with the measured flutter speeds. By comparison, the flutter speeds predicted by the assumed mode methods are very much higher than themeasured values, even when four modes are used. But for positions of the mass outboard of the 1/3 span posttion, the flutter speeds predicted by the Direct Matrix Method are very much lower than the speeds predicted by the exact analysis (Ref.337) and the Analogue Solution (Ref. 10).

Two more wing-weight combinations were also investigated by the Direct Matrix Method (using the same collocation stations as above). These are weights 7c and 7 e.

The characteristics of these two weights are given below:

Designation	$\bar{M}$	$\bar{I}$	$\bar{X}$
7 c	0.96	2.04	-0.18
7 e	0.954	1.56	+0.034

The flutter speeds predicted by the Direct Matrix Method for these two weights are shown in Fig. 8.3 . For weight 7 c, the flutter speeds estimated by this method are all lower than the measured values. For weight 7e, some values are lower than the measured values while the flutter speed for the mid span position and the 2/3 span position are higher than the measured speeds.

8.3

For both the wings (Ref. 9 and Ref. 38) the values of the flutter speeds predicted by the Direct Matrix Method for most wing-mass combinations are in good agreement with the measured flutter speeds. In general, the flutter speeds predicted by this method are lower than the measured values. The agreement is not good for outboard locations of weight 7 a of Ref. (5). Fig (8.2). It is possible that better agreement would have been obtained if a larger number of control stations ~~were~~ had been used in the analysis.

The three weights investigated here for the wing of Ref.38 also illustrate the disadvantages of the assumed mode methods. It used to be assumed that the flutter speeds predicted by the assumed mode methods were always on the conservative side - i.e. gave a lower estimate of the flutter speed. For these wing-mass systems, the assumed mode methods predict that flutter would occur at much higher speeds than the actual flutter speed. However, the trends for the flutter speed with spanwise locations of the mass are closely predicted by these methods.

These results show that the Direct Matrix Method can be used with confidence to predict the flutter speeds of similar wing - mass comibnations. The flutter speeds will be generally on the conservative side. However, for

some weights, the estimates of the flutter speeds are much lower than the actual flutter speed.

CHAPTER 9

DISCUSSION OF RESULTS

9.1 General Trends

The results of both the Direct Matrix and the experimental analyses are shown in Figs.(6.5) to (6.27) and in Figs.(7.9) to (7.19). In all these graphs, the flutter speed and frequency are presented as functions of the spanwise positions of the concentrated inertia, with the individual curves representing different conditions of the concentrated mass parameters.

These results will be examined to obtain the influence of the different parameters of the concentrated mass on the flutter speed of the wing-mass combinations.

9.1.1 Effect of Spanwise Position

From Figs.(6.5) to (6.27) amd Figs.(7.9) to (7.19) the effect of the spanwise position of a given concentrated mass on the flutter speed can be obtained.

In general, for most concentrated masses, there is a decrease in the flutter speed as the spanwise position is varied from root to tip. After reaching a minimum value around the midspan position, the flutter speed increases again, to reach a maximum value for the tip location. This trend is shown both by experimental and the analytical results.

Concentrated masses with zero pitching moment of inertia show a different trend when the centre of gravity is ahead of the elastic axis. (Fig. 6.5 and Fig.6.14). In these cases, the flutter speed shows a continuous increase as the concentrated mass is moved outboard from the root. Fig.(6.11) shows the effect of a concentrated mass(zero pitching moment of inertia) placed on the elastic axis. In this case also there is an increase in the flutter speed as

the concentrated mass is moved outboards from the root.

In general, for all the values of concentrated mass parameters ($\bar{M}$, $\bar{I}$ and $\bar{x}_p$) considered here, the spanwise location to obtain the maximum possible flutter speed is at the tip or at locations very near the wing root. For most concentrated masses, the locations near the midspan region give low values of flutter speed (compared to the bare wing flutter speed).

The hypothetical wing B4 also shows a similar trend. However, the effect of the concentrated mass (with zero pitching moment of inertia) is different on the hypothetical wing B5. For this wing, the maximum value of the flutter speed is obtained when the concentrated mass is located at about a spanwise position of 0.5 (Fig. 6.27).

9.12 Effect of Chordwise position

In Figs (9.1 a) to (9.1d) the results from the Direct Matrix Analysis are plotted as follows: For given values of the parameters $\bar{M}$ and $\bar{I}$ the flutter speed is plotted against the chordwise position of the centre of gravity of the concentrated mass, with the spanwise location of the mass as a parameter. For all the values investigated here, the general trend is for the flutter speed to increase as the centre of gravity of the concentrated mass is moved ahead of the elastic axis.

9.1.4 Effect of Mass Ratio

For the wings A2 and A3, the mass ratios ($\bar{M}$) of the pods were 1.0 and 0.833 respectively. These two results are not directly comparable since the values of the pitching moments of inertia of the basic wings were different.

In Fig (9.2) an attempt is made to obtain the effect of the mass ratio on the flutter speed. In this figure, the flutter speed is plotted at each of the spanwise stations as a ratio of the bare wing flutter speed. (All the results presented are results from the Direct Matrix analysis). In general, the flutter speed ratios for the concentrated mass on wing A3 ($\bar{M}$ = 0.83) are greater than the flutter speed ratios for the concentrated mass on wing A2 ($\bar{M}$ = 1.0). This is true for both chordwise positions ($\bar{x}$ = 0.1 c and o c aft of the elastic axis), except for $\bar{x}$ = 0.33 and 0.5 for the mass on the elastic axis.

9.1.5 Effect of Inertia Ratio

In Figs (9.3.a) to (9.3.g) the flutter speed is plotted against the pitching moment of inertia ratio ($\bar{I}$) of the concentrated mass. A detailed study was made only for the concentrated mass on the wing A2, only two values of the inertia ratio ($\bar{I}$) being used for the wing A3. For the curves of wing A2, the value of the mass ratio ($\bar{M}$) is unity. The graphs show the flutter speed plotted against the inertia ratio ($\bar{I}$) with the spanwise location of the concentrated mass as parameter. For the wing A2 five different chordwise locations of the concentrated mass centre of gravity are considered.

For all these values of the centre of gravity (both spanwise and chordwise locations) the flutter speed shows a large decrease as the value of the inertia ratio is increased zero to 10.0.

The reductions are largest for the value of $\bar{I}$ = 10.0 and when the chordwise position of the centre of gravity of the concentrated mass is aft of the elastic axis.

For all the cases considered, the principal modes

participating in the flutter were the fundamental bending and the fundamental torsion modes.

9.2 Influence of Pod Aerodynamics and Fins

Figs (9.4.a) to (9.4.c) show the influence of the pod aerodynamic shape on the flutter speed. In each of these figures, the flutter speeds due to the pods with the same inertial properties but with different aerodynamic shpaes are compared at each of the spanwise stations.

Fig. (9.4.a) refers to Wing A2. The relevant pod inertial parameters are: $\bar{M} = 1$, $\bar{I} = 8.5$ and $\bar{x}_p = +0.1$. The flutter speeds due to two pods - pods A and B - are presented. The flutter speeds show similar trends with changes in the spanwise position of the pod. At each of the span locations, the flutter speeds do not show exact agreement, but all locations, except near the mid-span region, the differences are small. At the outboard positions ($\eta > 0.75$), pod B gives a higher flutter speed. Around $\eta = 0.5$, pod A gives a higher flutter speed.

Fig (9.4.b) also refers to wing A2. For this case, the inertial details of the pod are: $\bar{M} = 1.0$, $\bar{I} = 8.5$ and $\bar{x}_p = 0$. Again, for both the pods, the flutter speed exhibits a similar trend with changes in the spanwise position of the pod. In this case, the flutter speeds due to the pods exhibit a larger difference than in the corresponding cases in Fig (9.4.a).

In Fig. (9.4.c) four different pods are compared for their influence on the flutter speed. In this figure, which refers to wing A3, the inertial details of the pods are: $\bar{M} = 0.83$, $\bar{I} = 10$, $\bar{x}_p = +0.1$. The flutter

speeds due to the different pods show similar trends with changes in the spanwise position of the pods, though they do not have the same values at each of the spanwise stations. Flutter was obtained at the spanwise location of η = 0.917 only for the pod A, and for the wings with the other pods flutter was not obtained upto the maximum tunnel speed.

From the above results it appears that even drastic changes in the aerodynamic shape of the pods has very little influence on the flutter speed.

9.3 Influence of Ailerons

A preliminary set of calculations was carried out to examine the influence of the aileron degree of freedom on th flutter speed. These showed that a combination of the degrees of freedom of wing twisting and (free) aileron-rotation resulted in a flutter speed which was lower than in the case of the wing-pod combination with rigid controls.

Though the aileron had dimensions which would be considered as being representative of the conditions on a full scale aeroplane, the assumed inertial properties may not be representative. However, it is felt that the result obtained could be considered as providing a guide to the importance of including the aileron degree of freedom in a flutter analysis of a given wing-mass combination.

9.4 Comparison Between Theory and Experiment

9.4.1 Bare Wings

For the bare wings, wind tunnel results are available only for the wing A1(and for the wing of Ref. 38)

From the results shown in sections (6.4.1) and (8.2), all the analytical methods considered - assumed mode method the exact analysis of Ref (37), the iterative transformation procedure of (Ref.(43') and the Direct Matrix Method - gave flutter speeds which are in very close agreement with the measured speeds. In the assumed mode method, the use of two modes - the fundamental bending and the fundamental torsion modes of the bare wing - were used. These give very good results for the flutter speed. Molyneux's approximate formula (Ref. 39) also gives a good approximation to the flutter speed.

In all the above analyses, two dimensional strip theory aerodynamic derivatives were used.

The excellent agreement between all these methods can be attributed to the fact that the wings had uniform properties along the span.

These results show that the Direct Matrix Method can be used with confidence to obtain the flutter speeds of uniform cantilever wings. (In the Direct Matrix Method, ten control points were used.).

9.4.2 Wing A2 with Pods

Figs (9.5. a), (9.5.b),(9.5.c) and(9.5.d) show the flutter speed plotted as a function of the spanwise position of the pod. Both the wind tunnel test results and the analytical results are shown.

The results for Pod A are shown in Fig. (9.5.a), and the relevant inertial parameters of the pod are: $\bar{M} = 1.0$,

$\bar{I}$ = 10.0 and $\bar{x}_p$ = 0. Also shown in the figure are the results of a Direct Matrix Analysis and the results obtained by the assumed mode method. In the assumed mode method, only two modes were used. These were the fundamental bending and the fundamental torsion modes of the wing with the appropriate concentrated mass.

For the outboard locations (η = 0.67 and η = 0.875), the results of the Direct Matrix Method show good agreement with the measured flutter speeds. The agreement is not so good for inboard locations of the pod. At the midspan location, the flutter speed predicted by the Direct Matrix Method is higher than the measured speed. For this case, the results of the Direct Matrix Method indicate a spurious trend for the flutter speed as the pod is moved outboard from the root.

For all these cases, the important modes at flutter were the fundamental bending and the fundamental torsion modes.

In this figure the results of an assumed mode method analysis are also given. For this wing pod configuration, flutter speeds predicted by the assumed mode method (using only two modes), show a much better agreement with the measured flutter speeds than the results from the Direct Matrix Method.

Fig. (9.5.b) is also for the wing A2. The relevant pod parameters are: $\bar{M}$ = 1.0, $\bar{I}$ = 10.0 and $\bar{x}_p = \pm 0.1$. For this case, the Direct Matrix Method gives values for the flutter speed which are always lower than the measured speeds. They also predict the correct trend for the variation of the flutter speed due to changes in the spanwise position of the pod.

The flutter speeds predicted by the assumed mode method show a better agreement with the measured flutter speeds than the results from the Direct Matrix Method. However, they predict an incorrect trend for the behaviour of the flutter speed curve with variations in the spanwise position of the pod.

In Fig (9.5.c) the measured flutter speeds for the pods A and B are compared with the flutter speeds obtained by using the Direct Matrix Method and also by using the assumed mode method. In this case, the pod inertia parameters are: $\bar{M} = 1.0$, $\bar{I} = 8.5$ and $\bar{x}_p = 0$. As in Fig (9.5.a), the results of the Direct Matrix Method show a spurious trend at $\eta = 0.5$. For the outboard positions of the pod, the values of the flutter speed predicted by the Direct Matrix Method show good agreement with the measured speeds.

For all the spanwise positions of the pod considered, the assumed mode method gives good agreement with the measured flutter speeds. They also show the correct trend for the flutter speed when the pod is moved spanwise.

Fig. (9.5.d) also refers to the Wing A2. In this case the pod inertia parameters are: $\bar{M} = 1.0$, $\bar{I} = 8.5$ and $\bar{x}_p = 0.1$. The values predicted by the Direct Matrix Method are lower than the measured flutter speeds but they predict the correct trend for the variation of the flutter speed with the spanwise position of the pod.

For this wing-pod configuration also the assumed mode method predicts values for the flutter speed which show the correct trend, and are reasonably accurate, especially around the midspan position. For both the inboard and outboard positions, the flutter speeds are much lower than the measured speeds.

9.4.3 Wing A3 with Pods

Fig. (9.5.e) refers to the wing A3, carrying a pod whose inertial parameters are: $\bar{M}$ = 0.83, $\bar{I}$ = 10 $\bar{x}$ = 0. The measured flutter speeds for the pod B are compared with the values predicted by using the Direct Matrix Method and the assumed mode method. The results predicted by the Direct Matrix Method are much lower than the measured speeds for inboard locations of the pod ($\eta < 0.5$). For outboard locations the difference in the two flutter speeds is lower and the Direct Matrix Method results show the correct trend for the flutter speed.

In Fig (9.5.f) the pod has the following inertial parameters: $\bar{M}$ = 0.83, $\bar{I}$ =10, $\bar{x}$ = + 0.1. The measured flutter speeds for the pods A and B are compared with the values predicted by using the Direct Matrix Method, the assumed mode method and the exact solution of Ref. (37).

For this pod the values of the flutter speed predicted by the Direct Matrix Method show good agreement with the measured flutter speeds, except at the span location of η = 0.33 where the value is much lower than the measured flutter speed.

For both these pods, the results of the assumed mode analyses show good agreement with the measured speeds. For the pod condition shown in Fig. (9.5.f) the assumed mode results do not exhibit the correct trend for the behaviour of the flutter speed with variations in the spanwise position of the pod.

The results of the "exact" analysis of Ref 37 show very good agreement with the measured speeds at both the spanwise locations considered. From (Fig 9.5.f) it

can be seen that the speeds predicted by the exact analysis are closer to the measured speeds than the speeds predicted by the assumed mode or the Direct Matrix methods.

The analytical results indicate that the flutter speeds obtained by including the pod aerodynamic loads in the analysis are generally lower than the flutter speeds obtained by an analysis which neglects these loads. Though there is no consistent trend, at most of the spanwise positions considered the flutter speeds due to the pod D are higher than the flutter speeds due to the other pods (Fig.9.4.c). Since this pod had the same shape as the wing cross section, the flutter speed can be compared with the theoretical results in which the pod aerodynamic loads have been neglected. From this limited evidence, it can be argued that the theoretical results about the effects of the pod aerodyanimi loads (predicted by the momentum theory) as the flutter speeds show approximately the same trend as the experimental results. For pods without fins, inclusion of the pod aerodynamic loads made very little difference in the flutter speeds and from the experimental results it can be seen that the pod aerodynamic loads do not seem to have any marked effect on the flutter speed. In the theoretical analysis, the inertial terms due to the pod dominate the equations of motion, and the inclusion of the aerodynamic loads due to the pods makes only a slight change in the equations of motion.

The analytical results for the pods with fins give the same trend a for the flutter speeds (due to an ~~increase~~ increase in the fin size) as the experimental results (Fig.6.8).

But the increases predicted by the results of the Direct Matrix analysis are much less than the measured increases in the flutter speeds.

This may again be due to the fact that the large values of the pod inertia dominate theequations of motion and the flutter speeds are not very sensitive to changes in the aerodynamic terms of the pods. It is also possible that the momentum theory does not give the correct aerodynamic loads of the oscillating pod-fin combination. So, if a more sophisticated aerodynamic theory, which gives the correct aerodynamic loads of the pod-fin combination and which also takes into account the interference effect of the wing-pod configuration, were used, the results may show better agreement.

9.4.4. Wings of Ref (9) and Ref (38)

In Chapter 8, the Direct Matrix Method was used to obtain the flutter speeds and frequencies for the wings of Ref (9) and Ref (38), under different conditions of concentrated mass. For the bare wings, the Direct Matrix Method gave very good agreement with the measured speed for the wing of Ref. 38.

When different concentrated masses were attached to the wings, the Direct Matrix Method predicted values for the flutter speed which were in good agreement with the measured flutter speeds (Ref. 38) and with the values predicted by the assumed mode method (Ref. 9).

9.4.5

In applying the Direct Matrix Method to the wings referred to above, ten control stations were used (as in Fig. 6.4). In all the cases, two dimensional strip theory derivatives were used. It is probable that better agreement

could have been obtained if a larger number of control stations were used and if a more sophisticated aerodynamic theory was used to predict the aerodynamic loads of the oscillating wing.

9.5 Implications on Design Procedure

For wings of conventional planform, (without any discontinuities or concentrated masses), it is possible to obtain approximate formulae for the flutter speed in terms of their geometric, structural and inertial parameters. However, as was seen in Chapter 2, this is no longer possible when the wing carries concentrated masses. In general, each concentrated mass requires a separate analysis to obtain the corresponding flutter speed. From the results obtained so far and from the results discussed in Chapter 2, it is, however, possible to perceive some general trends.

(a) For wings A2 and A3 (with concentrated masses), an increase in the inertia ratio ($\bar{I}$) results in a decrease in the flutter speed.

(b) Locations of the concentrated mass centre of gravity ahead of the spar result in higher values of the flutter speed than when the centre of gravity is located aft of the spar.

(c) In general, for all chordwise locations of the concentrated mass c.g., the mid span position gives the lowest value for the flutter speed when the concentrated mass has a finite pitching moment of inertia.

(d) When the concentrated mass c.g. is ahead of the spar, the best spanwise location (for the wings A 2 and A3) is at the tip. At these locations, the flutter speed of the wing-mass combination is higher than the bare wing flutter speed.

(e) From the results for wings B4 and B5, it can be seen that it is possible to obtain the maximum flutter speed at a location other than at the tip by a suitable modification of the relative values of the bending and torsional stiffnesses.

(f) By adding suitable fins to thepod, it is possible to obtain large increases in the flutter speed. These fins have a stabilising effect with regard to the static stability of the pod.

From the above observations, it can be seen that by a proper location of the concentrated mass (both in the spanwise and in the chordwise directions), large increases in the flutter speed can be obtained (compared with the bare wing flutter speed). This can be used as a cure for the bare wing flutter.

If the spanwise position of the pod has been fixed by other considerations such as the location of the control surfaces, it may still be possible to obtain useful increases in the flutter speed by a proper location of the chordwise position of the centre of gravity of the concentrated mass. Positions of the centre of gravity forward of the spar give higher values for the flutter than aft positions.

By adding suitable fins to the pods, it is possible to obtain increases in the flutter speed. The increases in flutter speed which can be obtained by this may be limited by possible limitations on the size of the fins.

Another possible method of obtaining increases in the flutter speed is by altering the relative values of the bending and torsional stiffnesses so that an optimum value is obtained for the flutter speed, which is governed by the relative values of the bending and torsional frequencies.

All the above recommendations are applicable to straight cantilever wings. The increases in flutter speed obtained by a proper positioning of the concentrated mass can be nullified when the root degrees of freedom are allowed. Also, care should be exercised when other factors such as flexibility in the attachment of the concentrated mass, sweepback, movable fuel (in the case of fuel tanks), etc. are introduced. Each of these conditions can bring about large, detrimental effects on the flutter speed.

CHAPTER 10

CONCLUSIONS

10.1 Literature Survey

A survey of the previous studies of the physical problem (both experimental and theoretical) showed that the flutter of wings with concentrated masses is influenced by a number of parameters which can be varied over a very wide range.

At a given spanwise position, the influence of the mass ratio ($\bar{M}$) is governed by the chordwise position of its centre of gravity with respect to the wing elastic axis. When the centre of gravity of the mass is ahead of the elastic axis, the flutter speed increases at first as the mass ratio is increased from low values. After reaching a maximum value, (at a critical value of the mass ratio) the flutter speed decreases when the mass ratio is increased. In general, for all values of $\bar{M}$, the flutter speed of the wing-mass combination is higher than the bare wing flutter speed (when the centre of gravity of the concentrated mass is ahead of the elastic axis).

When the concentrated mass is located on the elastic axis, the flutter speed does not seem to show a well defined trend with changes in the mass ratio.

When the centre of gravity of the concentrated mass is aft of the elastic axis, the flutter speed of the wing-mass combination decreases with increases in the mass-ratio. For all values of the mass ratio ($\bar{M}$), the flutter speeds are generally lower than the bare wing flutter speed.

In general, when the inertia ratio ($\bar{I}$) is increased, there is a decrease in the flutter speed. The actual behaviour of the curve of $\bar{V}$ vs $\bar{I}$ is influenced mainly by the value of the mass ratio ($\bar{M}$) and the spanwise location of the concentrated mass.

The chordwise position of the centre of gravity of the concentrated mass seems to have the strongest influence on the value of the flutter speed. For the wing-mass combinations reviewed in Chapter 2, the general trend is for the flutter speed to increase as the centre of gravity position of the concentrated mass is moved forward from a location aft of the elastic axis. At a certain centre of gravity location forward of the elastic axis a maximum value is reached and any further (forward) movements of the centre of gravity tend to decrease the flutter speed.

The influence of the spanwise location of the concentrated mass seems to be governed mainly by the chordwise position of the concentrated mass centre of gravity and to a lesser extent by the value of the mass ratio $\bar{M}$. When the centre of gravity of the concentrated mass is ahead of the elastic axis, the flutter speed increases as the concentrated mass is moved outboard from the root.

After reaching a maximum value at a location between the midspan and the tip, the flutter speed decreases as the mass is moved further towards the tip.

For locations of the centre of gravity of the concentrated mass aft of the elastic axis, the flutter speed decreases initially and after reaching a minimum value at around the midspan region, it increases again

as the concentrated mass is moved further outboards.

For a concentrated mass which is rigidly attached to the wing, it is possible to find an optimum position for the location of its centre of gravity (both spanwise and chordwise). At this position, it is possible to obtain large increases in the flutter speed (compared to the bare wing flutter speed). This suggests a method of curing the flutter problem of bare wings.

The conclusions drawn so far have been concerned mainly with concentrated masses which are attached rigidly to a cantilever wing (with rigid control surfaces). It is possible that these will have to be modified when some or all of the following parameters are varied:

(a) Flexibility of the wing-mass attachment

(b) Root degrees of freedom

(c) Fuel sloshing

(d) Control surface flexibility

If the values of the parameters are in certain critical ranges, these can have large detrimental effects on the flutter speed.

In general, introducing sweepback to a concentrated mass cantilever wing combination seems to have a beneficial effect on the flutter speed.

An examination of the available data on the influence of the aerodynamic shape of the concentrated mass showed that at subsonic speeds, the aerodynamic shape had very little influence on the flutter speed.

10.2 Experimental Results

The experimental work was mainly concerned with investigating the effects of the inertia ratio of the concentrated mass at a number of spanwise and chordwise positions. An investigation was also made of the influence of the aerodynamic shape of the concentrated mass on the flutter speed of the wing-mass combination.

Four pods having different aerodynamic shapes were tested. These tests showed that for given values of the parameters $\bar{M}$, $\bar{I}$, $\bar{x}_p$ and η , the aerodynamic shape of the concentrated mass has no significant or consistent influence on the flutter speed.

This could be due to the fact that the aerodynamic loads due to the oscillating pods were not sufficiently large in comparison with the inertial parameters of the wing-mass combinations.

By attaching horizontal fins to the trailing edge of the pods, it was found that the flutter speeds could be increased. The results showed a consistent trend in that the flutter speed increased with increases in the size of these fins.

The design of the wing and the pods allowed the pods to be attached to the wing at a number of spanwise locations. At all the spanwise locations, it was found that the flutter speeds of the wing-pod combinations were much lower than the (theoretically calculated) bare wing flutter speeds. When the other parameters ($\bar{M}$, $\bar{x}_p$ and) were fixed, it was found that increasing the inertia ratio ($\bar{I}$) resulted in a decrease in the flutter speed. For the two chordwise locations of the pod centre of gravity considered, it was found that regions near the wing tip or the wing root gave higher flutter speeds than the midspan

locations.

10.3 Theoretical Results

10.3.1 An in-vacuo vibration analysis has been developed which gives closed-form solutions for the vibration fr quencies and modes of uniform beams (or shafts) carrying a concentrated mass (or moment of inertia). In the assumed mode flutter calculations, the mode shapes obtained by this method were used.

The Direct Matrix Method was also used to obtain the coupled frequencies and mode shapes of the wing -mass combinations. With ten control stations in the Direct Matrix Method, the calculated frequencies (using measured stiffness distributions) showed good agreement with the measured values

10.3.2 The flutter speeds of the different wing-inertia combinations were obtained by three different methods.

The results of the 'exact' analysis of Ref.(37) gave very good estimates of the flutter speed. One major disadvantage of this method is the large amount of numerical work which is necessary for calculating the flutter speeds.

10.3.3 In all the assumed mode analyses, only two modes were used. These were the uncoupled bending and torsion modes for the particular wing-mass configuration and were obtained by the method of Appendix III, as mentioned in Section 10.3.1.

The flutter speeds predicted by this method showed good agreement with the measured values. In general, the assumed mode analyses gave values for the flutter speeds which were lower than the measured speeds.

The preliminary investigations into the influence of the control surface dgree of freedom or the flutter speeds of a specific wing-mass combination showed that this may have a detrimental influence on the flutter speed.

10.3.4 The Direct Matrix Method was used extensively to obtain the flutter speeds and frequencies. Ten collocation statinns were used in the analyses. This meant that the influence of the concentrated masses on the flutter speed could be assessed at only five spanwise stations. Strip theory aerodynamic loads were used in all the cases for obtaining the aerodynamic influence coefficient matrices.

The vibration frequencies predicted by the Direct Matrix Method for the wing-mass combinations showed good agreement with the measured frequencies. The flutter speeds predicted were by lower than both the measured flutter speeds and the assumed mode results.

The Direct Matrix Method was also used to obtain the flutter speeds and frequencies of some wing-mass combinations treated in Refs. (9) and (38). In these cases the Direct Matrix results showed good agreement with the measured speeds of Ref (38) and the analogue solutions of Ref. (9) For a certain wing-mass combination of Ref. (38), assumed-mode methods predicted higher values for the flutter speed, even when four modes were used in the analysis. The results of the Direct Matrix Method showed better agreement with the measured values of the flutter speed in this case.

It is possible that a better agreement could have been obtained if a larger number of collocation stations were used in the Direct Matrix analysis.

A major attraction of using the Direct Matrix Method is that it is not necessary to prescribe the mode shapes of the vibrating structure in advance. On the other hand, the mode shapes are obtained as part of the analysis.

10.3.5 When the aerodynamic loads due to the pods (as obtained from the momentum theory) were included in the Direct Matrix analyses, it was found that the resulting flutter speeds were slightly lower than the flutter speeds predicted by this method when the aerodynamic loads were neglected.

When the aerodynamic loads due to the finned-pods were also included in the analyses, the results showed the correct trend for the flutter speed to increase with increases in the fin size. However, it was again found that these values were much lower than the measured flutter speeds.

10.4 General

The results show that the Direct Matrix Method could be used with confidence to obtain the flutter speeds of wing mass combinations since there was a 'built-in' degree of conservatism in these results.

It is especially useful when the influence of varying a large number of parameters is to be assessed.

The preliminary investigation into the influence of the aileron degree of freedom on the flutter characteristics of the wing-mass combination indicated that this could have a significant influence on the flutter speed. This effect needs further investigation.

It should be emphasized that the conclusions drawn here apply to the specific wing. The influence of a concentrated mass on the flutter appears to be dependent on the (torsion/bending) frequency of the particular wing. However, the

results serve as a guide to the influence of concentrated masses on the flutter speed.

CHAPTER II

SUGGESTIONS FOR FURTHER RESEARCH

1. The investigations undertaken in this report were all concerned with uniform cantilever wings. Investigations of the influence of the root flexibilities (in normal translation, pitch and roll) should be made, mainly with a view to checking the accuracy of the results predicted by the Direct Matrix Method.

2. The influence of the flexibilities (in normal translation, pitch and roll) of the attachment of the concentrated masses on the flutter speed have not been investigated in this report. At the large values of the pitching moments of inertia considered here, these may have considerable influences on the flutter speed.

3. The effect of the chordwise flexibilities of the wing have not been considered here. For thin wings with concentrated masses, the influence of this factor may be significant.

4. The influence of the aerodynamic shape of the concentrated masses does not seem to be very significant. However, these may become significant at high speeds. At low speeds, a method of obtaining an estimate of the influence of the pod aerodynamic shape on the flutter speed may be to test pods having negligible mass and moment of inertia. If a number of different pods are tested, it may be possible to assess the influence of the aerodynamic shape, independently of changes in mass distribution, etc.

4. Further work should be carried out on determining the nature of the influence of finned pods. Both experimental and analytical work should be undertaken to determine the oscillatory aerodynamic loads on finned pods, especially when the pods have unorthodox cross sections.

5. In all the Direct Matrix results reported here, ten collocation stations were used. Further work is needed to assess the convergence of the results as the number of collocation stations is increased.

6. For quickly assessing the changes in the flutter characteristics due to changes in the concentrated mass parameters, a sensitivity analysis can be envisaged, to be used in conjunction with the Direct Matrix Method. Existing analyses can only take into account the results of only small changes in the parameters. Large changes in the parameters will affect the character of the matrices. It may be possible to develop some approximate formulae which would evaluate the changes in the flutter characteristics even for large changes in the parameters,

7. Further work is needed to asses the influence of control surface degrees of freedom on the flutter characteristics of wing-mass combinations.

8. The results obtained in this report indicate that the Direct Matrix Method can be used with confidence to obtain the flutter speeds of bare wings and of wing-mass combinations. It would therefore be useful to extend the computer programme used in these investigations. Subroutines which can calculate the structural influence coefficient matrix in the desired form by using sophisticated theories (such as plate theory etc.) would make the programme more useful. Subroutines to calculate the aerodynamic influence coefficients by using sophisticated theories (such as lifting surface theories for the various Mach Number regimes) can be incorporated in the programme. These additions would make the computer programme more useful in the vibration and flutter analysis of practical configurations.

REFERENCES.

1. HOWE, D. — "Aeroplane Design Studies - Conventional and VTOL Freighter Aircraft". CoA Rep. Aero. No 171, Nov. 1963.

2. MOMIRSKY, M. — "Flutter Characteristics of the VTOL F-61 Strategic Freighter Wing." CoA Unpublished Thesis, 1962.

3. JOHNS, D.J. — "Recent Aeroelastic Investigations at the College of Aeronautics". CoA Note Aero. No 168, Jan. 1965.

4. MOLYNEUX, W.G. — "Flutter of Wings with Localised Masses". J. Roy. Aero. Soc. 61, Oct.1957, p.p. 667-668.

5. MOLYNEUX, W.G. — "Flutter of Wings with Localised Masses". RAE Rep. Struct. No. 214, 1956.

6. LAMBOURNE, N.C. WESTON, D. — "An Experimental Investigation of the Effect of Localised Masses on the Flutter and Resonances of a Model Wing". A.R.C. R & M No. 2533, 1944.

7. GAUKROGER, D.R. — "Wind Tunnel Tests on the Effect of a Localised Mass on the Flutter of a Swept Back Wing with Fixed Root." A.R.C. R & M No. 3141, 1960.

8. ROCKLIFF, R.J. et al. — "An Investigation of the Flutter of Rectangular Wings with Tip Masses". W.R.E. (Aust.) Reps. HSA 5,6, and 7, 1956.

9. GAUKROGER, D.R. — "A Theoretical Treatment of the Flutter of a Wing with a Localised Mass." R.A.E. Rep. Struct. No. 213, 1956.

10. WILTS, C.H. — "Incompressible Flutter Characteristics of Representative Aircraft Wings". NACA Rep. No. 1390, 1957.

11. YOUNG, L.S. RUHLIN, C.L. — "Effect of Store Pitch Flexibility on Flutter Characteristics of a Wing-Store Configuration at Mach. Numbers Near 0.85". NASA TN D-2479,

12. GAUKROGER, D.R. — "Flutter Characteristics of a Wing Carrying a Flexibly Mounted Mass". RAE Rep. Struct. No. 261, March 1961.

13. YFF, J. — "The Influence of External Fuel Tanks on Wing Flutter of Slender Unswept Wings". Delft, 1960.

14. MARTIN. SEWALL, J. L. — "Tunnel Experiments with Dynamic Models Relating to the Effects of External Stores". NACA - Industry Conference on Aircraft Loads, Flutter and Structures. 1953. pp. 303-311.

15. CAYMAN, W.H. "An Investigation of the Effect of a Varying Tip Weight Distribution on the Flutter Characteristics of a Straight Wing". J. Aero. Sci., 19, 5, May 1952, pp 289-301.

16. SEWALL, J.L. WOOLSTON. "Preliminary Experimental Investigation of the Effect of Aerodynamic Shape of Concentrated Weights on the Flutter Characteristics of a Straight Cantilever Wing". NACA RM L9E17, 1949.

17. GAUKROGER, D.R. "Wind Tunnel Tests on the Effects of Body Freedoms on the Flutter of a Model Wing Carrying a Localised Mass". ARC R & M No. 3081, 1958.

18. GAUKROGER, D.R. "Wind Tunnel Tests on the Symmetric and Anti Symmetric Flutter of Swept-back Wings." ARC R & M No. 2911, 1953.

19. GAUKROGER, D.R. CHAPPLE, E.W. MILLN, A. "Wind Tunnel Tests on a Model Delta Wing Under Fixed and Free Root Conditions". ARC R & M No. 2826, 1950.

20. SEWALL, J.L. "An Experimental and Theoretical Study of the Effect of Fuel on Pitching Translation Flutter". NACA Tech. Note No. 4166, 1957.

21. MOLYNEUX, W.G. "The Flutter of Swept and Unswept Wings with Fixed Root Conditions". RAE Rep. Struct. No.58, Jan, 1950.

22. SANDFORD, M.C. RUHLIN, C.L. ABEL, I. "Flutter Studies of Simplified Component Models of a Variable-Sweep Wing Airplane at Mach. Numbers Up to 3.0". NACA TN D-3501.

23. BISPLINGHOFF, R.L. ASHLEY, H. HALFMAN, R.L. "Aeroelasticity". Addison-Wesley Publishing Co., Cambridge, Mass., 1955.

24. MOLYNEUX, W.G. "Aero elastic Modelling". RAE TN Struct. No.353, 1964.

25. MINHINNICK, I.T. "Tables of Functions for Evaluation of Wing and Control Surface Flutter Derivatives for Incompressive Flow". RAE Rep. Struct. No.86, 1950.

26. VAN DE VOOREN "Collected Tables and Graphs". Part VI of "AGARD Manual or Aeroelasticity" 1959.

27. TEMPLETON, H. "Technique of Flutter Calculations". RAE Rep Struct. No.142, 1953.

28. SCANLAN, R.H. ROSENBAUM, R. "Introduction to the Study of Aircraft Vibration and Flutter". The Macmillan Company, N.Y., 1960.

29. MINHINNICK, I.T. "Subsonic Aerodynamic Flutter Derivatives for Wings and Control Surfaces (Compressible and Incompressible Flows)". RAE Rep. No.87, 1950.

30. REISSNER, E. STEVENS, J.E. "Effect of Finite Span on Airload Distributions for Oscillating Wings. Part II Methods of Calculation and Examples of Application". NACA TN 1195, 1947.

31. WOOLSTON, D.S. CASTILE, G.E. "Some Effects of Variations in SeveralParameters Including Fluid Density on the Flutter Speed of Light Uniform Cantilever Wings". NACA TN 2558, Dec. 1951.

32. REISSNER, E. "Effect of Finite Span on Airload Distributions for Oscillating Wings: Part II Methods of Calculation and Examples of Applications". NACA TN 1195, 1947.

33. GUYETT, P.R. "Empirical Values of Derivatives" Part II, Chap. 11 of 'AGARD Manual on Aeroelasticity.' 1959.

34. MOLYNEUX, W.G. HALL, H. "The Aerodynamic Effect of Aspect Ratio and Sweepback on Wing Flutter" ARC R & M 3011, Feb. 1955.

35. GOLAND, M. " The Flutter of a Uniform Cantilever Wing" J. App. Mech. 12, No.4, Dec. 45. pp A197-A208

36. GOLAND, M. & Luke, Y.L. "The Flutter of a Uniform Wing with Tip Weights". Jour. App. Mech. March 1948, pp 13-20.

37. RUNYAN, H.L. WATKINS, C.E. "Flutter of a Uniform Wing with an Arbitrarily placed Mass According to a Differential Equation Analysis and a Comparison with Experiment". NACA Rep. No.966.

38. RUNYAN, H.L. & SEWALL, J.L. "Experimental Investigation of the Effects of Concentrated Weights on Flutter Characteristics of a Straight Cantilever Wing". NACA TN 1594, 1948.

39. PARKS, P.C. "A Stability Criterion for a Panel Flutter Problem via the Second Method of Lyapunov" Proceedings of AIAA Symposium on Structural Dynamics and Aeroelasticity, Boston, Mass. Aug-Sept. 1965, pp 92-95.

40. WANG, P.K.C. "Stability Analysis of a Simplified Flexible Vehicle via Lyapunov's Direct Method". AIAA Jour. No 13, No. 9, Sept. 1965 pp. 1764-5

41. WANG, P.K.C. "Stability Analysis of Elastic and Aeroelastic Systems via Lyapunov's Direct Method." J. Franklin Inst., 281, 1 Jan. 1966, pp 51-72.

42. VANDE VOOREN, A.I. "Flutter Calculation with Many Degrees of Freedom for Modern Aircraft." in "Aeroelasticity Symposium" Gottingen, April 16-17, 1957. (NASA T.T. F.81, Sept. 1963).

43. GOSSARD., M.L. "Iterative Transformation Procedure For Numerical Solution of Flutter and Similar Characteristic Value Problems" NACA Rep No.1073.

44. WOOLSTON, D.S. RUNYAN, H.L. "Appraisal of Method of Flutter Analysis Based on Chosen Modes by Comparison with Experiment for Cases of Large Mass Couplings" NACA TN No. 1902, 1949.

45. FRAZER, R.A. DUNCAN, W.J. & COLLAR, A.R. "Elementary Matrices and Some Applications to Dynamics and Differential Equations". Cambridge University Press, 1963.

46. DUNCAN. "Flutter of Sustems with Many Degrees of Freedom" CoA Rep. No. 19. College of Aeronautics, Cranfield.

47. CRISP, J.D.C. "On the Stability Criteria for Fluttering Systems." (Australian) Aero. R.E.S. Labs. Rep. SM 250.

48. BOLLAY, "Aerodynamic Stability and Automatic Control." J. Aero. Sci. 18, 1951, pp.569-623.

49. SERBIN, H. CASTILOW, E.L. "Application of Response Function to Calculation of Flutter Characteristics of a Wing Carrying Concentrated Mass". NACA TN 2540, Nov. 1951.

50. LORING, S. "General Approach to the Flutter Problem". SAE Jour. 49, No.2, August 1941.

51. LORING, S. "Use of Generalized Co-ordinates in Flutter Analysis." SAE Jour. 52, No.4, April 1944.

52. LANCASTER, P. "Direct Solution of the Flutter Problem" ARC R & M. 3206, Dec. 1956.

53. HERRESHOFF, J.B. "Flutter Analysis Using Influence Matrices and Steady-State Aerodynamics." AIAA Jour. Dec. 1963, p.2853.

54. MAZELSKY, B.
O' CONNELL, R.F.
"The Integrated Use of Analog and Digital Computing Machines for Aircraft Dynamic Load Problems".
J. Aero. Sci. 23, August 1956. pp.721-780.

55. RODDEN, W.P.
"A Matrix Approach to Flutter Analysis".
SMF FUND Paper No. FF-63, Inst. of the Aero. Sci., NY, May 1959.

56. PARKS, P.C.
"Lyapunov Functionals for Aeroelstic Problems"
J. Franklin Inst., 283, 5, May 1967. p
(See also: WANG, P.K.C. "Reply to the above"
J. Franklin Inst., 283, 5, May 1967, p)

57. RODDEN, W.P.
FARKAS, E.F.
MALCOM, H.A.
"Flutter and Vibration Analysis by a Modal Method: Analytical Development and Computational Procedure"
Report No. TDR 169 (3230-11), TN - 15,
Aerospace Corporation, Calif. July 1963.

58. RODDEN, W.P.
FARKAS, E.F.
MALCOM, H.A.
"Flutter and Vibration Analysis by a Collocation Method: Analytical Development and Computational Procedure".
Rep. No. TDR 169 (3230-11) TN-14
Aerospace Corporation, Calif, July 1963.

59. SCHMITT.
"A Least Squares Matrix Interpolation of Flexibility Influence Coefficients"
J. Aero. Sci. 1956, p.980.

60. RODDEN, W.P.
REVELL, J.D.
"The Status of Unsteady Aerodynamic Influence Coefficients".
Rep. No. TDR-930 (2230-09) TN - 2
Aerospace Corporation, Calif, Nov. 1961.

61. BRYSON, A.E.
"Stability Derivatives for a Slender Missile with Application to a Wing-Body-Vertical Tail Configuration".
J. Aero. Sci. 20, 5, May 1963. p.

62. LAMB, H.
"Hydrodynamics".
6th Ed. Dover Publications, NY, 1945. pp 139-156.

63. MILES, J.W.
"On Non-Steady Motion of Slender Bodies."
Aero Quarterly, 2, Nov. 1950 pp 183 - 194.

64. MILES, J.W.
"The Potential Theory of Unsteady Supersonic Flow"
Cambridge University Press. 1959, pp 158 et seq.

65. WOODS, R.M.
MURPHY, C.H.
"Aerodynamic Derivatives for both Steady and Non-Steady Motion of Slender Bodies."
J. Aero. Sci. Dec. 1955. pp 870-871.

66. BOND, R.
PACKARD, B.B.
"Unsteady Aerodynamic Forces on a Slender Body of Revolution in Supersonic Flow".
NASA T.N. D-859, May 1959.

67. "USAF Stability and Control DATCOM",
July 1963.

68. DWYER, P.S. "Linear Computations".
John Wiley and Sons, N.Y. 1951.

69. JOHNS, D.J.
NAGARAJ, V.T. "On the Fundamental Frequency of a Square Plate Symmetrically Supported at Four Points."
To Be Published (Also Appendix VIII)

70. LANCZOS, C. "Applied Analysis"
Pitman and Sons, London,1957

71. GREGORY, R. "Results using Lanzos's Method for finding eigenvalues of Arbitrary Matrices".
J. Soc. Indust. Appl. Math. 6 (1958) pp 182-188.

72. YOUNG, R.
McCALLUM, H. "The Frequencies and Modes of Undamped Structures Using Finite Element Stiffness and Consistent- Mass Matrices".
ASRL TR 121 - 8,

73. BODEWIG, E. "Matrix Calculus"
Interscience Publishers Inc. N.Y. 1959.

74. AITKEN, A.C. "The Evaluation of the Latent Roots and Latent Vectors of a Matrix."
Proc. Roy. Soc. Edinburgh., Sect. A, 57, 1937 pp 268 - 304.

75. SEWALL, J.L. "Experimental and Analytical Investigations of Flutter of a Non-Uniform Sweptback Cantilever Wing with two cencentrated Weights."
NACA RM L51 4090, 1951.

76. HARRIS, C.H
CREDE,C (Editors) " Shock and Vibration Handbook"
McGraw-Hill, NY, 1961 (Published in 3 Vols.)

77. GOLLNITZ, H.
WILLE, F. "Calculation of Eigenvalues and Eigenvectors of large Non-Hermitian Matrices".
AGARD Rep. No.511, NATO, AGARD.

APPENDIX I

GEOMETRIC, INERTIAL AND STRUCTURAL DETAILS OF WINGS REFERRED TO IN CHAPTER 2

1.1 Wing of Ref (6)

(a) Geometry:

b = span = 6ft

c_r = root chord = 2.7 ft

λ = taper ratio = 0.524 (Tip chord/Root chord)

A.R = aspect ratio = 2.92

Λ = sweepback = 0^o

Aerofoil: $t/c = 0.3898\left(1-\frac{x}{c}\right)\sqrt{\frac{x}{c}}$, symmetric

Elastic Axis = 0.32c aft of leading edge

(b) Inertia

Weight of wing = 127 lb

(Wing density = 0.5 lb/ft^3)

Inertia Axis 0.4c aft of leading edge

Radius of gyration 0.28c about an axis 0.3c aft of leading edge

(c) Structural

No data available

(d) Concentrated Mass

Spanwise locations = 0.1, 0.3, 0.5 and 1.0

Chordwise locations of c.g. $\bar{x}$ = -0.29c, 0.30c, 0.69c aft of leading edge

Range of Mass Ratios $\bar{M}$ = 0 to

All masses were considered to have negligible moment of inertia about their own axis.

(e) Speed Range of Tests 0 to 160 f.p.s.

Max. Re. No. = 2.14×10^6 (based on mean chord)

(f) General

Effect of flexibility of attachment was also investigated. The flutter mode shapes were measured for some cases and are presented in the report.

The effect of adding more than one mass at the same time to the wing was investigated.

1.2 Wing of Ref. 38

(a) Geometry

b = 4ft

c_r = 2/3 ft

λ = 1.0

A.R. = 6

Λ = 0

Aerofoil section NACA 16010

Elastic Axis 0.437c aft of LE

(b) Inertia

Weight of Wing = 3.48 lb

Inertia Axis = 0.45c aft of LE

Radius of Gyration = 0.258c about inertia axis

(c) Structural

$EI = 0.1407 \times 10^6$ lb in^2

$GI = 0.0692 \times 10^6$ lb in^2

(Bare wing) Fundamental Bending Frequency = 6.44 cps

(Bare wing) Fundamental Torsion Frequency = 39.2 cps

(Bare wing) First overtone bending frequency = 48.4 cps

(d) Concentrated Mass

Spanwise locations = 0.22 to 1.0

Chordwise locations of c.g. x = - 0.468c to 0.34c aft of the axis.

Range of Mass Ratios $\bar{M}$ = 0.375 to 1.04

Range of Inertia Ratios $\bar{I}$ = 0.883 to 7.50

(e) Speed Range of tests M.No = 0 to 0.74

Re. N_c = 0.92×10^6 to $4,2 \times 10^6$

(f) General

The model was suspended vertically from the roof of the wind tunnel. A set of twelve different weights were tested.

.3 Wing of Ref 16

(a) Geometry

b = 3.33 ft.

c_r = 2/3 ft

λ = 1.0

A.R = 5.0

Λ = 0

Aerofoil section NACA 16 - 004

Elastic Axis 0.45c aft

(b) Inertia

Weight of Wing = 4.89 lb

Inertia Axis = 0.475c aft of E.A.

Rad. of Gyration = 0.23c about inertia axis

(c) Structural

EI = 0.0608×10^6 lb in^2

GI = 0.0944×10^6 lb in^2

ω_{b_1} = 4.94 cps

ω_{t_1} = 58.3 cps

ω_{b_2} = 30.9 cps

(d) Concentrated Mass

Spanwise location = 0 to 1.0

Chordwise locations -0.256c to +0.022c aft of elastic axis.

Range of Mass Ratios $\bar{M}$ = 0.0485 to 0.0755

Range of Inertia Ratios $\bar{I}$ = 0.07 to 0.509

(e) Speed Range Up to 447 fps

Re NO = 1.42×10^6 to 1.68×10^6

(f) General

The object of these tests was to investigate the effect of the aerodynamic shape of the concentrated mass on the flutter speed and a number of different shapes were tested.

I.4 Wing of Ref 75

(a) Geometry

b = 4.025 ft

c_r = 0.433 ft

λ = 0.454

A.R = 12.8

Λ = 34.5° on the 0.38 chord line

Aerofoil NACA 65_1 - 012 parallel to the air stream

Elastic Axis = 0.38c aft of Leading Edge (approximate)

(b) Inertia

Weight of wing = 3.79 lb

Inertia axis = Variable: Average:- 0.441c

Radius of Gyration = 0.216c (average)

(c) Structural

$EI = 2.89 \times 10^3$ lb-ft^2 (Root) to 0.075×10^3 lb-ft^2 (tip)

$GJ = 2.18 \times 10^3$ lb-ft^2 (Root) to 0.075×10^3 lb-ft^2 (tip)

$\omega_{b_1} = 6.97$ cps

$\omega_{b_2} = 30.9$ cps

$\omega_{t_1} = 37.9$ cps

(d) Concentrated Mass

Spanwise location: = 0.33 and 0.75

Chordwise location: —

Mass Ratios: Inboard mass $\bar{M} = 0.784$

Outboard mass $M = 0.42$

Inertia Ratios: —

(e) Speed range Upto 290 fps

Re NO : 5.19×10^6 to 5.77×10^6

(f) General

The object was to test the influence of adding two concentrated masses simultaneously to the wing two types of root restraints were used: in the first, the root section was clamped parallel to the air stream. In the second, a triangular shaped area at the root was restrained so that the wing behaved structurally as an unswept cantilever beam.

I.5 Wing of Ref 15

(a) Geometry

b = 2.94 ft

c_r = 0.88 ft

λ = 0.51

A.R. = 4.43

Λ = 0° at the 0.3 chord line

Aerofoil : NACA 0009 - 64

Elastic Axis : 0.3c aft of the leading edge

(b) Inertia

Weight of wing = 10.682 lb

Inertia Axis = Variable (average: 0.467c)

Moment of inertia of wing = 134.8 lb in^2

(c) Structural

EI = 0.98×10^5 lb-in^2 (Root) to 0.11×10^5 lb-in^2 (tip)

GJ = 0.98×10^5 lb-in^2 (Root) to 0.08×10^5 lb-in^2 (tip)

ω_{b_1} = —

ω_{t_1} = —

ω_{b_2} = —

(d) Concentrated Mass

Spanwise location : = 1.0

Chordwise location

Mass Ratios $\bar{M}$ = 0.0245 to 0.234

Inertia Ratios $\bar{I}$ = 0.0545 to 153.2

(e) Speed Range upto 250 fps

Re No = 12.7×10^6

(f) General

The wing was tested as a cantilever. The effect of a variable tip tank fuel content

were simulated. Four different types of pod were tested in order to assess the effect of the pod aerodynamic loads on the flutter speed.

I.6 Wing of Ref. 9

(a) Geometry

b = 4.0 ft

c_r = 1.0 ft

λ = 1.0

A.R. = 4

Λ = 0, 15°, 30°, 45°

Aerofoil = —

Elastic Axis = 0.25c aft of leading edge

(b) Inertia

Weight of Wing = 4.8 lb

Inertia Axis = 0.35c aft of leading edge

Moment of inertia of wing = 0.258 lb ft^2

(c) Structural

EI = —

GJ = —

ω_{b_1} = 3.6 cps

ω_{t_1} = 14.5 cps

ω_{b_2} = —

(d) Concentrated Mass

Range of spanwise locations : 0, 0.5, 0.67, 0.75, 1.0

Range of Chordwise locations $\bar{x}$ = -0.3c to +0.1c aft of elastic axis

Mass Ratios : $\bar{M}$ = 0 to 1.0

Inertia Ratios : The pitching radius of gyration of the concentrated mass was

varied between 0 and 0.7c

(e) Speed Range =

Re No. =

(f) General

The investigations were by the 'assumed - mode' method.

I.7 Wing of Ref 8

(a) Geometry

b = 3.0 ft

c_r = 1.5 ft

λ = 1.0

A.R. = 2.0

Λ = 0.0

Aerofoil = NACA 65 - 012

Elastic Axis = 0.319c aft of the leading edge

(b) Inertia

Weight of Wing = 13.27 lbs.

Inertia Axis = 0.431c aft of leading edge

Moment of inertia of wing =

(c) Structural

$EI = 1.534 \times 10^4$ lb ft^2

$G.J = 1.274 \times 10^4$ lb ft^2

ω_{b_1} = —

ω_{t_1} = —

ω_{b_2} = —

(d) Concentrated Mass

Spanwise position : Wing Tip

Range of chord wise positions -0.533c to 0.267c aft of the elastic axis.

Mass Ratios : $\bar{M}$ = 0.22, 0.44, 0.66

Inertia Ratios: $\bar{I}$ =

(e) Speed Range : Up to 2500 ft/sec

Re No : 24×10^6

(f) General

The tests were carried by means of ground launched rockets. Thus both symmetric and anti-symmetric degrees of freedom were allowed. All the concentrated masses were completely enclosed within the wing contour.

I.8 Wing of Ref(19)

(a) Geometry

$b_{/2} = 3.75$ ft

$c_r = 4.0$ ft

$\lambda = 1/16$

A.R. = 1.76

$\Lambda = 45^\circ$ on the leading edge

Aerofoil

Elastic Axis = 0.15 c aft of wing leading edge.

(b) Inertia

Weight of bare wing = 15.57 lb

Inertia Axis : overall wing c.g. between 0.4 and 0.5

MI of Wing = 1916 to 2540 lb in^2 =

(c) Structural

EI := ℓ_φ = 375 lb ft/rad } measured at

G.J := m_θ = 62 lbft /rad } span position

$\omega_{b_1} = 3.3$ cps

$\omega_{t1} = 9.7$ cps

$\omega_{b2} = 7.6$ cps

(d) Concentrated Mass

No concentrated mass was attached to the wing, but the body mass and pitching inertia at root were varied.

Body Mass Ratio

Body Pitch Inertia Ratio - 1 to + 2

Body c g

(e) Speed Range of the tests Up to 175 fps

Re No. = 2.4×10^6

(f) General

The tests were conducted to assess the influence of allowing the root degrees of freedom of pitch and normal translation.on the flutter speed of a delta wing model.

I.9 Wing on Ref.7

(a) Geometry

b = 3.0 ft

c_r = 1.75 ft

λ = 0.3

Sweepback Angles = 13°, 23°, 33° and 43°

Aerofoil RAE 101

Elastic Axis 0.3c aft of wing leading edge

(b) Inertia

Weight of Wing = 3.81 lb

Inertia Axis = 0.43c aft of wing leading edge

Moment of Inertia of Wing =

(c) Structural

EI = –

GJ = –

ω_{b1} = 3.9 cps

ω_{ti} = 15.3 cps

ω_{b2} = 11.4 cps

(d) Concentrated Mass

Spanwise locations = 0.25, 0.50, 0.75 and 1.0

Chordwise locations - 1.0c to 0.5c aft of the Elastic Axis.

Mass Ratios $\tilde{M}$ = 0.13 to 1.3

Inertia Ratios $\bar{I}$ =

(e) Speed Range

Up to 120 fps

Re No = 0.86×10^6

(f) General

The tests were made on a wing which could be set at four different sweepback angles. No root degrees of freedom were allowed. The influence of the aerdynamic shape of the concentrated mass was also tested.

I.10 Wing of Ref.11

(a) Geometry

b = 0.458 ft

c_r = 0.252 ft

Λ = 45° on the leading edge

Aerofoil NACA 65A 004

Elastic Axis

(b) Inertia

Weight of wing = 0.004875 slug =

Inertia axis = 0.538 c aft of wing Leading Edge

Moment of inertia of wing = 8.96×10^{-5} slug-ft^2/ft =

(c) Structural

EI = ~

GJ = —

ω_{b1} = 45.4 cps

ω_{t1} = 397 cps

ω_{b2} = 353 cps

(d) Concentrated Mass

Spanwise location = 0.755

Chordwise locations - 0.13c to 0.32 c aft of the ea

(In addition the position of the concentrated mass centre of gravity vertically below the wing was also varied between 0.09c and 0.13c)

Mass Ratios $\bar{M}$ = 0.039 to 1.019

Inertia Ratios $\bar{I}$ = 1.0 to 2.09

(e) Speed Range M = 0.8 to 1.3

Re NO ——

(f) General

The experiments were concerned with the effect of the pitching flexibility of the concentrated mass on the flutter speed. The value of the ratio (mass pitching frequency/ wing torsional frequency) was varied between the values of 0.1 and 1.4.

In addition, the effect of varying the aerodynamic shape of the mass was also investigated.

I.11 Wings of Ref 10

In this report, four different wings were investigated by using an analogue computer. The details of the wings are given below:

I.11.1 "Basic Fighter A"

b = 17.0 ft (exposed wing semi-span)

c_r = 8.2 ft

λ = 0.54

A.R =

Λ = 0 (40% chord line)

Aerofoil Assumed to be a flat plate

Elastic Axis 0.4c aft of the elastic axis

(b) Inertia

Weight of wing = 2065 lb

Inertia axis = 0.4c aft of wing leading edge

Moment of Inertia of wing = 2100 lb-in^2

(c) Structural

EI = 1.25×10^{10} lb-in^2 (Root) to 0.025×10^{10} lb-in^2 (tip)

GH = 0.33×10^{10} lb-in^2 (Root) to 0.019×10^{10} lb-in^2 (Tip)

ω_{b1} = -

ω_{t1} = -

ω_{b2} = -

(d) Concentrated Mass

Range of spanwise Positions = 0.214 to 1.0

Range of chordwise positions

Mass Ratios $\bar{M}$ = 0 to 4.0

Inertia Ratios: Pitching Radius of Gyration Varied from 6ins. to 30 .

(e) Speed Range:

I.11.2 "Basic Fighter B"

(a) Geometry

b = 19.38 ft (Exposed wing span)

c_r = 8.83 ft

λ = 0.5

Λ = 30°

Aerofoil : Assumed to be a flat plate

Elastic axis : 0.4c aft of the wing leading edge

(b) Inertia

Weight of wing = 2714 lbs.

Inertia axis = 0.4c aft of wing leading edge

Moment of inertia of wing = 2633 lb-in^2

(c) Structural

EI = 0.67×10^{10} lb-in^2 (Root) to 0.065×10^{10} lb-in^2 (Tip)

GJ = 0.27×10^{10} lb-in^2 (Root) to 0.075×10^{10} lb-in^2 (Tip)

ω_{b1} = —

ω_{t1} = —

ω_{b2} = —

(d) Concentrated Mass

Same as for the wing of I.11.1

(e) Speed Range

I.11.3 "Basic Bomber A"

(a) Geometry

b = 70.4 ft

c_r = 16.67 ft

λ = 0.4

A.R. =

Λ = 0

Aerofoil : Flat Plate

Elastic Axis : 0.4c aft of wing leading edge

(b) Inertia

Weight of wing = 7662 lb.

Inertia axis = 0.4c aft of wing leading edge

Moment of inertia of wing = 36 220 lb-in^2

(c) Structural

EI = 10×10^{10} lb-in^2 (Root) to 0.109×10^{10} lb-in^2 (Tip)

G = 3.3×10^{10} (Root) to 0.09×10^{10} lb-in^2 (Tip)

ω_{b1} = —

ω_{t1} = —

ω_{b2} = —

(d) Concentrated Mass

Range of spanwise positions = 0.154 to 1.0

Range of Chordwise positions :

Mass Ratios : $\hat{M}$ = 0 to 4.0

Inertia Ratios Pitching Radius of Gyration = 35 in^2

(e) Speed Range

I.11.4 "Basic Bomber B"

The details of this wing are essentially similar to those of (I.11.3) except that this wing had a sweepback angle of 30°

For all the wings the root degrees of freedom were allowed. The symmetric and anti-symmetric degrees of freedom were allowed separately.

I.12 Wing of Ref 21

This wing is the same as that of Ref 5 (I.2) only one of the weights tested there was investigated by the "exact" analysis of this report.

APPENDIX II

DETAILS OF THE UNIFORM CANTILEVER WINGS AND PODS USED IN THE EXPERIMENTAL THEORETICAL ANALYSES

II.1 Wings

In the early experiments two wings, identical in all details, were built. The first wing was tested in the bare condition and this wing destroyed itself at the flutter speed. When a pod was attached to the second wing, no accurate flutter speed could be obtained as the flutter speeds were too low to be measured in the wind tunnel. In a test on the bare wing, this wing also suffered destruction. These two wings are designated as Wing A1. The details of these wings are given below:

Designation: Wing A1

Weight = 0.369 lb/ft

Pitching Moment of inertia = 0.0056 $lbft^2/ft$ (about the inertia axis)

c.g. location: 0.45c aft of the leading edge

Spar location: 0.35c aft of the leading edge

EI = 66.67 $lbft^2$

GJ = 3.06 $lbft^2$

Aerofoil: NACA 0018

Fundamental bending frequency = 9.5 cps

Fundamental Torsion frequency = 21.5 cps

As a result of the experiments on wing A1, it was decided to replace the wing spar with another spar of greater torsional stiffness. This wing is designated as Wing A2 and the relevant details are given below:

Designation: Wing A2

Weight: 0.396 lb/ft

Pitching Moment of Inertia 0.0066 $lbft^2/ft$ about the inertia axis

c.g. location: 0.35c

Spar location: 0.35c

EI = 51.4 lb ft^2

GJ = ~~5.24~~ 17.1 lb ft^2

Spar Details: Channel Section

Dimensions 0.75in. x 0.292in x 0.125in

Fundamental bending frequency ~~9.06~~ 9.10 cps

Fundamental torsion frequency 35.3 cps

After a series of experiments with Wing A2, it was found that the attachment points on some of the wing sections were deteriorating and it was felt necessary to replace these sections.

For the new sections, it was found difficult to obtain the same inertial properties as for the sections of wing A2. The weight and centre of gravity locations of the wing sections were maintained at the same value as in the case of wing A2, but a pitching moment of inertia of 0.0055 lbft^2/ft was obtained. Details of this wing (Wing A3) are given below:

Designation: Wing A3

Weight: 0.396 lb/ft

Pitching moment of inertia: 0.0055 lbft^2/ft about the inertia axis

c.g. location: 0.45c aft of the wing leading edge

Spar location 0.35c

EI 51.4 lbft^2

GJ ~~5.24~~ 17.1 lbft^2

Spar same as for wing A2

Fundamental bending frequency 9.1 cps

Fundamental torsion frequency 38.9 cps

During the course of the theoretical calculations (by the Direct Matrix Method) it was decided to investigate the influence of the changes in the stiffnesses on the flutter speed. (The other parameters were not altered).

First, only the bending stiffness was changed. This hypothetical wing was designated as Wing B4. This had the sameproperties as wing A3, except that the value of EI was 6.61 lb ft^2 (instead of 51.4 $lbft^2$).

The second hypothetical wing, Wing B5 is similar to wing B4, except that the value of GJ is set to 6.61 $lbft^2$ (instead of 5.24 $lbft^2$).

II.2 Pods

Four pods each having a different aerodynamic shape were used,

Pods A and B were designed so that they had approximately the same cross sectional area distribution along the pod length. Figs. 7.1 and 7.2 are photographs of pod A and B, respectively, and show these pods mounted on the model wing. Fig. 7.4 shows details of pod A and details of pod B are shown in Fig. 7.5.

Pod C was similar to pod A, except that the portion of the pod immediately aft of the wing trailing edge was removed. Thus the pod had a length of only 13.9 ins., compared to 20 ins. for pod A.

Pod D was constructed out of Wood's metal and a photograph of this pod is shown in Fig. 7.3.

II.3 Fins

Some preliminary tests showed that by attaching horizontal fins to the trailing edge of pods A and B, the flutter speeds could be increased.

A systematic study was made to obtain an estimate of the influence of the fins on the flutter speed. For this, five different fins were used. The details of the fins are shown in Fig. 7.5 ~~7.21~~.

The fins were constructed out of sheet balsa and were attached to the pods by balsa cement.

APPENDIX III

Vibration Analysis of Wings with Concentrated Inertias.

The details of the operational method applied to the solution of the vibration problem of uniform beams and shafts with concentrated inertias is given in this appendix. These results were presented as a paper at the 20th Annual Meeting of the Aeronautical Society of India, held in Bangalore, India (3-5 May, 1968).

In this analysis, the basic differential equations of motion of uniform beams and shafts are solved by an operational approach. The details of this method and some results obtained for the vibration frequencies and modes of uniform beams and shafts with concentrated inertias are presented in this appendix.

THE INFLUENCE OF CONCENTRATED INERTIAS ON THE FREE VIBRATIONS OF UNIFORM BEAMS AND SHAFTS †

V. T. NAGARAJ*

Loughborough University of Technology, Loughborough, Leics.

SUMMARY

In part A, an analytical method is developed for determining the natural frequencies and modes of vibration of uniform beams in bending vibrations with a concentrated mass attached at any point along the span. The method makes use of the operational calculus for solving the equations of motion and for obtaining the exact solutions for the natural frequencies and is applicable for uniform beams with any type of end conditions. Numerical results are given for the case of a cantilever beam for a wide range of mass ratios (concentrated mass to beam mass) and for a range of mass positions along the span of 1/4, 1/2, 2/3, 3/4 of the beam span and at the tip. The modes of vibration are obtained for one specific case.

In part B, the method is extended to cover the case of torsional vibrations of a uniform shaft with a discrete inertia at any point along the span. Numerical results are given for a similar range of inertia ratios and locations along the span as in part A.

The case when the mass has a rotary inertia is considered in the Appendix. The frequency equations are derived for a) a uniform cantilever beam and b) for a uniform beam with simply supported ends. For both these cases, the arbitrarily placed mass has also a rotary inertia.

NOTATION

Part A

EI	Bending Stiffness of beam, lb-in^2
L	Length of beam, in.
M	Concentrated Mass, lb-sec^2/in.
mL	Total Mass of beam, lb-sec^2/in.
$\bar{M}$	M/mL
RL	Distance from one end of beam, of Concentrated Mass, in.
T	See Eqn. 2.
t	Time, sec.
X_1, X_2, X_3, X_4	See Eqn. 12.

*Mature Research Student, Department of Transport Technology.

† Paper presented at the 20th Annual Session of the Aeronautical Society of India, 5th May 1968 in Bangalore, India.

y Co-ordinate distance measured along the span, in.

z Lateral deflection of beam, in.

$Z(s)$ Laplace transform of z

αL Frequency Parameter $(m\omega^2 L^4 / EI)^{\frac{1}{4}}$

ω Natural Frequency of the beam, rad/sec.

Part B

GJ Torsional Stiffness of Shaft, lb-in^2.

I Concentrated Moment of Inertia, lb-sec^2.

iL Total Moment of Inertia of Shaft about its Centroidal Longitudinal axis, lb-sec^2.

$\bar{I}$ I/iL

βL Frequency Parameter $(i\omega^2 L^2 / GJ)^{\frac{1}{2}}$

θ Torsional deflection, about the longitudinal axis, rad.

ϕ See Eqn. 16.

Appendix Ig Rotary Inertia of concentrated mass lb-in^2

β $(= I_g / mL^3)$ Non Dimensional Rotary Inertia.

INTRODUCTION

Analyses of the influence of concentrated inertias on the free vibrations of beams and shafts has been reported previously in Refs. (1) to (7). Refs. (1), (2) and (7) refer specifically to cantilever beams (shafts) with additional tip inertias, whereas Refs (3) to (6) also consider the addition of masses at intermediate spanwise stations. These latter references have relied directly on the satisfaction of the governing differential equation for free vibration of uniform beam sections, with the appropriate boundary conditions satisfied at the concentrated mass or inertia.

The present paper presents corresponding results for similar problems using a Laplace Transform technique which is briefly described below. The graphical results obtained for the frequencies of the beams (in bending) and shafts (in torsion) are of course equivalent to those presented earlier, e.g. Refs. 3 and 4. However, it is worth noting that the present technique enables a more precise representation of the general mode shapes for a given problem. Also, as shown in the Appendix, the inclusion of the rotary inertia of the concentrated mass is a relatively easy procedure with this technique.

This general problem can be most conveniently handled by the use of the Laplace Transform (Ref. 8). Briefly, this consists of applying the Laplace

Transform to the equations of motion, using the root conditions and certain other boundary conditions. The resulting system of equations are then solved for the dependent variable and the inversion integral applied to the results. The remaining boundary conditions are then used to set up relations between the undetermined parameters and hence obtain the frequency equation.

In this investigation, the non-dimensional frequency parameter (αL) is obtained as a function of the mass ratio ($\bar{M}$) and the non-dimensional spanwise position of the mass (R). The beam may be supported in any fashion at the ends and the concentrated mass may be located at any point along the span of the beam. The problem solved in Part A is that of a cantilever carrying a concentrated mass (Fig. 1). Numerical results have been obtained using the IBM 1620 computer, for a range of mass ratios ($\bar{M}$) with each mass located successively at R = 1/4, 1/2, 2/3, 3/4 and 1.0. Also, the first four modes of vibration have been obtained for all these spanwise positions for the mass ratios of $\bar{M}$ = 1.0 and 2.0 respectively.

In Part B, the method is extended to cover the case of a uniform cantilever shaft carrying a concentrated inertia (Fig. 2). Numerical results for the frequencies and modes have been obtained for a similar range of inertia ratios and positions.

It may be of interest to mention the need for this study. The main problem was the determination of the flutter speed and frequency of a uniform wing carrying a pod of appreciable mass and of a very large mass moment of inertia (in the pitch sense) compared to the values of the basic wing. The modes and frequencies obtained in this study have been used to set up the flutter determinant by the 'assumed mode' method.

Though the analysis is carried out only for the case of a uniform cantilever beam, the procedure is quite general and can be applied for uniform beams with any type of end conditions.

Using this, equation (3b) becomes:

$$EI\left[S^4\bar{z}(s) - s^3 z(0) - s^2 z'(0) - s\,z''(0) - z'''(0) - e^{-SRL}\left\{z'''(RL_+) - z'''(RL_-)\right\}\right] - m\omega^2\bar{z}(s) = 0 \tag{5}$$

where the primes indicate differentiation with respect to y.

Let

$$\alpha^4 = m\omega^2/EI \tag{6}$$

Solving equation (5) for $\bar{z}(s)$,

$$\bar{z}(s) = \frac{\left[s^3 z(0) + s^2 z'(0) + s\,z''(0) + z'''(0) + e^{-SRL}\left\{z'''(RL_+) - z'''(RL_-)\right\}\right]}{(s^4 - \alpha^4)} \tag{7}$$

For a uniform cantilever carrying a point mass as in Fig. (1), the boundary conditions are:

At y = 0

$$z(0) = 0 \quad , \quad z'(0) = 0 \tag{8}$$

At y = L

$$z''(L) = 0 \quad , \quad z'''(L) = 0 \tag{8a}$$

At y = RL

$$EI\left\{z'''(RL_-) - z'''(RL_+)\right\} = -M\omega^2 z(RL) \tag{9}$$

In view of the boundary conditions at y = 0 the first two terms on the right hand side of equation (7) vanish. If we now use the last condition (at y = RL) and apply the inverse transform, we have:

$$z(y) = \frac{z''(0)}{2\alpha^2}(\cosh\alpha y - \cos\alpha y) + \frac{z'''(0)}{2\alpha^3}(\sinh\alpha y - \sin\alpha y) + \left\{\sinh\alpha(y-RL) - \sin\alpha(y-RL)\right\}\left\{\frac{M}{2}\alpha L\, z(RL)\right\} \tag{10}$$

In equation (10) it should be remembered that the last term vanishes for $y \leq RL$.

The value for z at y = RL can be obtained from equation (10) itself. If we now use the second set of boundary conditions (for y = L) we obtain two homogeneous equations for $\left[z''(o)/_{2\alpha^2}\right]$ and $\left[z'''(0)/2\alpha^3\right]$. The condition that these should yield nontrivial solutions leads us to the frequency determinant:

$$\begin{vmatrix} X_1 & X_2 \\ X_3 & X_4 \end{vmatrix} = 0 \qquad (11)$$

where

$$X_1 = \cosh \alpha L + \cos \alpha L + \frac{\bar{M}}{2} \alpha L \cdot \{\sinh \alpha(L-RL) + \sin \alpha(L-RL)\} (\cosh \alpha RL - \cos \alpha RL$$

$$X_2 = \sinh \alpha L + \sin \alpha L + \frac{\bar{M}}{2} \alpha L \{\sinh \alpha(L-RL) + \sin \alpha(L-RL)\} (\sinh \alpha RL - \sin \alpha RL)$$

$$X_3 = \sinh \alpha L - \sin \alpha L + \frac{\bar{M}}{2} \alpha L \{\cosh \alpha(L-RL) + \cos \alpha(L-RL)\} (\cosh \alpha RL - \cos \alpha RL$$

$$X_4 = \cosh \alpha L + \cos \alpha L + \frac{\bar{M}}{2} \alpha L \cdot \{\cosh \alpha(L-RL) + \cos \alpha(L-RL)\} (\sinh \alpha RL - \sin \alpha R$$

(12)

In equation (10) the fact that $(M\omega^2 / EI.\alpha^3) = \bar{M}.\alpha L$ has been used.

As a check on equation (11) the limiting cases will be considered. For either R = 0 or $\bar{M}$ = 0, i.e. for a bare cantilever, equation (11) becomes the familiar equation:

$$1 + \cosh \alpha L . \cos \alpha L = 0 \qquad (13)$$

For R = 1.0, i.e. for a cantilever with the mass at the tip, equation (11) becomes:

$$\bar{M} = \frac{1 + \cosh \alpha L \cos \alpha L}{\alpha L [\sin \alpha L \cosh \alpha L - \sinh \alpha L \cos \alpha L)} \qquad (14)$$

which is the same as the one obtained by Pipes (Ref.2).

Solutions were obtained for Eqn. (11) using an IBM 1620 digital computer for a cantilever beam with the following combinations of R and $\bar{M}$. R = ~/4, 1/2, 2/3, 3/4 and 1.0 and for each R, $\bar{M}$ was varied from 0 to 50. These are presented in Table 1 and Fig. 3.

As an approximate check on the frequency parameters (αL) they were compared with values obtained from a Rayleigh analysis for a similar beam. As can be seen from Table 1, these values are in close agreement with the exact values.

The mode shape used in the Rayleigh analysis was:

$$Z = Z_0 \left(1 - \cos \frac{\pi}{2} \frac{y}{L}\right)$$

In Fig. 3, the values of $\bar{M}$ are plotted on a logarithmic scale and those of αL on a linear scale. For $\bar{M} = 0$, the fundamental frequency is equal to 1.8751 and the first overtone is equal to 4.6941 for all values of R.

PART B. TORSIONAL FREQUENCIES

The analysis of the torsional vibrations of a shaft carrying a discrete Moment of Inertia follows the same lines as in Part A. Again, though the analysis is presented for the case of a uniform cantilever shaft, it is equally applicable to a uniform shaft with any set of end conditions.

Subject to the usual assumptions, the equation of motion of a uniform shaft such as the one in Fig. 2, is (*Ref.* 5):

$$i. \frac{\partial^2 \phi}{\partial t^2} - GJ \frac{\partial^2 \phi}{\partial y^2} = 0 \qquad (15)$$

where $\phi = \phi(y, t)$

If we put $\phi(y,t) = \theta(y).T(t)$ (15a)

in Eqn. (15), we obtain the two equations: (16)

$$d^2T/dt^2 + \omega^2 T = 0 \qquad (17a)$$

$$d^2\theta/dy^2 + \frac{\omega^2}{a^2}\theta = 0$$

In Eqn. (17b), $a^2 = (GJ/i)$ (17b)

Using the relation (4), and applying the Laplace Transform to Eqn. (17b), (18)
we obtain for $\bar{\theta}(s)$,

$$\bar{\theta}(s) = \left(\frac{1}{s^2+\beta^2}\right)\left[s.\theta(0) + \theta'(0) + e^{-sRL}\{\theta'(RL_+) - \theta'(RL_-)\}\right] \qquad (19)$$

where

$$\beta^2 = \frac{\omega^2}{a^2} = \frac{i\omega^2}{GJ} \qquad (20)$$

The boundary conditions on the cantilever shaft of Fig. (2) are:

At $y = 0$ $\quad \theta = 0$

At $y = L$ $\quad \theta' = 0$

At $y = RL$ $\quad GJ\{\theta'(RL_-) - \theta'(RL_+)\} = I\omega^2\theta(RL)$ (21)

In view of the first and the last boundary conditions, Eqn. (19) becomes:

$$\bar{\theta}(s) = \frac{\theta'(0)}{s^2+\beta^2} - \frac{e^{-sRL}}{s^2+\beta^2}\,\frac{I\omega^2}{GJ}\,\theta(RL) \qquad (22)$$

Applying the inverse transform:

$$\theta(y) = \frac{\theta'(0)}{\beta}\sin\beta y - \frac{I\omega^2}{GJ\beta}\,\theta(RL)\cdot\sin\beta(y-RL) \qquad (23)$$

It should be remembered that in Eqn. (23) the last term vanishes for $y \leq RL$.

If we now substitute for θ at $y = RL$, and use the second boundary condition, we obtain the frequency equation:

$$\frac{I}{iL} = (\cos\beta L) \Big/ \{\beta L \cdot \sin\beta RL \cdot \cos\beta(L-RL)\} \qquad (24)$$

In Eqn. (24), use is made of the fact that

$$\frac{I\omega^2}{GJ\beta} = \frac{I}{iL}\,\beta L \qquad (25)$$

From Eqn. (24) one can easily derive the equations for the simpler cases. For example, for $R = 0$, (or $\bar{I} = 0$) i.e., for a uniform shaft, the frequency equation is:

$$\cos\beta L = 0 \qquad (26)$$

For a uniform shaft with an Inertia at the tip, i.e. for $R = 1$,

$$(I/iL) = 1/\beta L.\tan\beta L \qquad (27)$$

Solutions to equation (24) have been obtained for the following combinations of R and $\bar{I}$: $R = 1/4,\ 1/3,\ 1/2,\ 2/3,\ 3/4$, and 1.0. For each R, $\bar{I}$ was varied from 0 to 50. These are presented in Table 2 and Figure 4.

The frequencies were also checked by a Rayleigh analysis. These are also shown in Table 2 [illegible] and it can be seen that the agreement between the two sets of frequency parameters is quite close. The mode shape used for the Rayleigh analysis was:

$$\Theta = \sin \frac{\pi}{2} \frac{y}{L}$$

PART C. MODE SHAPES

a) BENDING: Once the values of αL are obtained for a given beam, Eqn. (10) provides a convenient means of obtaining the corresponding mode shape. While evaluating the mode shape, it should be remembered that the last term should be set to zero for values of $y \leq RL$.

Fig. 5 shows the mode shapes for a uniform cantilever beam with $\bar{M} = 1.0$, and for values of R ranging from 0 to 1.0. The first four natural modes are presented for each case. Even for this value of $\bar{M}$, the influence of the concentrated mass on the mode shape is quite considerable.

b) TORSION: Eqn. (23) is used for obtaining the torsional modes. Fig. 6 shows the mode shapes for values of R from 0 to 1.0. For all these inertia locations, $\bar{I} = 10.0$. The first four modes are shown for each case. The influence of the concentrated inertia is even more pronounced than in the corresponding case for the beam vibrations, mainly due to the high value of the concentrated inertia. The mode shapes for R = 2/3 are of particular interest from the flutter point of view. For a uniform shaft, this station is a node for the first overtone mode, and the placing of a concentrated inertia here does not influence the frequency parameter. The frequency parameter has its maximum value when the inertia is placedhere. These considerations suggest that the best location for a concentrated inertia is at 2/3rds., the span from the root in order to obtain the most favourable influence on the flutter speed.

(In the torsion mode shapes, some of the overtone modes are shown as having zero amplitudes. This is not strictly correct, but the amplitudes are so small that they cannot be shown to scale in the graphs.)

CONCLUSIONS

The method presented above for the analysis of vibrations of uniform beams is seen to be versatile and can be applied to beams with any general boundary conditions. In the main text only the vibrations of a uniform cantilever beam with a point mass and the vibrations of a uniform cantilever shaft with an arbitrary placed inertia have been considered. In the appendix, the case when the concentrated mass has a rotary inertia has been solved for a uniform cantilever beam and for a simply supported beam. In both these cases, the mass can be placed arbitrarily at any point along the span.

Some of the problems which can be solved by applying this method are:

i) Beams with different boundary conditions (fixed-fixed, free-free, hinged-free flexibly supported ends etc.)

ii) Beams carrying more than one concentrated mass (or concentrated mass with rotary inertia)

iii) Beams carrying flexibly mounted masses

iv) Beams with uniformly varying cross sections

and v) Coupled vibrations of uniform wings carrying a mass (with rotary inertia).

The mass (or masses) could be at any arbitrary position along the span and its static unbalance can be arbitrary.

(In solving the last problem (coupled vibrations of wings) it will not, in general, be possible to obtain closed form solutions for the frequencies as the inversion for the mode shape function has to be done by a series approximation.)

It is also worth noting that the mode shape of the beam with a given mass can be obtained concisely as part of the calculation.

REFERENCES

1. PIPES, L.A. "Applied Mathematics for Engineers and Physicists" (Mc.Graw-Hill Book Co., N.Y., 1958) p. 263

2. BISPLINGHOFF, R.L. ASHLEY, H. HALFMANN, R.L. "Aeroelasticity" (Addison-Wesley Publishing Co., Inc.Camb.Mass., 1955) p.98

3. MALTBAEK, J.C. "The Influence of a Concentrated Mass on the Free Vibrations of a Uniform Beam", International Journal of Mechanical Sciences, Pergamon Press Ltd., 1961, Vol. 3 pp 197-218

4. MALTBAEK, J.C. "The Influence of a Discrete Inertia on the Free Torsional Vibrations of a Uniform Bar", International Journal of Mechanical Sciences, Pergamon Press Ltd., Vol. 4, 1962, pp 25-34

5. SRINATH, L.S.
DAS, Y.C.
"Vibrations of Beams Carrying Mass"
Journal of Applied Mechanics, Vol. 34, 1967,
pp 784-785

6. YOSHIMURA, J.
HAMAYOSHI, F.
"Exact Solutions of the Free Lateral Vibration Period of Beams Subjected to a Concentrated Load and a Full Uniform Load Simultaneously", Memoirs of the Faculty of Engineering of Hokkaido University, Vol. 10, 1958, pp 505-521.

7. DURVASULA, S.
"Vibrations of a Uniform Cantilever Beam Carrying a Concentrated Mass and Moment of Inertia at the Tip", Journal of the Aeronautical Society of India, 1966, Vol. 18, No. 1, pp 17-25

8. RUNYAN, H.L.
WATKINS, C.E.
"Flutter of a uniform Wing with an Arbitrarily Placed Mass According a Differential Equation Analysis and a Comparison with Experiment", NACA Report No. 966, 1950.

9. CHURCHILL, R.
"Modern Operational Mathematics in Engineering"
(McGraw-Hill Book Co., N.Y., 1944) p 7.

THE INFLUENCE OF THE ROTARY INERTIA OF A DISCRETE MASS ON UNIFORM BEAM VIBRATIONS

In the main text, the concentrated mass was treated as being with no rotary inertia(i.e., a point mass). In order to assess the influence of the rotary inertia, we follow the same procedure as in the main text, except that we now have to take into account one more discontinuity (in the bending moment).

In this appendix, the vibrations of a uniform beam with a discrete mass (a concentrated mass which has a rotary inertia) will be considered. The mass can be attached at any point along the beam span and the end conditions can be arbitrary.

Neglecting the rotary inertia of the beam sections in comparison with the other terms, the equation of motion is the same as Eqn.(3a) of the main text,i.e.,

$$EI \frac{d^4 z}{dy^4} - m\omega^2 z = 0 \qquad (3.a)$$

If we take the Laplace Transform of this equation,remembering that we now have a discontinuity in the second derivative of z as well as in the third derivative, and solve for $\bar{z}(s)$, we get

$$\bar{z}(s) = \frac{1}{(s^4 - \alpha^4)} \Big[s^3 z(0) + s^2 z'(0) + s\, z''(0) + z'''(0) + e^{-sRL}\{ z'''(RL+) - z'''(RL-)\} + e^{-sRL}\, s\, \{ z''(RL+) - z''(RL-)\} \Big] \qquad (A.1)$$

Equation (A.1) is the starting point in the analysis for uniform beams with any type of end conditions. Two cases will now be considered: a) A uniform cantilever beam and b) a uniform simply supported beam, each carrying a discrete mass placed

arbitrarily along their spans.

a) UNIFORM CANTILEVER BEAM.

The boundary conditions for this beam are (Fig. A.1)

$$\begin{aligned} &\text{At } y = 0 && z(0) = z'(0) = 0 \\ &y = L && z''(L) = z'''(L) = 0 \\ &y = RL && EI\,[z'''(RL-) - z'''(RL+)] = -M\omega^2 z(RL) \\ & && EI\,[z''(RL-) - z''(RL+)] = I_g \omega^2 z'(RL) \end{aligned} \tag{A.2}$$

If we now make use of the symbols

$$\bar{M} = M/mL \,, \quad \beta = I_g/mL^3 \tag{A3}$$

the boundary conditions can be written as:

$$\begin{aligned} &z(0) = z'(0) = 0 \quad ; \quad z''(L) = z'''(L) = 0 \\ &\{z'''(RL+) - z'''(RL+)\} = -\bar{M}\cdot\alpha^4 L.\, z(RL) \\ &\{z''(RL-) - z''(RL+)\} = \beta.\,\alpha^4 L^3.\, z'(RL) \end{aligned} \tag{A.4}$$

Using the conditions at $y = 0$ abd at $y = RL$ in Eqn.(A.1) and applying the inverse transform, we obtain the mode shape as:

$$\begin{aligned} z(y) = {} & \frac{z''(0)}{2\alpha^2}(\cosh\alpha y - \cos\alpha y) + \frac{z'''(0)}{2\alpha^3}(\sinh\alpha y - \sin\alpha y) \\ & + \tfrac{1}{2}\bar{M}\,\alpha L.\, z(RL)\,\{\sinh\alpha(y-RL) - \sin\alpha(y-RL)\} \\ & - \tfrac{\beta}{2}.\,\alpha^2 L^3.\, z'(RL)\,\{\cosh\alpha(y-RL) - \cos\alpha(y-RL)\} \end{aligned} \tag{A.5}$$

In Eqn.(A.5), it should be remembered that the last two terms vanish for $y \leq RL$.

The values of $z(RL)$ and $z'(RL)$ can be obtained from Eqn.(A.5) itself. If we now use the boundary conditions at the tip ($y = L$) we obtain two homogeneous equations for $(z''(0)/2\alpha^2)$ and $(z'''(0)/2\alpha^3)$. The condition that these should yield nontrivial solutions leads to the frequency equation:

$$\begin{vmatrix} X_5 & X_6 \\ X_7 & X_8 \end{vmatrix} = 0 \tag{A.6}$$

where:

$$X_5 = (\cosh\alpha L + \cos\alpha L) + \frac{\bar{M}}{2}\cdot\alpha L\cdot[\sinh\alpha(L-RL) + \sin\alpha(L-RL)](\cosh\alpha RL - \cos\alpha RL)$$
$$- \frac{\beta}{2}\cdot(\alpha L)^3\cdot[\cosh\alpha(L-RL) + \cos\alpha(L-RL)](\sinh\alpha RL + \sin\alpha RL)$$

$$X_6 = (\sinh\alpha L + \sin\alpha L) + \frac{\bar{M}}{2}\cdot\alpha L\cdot[\sinh\alpha(L-RL) + \sin\alpha(L-RL)](\sinh\alpha RL - \sin\alpha RL)$$
$$- \frac{\beta}{2}\cdot(\alpha L)^3\cdot[\cosh\alpha(L-RL) + \cos\alpha(L-RL)](\cosh\alpha RL - \cos\alpha RL)$$

$$X_7 = (\sinh\alpha L - \sin\alpha L) + \frac{\bar{M}}{2}\alpha L[\cosh\alpha(L-RL) + \cos\alpha(L-RL)](\cosh\alpha RL - \cos\alpha RL)$$
$$- \frac{\beta}{2}\cdot(\alpha L)^3\cdot[\sinh\alpha(L-RL) - \sin\alpha(L-RL)](\sinh\alpha RL + \sin\alpha RL)$$

$$X_8 = (\cosh\alpha L + \cos\alpha L) + \frac{\bar{M}}{2}\alpha L[\cosh\alpha(L-RL) + \cos\alpha(L-RL)](\sinh\alpha RL - \sin\alpha$$
$$- \frac{\beta}{2}\cdot(\alpha L)^3[\sinh\alpha(L-RL) - \sin\alpha(L-RL)](\cosh\alpha RL - \cos\alpha R$$

(A.7)

As a check on Eqn.(A.6), when $\bar{M} = \beta = 0$ i.e., a uniform cantilever beam, we get the familiar equation

$$1 + \cosh\alpha L\cos\alpha L = 0 \qquad (A.8)$$

When only $\beta = 0$, we get Eqn.(11) of the main text.

When $R = 1$ i.e., the mass is at the tip, we get:

$$(1 + \bar{M}\beta\alpha^4L^4) + \cosh\alpha L\cos\alpha L(1 - \bar{M}\beta\alpha^4L^4)$$
$$+ \bar{M}\cdot\alpha L\cdot(\cos\alpha L\sinh\alpha L - \cosh\alpha L\sin\alpha L)$$
$$- \beta\cdot\alpha^3L^3\cdot(\sinh\alpha L\cos\alpha L + \cosh\alpha L\sin\alpha L) = 0 \qquad (A.9)$$

This is the same equation as the one obtained by Durvasula (Eqn.11 of Ref.7).

b) UNIFORM SIMPLY SUPPORTED BEAM

The boundary conditions for this beam are (Fig.A.2)

$$\left.\begin{aligned} Z(0) &= Z''(0) = 0 \\ Z(L) &= Z''(L) = 0 \\ \{Z'''(RL-) - Z'''(RL+)\} &= -\bar{M}\alpha^4L\,Z(RL) \\ \{Z''(RL-) - Z''(RL+)\} &= \beta\alpha^4L^3\,Z'(RL) \end{aligned}\right\} \qquad (A.10)$$

Following a procedure similar to that outlined for the cantilever beam, we obtain the mode shape as:

$$Z(y) = \frac{Z'(0)}{2\alpha}\left(\sinh \alpha y + \sin \alpha y\right) + \frac{Z'''(0)}{2\alpha^3}\left(\sinh \alpha y - \sin \alpha y\right)$$
$$+ \frac{\overline{M}}{2}\alpha L \cdot Z(RL)\left\{\sinh \alpha (y-RL) - \sin \alpha (y-RL)\right\}$$
$$- \frac{\beta}{2}\cdot (\alpha L)^3 \cdot Z'(RL)\left\{\cosh \alpha (y-RL) - \cos \alpha (y-RL)\right\} \qquad (A.11)$$

and the frequency determinant as:

$$\begin{vmatrix} X_9 & X_{10} \\ X_{11} & X_{12} \end{vmatrix} = 0 \qquad (A.12)$$

where:

$$X_9 = (\sinh \alpha L + \sin \alpha L) + \frac{\overline{M}}{2}\cdot \alpha L \cdot \left[\sinh \alpha (L-RL) - \sin \alpha (L-RL)\right](\sinh \alpha RL + \sin \alpha RL)$$
$$- \frac{\beta}{2}\cdot (\alpha L)^3 \left[\cosh \alpha (L-RL) - \cos \alpha (L-RL)\right](\cosh \alpha RL + \cos \alpha RL)$$

$$X_{10} = (\sinh \alpha L - \sin \alpha L) + \frac{\overline{M}}{2}\cdot \alpha L \cdot \left[\sinh \alpha (L-RL) - \sin \alpha (L-RL)\right](\sinh \alpha RL - \sin \alpha RL)$$
$$- \frac{\beta}{2}\cdot (\alpha L)^3 \cdot \left[\cosh \alpha (L-RL) - \cos \alpha (L-RL)\right](\cosh \alpha RL - \cos \alpha RL)$$

$$X_{11} = (\sinh \alpha L - \sin \alpha L) + \frac{\overline{M}}{2}\alpha L \left[\sinh \alpha (L-RL) + \sin \alpha (L-RL)\right](\sinh \alpha RL + \sin \alpha RL)$$
$$- \frac{\beta}{2}(\alpha L)^3 \left[\cosh \alpha (L-RL) + \cos \alpha (L-RL)\right](\cosh \alpha RL + \cos \alpha RL)$$

$$X_{12} = (\sinh \alpha L + \sin \alpha L) + \frac{\overline{M}}{2}\alpha L \left[\sinh \alpha (L-RL) + \sin \alpha (L-RL)\right](\sinh \alpha RL - \sin \alpha RL)$$
$$- \frac{\beta}{2}(\alpha L)^3 \left[\cosh \alpha (L-RL) + \cos \alpha (L-RL)\right](\cosh \alpha RL - \cos \alpha RL) \qquad (A.13)$$

As a check on Eqn (A.12), when $\overline{M} = \beta = 0$, i.e., for a uniform beam, we have

$$\sin \alpha L = 0 \qquad (A.14)$$

When only $\beta = 0$, i.e., when we have a concentrated (point) mass with no rotary inertia, we have

$$\overline{M} = \frac{2}{\alpha L\left[\left(\frac{\sin \alpha (L-RL)\,\sin \alpha RL}{\sin \alpha L}\right) - \left(\frac{\sinh \alpha (L-RL)\,\sinh \alpha RL}{\sinh \alpha L}\right)\right]} \qquad (A.15)$$

which is the same equation (but in a different notation)

as that obtained by Malmbaek (Eqn.19 of Ref.3)

When Eqn.(A.13) is expanded, we get an equation which is the same (allowing for differences in notation) as that obtained by Srinath and Das (Eqn.10 of Ref.5).

Frequency equations and mode shapes for uniform beams with other types of boundary conditions can be obtained in a similar way.

Table 1 Values of $\alpha_1 L$ for Cantilever Banding

a) Fundamental Mode Frequencies

β \ λ	0		0.25		0.50		0.67		0.75		1.00	
	Exact	Rayleigh	Exact	Rayleigh	Exact	Rayleigh	Exact	Rayleigh	Exact	Rayleigh	Exact	Rayleigh
0.5			1.8662	1.910	1.7784	1.832	1.6665	1.715	1.6041	1.647	1.4200	1.428
1.0			1.8573	1.902	1.7004	1.769	1.5378	1.590	1.4580	1.499	1.2479	1.256
2.0			1.8361	1.889	1.5812	1.660	1.3782	1.430	1.2882	1.321	1.0761	1.084
5.0			1.7868	1.860	1.3709	1.470	1.1492	1.199	1.0628	1.092	0.8702	0.872
10.0		1.914	1.7048	1.810	1.1950	1.292	0.9839	1.030	0.9056	0.950	0.7382	0.739
25.0			1.6329	1.768	1.0939	1.190	0.8946	0.935	0.8220	0.840	0.6662	0.668
50.0			1.5712	1.728	1.0248	1.119	0.8352	0.874	0.7668	0.790	0.6205	0.622
100.0			1.5181	1.695	0.9732	1.063	0.7914	0.815	0.7262	0.747	0.5872	0.588
∞			1.3358	1.560	0.8252	0.906	0.6681	0.692	0.6124	0.630	0.4944	0.495

Table 1 cont. b) First Overtone Frequency

M \ R	0	0.25	0.50	0.67	0.75	1.00
	Exact	Exact	Exact	Exact	Exact	Exact
0.50	↑	4.3206	4.0327	4.4513	4.6701	4.1111
1.00		4.0360	3.7717	4.3550	4.6608	4.0311
2.00		3.6594	3.5399	4.2710	4.6530	3.9899
5.00		3.1356	3.3304	4.2006	4.6458	3.9500
10.00	4.6941	2.8085	3.2422	4.1716	4.6429	3.9384
15.00		2.6645	3.2099	4.1611	4.6419	3.9346
20.00		2.5857	3.1941	4.1557	4.6413	3.9323
25.00		2.5332	3.1834	4.1524	4.6410	3.9314
50.00	↓	2.4288	3.1627	4.1457	4.6404	3.9290

Table 2 Values of βL for Torsional Vibration

a) FUNDAMENTAL

J \ R	0		0.25		0.33		0.50		0.67		0.75		1.00	
	Exact	Rayleigh	Exact	Rayleigh	Exact	Rayleigh	Exact	Rayleigh	Exact	Rayleigh	Exact	Rayleigh	Exact	Rayleigh
0.50	↑		1.4510	1.4671	1.3840	1.4050	1.2646	1.2825	1.1766	1.1874	1.1432	1.1538	1.0769	1.0[illegible]
1.00			1.3329	1.3794	1.2302	1.2825	1.0769	1.1107	0.9761	0.9934	0.9386	0.9547	0.8703	0.9[illegible]
2.00			1.1376	1.2474	1.0169	1.1107	0.8603	0.9069	0.7644	0.7854	0.7291	0.8507	0.6933	0.7[illegible]
5.00			0.8203	1.0007	0.7174	0.8396	0.5932	0.6413	0.5192	0.5388	0.4922	0.5087	0.4388	0.4[illegible]
10.00	1.5709	1.5708	0.6061	0.7926	0.5271	0.6413	0.4329	0.4736	0.3768	0.3927	0.3563	0.3695	0.3113	0.3[illegible]
15.00			0.5022	0.6765	0.4370	0.5388	0.3581	0.3927	0.3106	0.3240	0.2940	0.3045	0.2540	0.2[illegible]
20.00			0.4379	0.5999	0.3800	0.4736	0.3110	0.3428	0.2701	0.2821	0.2553	0.2650	0.2218	0.2[illegible]
25.00			0.3933	0.5446	0.3412	0.4275	0.2791	0.3080	0.2423	0.2532	0.2287	0.2377	0.1987	0.2[illegible]
30.00	↓		0.2805	0.3972	0.2432	0.3080	0.1987	0.2200	0.1772	0.1802	0.1625	0.1690	0.1406	0.1[illegible]

Table 2 Values of βL for Torsion

b) FIRST OVERTONE

$\bar{I}$ \ R	0	0.25	0.33	0.50	0.67	0.75	1.00
	Exact	Exact	Exact	Exact	Exact	Exact	Exact
0.50	↑	3.3281	3.3862	3.9352	↑	4.4916	3.6436
1.00		2.8218	2.9685	3.6436		4.3968	3.4256
2.00		2.4639	2.6802	3.4256		4.3154	3.2940
5.00		2.2333	2.4860	3.2636		4.2467	3.2039
10.00	4.7124	2.1612	2.4207	3.2039	4.7124	4.2191	3.1731
15.00		2.1383	2.3990	3.1837		4.2094	3.1628
20.00		2.1270	2.3882	3.1731		4.2043	3.1574
25.00		2.1204	2.3806	3.1668		4.2013	3.1543
50.00	↓	2.1073	2.3678	3.1543	↓	4.1951	3.1480

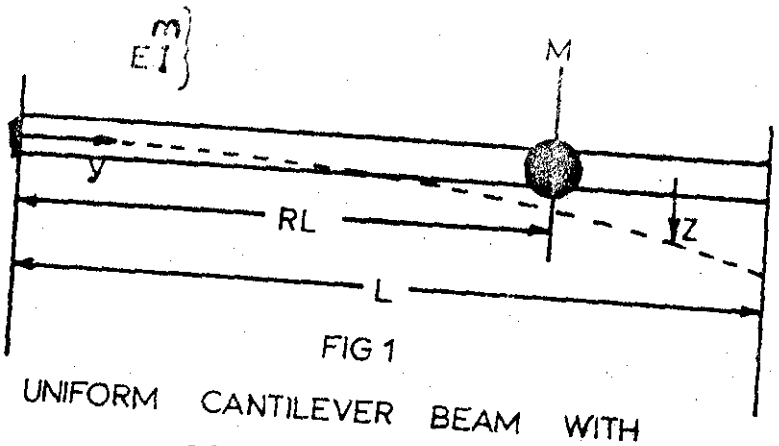

FIG 1

UNIFORM CANTILEVER BEAM WITH CONCENTRATED MASS

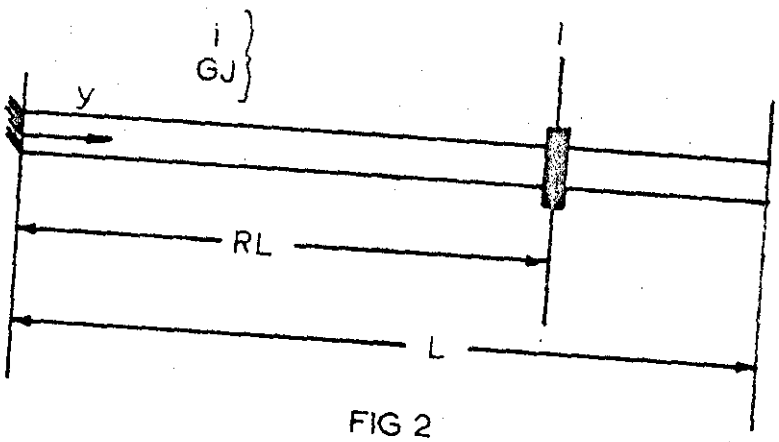

FIG 2

UNIFORM CANTILEVER SHAFT WITH CONCENTRATED INERTIA

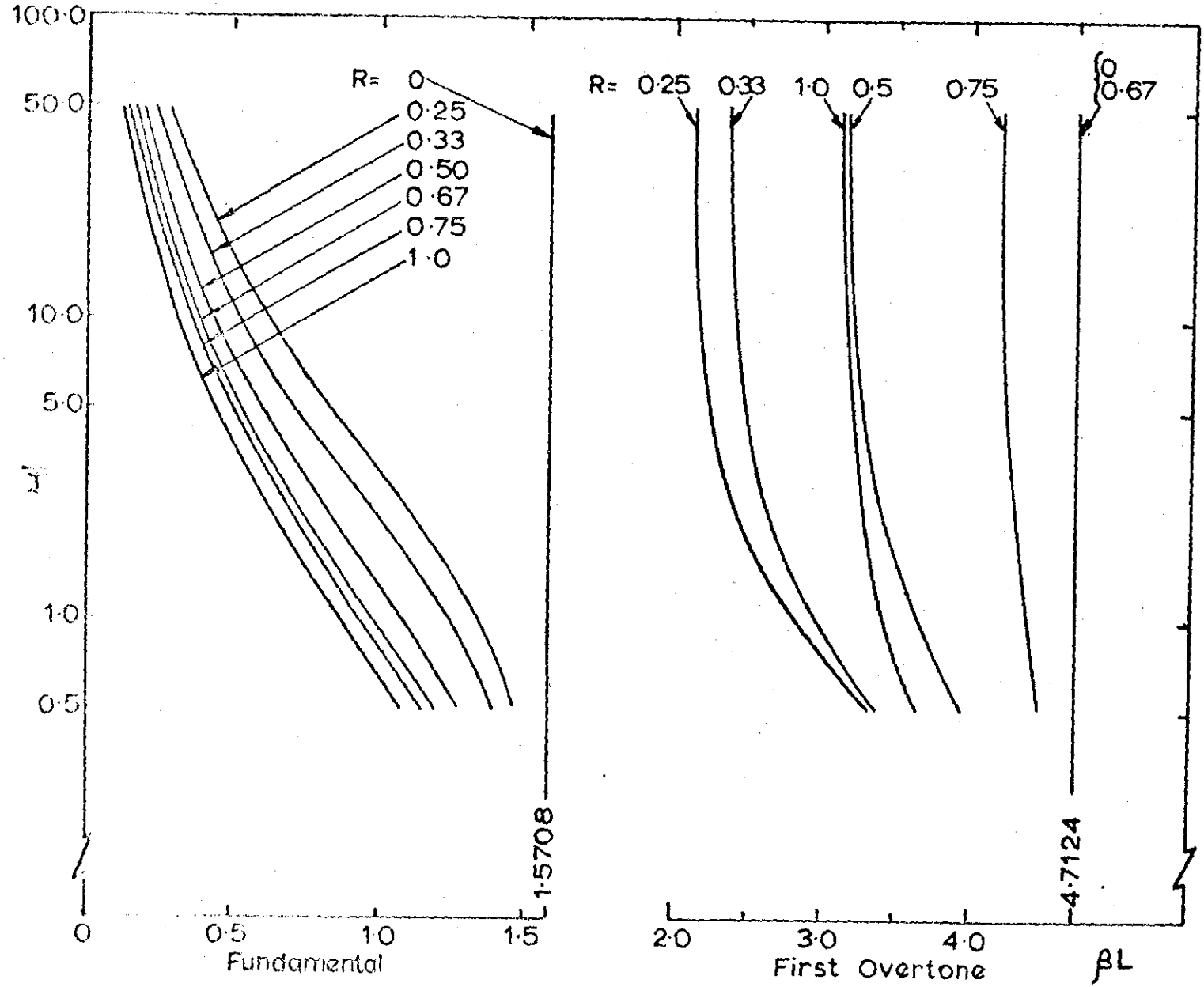

FIG. 4. TORSIONAL FREQUENCIES

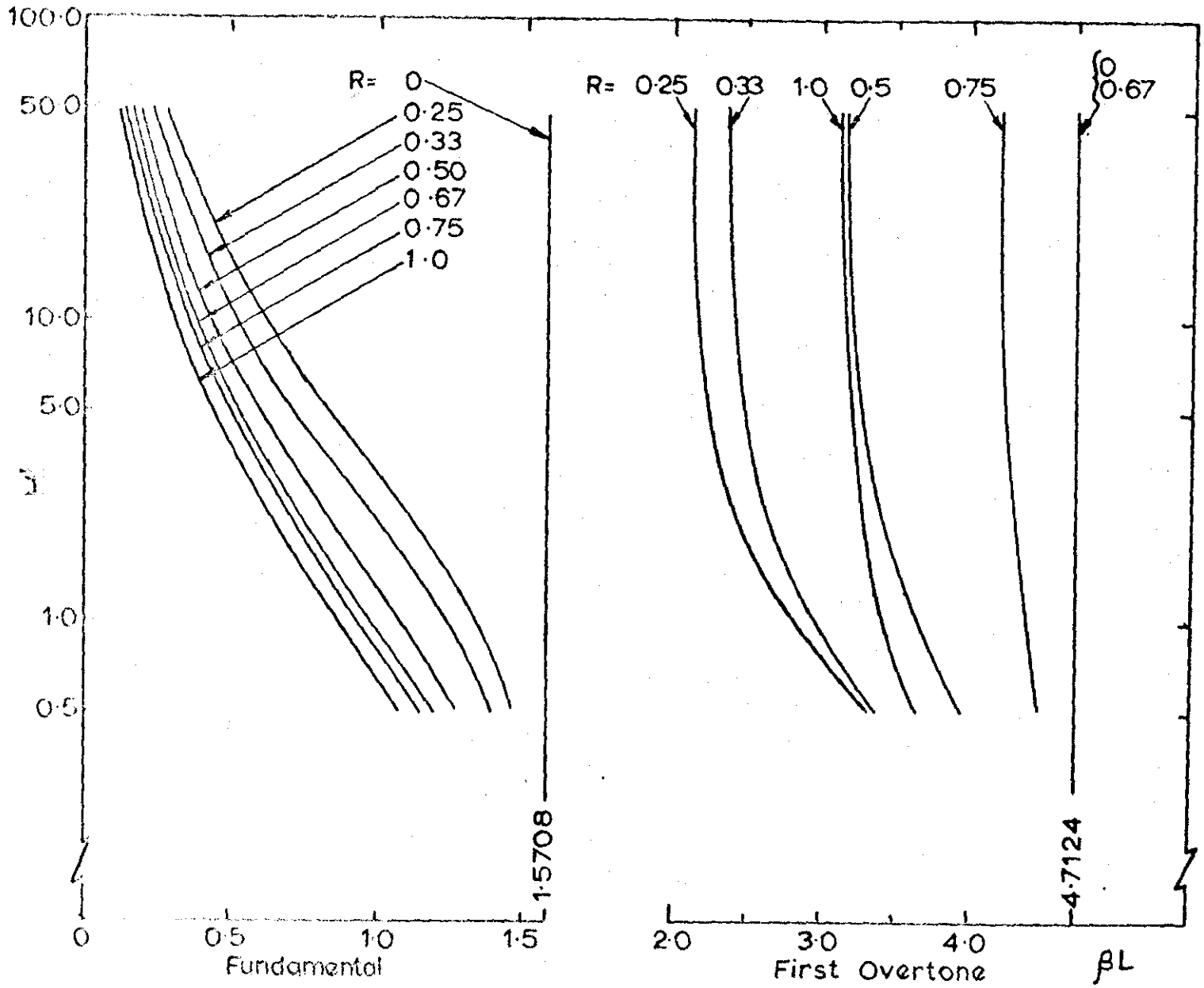

FIG. 4. TORSIONAL FREQUENCIES

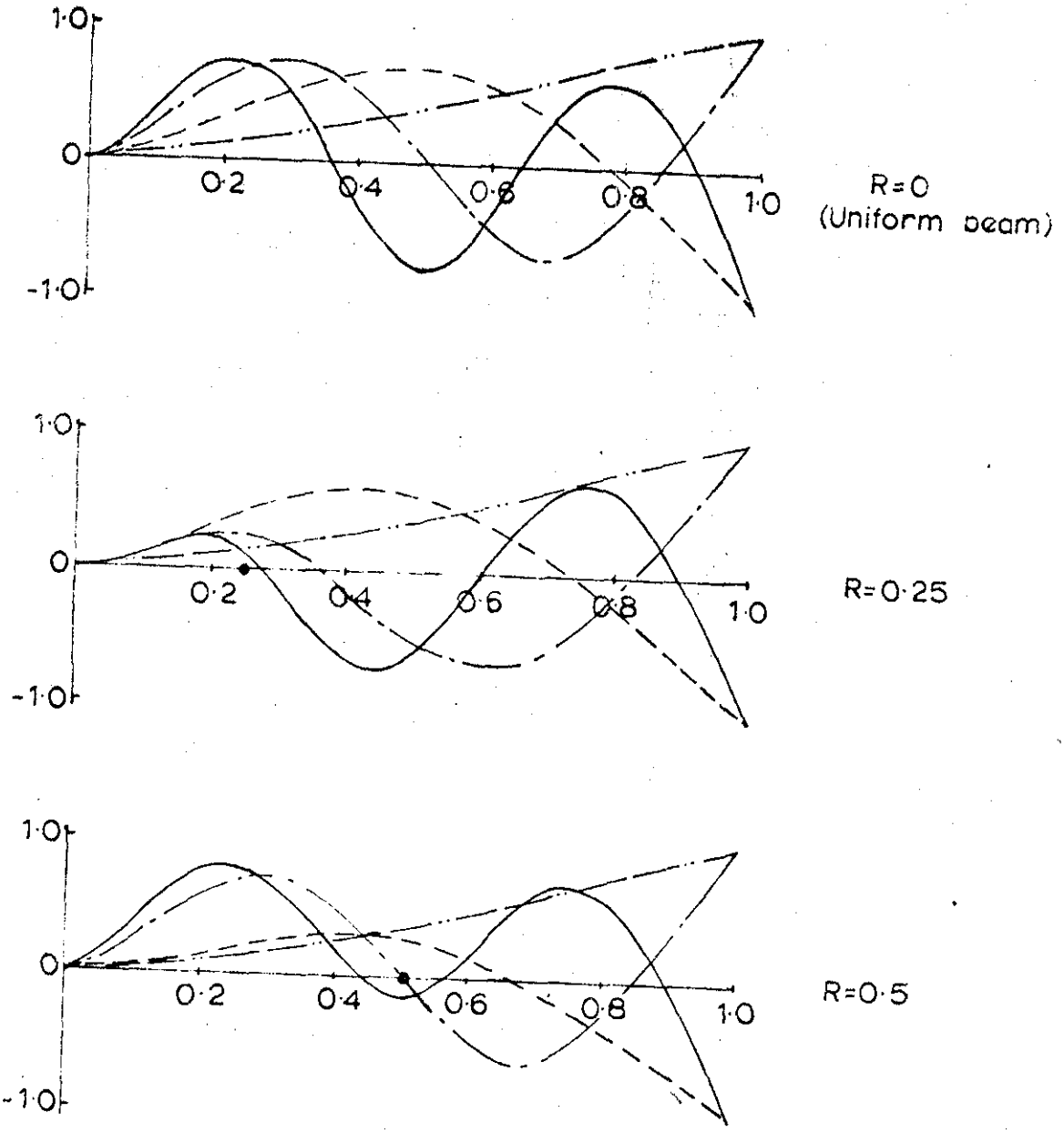

Fig.5.
FIRST FOUR NATURAL MODES OF A UNIFORM BEAM, WITH $\bar{M} = 1{\cdot}0$.

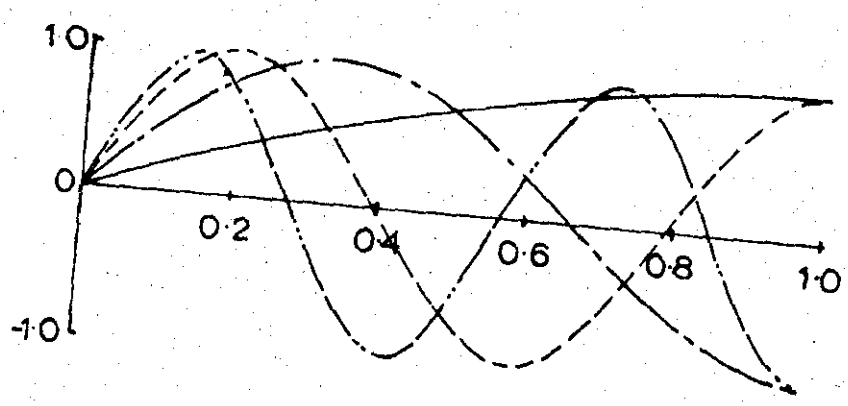

R=0
(Uniform shaft)

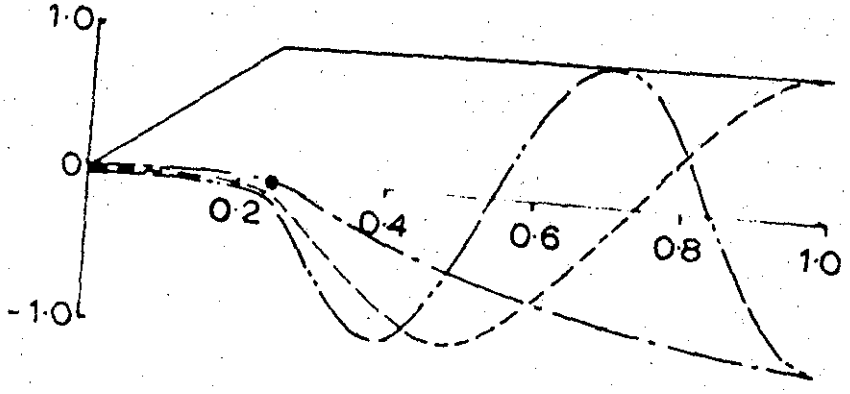

R=0·25

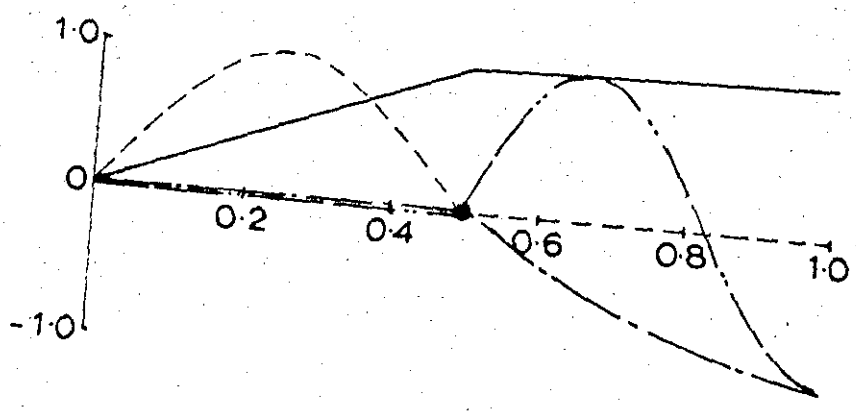

R=0·5

Fundamental
2nd. Mode
3rd. Mode
4th. Mode

FIG.6 TORSION MODES FOR SHAFT WITH $\bar{I}$=10·0

APPENDIX IV

A LEAST SQUARES CURVE FITTING PROCEDURE FOR THE MODE SHAPES OF VIBRATION

The problem of fitting a given expression to a curve can be stated as follows:

Let (x_i, y_i), $(i = 1,2 \ldots\ldots n)$, define the curve on the $(x\ y)$ plane. If $f_i(x)$, $(i = 1, \ldots\ldots m)$, be a set of known functions of x, it is required to find a function y such that

$$y = c_1 f_1(x) + c_2 f_2(x) + \ldots + c_m f_m(x) \qquad \text{IV.1}$$

where the c_i's are, as yet, undetermined constants, so that y represents the given curve with the least possible error.

Since we have n sets of points to define the curve, each of the values (x_i, y_i) must satisfy Eqn (IV.1).

$$\begin{aligned} y_1 &= c_1 f_1(x_1) + c_2 f_2(x_2) + \ldots + c_m f_m(x_1) \\ y_2 &= c_1 f_1(x_2) + c_2 f_2(x_2) + \ldots + c_m f_m(x_2) \\ &\vdots \\ y_n &= c_1 f_1(x_n) + c_2 f_2(x_n) + \ldots + c_m f_m(x_n) \end{aligned} \qquad \text{(IV.2)}$$

Since it is not always possible to satisfy the above equations let δ_i $(i = 1, \ldots\ldots n)$ represent the residuals in the above equations, i.e.

$$\left.\begin{aligned} \delta_1 &= c_1 f_1(x_1) + c_2 f_2(x_1) + \ldots + c_m f_m(x_1) - y_1 \\ &\vdots \\ \delta_n &= c_1 f_1(x_n) + c_2 f_2(x_n) + \ldots + c_m f_m(x_n) - y_n \end{aligned}\right\}$$

or $$\delta_j = \sum_{i=1}^{m} c_i f_i(x_j) - y_j \qquad \text{IV.3}$$

To minimise the errors, we choose the constants c_i such that the sum $\left(\sum_{j=1}^{n} \delta_j^2\right)$ is a minimum, i.e.

$$\frac{\partial}{\partial c_k} \sum_{j=1}^{n} \delta_j^2 = 0 \quad \text{for } k=1,2,\ldots m \qquad \text{(IV.4)}$$

or

$$\sum_{j=1}^{n} \delta_j \frac{\partial \delta_j}{\partial c_k} = 0 \quad \text{for } k=1,2,\ldots m \qquad \text{(IV.5)}$$

Now

$$\frac{\partial \delta_j}{\partial c_k} = f_k(x_j) \qquad \text{(IV.6)}$$

Substituting Eqn. (IV.3) and Eqn. (IV.6) into Eqn. (IV.5), we have

$$\sum_{j=1}^{n}\left[\sum_{i=1}^{m} c_i f_i(x_j) - y_j\right] f_k(x_j) = 0, \qquad k=1,2,\ldots m \qquad \text{(IV.7)}$$

This can be expressed as a system of m linear equations for the C_i's.

$$\sum_{i=1}^{n} c_i \sum_{j=1}^{m} f_i(x_j) f_k(x_j) = \sum_{j=1}^{n} y_i f_k(x_j) \qquad \text{(IV.8)}$$

$$k=1,2\ldots m$$

Let $[F]$ represent the (n x m) matrix

$$[F] = \begin{bmatrix} f_1(x_1) & f_2(x_1) & \ldots & f_m(x_1) \\ f_1(x_2) & f_2(x_2) & \ldots & f_m(x_2) \\ \vdots & & & \\ f_1(x_n) & f_2(x_n) & \ldots & f_m(x_n) \end{bmatrix} \qquad \text{(IV.9)}$$

Define two more matrices $\{c\}$ and $\{y\}$ where:

$$\{c\} = \begin{Bmatrix} c_1 \\ c_2 \\ \vdots \\ c_m \end{Bmatrix} \quad , \quad \{y\} = \begin{Bmatrix} y_1 \\ y_2 \\ \vdots \\ y_n \end{Bmatrix} \qquad \text{(IV.10)}$$

Equation IV.8 can be written as

$$[F]^T [F] \{c\} = [F]^T \{y\} \qquad \text{(IV.11)}$$

Where the "T" denotes the transposed matrix. The coefficients $\{c\}$ can be obtained by solving the system of linear equations (IV.11).

The accompanying flow chart gives the general outline of the method of the least squares curve fitting procedure.

The computer programme which follows this is in the Fortran II language. The system of Equations (IV.11) is solved by the Gaussian Elimination Technique.

(A standard library routine was used to solve this system of equations).

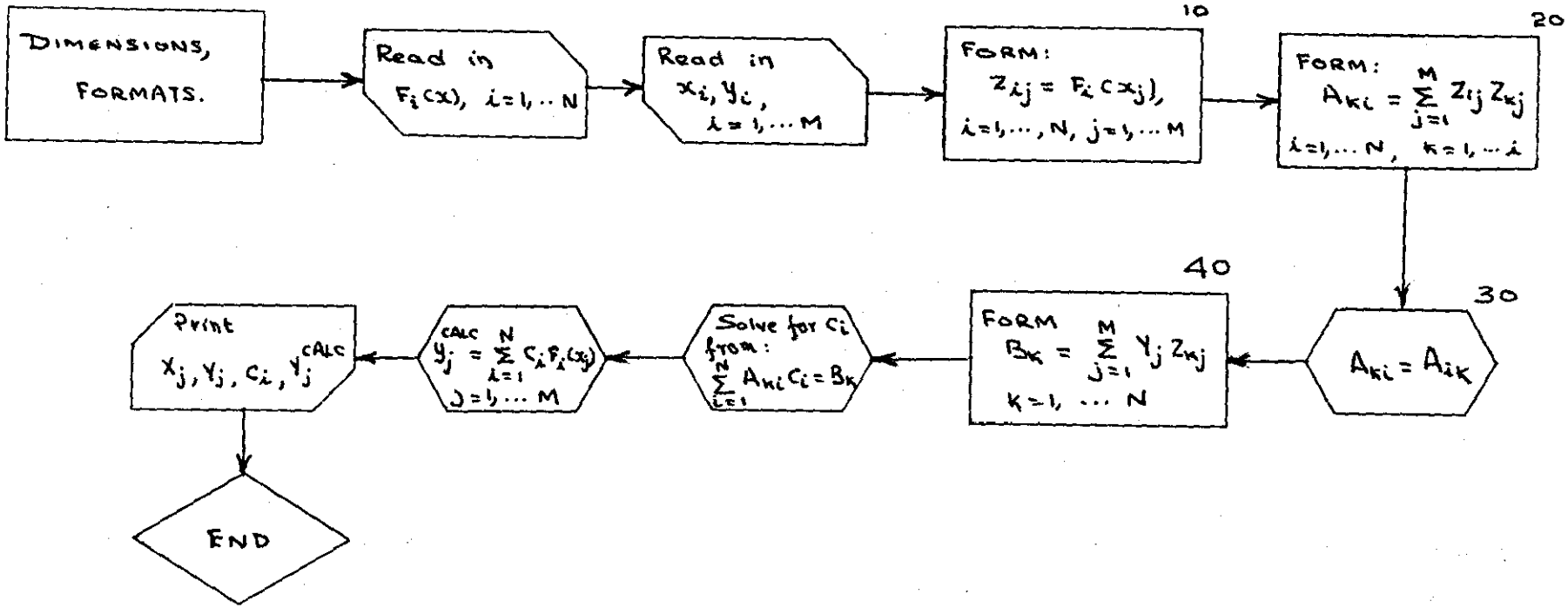

FLOW CHART FOR LEAST SQUARES CURVE FIT

```
ZZJOB 5
ZZFORX
C       V.T.NAGARAJ , TRANSPORT TECHNOLOGY
C      PROGRAMME FOR LEAST SQUARES CURVE FIT
C    N = NUMBER OF POLYNOMIALS     M = NUMBER OF POINTS IN DATA
C       THE FUNCTIONS FU1(S) ETC.( SHOULD BE DEFINED
C         FITS CURVES UPTO 25 POINTS
C         UPTO 5 FUNCTIONS MAY BE USED
C         THESE CAN BE INCREASED BY CHANGING THE DIMENSION STATEMENTS
      DIMENSION X(25),Y(25),C(5),A(5,5), F(5,25),B(5),YCALC(25)
      FU1(S) = S
      FU2(S) = S**2.
      N = 2
      M = 21
      DO 1 I = 1,M
    1 READ 2,X(I),Y(I)
    2 FORMAT (F5.2,F9.6)
      DO 10 J=1,M
      F(1,J) = FU1(X(J))
   10 F(2,J) = FU2(X(J) )
      DO 30 I = 1,N
      DO 30 K = 1,I
      A(K,I) =0.
      DO 20 J = 1,M
   20 A(K,I) = A(K,I)+F(I,J)*F(K,J)
   30 A(I,K) = A(K,I)
      DO 40 K = 1,N
      B(K) = 0.
      DO 40 J = 1,M
   40 B(K) =  B(K) + Y(J)*F(K,J)
      DO 1000 I=1,N
      DO 1000 J=1,N
 1000 PUNCH 1100,A(I,J),B(I)
 1100 FORMAT (E12.6,2XE12.6,2XE12.6)
```

```
      NM1 = N-1
      DO 300 K= 1,NM1
      KP1 = K+1
      L=K
      DO 400 I = KP1,N
      IF(ABSF(A(I,K))-ABSF(A(L,K))) 400,400,401
  401 L=I
  400 CONTINUE
      IF (L-K) 500,500,405
  405 DO 410 J = K,N
      TEMP = A(K,J)
      A(K,J)=A(L,J)
  410 A(L,J)=TEMP
      TEMP = B(K)
      B(K) = B(L)
      B(L) = TEMP
  500 DO 300 I = KP1,N
      FACTOR = A(I,K)/A(K,K)
      A(I,K)=0.
      DO 301 J = KP1,N
  301 A(I,J) = A(I,J)-FACTOR*A(K,J)
  300 B(I) = B(I)-FACTOR*B(K)
      C(N)=B(N)/A(N,N)
      I = NM1
  710 IPI = I+1
      SUM = 0.
      DO 700 J = IPI,N
  700 SUM = SUM + A(I,J)*C(J)
      C(I)=(B(I)-SUM)/A(I,I)
      I= I-1
      IF (I) 800,800,710
  800 DO 900 I = 1,N
  900 PUNCH 901,I,C(I)
  901 FORMAT (I5,E12.6)
      DO 950 J = 1,M
      YCALC(J) = 0.
      DO 9500 I = 1,N
 9500 YCALC(J) = YCALC(J) + F(I,J)*C(I)
  950 PUNCH 960,YCALC(J)
  960 FORMAT (E12.6)
      DO 550 I = 1,N
  550  PUNCH 551,J,X(J),Y(J),YCALC(J)
  551 FORMAT (I4,3(1X E12.6))
      END
```

APPENDIX V

FLUTTER ANALYSIS OF WINGS WITH CONCENTRATED INERTIAS BY THE ENERGY METHOD

In the following analysis, it is assumed that the pod is rigidly attached to the wing so that its movement (both translational and rotational) exactly corresponds to that of the spar station to which it is attached. In the general analysis, the pod aerodynamic loads are included. For wings without pods, the pod inertial and aerodynamic terms are set equal to zero.

It is assumed that all the modes included in the analysis are uncoupled that there is no chordwise bending of the wing. Hence the displacement of any point on the wing can be expressed in terms of the bending displacement, Zo, of the reference axis (the flexural axis) and the rotation α, about this axis, where both Z_o and α are measured with respect to the equilibrium position.

V.1 The Classical British Technique

Let the motion of the wing be completely defined by a certain number, say r, of bending modes and by (n - r) torsion modes. If we assume that all the modes are uncoupled and that no chordwise wing distortion takes place, the displacement of any point on the wing can be expressed in terms of Z_o (the downwards displacement of the reference axis) and α the rotation about the reference axis; both Z_o and α are measured relative to the equilibrium position (Fig. V.1).

In terms of the assumed modes, Z_o and α become

$$Z_o = \sum_{\lambda=1}^{r} Z_{o_\lambda} \Phi_\lambda(\eta)$$

$$\alpha = \sum_{\lambda=r+1}^{n} \alpha_{o_\lambda} \Theta_\lambda(\eta) \qquad (V.1)$$

where $\eta = y/0.7s$

s = semispan.

z_{o_i} and α_{o_j} are the displacements of and about the reference section (η = 1.0) in the ith and jth modes, respectively.

$\Phi_i(\eta)$ and $\Theta_i(\eta)$ are the displacement functions which have unit value at the reference section.

We now define the generalized co-ordinates, q as:

$$q_i = \frac{z_{o_i}}{b}, \quad i = 1, 2, \ldots, r$$
$$q_j = \frac{c \cdot \alpha_{o_j}}{b}, \quad j = r+1, \ldots, n \qquad \text{(V.2)}$$

where $b = 0.75\,S$.

Substituting (V.2) in (V.1)

$$z_o = b \sum_{i=1}^{r} q_i \Phi_i(\eta)$$
$$\alpha = \frac{b}{c} \sum_{i=r+1} q_i \Theta_i(\eta) \qquad \text{(V.3)}$$

The displacement z of any point (x, y) is given by

$$z = z_o(\eta) + x \cdot \alpha(\eta) \qquad \text{(V.4)}$$

The Kinetic energy of the fluttering wing is given by

$$T = \int_{WING} \tfrac{1}{2} \dot{z}^2 \delta m + \tfrac{1}{2} M_p \dot{z}_p^2 + \tfrac{1}{2} I_p \dot{\alpha}_p^2 \qquad \text{(V.5)}$$

where Z = the displacement of the elemental mass of the wing

M_p = Mass of the pod

$I_p = M_p k_p^2$ = pi ching moment of inertia, about the pod centroid of the pod

z_p = Bending displacement of pod

α_p = Torsional displacement of pod

The total strain energy of the vibrating wing can be written as

$$V = \frac{EI}{2}\int_0^S \left(\frac{d^2z}{dy^2}\right)^2 dy + \frac{GJ}{2}\int_0^S \left(\frac{d\alpha}{dy}\right)^2 dy \qquad (V.6)$$

We now consider the generalized forces Q_i due to the aerodynamic loads. The generalized force Q_i is appropriate to the co-ordinate q_i and is defined as follows. If, due to a small virtual displacement δq_i the work done by the aerodynamic loads is δW_i,

$$Q_i = \frac{\delta W_i}{\delta q_i} \qquad (V.7)$$

In this case, the aerodynamic forces are the lift and moment forces on the wing and pod.

In terms of the strip theory derivatives, the aerodynamic lift and moment per unit span of ahe wing can be written as (eg Ref: 23, 25, etc)

$$\frac{L_W}{\rho c V^2} = \left(-\nu^2 l_{w\ddot{z}} + i\nu\, l_{w\dot{z}} + l_{wz}\right)\frac{z_0}{c} + \left(-\nu^2 l_{w\ddot{\alpha}} + \cdots\right)\alpha$$

$$\frac{M_W}{\rho c^2 V^2} = \left(-\nu^2 m_{w\ddot{z}} + i\nu\, m_{w\dot{z}} + m_{wz}\right)\frac{z_0}{c} + \left(-\nu^2 m_{w\ddot{\alpha}} + \cdots\right)\alpha \qquad (V.8)$$

In terms of the generalized co-ordinates, (Eqn V.3), these can be written as

$$\frac{L_W}{\rho c V^2} = \frac{l}{c}\left[\left(-\nu^2 l_{w\ddot{z}} + i\nu\, l_{w\dot{z}} + l_{wz}\right)\left(\sum_{i=1}^{n} q_i \Phi_i(\eta)\right) + \left(-\nu^2 l_{w\ddot{\alpha}} + \cdots\right)\left(\sum_{i=n+1}^{n} q_i \Theta_i(\eta)\right)\right]$$

$$\frac{M_W}{\rho c^2 V^2} = \frac{l}{c}\left[\left(-\nu^2 m_{w\ddot{z}} + \cdots\right)\sum_{i=1}^{n} q_i \Phi_i(\eta) + \left(-\nu^2 m_{w\ddot{\alpha}} + \cdots\right)\sum_{i=n+1}^{n} q_i \theta_i(\eta)\right] \qquad (V.9)$$

The body aerodynamic forces can be found from one of the theories outlined in Sectinn 5.6. The lift and moment forces can be reduced to the form:

$$\frac{L_p}{\rho c V^2} = \frac{l}{c}\left[\left(-\nu^2 l_{p\ddot{z}} + i\nu l_{p\dot{z}} + l_{pz}\right)\sum_{i=1}^{n} q_i \phi_i(\eta_p) + \left(-\nu^2 l_{p\ddot{\alpha}} + \cdots\right)\sum_{i=n+1}^{n} q_i \theta_i(\eta_p\right.$$

$$\frac{M_p}{\rho c V^2} = \frac{l}{c}\left[\left(-\nu^2 m_{p\ddot{z}} + \cdots\right)\sum_{i=1}^{n} q_i \phi_i(\eta_p) + \left(-\nu^2 m_{p\ddot{\alpha}} + \cdots\right)\sum_{i=n+1}^{n} q_i \theta_i(\eta_p)\right. \tag{V.10}$$

It should be noted that the aerodynamic derivatives in (Eq. V.10) are not non-dimensional, but will have the dimension of a length. This is because while the values of L_w and M_w are the values per unit span of the wing, L_p and M_p represent the total lift and moment on the pod.

The equations of motion can now be derived using Lagrange's Equation:

$$\frac{d}{dt}\left(\frac{\partial T}{\partial \dot{q}_r}\right) + \frac{\partial V}{\partial q_r} + Q_r = 0, \qquad r = 1, 2, \ldots n \tag{V.11}$$

Using the values for T, V and Q_r from the previous equations, the equations of motion can be written in the form:

$$\rho V^2 l^3 \left[-\left(\sum_{s=1}^{n} a_{rs} q_s\right)\nu^2 + \sum_{s=1}^{n} e_{rs} q_s + \sum_{s=1}^{n} \left(-\nu^2 \gamma_{rs} + i\nu b_{rs} + c_{rs}\right) \cdot q_s = 0\right.$$

$$r = 1, 2, \ldots n \tag{V.12}$$

where

ρ = the local air density

$[a_{rs}]$ = matrix of the non-dimensional structural inertia coefficients,

$[b_{rs}]$ = matrix of the aerodynamic damping coefficients

$[C_{rs}]$ = matrix of the aerodynamic stiffness coefficients

$[e_{rs}]$ = matrix of the structural stiffness coefficients

$[\gamma_{rs}]$ = matrix of aerodynamic inertia coefficients

For a binary analysis, we assume only two modes, so that the bending and torsional deflections are specified by:

$$z_0 = l \cdot q_1 \cdot \Phi_1(\eta)$$
$$\alpha = \frac{l}{c} q_2 \theta_2(\eta) \qquad (V.13)$$

For the binary system the matrices ars, brs ..... γrs are given by the equations

$$[a_{rs}] = \begin{bmatrix} \frac{m}{\rho c^2}\int_0^{1/0.7} \Phi_1^2 d\eta + \frac{M_p}{\rho l c^2}\Phi_1^2(\eta_p) & \frac{m\bar{x}_w}{\rho c^3}\int_0^{1/0.7}\Phi_1\theta_2 d\eta + \frac{M_p \bar{x}_p}{\rho l c^3}\Phi_1(\eta_p)\theta_1(\eta_p) \\ \frac{m\bar{x}_w}{\rho c^3}\int_0^{1/0.7}\Phi_1\theta_1 d\eta + \frac{M_p\bar{x}_p}{\rho l c^3}\Phi_1(\eta_p)\theta_1(\eta_p) & \frac{m\bar{k}_w^2}{\rho c^4}\int_0^{1/0.7}\theta_2^2 d\eta \\ & + \frac{M_p(\bar{x}_p^2+k_p^2)}{\rho l c^4}\theta_2^2(\eta_p) \end{bmatrix}$$

$$[e_{rs}] = \begin{bmatrix} \frac{EI}{\rho V^2 (0.75)^2}\int_0^{1/0.7}\left(\frac{d^2\Phi_1}{d\eta^2}\right)^2 d\eta & 0 \\ 0 & \frac{GJ}{\rho V^2 c^2 (0.75)^2}\int_0^{1/0.7}\left(\frac{d\theta_2}{d\eta}\right)^2 d\eta \end{bmatrix}$$

$$[b_{rs}] = \begin{bmatrix} (l_{w\dot{z}} + l_{p\dot{z}})\int_0^{1/0.7}\Phi_1^2 d\eta & (l_{w\dot{\alpha}} + l_{p\dot{\alpha}})\int_0^{1/0.7}\Phi_1\theta_2 d\eta \\ -(m_{w\dot{z}} + m_{p\dot{z}})\int_0^{1/0.7}\Phi_1\theta_2 d\eta & -(m_{w\dot{\alpha}} + m_{p\dot{\alpha}})\int_0^{1/0.7}\theta_2^2 d\eta \end{bmatrix}$$

$[C_{rs}]$: Similar to $[b_{rs}]$, except that the derivatives $l_{w\dot{z}}$, $m_{w\dot{z}}$, $l_{p\dot{z}}$, .. etc. are replaced by l_{wz}, m_{wz}, l_{pz} ... etc.

$[\gamma_{rs}]$: Similar to $[b_{rs}]$, except that the derivatives are now replaced by $l_{w\ddot{z}}$, $m_{w\ddot{z}}$ .. etc

In the flutter equiations, the coefficient matrices b_{rs} , c_{rs} and γ_{rs} depend on the value of the reduced frequency $(\nu = c\omega/V)$ and for a given value of ν they can be considered as known quantities. The matrix e_{rs} contains the velocity V.

For non-trivial solutions of the flutter equation, the determinant of the bracketed terms in Eqn. (V.12) must vanish. If we assume a reference speed V_r and define

$$\Xi = V/V_r \tag{V.18}$$

The flutter determinant can be written as

$$-\nu^2 \sum_{s=1}^{n} (a_{rs}+\gamma_{rs}) + i\nu \sum_{s=1}^{n} b_{rs} + \sum_{s=1}^{n} c_{rs} + \Xi \sum_{s=1}^{n} e_{rs} \qquad (r = 1, 2, 3, \ldots n) \tag{V.19}$$

This system of equations can be solved for the values of ν and Ξ by one of the methods described in Chapter 4 Section 4.5.3. Possibly the easiest method would be to expand the determinant into a polynomial in $\lambda = i\nu$. By separating the real and imaginary parts of this polynomial and equating them to zero, the value of λ and Ξ can be obtained. The derived value of ν should be in reasonable agreement with the assumed value of ν. Considerable differences between the assumed and derived values of can be tolerated so long as both of them are above about 0.6. In this range the solution is comparitively insensitive to the value of ν in so far as it affects the aerodynamic coefficients.

V.2 The Classical American Technique

The main departure from the classical British Technique are in the definitions of the aerodynamic lift and the

definition of the reduced frequency. The reduced frequency, ν is defined based on the semi-chord:

$$\nu = b\omega/V \qquad \text{(V.20)}$$

The aerodynamic lift and moment per unit span of the wing are defined by:

$$L_W = \pi \rho b^3 \omega^2 \left[L_{wz} \frac{z_0}{b} + L_{w\alpha} \alpha \right]$$

$$M_W = \pi \rho b^4 \omega^2 \left[M_{wz} \frac{z_0}{b} + M_{w\alpha} \alpha \right] \qquad \text{(V.20a)}$$

where the non-dimensional derivatives are appropriate to a given reference axis.

The lift and moment on the pod can be defined in a similar way:

$$L_p = \pi \rho b^3 \omega^2 \left[L_{pz} \frac{z_0}{b} + L_{p\alpha} \alpha \right]$$

$$M_p = \pi \rho b^4 \omega^2 \left[M_{pz} \frac{z_0}{b} + M_{p\alpha} \alpha \right] \qquad \text{(V.21)}$$

Where again the derivatives L_{pz}, $L_{p\alpha}$, M_{pz} and $M_{p\alpha}$ are not non-dimensional.

The equations of motion, derived by using Lagrange's equations of motion and the values of the Kinetic energy and the aerodynamic forces, can be written in the form

$$\left[A + P - \left(\frac{1 + ig}{\omega^2} \right) E \right] q = 0 \qquad \text{(V.22)}$$

Where g is the coefficient of artificial damping.

For a binary analysis, the flutter determinant becomes

$$\begin{vmatrix} a_{11} & a_{12} \\ a_{21} & a_{22} \end{vmatrix} = 0 \qquad \text{(V.23)}$$

where

$$a_{11} = \frac{m}{\pi\rho b^2}(1-\Omega^2 z) f_{11} + \frac{M_p}{\pi\rho b^3 L}\Phi_1^2(\eta_p) + L_h f_1$$

$$a_{12} = -\frac{m\bar{x}_w}{\pi\rho b^3} f_{12} - \frac{M_p \bar{x}_p}{\pi\rho b^3 L}\Phi_1(\eta_p)\Theta_1(\eta_p) - L_\alpha f_{12}$$

$$a_{21} = -\frac{m\bar{x}_w}{\pi\rho b^3} f_{12} - \frac{M_p \bar{x}_p}{\pi\rho b^3 L}\Phi_1(\eta_p)\Theta_1(\eta_p) - M_h f_{12}$$

$$a_{22} = \frac{m\bar{k}_w^2}{\pi\rho b^4} f_2(1-z) + \frac{M_p(\bar{x}_p^2+\bar{k}_p^2)}{\pi\rho b^4 L}\Theta_1^2(\eta_p) + M_\alpha f_2$$

$$f_1 = \int_0^1 \Phi_1^2 d\eta, \quad f_{12} = \int_0^1 \Phi_1\Theta_1 d\eta, \quad f_2 = \int_0^1 \Theta_1^2 d\eta, \quad z = \left(\frac{\omega_\theta}{\omega}\right)^2 (1+ig) \qquad (V.23)$$

For a given value of the reduced frequency, all the coefficients in Eq. V.23 are known, with Z being the only unknown quantity. The flutter determinant is expanded into a quadratic equation in Z which has complex coefficients. When this equation is solved for the two values of Z, the frequency ω and the artificial damping g are found as

$$\omega_{1,2} = \omega_\theta/\sqrt{z_R}, \qquad g = z_I/z_R \qquad (V.24)$$

Since a value was previously assumed for ν the corresponding velocity can be found as:

$$V = b\omega/\nu \qquad (V.25)$$

For a number of assumed values of ν the flutter determinant is solved and the values of g, ω and V are found. The value of the flutter speed is found as the speed corresponding to the value where $g = 0$.

V.3 The Aerodynamic Derivatives

The strip theory derivatives L_{wz}, $L_{w\alpha}$, M_{wz} and $M_{w\alpha}$ can be obtained in terms of the Theodoresen circulation function $C(\nu) = F(\nu) + iG(\nu)$ as follows: (Eg Ref. 23)

$$L_{wz} = 1 - 2i \frac{V}{b\omega} (F + iG)$$

$$L_{w\alpha} = 0.5 - i \cdot \frac{V}{b\omega} (1 + 2F + 2iG) + 2\frac{V^2}{b^2\omega^2} (F + iG)$$

$$M_{wz} = 0.5$$

$$M_{w\alpha} = 0.375 - i \frac{V}{b\omega}$$

For the wings used in the experiments, the reference axis is at 0.35c aft of the LE. With respect to this axis, the derivatives aredobtained as

$$L_{wz} = \left(1 + \frac{2G}{\nu}\right) - i \frac{2F}{\nu}$$

$$L_{w\alpha} = \left(0.3 + 1.6\frac{G}{\nu} + \frac{2F}{\nu^2}\right) - i\left(\frac{1}{\nu} + 1.6\frac{F}{\nu} - \frac{2G}{\nu^2}\right)$$

$$M_{wz} = \left(0.3 - 0.4\frac{G}{\nu}\right) + i\, 0.4\frac{F}{\nu}$$

$$M_{w\alpha} = \left(0.215 - 0.32\frac{G}{\nu} - 0.4\frac{F}{\nu^2}\right) - i\left(\frac{1.2}{\nu} + 0.48\frac{F}{\nu} - 0.4\frac{G}{\nu^2}\right) \quad (V.27)$$

where $\nu = b\omega/V$

Using the approximate values for F and G from Ref. 26 (Eqns. 3.8 ~~and 3~~.), the values of the derivatives have been tabulated for several values of in Table V.1.

ν	$Re(L_h)$	$Im(L_h)$	$Re(L_\alpha)$	$Im(L_\alpha)$
.100	.444611E+01	-.166384E+02	.169441E+03	.111503E+02
.200	.288625E+01	-.727578E+01	.381879E+02	-.138933E+01
.300	.219545E+01	-.443314E+01	.160335E+02	-.289500E+01
.400	.182492E+01	-.312488E+01	.877216E+01	-.293760E+01
.500	.160284E+01	-.239174E+01	.556576E+01	-.270770E+01
.600	.145928E+01	-.192933E+01	.388298E+01	-.244465E+01
.700	.136119E+01	-.161359E+01	.289409E+01	-.220344E+01
.800	.129125E+01	-.138536E+01	.226470E+01	-.199422E+01
.900	.123966E+01	-.121317E+01	.183969E+01	-.181535E+01
1.000	.120054E+01	-.107886E+01	.153930E+01	-.166255E+01

ν	$Re(M_h)$	$Im(M_h)$	$Re(M_\alpha)$	$Im(M_\alpha)$
.100	-.389222E-00	.332768E+01	-.336132E+02	-.910100E+01
.200	-.772516E-01	.145515E+01	-.736258E+01	-.585992E+01
.300	.609096E-01	.886628E-00	-.293170E+01	-.426698E+01
.400	.135015E-00	.624977E-00	-.147943E+01	-.333751E+01
.500	.179430E-00	.478349E-00	-.838153E-00	-.273288E+01
.600	.208142E-00	.385867E-00	-.501597E-00	-.230994E+01
.700	.227760E-00	.322718E-00	-.303818E-00	-.199834E+01
.800	.241749E-00	.277072E-00	-.177941E-00	-.175967E+01
.900	.252067E-00	.242634E-00	-.929395E-01	-.157123E+01
1.000	.259891E-00	.215773E-00	-.328603E-01	-.141882E+01

TABLE V.1

APPENDIX VI

FLUTTER ANALYSIS OF THE MODEL WINGS BY THE DIRECT MATRIX METHOD

VI.1 Mathematical Model of the Wing

For the calculations, the model wings were approximated by a ten degree of freedom wing. (Fig 6.4). The inertial structural and aerodynamic forces acting on the wing were lumped at 10 control stations located at 3", 8", 12", 16" and 21" from the root.

At each spanwise control section, two control stations are located, the forward one at the $\frac{1}{4}$ chord point and the rear one at the $\frac{3}{4}$ chord point. For obtaining the mass matrix, the mass, moment of inertia and the chordwise centre of gravity location of each panel are replaced by three masses located at the $\frac{1}{4}$, $\frac{1}{2}$ and $\frac{3}{4}$ chord points respectively.

Since the model wing was designed such that all the structural stiffnesses are contributed by the spar only, the structural influence coefficient matrix can be constructed from a knowledge of the bending and torsional stiffnesses of the spar.

The construction of the aerodynamic matrix also simplified since the wing has a constant chord along the span.

VI.2 The Mass Matrix

In deriving the mass matrix, the mass, pitching moment of inertia and the chordwise position of the c.g. of each strip of the wing (in Fig. 6.4) were replaced by a system of three masses located at the control points. The rolling

moment of inertia was not considered in the mass matrix as all the analyses were for cantilever wings. Thus the masses M_{13}, M_{24}, M_{35}, M_{46} etc. in Fig. 5.3 do not enter the mass matrix and the mass matrix has a tri-diagonal form.

As an illustration, the derivation of the mass matrix for the uniform wing A2 will now be illustrated. In Fig. 6.7 the values of the weight and moment of inertia of each panel are given, together with the corresponding values of the equivalent control point weights. From the values of M_i, M_{ij}, M_j, ($i = 1,3,5,7,9$ $j = 2,4,6,8,10$) the elements of the mass matrix are derived using (Eqn. 5.27). The mass matrix is given in Table VI.2. Since there are ten control points, the mass matrix is of the tenth order and is a symmetric matrix.

VI.3 The Structural Influence Coefficient Matrix

The model was designed and constructed so that all the stiffnesses were contributed by the spar.

To obtain the SIC matrix, the bending and torsion flexibility influence coefficients have to be determined first.

For the cantilever wing, the flexibility influence coefficients are obtained directly by the application of the cantilever bending and torsion formulae. The bending influence coefficients are given by (Eg. Ref 23, p.42)

$$c^z(y,\eta) = \int_0^y \frac{(\eta-\lambda)(y-\lambda)}{EI}\, d\eta \quad : \quad y \le \eta$$

$$c^z(y,\eta) = \int_0^\eta \frac{(\eta-\lambda)(y-\lambda)}{GJ}\, d\eta \quad : \quad y \ge \eta \qquad \text{(VI.1)}$$

The torsion influence coefficients are given by

$$c^\theta(y,\eta) = \int_0^y d\lambda/GJ \quad : \quad y \le \eta$$

$$= \int_0^\eta d\lambda/GJ \quad : \quad y \ge \eta \qquad \text{(VI.2)}$$

$C^z(y,\eta)$ and $C^\theta(y,\eta)$ represent the bending and torsion influence coefficients, respectively, and EI and GJ are the corresponding stiffnesses.

The SIC matrix for the wing is obtained by using the scheme described in section 5.4. The SIC matrix for wing A2 is given in Table VI.3. This is a tenth order square, symmetric matrix.

For all the wings $e_1 = 0.6"$ and $e_2 = 2.4"$.

Any local changes in the stiffnesses affects the influence coefficients of the other stations. Hence, to take into account the effects of local changes in stiffness it may be necessary to re-derive the entire SIC matrix.

VI.4 The Aerodynamic Influence Coefficient Matrix

For the aerodynamic influence coefficient matrix, two dimensional strip theory derivatives were used. These are

$$L = \pi\rho\omega^2 b^3 \Delta y \left(L_h \frac{h}{b} + L_\alpha \alpha\right)$$

$$M = \pi\rho\omega^2 b^4 \Delta y \left(M_h \frac{h}{b} + M_\alpha \alpha\right) \qquad \text{(VI.3)}$$

where the aerodynamic derivatives $L_h, L_\alpha, M_h, M_\alpha$ are given by

$$L_h = 1 - 2i\frac{V}{b\omega}(F + iG)$$

$$L_\alpha = \frac{1}{2} - i\left(\frac{V}{b\omega}\right)\left(1 + 2\overline{F+iG}\right) - 2\left(\frac{V}{b\omega}\right)^2 (F+iG)$$

$$M_h = \frac{1}{2}$$

$$M_\alpha = \frac{3}{8} - i\left(\frac{V}{b\omega}\right)$$

and $C\left(\frac{b\omega}{V}\right) = F\left(\frac{b\omega}{V}\right) + iG\left(\frac{b\omega}{V}\right)$ is the (VI.4)

Theodoresen circulation function.

From Eq (5.51) the individual aerodynamic influence

coefficients are given by:

$$[C_h]_{\lambda} = \pi\rho \frac{\Delta y}{S} \begin{bmatrix} 1 & -b/d \\ 0 & b/d \end{bmatrix} \begin{bmatrix} L_h & L_\alpha \\ M_h & M_q \end{bmatrix} \begin{bmatrix} 1 & 0 \\ -b/d & b/d \end{bmatrix}$$

(Since $b = b_f$) VI.5

As an illustration, the aerodynamic influence coefficients matrix is illustrated in Table VI.2. This refers to wing A2 and the value of the reduced frequency is 0.1

VI.5 The Flutter Equation

The procedure for constructing the flutter equation is as follows:

The elements of the mass and the SIC matrices are first derived. The elements of the AIC matrix are then obtained for a particular value of ν. From these three the dynamic matrix U is found from Eq. (5. 14).

The eigenvalues and eigenvectors of U can now be derived. To do this the iterative method of Gollnitz et al was used. (Section 5.9 and Appendix VII).

APPENDIX VII

A COMPUTER PROGRAM FOR VIBRATION AND FLUTTER ANALYSIS BY THE DIRECT MATRIX METHOD

VII.1

This appendix gives the details of the computer programme which was used for the setting up of the characteristic matrix and for the determination of the flutter speeds and frequencies.

The programme can be divided into three major parts:

(a) The part which calculates the characteristic matrix

(b) The subroutine for the calculation of the eigenvalues and eigenvectors of the characteristic matrix

and (c) The subroutine for calculating the flutter speeds, frequencies etc., and for printing these results.

These steps are achieved in this programme by means of the following:

(a) The Main Programme

(b) A subprogram, UTM4, for multiplying two matrices

(c) Subroutines Eigwrt, Doppel and Doplwz, for the calculation of the eigenvalues and eigenvectors of a complex matrix by Gollnitz's method.

and (d) Subroutine Shribe, which outputs the results.

VII.2

Even though the aerodynamic matrix and consequently the characteristic matrix are complex, all the computations are carried out with real numbers, (giving proper attention to the rules of complex algebra).

As it stands, the programme can solve the flutter problem by the direct matrix method, of systems with upto ten degrees of freedom. It is possible to treat the case of systems with a larger number of degrees of freedom, by

making appropriate changes to the DIMENSION and DOUBLE PRECISION statements in the main programme and in all the subroutines.

The different parts of the programme will now be described.

VII.3 Main Programme

This programme reads the data and computes the characteristic matrix. The data deck is set up as follows:

1st card· Title (Format 10 A 8) This reads in the description of the programme. It is not necessary to fill in all the spaces in this card.

2nd card NAERO, VELCTY (Format I4, F 10.6)· This card reads in the control numbers for each pass.

NAERO should be set equal to the number of roots which are to be computed.

VELCTY is a control number:

For flutter analysis, VELCTY = $\nu = \frac{b\omega}{V}$ = the frequency parameter

For Vibration Analysis, VELCTY = 0

If VELCTY is set equal to a negative value, this indicates that the programme is to be terminated and no further eases will be considered.

If VELCTY $\geq$ 0, the analysis proceeds further.

3rd card (LOW(J),LHIGH (J), J = 1, 10) : FORMAT (20 I 4)

Since the mass matrix and the AIC matrices are sparsely po ulated, it was felt that it would be more convenient to read in only the non zero elements. LOW (J) and LHIGH (J) indicate the first and last columns in each row J, which contain the nonzero elements. For example, consider the following (4 x 4) matrix·

$$\begin{bmatrix} a_{11} & 0 & a_{13} & 0 \\ 0 & a_{22} & a_{23} & 0 \\ 0 & 0 & a_{33} & a_{34} \\ a_{41} & 0 & a_{43} & 0 \end{bmatrix}$$

In this case, LOW (1) = 1, LHIGH (1) = 3

LOW (2) = 2, LHIGH (2) = 3

LOW (3) = 3, LHIGH (3) = 4

LOW (4) = 1, LHIGH (4) = 3

In rows 1 and 4, the zeros in the second column must also be punched in the appropriate data card.

4th Set: SM: FORMAT (4 E 12.6)

This is the mass matrix. This matrix is input by rows and in each row, only the nonzero elements are read in. Any null elements in between the nonzero elements are also read in, as described previously.

5th Set: S FORMAT (10 F 8.6). This reads in the flexibility matrix, again by rows. All the elements are read in, though it is possible to simplify this by taking account of the symmetric nature of this matrix.

It was felt that, to avoid working with very small order numbers, the SIC matrix should be multiplied by an (arbitrary) factor of 10^4. This is not compulsory as it was found by a number of examples that the accuracy did not suffer by not introducing this factor.

6th Set: AR FORMAT (4 E 12.6). This is the real part of the AIC matrix:

$$AR = \rho b_r^2 s \left(\text{Real}\left[C_h\right]\right)$$

As in the case of the mass matrix, only the nonzero elements are read-in.

7th Set: AI FORMAT (4 E 12.6). The imaginary part of the AIC matrix is also read-in in the same way as the AR Matrix.

(Note AI = $\rho b_1^2 S \left(\mathrm{Im} [C_h] \right)$

After all these data are read-in, the main programme computes the real and imaginary parts of the characteristic matrix separately. The complete characteristic matrix is then computed.

This is done as follows:

Real part UR = S * (SM + AR)

Imaginary part UI = S * AI

The characteristic matrix $U = UR + \lambda UI$ is now set up by putting

$U(I, 2J-1) = UR(I, J)$

$U(I, 2J) = UI(I, J)$

and J = 1, 2..... 10

for II = 1, 2 ..... 10 and J = 1,2 10

VII.4 UTM4 The multiplications indicated above are performed by using a library routine which computes the product C of two matrices A and B.

VII.5 EIGWRT, DOPPEL, DOPLWZ : This set of subroutines is used for the calculation of the eigenvalues and eigenvectors of complex matrices. This has also been used for the calculation of the eigenvalues and eigenvectors of real matrices (e.g. for vibration problems), though it might have been more economical to use the specific routines available for real matrices.

These three routines are based on the method of Goll itz et al (Section 5.8.2.) and are set out in the flow charts which follow.

VII.6 The Outputs

1. The Title card: The alphameric data input in the title card is printed first.
2. The values of NAERO, VELCTY
3. The Mass Matrix,
4. The flexibility Matrix
5. The real part of the AIC matrix
6. The Imaginary part of the AIC matrix
7. The characteristic matrix

(All the matrices are output by rows).

8. The values of the roots obtained by the power method and from the two root procedure.
9. After these values have been output, the following data is output for each root :-

(a) The value of the root obtained by the Wielandt iteration and the associated eigenvector

(b) The values of the flutter frequency, damping and flutter speed.

(Note: the values of the flutter frequency and speed are controlled by the values of b and ν For each given wing planform the statements controlling these parameters in the subroutine SHRIBE have to be changed).

The flow chart and the listing of the computer programme are given in the following pages.

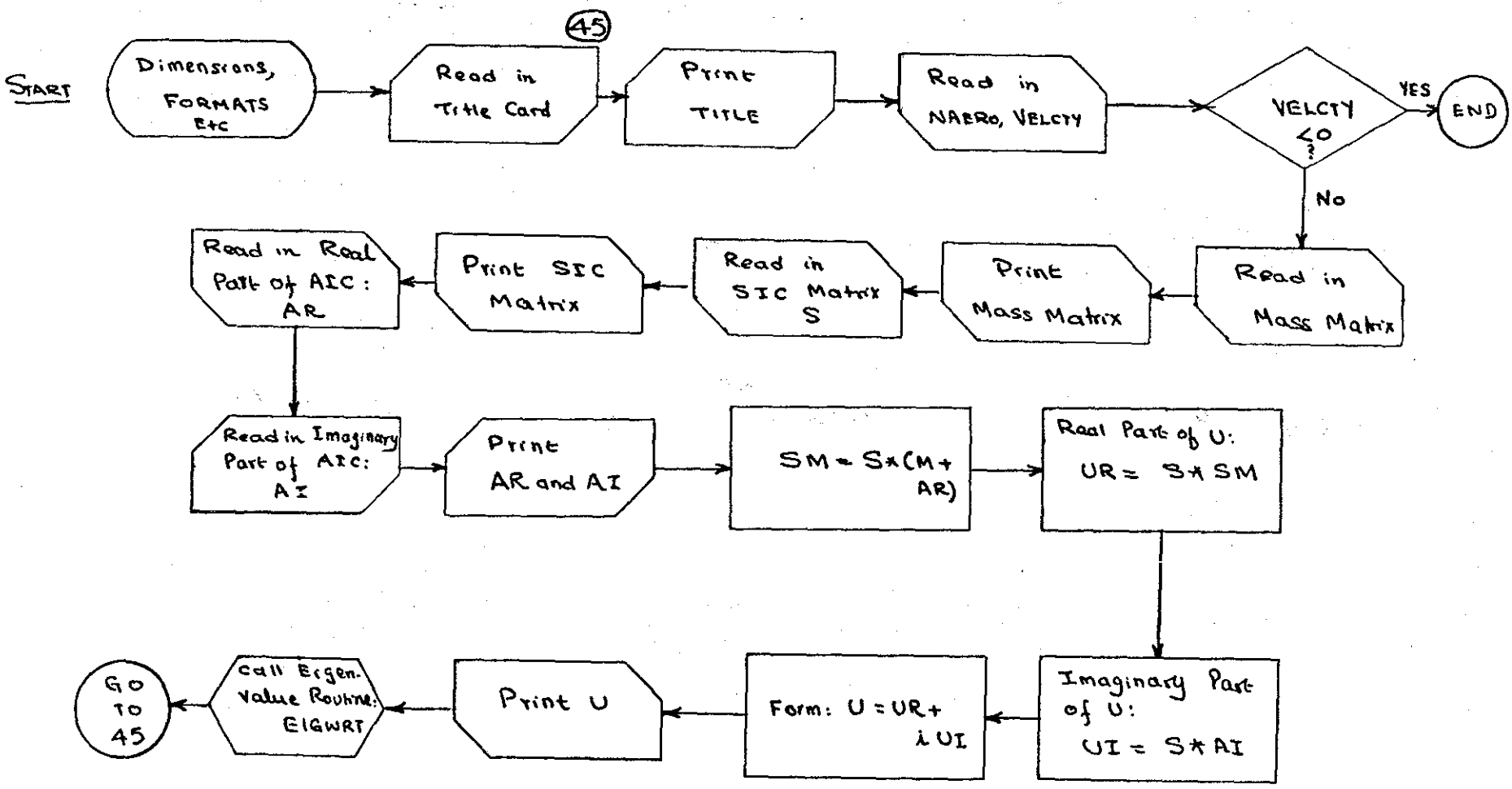

MAIN ROUTINE

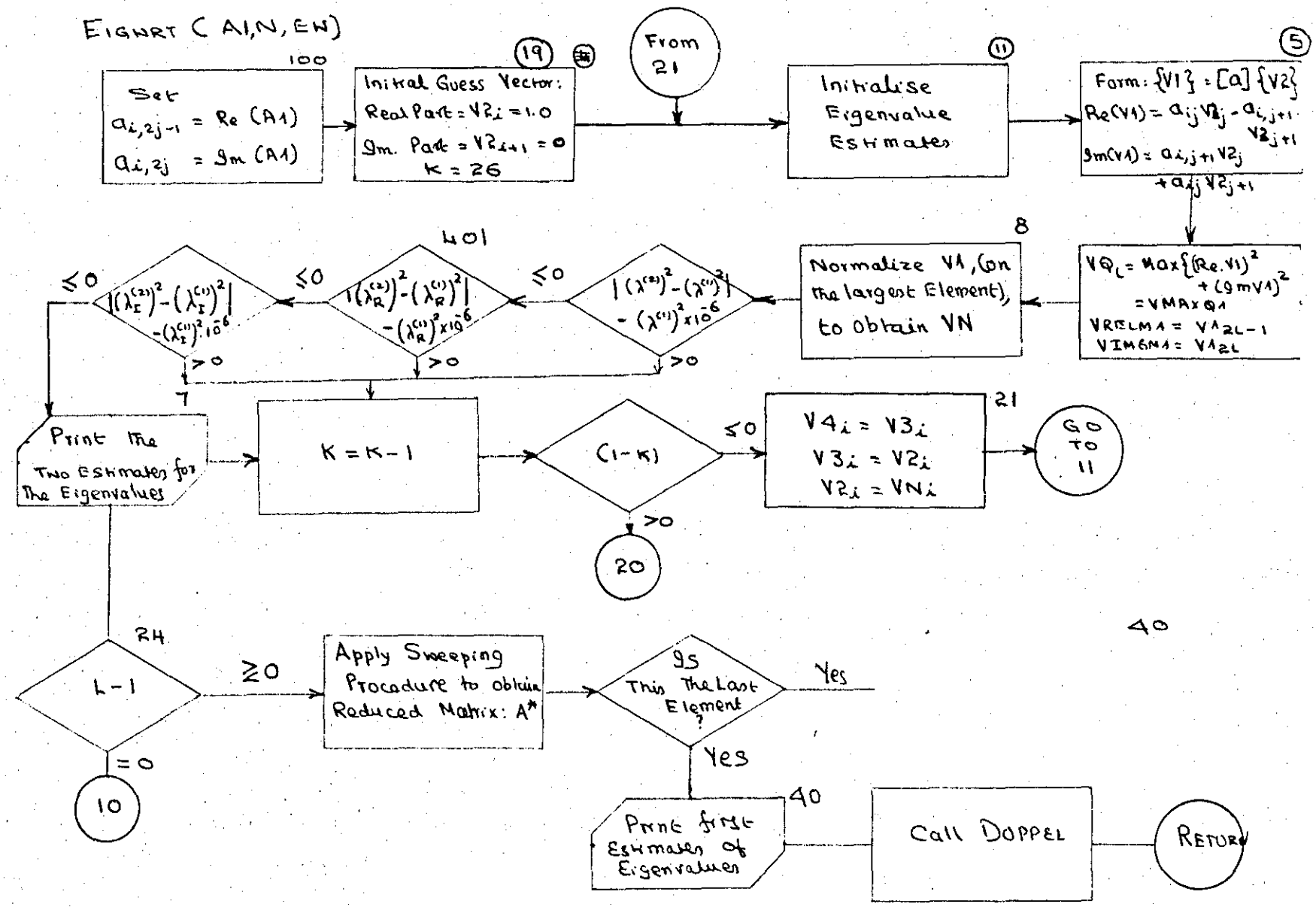
EIGNRT (A1,N,EN)
100
Set
$a_{i,2j-1}$ = Re (A1)
$a_{i,2j}$ = Im (A1)
19
Initial Guess Vector:
Real Part = $V2_i$ = 1.0
Im. Part = $V2_{i+1}$ = 0
K = 26
From 21
11
Initialise Eigenvalue Estimates
5
Form: {V1} = [a] {V2}
$Re(V1) = a_{ij} V2_j - a_{i,j+1} V2_{j+1}$
$Im(V1) = a_{i,j+1} V2_j + a_{ij} V2_{j+1}$
8
Normalize V1, (on the largest Element), to obtain VN
VQ_L = Max {$(Re.V1)^2 + (Im V1)^2$} = VMAXQ_1
VRELM_1 = $V1_{2L-1}$
VIMG_{M1} = $V1_{2L}$
401
$|(\lambda_I^{(2)})^2 - (\lambda_I^{(1)})^2| - (\lambda_I^{(1)})^2 \cdot 10^{-6}$
$|(\lambda_R^{(2)})^2 - (\lambda_R^{(1)})^2| - (\lambda_R^{(1)})^2 \times 10^{-6}$
$|(\lambda^{(2)})^2 - (\lambda^{(1)})^2| - (\lambda^{(1)})^2 \times 10^{-6}$
≤0
>0
7
Print the Two Estimates for the Eigenvalues
K = K-1
(I-K)
≤0
>0
21
$V4_i = V3_i$
$V3_i = V2_i$
$V2_i = VN_i$
GO TO 11
20
24
L-1
≥0
=0
10
Apply Sweeping Procedure to obtain Reduced Matrix: A*
Is This the Last Element?
Yes
Yes
40
40
Print first Estimates of Eigenvalues
Call DOPPEL
RETURN

EIGWRT - CONTD.

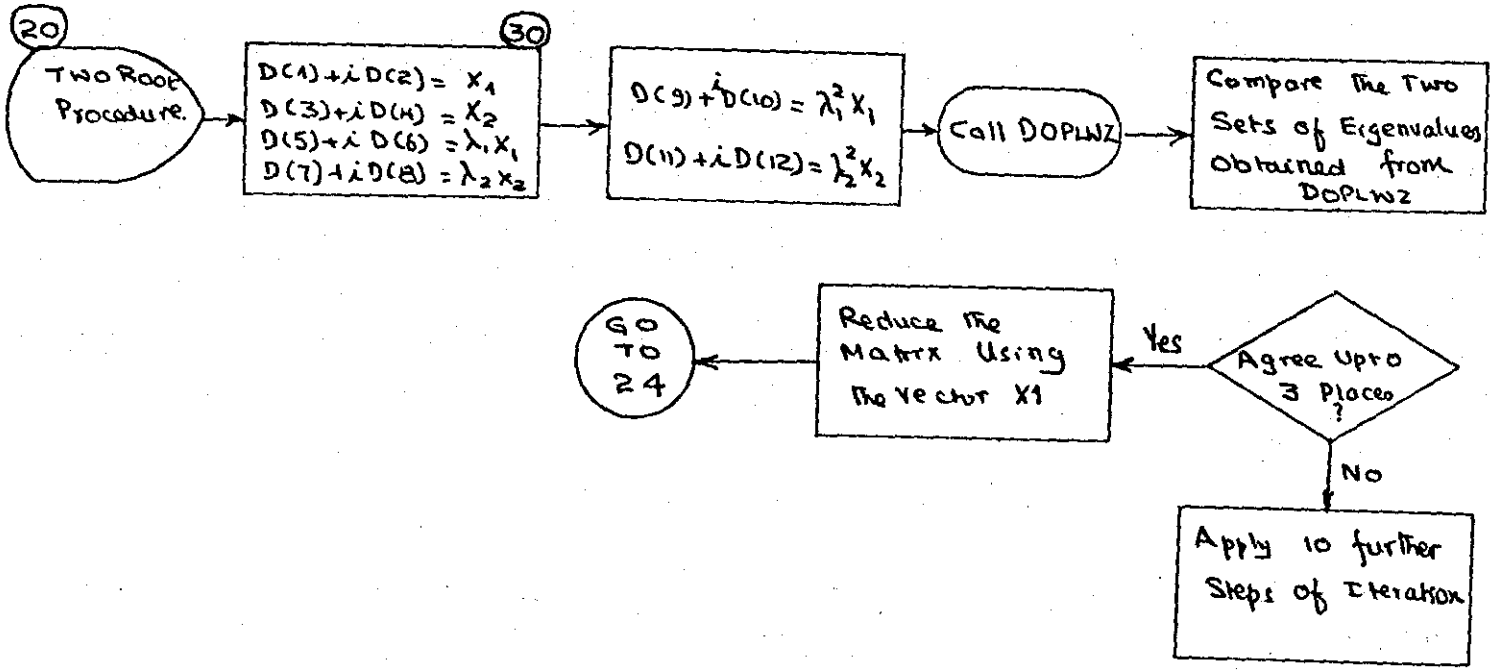

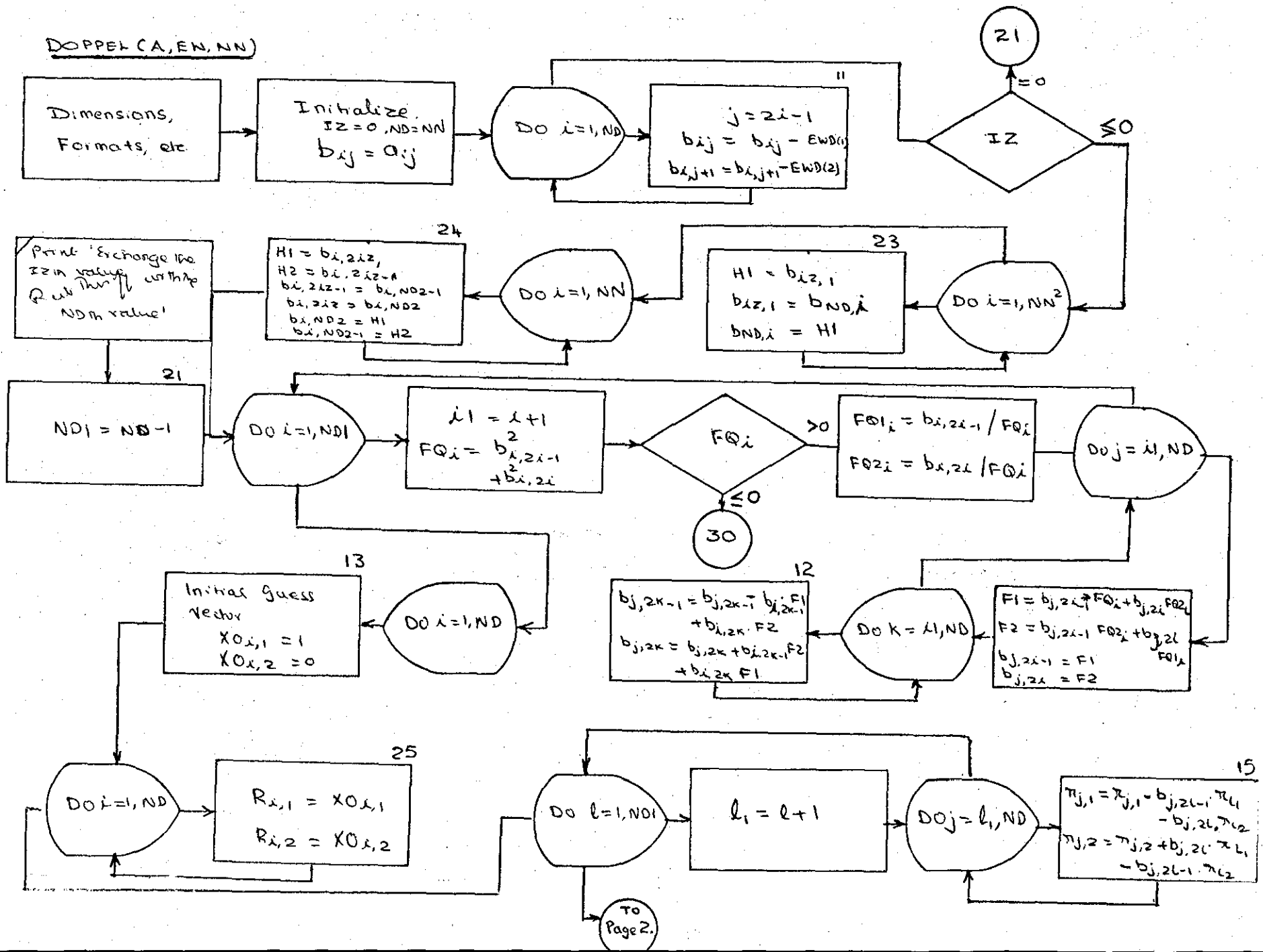
DOPPEL (A, EN, NN)
Dimensions, Formats, etc.
Initialize
IZ = 0, ND = NN
$b_{ij} = a_{ij}$
DO i=1, ND
j = 2i-1
$b_{ij} = b_{ij} - EWD(1)$
$b_{i,j+1} = b_{i,j+1} - EWD(2)$
21
IZ
=0
≤0
Print 'Exchange the IZ in value with the Q with the NDth value'
24
H1 = $b_{i,2iz}$,
H2 = $b_{i,2iz-1}$
$b_{i,2iz-1} = b_{i,ND2-1}$
$b_{i,2iz} = b_{i,ND2}$
$b_{i,ND2} = H1$
$b_{i,ND2-1} = H2$
DO i=1, NN
23
H1 = $b_{iz,1}$
$b_{iz,1} = b_{ND,i}$
$b_{ND,i} = H1$
DO i=1, NN^2
21
NDI = ND-1
DO i=1, NDI
i1 = i+1
$FQ_i = b^2_{i,2i-1} + b^2_{i,2i}$
FQi
>0
$FQ1_i = b_{i,2i-1} / FQ_i$
$FQ2_i = b_{i,2i} / FQ_i$
DO j = i1, ND
30
13
Initial Guess Vector
$XO_{i,1} = 1$
$XO_{i,2} = 0$
DO i=1, ND
12
$b_{j,2k-1} = b_{j,2k-1} - b_{j,2i-1} \cdot F1 + b_{i,2k} \cdot F2$
$b_{j,2k} = b_{j,2k} + b_{j,2k-1} \cdot F2 + b_{i,2k} \cdot F1$
DO K = i1, ND
$F1 = b_{j,2i} \cdot FQ_i + b_{j,2i} \cdot FQ2_i$
$F2 = b_{j,2i-1} \cdot FQ2_i + b_{j,2i} \cdot FQ1_i$
$b_{j,2i-1} = F1$
$b_{j,2i} = F2$
25
$R_{i,1} = XO_{i,1}$
$R_{i,2} = XO_{i,2}$
DO i=1, ND
DO l=1, NDI
$l_1 = l+1$
DOj = l_1, ND
15
$\pi_{j,1} = \pi_{j,1} - b_{j,2l-1} \cdot \pi_{l1} - b_{j,2l} \cdot \pi_{l2}$
$\pi_{j,2} = \pi_{j,2} + b_{j,2l} \cdot \pi_{l1} - b_{j,2l-1} \cdot \pi_{l2}$
TO Page 2.

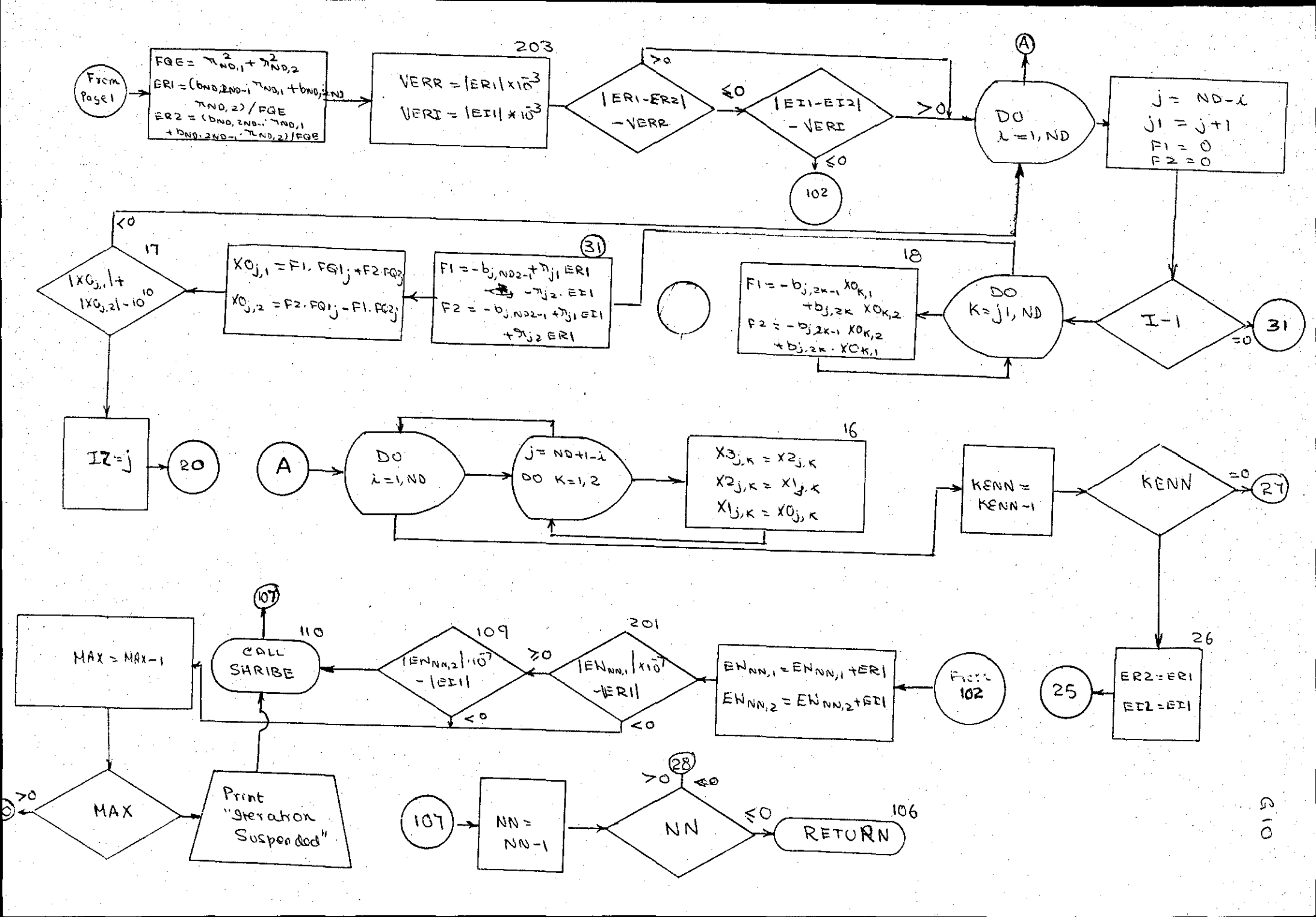
From Page1
FQE = $\pi^2_{ND,1} + \pi^2_{ND,2}$
ER1 = ($b_{ND,2ND-1}\,\pi_{ND,1} + b_{ND,2ND}\,\pi_{ND,2}$) / FQE
ER2 = ($b_{ND,2ND-1}\,\pi_{ND,1} + b_{ND,2ND}\,\pi_{ND,2}$) / FQE
203
VERR = |ER1| x 10^-3
VERI = |EI1| * 10^-3
|ER1-ER2| - VERR
>0
≤0
|EI1-EI2| - VERI
>0
≤0
102
A
DO I = 1, ND
J = ND-I
J1 = J+1
F1 = 0
F2 = 0
I-1
=0
31
DO K = J1, ND
18
F1 = -$b_{J,2K-1}$ $XO_{K,1}$ + $b_{J,2K}$ $XO_{K,2}$
F2 = -$b_{J,2K-1}$ $XO_{K,2}$ + $b_{J,2K}$ · $XO_{K,1}$
(31)
F1 = -$b_{J,ND2-1}$ + π_{J1} ER1 - π_{J2} · EI1
F2 = -$b_{J,ND2-1}$ + π_{J1} EI1 + π_{J2} ER1
$XO_{J,1}$ = F1 · FQ1J + F2 · FQ2J
$XO_{J,2}$ = F2 · FQ1J - F1 · FQ2J
17
|$XO_{J,1}$| + |$XO_{J,2}$| - 10^{10}
<0
IZ = J
20
A
DO I = 1, ND
J = ND+1-I
DO K = 1, 2
16
$X3_{J,K}$ = $X2_{J,K}$
$X2_{J,K}$ = $X1_{J,K}$
$X1_{J,K}$ = $XO_{J,K}$
KENN = KENN-1
KENN
=0
27
26
ER2 = ER1
EI2 = EI1
25
From 102
$EN_{NN,1}$ = $EN_{NN,1}$ + ER1
$EN_{NN,2}$ = $EN_{NN,2}$ + EI1
201
|$EN_{NN,1}$| x 10^7 - |ER1|
<0
≥0
109
|$EN_{NN,2}$| · 10^7 - |EI1|
<0
110
CALL SHRIBE
107
MAX = MAX-1
MAX
>0
Print "Iteration Suspended"
107
NN = NN-1
28
>0
<0
NN
≤0
106
RETURN

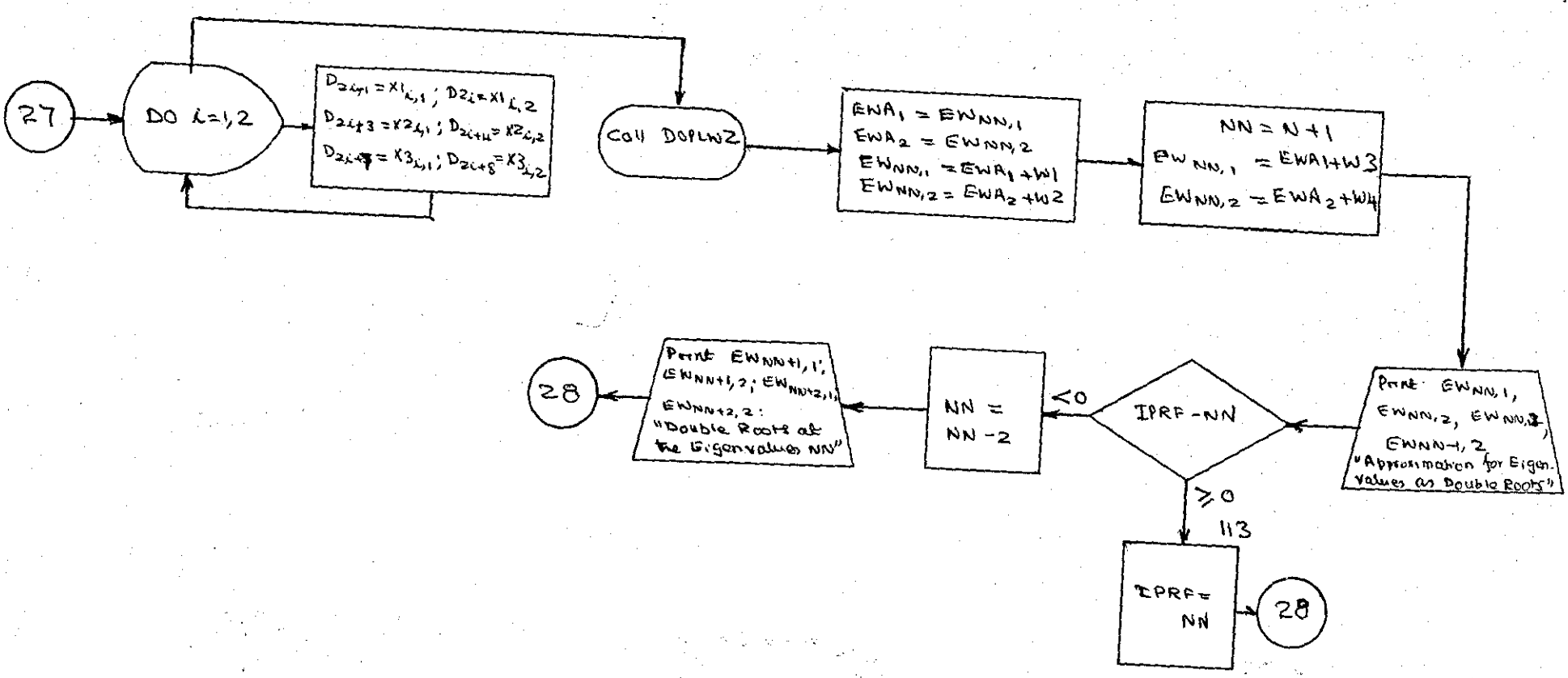
27
DO I=1,2
D2I+1 = X1I,1 ; D2I = X1I,2
D2I+3 = X2I,1 ; D2I+4 = X2I,2
D2I+6 = X3I,1 ; D2I+8 = X3I,2
Call DOPLW2
EWA1 = EWNN,1
EWA2 = EWNN,2
EWNN,1 = EWA1 + W1
EWNN,2 = EWA2 + W2
NN = N + 1
EWNN,1 = EWA1 + W3
EWNN,2 = EWA2 + W4
Print EWNN,1, EWNN,2, EWNN+1,1, EWNN+1,2 "Approximation for Eigen. Values as Double Roots"
IPRF - NN
< 0
NN = NN - 2
Print EWNN+1,1; EWNN+1,2; EWNN+2,1; EWNN+2,2: "Double Roots at the Eigenvalues NN"
28
≥ 0
113
IPRF = NN
28

DOPLN2

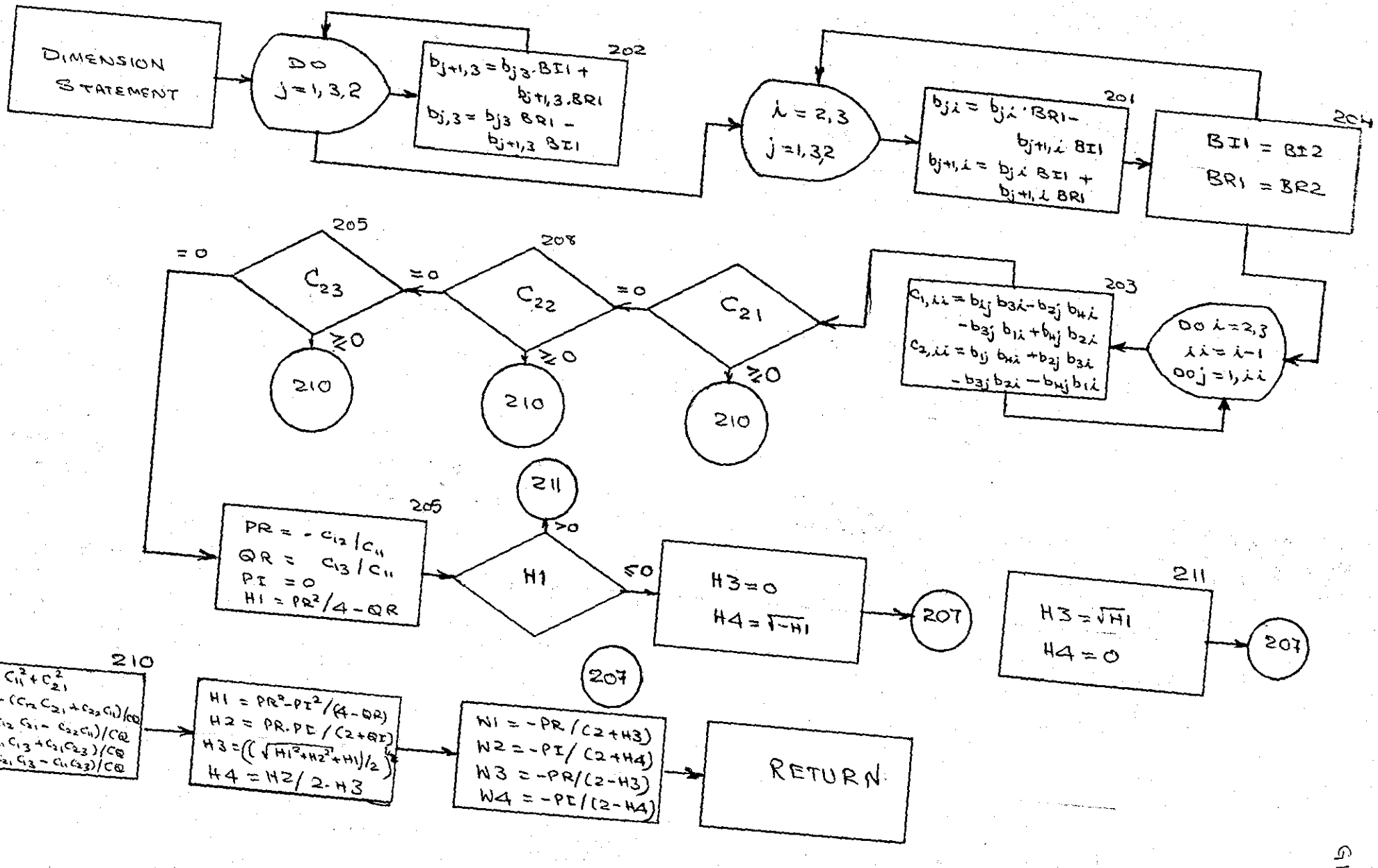
DIMENSION STATEMENT
DO j=1,3,2
202
$b_{j+1,3} = b_{j3} \cdot BI1 + b_{j+1,3} \cdot BR1$
$b_{j,3} = b_{j3} BR1 - b_{j+1,3} BI1$
$\lambda = 2,3$
$j = 1,3,2$
201
$b_{j\lambda} = b_{j\lambda} \cdot BR1 - b_{j+1,\lambda} BI1$
$b_{j+1,\lambda} = b_{j\lambda} BI1 + b_{j+1,\lambda} BR1$
204
BI1 = BI2
BR1 = BR2
205
C_{23}
=0
≠0
208
C_{22}
=0
≠0
C_{21}
≠0
210
210
210
203
$C_{1,\lambda i} = b_{1j} b_{3\lambda} - b_{2j} b_{4\lambda} - b_{3j} b_{1\lambda} + b_{4j} b_{2\lambda}$
$C_{2,\lambda i} = b_{1j} b_{4\lambda} + b_{2j} b_{3\lambda} - b_{3j} b_{2\lambda} - b_{4j} b_{1\lambda}$
DO $\lambda = 2,3$
$\lambda i = \lambda - 1$
DO $j = 1, \lambda i$
205
$PR = -C_{12}/C_{11}$
$QR = C_{13}/C_{11}$
$PI = 0$
$H1 = PR^2/4 - QR$
211
H1
>0
≤0
H3=0
$H4 = \sqrt{-H1}$
207
211
$H3 = \sqrt{H1}$
H4 = 0
207
210
$CQ = C_{11}^2 + C_{21}^2$
$PR = -(C_{12}C_{21} + C_{22}C_{11})/CQ$
$PI = (C_{12}C_{21} - C_{22}C_{11})/CQ$
$QR = (C_{11}C_{13} + C_{21}C_{23})/CQ$
$(QI) = (C_{21}C_{13} - C_{11}C_{23})/CQ$
$H1 = PR^2 - PI^2/(4 - QR)$
$H2 = PR \cdot PI/(2 + QI)$
$H3 = \left(\sqrt{H1^2 + H2^2} + H1\right)/2$
$H4 = H2/2 \cdot H3$
207
$W1 = -PR/(2 + H3)$
$W2 = -PI/(2 + H4)$
$W3 = -PR/(2 - H3)$
$W4 = -PI/(2 - H4)$
RETURN

SHRIBE

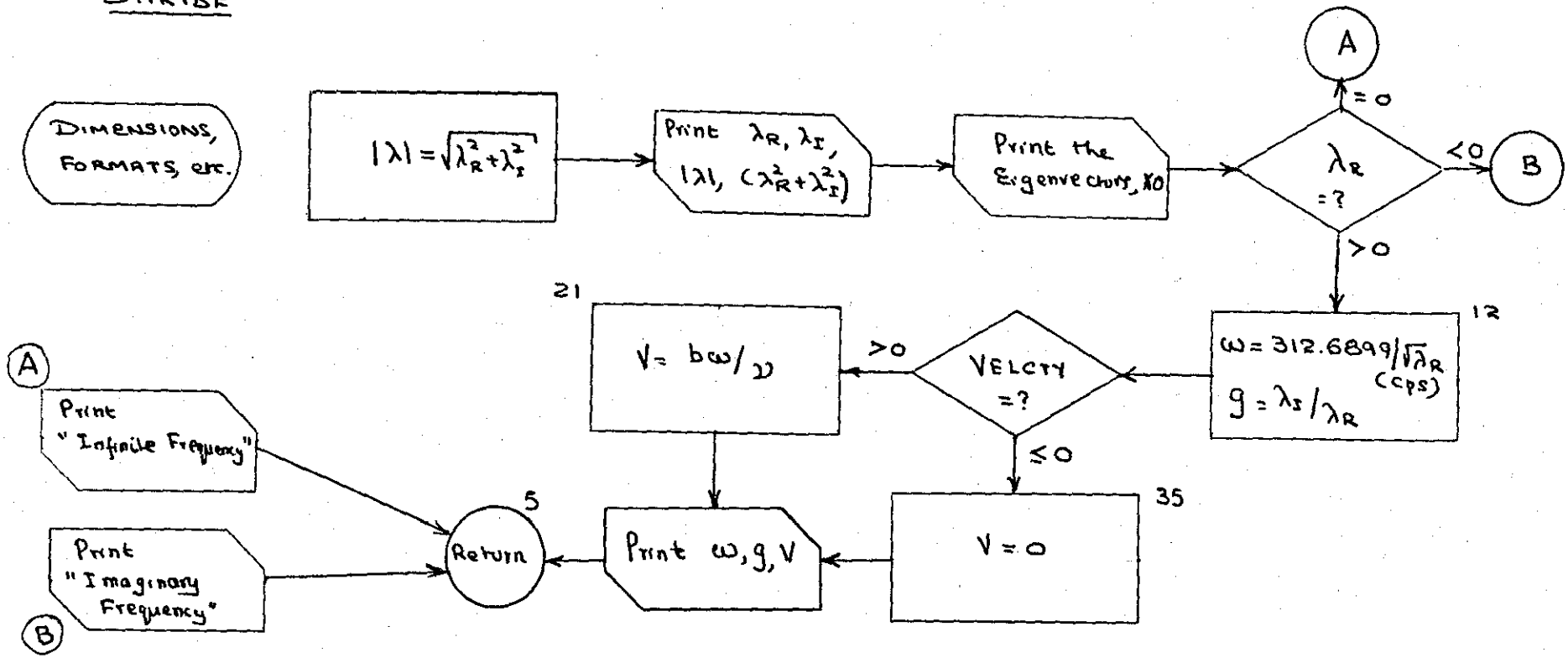
DIMENSIONS, FORMATS, etc.
$|\lambda| = \sqrt{\lambda_R^2 + \lambda_I^2}$
Print λ_R, λ_I, $|\lambda|$, $(\lambda_R^2 + \lambda_I^2)$
Print the Eigenvectors, XO
A
= 0
λ_R =?
< 0
B
> 0
12
$\omega = 312.6899/\sqrt{\lambda_R}$ (cps)
$g = \lambda_I / \lambda_R$
VELCTY =?
> 0
21
$V = b\omega/\nu$
≤ 0
35
V = 0
Print ω, g, V
5
Return
A
Print "Infinite Frequency"
B
Print "Imaginary Frequency"

```
*FORTRAN B128,V.T.NAGARAJ.TRANSPORT TECH
      NO TRACE
       MASTER(B134)
C      FLUTTER ANALYSIS BY THE DMM. **  MAIN PROGRAMME
C      ALL MATRICES INPUT BY ROWS
C      SM = MASS MATRIX (LB)     S = STC MATRIX (IN/LB)     A = AIC MATRIX(NON-
C     DIMENSIONAL)
C      VELCTY = 1/KR
C     AIC MATRIX = AR + I.AI
C      1ST CARD  TITLE
C      2ND CARD   NAERO,VELCTY
C      NAERO   NUMBER OF ROOTS DESIRED
C      3RD CARD  LOW(J),LJIGH(J)
C      4TH SET  MASS MATRIX  INPUT BY ROWS  ONLY NON-ZERO ELEMENTS
C      5TH SET:  FLEXIBILITY MATRIX  INPUT BY ROWS
C      6TH SET  AR MATRIX
C      7TH SET  AI MATRIX
C      TO TERMINATE PROGRAM  THE VALUE OF VELCTY MUST BE SET TO (-VE) VALUE
C    UTM4 IS A LIBRARY SUBROUTINE FOR MULTIPLYING TWO MATRICES : A*B=C
      DIMENSION SM(10,10),S(10,10),AR(10,10),AI(10,10),UR(10,10),UI
     1 (10,10)
       DIMENSION TITLE (10)
      DIMENSION EW(10,2)
      DIMENSION U(10,20),LOW(10),LHIGH(10)
       COMMON NAERO,VELCTY
C    ***************************                                  ***********
C
  325  FORMAT (10A8)
  326  FORMAT (1X,10A8)
   12  FORMAT(I4,F10.6)
```

```
   77 FORMAT (2014)
   30 FORMAT (4E12.6)
      WRITE (2,1000)
 1000 FORMAT (50X 11HMASS MATRIX/)
  999 FORMAT (10E12.6)
    1  FORMAT (10F8.6)
 1001 FORMAT (50X 11H SIC MATRIX/)
 1002 FORMAT (50X 10HAIC MATRIX, 12H***REAL PART/)
 1008 FORMAT (50X 17H***IMAGINARY PART/)
   43 FORMAT ( 48X 14HDYNAMIC MATRIX/)
   45  READ (1,325) TITLE
      WRITE (2,326) TITLE
C      READ IN MASS MATRIX FOR WING
       READ (1,12) NAERO,VELCTY
      WRITE (2,12) NAERO,VELCTY
       IF (VELCTY) 47,48,48
   48  DO 118 I = 1,10
      DO 118 J = 1,10
  118 SM(I,J) = 0.
      READ (1,77) (LOW(J),LHIGH(J),J=1,10)
      DO 21 N = 1,10
      N1 = LOW(N)
      N2 = LHIGH(N)
   21 READ (1,30) (SM(N,J),J=N1,N2)
      WRITE (2,999) ((SM(I,J),J=1,10),I=1,10)
C      READ IN FLEXIBILITY MATRIX (S)
      DO 119 I = 1,10
      DO 119 J = 1,10
  119 S(I,J) = 0.
       READ (1,1) ((S(I,J),J=1,10),I=1,10)
```

```
C       THERE IS A FACTOR OF 0.1E+05 ON THE SIC MATRIX.
        DO 250 I = 1,10
             DO 250 J = 1,10
  250   S(I,J) = S(I,J) * 0.1E+05
        WRITE (2,1001)
        WRITE (2,999) ((S(I,J),J=1,10),I=1,10)
C       READ IN COMPLEX AIC   A
  166   DO 191 M = 1,10
        DO 191 L = 1,10
        AR(L,M) = 0.
  191   AI(L,M) = 0.
        DO 31 N = 1,10
        N1 = LOW(N)
        N2 = LHIGH(N)
   31   READ (1,30) (AR(N,J),J=N1,N2)
        DO 32 N = 1,10
        N1 = LOW(N)
        N2 = LHIGH(N)
   32   READ (1,30) (AI(N,J),J=N1,N2)
        WRITE (2,1002)
        WRITE (2,999) ((AR(I,J),J=1,10),I=1,10)
        WRITE (2,1008)
        WRITE (2,999) ((AI(I,J),J=1,10)I=1,10)
  215   DO 216 I = 1,10
        DO 216 J = 1,10
        UR(I,J) =0.
  216   UI(I,J) = 0.
        DO 228 I = 1,10
        DO 228 J = 1,10
  228   SM(I,J) = SM(I,J) + AR(I,J)
```

```
C       UR = S*RM          UI = S*AI                          U = UR + I.UI
        CALL UTM4(S,SM,UR,10,10,10)
        CALL UTM4 (S,AI,UI,10,10,10)
        DO 41 I = 1,10
        DO 41 J = 1,20
   41   U(I,J) = 0.
        DO 42 I = 1,10
        DO 42 J = 1,10
        IJ = 2*J
        JJ = 2*J -1
        U(I,JJ) = UR(I,J)
   42   U(I,IJ) = UI(I,J)
        WRITE (2,43)
        WRITE (2,44) ((U(I,J),J=1,20),I=1,10)
   44 FORMAT (8(1X E12.6))
        NN = 10
         CALL EIGWRT (U,NN,EW)
        GO TO 45
   47   STOP
           END
```

```
      SUBROUTINE UTM4(A,B,C,N,M,L)
C     MATRIX MULT   C=A*B
      ML=M*L
      NM=N*M
      NL=N*L
      DIMENSION A(NM),B(ML),C(NL)
      IR=0
      IK=-M
      DO 1 K=1,L
      IK=IK+M
      DO 1 J=1,N
      IR=IR+1
      JI=J-N
      IB=IK
      C (IR)=0.
      DO 1 I=1,M
      JI=JI+N
      IB=IB+1
    1 C(IR)=C(IR)+A(JI)*B(IB)
      RETURN
      END
```

```
      SUBROUTINE EIGWRT(A1,N,EW)
C       EIGWRT IS THE SUBPROGRAMME FOR OBTAINING THE EIGENVALUES
C         OF REAL OR COMPLEX MATRICES  BY THE METHOD OF GOLUNIT?
      DIMENSION A1(10,20),EW(10,2),A(10,20),V1(40),V2(40),V3(40),V4(40),
     1  W1(4),W(4),D(12),VN(40),VQ(20)
    3 FORMAT (14H DOUBLE ROOTS.,6E17.8)
   40 FORMAT (8H EIGVAL ,6(2H  E15.8))
      ND=N
      N2=N*2
  115 DO 100 I=1,N
      DO 100 J=1,N
       A(I,2*J) = A1(I,2*J)
  100  A(I,2*J-1) = A1(I,2*J-1)
   19 N2M1=N2-1                                                          01
      DO 4 I=1,N2M1,2                                                    01
       V2(I)=1.                                                          02
    4  V2(I+1)=0.                                                        02
      K=26
   11  VMAXQ3=VMAXQ2                                                     02
      VMAXQ2=VMAXQ1                                                      02
       VRELM3=VRELM2                                                     02
      VRELM2=VRELM1                                                      02
       VIMGM3=VIMGM2                                                     02
      VIMGM2=VIMGM1                                                      02
        L=1                                                              02
      DO 6 I=1,N                                                         03
       V1(2*I-1)=0.                                                      03
      V1(2*I)=0.                                                         03
      DO 5 J=1,N2M1,2                                                    03
      V1(2*I-1)=V1(2*I-1)+A(I,J)*V2(J)-A(I,J+1)*V2(J+1)                  03
```

```
      5 V1(2*I)=V1(2*I)+A(I,J+1)*V2(J)+A(I,J)*V2(J+1)
        VQ(I)=V1(2*I-1)**2+V1(2*I)**2
        IF (VQ(I)-VQ(L))    6,6,408
    408 L=I
      6  CONTINUE
        VMAXQ1=VQ(L)
        VRELM1=V1(2*L-1)
        VIMGM1=V1(2*L)
        DO 8 I=1,N
        VN(2*I-1)=(V1(2*I-1)*    VRELM1+V1(2*I)*VIMGM1)/VMAXQ1
      8 VN(2*I)=(V1(2*I)*VRELM1-V1(2*I-1)*VIMGM1)/VMAXQ1
        VERGL=VMAXQ1*1.E-6
        VDIF=ABS(VMAXQ1-VMAXQ2)
        IF(VDIF-VERGL)    400,400,9
    400 VERGL=ABS(VRELM1)*1.E-6
        VDIF=ABS(VRELM1-VRELM2)
        IF(VDIF-VERGL)    401,401,9
    401 VERGL=ABS(VIMGM1)*1.E-2
        VDIF=ABS(VIMGM1-VIMGM2)
        IF(VDIF-VERGL)    7,7,9
      9 K=K-1
    202 IF(1-K)    90,90,20
     90 DO 21 I=1,N2
        V4(I)=V3(I)
        V3(I)=V2(I)
     21 V2(I)=VN(I)
        GOTO 11
      7 EW(N,1)=VRELM1
        EW(N,2)=VIMGM1
        WRITE (2,40) VRELM1,VRELM2,VIMGM1,VIMGM2,VMAXQ1,VMAXQ2
```

```
24   IF(L-1)     402,10,402
402  I2=2*L-2
     DO 12 I=1,L2
      LP=2*L+1-I
     LM=2*L-1-I
 12  VN(LP)=VN(LM)
     VN(1)=1
     VN(2)=0.
     LM1=L-1
     DO 13 I=1,N2
     HILF1=A(L,I)
     DO 14 J=1,LM1
       L1=L+1-J
     LJ=L-J
 14  A(L1,I)=A(LJ,I)
 13  A(1,I)=HILF1
     DO 15 I=1,N
     HILF1=A(I,2*L)
     HILF2=A(I,2*L-1)
      DO 16 J=1,L2
       LL=2*L+1-J
     LMJ=2*L-1-J
 16  A(I,LL)=A(I,LMJ)
     A(I,1)=HILF2
 15  A(I,2)=HILF1
 10   DO 17 I=2,N
     DO 17J=2,N
     A(J,2*I-1)=A(J,2*I-1)-VN(2*J-1)     *A(1,2*I-1)+VN(2*J)*A(1,2*I)
 17  A(J,2*I)=A(J,2*I)-VN(2*J-1)  *A(1,2*I)-VN(2*J)*A(1,2*I-1)
     N=N-1
```

```
      N2=2*N
       DO 18 I=1,N
       DO18 J=1,N2
   18   A(I,J)=A(I+1,J+2)
       IF(N-1)     19,403,19
  403  EW(1,1)=A(1,1)
       EW(1,2)=A(1,2)
       AMAX=A(1,1)**2+A(1,2)**2
        WRITE (2,40) A(1,1),VN(2),A(1,2),VN(2),AMAX,VN(2)
       CALL DOPPEL (A1,EW,ND)
       RETURN
   20  LN=1
       IF(L-1)    404,405,404
  404  LN=2*L-3
  405  LM=LN+3
       DO 30 I=LN,LM
       ILN=I-LN+1
       D(ILN)=V4(I)
       D(ILN+4)=V3(I)
   30  D(ILN+8)=V2(I)
       CALL DOPLW2(D,VRELM3,VRELM2,VIMGM3,VIMGM2,W1)
       W1Q1=W1(1)**2+W1(2)**2
       W1Q2=W1(3)**2+W1(4)**2
       WRITE (2,3)  (W1(I),I=1,4),W1Q1,W1Q2
       DO 31 I=LN,LM
       ILN=I-LN+1
       D(ILN)=V3(I)
       D(ILN+4)=V2(I)
   31  D(ILN+8)=V1(I)
       CALLDOPLW2(D,VRELM2,1.,VIMGM2,0.,W)
```

```
      WQ1=W(1)**2+W(2)**2
      WQ2=W(3)**2+W(4)**2
       WRITE (2,3) (W(I),I=1,4),WQ1,WQ2
      IF(WQ2-WQ1)     303,303,301
  303 EW(N,1) = W(1)
      EW(N,2) = W(2)
      VER1=ABS(W1(1)-W(1))
      VER2=ABS(W(1))/500.
      IF(VER1-VER2)      406,406,201
  406  VER1=ABS(W1(2)-W(2))
      VER2=ABS(W(2))/500
      IF(VER1-VER2)    302,302,201
  302 L=1
      DO 22 I=1,N
      V1(2*I-1)=W(3)*V2(2*I-1)-W(4)*V2(2*I)-V1(2*I-1)
      V1(2*I)=W(3)*V2(2*I)+W(4)*V2(2*I-1)-V1(2*I)
      VQ(I)=V1(2*I-1)**2+V1(2*I)**2
      IF(VQ(I)-VQ(L))      22,22,407
  407 L=I
   22 CONTINUE
      VMAXQ1=VQ(L)
      VRELM1=V1(2*L-1)
      VIMGM1=V1(2*L)
       DO 23 I=1,N
      VN(2*I-1) = V1(2*I-1)*VRELM1+V1(2*I)*VIMGM1)/VMAXQ1
   23 VN(2*I)= V1(2*I)*VRELM1-V1(2*I-1)*VIMGM1)/VMAXQ1
      GOTO 24
  201 K=10
      GOTO 202
  301 VER3=W(4)
```

```
W(4)=W(2)
W(2)=VER3
VER3=W(3)
W(3)=W(1)
W(1)=VER3
VER3=W1(3)
W1(3)=W1(1)
W1(1)=VER3
VER3=W1(4)
W1(4)=W1(2)
W1(2)=VER3
GOTO 303
END
```

```
      SUBROUTINE DOPPEL (A,EW,NN)
      DOUBLE PRECISION B(10,20),X0(10,2),R(10,2),F1,F2,F3,F4,
     1 ER1,EI1,FQ(20),FQ1(20),FQ2(20),FQF,EWD(2),H1,H2
      DIMENSION A(10,20),EW(10,2),D(12),W(4),EWA(2)   ,X1(20,2),X2(20,2),
     1X3(20,2)
       COMMON NAERO,VELCTY
    1 FORMAT (20H  DIAGONALELEMENT B(,I2,1H,,I2,4H)=0.)
    2 FORMAT (22H APPROXN FOR E.V.  RE=,E15.8,4H IM=,E15.8)
    6 FORMAT ( 19H APPROXN FOR L  RE=,E15.8,4H IM=,E15.8/
     1 10H XO(10,1)=,E15.8,9HXO(10,2)=,E15.8)
    5 FORMAT (4H NN=,I2,27HDOUBLE ROOTS AT THE EIGVALS ,
     1   2(E15.7,3H+I*,E15.7))
    3 FORMAT (14H EXCHANGE THE ,I2,18HTH VALUE WITH THE ,I2,32HT VALUE.L
     1AST EIGVECT COMPONENT=0)
   42 FORMAT (/20H ITERATION SUSPENDED?)
    4 FORMAT (19H APPROXN FOR EIGVAL,2(E15.8,3H+I*,E15.8))
      IPRF=NN+1
      ND=NN
      ND2=ND*2
   28 IZ=0
      MAX=5
   20 KENN=26
      ER2=0.
      EI2=0.
      DO330 I=1,ND
      DO 330 J=1,ND2
  330 B(I,J)=0.
      DO 10 J=1,ND
      DO 10 I=1,ND
        B(I,2*J) = A(I,2*J)
```

```
 10     B(I,2*J-1) = A(I,2*J-1)
        EWD(1)=EW(NN,1)
        EWD(2)=EW(NN,2)
        DO 11 I=1,ND
        J=2*I-1
        B(I,J)=B(I,J)-EWD(1)
 11     B(I,J+1)=B(I,J+1)-EWD(2)
        IF (IZ) 22,21,22
 22     DO 23 I=1,ND2
        H1=B(IZ,I)
        B(IZ,I)=B(ND,I)
 23     B(ND,I)=H1
        DO 24 I=1,ND
        H1=B(I,2*IZ)
        H2=B(I,2*IZ-1)
        B(I,2*IZ-1)=B(I,ND2-1)
        B(I,2*IZ)=B(I,ND2)
        B(I,ND2)=H1
 24     B(I,ND2-1)=H2
        WRITE (2,3) IZ,ND
 21     ND1=ND-1
        DO 12 L=1,ND1
        L1=L+1
        FQ(L)=B(L,2*L-1)**2+B(L,2*L)**2
        IF(FQ(L))   30,30,29
 30     WRITE (2,1) L,L
        GO TO 107
 29     FQ1(L)=B(L,2*L-1)/FQ(L)
        FQ2(L)=B(L,2*L)/FQ(L)
        DO 12 J=L1,ND
```

```
      F1=B(J,2*L-1)*FQ1(L)+B(J,2*L)*FQ2(L)
      F2=B(J,2*L-1)*FQ2(L)-B(J,2*L)*FQ1(L)
      B(J,2*L-1)=F1
      B(J,2*L)=F2
      DO 12 K=L1,ND
      B(J,2*K-1)=B(J,2*K-1)-B(L,2*K-1)*F1-B(L,2*K)*F2
   12 B(J,2*K)=B(J,2*K)+B(L,2*K-1)*F2-B(L,2*K)*F1
      DO 13 I=1,ND
      X0(I,1)=1.
   13 X0(I,2)=0.
   25 DO 14 I=1,ND
      R(I,1)=X0(I,1)
   14 R(I,2)=X0(I,2)
      DO 15 L=1,ND1
      L1=L+1
      DO 15 J=L1,ND
      R(J,1)=R(J,1)-B(J,2*L-1)*R(L,1)-B(J,2*L)*R(L,2)
   15 R(J,2)=R(J,2)+B(J,2*L)*R(L,1)-B(J,2*L-1)*R(L,2)
      FQE=R(ND,1)**2+R(ND,2)**2
      ER1=(B(ND,2*ND-1)*R(ND,1)+B(ND,2*ND)*R(ND,2))/FQE
      EI1=(B(ND,2*ND)*R(ND,1)-B(ND,2*ND-1)*R(ND,2))/FQE
  203 VERR=ABS (ER1)*1.E-3
      VERI=ABS (EI1)*1.E-3
      IF (ABS (ER1-ER2)-VERR) 100,100,101
  100 IF (ABS (EI1-EI2)-VERI) 102,102,101
  101 DO 17 I=1,ND1
      J=ND-I
      J1=J+1
      F1=0.
      F2=0.
```

```
      IF(I-1) 120,31,120
  120 DO 18 K=J1,ND1
      F1=-B(J,2*K-1)*X0(K,1)+B(J,2*K)*X0(K,2) +F1
   18                 F2=-B(J,2*K-1)*X0(K,2)-B(J,2*K)*X0(K,1)     +F2
   31         F1=-B(J,ND2-1)+R(J,1)*ER1-R(J,2)*EI1 +F1
              F2=-B(J,ND2)+R(J,1)*EI1+R(J,2)*ER1 +F2
      X0(J,1)= F1*FQ1(J)+F2*FQ2(J)
      X0(J,2)= F2*FQ1(J)-F1*FQ2(J)
   32 IF (ABS (X0(J,1))+ABS (X0(J,2))-1.E+10) 17,19,19
   19 I7=J
      GO TO 20
   17 CONTINUE
      DO 16 I=1,ND
      J=ND+1-I
      DO 16 K=1,2
      X3(J,K)=X2(J,K)
      X2(J,K)=X1(J,K)
   16 X1(J,K)=X0(J,K)
      KENN=KENN-1
      IF(KENN)  26,27,26
   26 ER2=ER1
      EI2=EI1
      GO TO 25
  102 EW(NN,1)=EW(NN,1)+ER1
      EW(NN,2)=EW(NN,2)+EI1
  201  IF (ABS(EW(NN,1)) * 1.E- 7 - ABS(ER1))  40,109,109
  109 IF (ABS(EW(NN,2))+1. E- 7 - ABS(EI1)) 40,110,110
   40 MAX=MAX-1
      IF(MAX) 41,41,20
   41  WRITE (2,42)
```

```
110 CALL SHRIBE (EW,ER1,EI1,NN,ND,XO,YO,N,OMN)
107 NN=NN-1
    IF (NN-NAERO) 106,106,28
106 RETURN
 27 DO 111 I=1,2
    D(2*I-1)=X1(I,1)
    D(2*I)=X1(I,2)
    D(2*I+3)=X2(I,1)
    D(2*I+4)=X2(I,2)
    D(2*I+7)=X3(I,1)
111 D(2*I+8)=X3(I,2)
    CALL DOPLWZ(D,ER1,EI1,ER2,EI2,W)
    EWA(1)=EW(NN,1)
    EWA(2)=EW(NN,2)
    EW(NN,1)=EWA(1)+W(1)
    EW(NN,2)=EWA(2)+W(2)
    NN=NN+1
    EW(NN,1)=EWA(1)+W(3)
    EW(NN,2)=EWA(2)+W(4)
    WRITE (2,4) EW(NN,1),EW(NN,2),EW(NN-1,1),EW(NN-1,2)
    IF(IPRF-NN)    112,113,113
113 IPRF=NN
    GOTO 28
112 NN=NN-2
    WRITE (2,5)  NN,EW(NN+1,1),EW(NN+1,2),EW(NN+2,1),EW(NN+2,
   12)
    IPRF=NN
    GOTO 28
    END
```

```
$IBFTC DOWU     DECK
CDOWU
      SUBROUTINE DOPLWZ (B,BR1,BR2,BI1,BI2,W)                          00
C       DOPLWZ  IS THE SUBPROGRAMME FOR CALCULATING NEARLY EQUAL ROOTS,( ROOT
C        WHICH CANNOT BE DETERMINED BY THE POWER METHOD ALONE)
      DIMENSION C(2,3),B(4,3),W(4)
       DO 202 J=1,3,2                                                  00
      BN=B(J,3)*BR1-B(J+1,3)*  BI1                                     00
      B(J+1,3)=B(J,3)*BI1+B(J+1,3)*BR1                                 00
  202 B(J,3)     =BN                                                   00
      DO 204 I=2,3                                                     10
      DO 201 J=1,3,2                                                   00
      BN=B(J,I)*BR1-B(J+1,I)*BI1                                       01
      B(J+1,I)=B(J,I)*BI1+B(J+1,I)*BR1                                 01
  201 B(J,I)=BN                                                        01
      BI1=BI2                                                          01
  204 BR1=BR2                                                          01
      DO 203 I=2,3                                                     01
      I1=I-1                                                           1
      DO 203 J=1,I1                                                    01
      II=I+J-2                                                         01
     1   +B(4,J)*B(2,I)                                                01
  203  C(2,II)=B(1,J)*B(4,I)+B(2,J)*B(3,I)-B(3,J)*B(2,I)
     1   -B(4,J)*B(1,I)
      IF(C(2,1))     210,208,210
  208 IF(C(2,2))     210,209,210
  209 IF(C(2,3))     210,205,210
  210 CQ=C(1,1)**2+C(2,1)**2
      PR=-(C(1,2)*C(1,1)+C(2,2)*C(2,1))/CQ
      PI=(C(1,2)*C(2,1)-C(2,2)*C(1,1))/CQ                              02
```

```
      QR=(C(1,1)*C(1,3)+C(2,1)*C(2,3))/CQ
      QI=(C(2,1)*C(1,3)-C(1,1)*C(2,3))/CQ
      H1=(PR**2-PI**2)/4.-QR
      H2=PR*PI/2.+QI
      H3=(((H1**2+H2**2)**0.5+H1)/2.)**0.5
      H4=H2/(2.*H3)
  207 W(1)=-PR/2.+H3
      W(2)=-PI/2.+H4
      W(3)=-PR/2.-H3
      W(4)=-PI/2.-H4
      RETURN
  205 PR=-C(1,2)/C(1,1)
      QR=C(1,3)/C(1,1)
      PI=0.
      H1=(PR**2)/4.-QR
      IF(H1)    206,206,211
  211 H3=H1**0.5
      H4=0.
      GOTO207
  206 H4=(-H1)**0.5
      H3=0.
      GOTO207
      END
```

```
      SUBROUTINE SHRIBE (EW,ER1,EI1,NNN,N,XO,YLN, OMN)
      DOUBLE PRECISION XO(20,2),BET,BETQ,WZ(2)
      DIMENSION EW(10,2),XBET(20),XARG(20)
      COMMON VELCTY
    1 FORMAT (/12H NEW EIGVAL ,2E12.6,6HERROR ,2E12.6,8HMODULUS ,2D17.8)
    2 FORMAT( 12H EIGENVECTOR,D15.8,3H+I(,D15.8,1H),
     1 D15.8,3H+I(,D15.8,1H),
     2 D15.8,3H+I(,D15.8,1H))
    3 FORMAT (11H SQRTF(EW,),2(E15.8,2H  ))
   14  FORMAT (42H ***THIS MODE GIVES IMAGINARY FREQUENCY***)
   16   FORMAT (23H **INFINITE FREQUENCY**)
   18  FORMAT (22H **FLUTTER FREQUENCY = E12.6,4H CPS,5X 12H **DAMPING =
     1, E12.6, 18H **FLUTTER SPEED =,E12.6,5H FPS/)
      BETQ=EW(NNN,1)**2+EW(NNN,2)**2
      BET=SQRT(BETQ)
       WRITE (2,1) EW(NNN,1),EW(NNN,2),ER1,EI1,BET,BETQ
      WRITE (2,2) ((XO(I,J),J=1,2),I=1,N)
       IF (EW(NNN,1)) 10,11,12
   10  WRITE (2,14)
       GO TO 5
   11  WRITE (2,16)
      GO TO 5
   12  A = SQRT (EW(NNN,1))
      FREQ = 0.3126899E 03 / A
      DAMP = EW(NNN,2) / EW(NNN,1)
      IF (VELCTY) 35,35,21
   35  SPEED = 0.
      GO TO 45
   21  SPEED = 0.1570796E 01 * FREQ / VELCTY
   45  WRITE (2,18) FREQ,DAMP,SPEED
    5  RETURN
       END
```

WING A3 UNIFORM WING VELCTY=0.1

4 0 100000

MASS MATRIX

0.124376E 00 -.543300E-02 0.000000E 00 0.000000E 00 0.000000E 00 0.000000E 00 0.000000E 00 0.000000E 00
0.000000E 00 0.000000E 00 -.543300E-02 0.847280E-01 0.000000E 00 0.000000E 00 0.000000E 00 0.000000E 00
0.000000E 00 0.000000E 00 0.000000E 00 0.000000E 00 0.000000E 00 0.000000E 00 0.829170E-01 -.366200E-02
0.000000E 00 0.000000E 00 0.000000E 00 0.000000E 00 0.000000E 00 0.000000E 00 0.000000E 00 0.000000E 00
-.362200E-02 0.564860E-01 0.000000E 00 0.000000E 00 0.000000E 00 0.000000E 00 0.000000E 00 0.000000E 00
0.000000E 00 0.000000E 00 0.000000E 00 0.000000E 00 0.829170E-01 -.366200E-02 0.000000E 00 0.000000E 00
0.000000E 00 0.000000E 00 0.000000E 00 0.000000E 00 0.000000E 00 0.000000E 00 -.362200E-02 0.564860E-01
0.000000E 00 0.000000E 00 0.000000E 00 0.000000E 00 0.000000E 00 0.000000E 00 0.000000E 00 0.000000E 00
0.000000E 00 0.000000E 00 0.829170E-01 -.366200E-02 0.000000E 00 0.000000E 00 0.000000E 00 0.000000E 00
0.000000E 00 0.000000E 00 0.000000E 00 0.000000E 00 -.362200E-02 0.564860E-01 0.000000E 00 0.000000E 00
0.000000E 00 0.000000E 00 0.000000E 00 0.000000E 00 0.000000E 00 0.000000E 00 0.000000E 00 0.000000E 00
0.124376E 00 -.543300E-02 0.000000E 00 0.000000E 00 0.000000E 00 0.000000E 00 0.000000E 00 0.000000E 00
0.000000E 00 0.000000E 00 -.543300E-02 0.847280E-01

SIC MATRIX

0.167000E 02 -.599000E 01 0.471100E 02 0.244200E 02 0.714300E 02 0.487400E 02 0.957600E 02 0.730700E 02
0.126160E 03 0.103470E 03 -.599000E 01 0.847600E 02 0.244200E 02 0.115170E 03 0.487400E 02 0.139490E 03
0.730700E 02 0.163820E 03 0.103470E 03 0.194220E 03 0.471100E 02 0.244200E 02 0.242730E 03 0.182230E 03
0.415700E 03 0.355200E 03 0.588680E 03 0.528180E 03 0.804890E 03 0.744390E 03 0.244200E 02 0.115170E 03
0.182230E 03 0.424240E 03 0.355200E 03 0.597210E 03 0.528180E 03 0.770190E 03 0.744390E 03 0.986400E 03
0.714300E 02 0.487400E 02 0.415700E 03 0.355200E 03 0.796530E 03 0.705780E 03 0.118572E 04 0.109497E 04
0.183555E 04 0.158145E 04 0.487400E 02 0.139490E 03 0.355200E 03 0.597210E 03 0.705780E 03 0.106980E 04
0.109497E 04 0.145799E 04 0.158145E 04 0.194447E 04 0.957600E 02 0.730700E 02 0.588680E 03 0.528180E 03
0.118572E 04 0.109497E 04 0.186924E 04 0.174823E 04 0.273411E 04 0.261310E 04 0.730700E 02 0.163820E 03
0.528180E 03 0.770190E 03 0.109497E 04 0.145799E 04 0.174823E 04 0.223227E 04 0.261310E 04 0.309714E 04
0.126160E 03 0.103470E 03 0.804890E 03 0.744390E 03 0.183555E 04 0.158145E 04 0.273411E 04 0.261310E 04
0.420338E 04 0.404456E 04 0.103470E 03 0.194220E 03 0.744390E 03 0.986400E 03 0.158145E 04 0.194447E 04
0.261310E 04 0.309714E 04 0.404456E 04 0.467985E 04

AIC MATRIX***REAL PART

```
 0.125262E 01 -.127475E 01 0.000000E 00 0.000000E 00 0.000000E 00 0.000000E 00 0.000000E 00 0.000000E 00
 0.000000E 00 0.000000E 00 0.938000E-03 0.281600E-02 0.000000E 00 0.000000E 00 0.000000E 00 0.000000E 00
 0.000000E 00 0.000000E 00 0.000000E 00 0.000000E 00 0.000000E 00 0.000000E 00 0.835078E 00 -.849830E 00
 0.000000E 00 0.000000E 00 0.000000E 00 0.000000E 00 0.000000E 00 0.000000E 00 0.000000E 00 0.000000E 00
 0.616000E-03 0.187800E-02 0.000000E 00 0.000000E 00 0.000000E 00 0.000000E 00 0.000000E 00 0.000000E 00
 0.000000E 00 0.000000E 00 0.000000E 00 0.000000E 00 0.835078E 00 -.849830E 00 0.000000E 00 0.000000E 00
 0.000000E 00 0.000000E 00 0.000000E 00 0.000000E 00 0.000000E 00 0.000000E 00 0.616000E-03 0.187800E-02
 0.000000E 00 0.000000E 00 0.000000E 00 0.000000E 00 0.000000E 00 0.000000E 00 0.000000E 00 0.000000E 00
 0.000000E 00 0.000000E 00 0.835078E 00 -.849830E 00 0.000000E 00 0.000000E 00 0.000000E 00 0.000000E 00
 0.000000E 00 0.000000E 00 0.000000E 00 0.000000E 00 0.616000E-03 0.187800E-02 0.000000E 00 0.000000E 00
 0.000000E 00 0.000000E 00 0.000000E 00 0.000000E 00 0.000000E 00 0.000000E 00 0.000000E 00 0.000000E 00
 0.125262E 01 -.127475E 01 0.000000E 00 0.000000E 00 0.000000E 00 0.000000E 00 0.000000E 00 0.000000E 00
 0.000000E 00 0.000000E 00 0.938000E-03 0.281600E-02
```

***IMAGINARY PART

```
-.273874E 00 0.133870E 00 0.000000E 00 0.000000E 00 0.000000E 00 0.000000E 00 0.000000E 00 0.000000E 00
 0.000000E 00 0.000000E 00 0.751160E-01 -.751160E-01 0.000000E 00 0.000000E 00 0.000000E 00 0.000000E 00
 0.000000E 00 0.000000E 00 0.000000E 00 0.000000E 00 0.000000E 00 0.000000E 00 -.182582E 00 0.892460E-01
 0.000000E 00 0.000000E 00 0.000000E 00 0.000000E 00 0.000000E 00 0.000000E 00 0.000000E 00 0.000000E 00
 0.500760E-01 -.500760E-01 0.000000E 00 0.000000E 00 0.000000E 00 0.000000E 00 0.000000E 00 0.000000E 00
 0.000000E 00 0.000000E 00 0.000000E 00 0.000000E 00 -.182582E 00 0.892460E-01 0.000000E 00 0.000000E 00
 0.000000E 00 0.000000E 00 0.000000E 00 0.000000E 00 0.000000E 00 0.000000E 00 0.500760E-01 -.500760E-01
 0.000000E 00 0.000000E 00 0.000000E 00 0.000000E 00 0.000000E 00 0.000000E 00 0.000000E 00 0.000000E 00
 0.000000E 00 0.000000E 00 -.182582E 00 0.892460E-01 0.000000E 00 0.000000E 00 0.000000E 00 0.000000E 00
 0.000000E 00 0.000000E 00 0.000000E 00 0.000000E 00 0.500760E-01 -.500760E-01 0.000000E 00 0.000000E 00
 0.000000E 00 0.000000E 00 0.000000E 00 0.000000E 00 0.000000E 00 0.000000E 00 0.000000E 00 0.000000E 00
-.273874E 00 0.133870E 00 0.000000E 00 0.000000E 00 0.000000E 00 0.000000E 00 0.000000E 00 0.000000E 00
 0.000000E 00 0.000000E 00 0.751160E-01 -.751160E-01
```

Application of a Direct Matrix Method to a Plate Vibration Problem

In this appendix, the fundamental frequencies of a square plate symmetrically supported at four points are obtained by a Direct Matrix method and also by using assumed mode methods. The results illustrate that the Direct Matrix method gives more satisfactory approximations to the fundamental frequency. The results from the assumed mode analysis show that it is not possible to assume a mode which yields satisfactory results for all positions of the support points.

(In this paper, the energy analyses were conducted by Prof D.J.Johns and the finite difference analyses by the present author).

On The Fundamental Frequency Of A Square Plate Symmetrically Supported At Four Points

D. J. Johns V. T. Nagaraj

University of Technology, Loughborough, Leics

SUMMARY

The title problem has been examined using (a) energy-type analyses involving the assumption of modal forms and (b) an alternative finite difference formulation of the governing differential equation of the problem.

Because of its simplicity in use and accuracy - the latter method is advocated. Over the entire range of symmetric supports (viz. 4 corner supports to 1 single central support) the finite difference method gives satisfactory results agreeing well with experimental data.

1. Introduction

A square plate symmetrically supported at four points has various practical applications which require a study to be made of its vibration characteristics.

Ref.1 present such results for rectangular plates supported at the four corners using a finite difference approach to the governing differential equation. For the particular case of a square plate Ref.2 employs an energy method and using a very simple assumed modal forms shows good agreement with Ref.1.

Alternative, more general modal forms are considered in Ref.3 when the four point supports lie at specified positions along the plate diagonals, and an attempt is made to correlate the results with those of corresponding experiments. Unfortunately, it is shown that none of the modal forms assumed is satisfactory for all possible support positions.

It is the authors' view that the finite difference approach should yield the more satisfactory set of results and the purpose of the present paper is to discuss results obtained recently for a square plate from both the energy method and the finite difference method for all possible symmetric support positions.

It should be remembered that energy methods always overestimate the fundamental frequency, so with more refined analyses the exact value can be approached from above. Conversely the finite difference method, established by Williams (ref. 4,5) underestimates the natural frequency and with increasing refinement in the analysis the exact value can be approached from below.

Thus it is hoped that sufficiently close upper and lower bounds can be obtained for the theoretical values of the natural frequency for all support positions and that closer correlation can be ontained with the available experimental data.

2. Plate Configuration

The plate configuration is shown in Fig.1 and the coordinates of the four support points are defined by the parameter α. The case of $\alpha/a = 0$ corresponds to corner supports and $\alpha/a = .5$ corresponds to a single, central support point. It is clear that in general the fundamental mode for a plate supported on diagonal point supports will have a nodal line crossing the plate co-ordinate axes and that the nodal points on these axes will provide an alternative set of four symmetric support points within the context of the present study.

3. Energy Analyses

Using classical thin plate theory the strain energy expression for the square plate is given by

$$U = \frac{D}{2} \int_{-a/2}^{a/2} \int_{-a/2}^{a/2} \left[\left(\frac{\partial^2 w}{\partial x^2}\right)^2 + \left(\frac{\partial^2 w}{\partial y^2}\right)^2 + 2\nu \frac{\partial^2 w}{\partial x^2} \frac{\partial^2 w}{\partial y^2} + 2(1-\nu)\left(\frac{\partial^2 w}{\partial x \partial y}\right)^2 \right] dxdy \quad (1)$$

and the kinetic energy is given by

$$T = \frac{\rho h}{2} \int_{-a/2}^{a/2} \int_{-a/2}^{a/2} \left(\frac{\partial w}{\partial t}\right)^2 dxdy \quad (2)$$

Where
- D = plate stiffness = $Eh^3/12(1-\nu^2)$
- E = Youngs modulus
- ν = Poissons Ratio
- h = Plate thickness
- ρ = Density
- w = Plate deflection

By assuming that $w_{(x,y,t)} = W_{(x,y)} \sin \omega t$ with the function W consisting of appropriate assumed deflection modes which satisfy the support constraints, it is possible to evaluate the frequency of vibration, ω, by the application of the Rayleigh - Ritz Method.

The following single deflection modes have been considered viz.

$$W_o = A \left(\cos \frac{k\pi x}{a} + \cos \frac{k\pi y}{a}\right) \quad (3)$$

$$W = B \left(2 - \frac{2^n k^n x^n}{a^n} - \frac{2^n k^n y^n}{a^n}\right) \qquad n \geq 2 \quad (4)$$

$$W = C \left(1 - \frac{4k^2x^2}{a^2}\right)\left(1 - \frac{4k^2y^2}{a^2}\right) \quad (5)$$

$$W = D \left(\cos \frac{k\pi x}{a} \cdot \cos \frac{k\pi y}{a}\right) \quad (6)$$

$$W = E \left(1 - \frac{16 k^4 x^2 y^2}{a^4}\right) \quad (7)$$

$$W = F \left(1 - \frac{2^n k^n x^n}{a^n}\right) \qquad n \geq 2 \quad (8)$$

Where $k = a/(a - 2\alpha)$ and A, B, C etc. are generalised co-ordinates. N.B.That mode F is independent of y.

In cases B & F the value $n = 2$ gave the lowest values of Ω

The corresponding expressions for the non-dimensional frequency parameter Ω ($= \omega^2 \rho h a^4/D$) are given below for those modal forms which gave the most acceptable results. The other single modal forms gave results which were in general far too high except for Mode A with $\alpha/a < .2$.

$$\Omega_B = 1440\,(1+\nu)\,k^4\left[45 - 30k^2 + 7k^4\right]^{-1} \qquad (9)$$

$$\Omega_F = 960\,k^4\left[15 - 10\,k^2 + 3\,k^4\right]^{-1} \qquad (10)$$

Numerical values of $\Omega^{\frac{1}{2}}$ based on these expressions are shown in Fig.2 together with other results including various binary and ternary solutions including those from Refs. 2,3.

The binaries A + C and B + C, (Ref. 3) do not give completely satisfactory results mainly due to the fact that Modes A and C alone gave unsatisfactory results. The binary A + D which gives a good result for $\alpha/a = 0$ as shown in Ref. 2 becomes increasingly unreliable as α/a increases thus showing the possible inadequacy of the energy method in assuming a simple combination of modes to cover all possible support points. The ternary A+B+C with n=2 (Ref.3) gives minimum results for $\Omega^{\frac{1}{2}}$ as shown by the thick line in Fig.2.

4. Finite Difference

The governing differential equation for small deflection behaviour of a thin uniform plate loaded normally to its surface by a pressure q is

$$\frac{\partial^4 w}{\partial x^4} + 2\,\frac{\partial^4 w}{\partial x^2 \partial y^2} + \frac{\partial^4 w}{\partial y^4} = q/D \qquad (11)$$

and the finite difference form of equation (11) can be written generally in terms of the deflections, w_n, at 13 stations in the neighbourhood of the loaded point as shown for a typical element, O, in Fig.3

Thus,

$$\frac{Ro\ell^2}{D} = 20\,w_o - 8\sum_{r=1}^{4} w_r + 2\sum_{r=5}^{8} w_r + \sum_{r=9}^{12} w_r \qquad (12)$$

For stations on or adjacent to the free edge of the plate the appropriate free edge boundary conditions are invoked to obtain expressions for those stations, w_r, off the plate in terms of those on the plate (Ref.4). This results in a less general form of equation (12) as will be seen later.

It is clear that this method becomes more accurate as the number of stations on the plate is increased and to this end the alternative mesh configurations shown in Fig.4 have been studied in detail. Because of the symmetry (assumed) of the fundamental mode about the diagonals and about the co-ordinate axes only a triangular portion of the plate would apparently need to be considered. It should be noted that cases III and V have previously been studied in Ref.1 for corner supports only.

The full details of the derivation of the relevant finite difference equations representing the oscillatory inertia force R_n on each station n are not presented here but a typical set of equations is given below for case IV. The effects of the free edge boundary conditions on the general form of equation (12) is clearly seen.

$$\frac{\ell^2 R_A}{D} = \frac{\lambda W_A}{4} = 2.31\, W_A - 4.62\, W_B + 1.4\, W_C + .91\, W_D \quad (13)$$

$$\frac{\ell^2 R_B}{D} = \frac{\lambda W_B}{2} = -2.31\, W_A + 8.23 W_B - 5.4\, W_C - 3.22\, W_D + 2.7\, W_E \quad (14)$$

$$\frac{\ell^2 R_C}{D} = \lambda W_C = 1.4\, W_A - 10.8\, W_B + 20.0 W_C + 3.4\, W_D - 16\, W_E + 2 W_F \quad (15)$$

$$\frac{\ell^2 R_D}{D} = \frac{\lambda W_D}{2} = .91 W_A - 6.44\, W_B + 3.4\, W_C + 6.53\, W_D - 5.4\, W_E + W_F \quad (16)$$

$$\frac{\ell^2 R_E}{D} = \lambda W_E = 5.4\, W_B - 16\, W_C - 5.4\, W_D + 24\, W_E - 8\, W_F \quad (17)$$

$$\frac{\ell^2 R_F}{D} = \lambda W_F = 8\, W_C + 4\, W_D - 32\, W_E + 20\, W_F \quad (18)$$

$$\text{Where } \lambda = \left(\frac{\rho h \omega^2}{D}\right) \cdot \ell^4 = \Omega \frac{\ell^4}{a^4} \quad (19)$$

If the corner only is supported then equation (13) is neglected and $W_A = 0$ in the remaining equations (13) - (16). For alternative diagonal support points e.g. C or F the correspondong equations (15) or (18) would be neglected together with W_C or W_F elsewhere.

It should be noted that if $W_A = W_B = W_D = 0$ simultaneously in the above equations then simply supported edges are simulated and λ the eigenvalue is determined by the solution of equations (15), (17) and (18). The results obtained may thus be compared with known exact solutions which has been done in Table I for cases I to IV. These show the improvement in accuracy obtained with decreasing mesh size . This problem has also been examined in Ref. 5.

From such finite difference solutions it is possible by means of Richardson's extrapolation formula (Ref.6) to predict a more exact solution. This procedure was followed in Ref. 1 and based on the results for Case III and Case V shown in Table 1 below an estimate of $\Omega_{\frac{1}{2}} = 7.117$ was obtained for the plate supported only at the corners whereas the energy method of Ref. 3 using the modes A + B + C with n = 2 gave 7.115. It may therefore be reasonably inferred that the exact value is 7.115.

TABLE 1

Values of Ω^2 by Finite Difference Method

Case	I	II	III	IV	V	VI	EXACT
ℓ/a	$\frac{1}{2}$	$\frac{1}{3}$	$\frac{1}{4}$	$\frac{1}{5}$	$\frac{1}{6}$	$\frac{1}{10}$	-
Simply Supported Plate	16	18	18.76[5]	19.04	19.6	-	19.74[5]
Corner Supported $\alpha/a=0; W_A=0$	6.47	6.85	6.98[1]	7.00	7.06[1]	7.092	7.115[3]

The numbers thus, (1) indicate the source reference if different from this paper.

The above results show that for the plate with corner supports only, Case VI gives consistent results and one can assume that the mesh size chosen viz. $\ell/a = \frac{1}{10}$ is sufficiently small to yield accurate results for all diagonal support points. These results are shown in Table 2 and Fig.2 together with a few additional results which indicate still further the increase in accuracy gained with decreasing mesh size.

TABLE 2

Values of Ω^2 by Finite Difference Method for Various α/a

	α/a = 0	.1	.2	.3	.4	.5
Case VI	Ω^2 = 7.092	12.58	22.26	18.31	15.32	26.82
	For Case VI Modified with Nodal Co-ordinate Axes					13.35

It is clear from Table 2 and Fig.2 that using the original finite difference Mesh for Case I, III and VI that an apparent anomaly has arisen. Although with decreasing mesh size the value of Ω^2 has increased the value for Case VI (Original) for $\alpha/a = .5$ is much greater than the corresponding energy solutions and shows an entirely unexpected trend for Ω^2 with α/a.

It was concluded that for the case of a single central support point for the plate the fundamental mode does not necessarily correspond to a situation in which the four quadrants of the plate vibrate in phase as was assumed in setting up the original finite difference equations. Instead a possible vibration mode could be visualised in which adjacent quadrants vibrate out-of-phase with nodal lines lying either along the co-ordinate axes of the plate or along the diagonals.

The detailed results obtained, assuming that the nodal lines lie along the coordinate axes are shown in Table 3, below and also in Fig.2 together with extrapolated results using corresponding pairs of individual results. Thus, whilst Case VI gives $\Omega^{\frac{1}{2}}$ = 13.35 the extrapolated result from Case III and VI is $\Omega^{\frac{1}{2}}$ = 13.56. This result gives much better agreement with the energy solution for α/a = .5 viz 13.56 cf. 16.22 than did Case VI (original). Results obtained assuming that the nodal lines lie along the diagonals were higher than those shown in Table.3

TABLE 3

Modified Results For α/a = .5

Case	I	III	VI
$\Omega^{\frac{1}{2}}$	9.48	12.1731	13.35
$\Omega^{\frac{1}{2}}$ extrapolated		12.9 13.48	13.56

Clearly the anomaly referred to above would not have arisen if no 'a priori' assumption had been made about the form of the fundamental vibration mode, and, instead, a general finite difference formulation had been derived for the entire plate.

5. Experimental Data

The experimental data shown in Fig.2 for cases α/a < .5 were presented in Ref.3. The result for α/a = .5 has been obtained by the present authors.

6. Discussion of Results and Conclusions

Fig. 2 shows the various results obtained for the frequency parameter $\Omega^{\frac{1}{2}}$ for a square plate supported successively at various diagonal points. The narrow band between the limiting results from both the energy and finite difference analyses indicates the region in which the various exact solutions would lie. The narrowness of this band is a measure of the close agreement with the exact solutions which has been achieved and this is supported by the correlation of the experimental results from Ref.3. with the band.

Since none of the energy methods was completely satisfactory over the range of values for α/a and because the energy methods give values of frequency which are higher than the exact solutions and are therefore unconservative in design it is believed that the finite difference method giving a frequency which is lower than the exact is to be preferred.

It is also worth noting that the amount of manual labour involved was far greater for the energy analyses.

7. Acknowledgements

Acknowledgement is made to H. Gollnitz (Max-Planck-Institut fur Physik und Astr Physik) who made available the computer programme used in the finite difference analyses and to Dr. D. Williams who made some useful comments in the early stages of this study.

References

1. Cox, H.L., Boxer, J., Vibration of Rectangular Plates Point-supported at the corners. Aero.Quart. 11 (1) : 41-50, February, 1960.

2. Kirk, C.L., A note on the lowest natural frequency of a square plate point-supported at the corners. J.Roy.Aero.Soc. 66 (4) : 240 - 241 April, 1962.

3. Tso, W.K., On the fundamental frequency of a four point-supported square elastic plate. A.I.A.A. Jour. 4 (4) : 733 - 735 April, 1966.

4. Williams, D., A general method (depending on the aid of a digital computer) for deriving the structural influence coefficients of aeroplane wings. A.R.C., R & M No. 3048, 1959.

5. Williams, D., A new method of obtaining lower limits for the solutions of eigenvalue problems for beams and plates, R.A.E. Report Structures 225, August, 1957.

6. Salvadori, M.G., Numerical computation of buckling loads by finite differences, Trans. Amer. Soc. Civil. Engs. Vol. 115 : 590 - 624 1951.

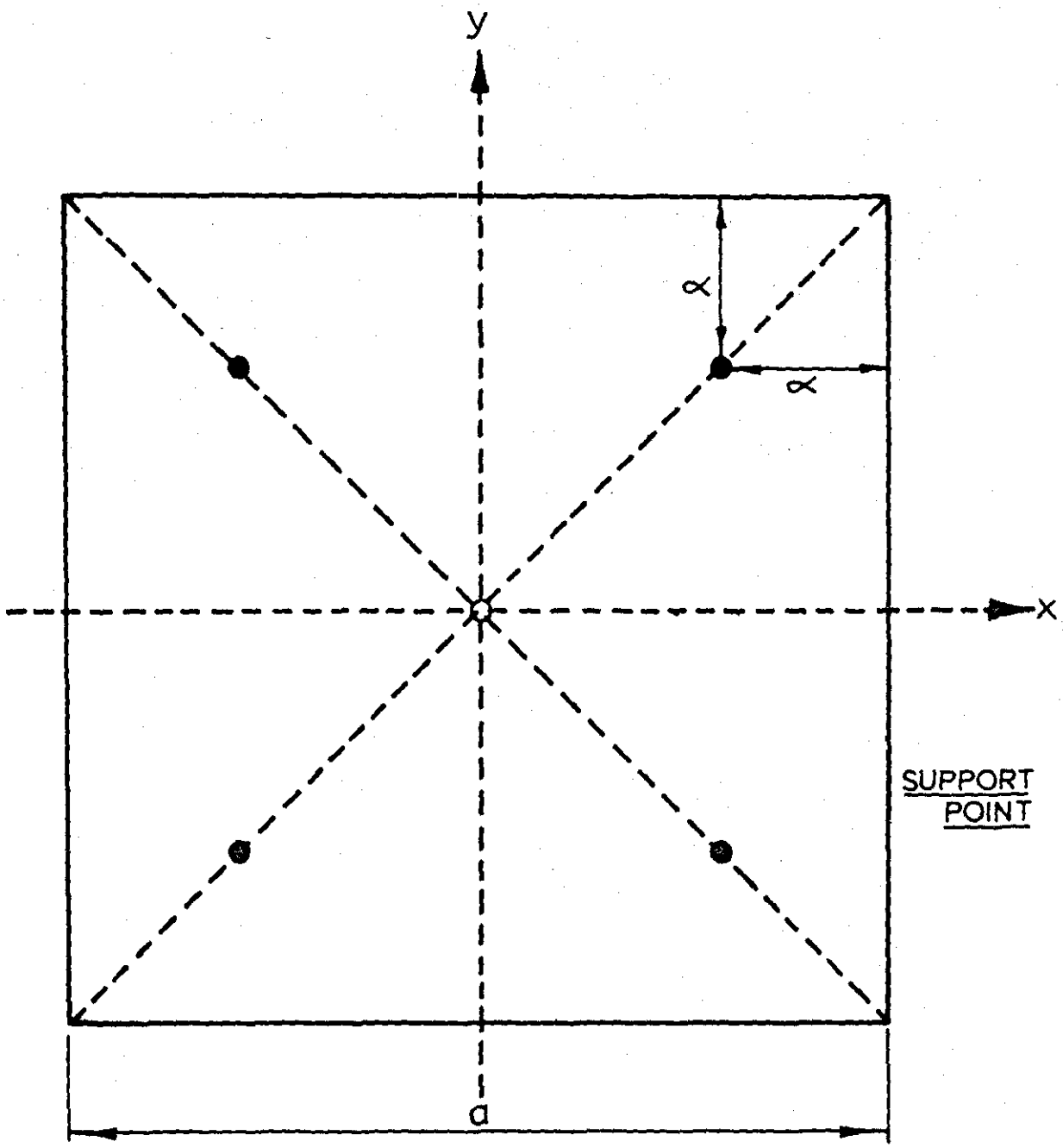

FIG.1. COORDINATES OF SQUARE PLATE SHOWING POINT SUPPORT LOCATIONS.

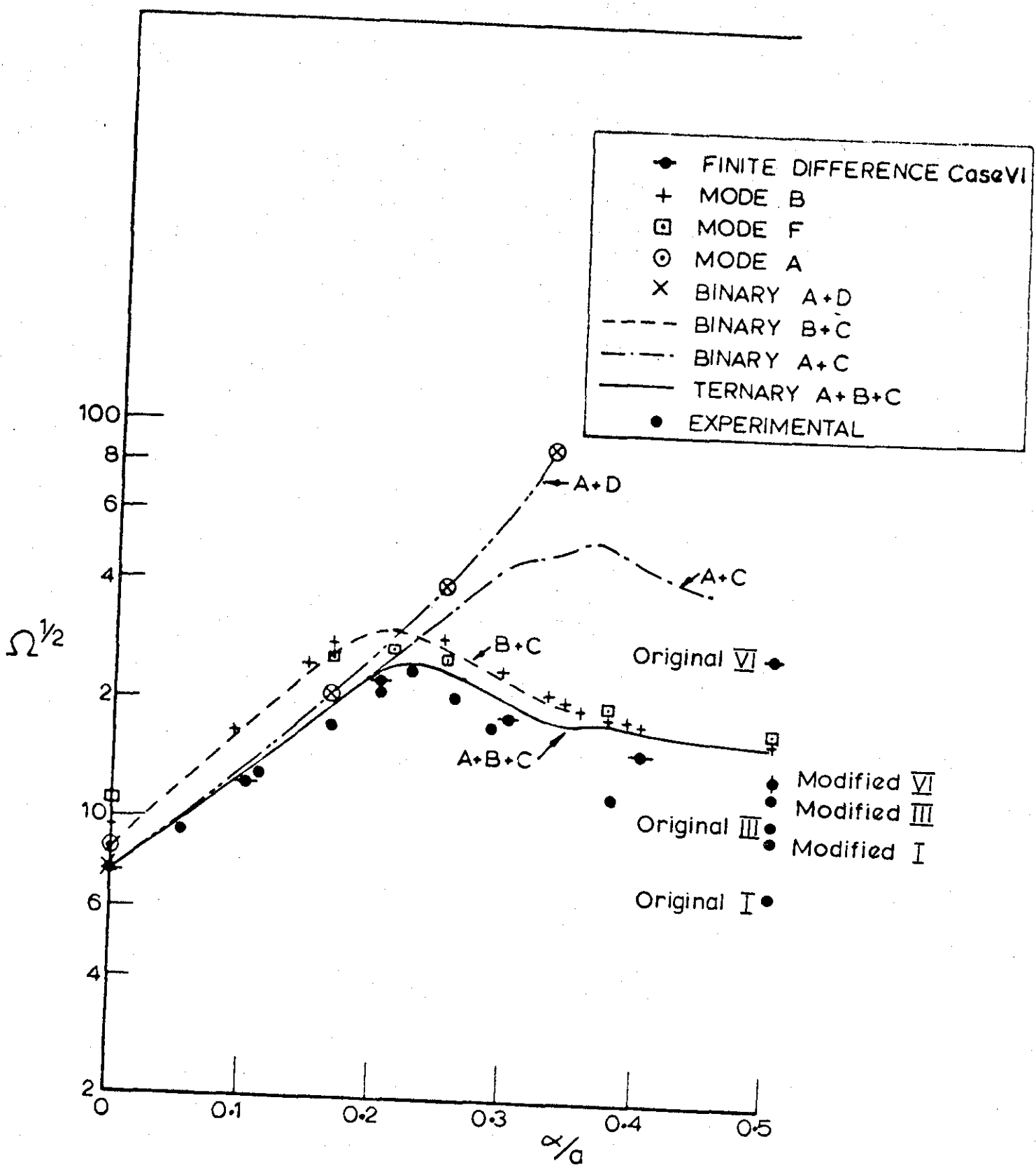

FIG. 2 PLOTS OF FUNDAMENTAL FREQUENCY VS SUPPORT LOCATIONS.

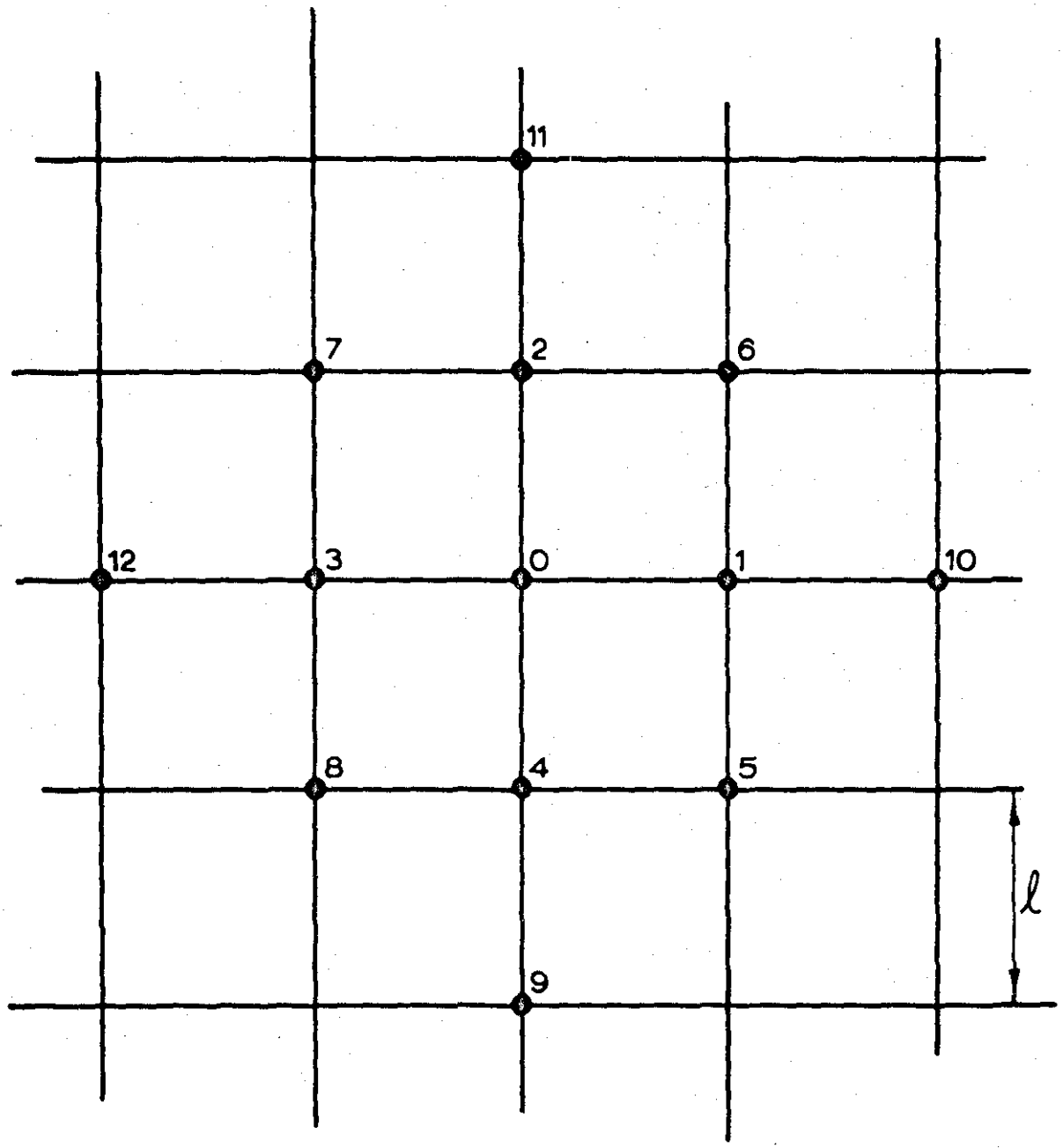

FIG.3. SQUARE MESH USED IN FINITE DIFFERENCE ANALYSES.

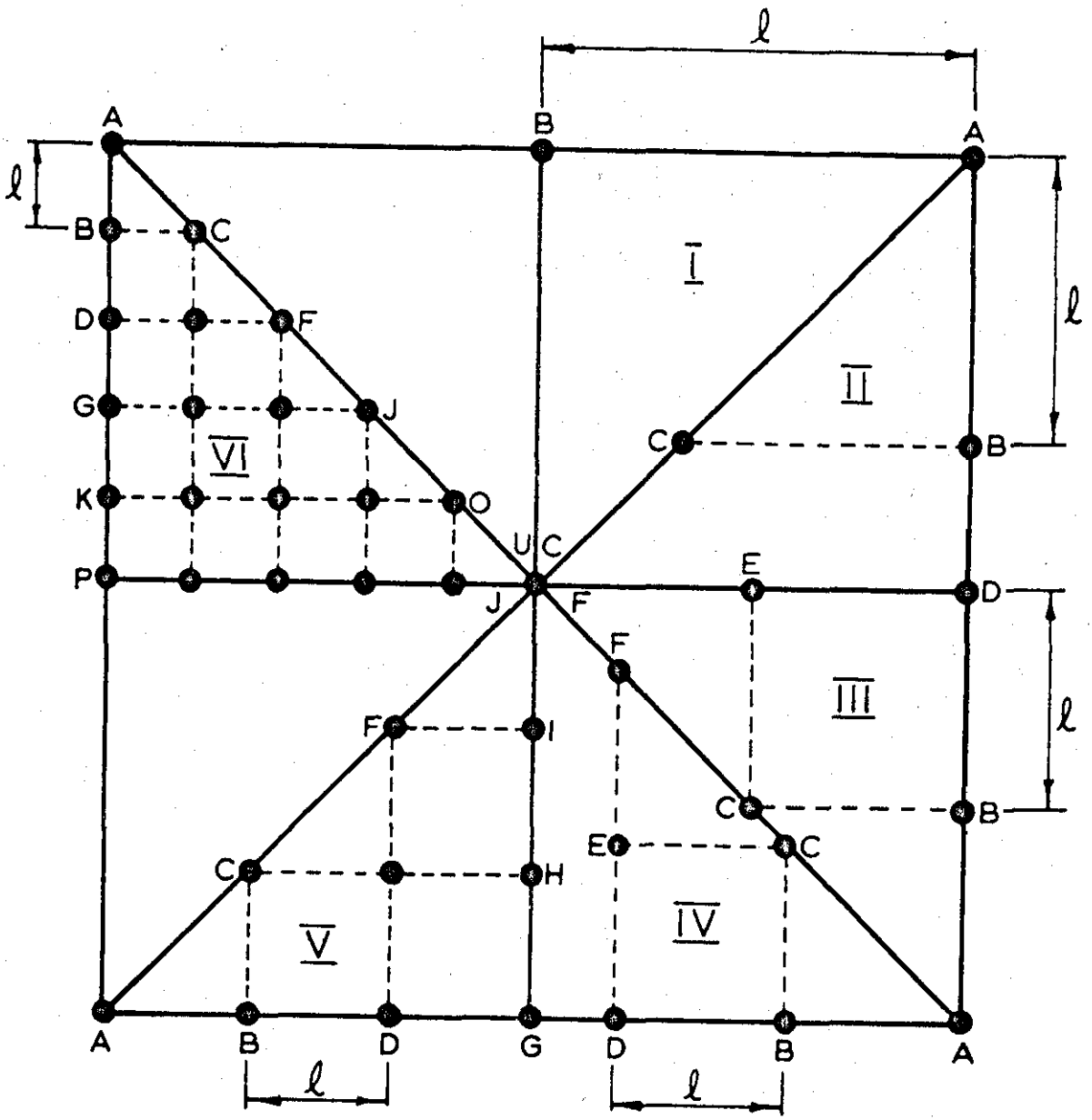

FIG. 4. ALTERNATIVE MESH CONFIGURATION FOR FINITE DIFFERENCE ANALYSES.

TABLE 6.1

Results of 'Exact' Analysis on Wing A3

η	Flutter Speed (fps)	Flutter Frequency (cps)
0.5	68.5 (75.2)	9.62 (10.1)
0.75	78.0 (82.5)	8.40 (7.8)

NOTE:

a) Pod attached to Wing A3

b) Pod Inertial Details:

$\overline{M} = 0.83$

$\overline{I} = 10.0$

$\overline{x}_p = 0.1$

c) Values in brackets refer to the experimental results

TABLE 6.2

Results of the Assumed Mode Analysis.

a) Wing A2

Details of the Concentrated Mass.	Span wise Location, η	Flutter Speed V, ft/sec
$\bar{M} = 1.0$ $\bar{I} = 10.0$ $\bar{X}_p = 0.0$	0.33	74.5
	0.50	64.2
	0.67	67.5
	0.875	75.8
$\bar{M} = 1.0$ $\bar{I} = 10.$ $\bar{X}_p = +0.1$	0.33	65.0
	0.50	58.2
	0.67	55.4
	0.875	64.5
$\bar{M} = 1.0$ $\bar{I} = 8.5$ $\bar{X}_p = 0.0$	0.33	82.2
	0.50	73.5
	0.67	77.5
	0.875	89.7
$\bar{M} = 1.0$ $\bar{I} = 8.5$ $\bar{X}_p = +0.1$	0.33	75.2
	0.50	68.6
	0.67	62.4
	0.875	72.7

b) Wing A3

$\bar{M} = 0.83$ $\bar{I} = 10$ $\bar{X}_p = 0$	0.33	88.0
	0.50	75.4
	0.67	82.6
	0.875	120.0
$\bar{M} = 0.83$ $\bar{I} = 10.$ $\bar{X}_p = +0.1$	0.33	84.5
	0.50	65.7
	0.67	62.0
	0.875	77.8

TABLE 6.3

Results of the Direct Matrix Method Applied to Wing A2

Concentrated mass details	η	ω_b (cps)	ω_t (cps)	V_F (fps)	ω_F (cps)
Uniform wing.		9.06	34.24	146.0	22.0
1. $\bar{M} = 1.0$, $\bar{I} = 0$, $\bar{X}_p = -0.1$	0.125	9.05	34.02	147.0	19.4
	0.33	8.59	30.74	166.0	18.4
	0.50	7.40	28.17	224.0	17.6
	0.67	6.10	29.74	230.0	13.2
	0.875	4.66	29.27	264.0	16.6
2. $\bar{M} = 1.0$, $\bar{I} = 5.0$, $\bar{X}_p = -0.1$	0.125	9.05	24.68	134.0	18.5
	0.33	8.59	15.81	108.9	13.9
	0.50	7.40	12.91	127.0	11.2
	0.67	6.10	11.47	168.0	10.0
	0.875	4.66	10.16	250.0	8.0
3. $\bar{M} = 1.0$, $\bar{I} = 10.0$, $\bar{X}_p = -0.1$	0.125	9.05	18.88	118.0	16.4
	0.33	8.57	11.71	65.0	11.2
	0.50	7.22	9.54	108.0	9.2
	0.67	6.04	8.37	115.0	7.8
	0.875	4.65	6.75	122.0	5.8
4. $\bar{M} = 1.0$, $\bar{I} = 0$, $\bar{X}_p = +0.1$	0.125	9.04	34.06	146.0	19.6
	0.33	8.56	32.52	145.0	18.5
	0.50	7.38	33.24	161.0	16.1
	0.67	6.06	34.11	164.0	10.4
	0.875	4.65	34.15	165.0	10.3
5. $\bar{M} = 1.0$, $\bar{I} = 5.0$, $\bar{X}_p = +0.1$	0.125	9.04	24.72	134.0	18.0
	0.33	8.56	16.09	93.0	14.4
	0.50	7.37	13.10	80.0	11.6
	0.67	6.05	11.77	85.2	10.0
	0.875	4.65	10.34	102.0	7.9
6. $\bar{M} = 1.0$, $\bar{I} = 10.0$, $\bar{X}_p = +0.1$	0.125	9.04	18.90	109.0	17.0
	0.33	8.53	11.92	59.25	11.3
	0.50	7.35	9.68	48.0	9.2
	0.67	6.03	8.58	51.0	8.0
	0.875	4.64	7.49	62.0	6.9
7. $\bar{M} = 1.0$, $\bar{I} = 0$, $\bar{X}_p = 0$	0.125	9.04	34.24	145.0	19.0
	0.33	8.58	34.00	156.0	18.0
	0.50	7.40	31.95	182.0	16.7
	0.67	6.09	33.29	180.0	14.0
	0.875	4.67	33.38	209.0	12.0

TABLE 6.3 - continued.

	Concentrated mass details	η	ω_b(cps)	ω_t(cps)	V_F(fps)	ω_F(cps)
8.	$\bar{M}$ = 1.0 $\bar{I}$ = 5.0 $\bar{X}_p$ = 0	0.125	9.04	24.96	137.2	
		0.33	8.57	16.14	95.0	
		0.50	7.39	13.09	96.0	
		0.67	6.09	11.66	96.3	
		0.875	4.67	10.26	127.4	
9.	$\bar{M}$ = 1.0 $\bar{I}$ = 10.0 $\bar{X}_p$ = 0	0.125	9.04	19.02	112.3	17.0
		0.33	8.56	11.90	66.4	11.1
		0.50	7.39	9.64	80.0	8.8
		0.67	6.04	8.72	63.1	8.0
		0.875	4.67	7.43	80.0	6.8
10.	$\bar{M}$ = 1.0 $\bar{I}$ = 0 $\bar{X}_p$ = -0.05	0.125	9.05	34.18	148.0	19.6
		0.33	8.59	32.61	161.1	18.6
		0.50	7.40	30.09	191.5	18.0
		0.67	6.10	31.72	198.0	14.5
		0.875	4.67	30.91	258.0	15.8
11.	$\bar{M}$ = 1.0 $\bar{I}$ = 5.0 $\bar{X}_p$ = -0.05	0.125	9.04	24.89	134.4	18.4
		0.33	8.58	16.02	101.0	12.2
		0.50	7.40	13.02	104.2	11.4
		0.67	6.10	11.57	94.0	10.6
		0.875	4.67	10.21	166.0	9.2
12.	$\bar{M}$ = 1.0 $\bar{I}$ = 10.0 $\bar{X}_p$ = -0.05	0.125	9.02	19.74	136.0	15.9
		0.33	7.92	12.50	71.2	11.6
		0.50	6.04	10.14	78.4	9.0
		0.67	4.52	8.96	86.0	7.6
		0.875	3.24	7.84	108.5	6.5
13.	$\bar{M}$ = 1.0 $\bar{I}$ = 0.0 $\bar{X}_p$ = +0.15	0.125	9.04	33.81	155.0	18.3
		0.33	8.55	30.62	144.3	18.3
		0.50	7.36	33.11	148.0	16.9
		0.67	6.04	33.22	144.0	15.2
		0.875	4.64	34.16	148.5	17.0
14.	$\bar{M}$ = 1.0 $\bar{I}$ = 5.0 $\bar{X}_p$ = +0.15	0.125	9.04	24.42	142.4	17.4
		0.33	8.53	15.92	134.0	12.3
		0.50	7.34	13.04	77.2	11.4
		0.67	6.02	11.80	88.0	9.6
		0.875	4.63	10.37	90.0	8.2
15.	$\bar{M}$ = 1.0 $\bar{I}$ = 10.0 $\bar{X}_p$ = +0.15	0.125	9.04	18.76	110.0	16.7
		0.33	8.50	11.88	58.8	11.2
		0.50	7.31	9.69	47.8	9.1
		0.67	5.99	8.63	50.0	8.0
		0.875	4.62	7.52	61.9	6.0

TABLE 6.4

Results of the Direct Matrix Method Applied to Wing A3

Concentrated Mass Details	η	ω_b(cps)	ω_t(cps)	V_F(fps)	ω_F(cps)
Uniform Wing		9.06	37.50	152.5	20.2
$\bar{M}$ = 0.83, $\bar{I}$ = 10.0, $\bar{X}_p$ = +0.1	0.125	9.04	20.68	124.0	17.8
	0.33	8.50	13.04	64.6	12.3
	0.50	7.26	10.60	63.0	10.2
	0.67	5.91	9.40	72.0	8.4
	0.875	4.51	8.21	87.0	7.8
$\bar{M}$ = 0.83, $\bar{I}$ = 10, $\bar{X}_p$ = 0	0.125	9.05	20.85	124.8	17.7
	0.33	8.64	13.05	65.2	12.4
	0.50	7.61	10.58	60.0	10.0
	0.67	6.39	9.31	80.0	8.5
	0.875	4.98	8.15	113.7	7.2
$\bar{M}$ = 0.83, $\bar{I}$ = 10, $\bar{X}_p$ = +0.15	0.125	9.04	19.07	123.8	17.9
	0.33	8.60	12.99	64.0	12.3
	0.50	7.55	10.59	52.0	9.9
	0.67	6.30	9.45	54.5	8.8
	0.875	4.93	8.25	75.0	7.5
$\bar{M}$ = 0.83, $\bar{I}$ = 5.0, $\bar{X}_p$ = +0.1	0.125	9.05	27.08	129.0	20.0
	0.33	8.63	17.62	100.0	15.2
	0.50	7.59	14.35	84.9	12.4
	0.67	6.36	12.91	107.5	10.0
	0.875	4.98	11.35	121.0	8.9
$\bar{M}$ = 0.83, $\bar{I}$ = 5.0, $\bar{X}_p$ = +0.15	0.125	9.05	26.75	138.0	19.5
	0.33	8.62	17.42	93.8	15.0
	0.50	7.57	14.26	80.0	12.6
	0.67	6.24	12.93	96.5	10.5
	0.875	5.0	11.20	107.0	9.2

TABLE 6.5

Results of the Direct Matrix Method Applied to Wing B4

Concentrated Mass Details.	η	ω_b(cps)	ω_t(cps)	V_F(fps)	ω_F(cps)
Uniform wing.		5.80	36.37	165.0	19.5
$\overline{M}$ = 0.83	0.125	5.79	27.09	135.0	17.8
$\overline{I}$ = 5.0	0.33	5.53	17.48	117.0	15.0
$\overline{X}_p$ = 0.10	0.50	4.88	14.63	104.0	12.5
	0.67	4.07	12.85	107.0	11.0
	0.875	3.17	11.36	126.8	8.1
$\overline{M}$ = 0.83	0.125	5.79	36.01	165.0	20.0
$\overline{I}$ = 0.	0.33	5.54	24.54	182.0	18.9
$\overline{X}_p$ = -0.1	0.50	4.90	23.96	209.5	16.8
	0.67	4.08	30.19	246.0	14.5
	0.875	3.18	40.29	291.2	24.2

TABLE 6.6

Results of the Direct Matrix Method Applied to Wing B5

Concentrated Mass Details	η	ω_b(cps)	ω_t(cps)	V_F(fps)
Uniform Wing		5.80	37.06	227.0
$\mathbb{M}$ = 0.83	0.125	5.73	29.25	194.8
$\mathbb{I}$ = 0.0	0.33	5.52	24.25	206.0
X_p = -0.1	0.50	4.90	24.54	275.0
	0.67	4.08	33.76	246.8
	0.875	3.18	31.73	216.2

TABLE 6.7

Effect of Inclusion of Pod Aerodynamics.

η	Flutter Speed (fps) With Pod Aerodynamics	Flutter Speed (fps) Without including Pod Aerodynamic Loads.
0.125	124.0	124.0
0.33	63.5	64.6
0.50	61.7	63.0
0.67	69.6	72.0
0.875	85.0	87.0

(These calculations refer to Wing A3. The inertial parameters of the pod are: $\bar{M}$ - 0.83, $\bar{I}$ = 10.0, $\bar{X}$ = +0.1 The pod aerodynamic loads were calculated for Pod A^p.)

TABLE 6.8

Influence Of Modifications To The Pod On The Flutter Speed

Method	V (FPS)		Pod Condition
	$\eta = 0.5$	$\eta = 0.67$	
D.M.M	63.0	72.0	No Fin
Expt.	75.2	72.5	
D.M.M	63.5	72.4	a = 2 ins. b = 1 in.
Expt	76.0	78.0	
D.M.M	64.2	73.5	a = 3 ins. b = 0.5 in.
Expt	78.0	76.0	

Notes: a) The experimental results refer to Pod A

b) The dimensions a and b are as shown in the following sketch.

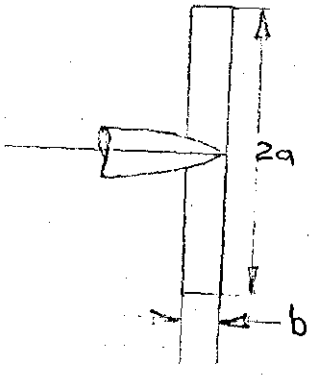

TABLE 7.1

Results of Wind Tunnel Tests on the Flutter of WING A2

Details of the Pod Inertia	η	ω_b(cps)	ω_t(cps)	V_F(fps)	ω_F(cps)
Pod A	0.33	8.75	14.50	92.0	11.00
	0.42	8.20	11.50	83.0	11.00
$\bar{M}$ = 1.0	0.50	7.75	10.75	75.2	10.00
$\bar{I}$ = 8.5	0.38	7.10	9.50	66.1	9.25
$\bar{X}_p$ = +0.1	0.67	6.50	8.80	72.5	8.75
	0.75	6.00	8.75	81.2	8.25
	0.83	5.50	8.25	84.8	7.00
	0.92	5.00	7.75	90.2	7.00
	0.33	8.60	16.40	- No Flutter -	
Pod A	0.42	8.00	13.50	85.5	9.75
$\bar{M}$ = 1.0	0.50	7.90	12.00	83.0	10.00
$\bar{I}$ = 8.5	0.58	7.00	10.75	66.2	8.50
$\bar{X}_p$ = 0	0.67	6.50	9.80	77.5	7.50
	0.75	6.25	9.40	85.0	7.00
	0.83	5.60	8.25	92.5	7.40
	0.92	5.00	8.00	97.0	6.75
	0.33	8.80	13.20	.	11.25
	0.42	8.25	12.25	68.0	9.75
Pod A	0.50	8.00	9.75	61.	9.25
$\bar{M}$ = 1.0	0.58	7.25	9.50		8.00
$\bar{I}$ = 10.0	0.67	6.30	8.60	62.0	7.75
$\bar{X}_p$ =+0.1	0.75	6.00	8.50	67.	7.30
	0.83	5.75	7.80	75.0	7.00
	0.92	5.00	7.60	82.0	7.10
	0.33	8.75	14.50	77.0	10.6
	0.42	8.20	12.00	77.0	9.75
Pod A	0.50	7.60	10.50		8.40
$\bar{M}$ = 1.0	0.58	7.00	9.60		8.50
$\bar{I}$ = 10.0	0.67	6.40	8.80	63.0	8.10
$\bar{X}_p$ = 0	0.75	5.75	8.25	72.	7.00
	0.83	5.00	8.00	78.0	7.20
	0.92	4.70	7.50	8	7.10
	0.33	8.50	16.50	90.1	11.70
	0.42	8.00	13.20	85.0	10.00
Pod B	0.50	8.00	11.70	71.2	9.60
$\bar{M}$ = 1.0	0.58	7.80	11.20	60.5	9.00
$\bar{I}$ = 8.5	0.67	6.50	10.00	67.8	8.70
$\bar{X}_p$ = +0.1	0.75	6.10	8.80	82.4	8.25
	0.83	5.60	8.50	86.1	7.60
	0.92	4.80	7.75	92.0	7.30

TABLE 7.1 continued.

Details of the Pod Inertia.	η	ω_b(cps)	ω_t(cps)	V_F(fps)	ω_F(cps)
Pod B	0.33	8.75	16.20	- No Flutter -	
$\bar{M}$ = 1.0	0.42	8.10	12.75	91.50	10.60
$\bar{I}$ = 8.5	0.50	7.80	11.75	80.0	9.80
$\bar{X}_p$ = 0.	0.58	7.25	11.00	71.2	9.00
	0.67	6.60	9.80	80.4	8.10
	0.75	6.00	8.50	88.5	7.60
	0.83	5.75	8.30	91.2	7.40
	0.92	5.00	8.10	94.6	7.00

Note:

η = Non dimensional span (=y/s)

ω_b = Fundamental bending frequency

ω_t = Fundamental torsional frequency

V_F = Flutter Speed.

ω_F = Flutter frequency

$\bar{X}_p$ = Distance of pod c.g. from elastic axis, non dimensionalized with respect to the wing chord. Positive aft of the elastic axis.

TABLE 7.2

Results of Wind Tunnel Tests on the Flutter of Wing A3.

Details of the Pod Inertia.	η	ω_b(cps)	ω_t(cps)	V_F(fps)	ω_F(cps)
Pod A	0.33	8.80	15.20	83.0	12.50
$\bar{M}$ = 0.83	0.42	8.25	12.75	73.7	10.60
$\bar{I}$ = 10.0	0.50	7.90	11.20	75.2	10.10
$\bar{X}_p$ = +0.1	0.58	7.20	10.00	66.1	9.25
	0.67	6.75	9.60	72.5	8.30
	0.75	6.25	8.90	82.5	7.80
	0.83	5.50	8.50	92.5	8.00
	0.92	5.20	8.25	98.0	7.50
Pod B	0.33	8.75	13.20	76.5	12.20
$\bar{M}$ = 0.83	0.42	8.20	12.50	83.0	11.40
$\bar{I}$ = 10.0	0.50	7.75	11.50	74.50	10.50
$\bar{X}_p$ = +0.1	0.58	7.20	10.25	68.00	9.40
	0.67	6.60	9.50	77.00	9.25
	0.75	6.20	9.25	79.2	8.75
	0.83	5.50	8.60	93.0	8.00
	0.92	4.80	8.50	- No Flutter -	
Pod B	0.33	9.00	14.50	92.0	13.25
$\bar{M}$ = 0.83	0.42	7.90	12.75	94.0	11.20
	0.50	7.80	11.50	82.9	10.10
	0.58	7.25	10.00	83.2	9.25
$\bar{I}$ = 10.0	0.67	6.80	9.20	91.2	8.75
$\bar{X}_p$ = 0	0.75	6.20	9.00	- No Flutter -	
	0.83	5.50	8.75	- No Flutter -	
	0.92	5.00	8.30	- No Flutter -	
Pod C	0.33	8.50	15.25	88.0	11.60
$\bar{M}$ = 0.83	0.42	8.20	12.60	81.2	11.20
$\bar{I}$ = 10.0	0.50	7.75	11.75	71.7	10.75
$\bar{X}_p$ = +0.1	0.58	7.20	10.10	72.5	9.60
	0.67	6.50	9.40	74.5	8.75
	0.75	6.25	8.75	86.5	8.40
	0.83	5.60	8.50	95.5	7.60
	0.92	5.00	8.20	- No Flutter -	
Pod D	0.33	8.60	15.50	85.0	12.50
$\bar{M}$ = 0.83	0.42	8.00	12.70	78.00	11.75
$\bar{I}$ = 10.0	0.50	7.60	11.50	76.5	10.20
$\bar{X}_p$ = +0.1	0.58	7.25	10.30	78.0	9.80
	0.67	6.50	9.40	80.0	8.75
	0.75	6.00	8.60	86.0	7.60
	0.83	5.50	8.40	95.0	7.80
	0.92	5.00	8.10	- No Flutter -	

TABLE 7.3

INFLUENCE OF MODIFICATIONS TO THE POD (Expeimental Results)

Fin Number			1	2	3	4	5
Fin Details / η	a(ins)	0.0	1.0	1.0	2.0	2.0	3.0
	b(ins)	0.0	0.5	1.0	1.0	0.5	0.5
0.33	POD A	83.0	83.0	84.0	85.8	84.5	86.0
0.42		73.7	73.0	74.5	75.0	73.5	76.0
0.50		75.2	76.0	75.5	76.0	75.5	78.0
0.67		72.5	73.5	74.0	78.0	74.0	76.0
0.75		82.5	82.5	84.0	91.7	85.0	92.2
0.83		92.5	95.0	98.5	*	*	*
0.33	POD B	76.5	76.0	77.5	78.0	78.0	80.0
0.42		83.0	84.0	84.5	91.7	85.0	92.2
0.50		74.5	75.0	74.5	76.5	76.5	78.0
0.67		68.0	65.5	67.5	69.5	68.5	70.0
0.75		77.0	78.0	80.0	80.0	82.0	82.0
0.83		93.0	95.0	97.0	98.0	97.5	*

NOTE: a) * Denotes that no Flutter could be obtained upto the maximum wind tunnel speed

b) All Flutter Speeds in ft/sec.

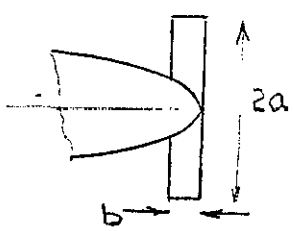

TABLE 8.2

Influence of Concentrated Masses on
the Flutter Speed of the Wing of Ref.(38)

η	$\overline{V}$				
	Experiment	Exact	2 Modes	3 Modes	4 Modes
0.0	1.0	1.0	1.0	1.0	1.0
0.23	0.97	0.985	1.105	-	-
0.355	1.13	1.22	-	2.01	1.49
0.625	*	1.575	-	-	-
0.935	*	1.20	-	-	-
0.965	1.065	1.10	-	-	-
1.00	0.965	0.90	-	1.065	1.065

Notes: a) These refer to Weight 7a.

b) * indicates Divergence.

TABLE 8.1

Flutter Speeds For the Wing of Ref.(9)

$\overline{x_p} = 0.15$

η	$\overline{V}$					
	$\overline{M} = 0.5$ $\overline{I} = 0$		$\overline{M} = 1.0, \overline{I} = 0$		$\overline{M} = 0.5, \overline{I} = 3.8$	
	Ref.(9)	DMM	Ref.(9)	DMM	Ref.(9)	DMM
0.0	1.0	1.0	1.0	1.0	1.0	1.0
0.125	1.1	1.02	1.05	1.0	1.02	1.0
0.33	1.25	1.17	1.12	1.17	1.10	1.00
0.50	1.38	1.25	1.20	1.12	1.11	1.57
0.67	2.60	2.50	2.50	2.37	2.65	1.75
0.875	1.58	1.78	1.50	1.00	2.08	1.42

NOTE. $\overline{V}$ = (Flutter Speed of Wing with Mass) / (Bare Wing Flutter Speed)

TABLE VI.I

Vibration Frequencies of Wings A2 and A3

(Comparison of the Direct Matrix Method and the Exact Solution)

(i) WING A2 DMM $\overline{M} = 1.0$ $\overline{I} = 5.0$ $\overline{x}_p = 0.5$

Exact $\overline{M} = 1.0$ $\overline{I} = 5.0$ (Uncoupled)

η	DMM		EXACT	
	ω_b (cps)	ω_t (cps)	ω_b (cps)	ω_t (cps)
0.0	9.06	34.24	9.04	36.12
0.125	9.04	24.96	8.94	26.60
0.33	8.57	16.14	8.60	16.45
0.50	7.39	13.09	7.50	13.62
0.67	6.09	11.66	6.01	11.95
0.875	4.67	10.26	4.72	10.48

(ii) WING A2 DMM $\overline{M} = 1.0$ $\overline{I} = 10.0$ $\overline{x}_p = 0$

Exact $\overline{M} = 1.0$ $\overline{I} = 10.0$ (Uncoupled)

η	DMM		EXACT	
	ω_b (cps)	ω_t (cps)	ω_b (cps)	ω_t (cps)
0.0	9.06	34.24	9.04	36.12
0.125	9.04	19.02	8.94	21.62
0.33	8.56	11.90	8.60	12.10
0.50	7.39	9.64	7.50	9.95
0.67	6.04	8.72	6.01	8.66
0.875	4.67	7.42	4.72	7.68

TABLE VI.I (Continued)

(iii) WING A3 DMM $\bar{M} = 0.83$ $\bar{I} = \cancel{10.0}\ 5.0$ $\bar{x}_f = 0.1$

Exact $\bar{M} = 0.83$ $\bar{I} = \cancel{10.0}\ 5.0$ (Uncoupled)

η	DMM		EXACT	
	ω_b (cps)	ω_t (cps)	ω_b (cps)	ω_t (cps)
0.0	9.06	37.50	9.04	39.50
0.125	9.05	27.08	8.96	29.10
0.33	8.63	17.62	8.62	18.00
0.50	7.59	14.35	7.70	14.91
0.67	6.36	12.91	6.45	13.10
0.875	4.98	11.35	5.05	11.47

(iv) WING A3 DMM $\bar{M} = 0.83$ $\bar{I} = 10.0$ $\bar{x}_f = 0.1$

Exact $\bar{M} = 0.83$ $\bar{I} = 10.0$ (Uncoupled)

η	DMM		EXACT	
	ω_b (cps)	ω_t (cps)	ω_b (cps)	ω_t (cps)
0.0	9.06	37.50	9.04	39.50
0.125	9.04	20.68	8.96	23.45
0.33	8.50	13.04	8.62	13.22
0.50	7.26	10.60	7.70	10.90
0.67	~~5.91~~ 5.91	9.40	6.45	9.60
0.875	4.51	8.21	5.05	8.40

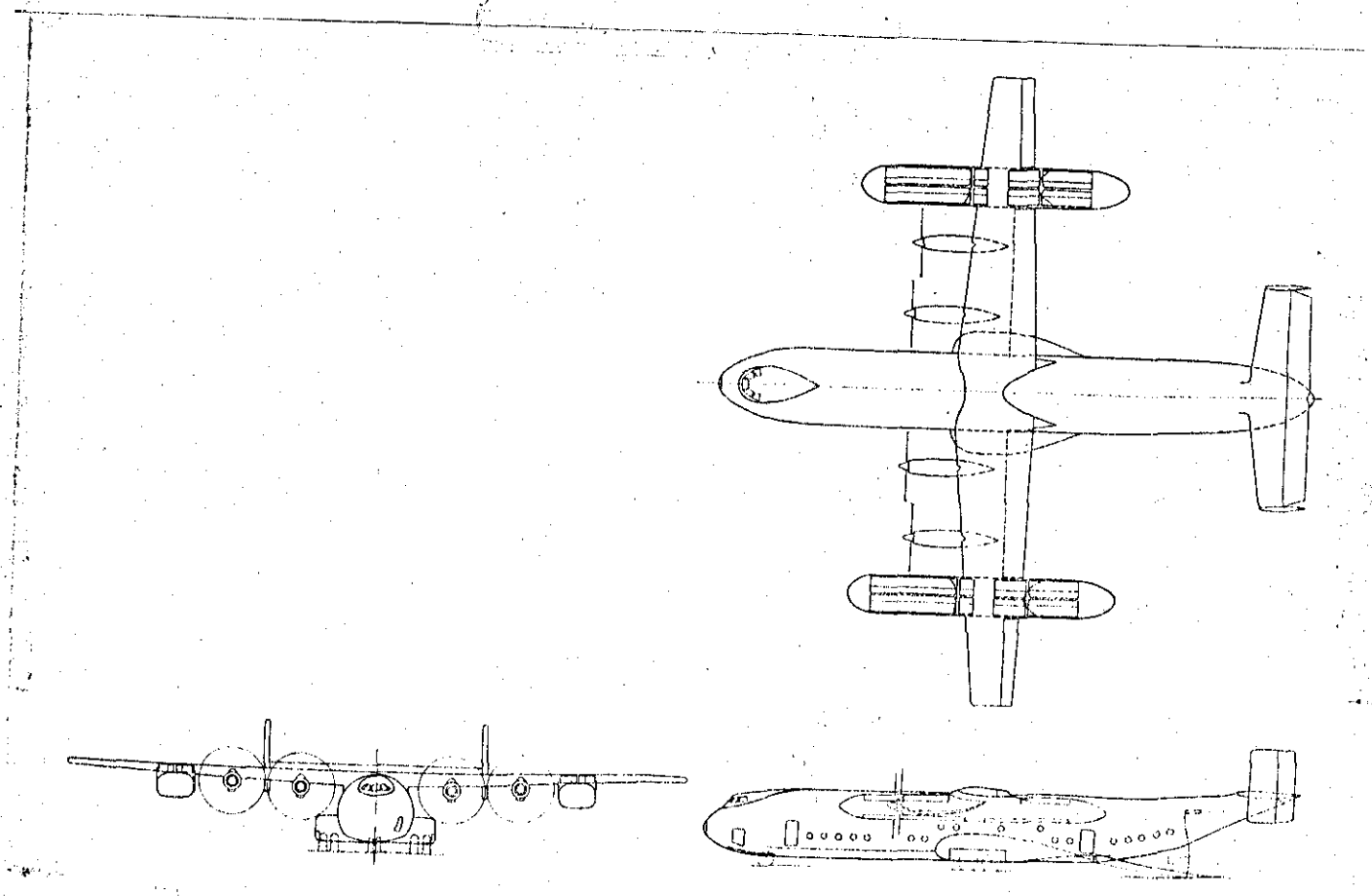

FIG 1.1 VTOL Aircraft of Ref(1)

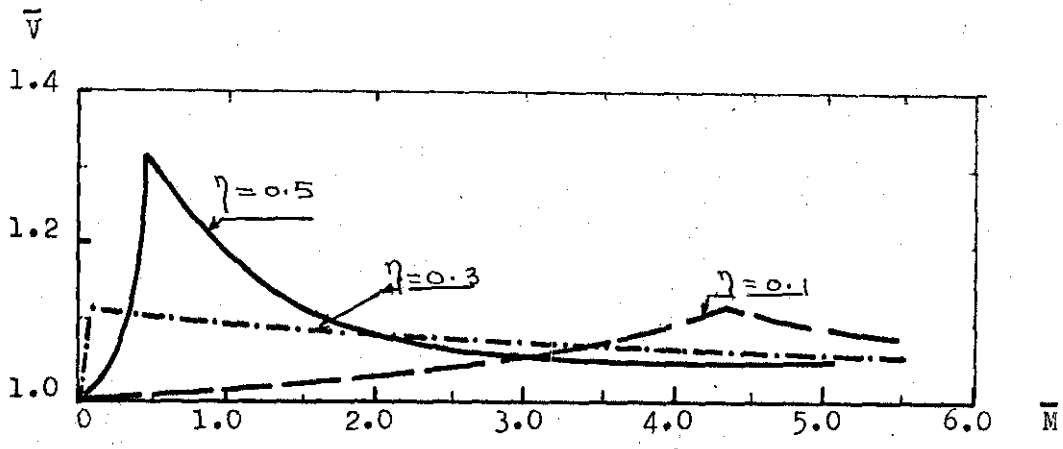

a) Mass 0.28c ahead of the Elastic Axis.

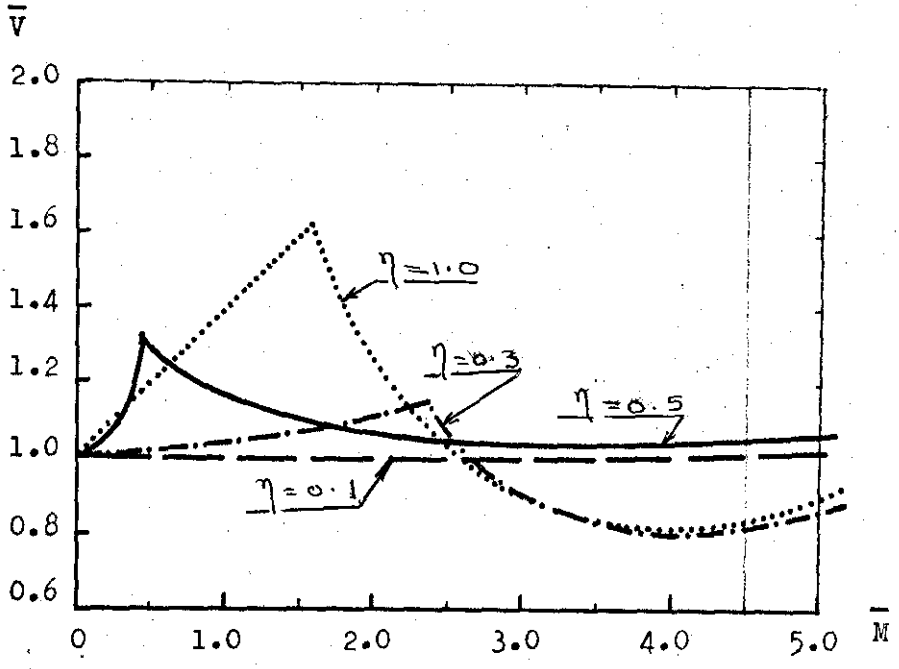

b) Mass on the Elastic Axis.

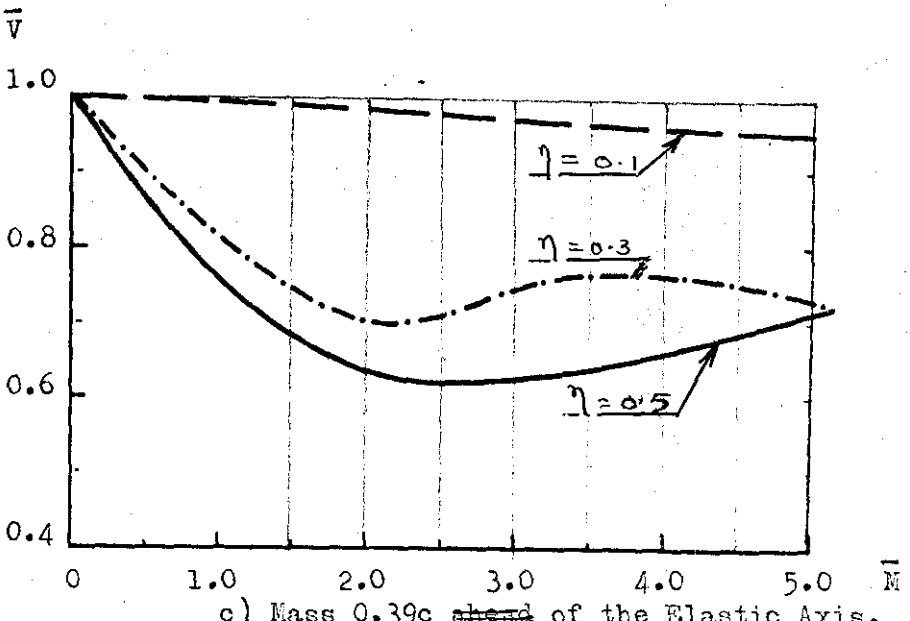

c) Mass 0.39c ~~ahead~~ aft of the Elastic Axis.

FIG. 2.1 Influence of M on the Wing of Ref(6)

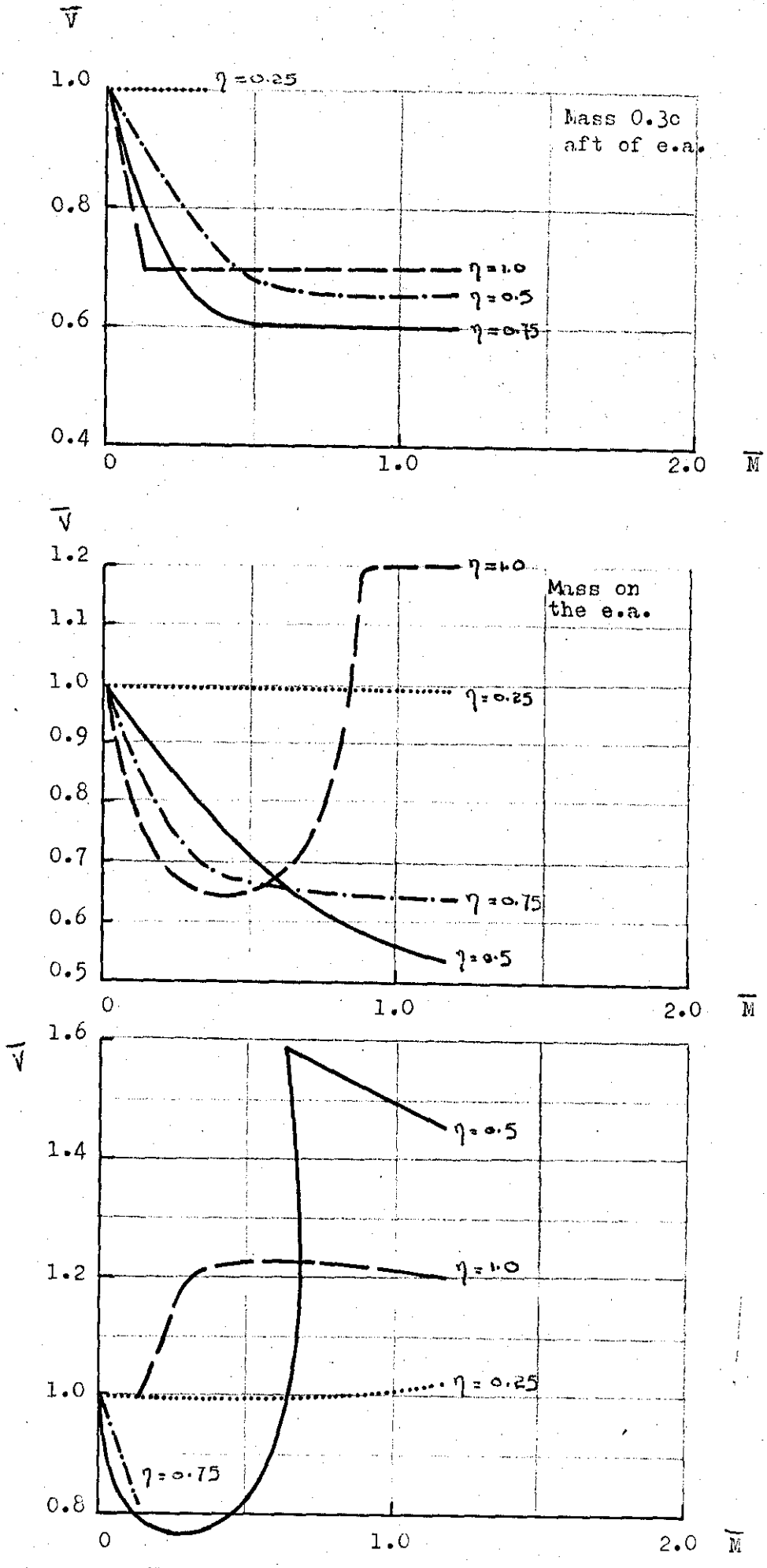

FIG. 2.2 Influence of $\overline{M}$ on the Wing Of Ref(7)

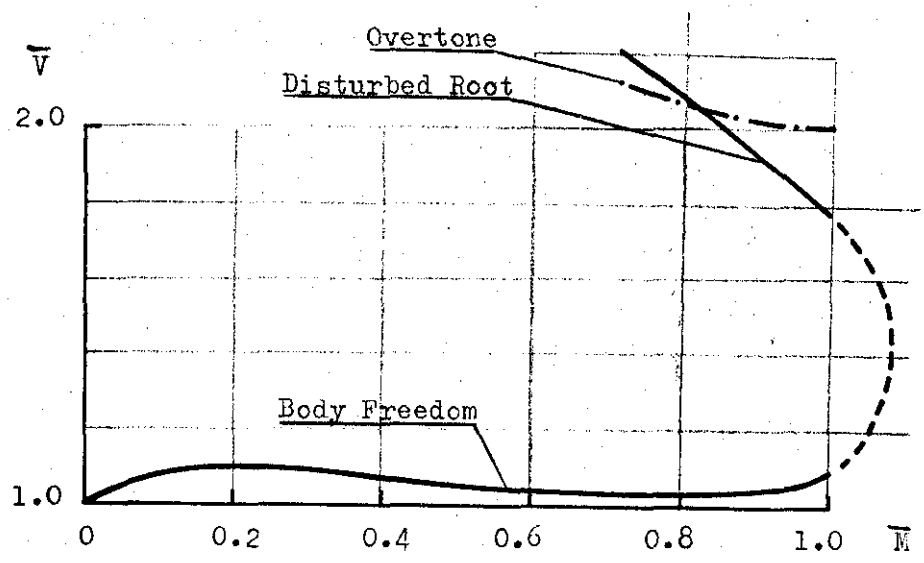

C.G. 0.467c
Forward of e.a.

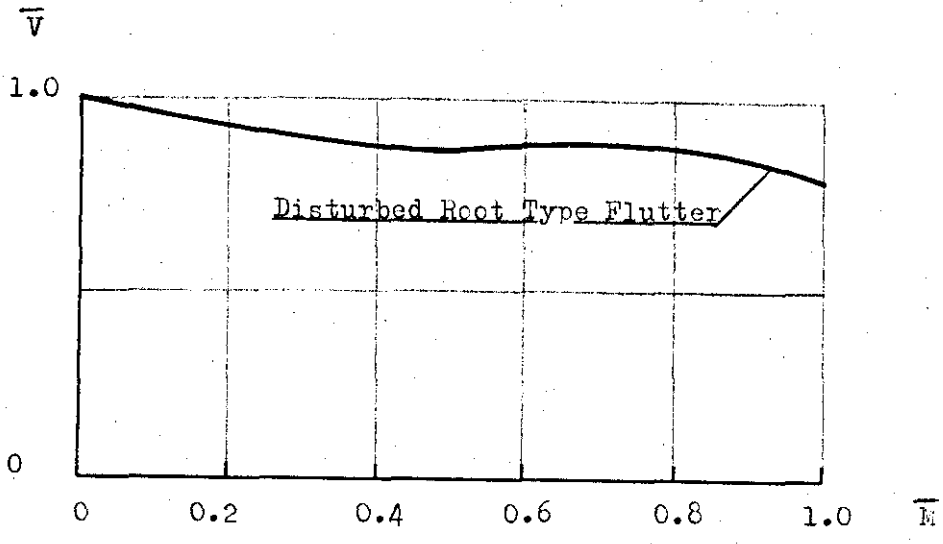

C.G 0.381c
Aft of e.a.

FIG.2.3 INFLUENCE OF M ON THE WING OF REF(8)

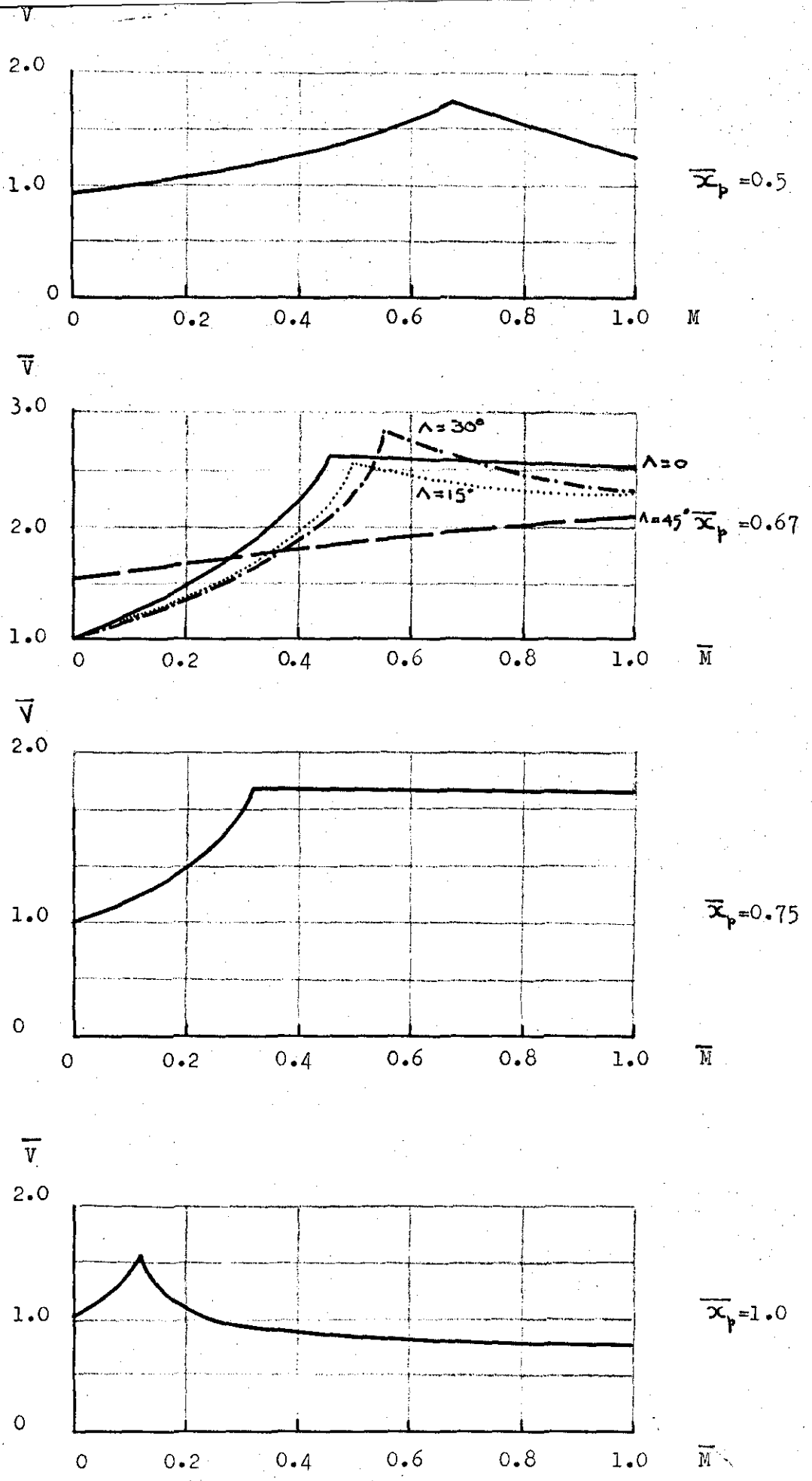

FIG 2.4 Influcnce of M: Wing of Ref(9)

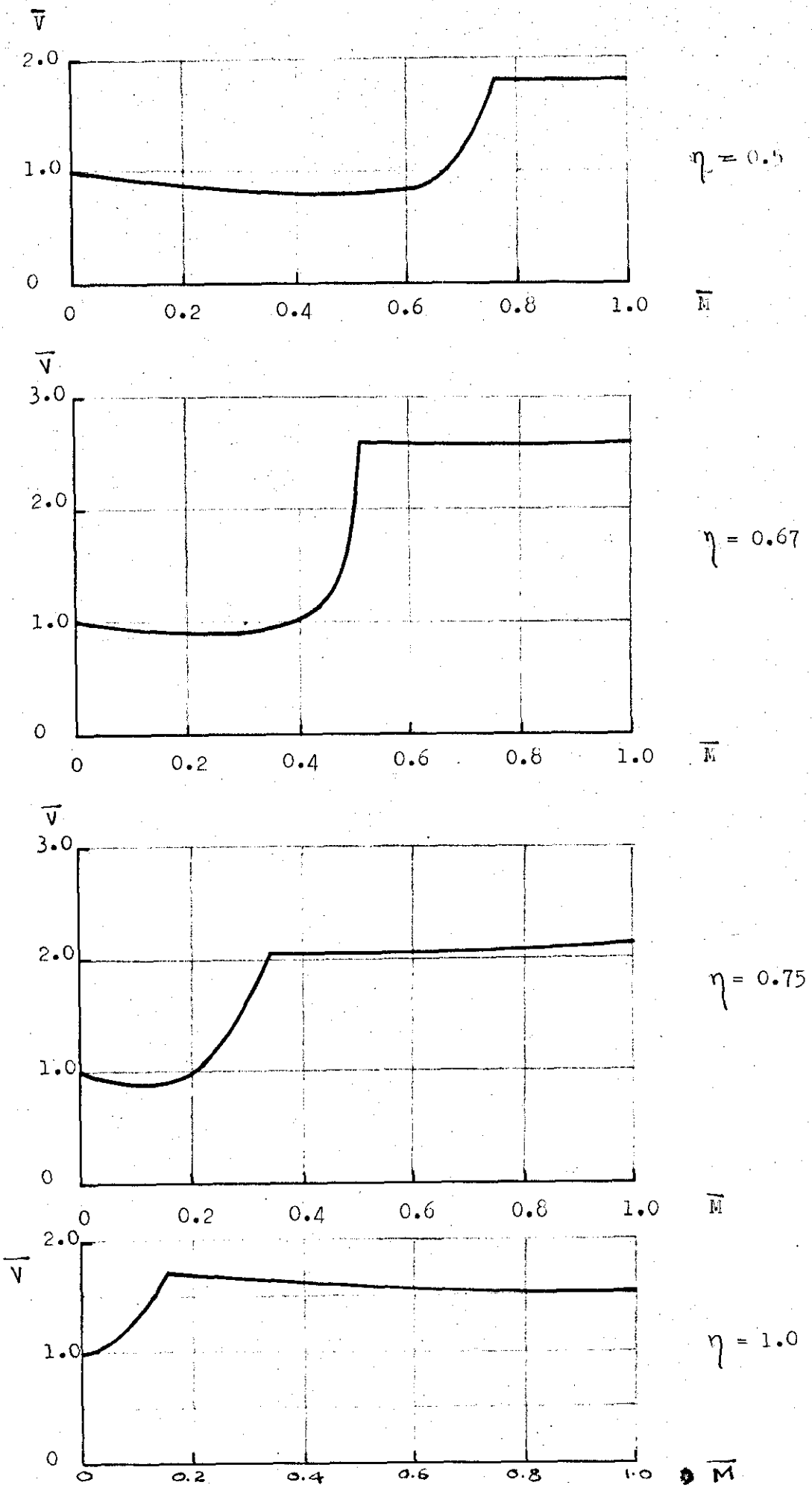

FIG 2.4a Influence of M: Wing of Ref(9) - $x_p = -0.1$

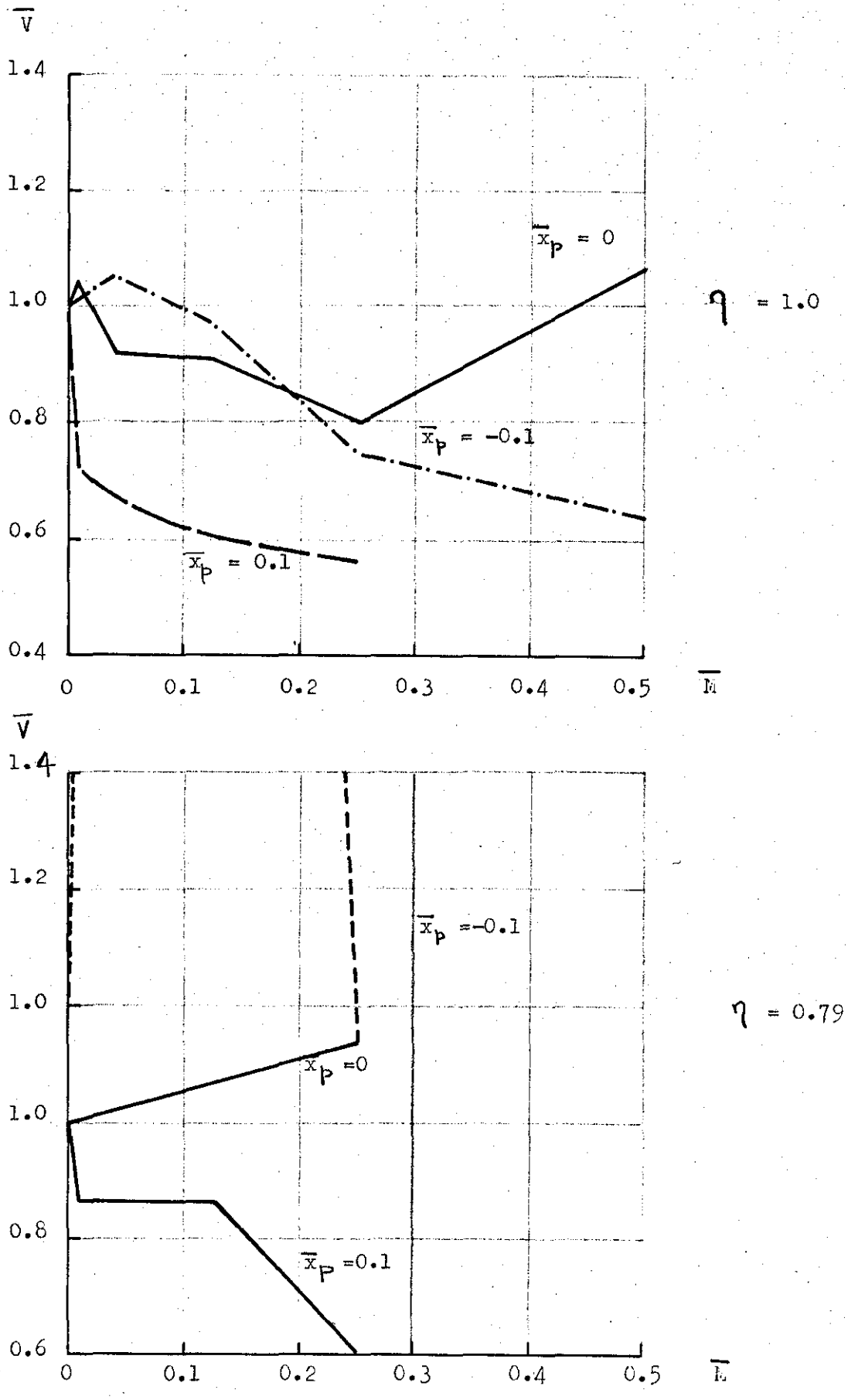

FIG 2.5 Influence of M: Wing of Ref(9)

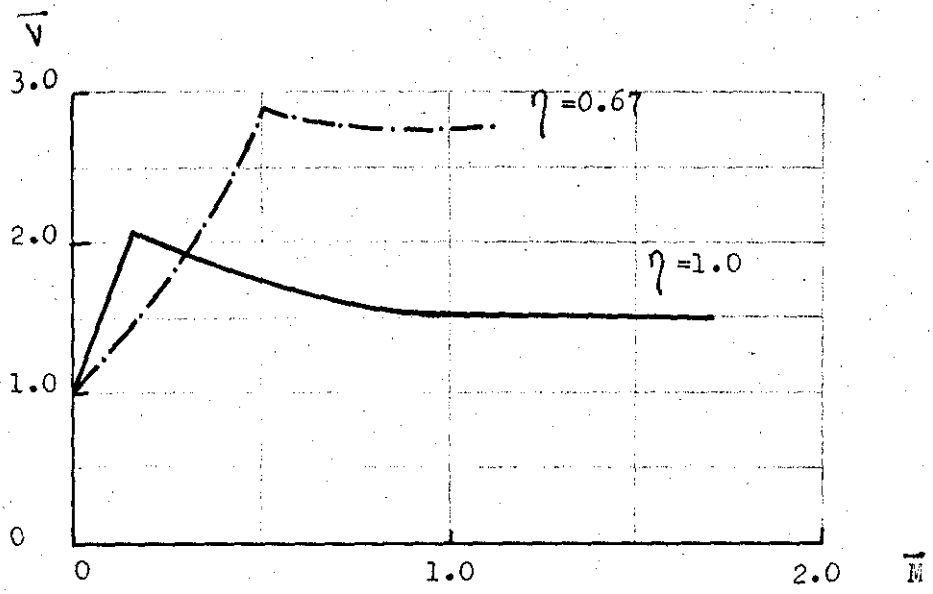

a) Mass on the Leading Edge.

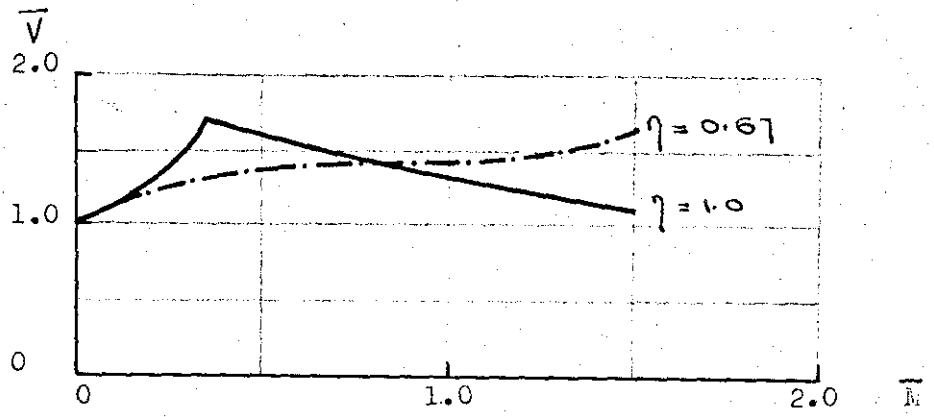

b) Mass on the Elastic Axis.

FIG. 2.6 Influence of M: Wing of Ref(5)

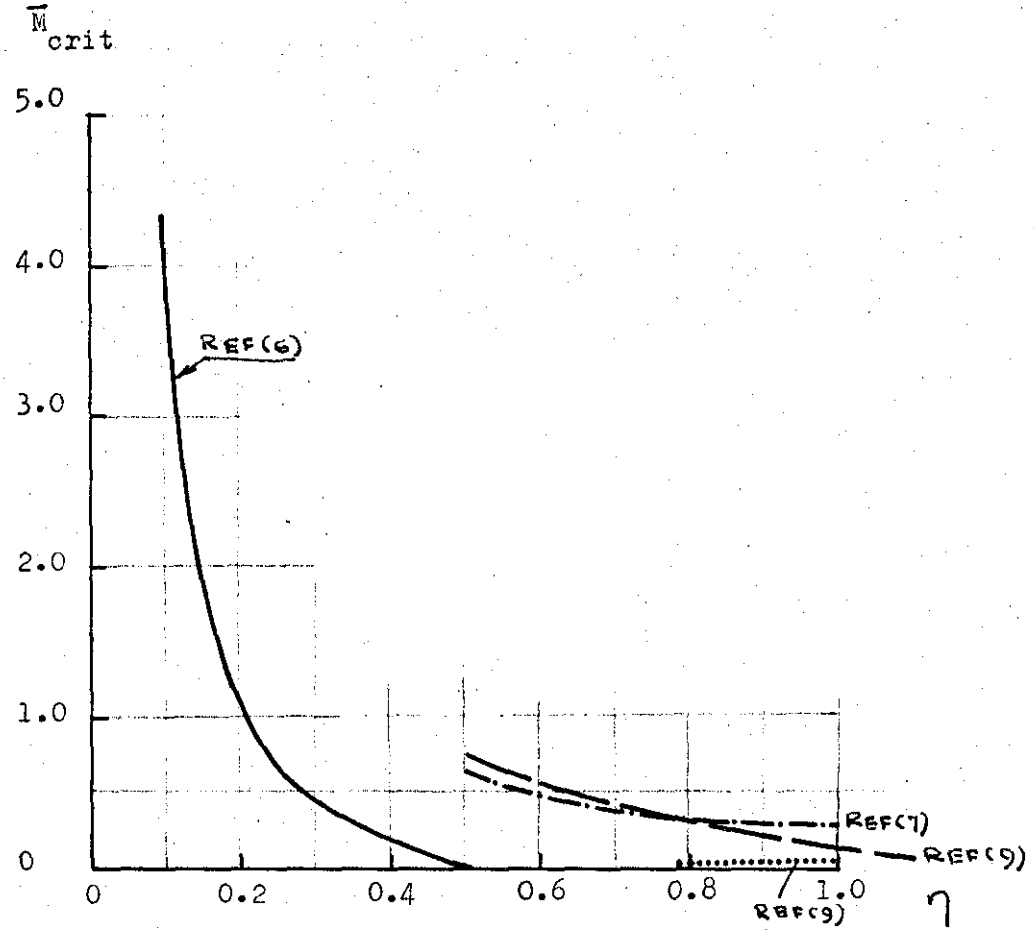

FIG.2.7 VALUE OF $\overline{M}_{crit}$ FOR MASS POSITIONS AHEAD OF E.A.

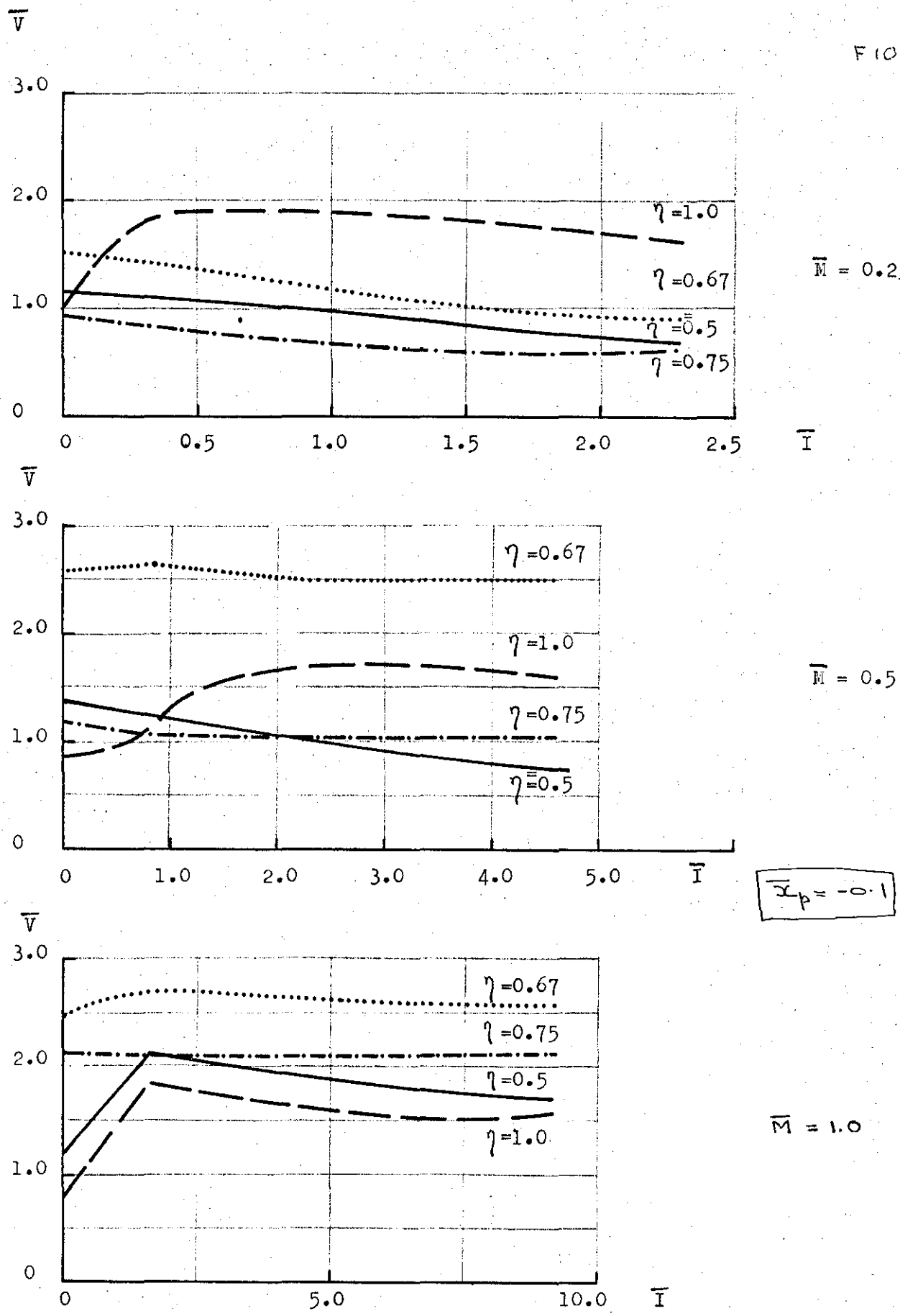

FIG. 2.8 Influence of I: Wing of Ref(9)

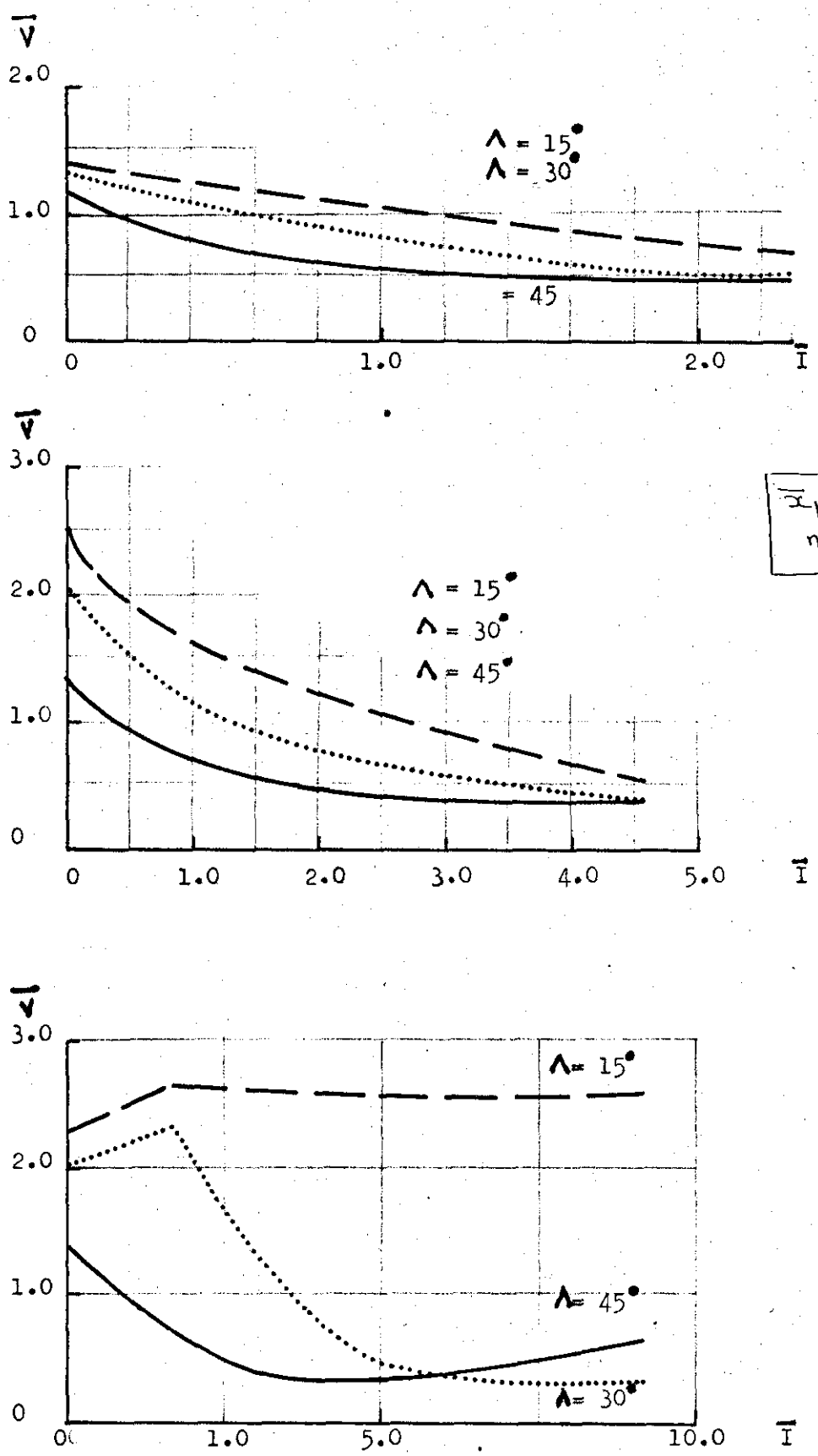

FIG. 2.9 Influence of I: Wing of Ref(9)

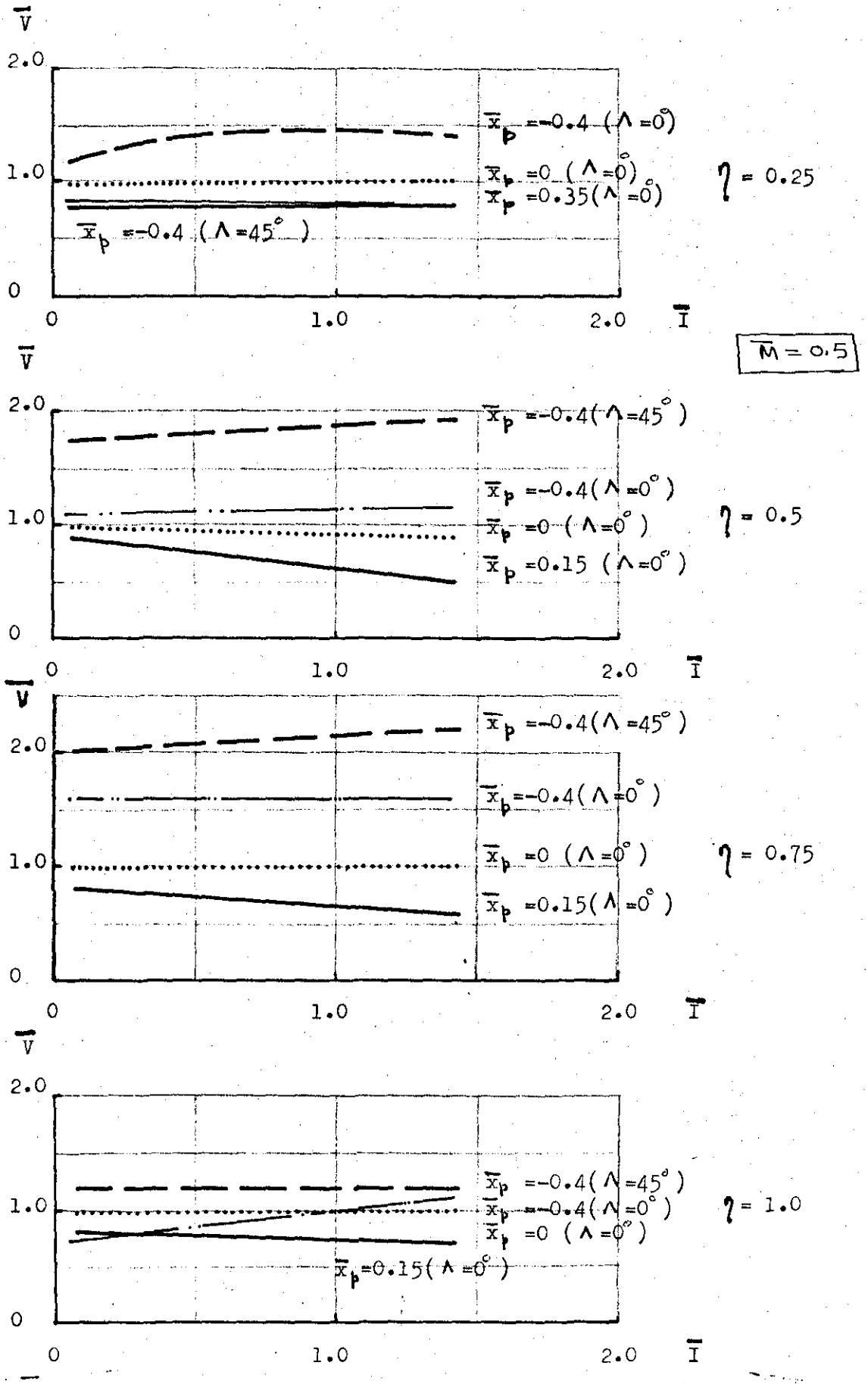

FIG. 2.10 Influence of I: Wing of Ref(10)

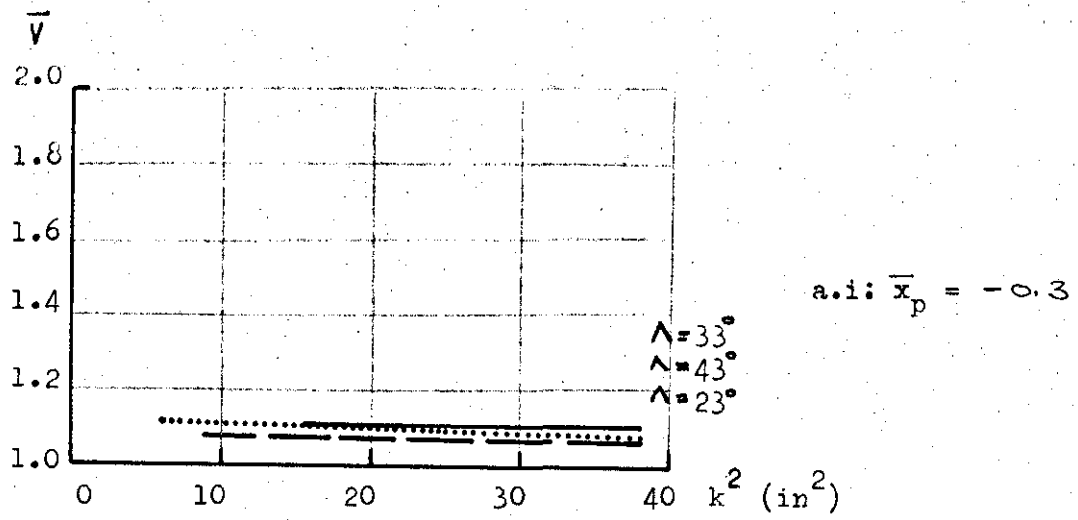

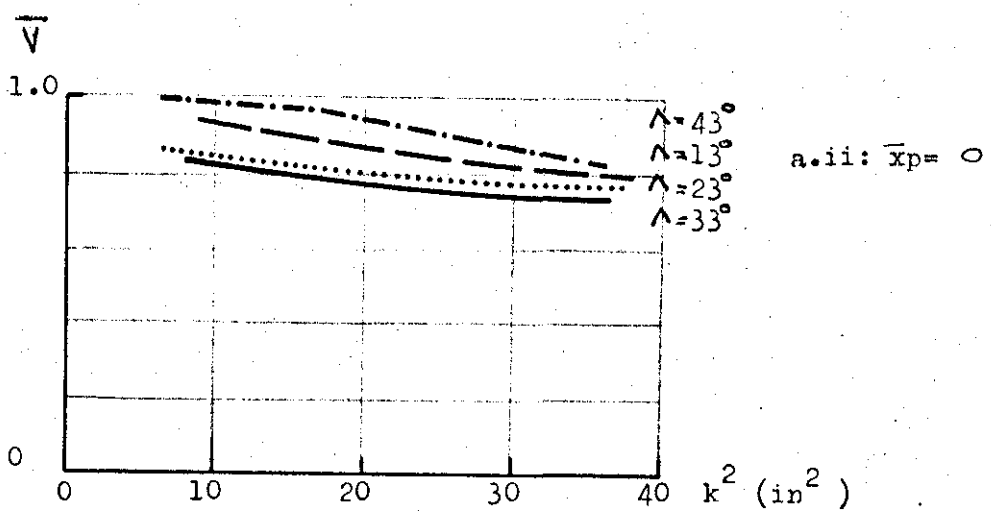

a) MASS AT WING TIP

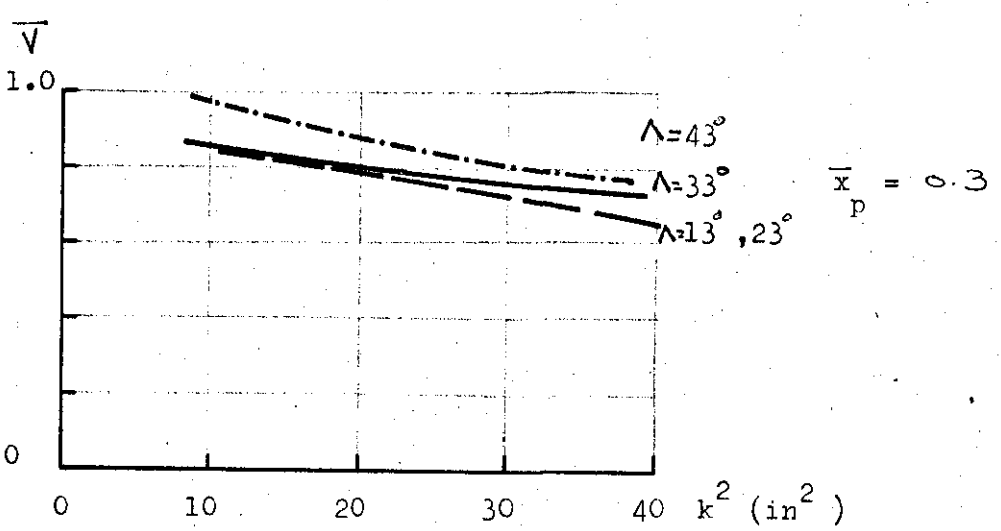

b) MASS AT 0.5 SPAN

FIG. 2.11 Influence of I: Wing of Ref(7)

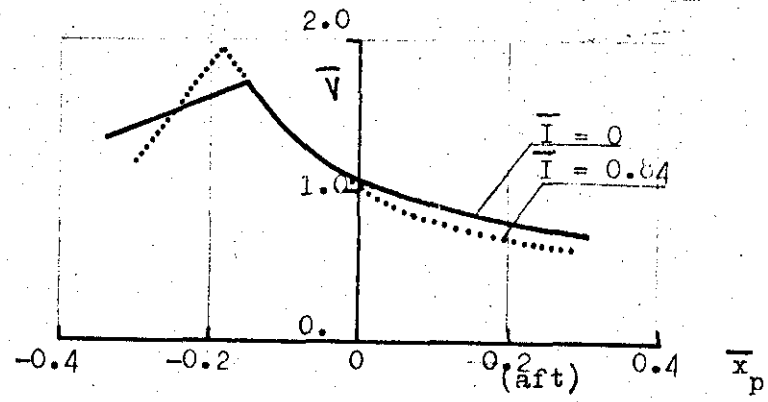

η = 0.5

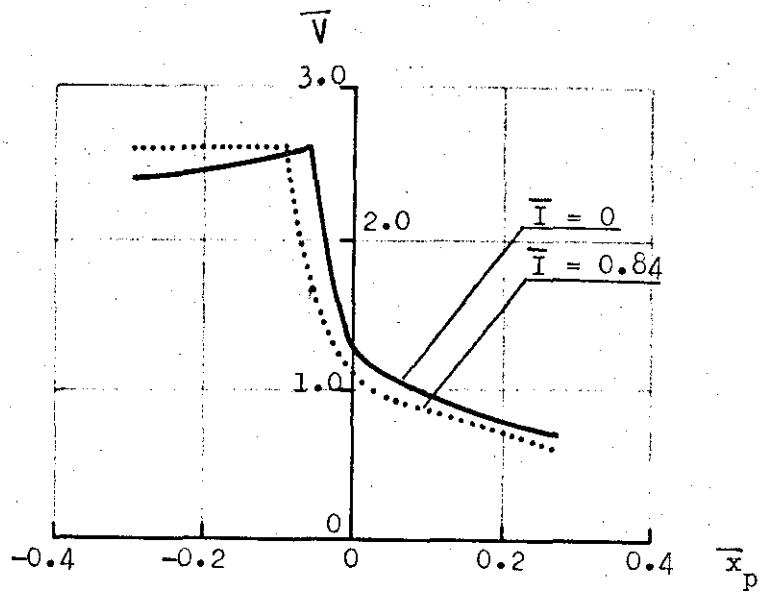

η = 0.67

$\overline{M}$ = 0.5

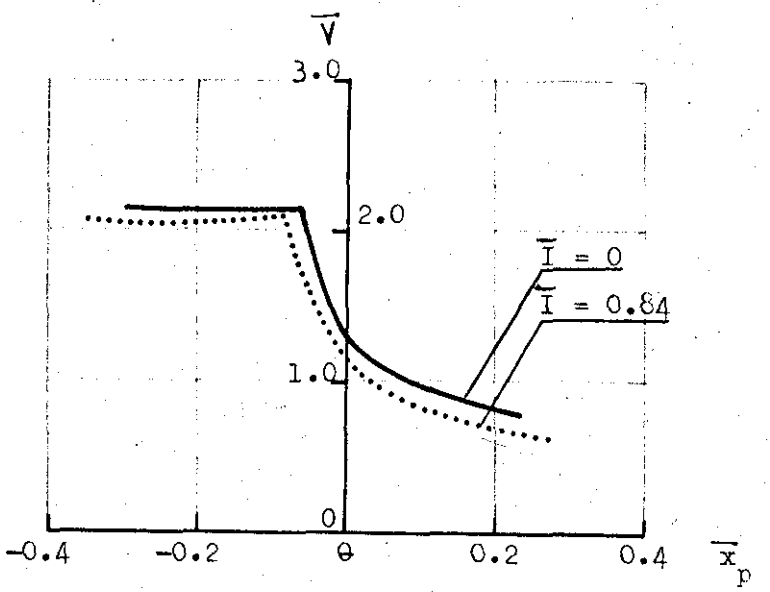

η = 0.75

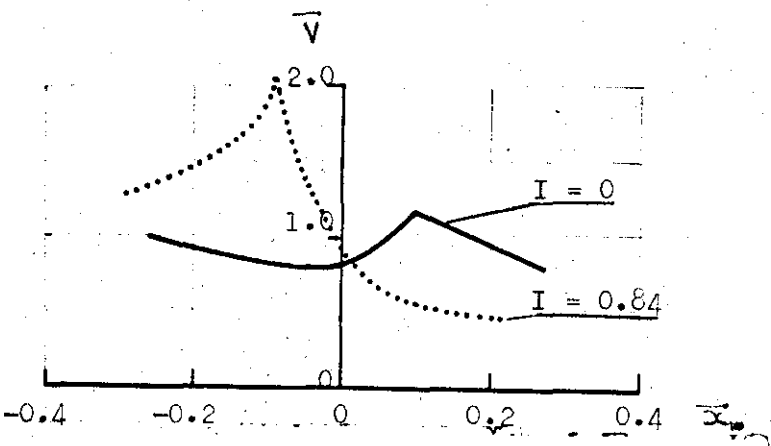

η = 1.0

FIG. 2.12 Influence of Chordwise Location: Wing of Ref(9)

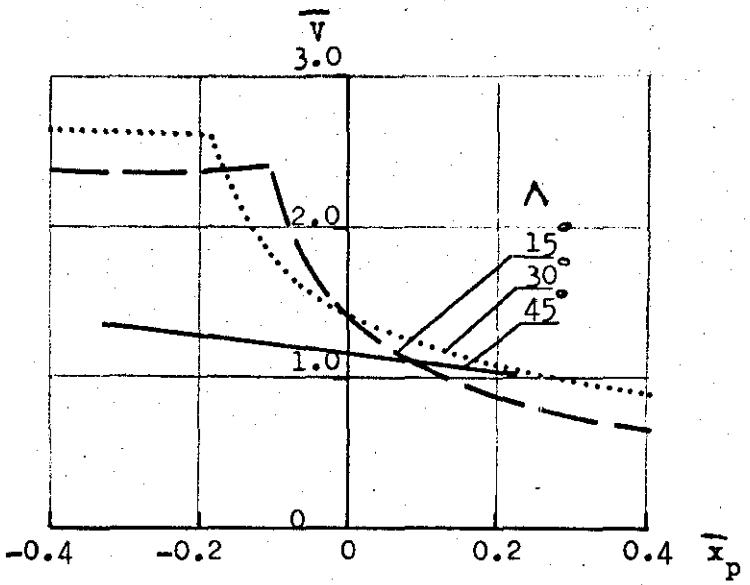

$\bar{I} = 0$

Mass at $\frac{2}{3}$ span position
$\bar{M} = 0.5$

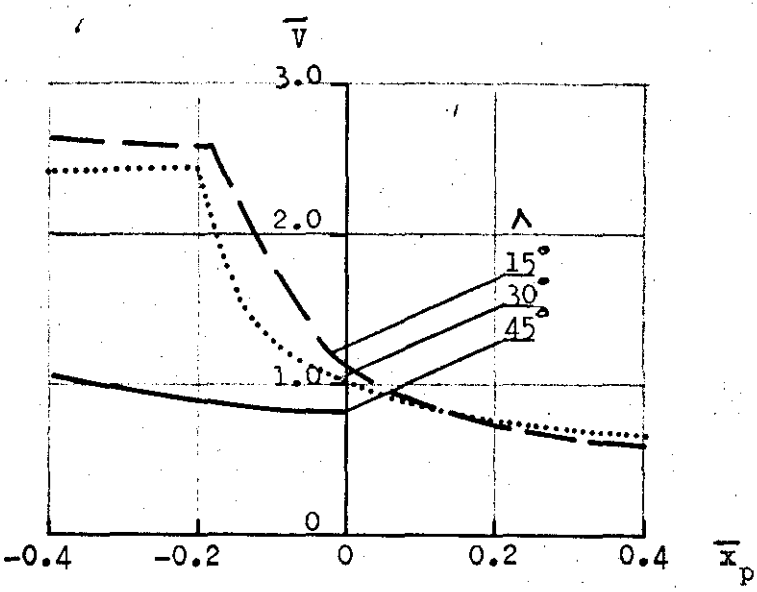

$\bar{I} = 0.84$

FIG.2.13 Influence of Chordwise Location of the c.g: Wing of Ref(9)

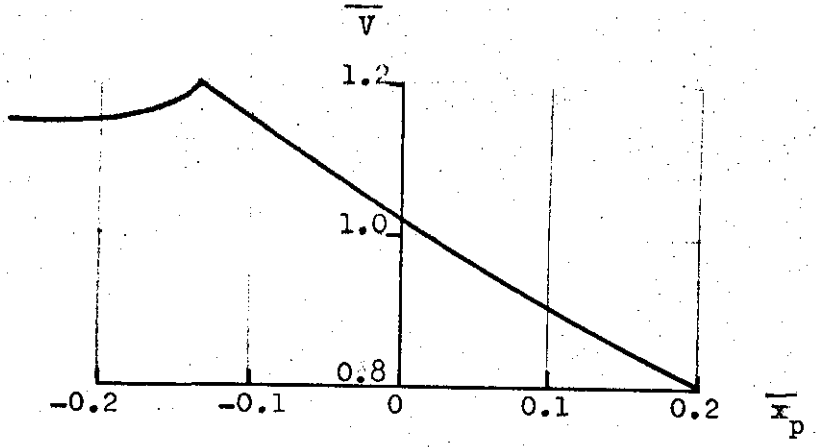

$\overline{M} = 0.5$

$\eta = 0.36$

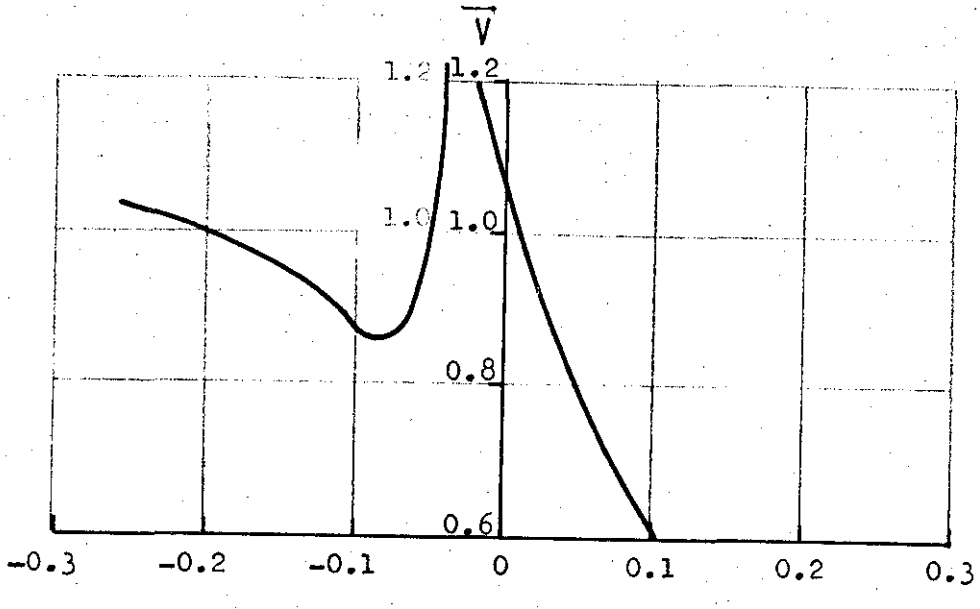

$\overline{M} = 0.5$

$\eta = 0.5$

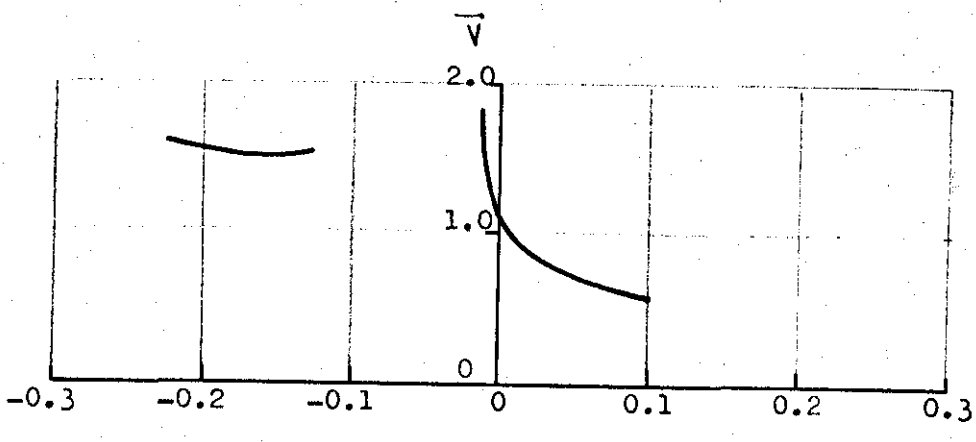

$\overline{M} = 0.5$

$\eta = 0.79$

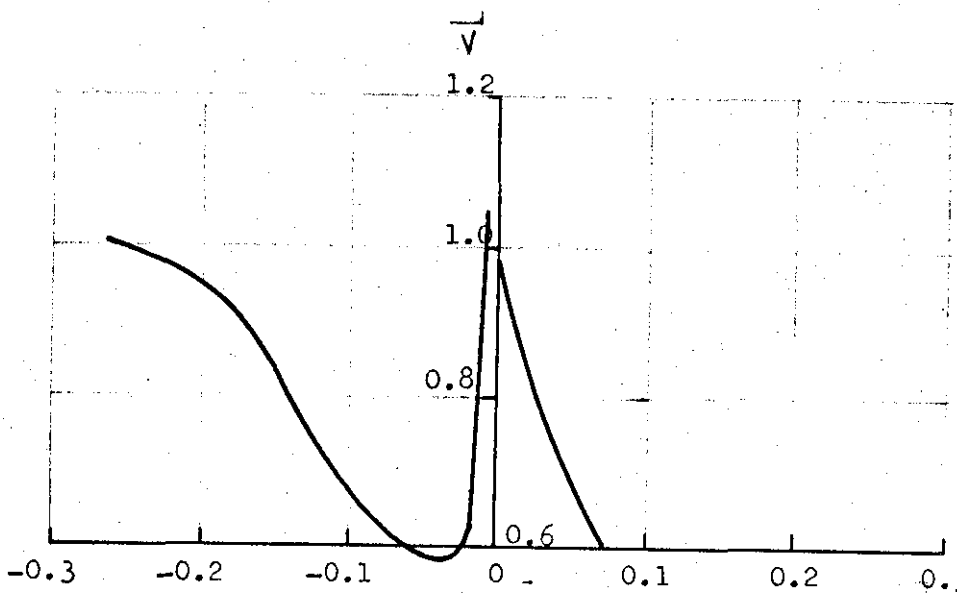

$\overline{M} = 0.5$

$\eta = 1.0$

FIG. 2.14 Influence of Chordwise Location: Wing of Ref(10) ("Fighter A")

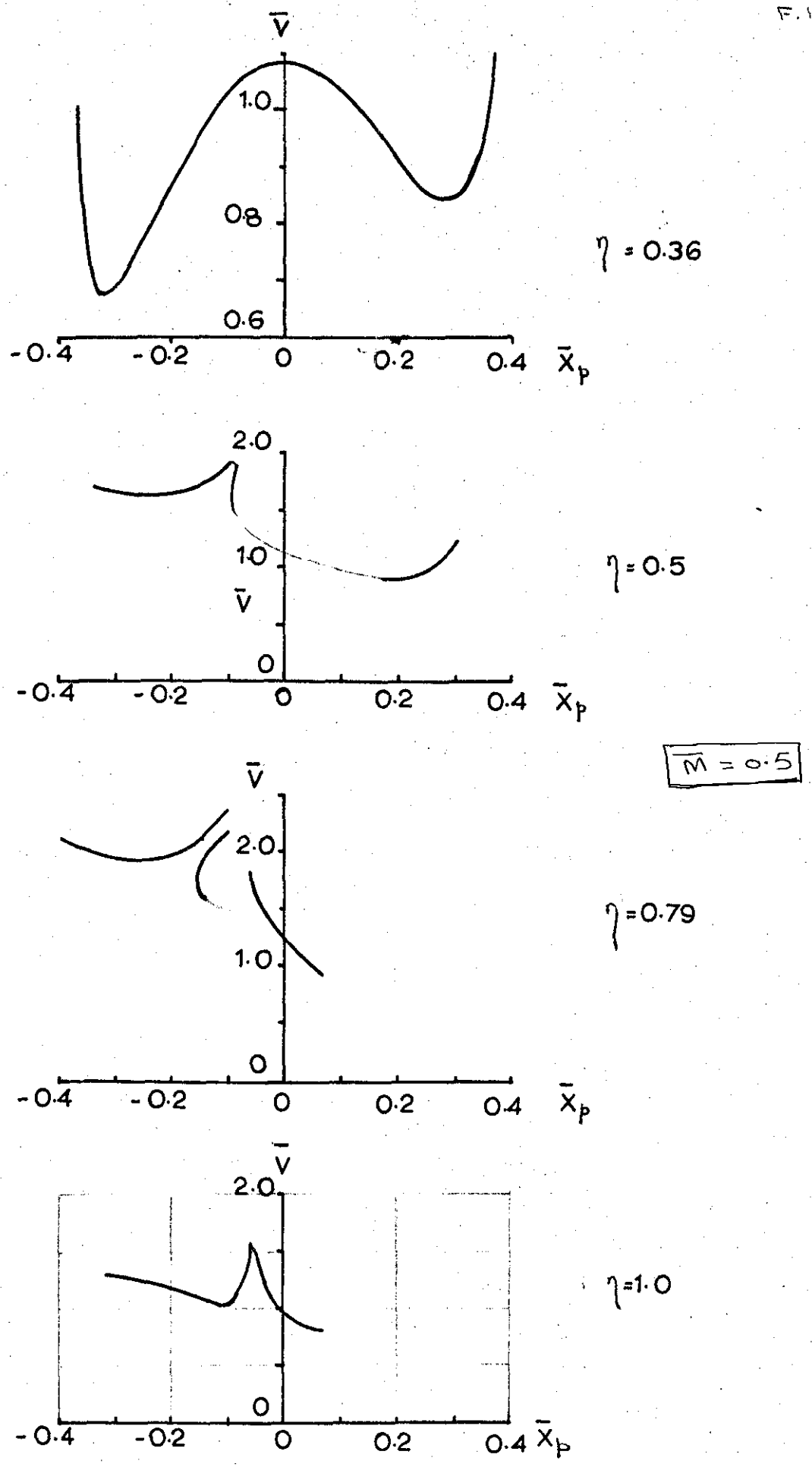

FIG. 2.15 Influence of Chordwise Location: Wing of Ref(10) ("Fighter-B" $\Lambda = 45°$)

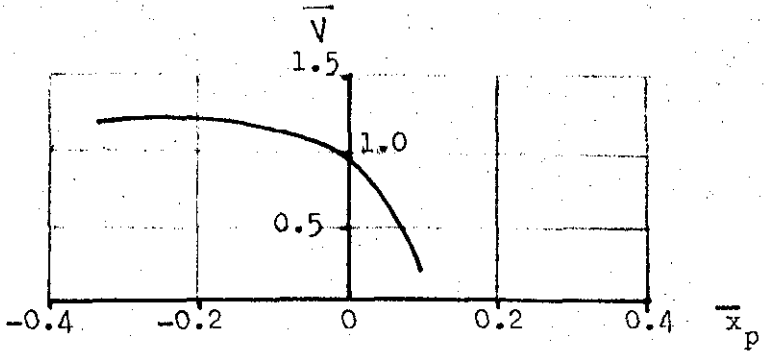

$\eta = 0.31$

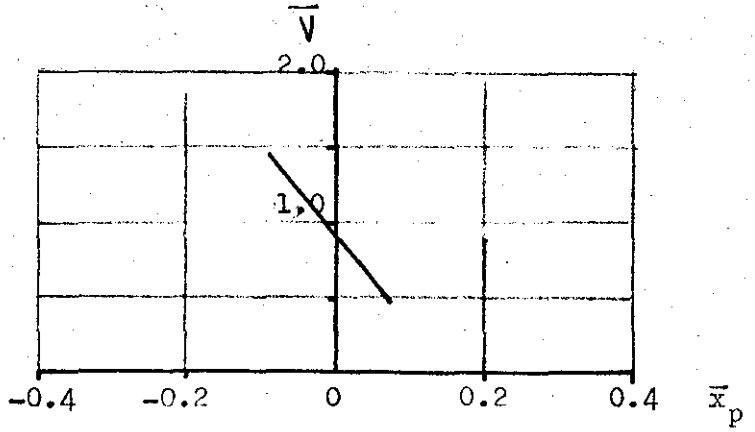

$\eta = 0.62$

$\overline{M} = 0.54$

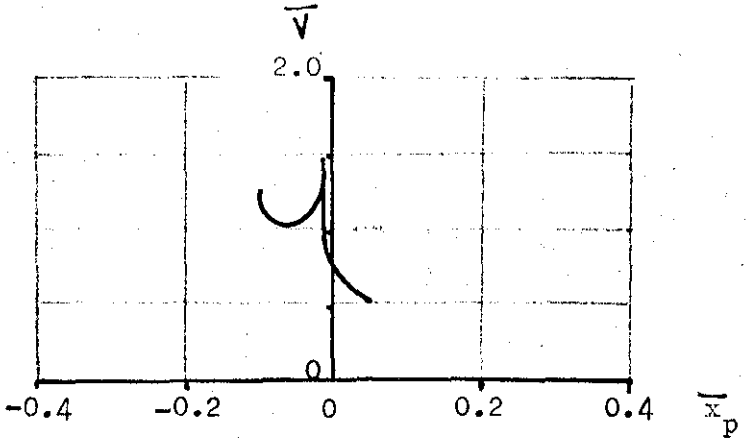

$\eta = 0.77$

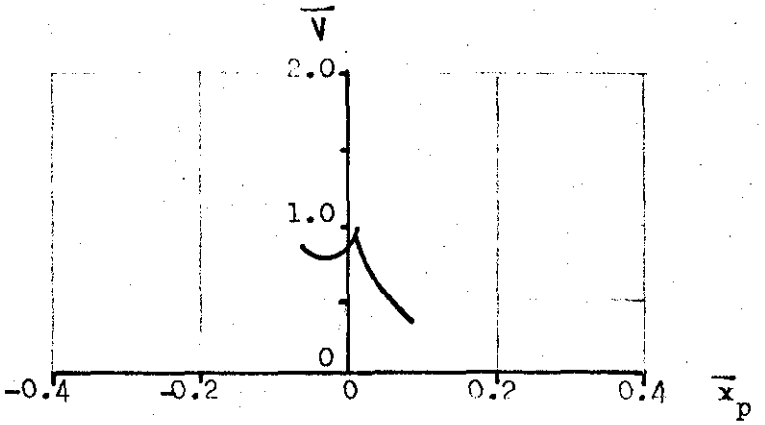

$\eta = 1.0$

FIG. 2.16 b Influence of Chordwise Location of c.g.

Wing of Ref (10) ("BOMBER. B")

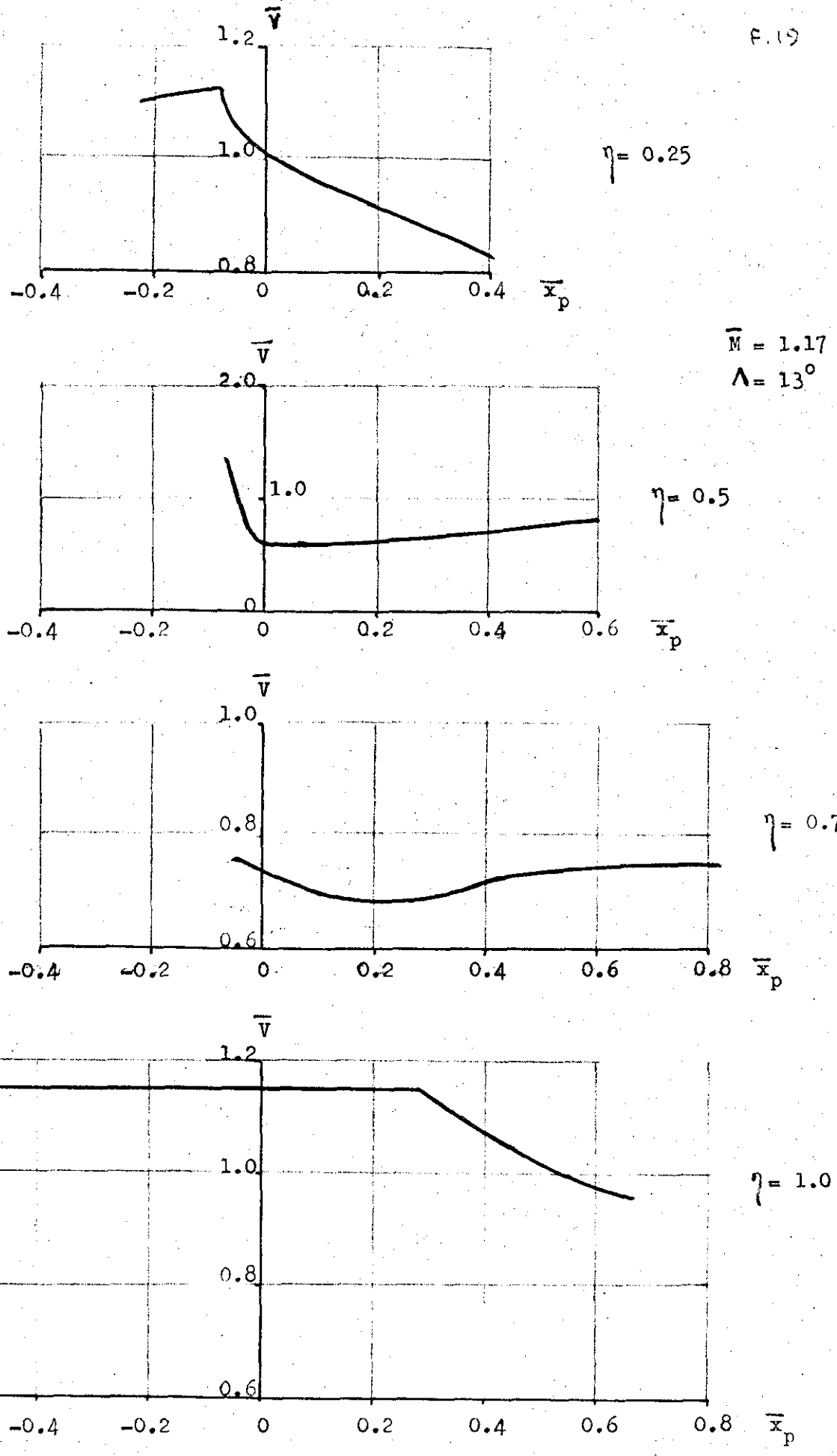

FIG. 2.17a Influence of Chordwise Location: Wing of Ref(7)

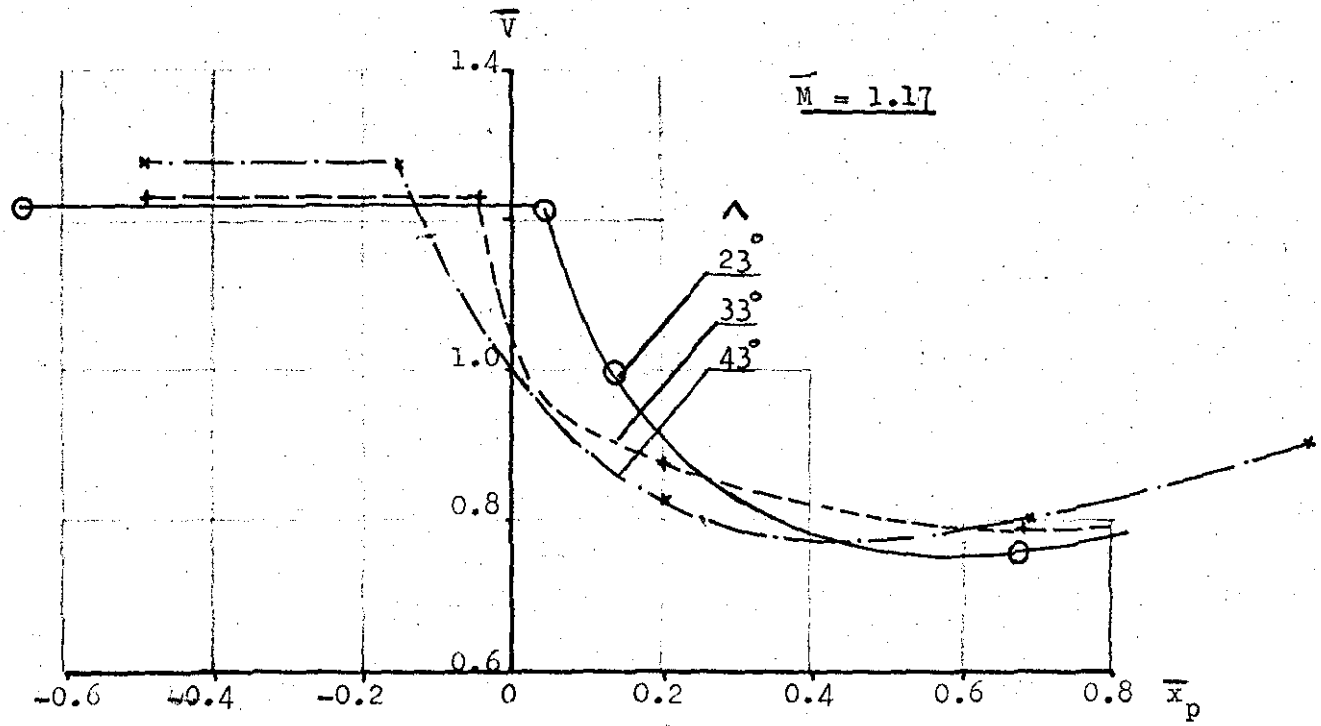

$\eta = 1$

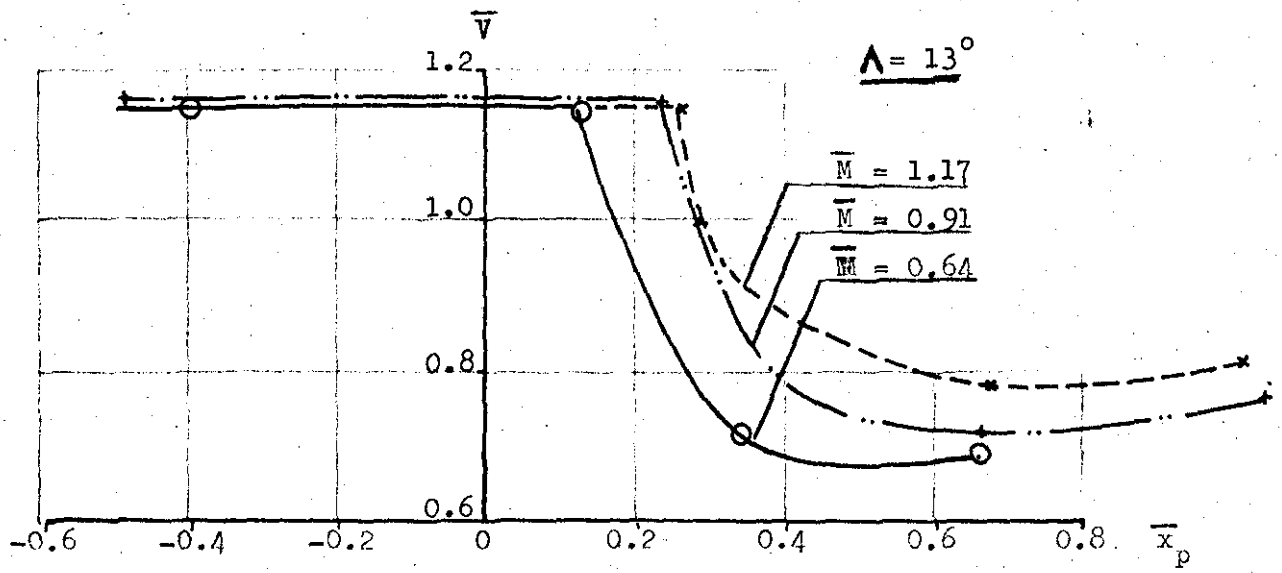

FIG. 2.17b Influence of Chordwise Location: Wing Ref(7)

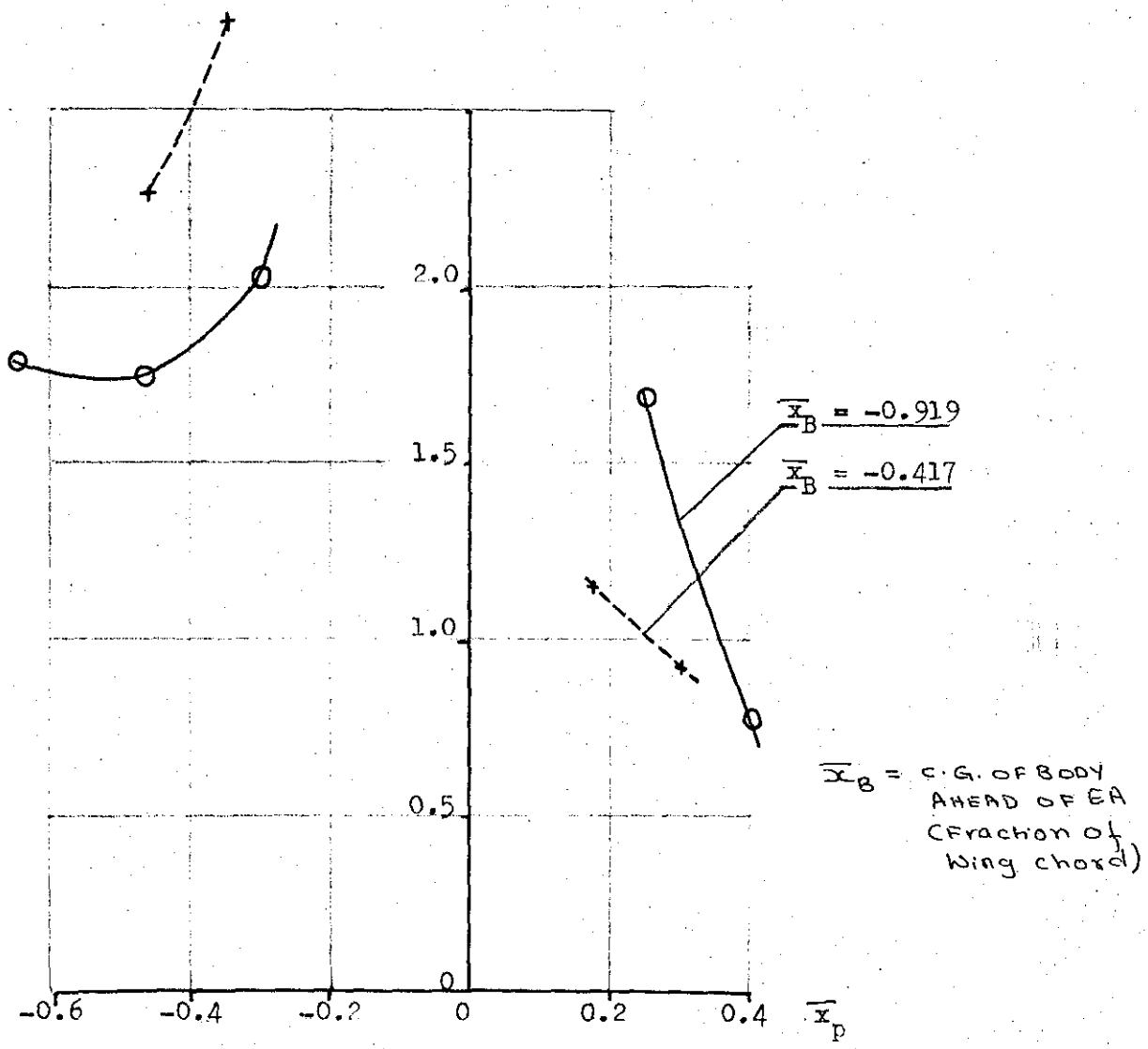

FIG 2.18 Influence of Chordwise Location of c.g. Wing of Ref(8)

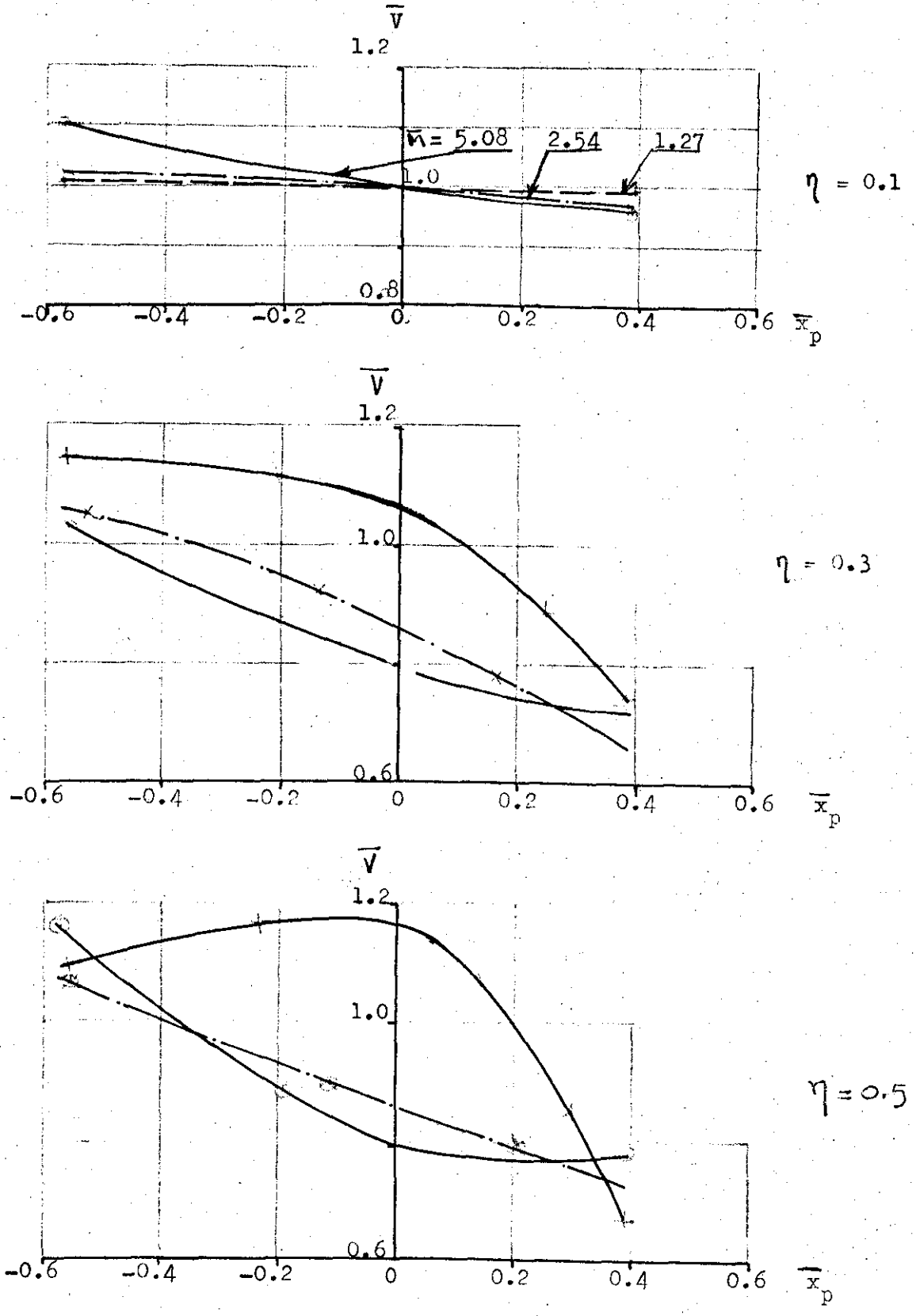

FIG.2.19 Influence of Chordwise Location of c.g. Wing of Ref(6)

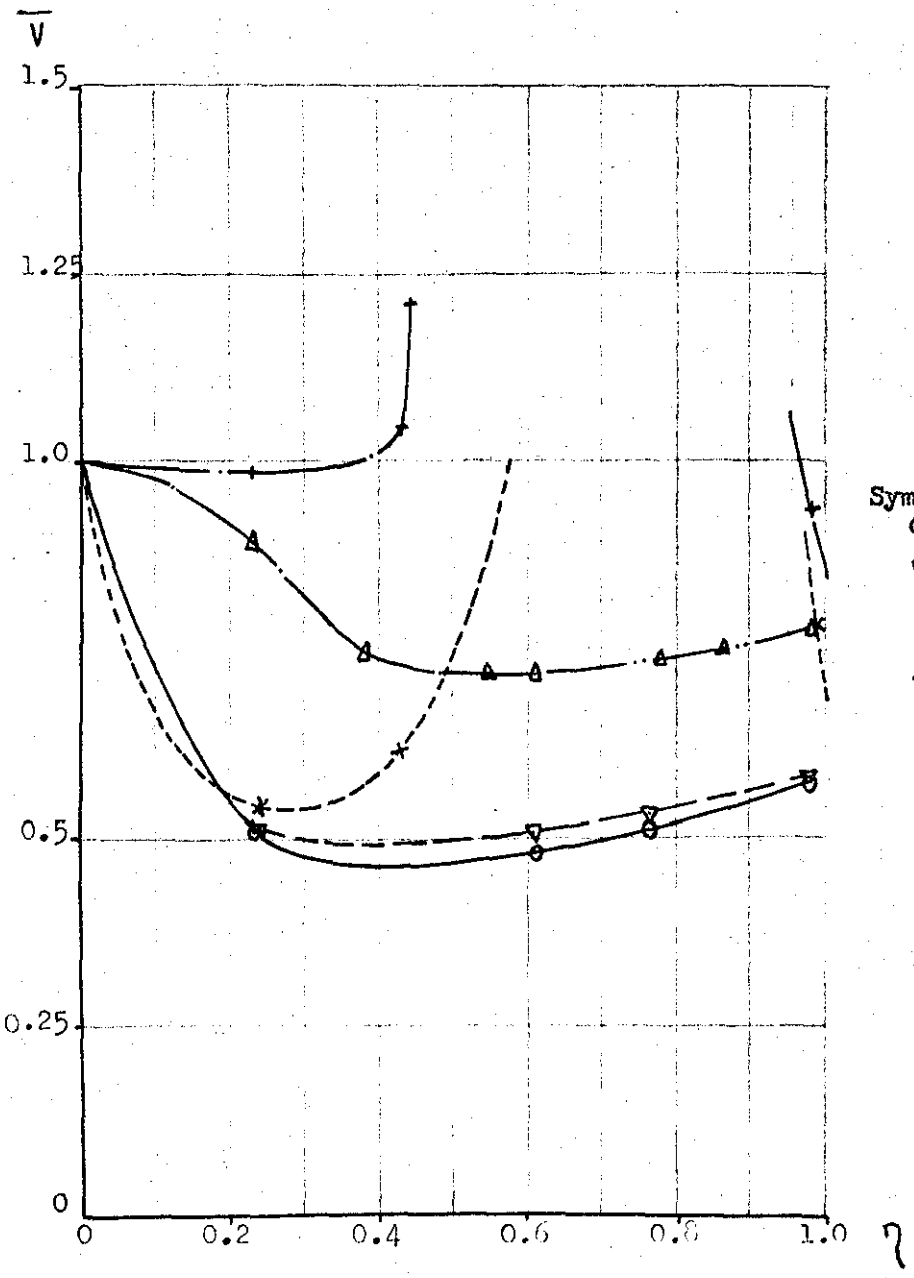

FIG.2.20 Influence of Spanwise Location: Wing of Ref(38)

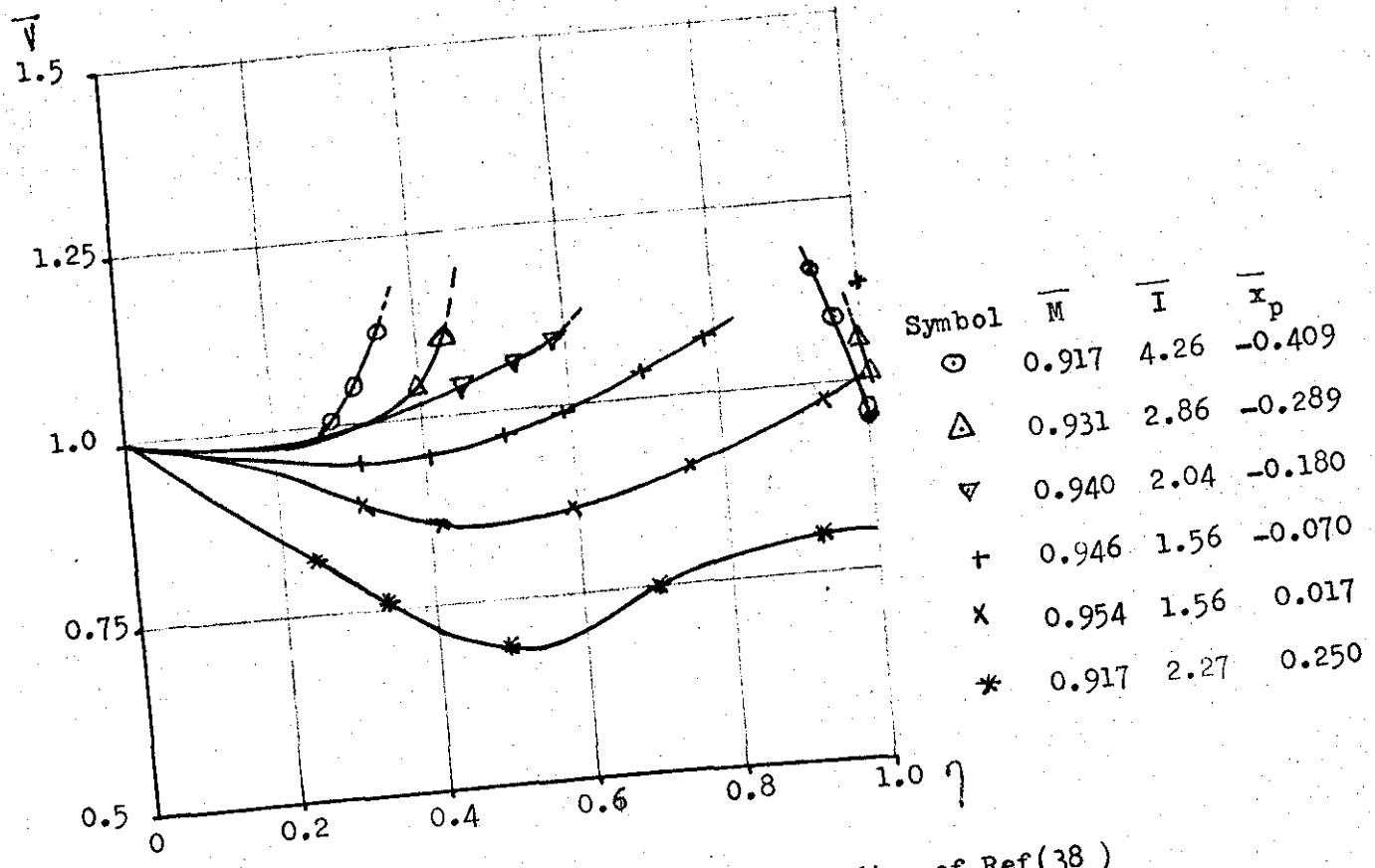

FIG 2.21 Influence of Spanwise Location: Wing of Ref(38)

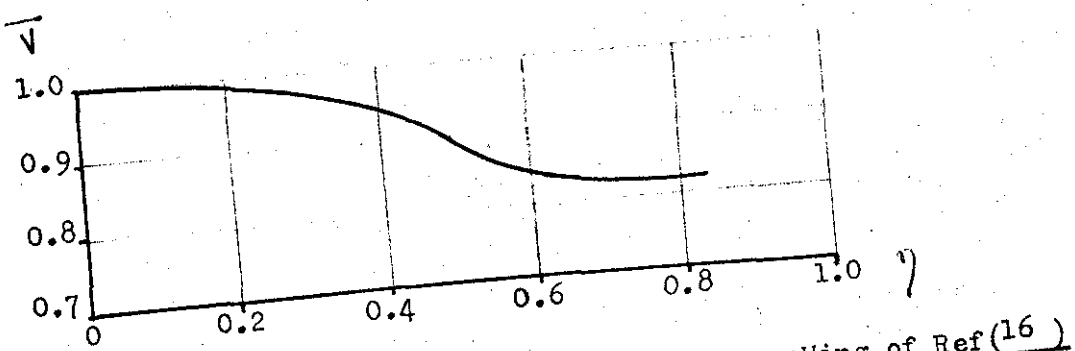

FIG.2.22 Influence of Spanwise Location: Wing of Ref(16)

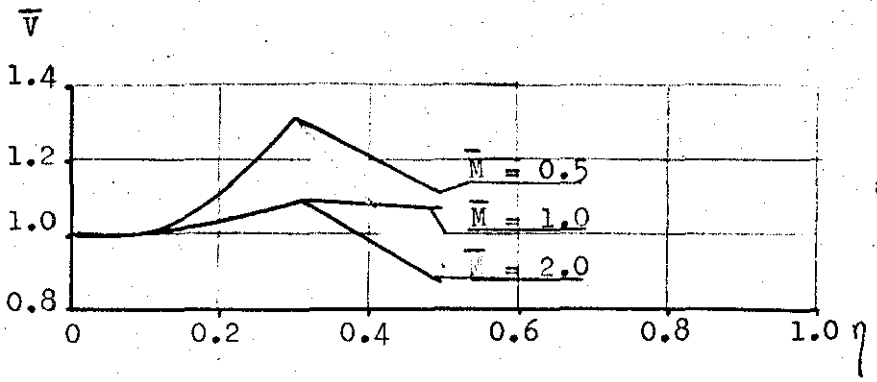

a) Mass 0.28c ahead of the Elastic axis.

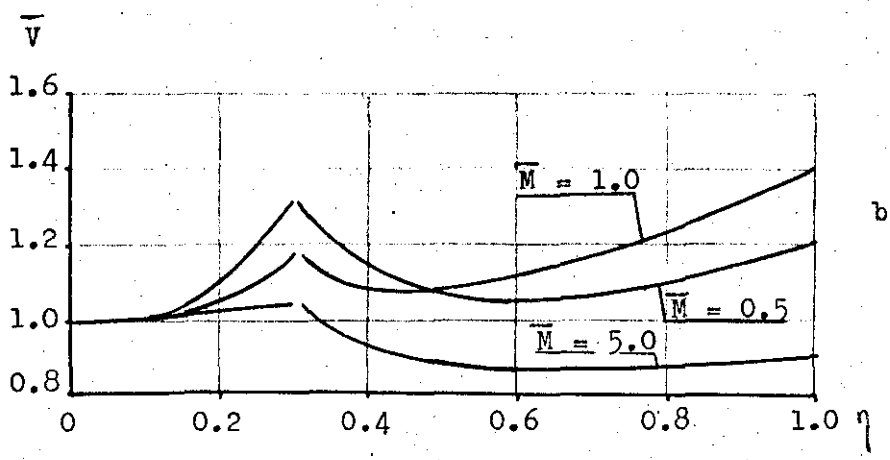

b) Mass on the Elastic Axis.

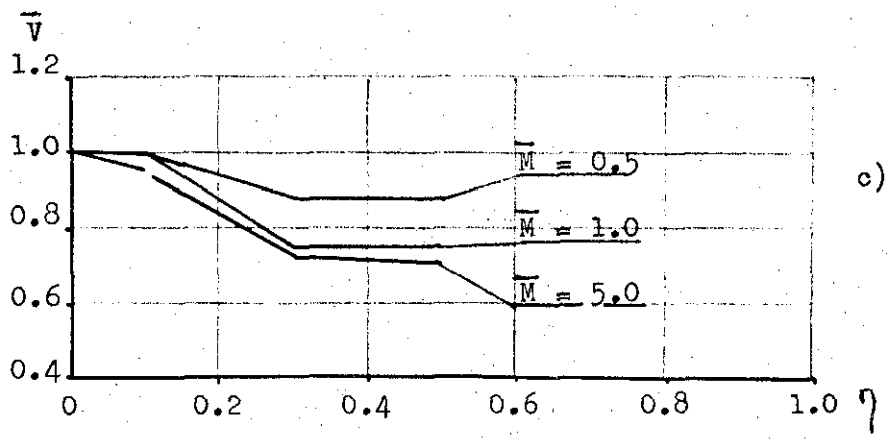

c) Mass 0.39c aft of the Elastic Axis.

FIG. 2.25 Influence of Spanwise Location: Wing of Ref(6)

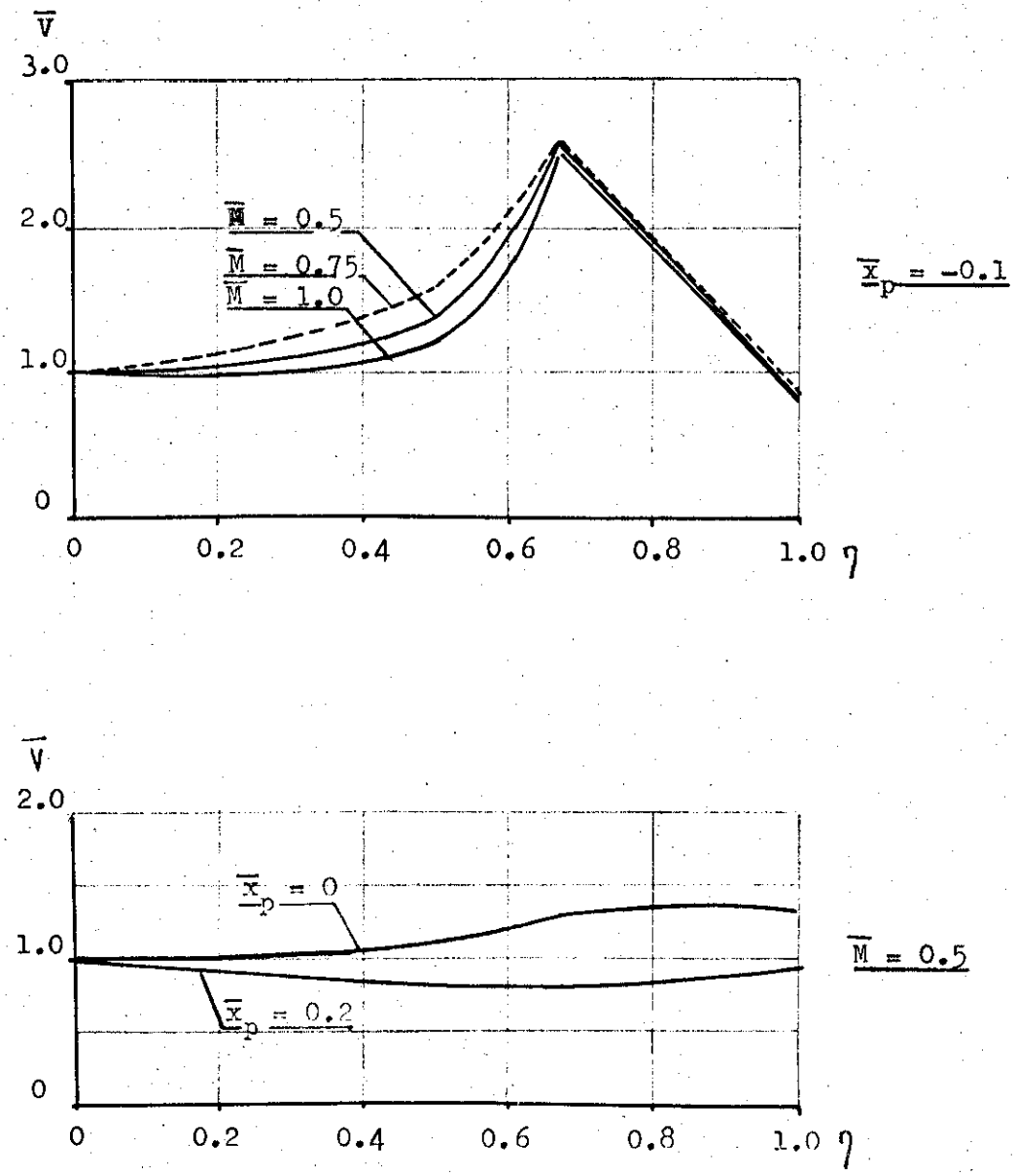

FIG.2.26 Influence of Spanwise Location: Wing of Ref(9)

$\overline{M}$ = 1.0

η = 0.755

$\overline{q}$ = (Dynamic Pressure at flutter of Wing+store)/(Dynamic Pressure at flutter of the bare wing)

$\overline{f}$ = (Flutter frequency of wing+store)/(Wing torsional frequency)

ω_N = Pitching Frequency of Mass

ω_t = Wing torsional frequency.

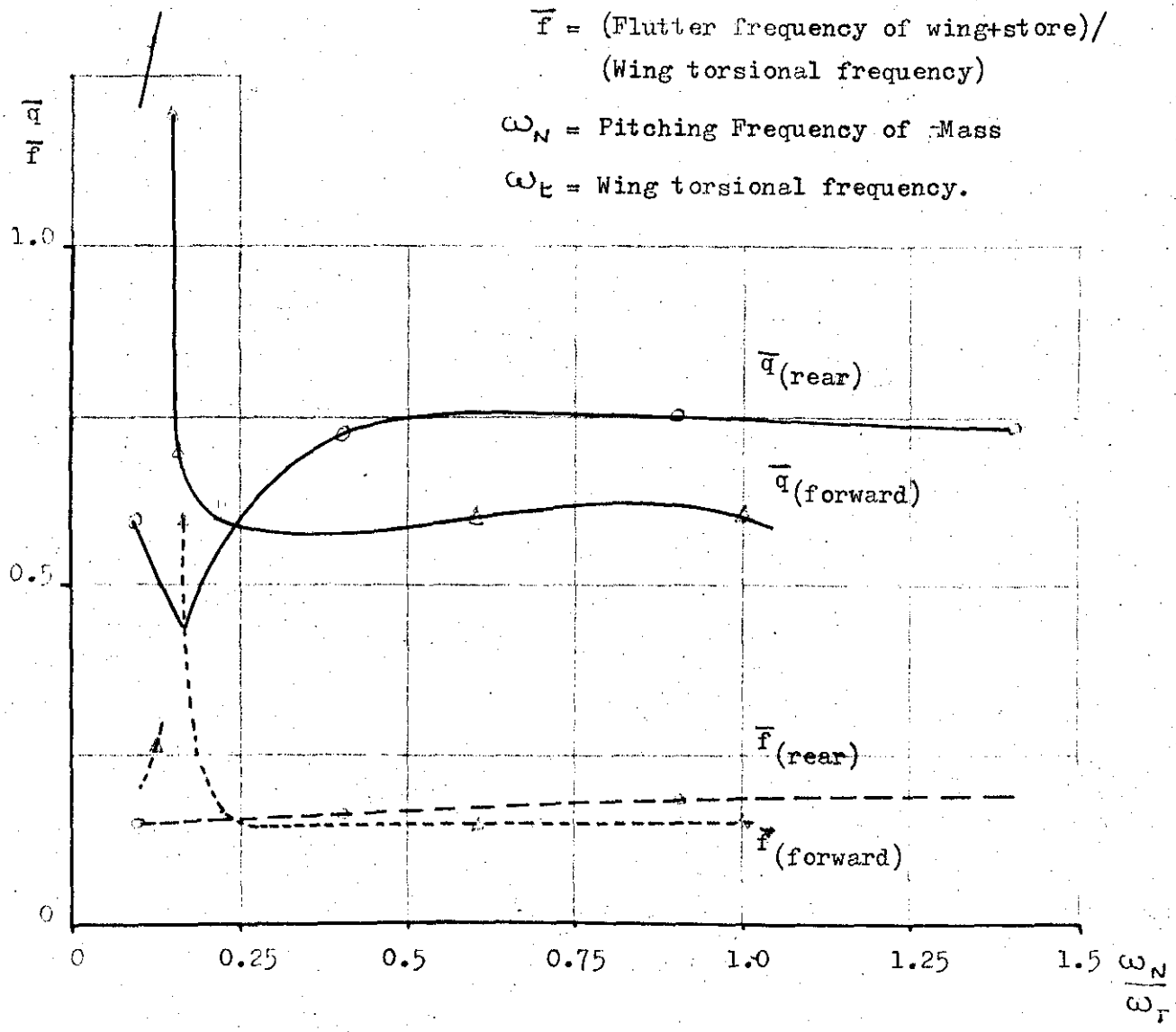

FIG. 2.27 Influence of Pitching Frequency: Wing of Ref(11)

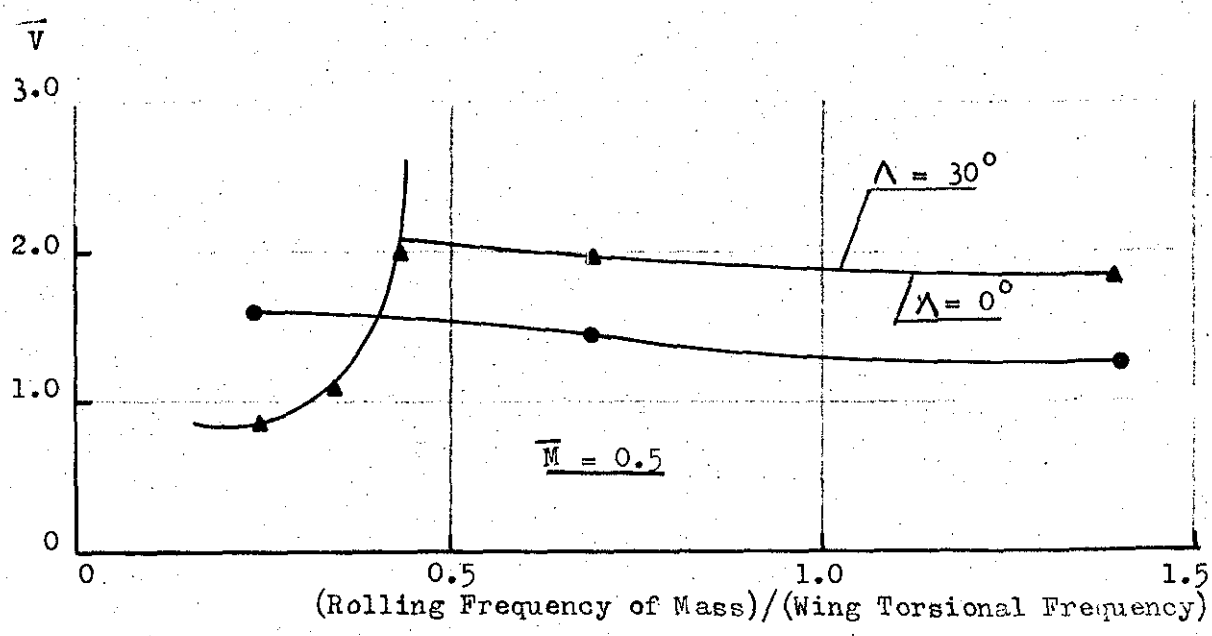

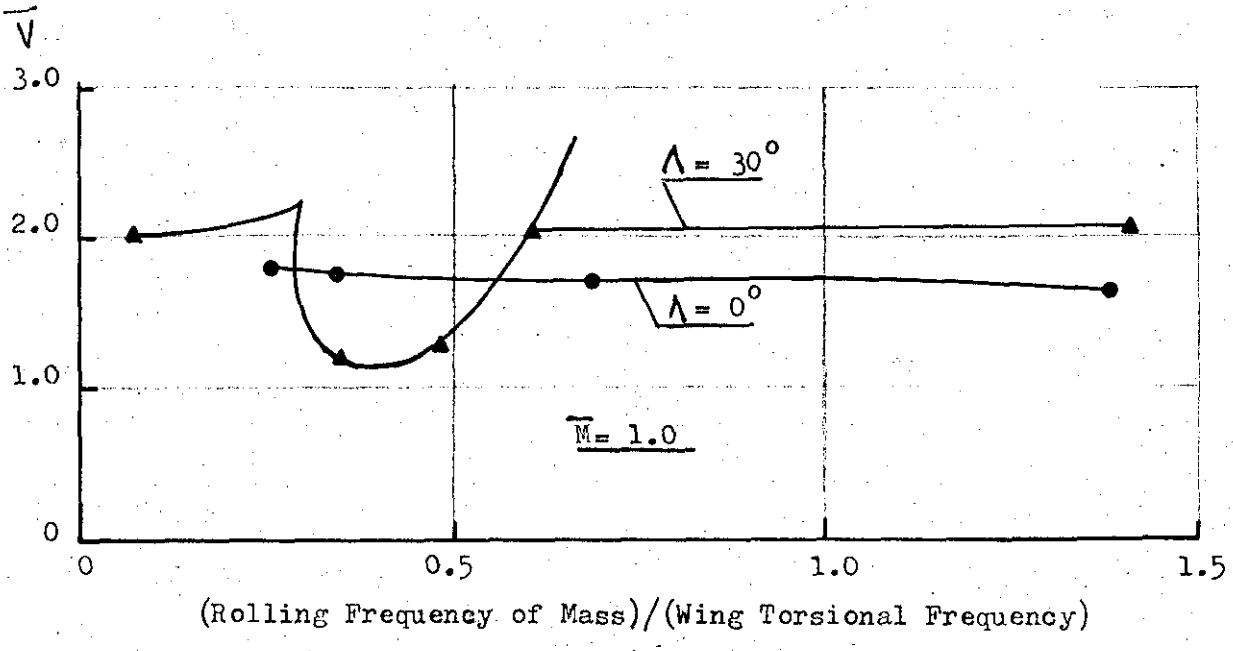

FIG. 2.29 Influence of Roll Frequency: Wing of Ref (12)

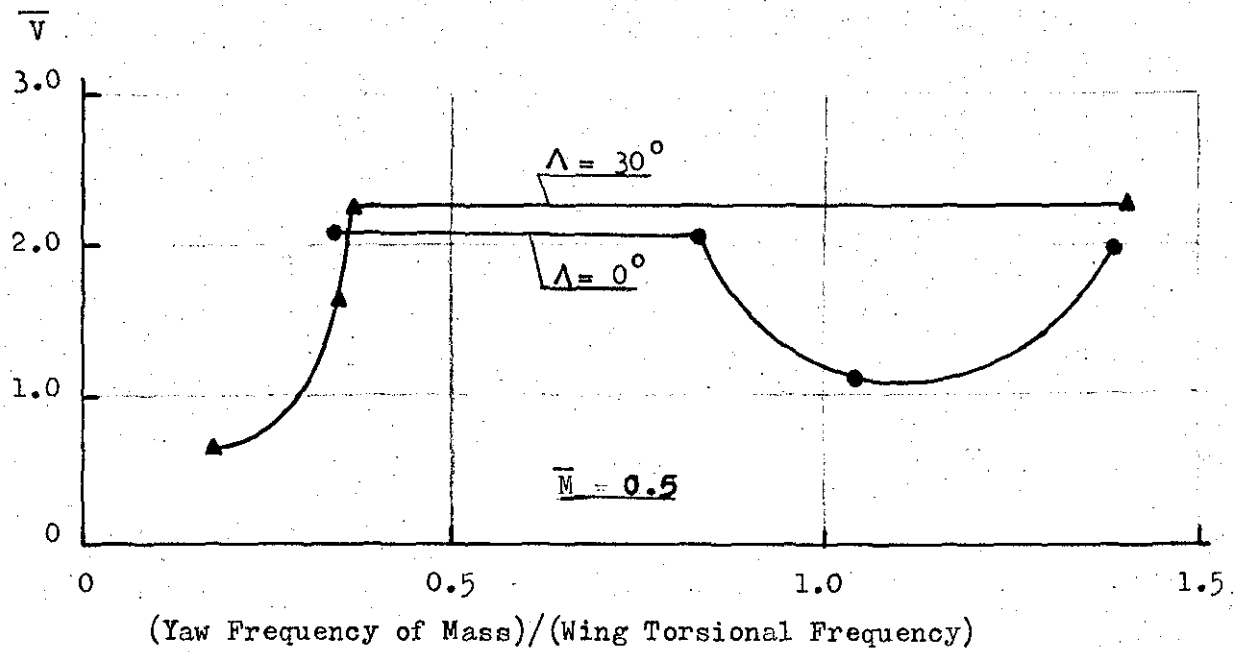

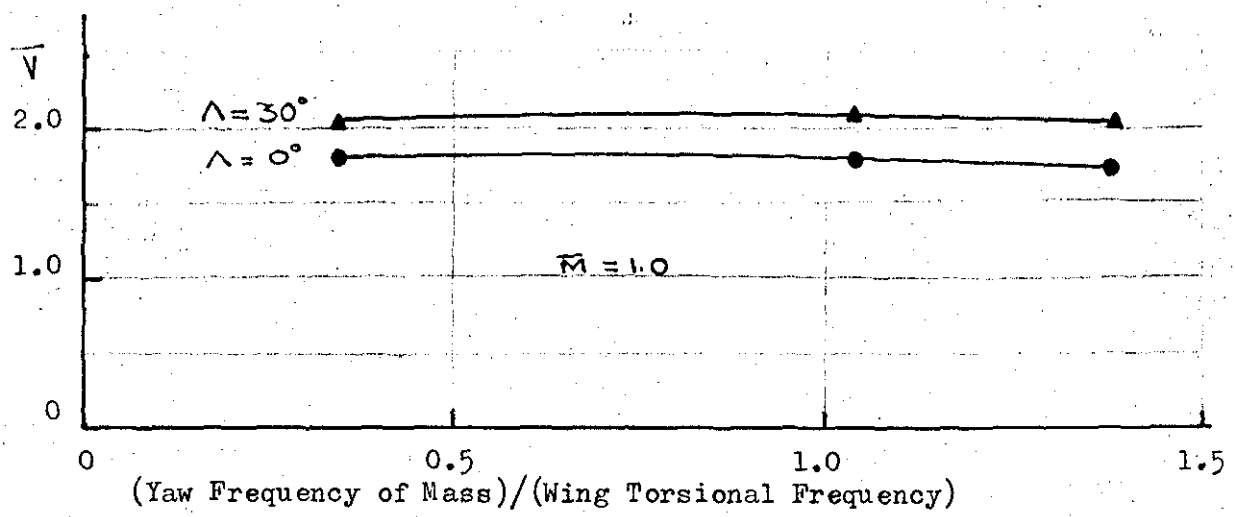

FIG. 2.30 Influence of Yaw Frequency: Wing of Ref(12)

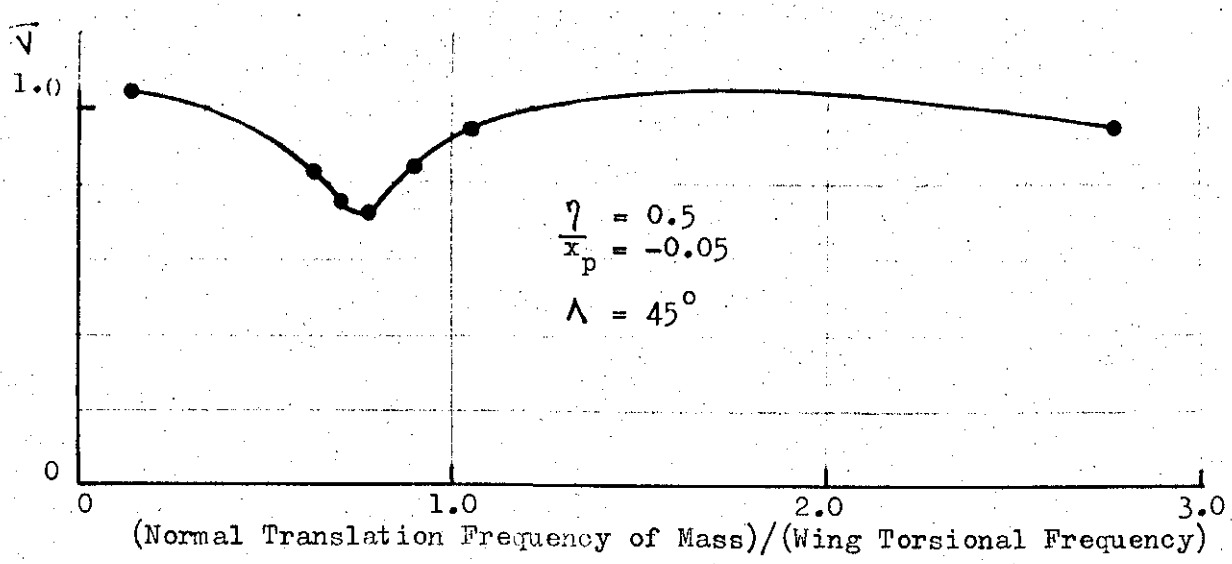

FIG. 2.31 Influence of Normal Translation Frequency: Wing of Ref(12)

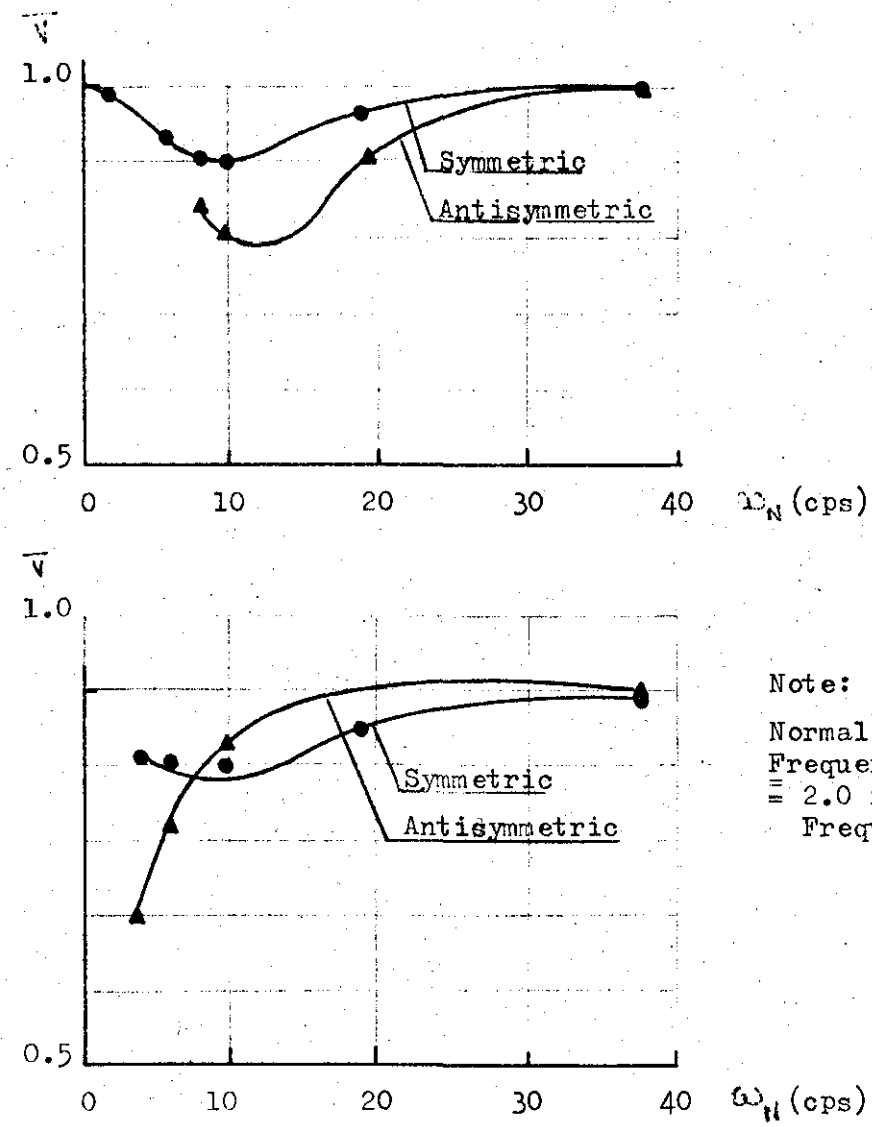

Note:

Normal Translation Frequency of Mass = 2.0 x (Pitching Frequency)

FIG. 2.32 Influence of (Normal Translation + Pitch) of Mass : Wing of Ref(10)

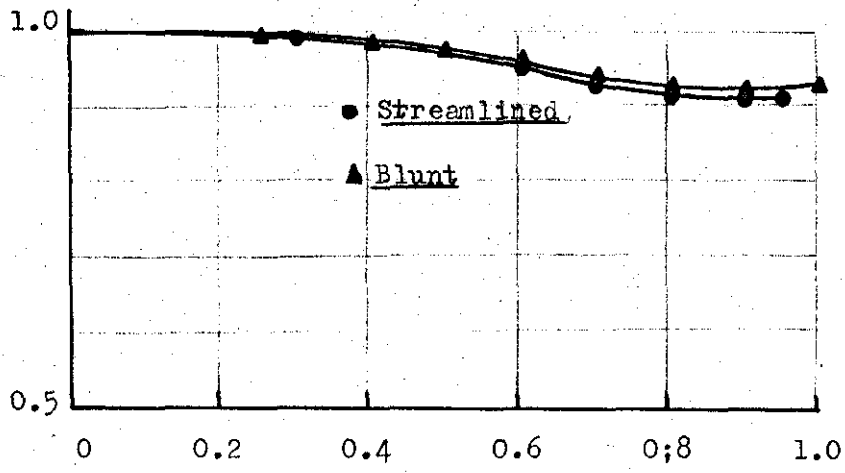

FIG. 2.33 Influence of Aerodynamic Shape: Wing of Ref(16)

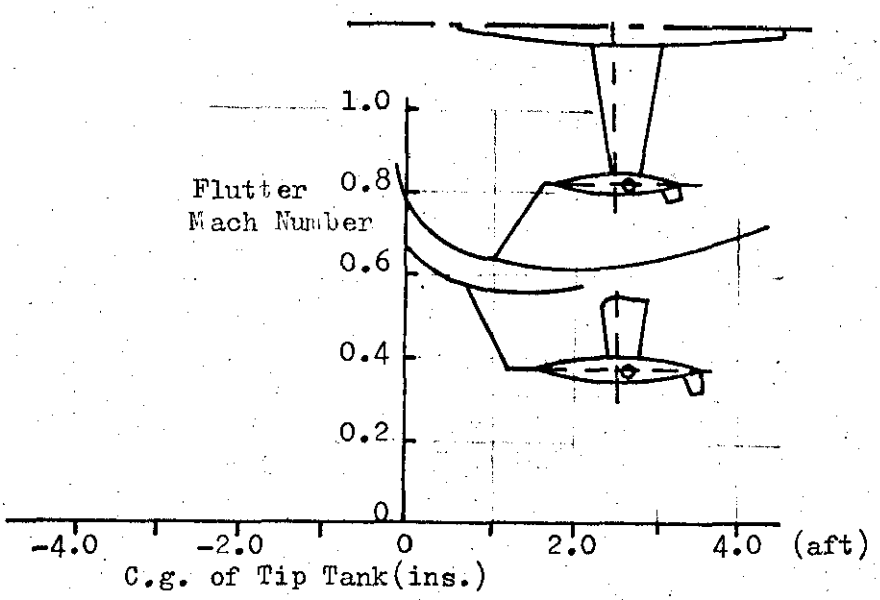

FIG. 2.34 Influence of Aerodynamic Shape: Wing of Ref(14)

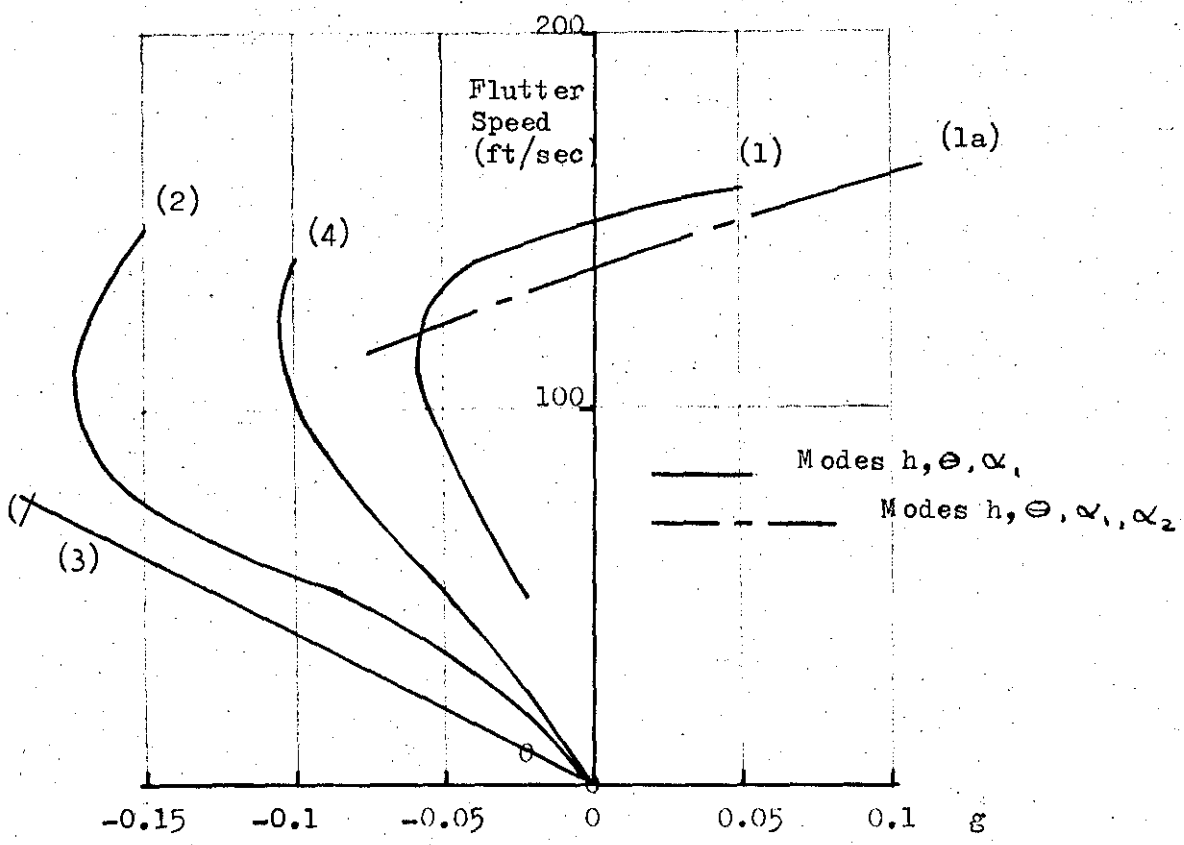

Case	Semi-Chord (in)	Span (in)	¼-chord (aft of e.a.) (in)
1	5.5	4.73	-0.88
2	16.5	2.77	-6.33
3	16.5	3.6	0
4	5.5	4.73	-6.33

FIG. 2.35 Influence of Aerodynamic Shape: Wing of Ref(15)

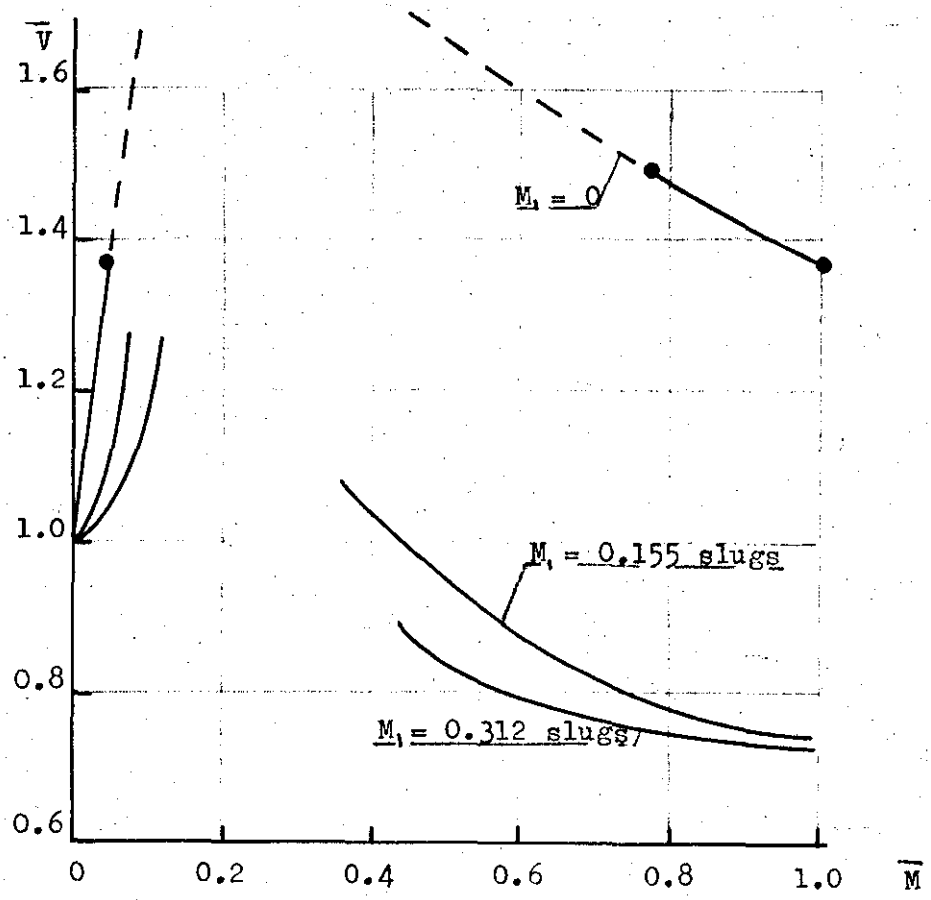

$\overline{M}$ = μ / Wing Mass = μ /0.394 (slug units)

V = (flutter speed of Wing+both masses)/(Flutter speed of Wing with M_1 only)

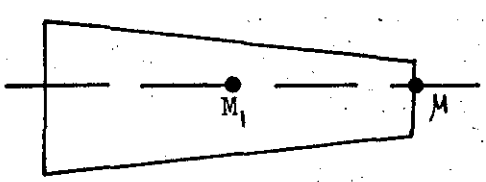

FIG. 2.36 Influence of Adding More than One Mass: Wing of Ref.6

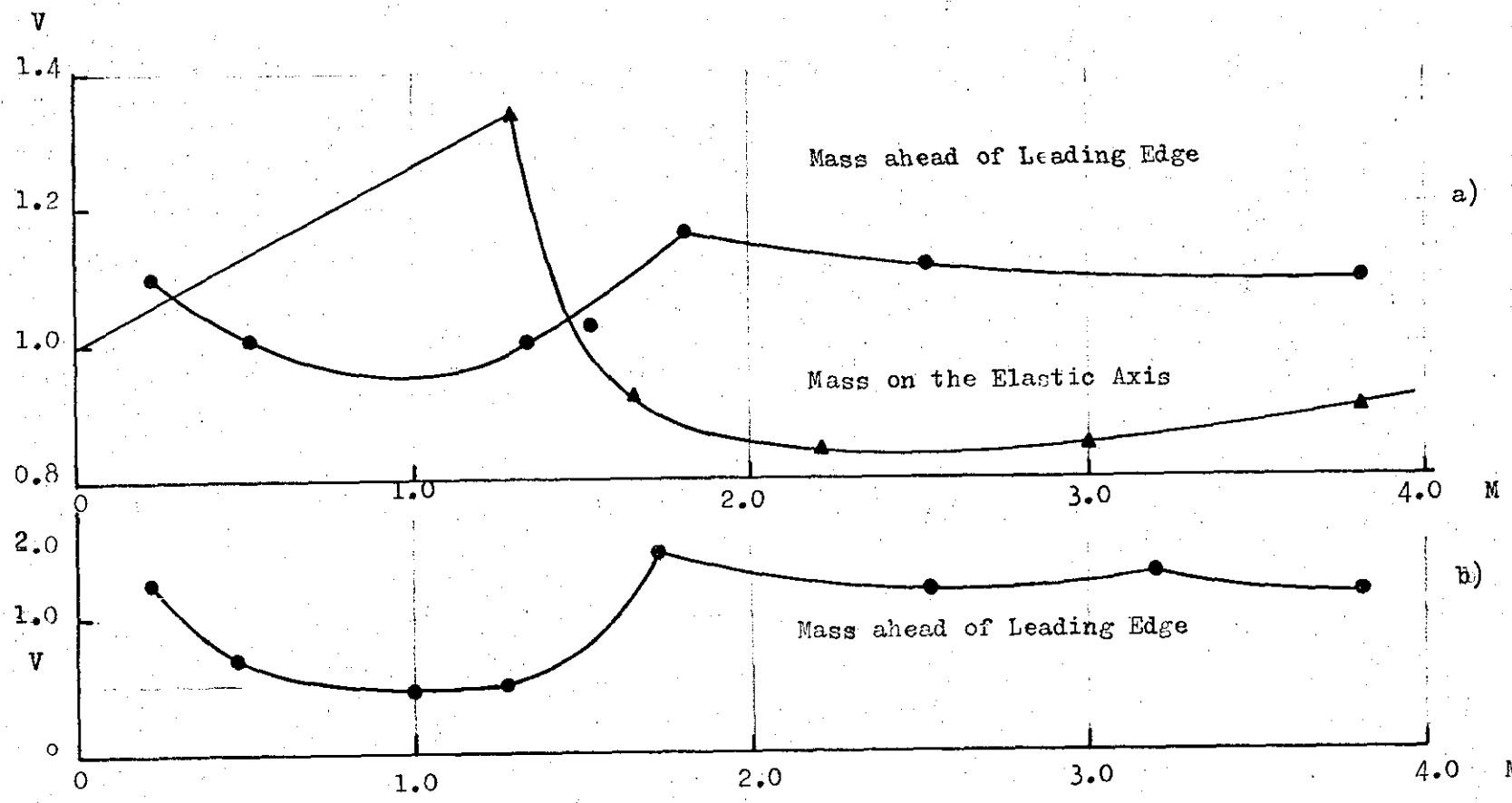

a) Mass Loading Simultaneously at = 0.3 and 0.5

b) Mass Loading Simultaneously at = 0.1,.0.3 amd 0.5

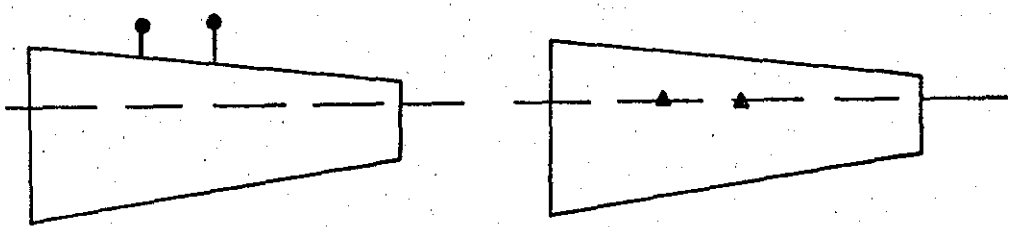

FIG. 2.37 Influence of adding More Than one Mass (Wing of Ref (6)

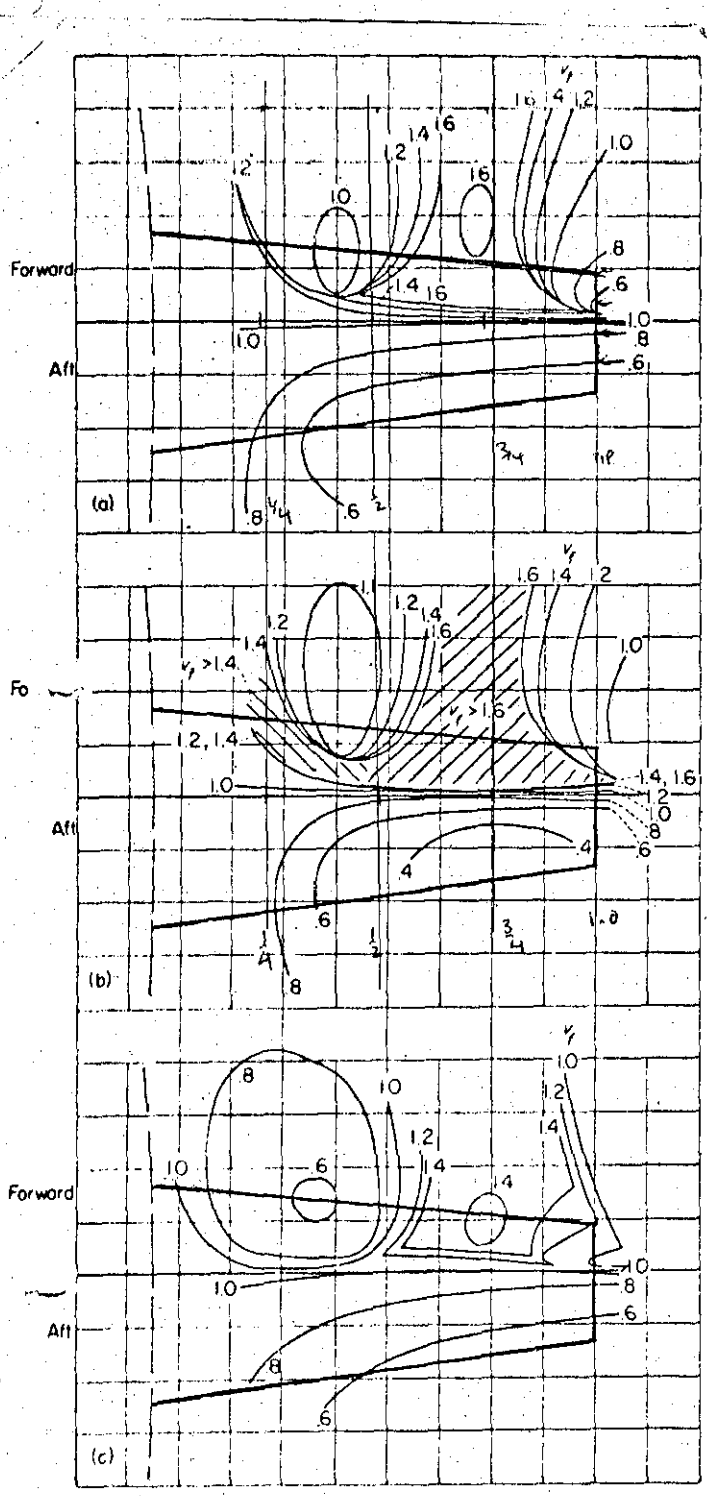

(a) Fighter A; $\Lambda = 0°$; symmetric; radius of gyration, 6 inches; $1.0 w_f$ = 989 miles per hour.
(b) Fighter A; $\Lambda = 0°$; symmetric; radius of gyration, 30 inches; $1.0 w_f$ = 989 miles per hour.
(c) Fighter A; $\Lambda = 0°$; antisymmetric; radius of gyration, 6 inches; $1.0 w_f$ = 1,091 miles per hour.

FIG 2.38 Influence of Root Degrees of Freedom: Wing Of Ref(10)

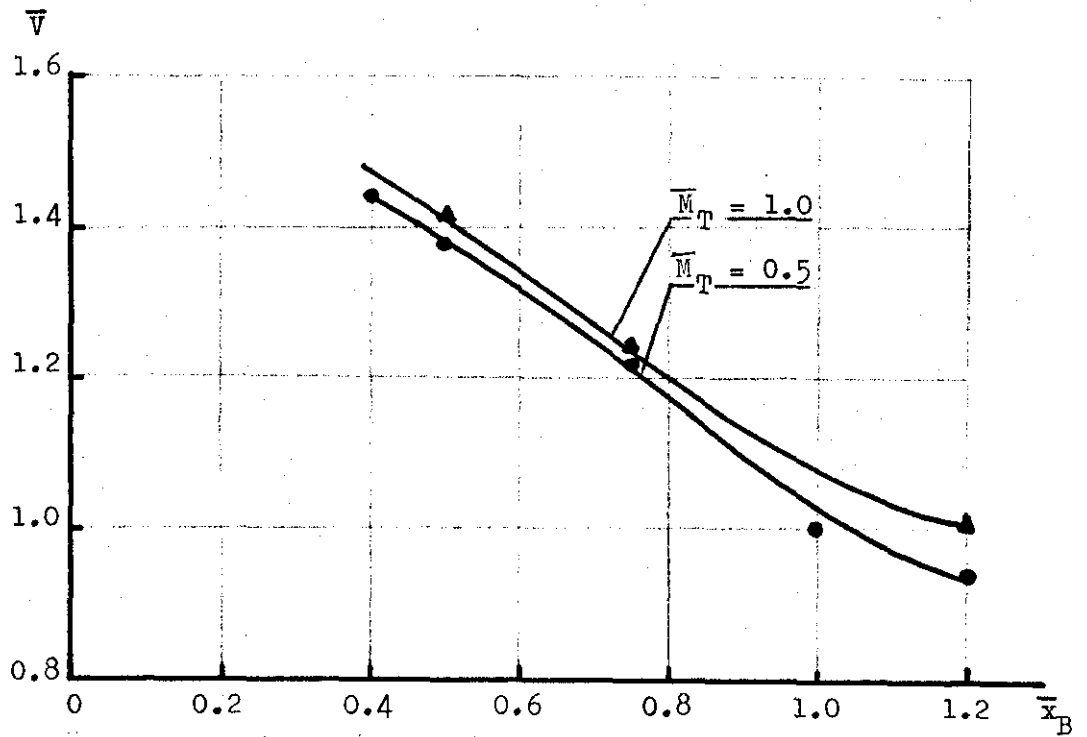

a) Radius of Gyration of tip mass = 0

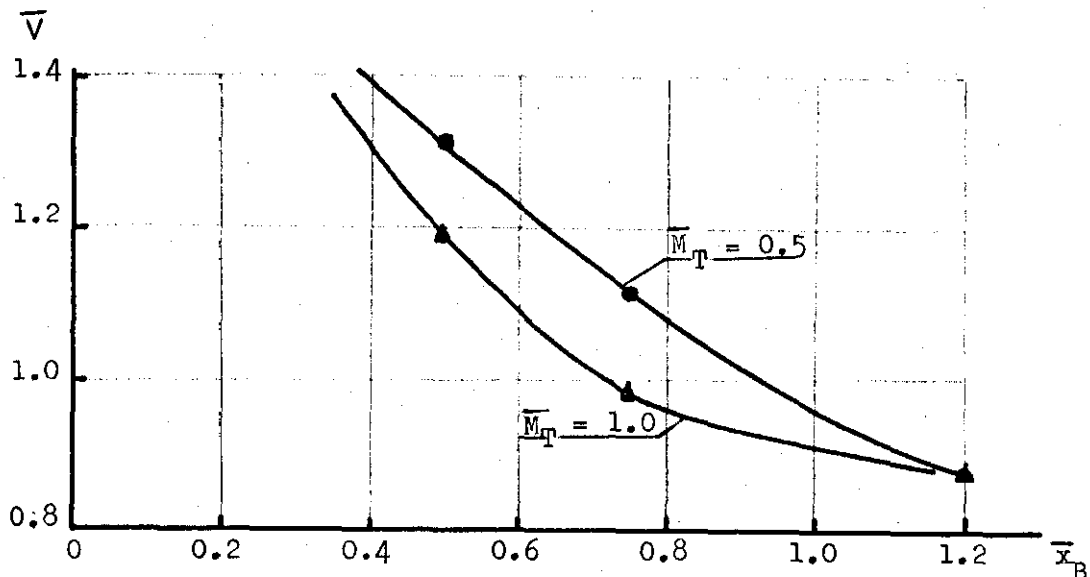

b) Radius of Gyration of tip mass = 1.5 ft.

Note:

$\overline{V}$ = (Body Freedom Flutter Speed)/(Bare Wing Flutter Speed)

$\overline{x}_B$ = C.G. Position ahead of Wing E.A. [Fraction of Wing Chord]

$\overline{M}_T$ = Tip Mass / Bare Wing Mass

FIG. 2.39 Influence of Root Degrees of Freedom: Wing of Ref(8)

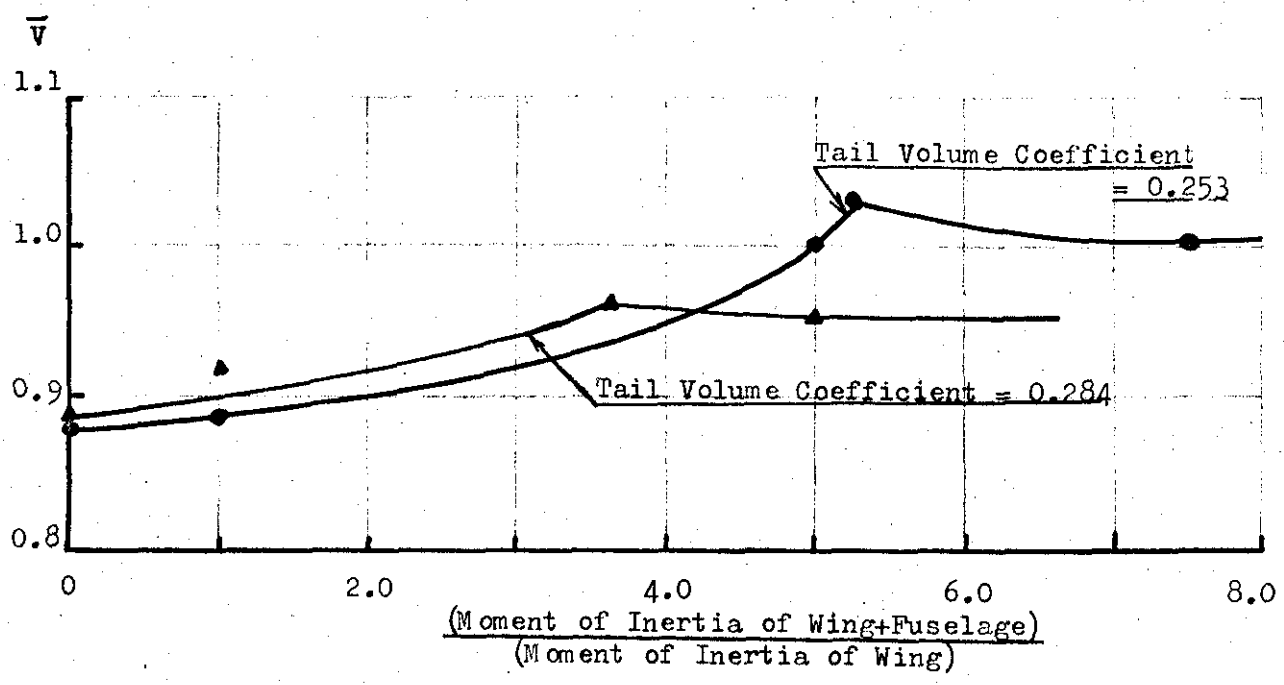

FIG. 2.40 Influence of Root Degrees of Freedom:Wing of Ref(18)

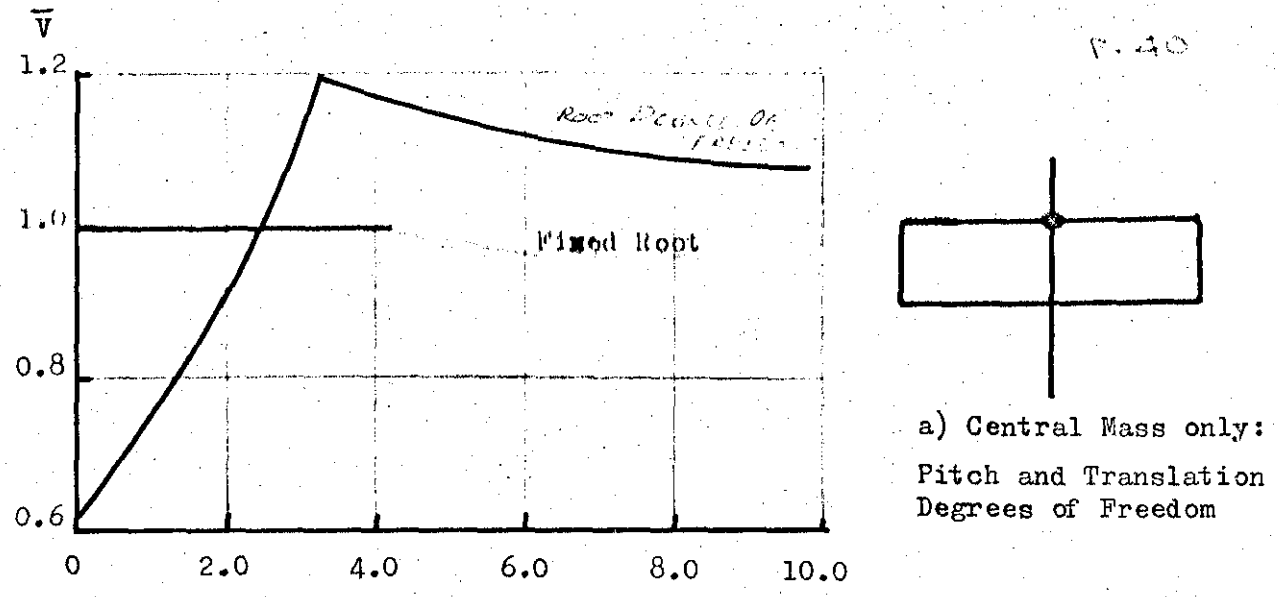

a) Central Mass only: Pitch and Translation Degrees of Freedom

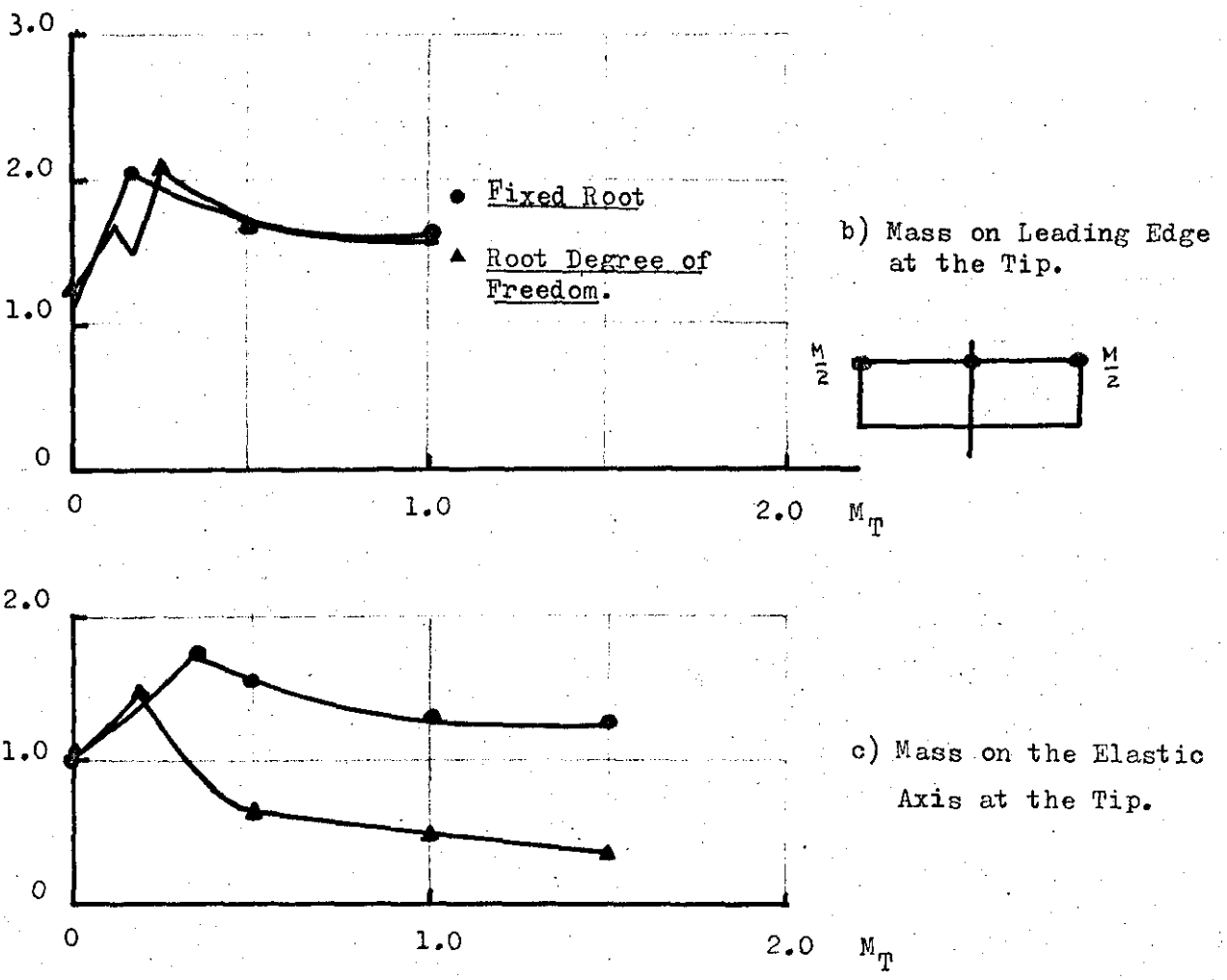

b) Mass on Leading Edge at the Tip.

c) Mass on the Elastic Axis at the Tip.

FIG. 2.41 Influence of the Root Degrees of Freedom: Wing of Ref(5) (Pitch and Translation Degrees of Freedom)

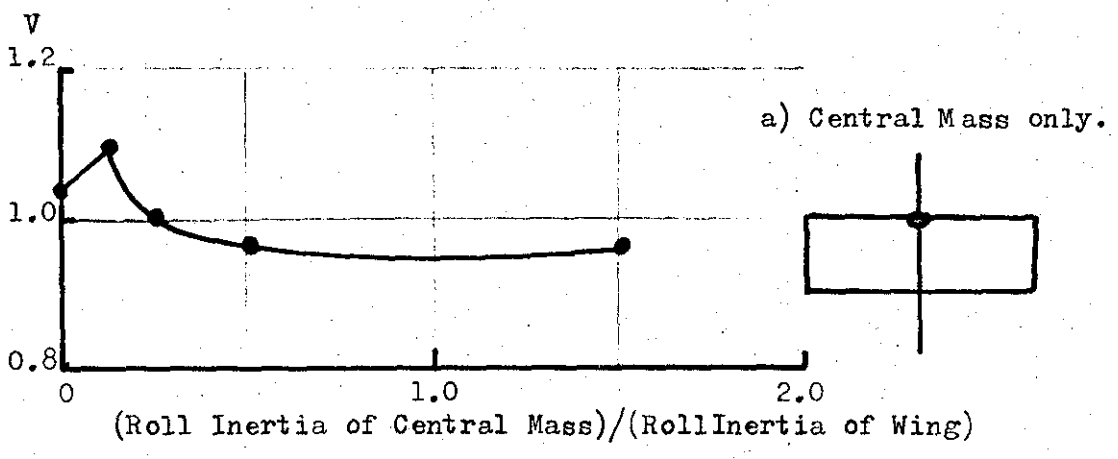

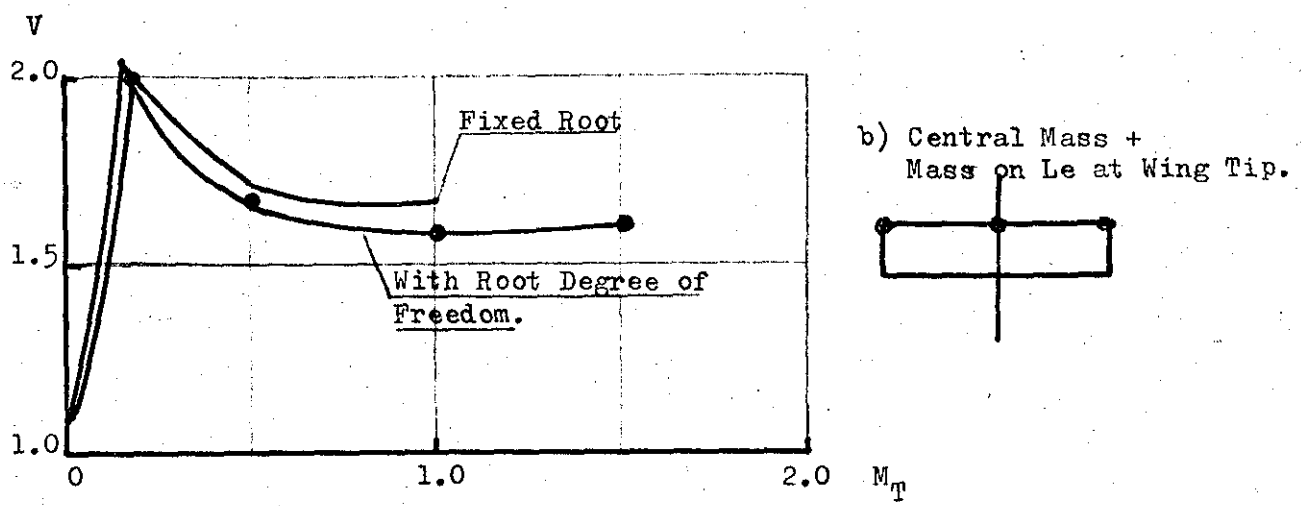

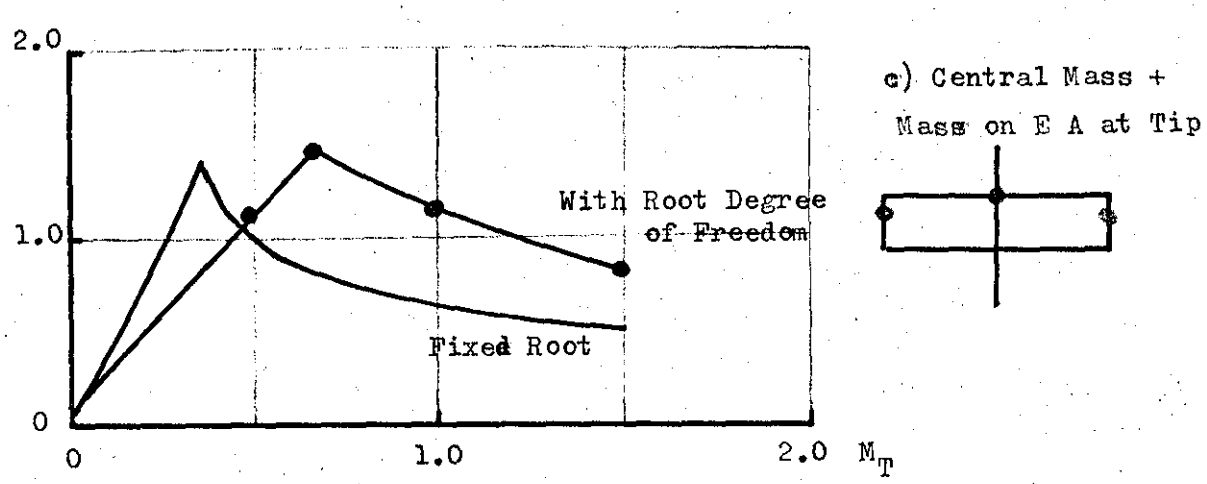

FIG 2.42 Influence of the Root Degrees of Freedom: Wing of Ref(5)

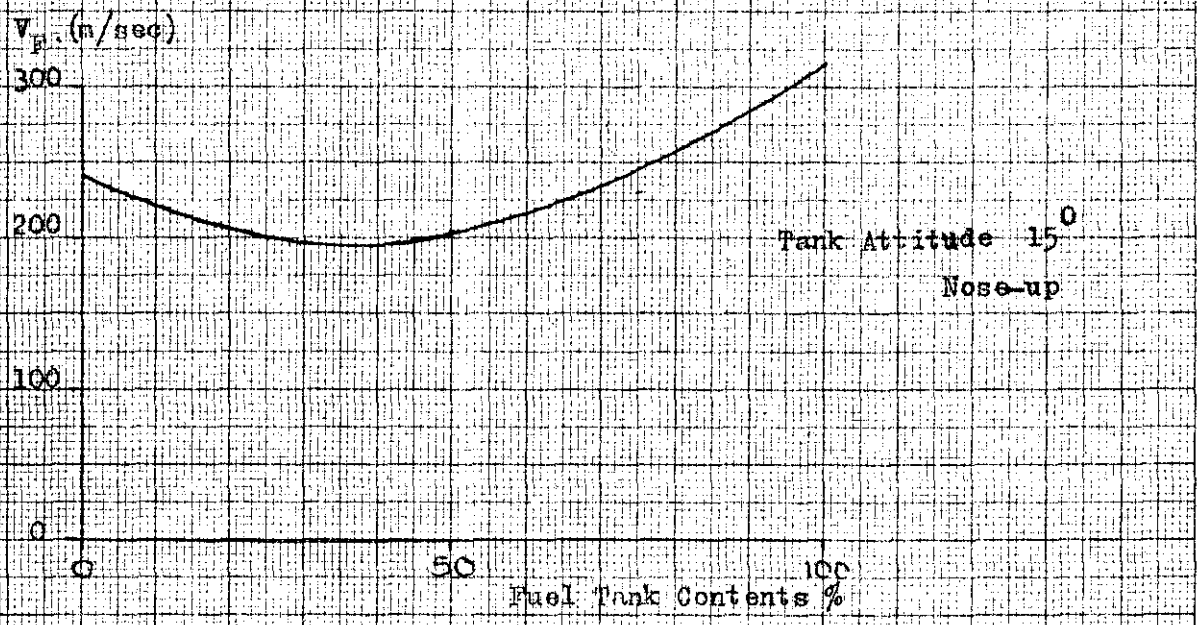

FIG 2.43 Influence of Variable Fuel Wing. of Ref(13)

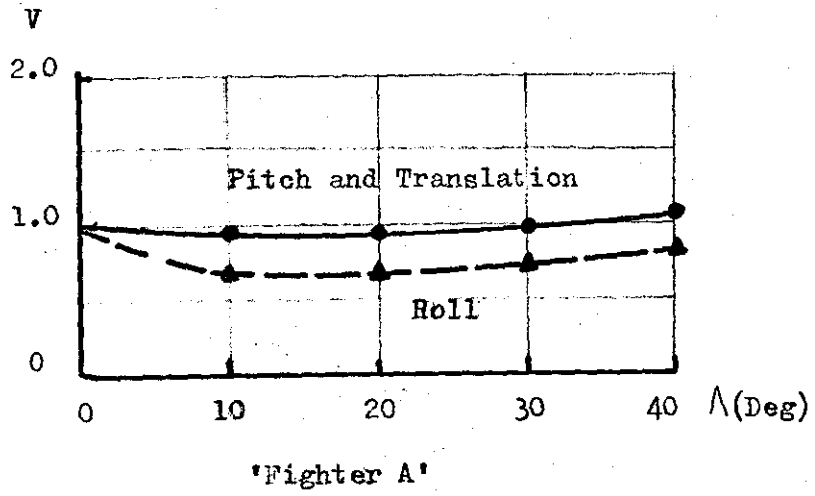

'Fighter A'

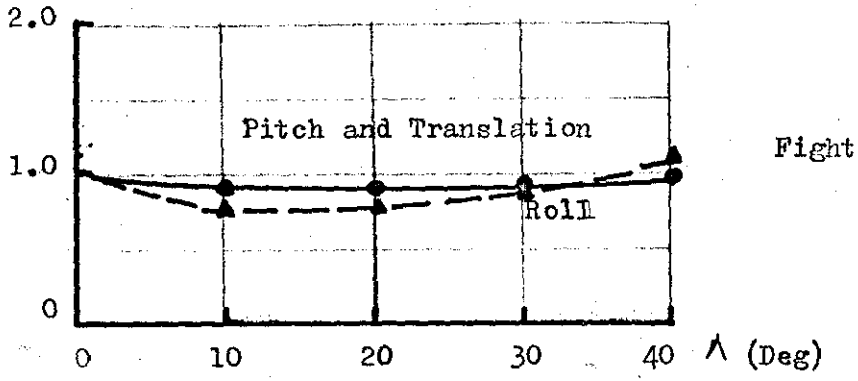

Fighter B

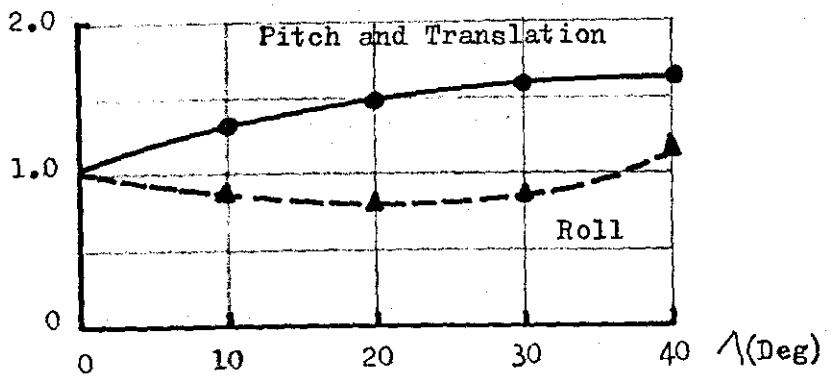

' Bomber A'

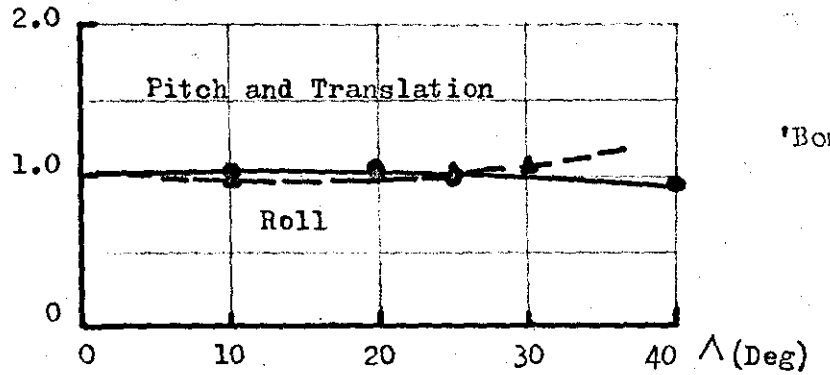

'Bomber B'

FIG. 2.44 Influence of Wing Sweepback: Wing Of Ref(10)

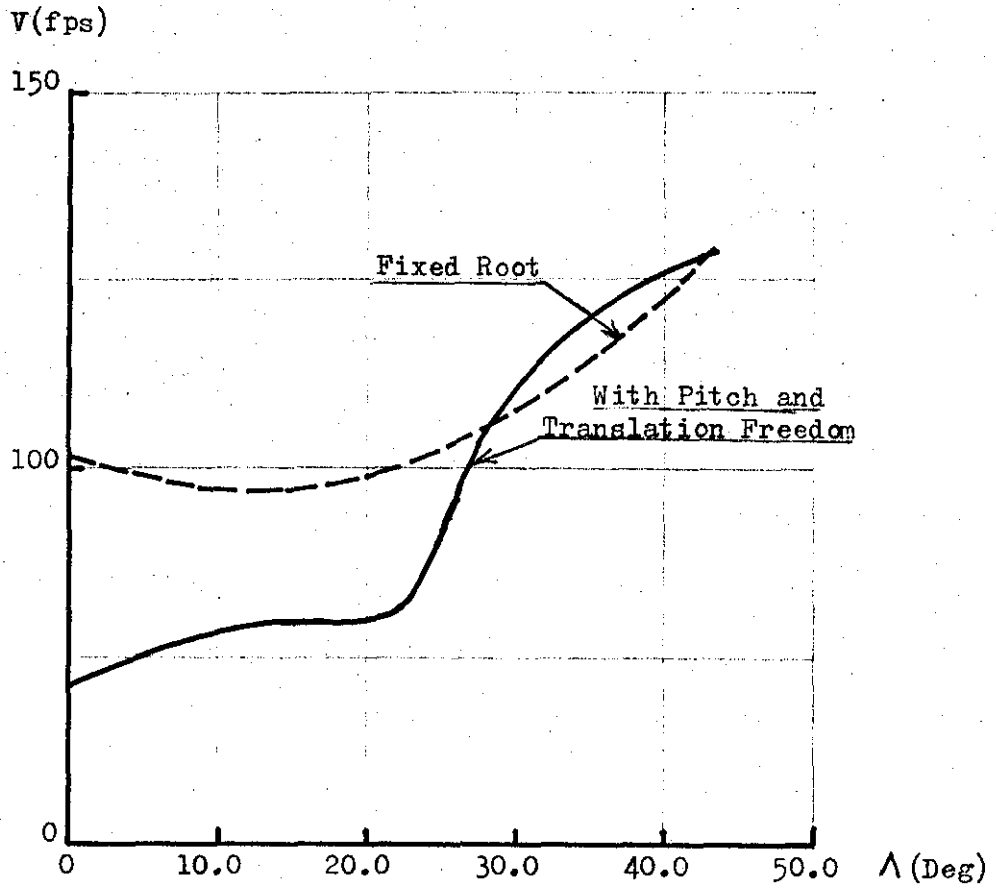

FIG 2.45 Influence of Wing Sweepback : Wing of Ref(18)

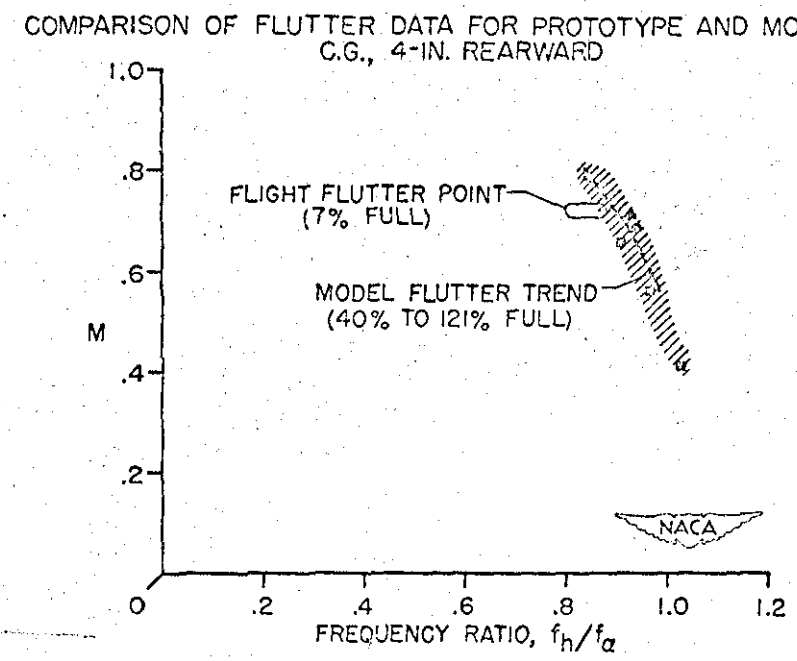

FIG 2.46 A Comparison between Flight and Wind Tunnel Results: (Wing of Ref(14))

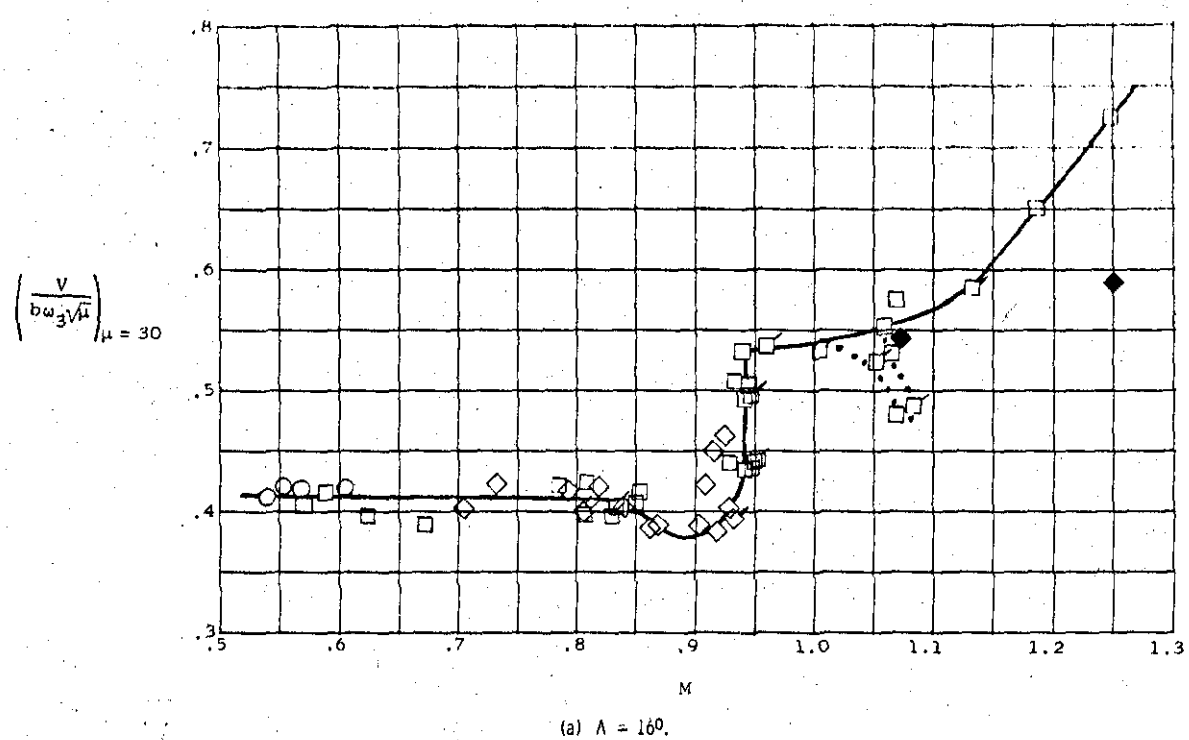

(a) $\Lambda = 16^0$.

FIG 2.47 Influence of Compressibility:Wing of Ref(22)

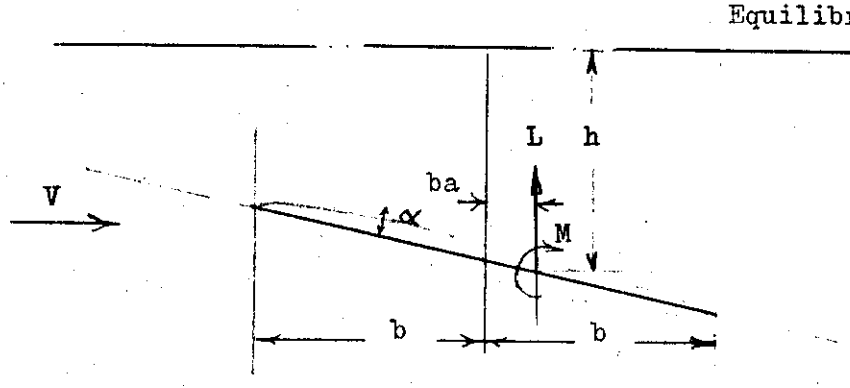

FIG 3.1 Lift and Moment on a Two Dimensional Wing.

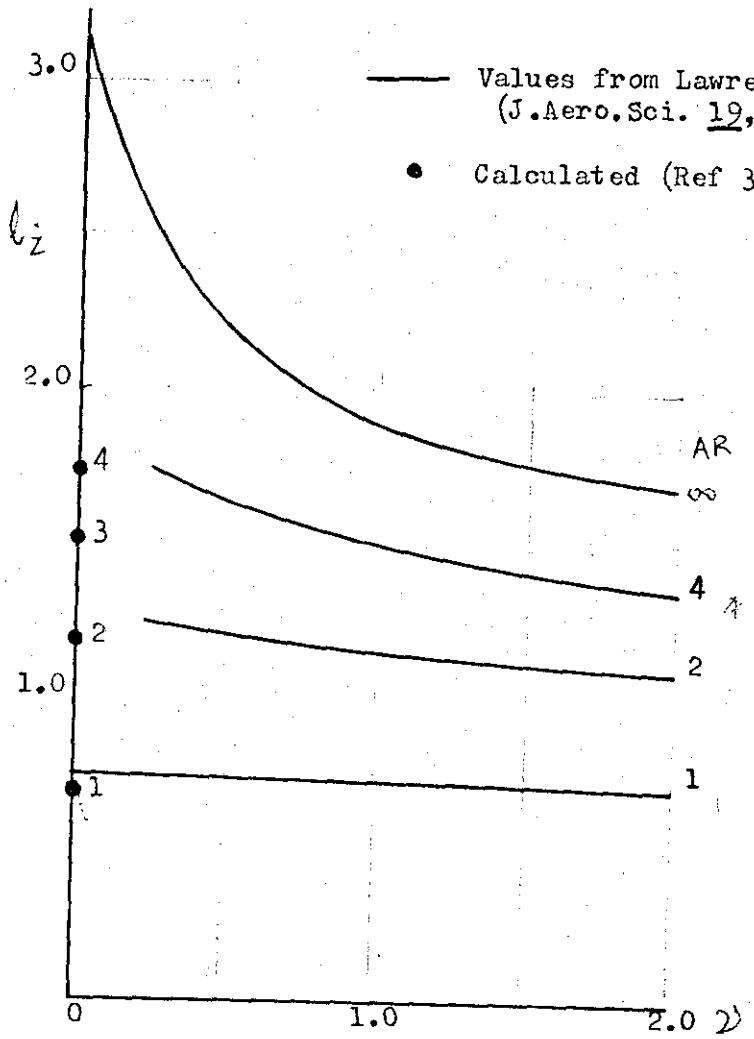

FIG. 3.2 l_i For Rectangular Wings

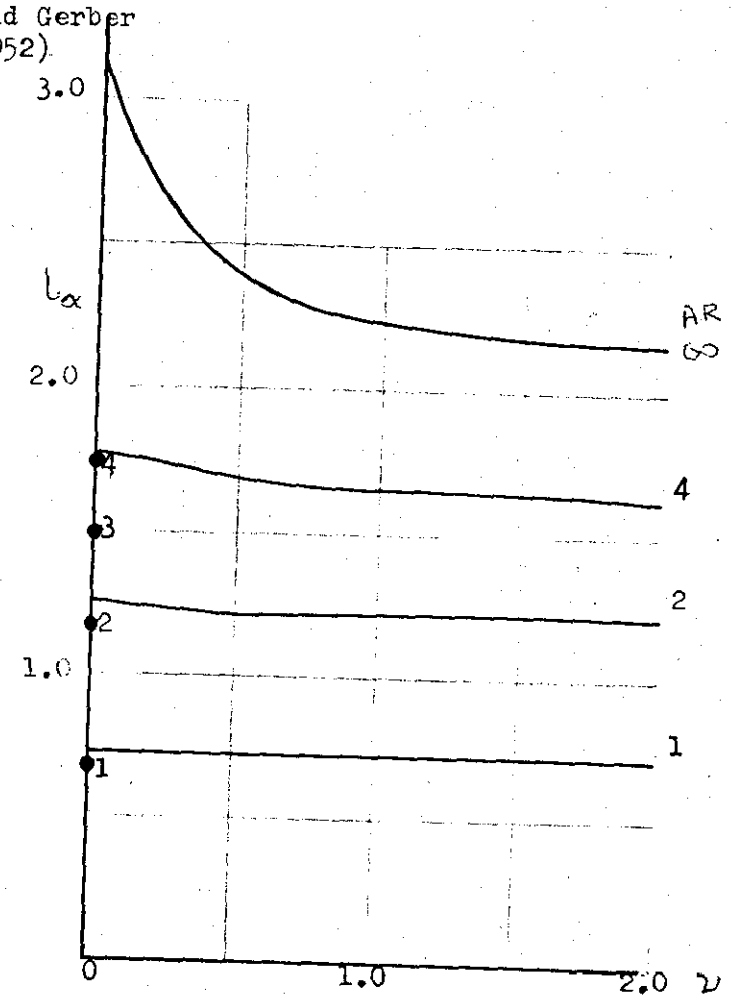

FIG 3.3 l_α For Rectangular wings

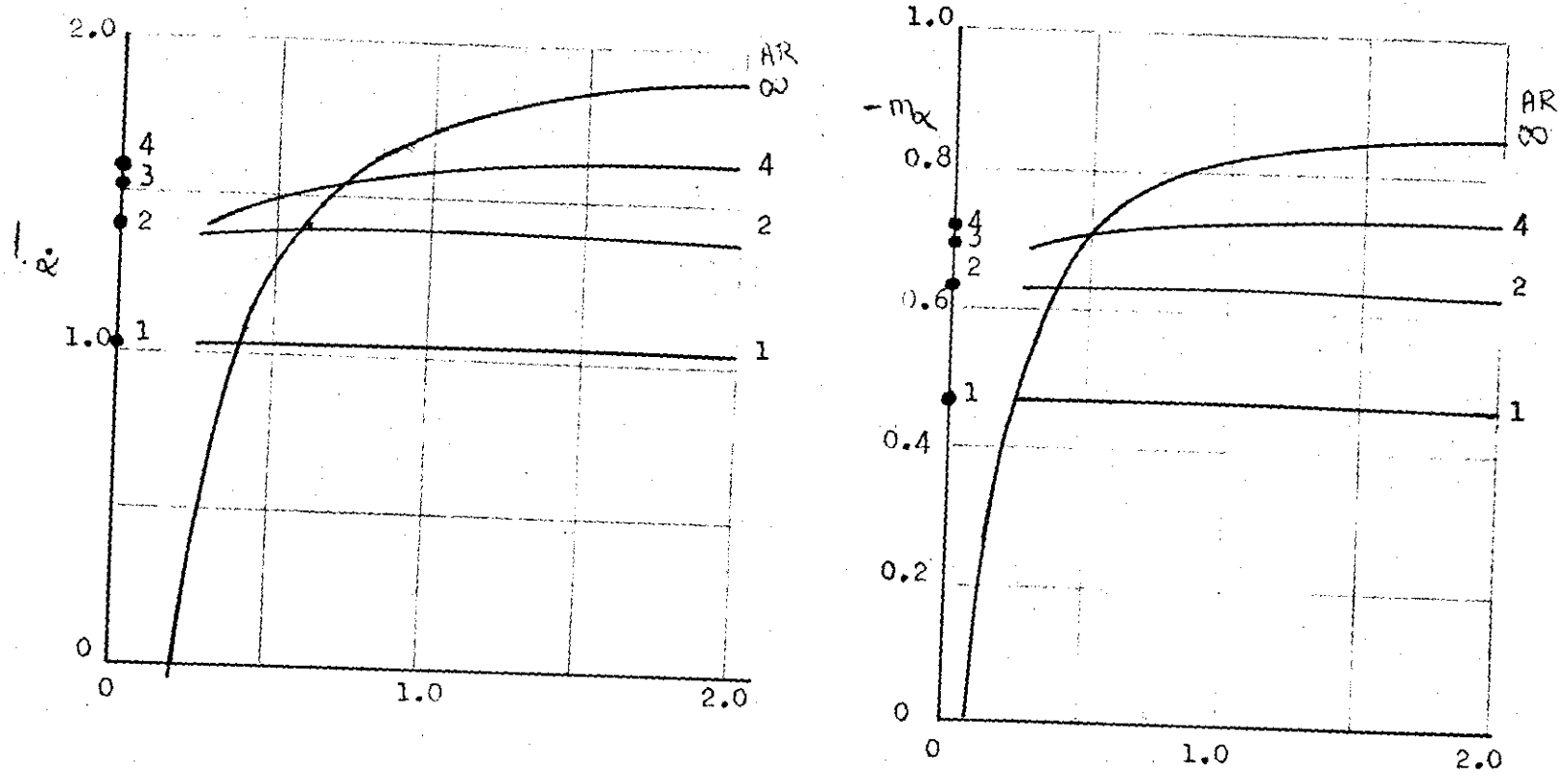

FIG 3.4 Derivatives $l_{\dot{\alpha}}$ and M_{α} for Rectangular Wings

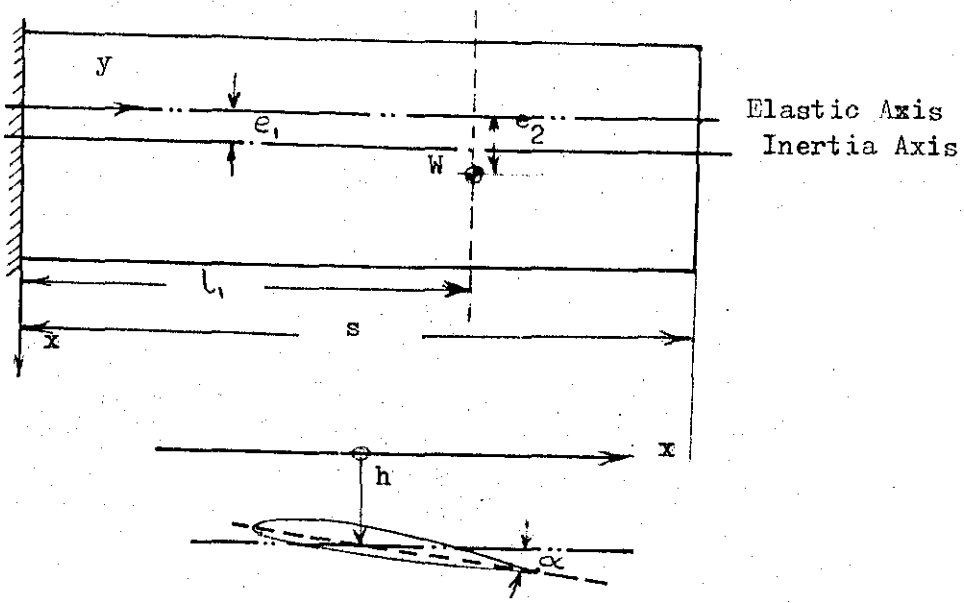

FIG. 4.1 Uniform Wing with Concentrated Mass

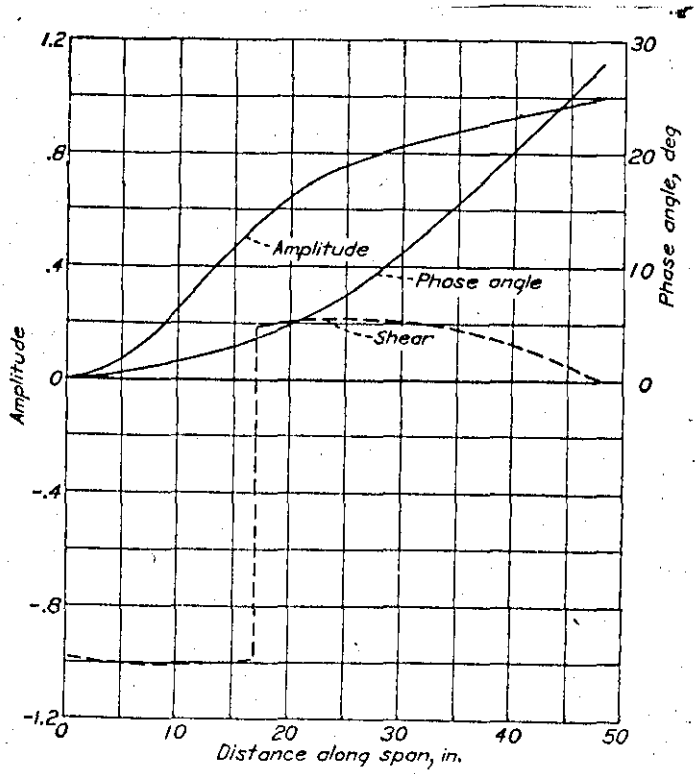

-Plot of amplitude and phase angle of displacement and shear curve for bending at flutter for l_1=17 inches (amplitude and shear referred to unit amplitude at tip in bending):

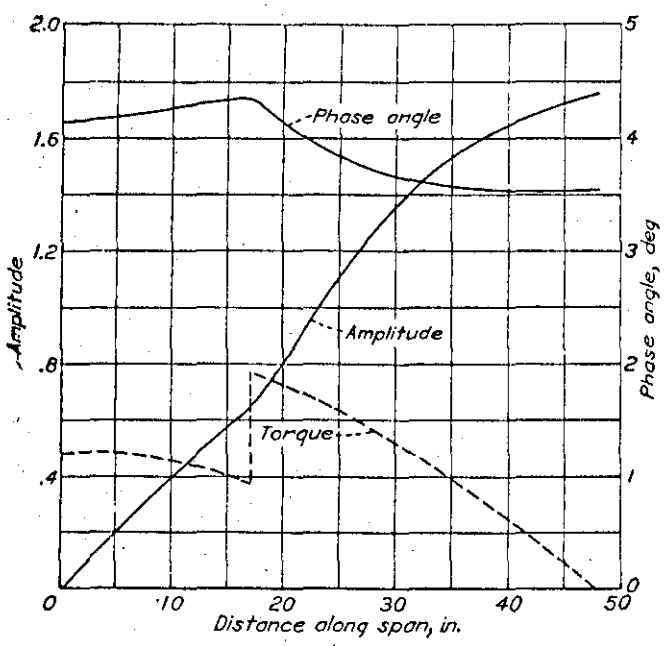

Plot of amplitude and phase angle of torsional displacement and torque for l_1=17 inches at flutter (amplitude and torque referred to unit amplitude at tip in bending).

FIG 4.2 Mode Shapes at Flutter: Wing of Ref(37)

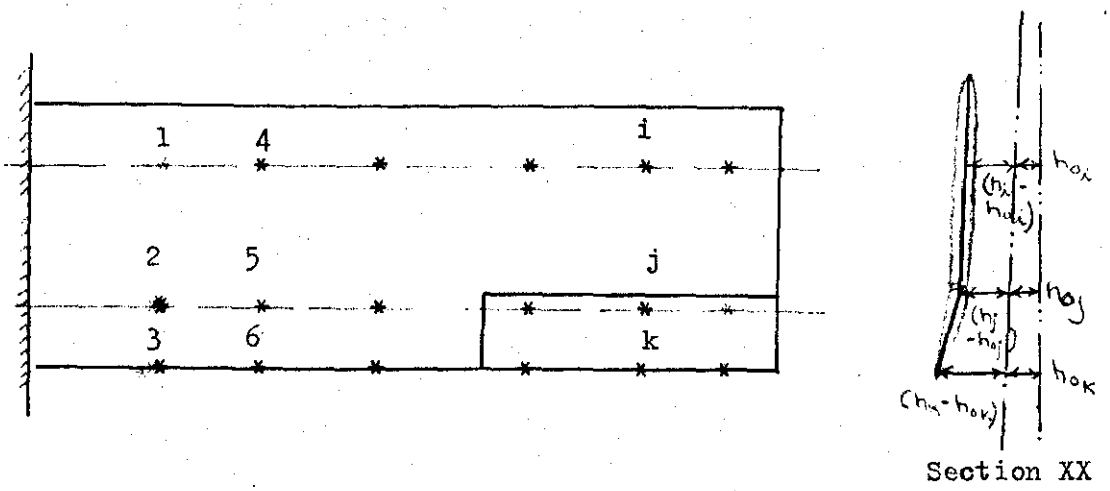

FIG. 5.1 Configuration for Direct Matrix Analysis.

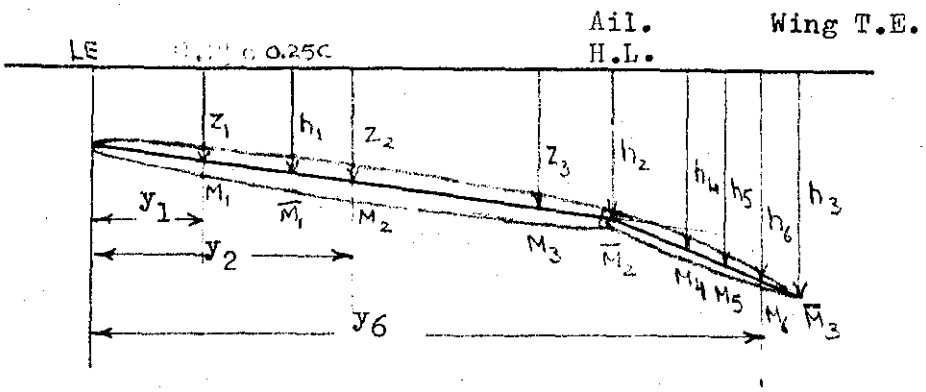

FIG. 5.2 Configuration for Mass Matrix.

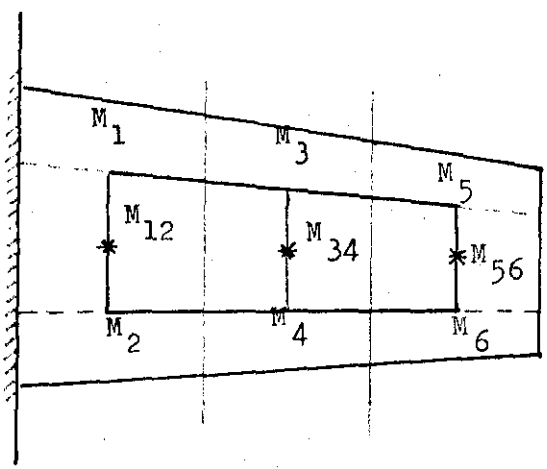

FIG. 5.3 Configuration for Mass Matrix (Example)

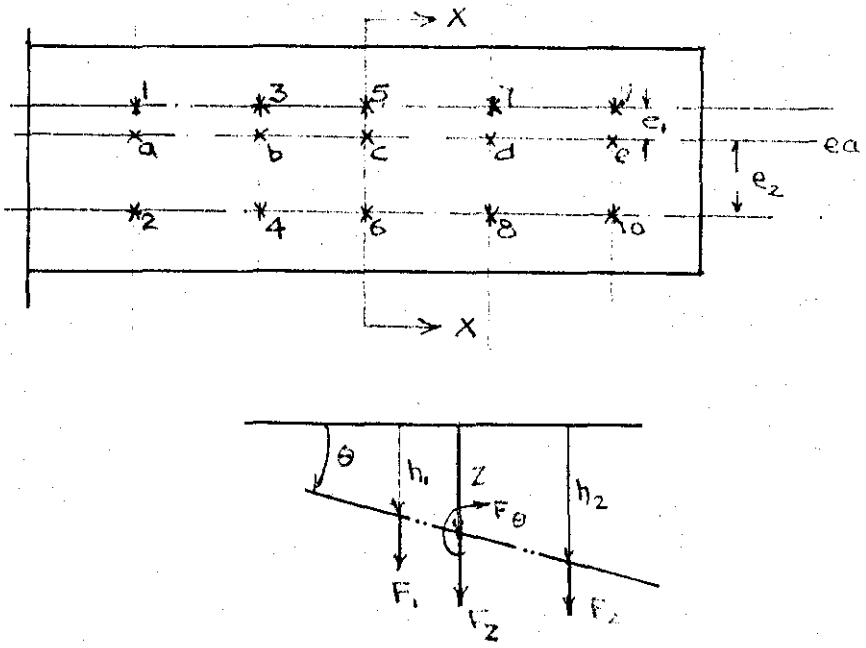

FIG. 5.4 Configuration for SIC Matrix

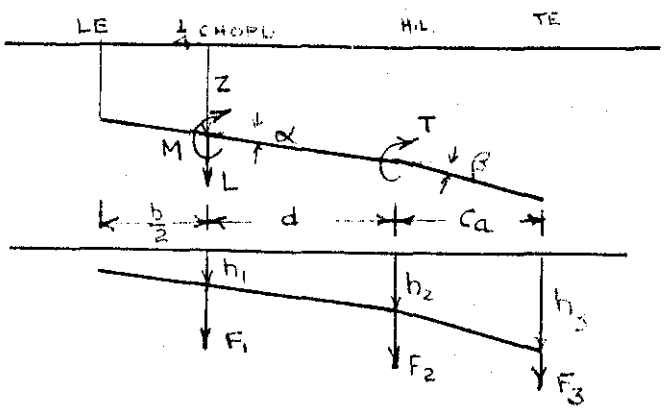

FIG. 5.5 Equivalent System for Aerodynamic Loads

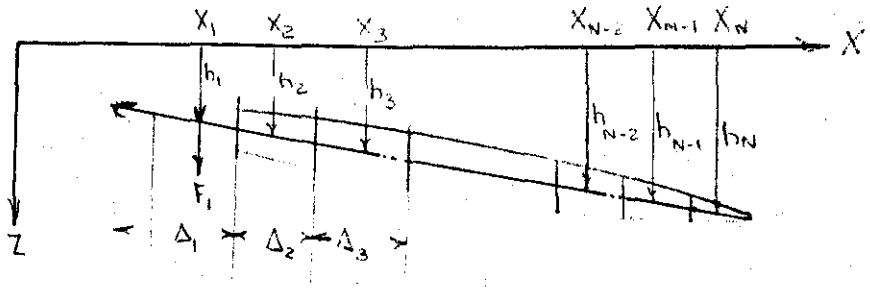

FIG. 5.6 Aerodynamic Loading on an Oscillating Body

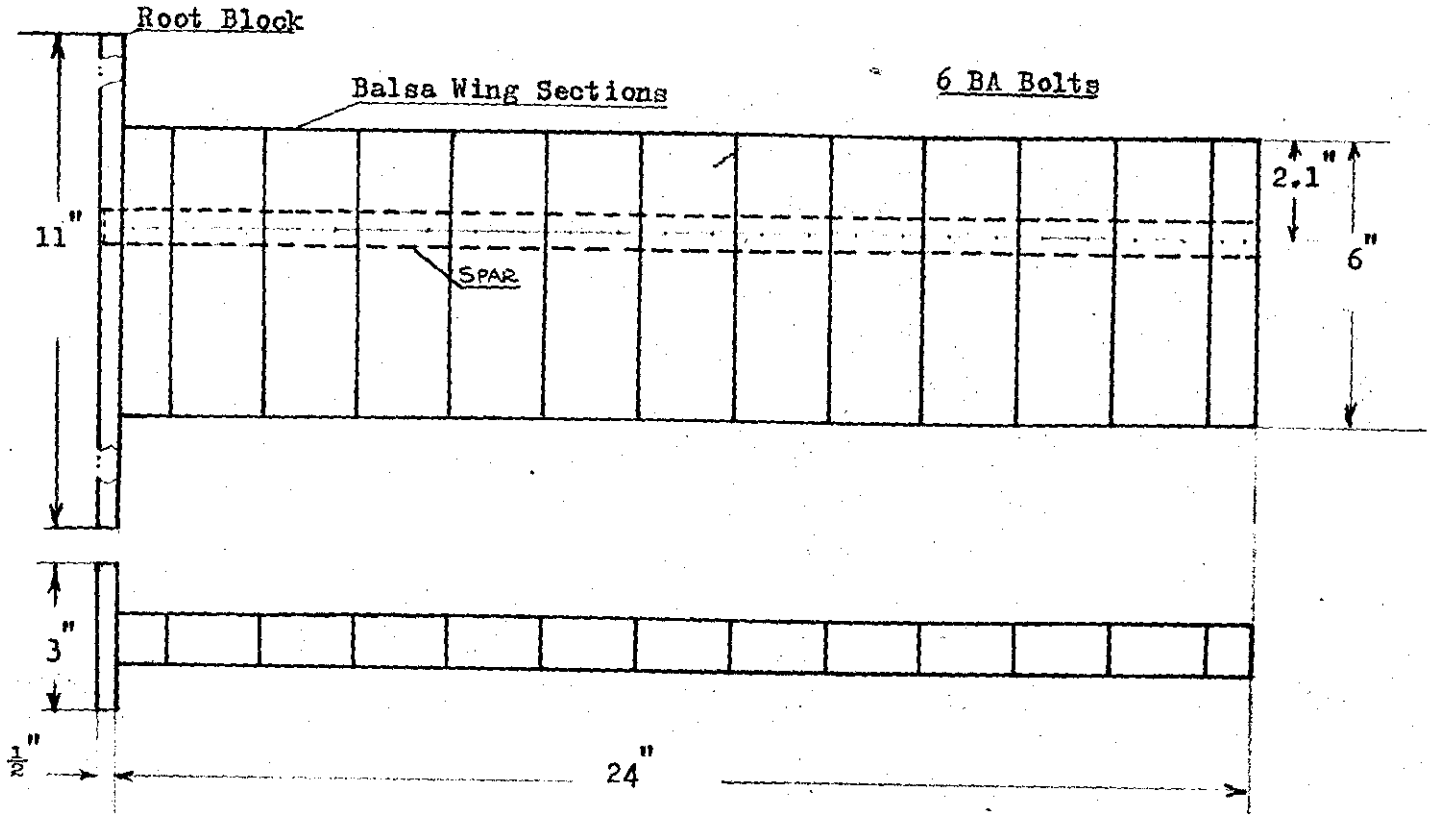

Notes:

a) Wing Profile NACA 0018

b) Spar Cross Section: Channel Section (Aluminium)

Wing A1 0.72in x 0.3in x 0.0625in

Wings A2 and A3 0.75in x 0.292in x 0.125in

c) There is a 1/16in. gap between the adjacent wing sections

FIG 6.1 Model Wing Used in the Wind Tunnel Tests.

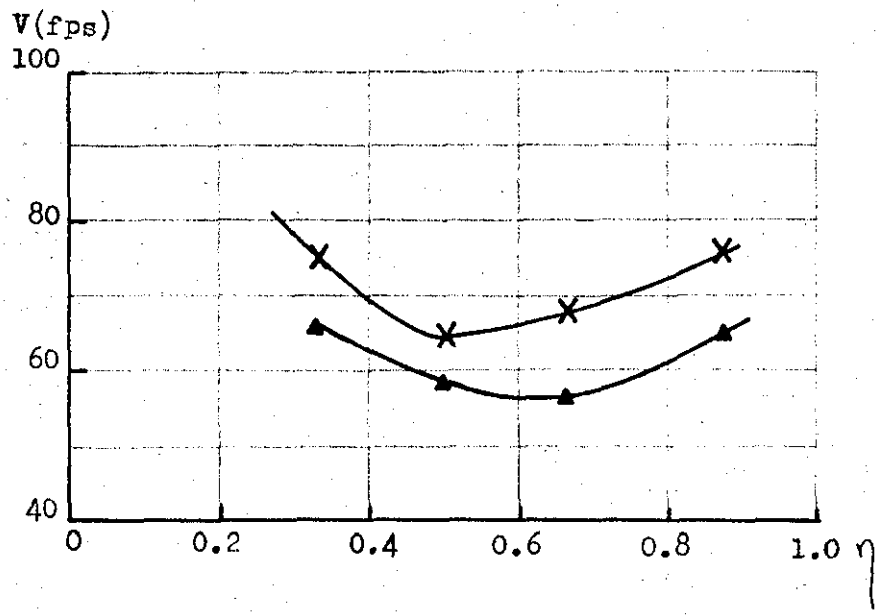

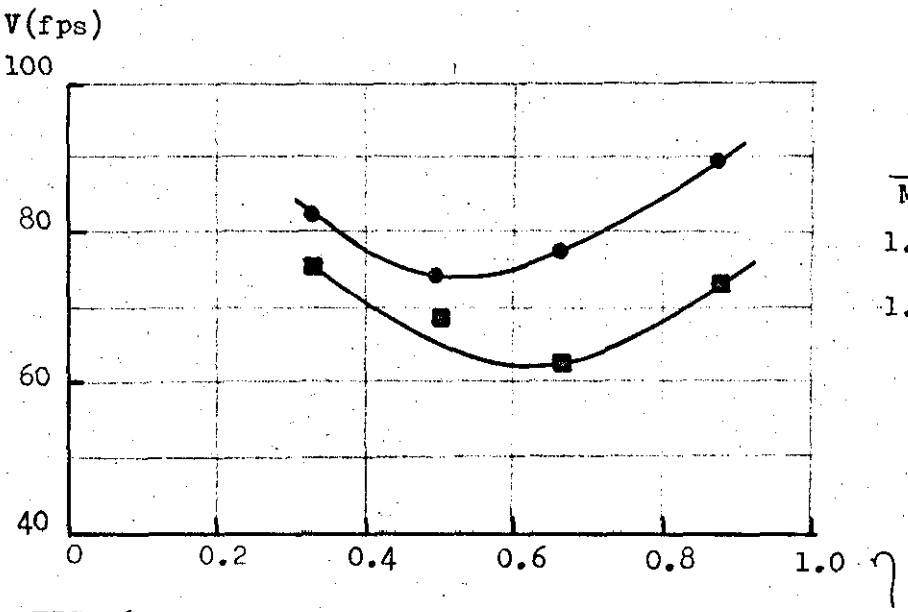

FIG. 6.2 Results of Assumed Mode Analysis: Wing A2

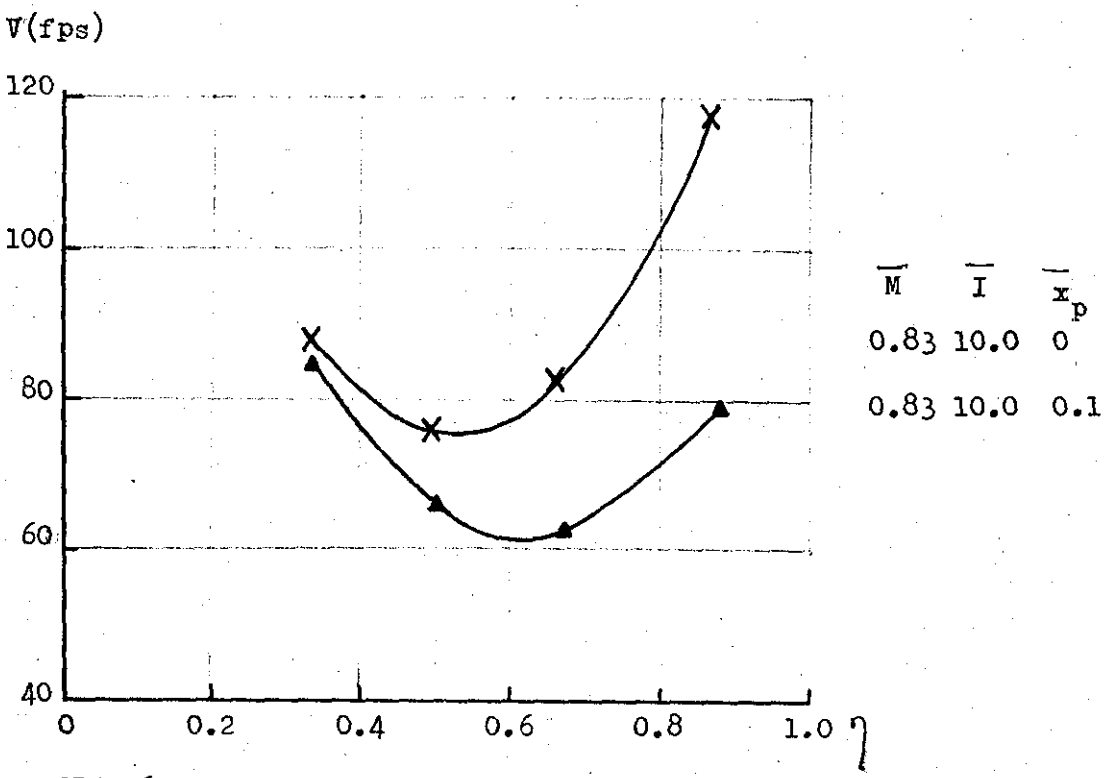

FIG. 6.3 Results of Assumed Mode Analyses: Wing A3

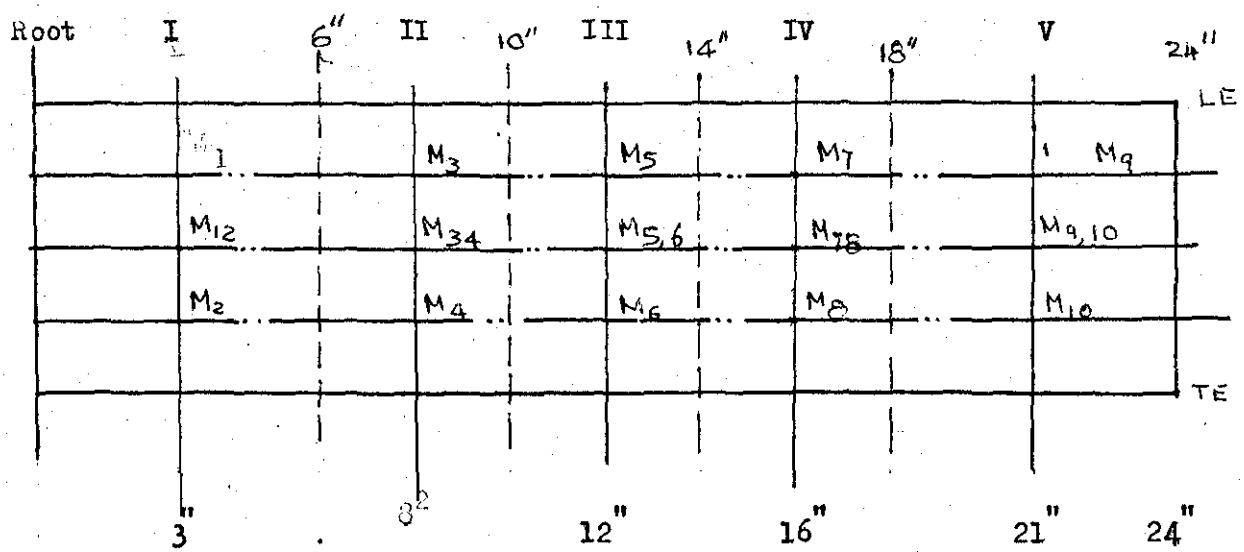

Panel Number (i)	Mass (lb)	Moment of Inertia ($lb\text{-}in^2$)	M_i	M_{ij}	M_j
I	0.193	0.475	0.1244	-.0054	0.0847
II	0.132	0.316	0.0829	-.0036	0.0565
III	0.132	0.316	0.0829	-.0036	0.0565
IV	0.132	0.316	0.0829	-.0036	0.0565
V	0.193	0.475	0.1244	-.0054	0.0847

FIG. 6.4 Location of Control Points for Direct Matrix Analysis

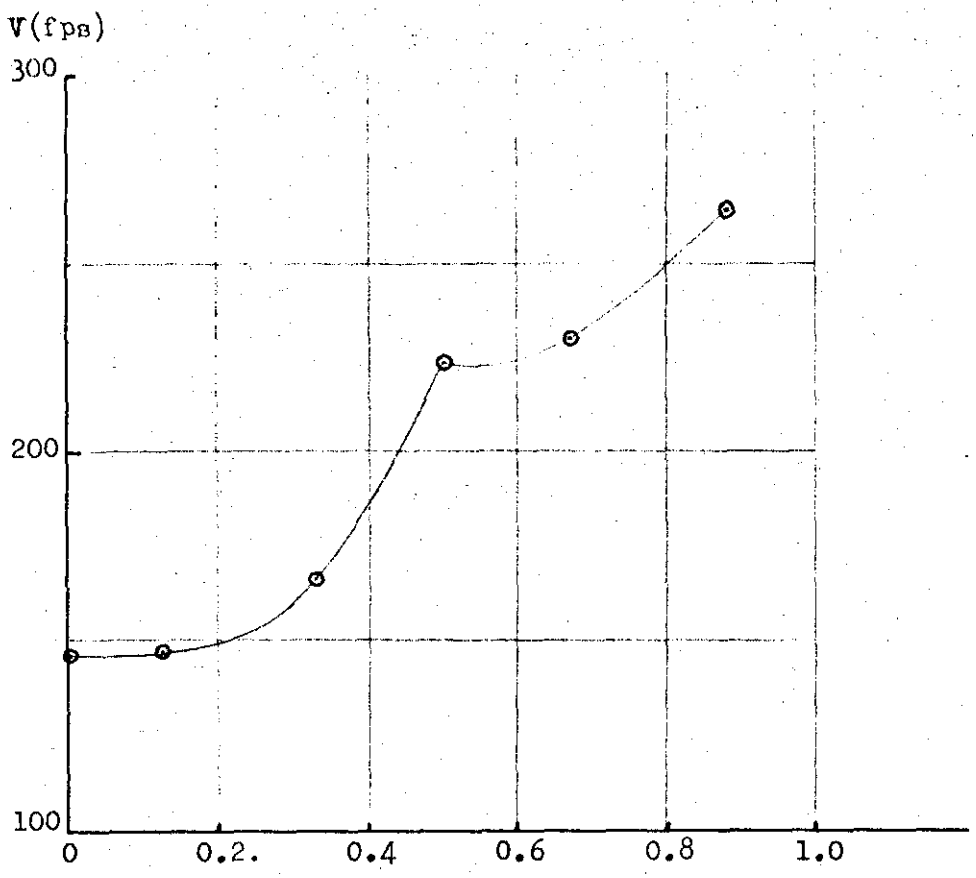

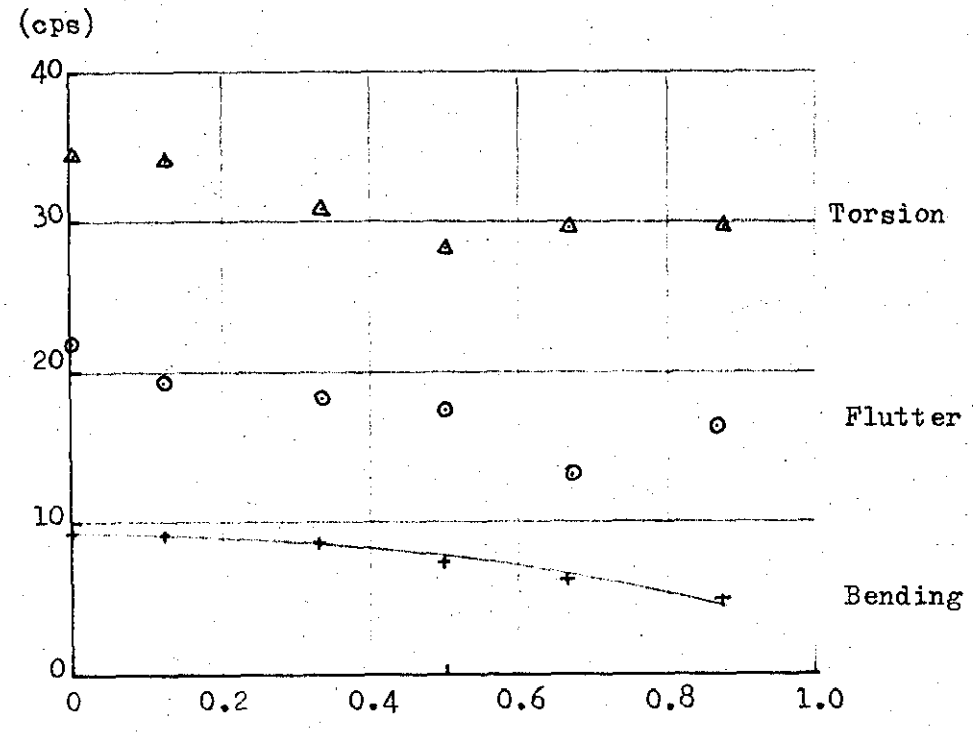

FIG. 6.5 DMM Results for Wing A2 $\overline{M}$ = 1.0, $\overline{I}$ = 0, $\overline{x}_p$ = -0.1

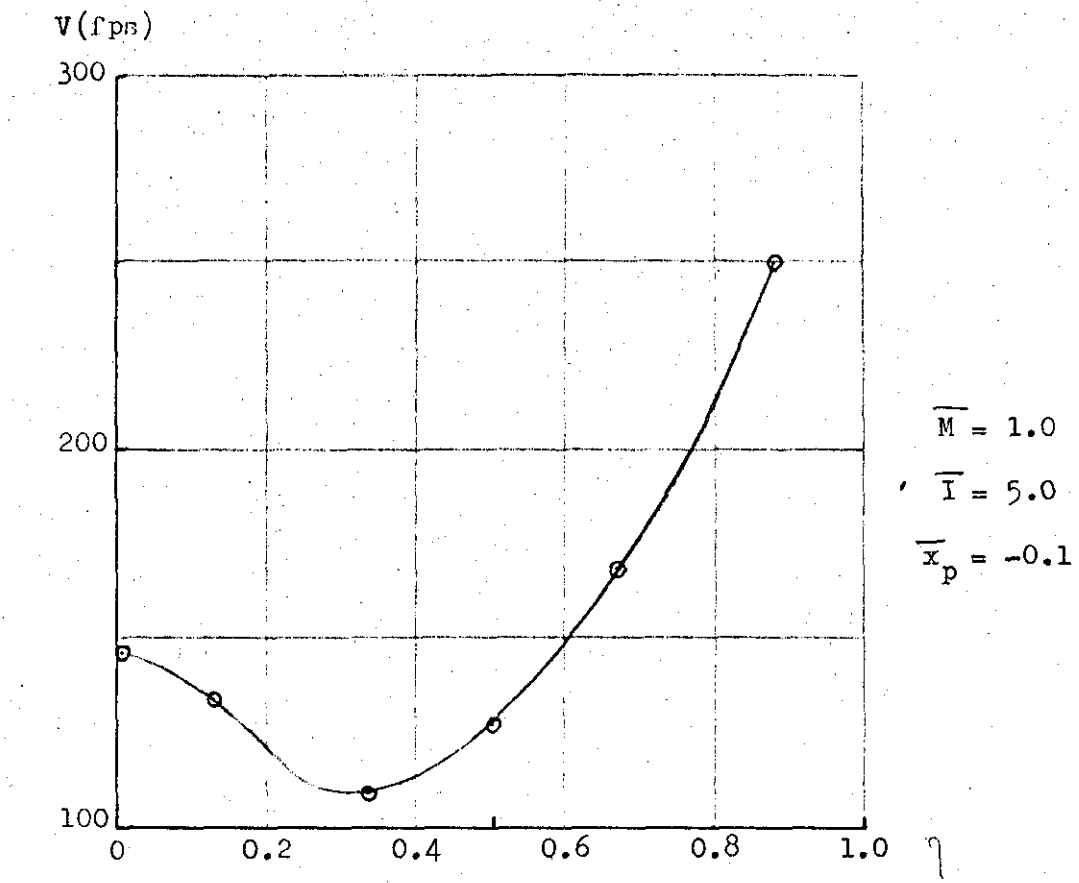

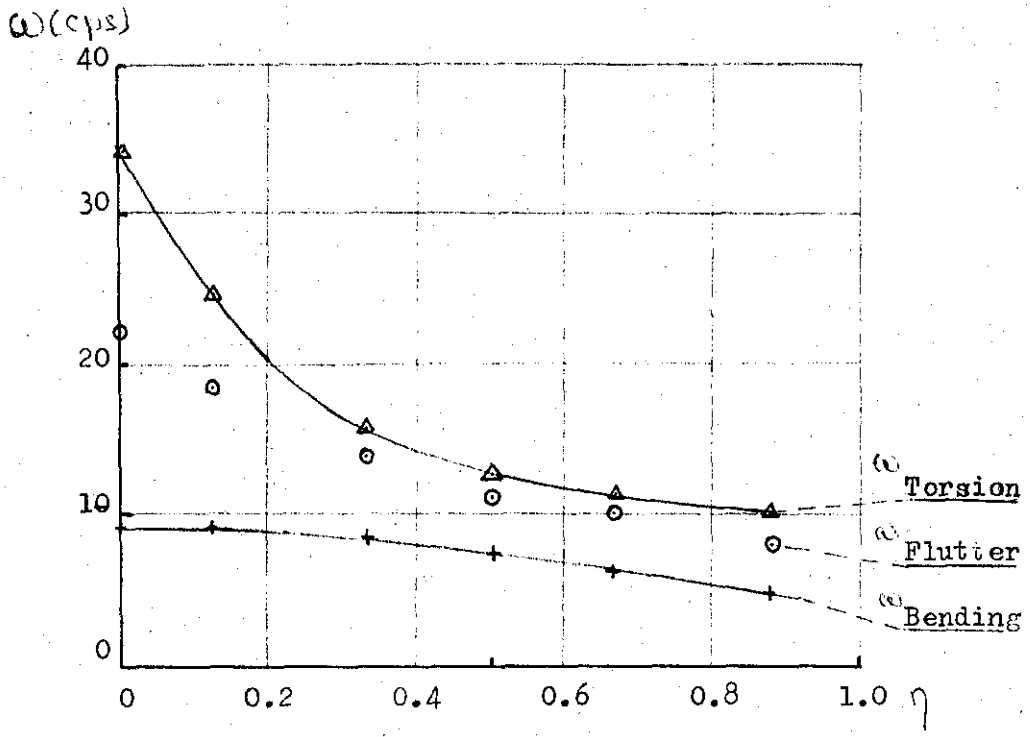

FIG. 6.6 Results of Direct Matrix Analysis:Wing A2

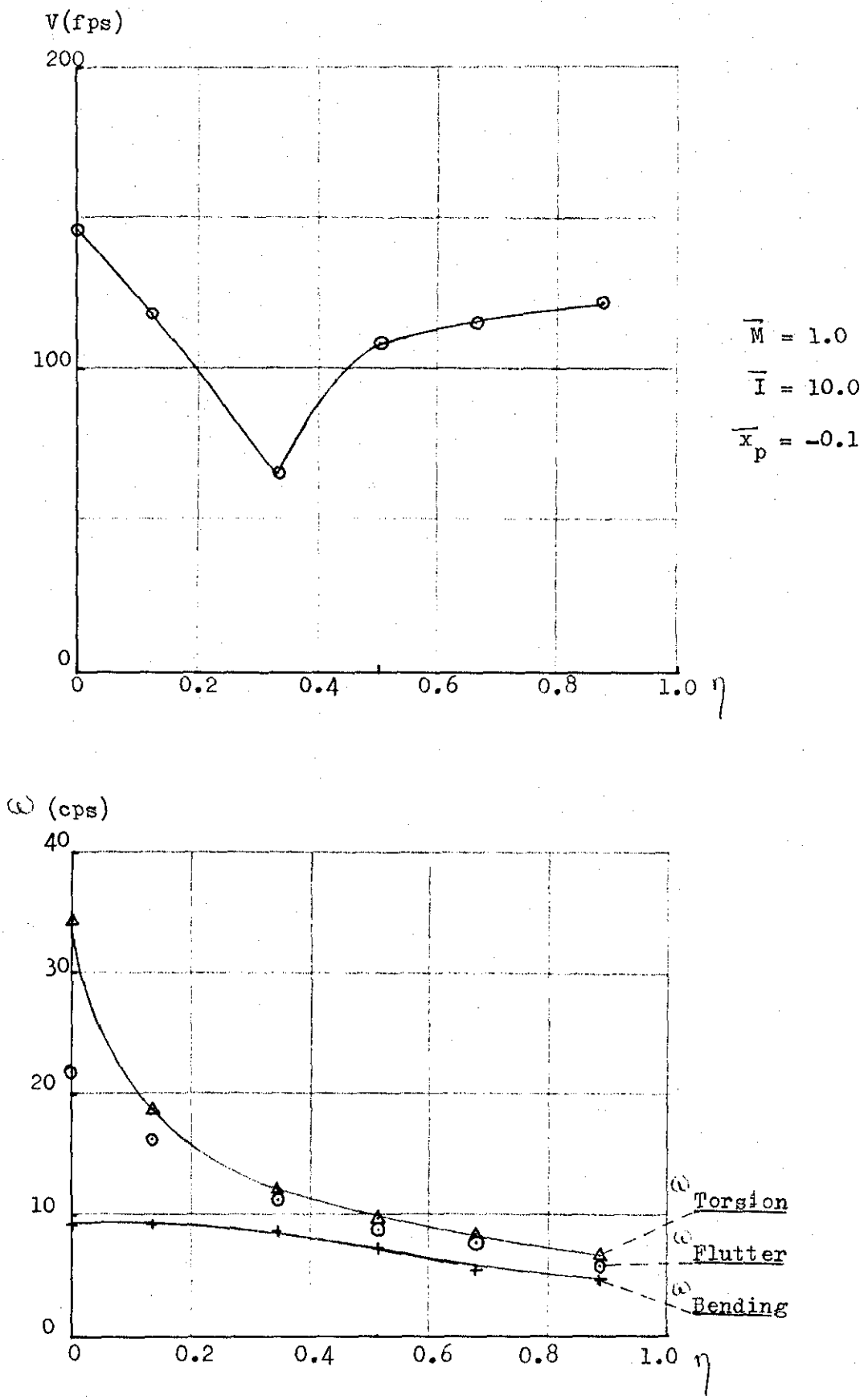

FIG 6.7 Results of Direct Matrix Analysis: Wing A2

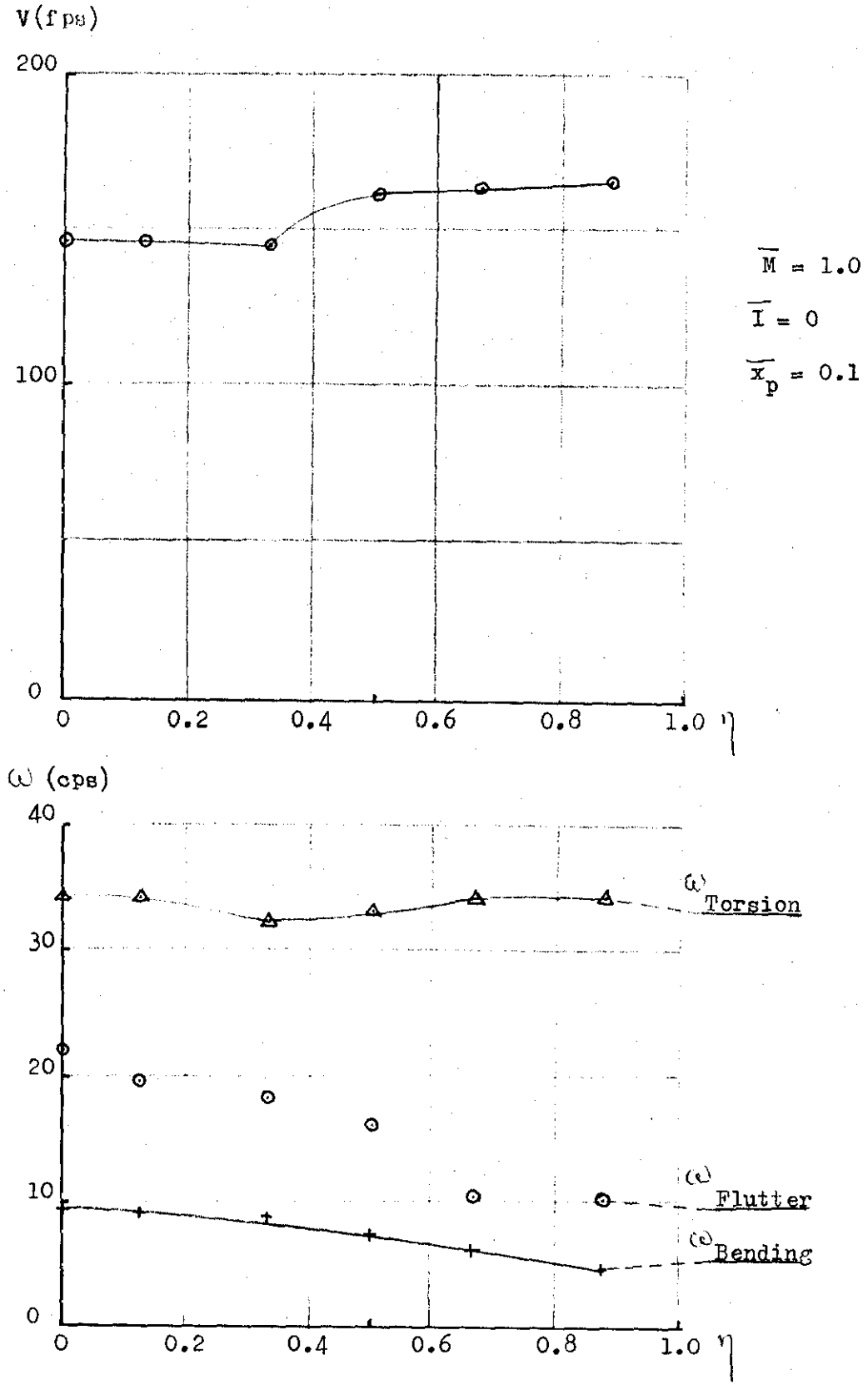

FIG 6.8 Results of Direct Matrix Analysis: Wing A2

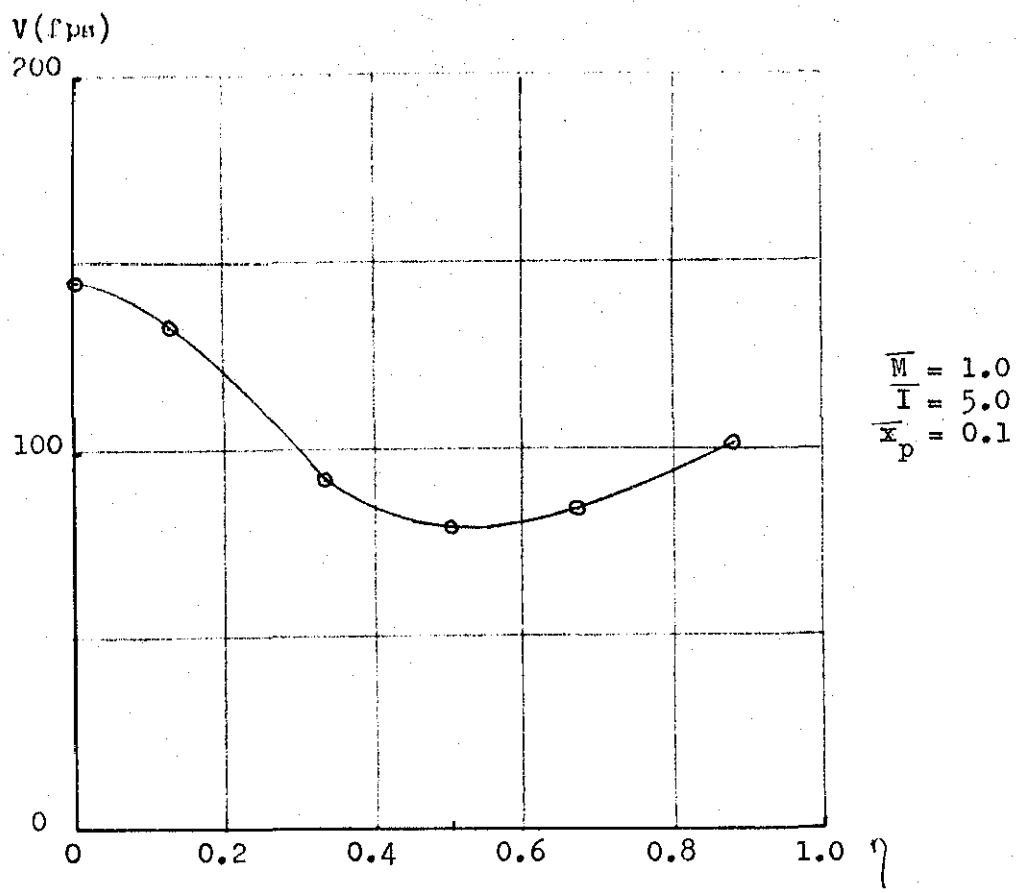

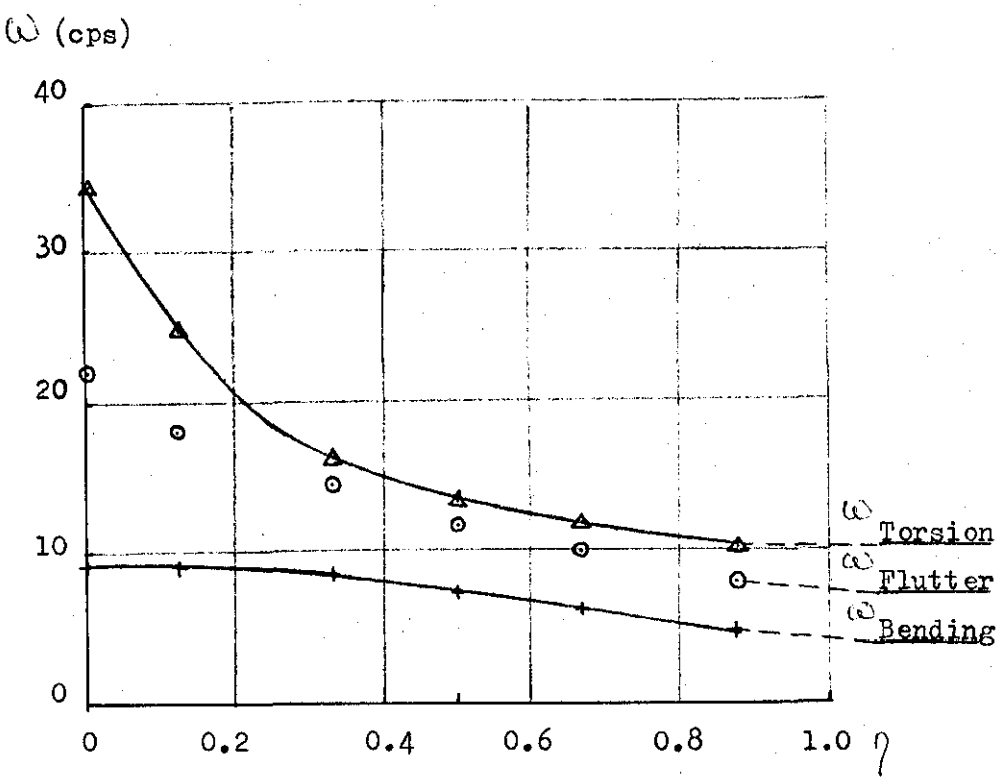

FIG. 6.9 Results of Direct Matrix Analysis: Wing A2

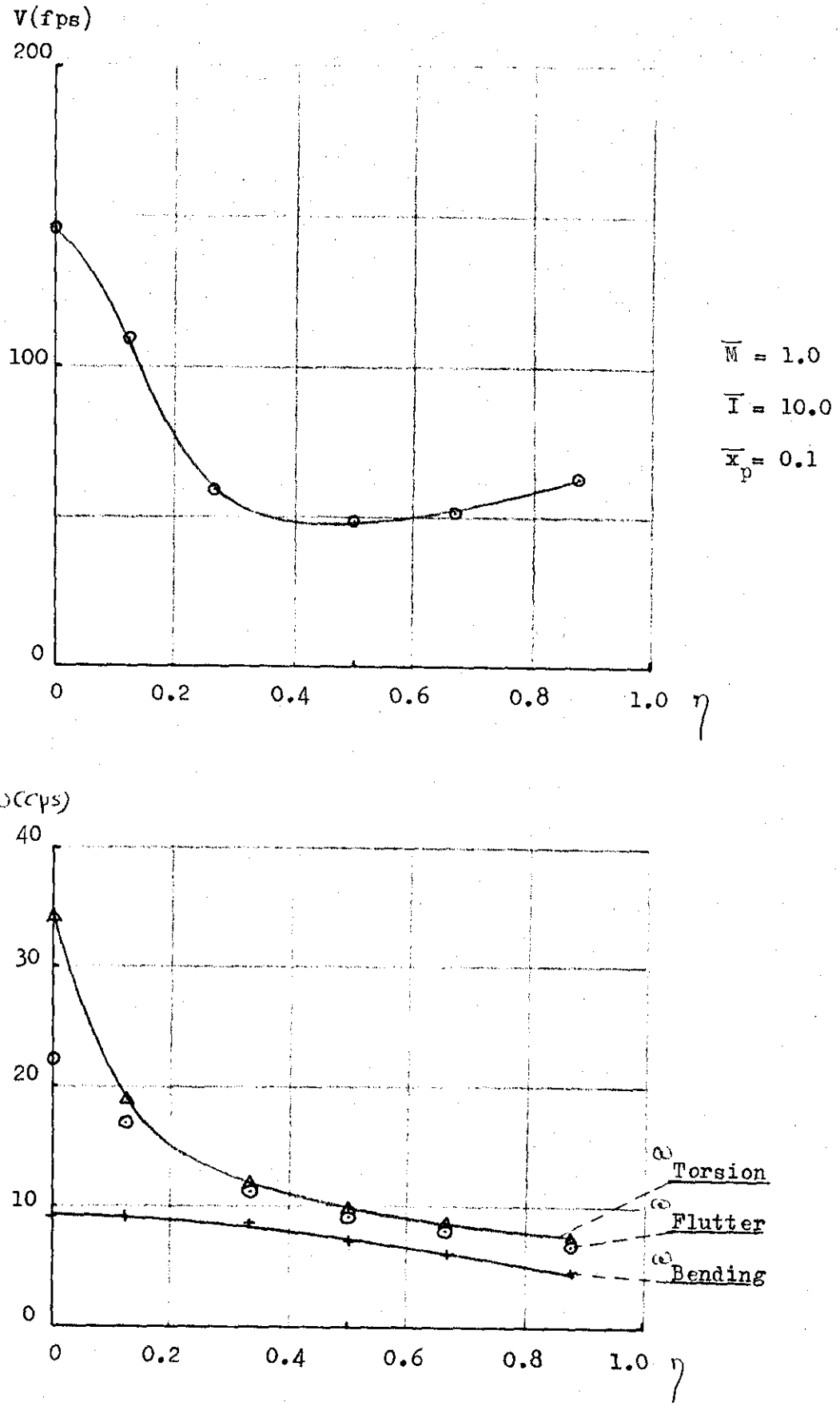

FIG. 6.10 Results of Direct Matrix Analysis: Wing A2

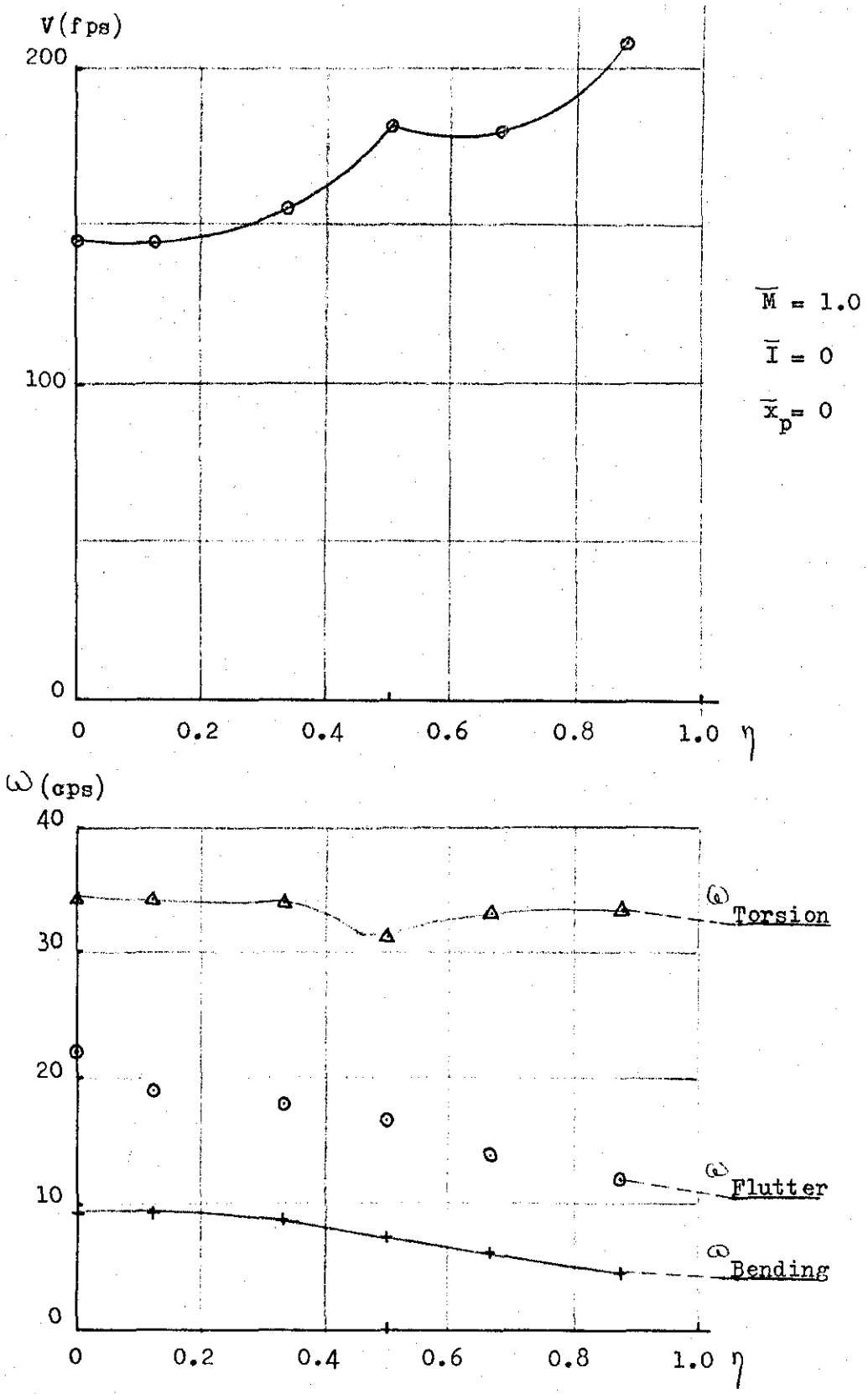

FIG. 6.11 Results of Direct Matrix Analysis: Wing A2

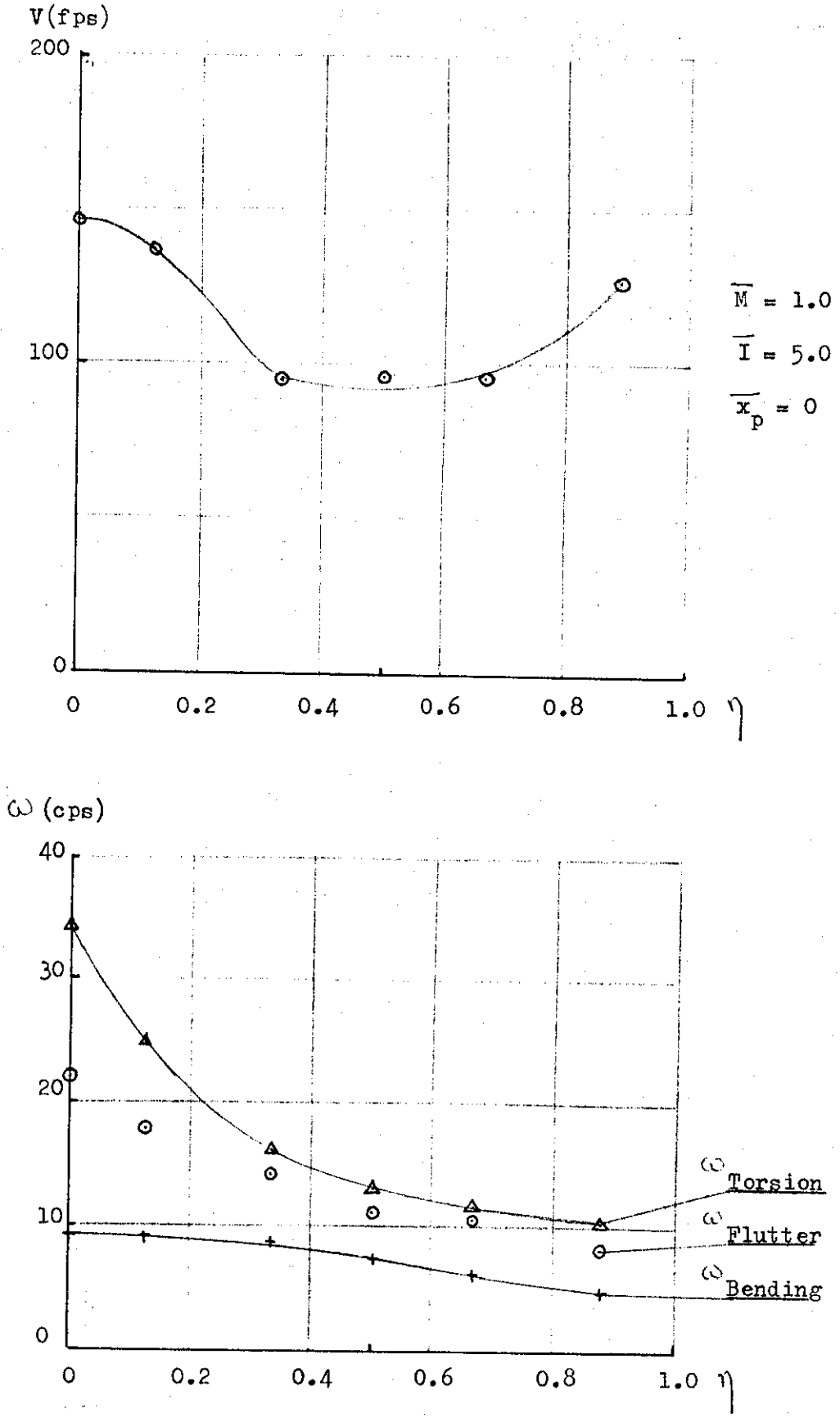

FIG. 6.12 Results of Direct Matrix Method: Wing A2

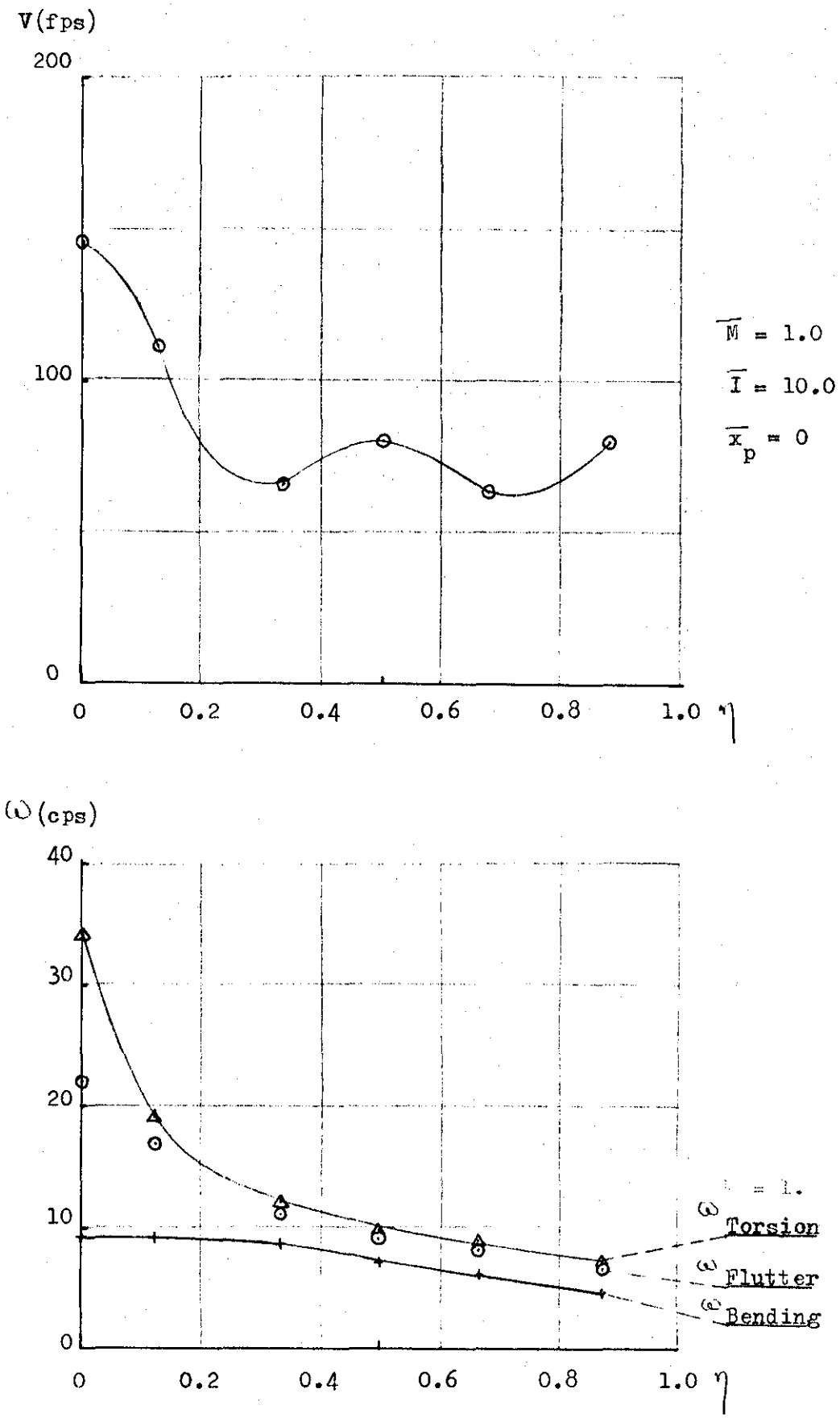

FIG. 6.13 Results of Direct Matrix Analysis: Wing A2

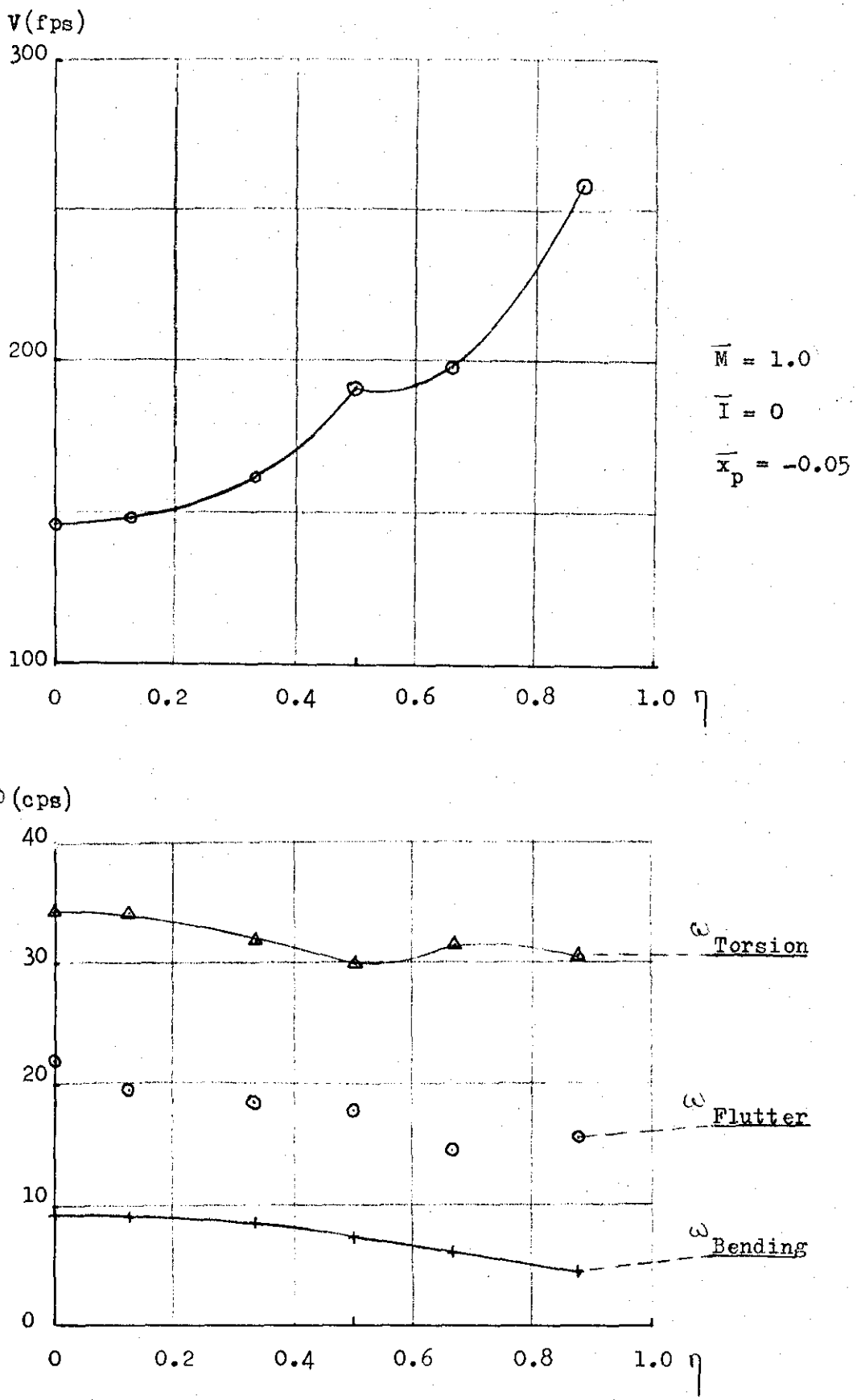

FIG. 6.14 Results of Direct Matrix Analysis: Wing A2

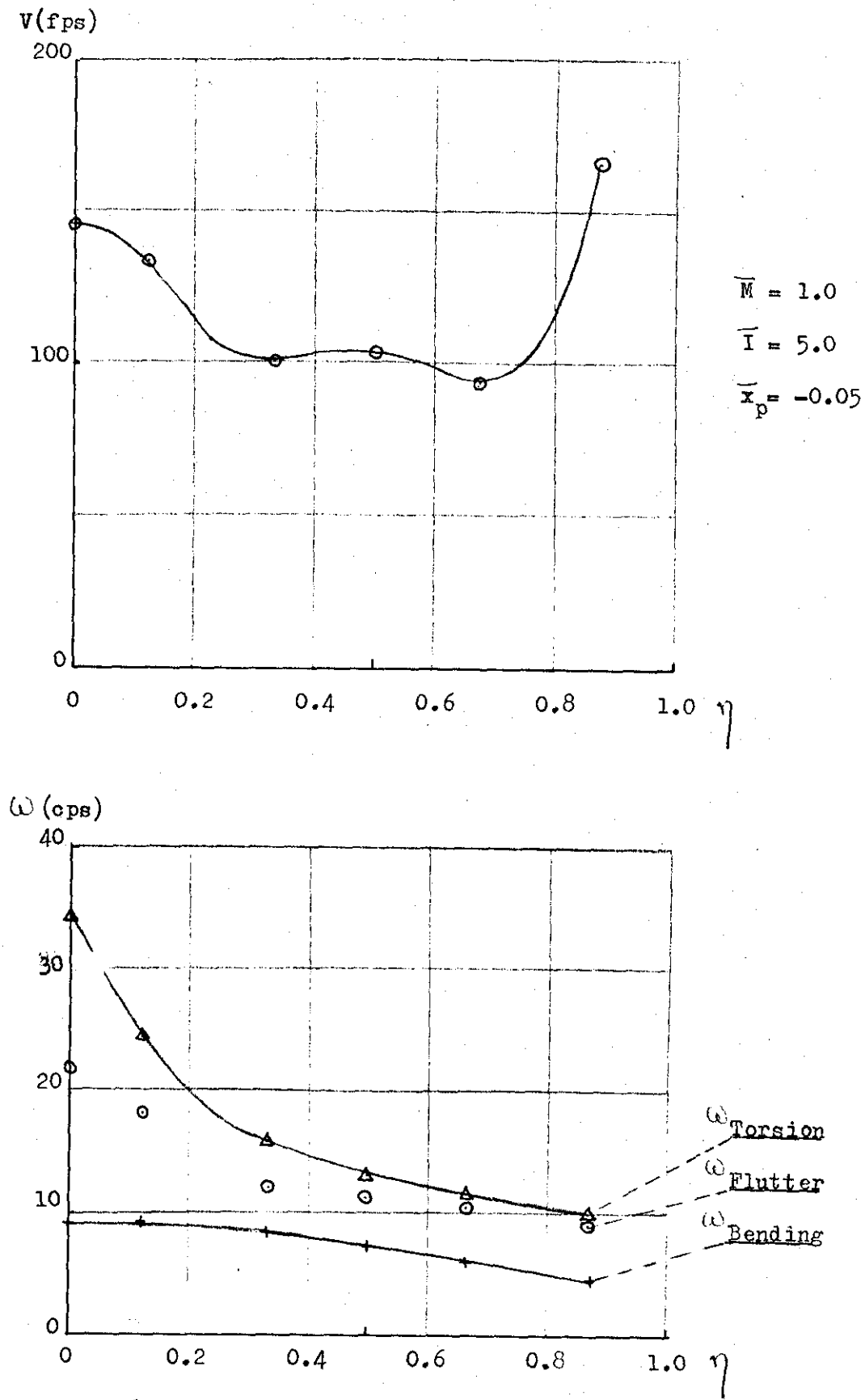

FIG. 6.15 Results of Direct Matrix Analysis: Wing A2

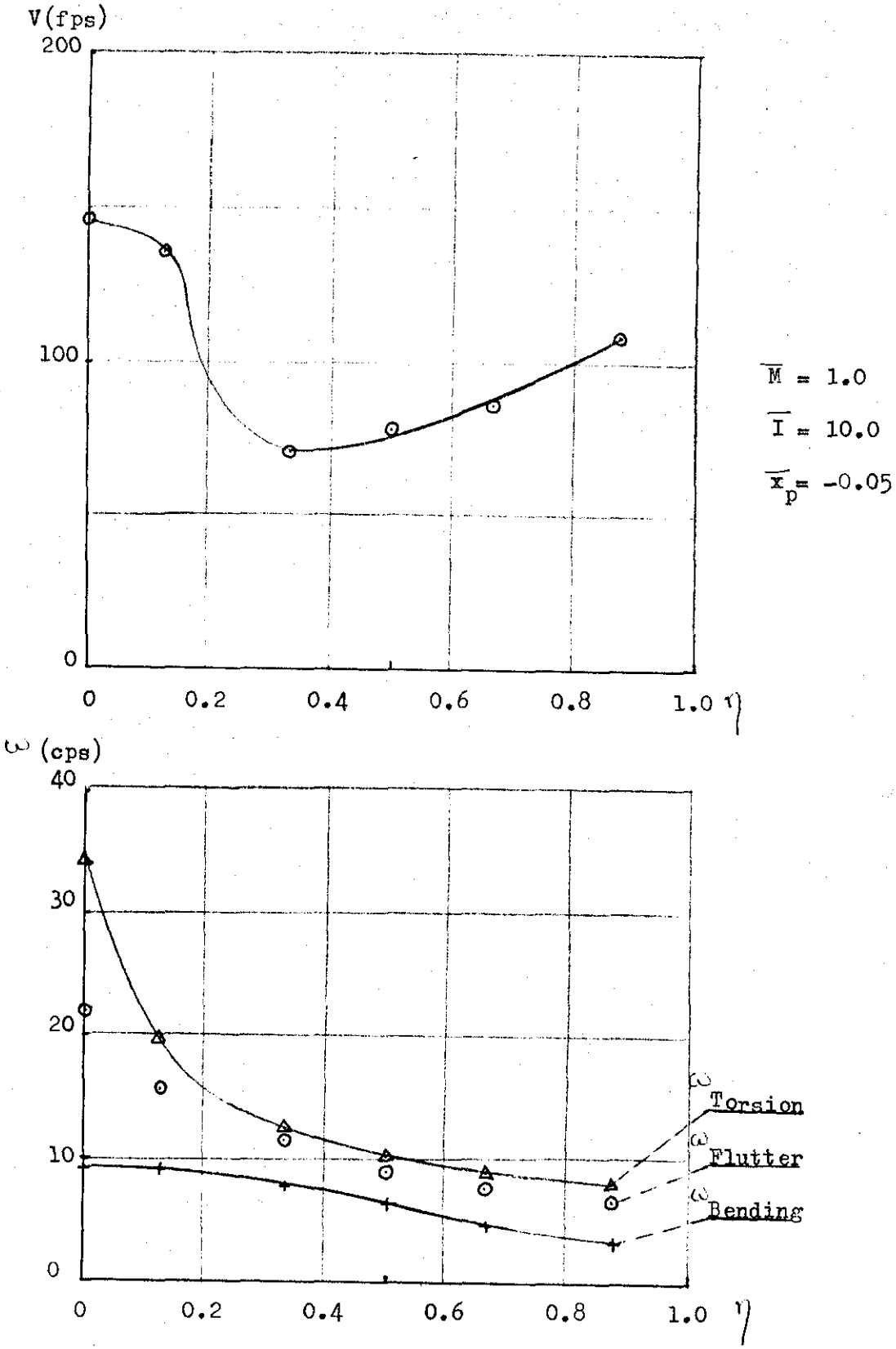

FIG. 6.16 Results of Direct Matrix Analysis: Wing A2

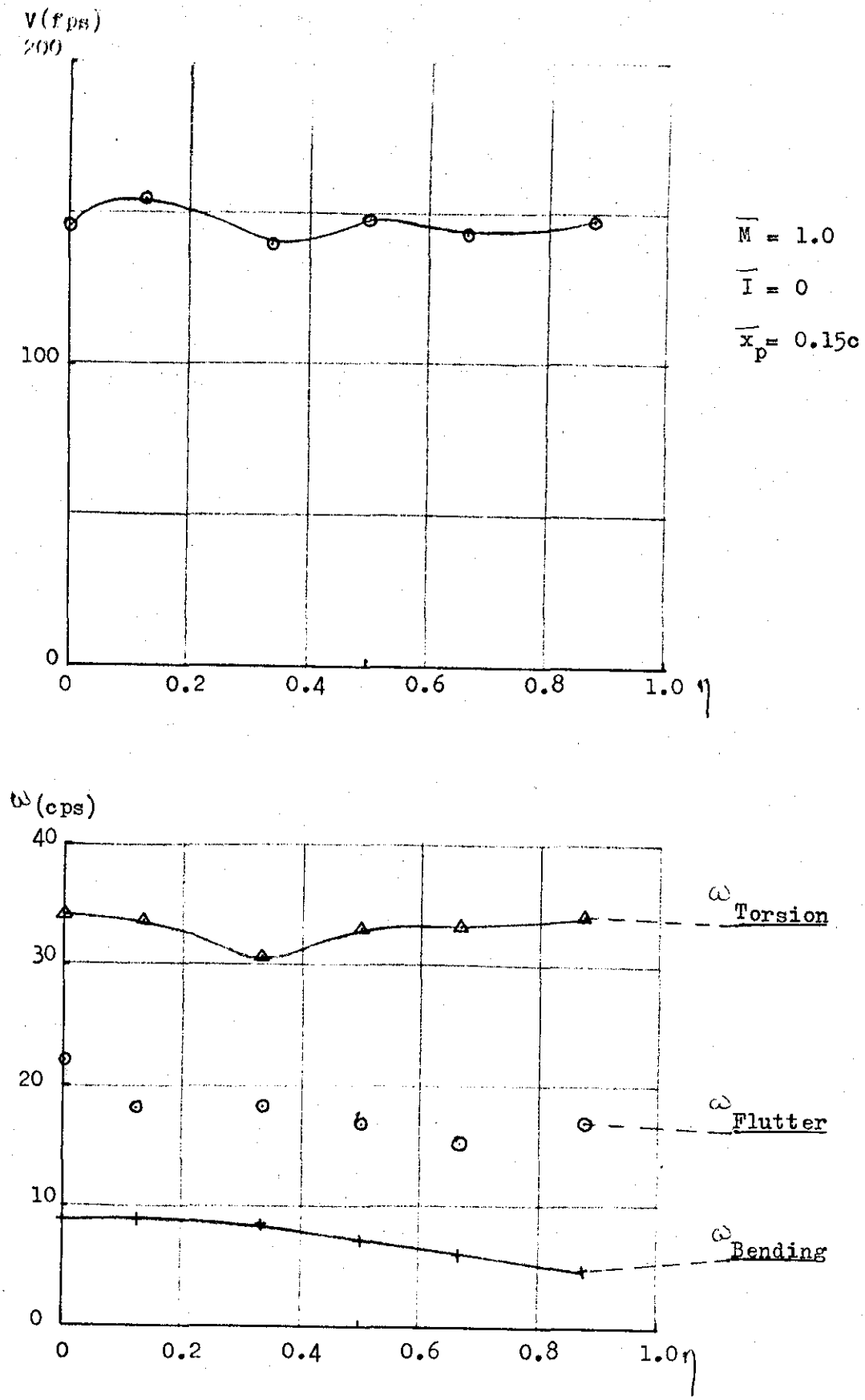

FIG. 6.17 Results of Direct Matrix Analysis: Wing A2

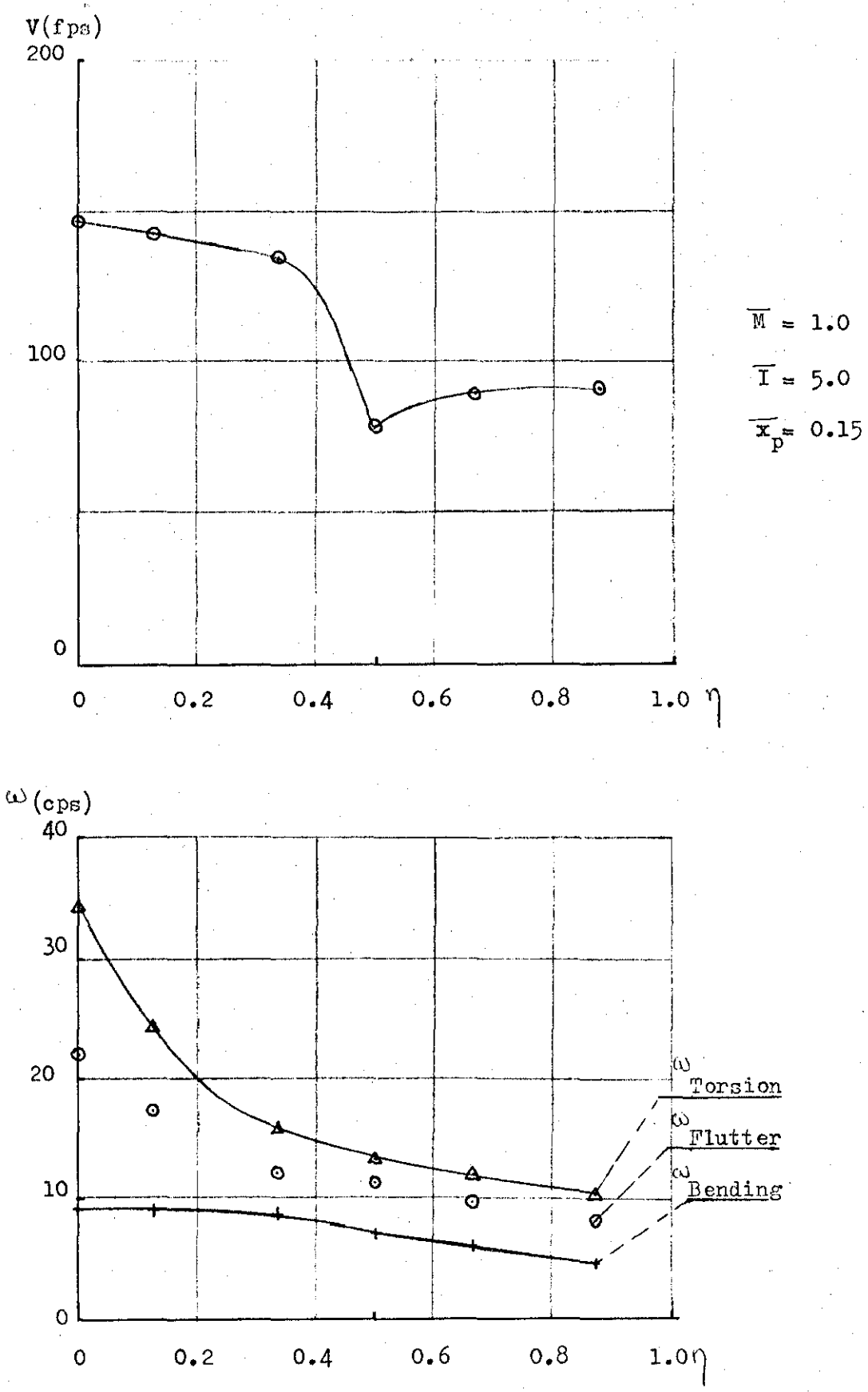

FIG. 6.18 Results of Direct Matrix Analysis: Wing A2

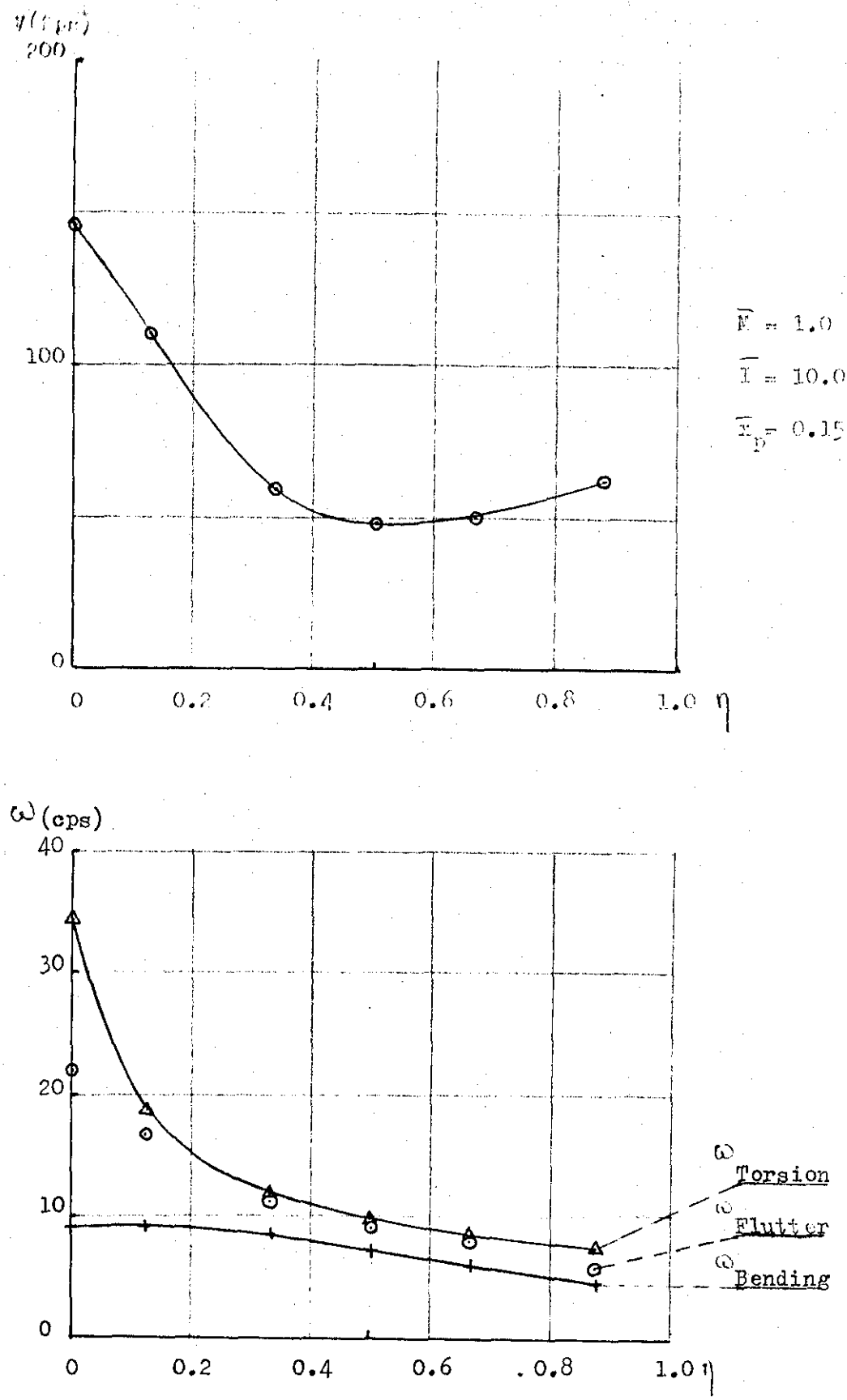

FIG. 6.19 Results of Direct Matrix Analysis: Wing A2

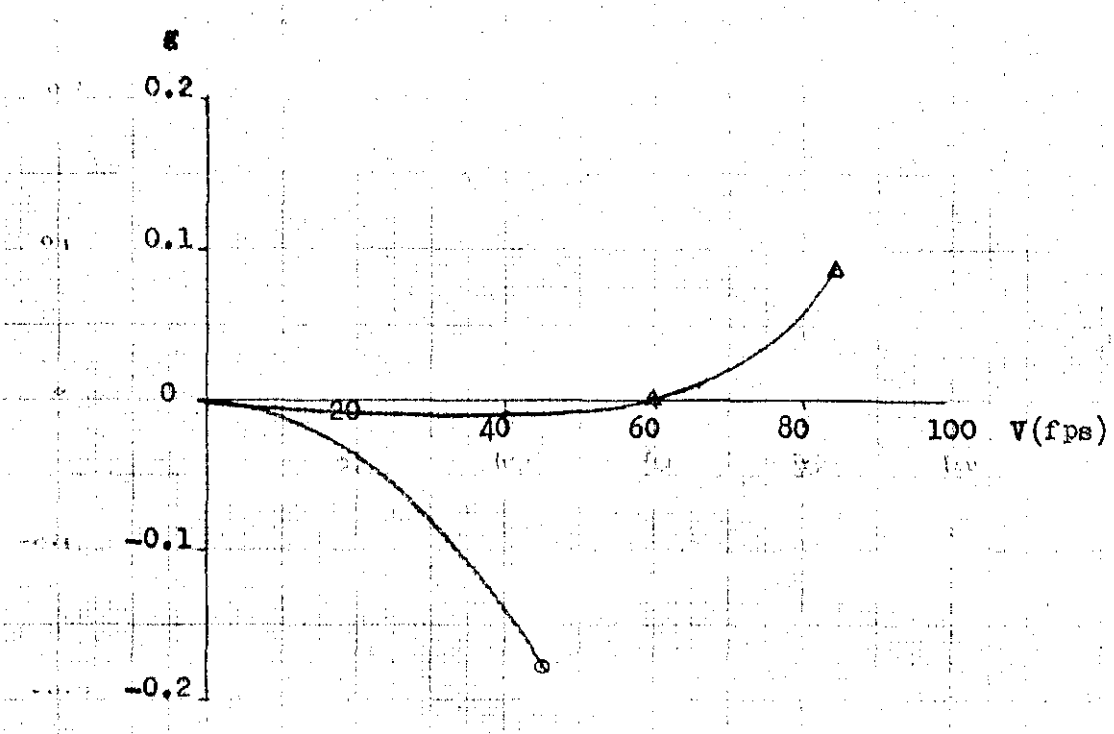

a) $M = 1.0 \quad I = 10.0 \quad x_p = 0.1 \quad \eta = 0.33$

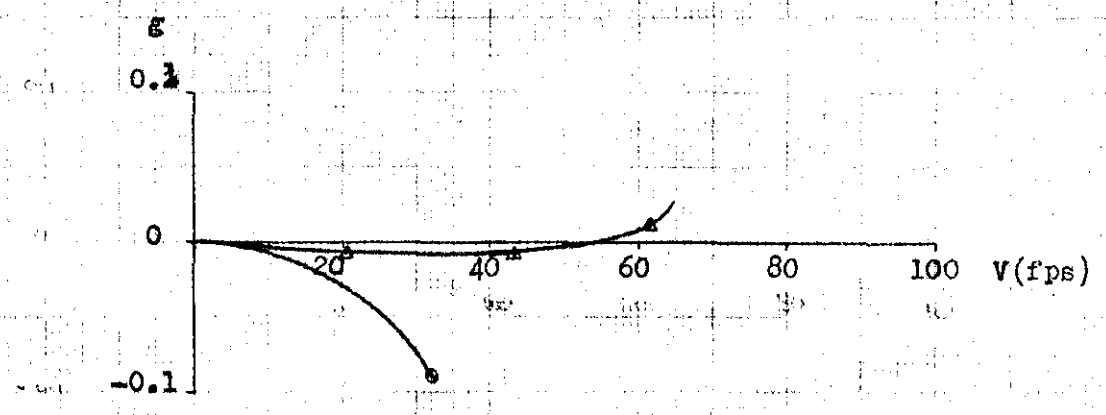

b) $\overline{M} = 1.0 \quad \overline{I} = 10.0 \quad \overline{x_p} = 0.1 \quad \eta = 0.67$

FIG 6.20 V-g Curve for Two Pods on Wing A2

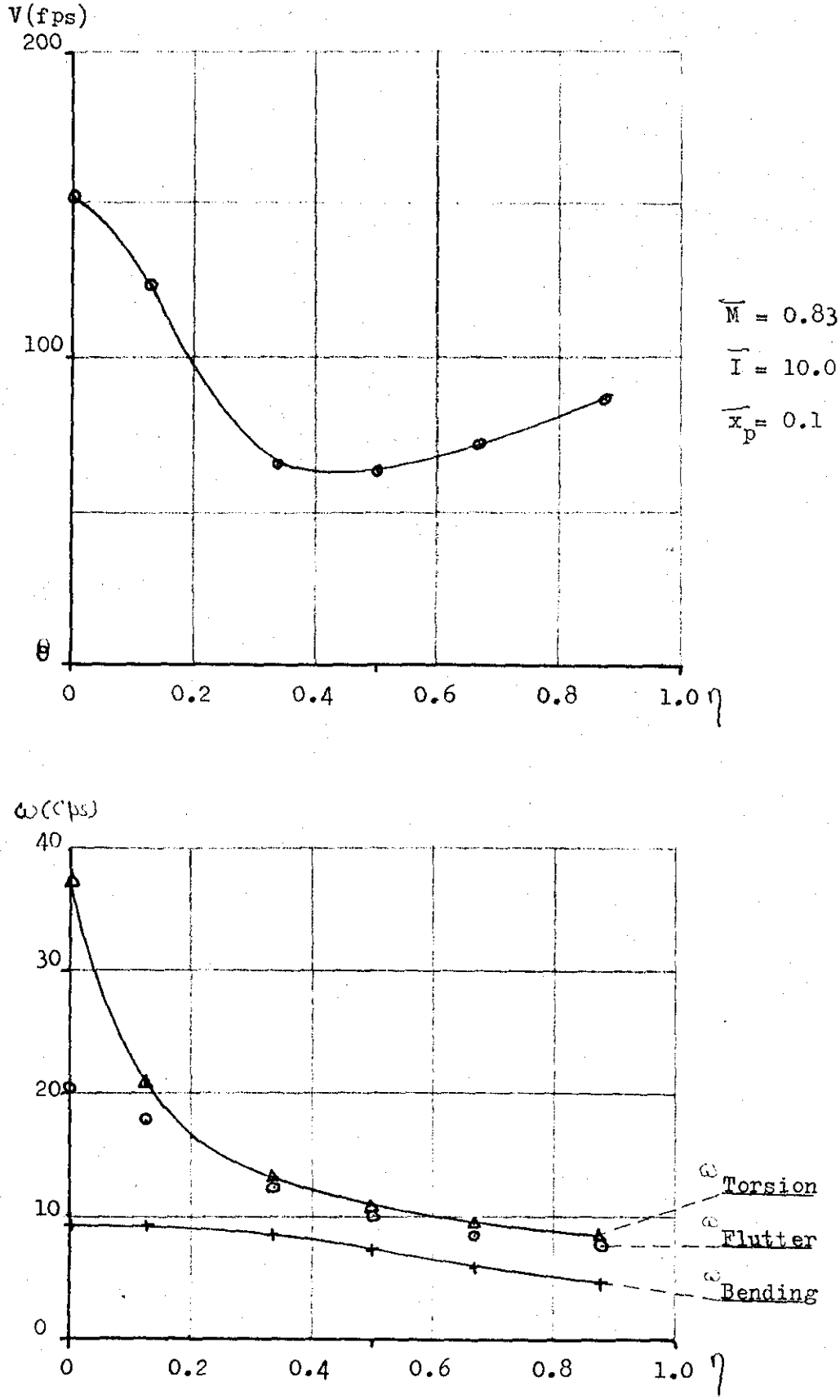

Fig 6.21 Results of Direct Analysis on Wing A3

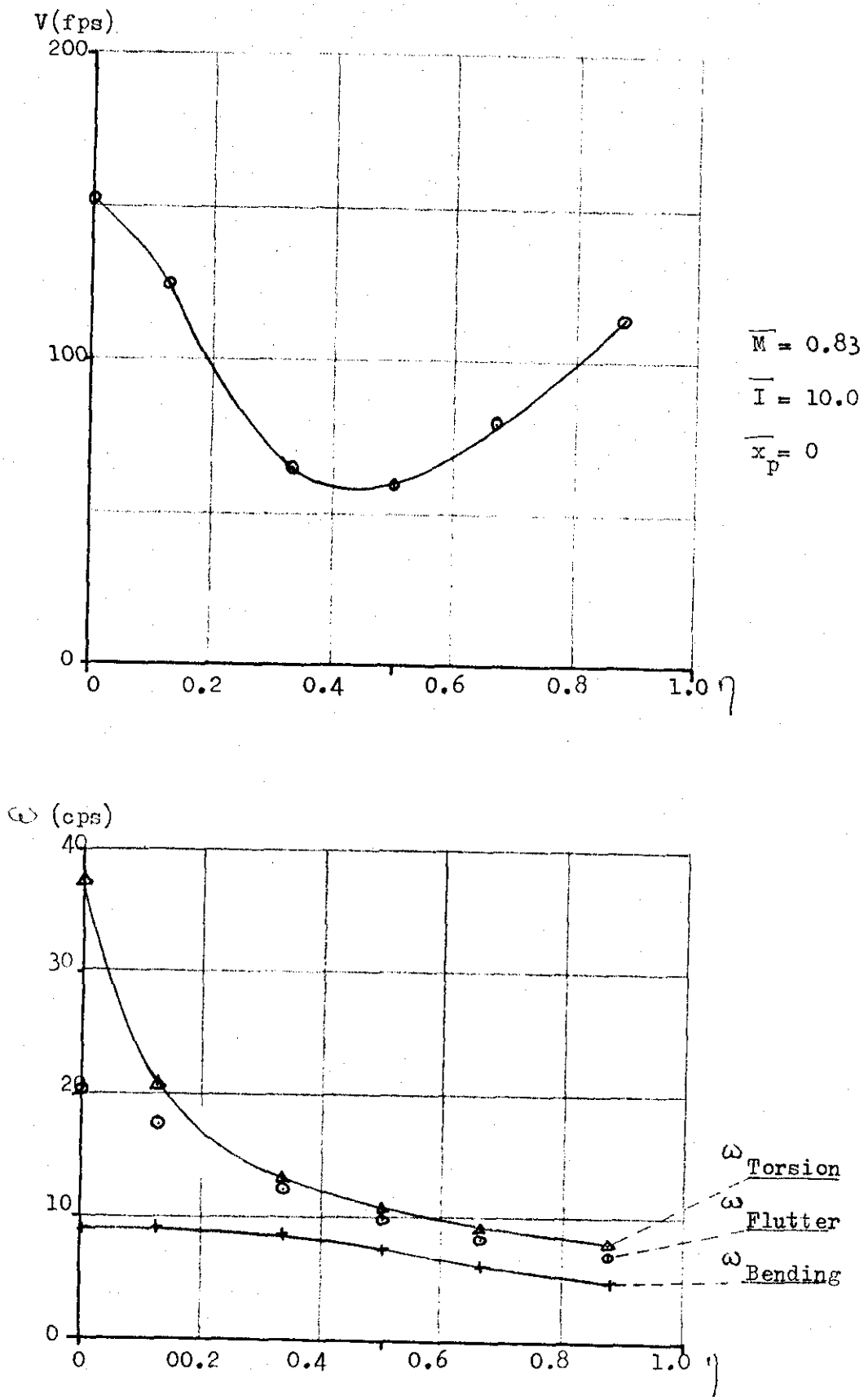

Fig. 6.22 Results of Direct Matrix Analysis: Wing A3

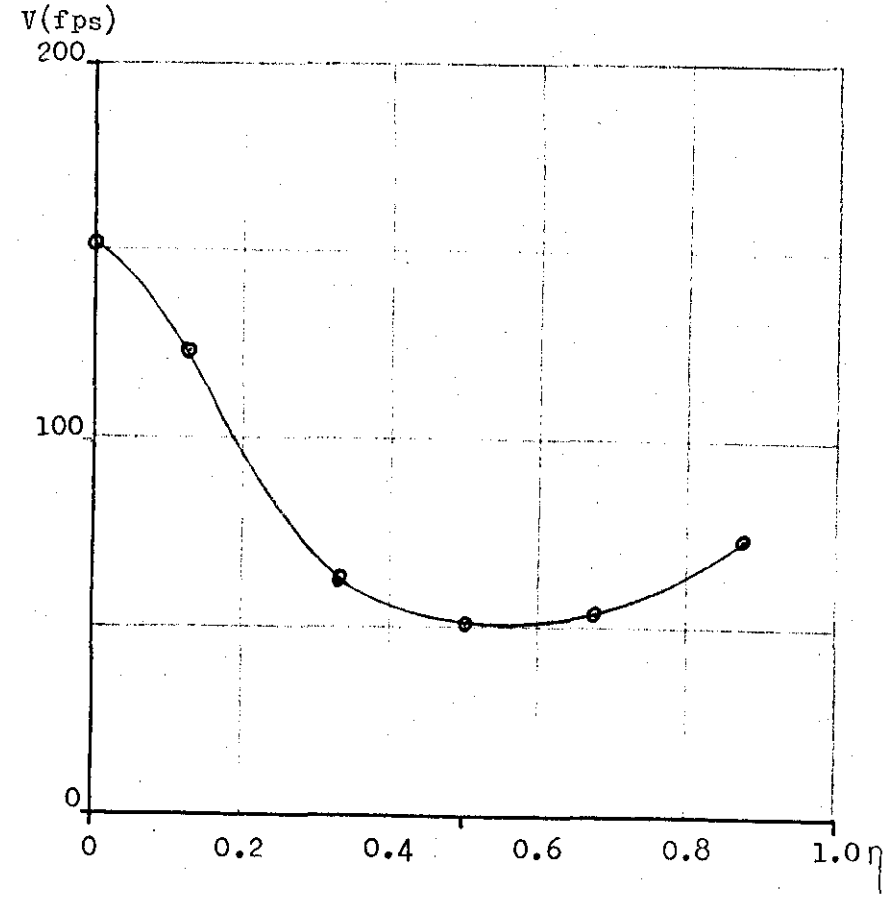

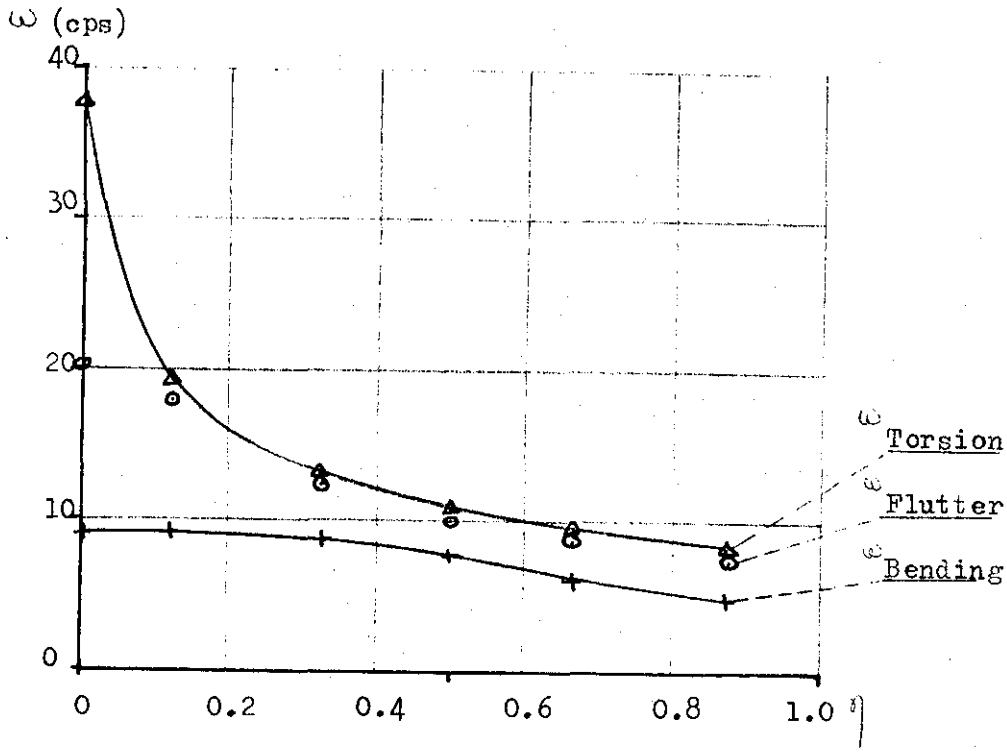

FIG. 6.23 Results of Direct Matrix Analysis: Wing A3

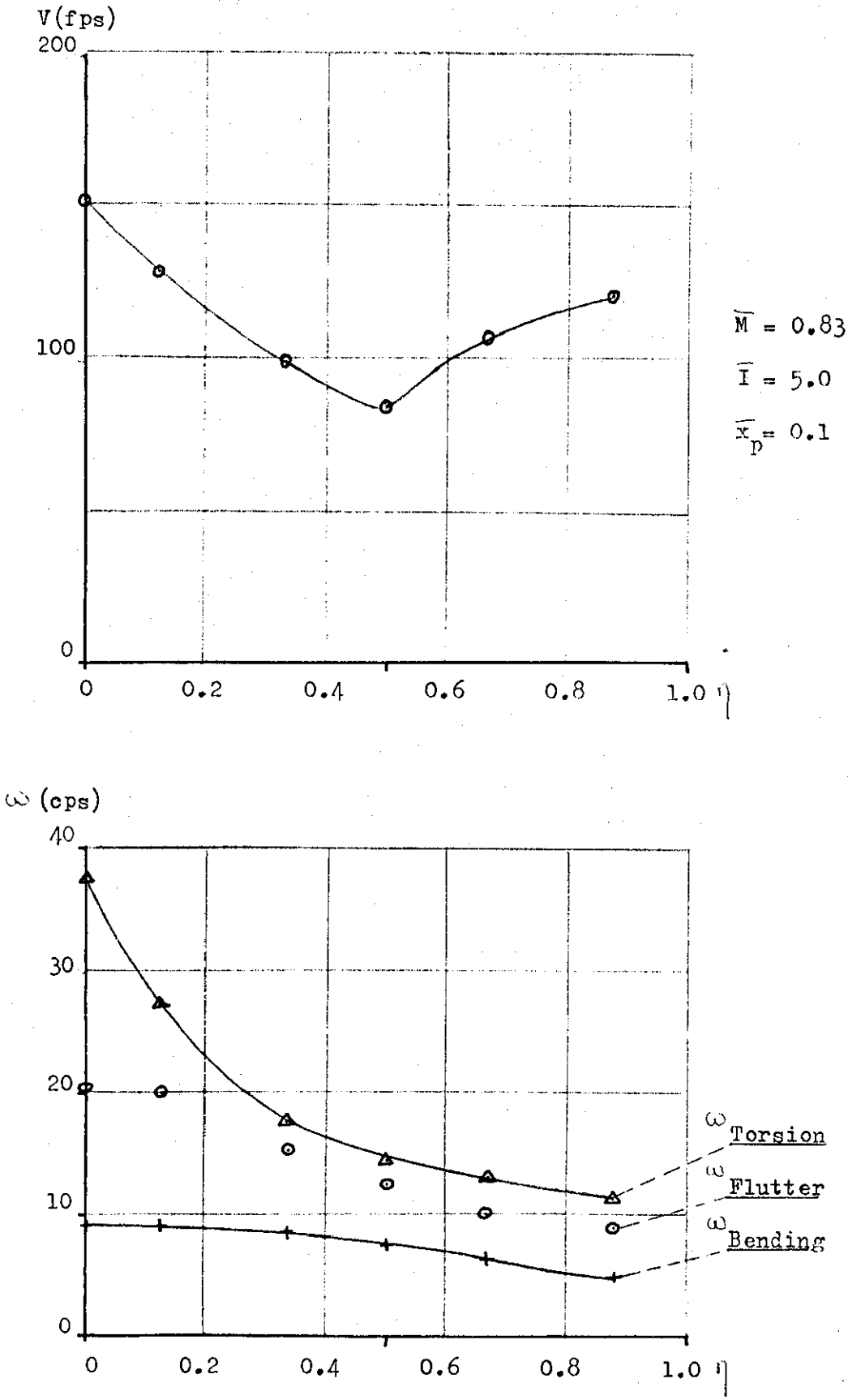

FIG. 6.24 Results of Direct Matrix Method: Wing A3

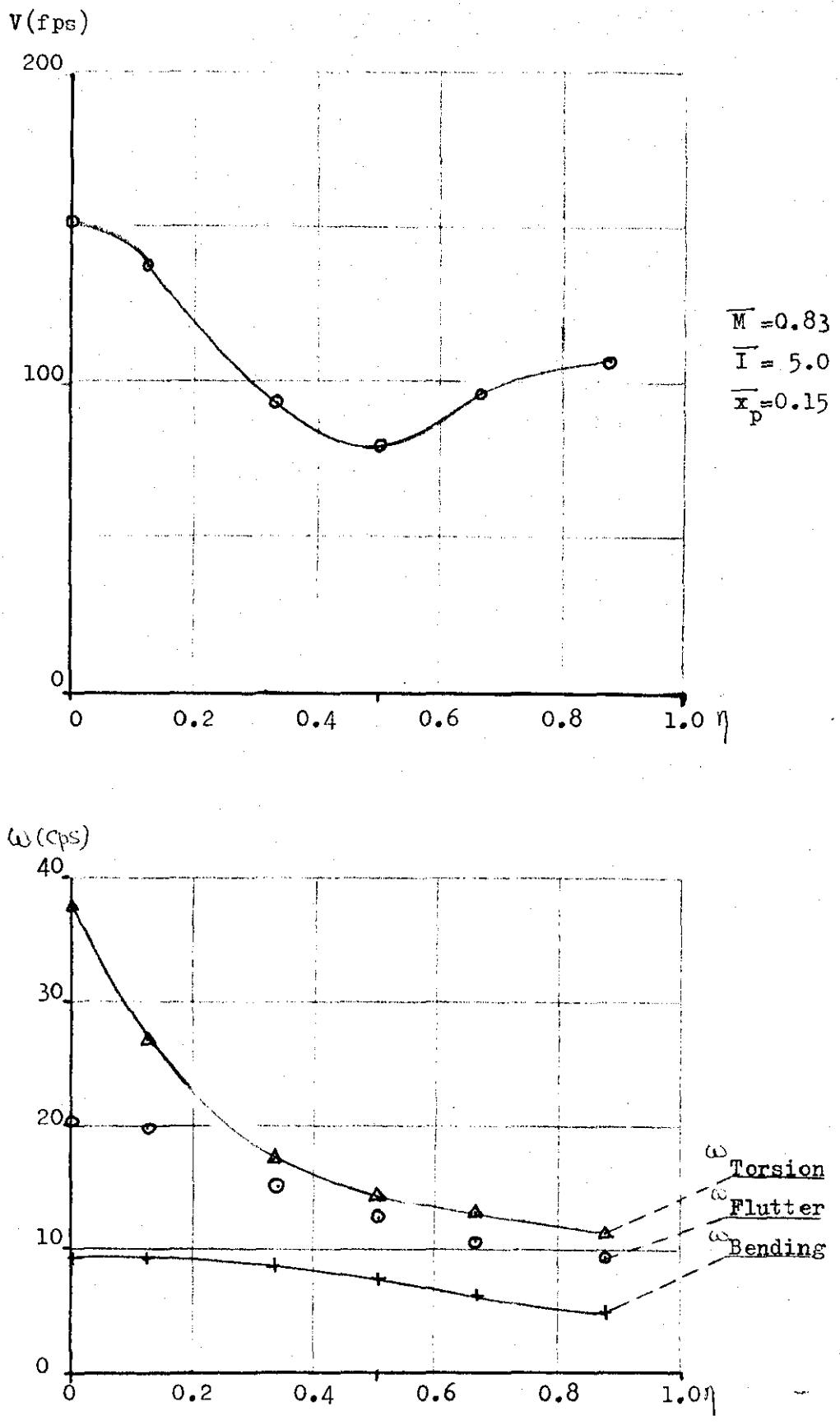

FIG. 6.25 Results of Direct Matrix Analysis: Wing A3

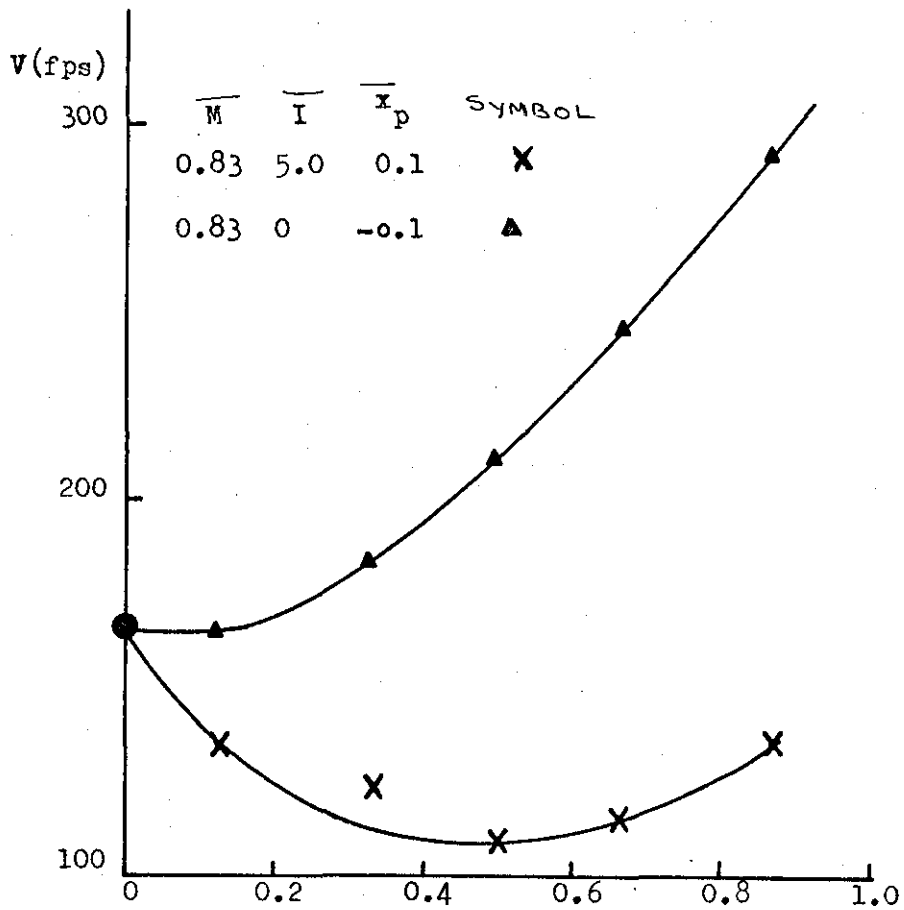

FIG. 6.26 Results of Direct Matrix Analysis: Wing B4

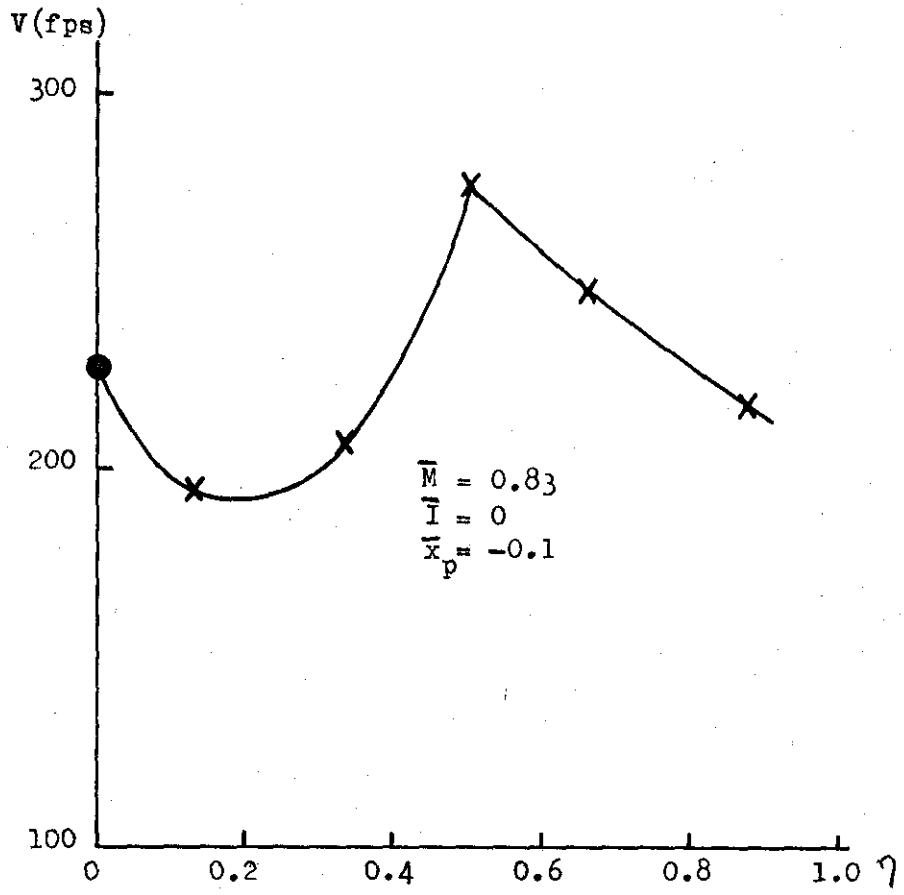

FIG. 6.27 Results of Direct Matrix Analysis: Wing B5

FIG 7.1 : POD A

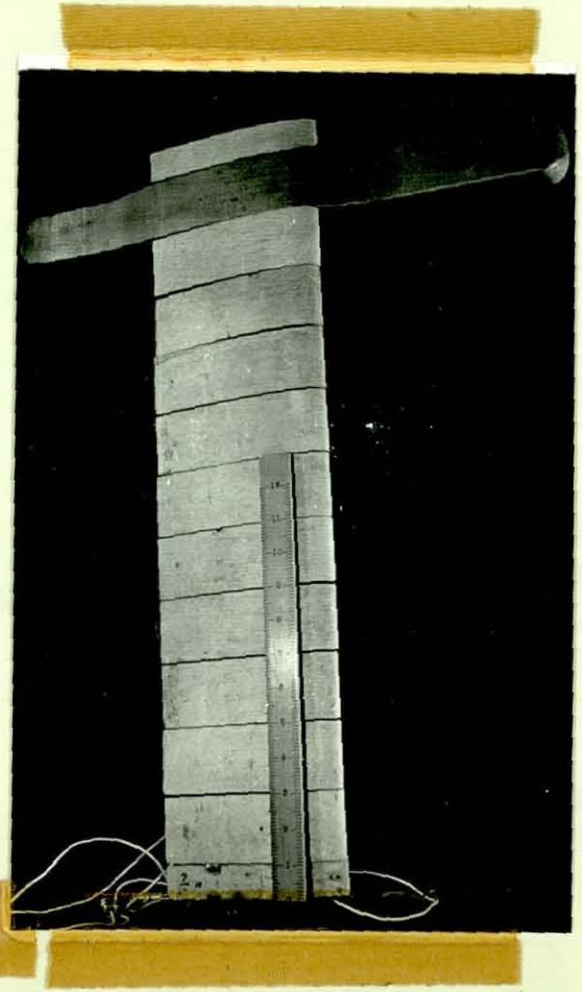

FIG 7.2 : POD B

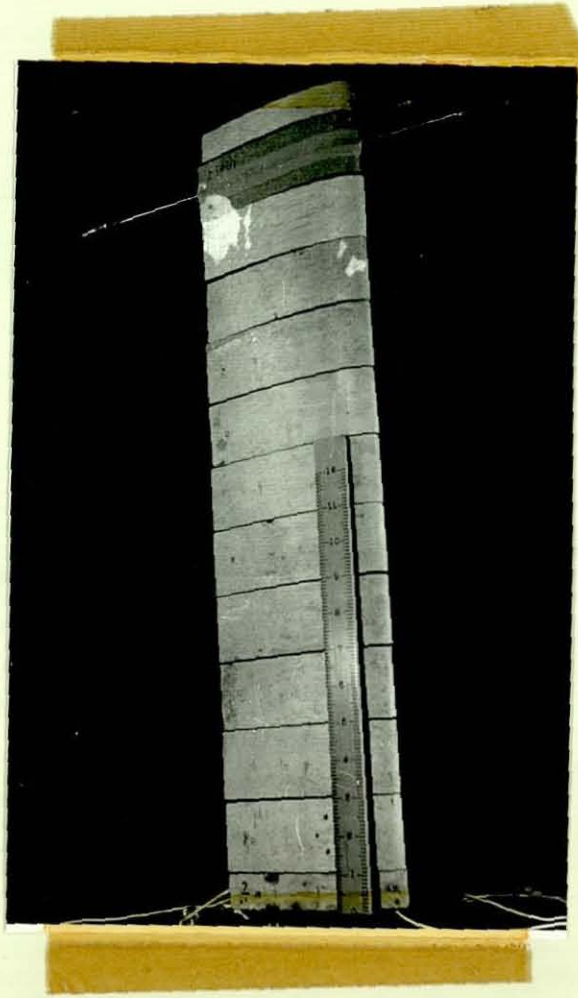

FIG 7.3 : POD D

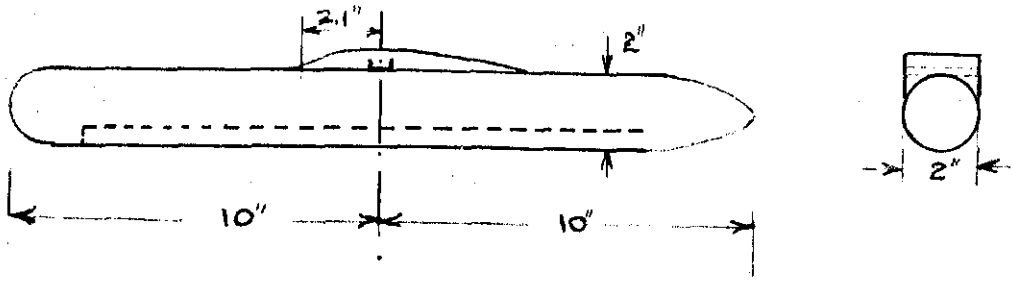

FIG 7.4 Details of Pod A

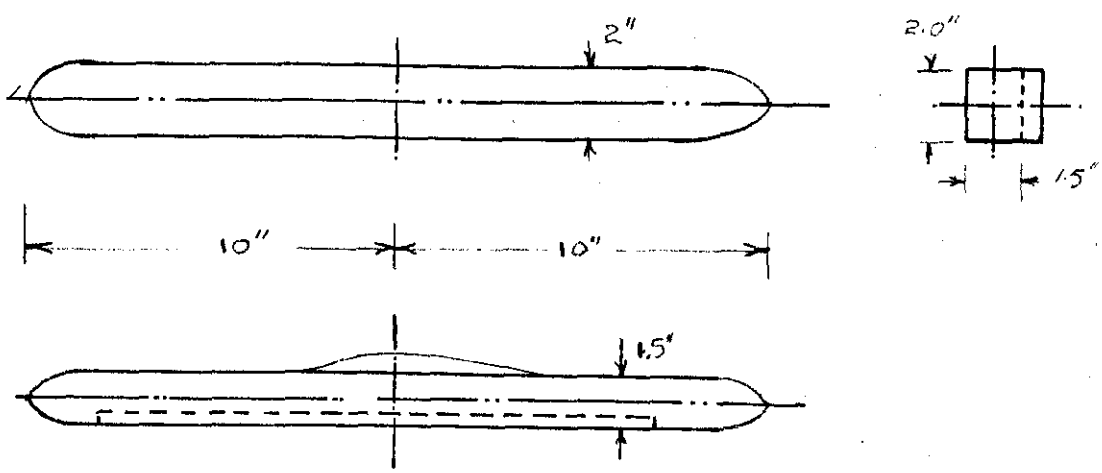

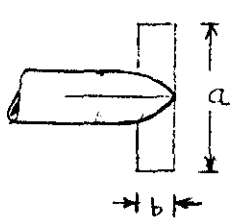

Fin No.	a(ins)	b(ins)
1	1.0	0.5
2	1.0	1.0
3	2.0	1.0
4	2.0	0.5
5	3.0	0.5

FIG 7.5 Details of Pod B and Fins.

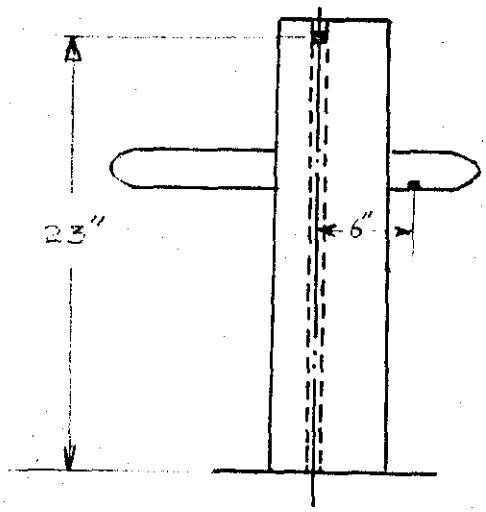

FIG.7.6 Location of Transducers

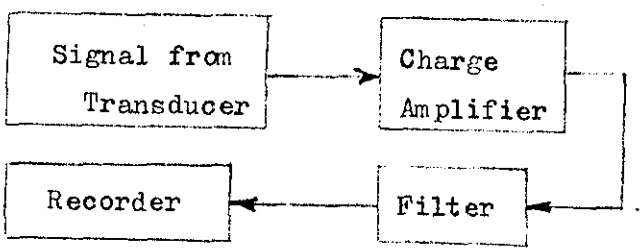

FIG 7.7 Instrumentation (Schematic)

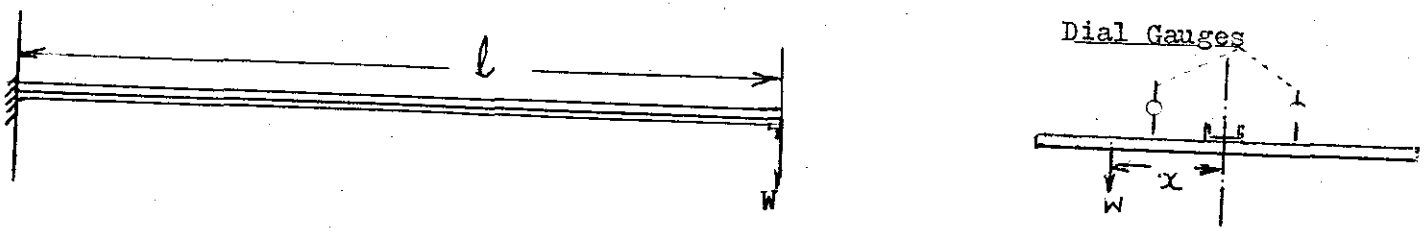

FIG 7.8 Rig For the Determination of EI and GJ

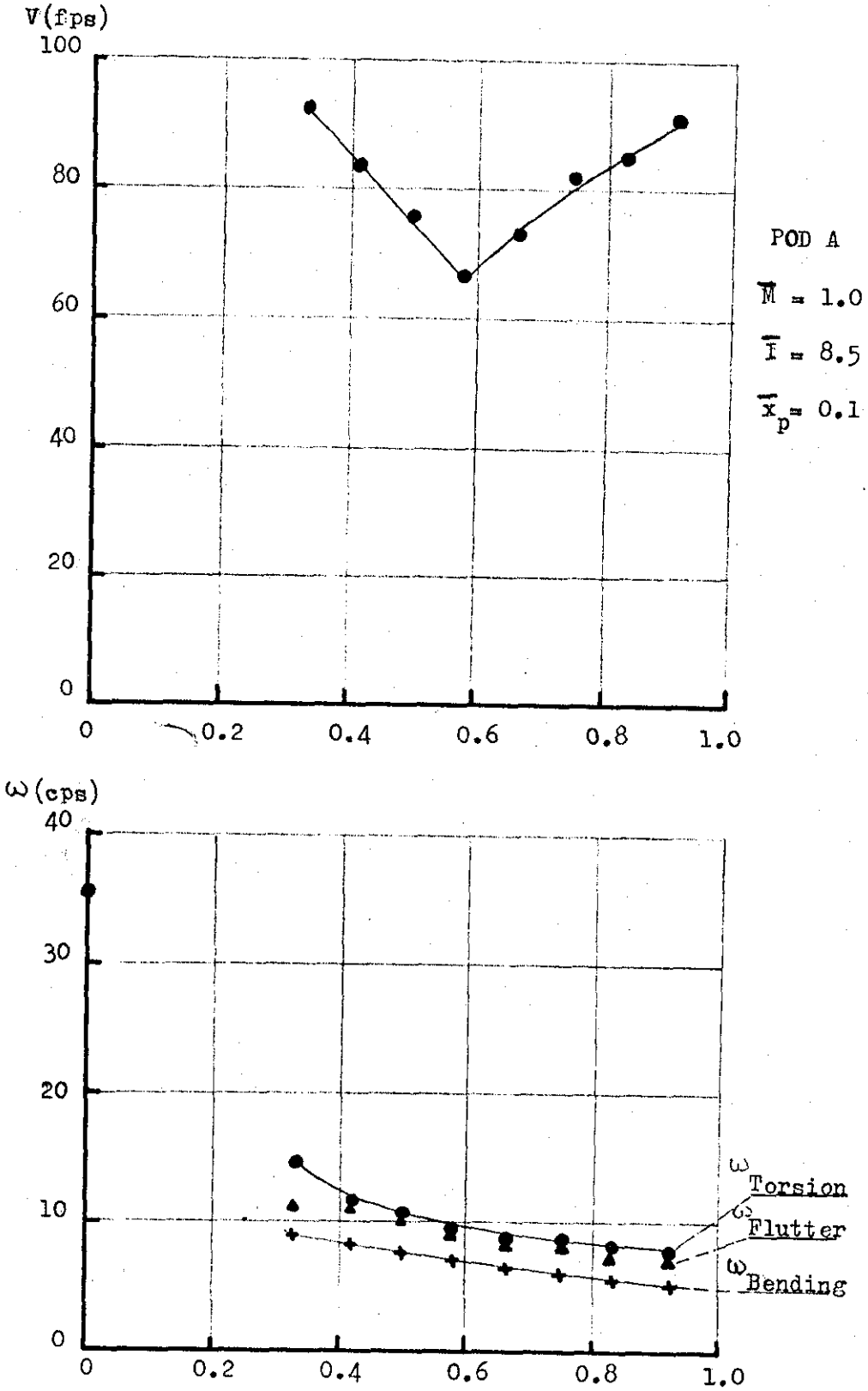

Fig. 7.9 Results of Wind Tunnel Tests: Wing A2

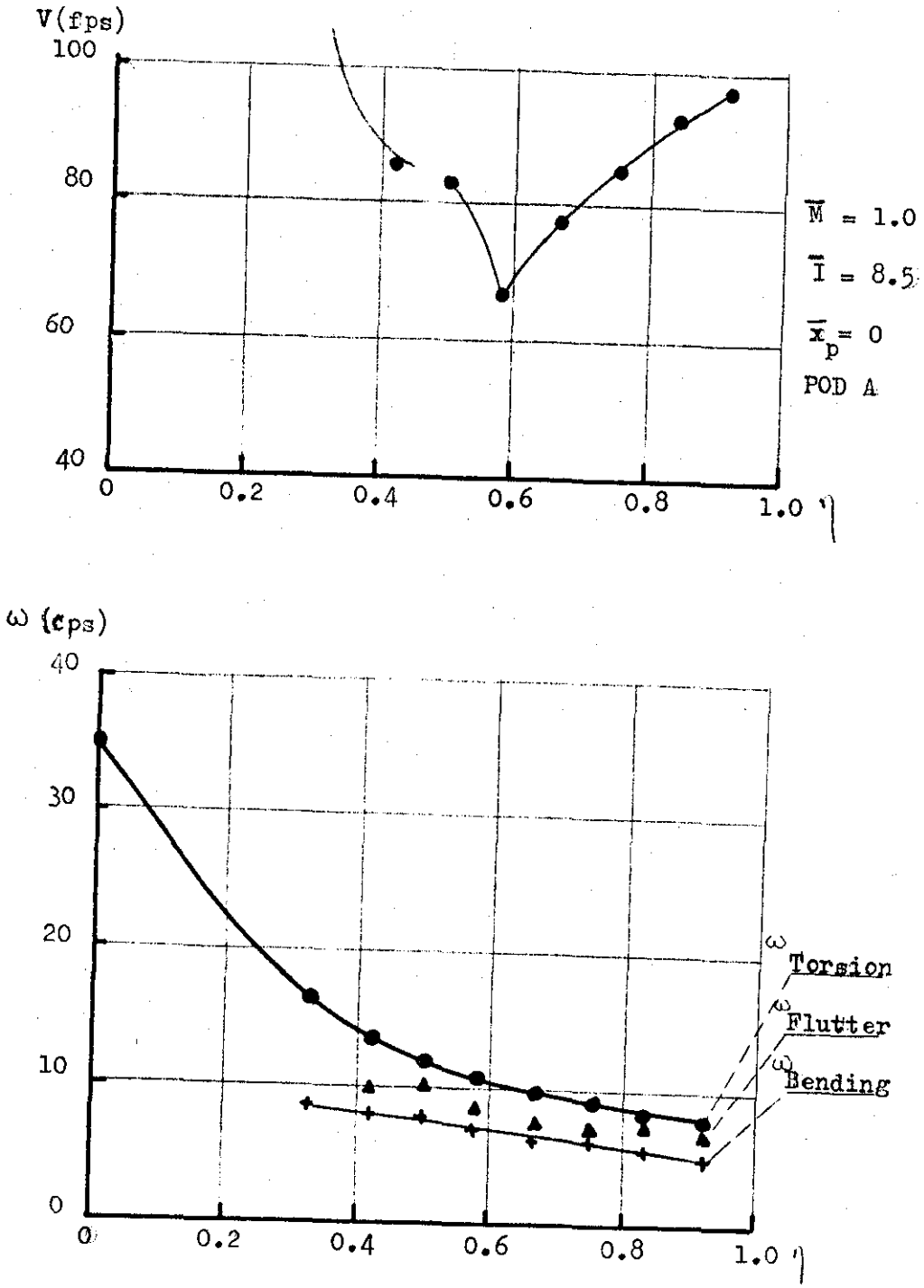

FIG. 7.10 Results of Wind Tunnel Tests: Wing A2

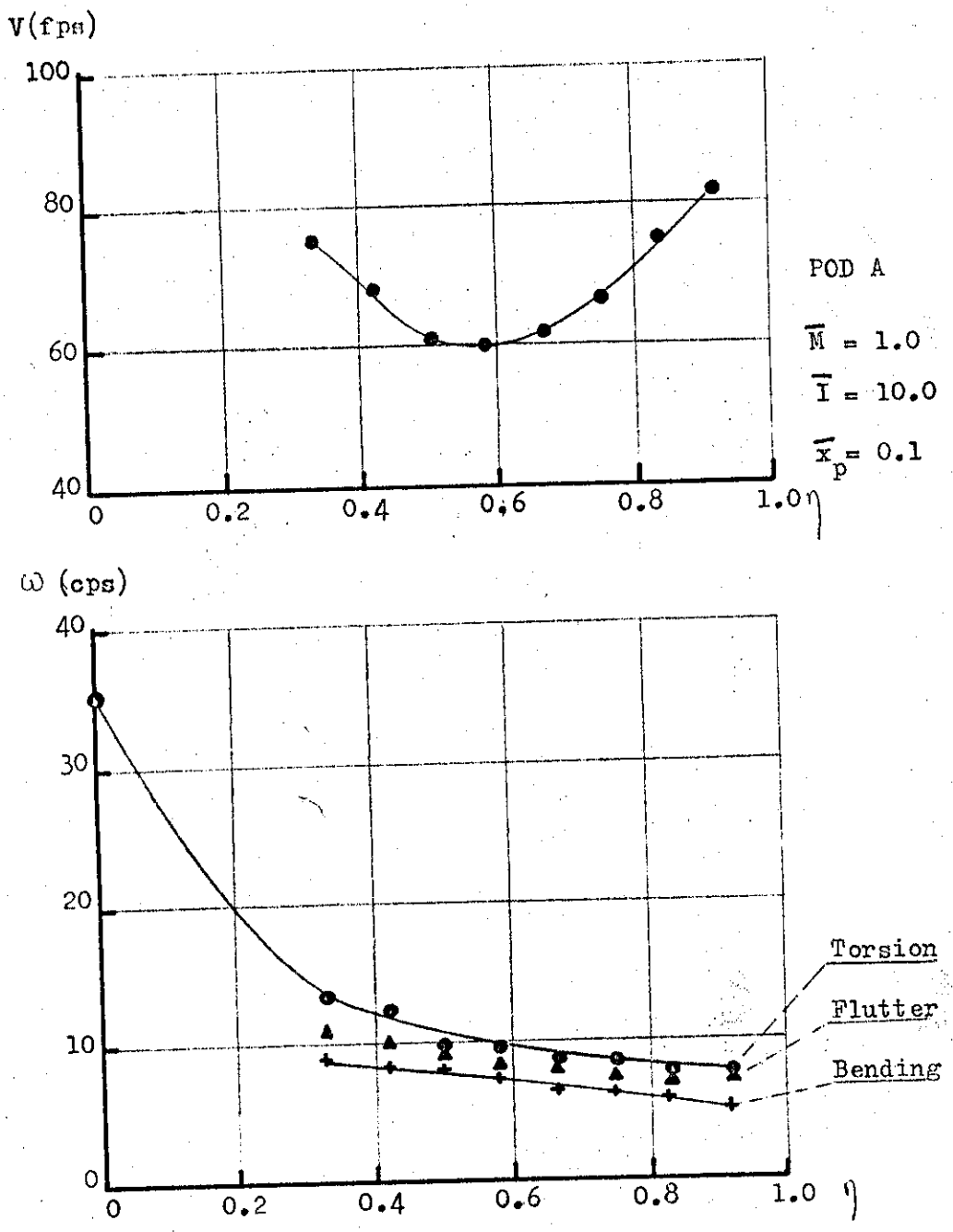

FIG. 7.11 Results of Wind Tunnel Tests: Wing A2

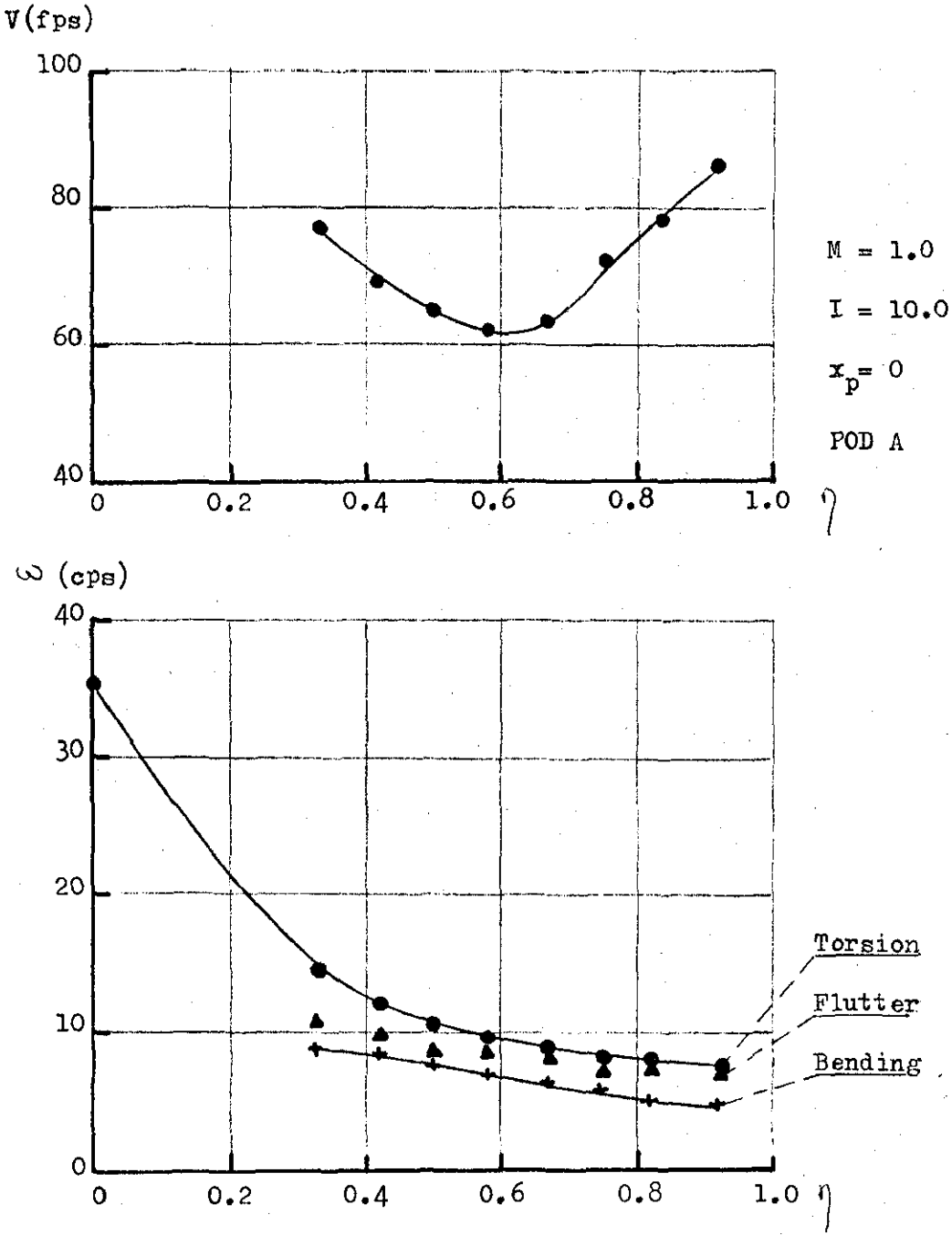

Fig. 7.12 Results of Wind Tunnel Tests: Wing A2

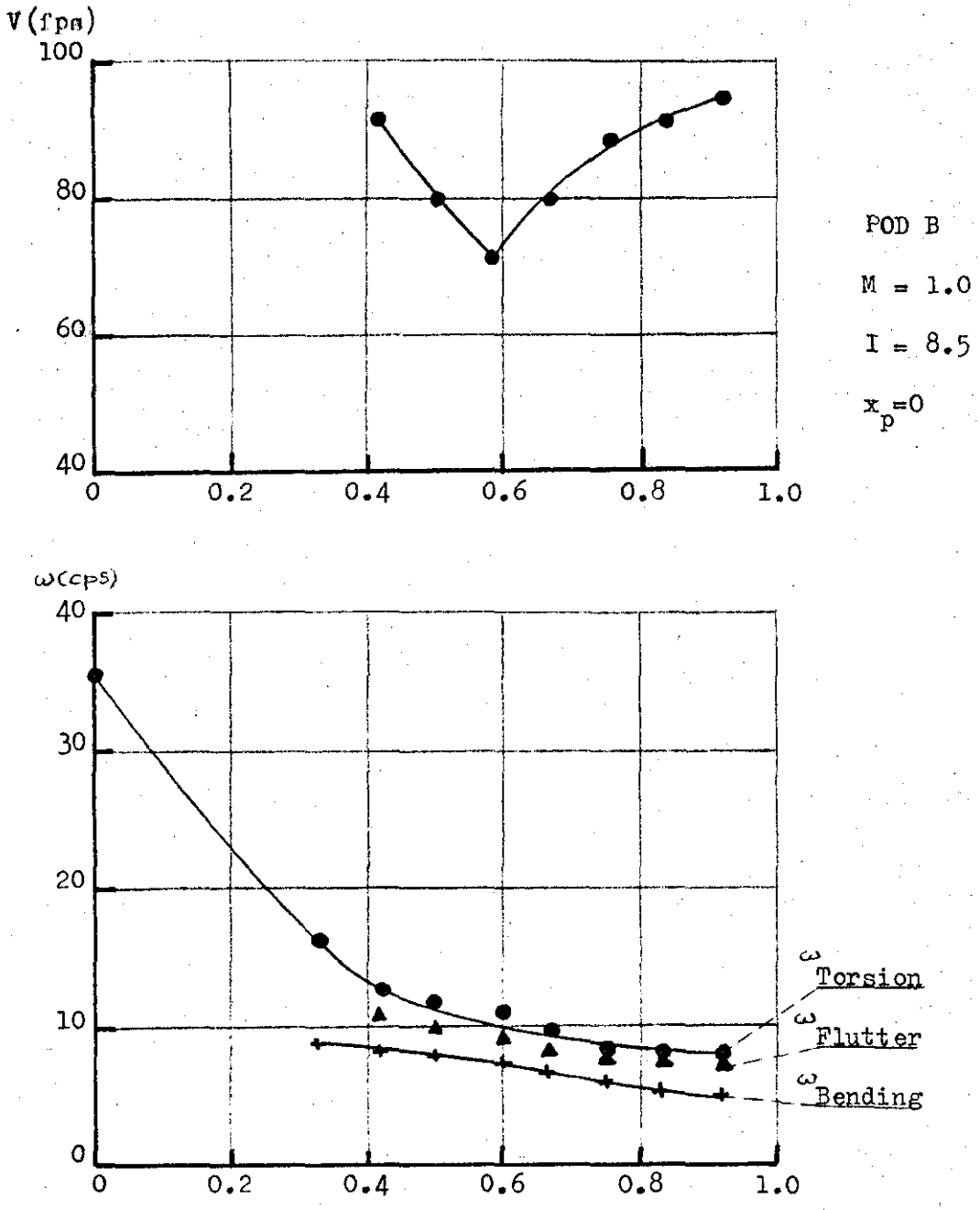

FIG. 7.13 Results of Wind Tunnel Tests: Wing A2

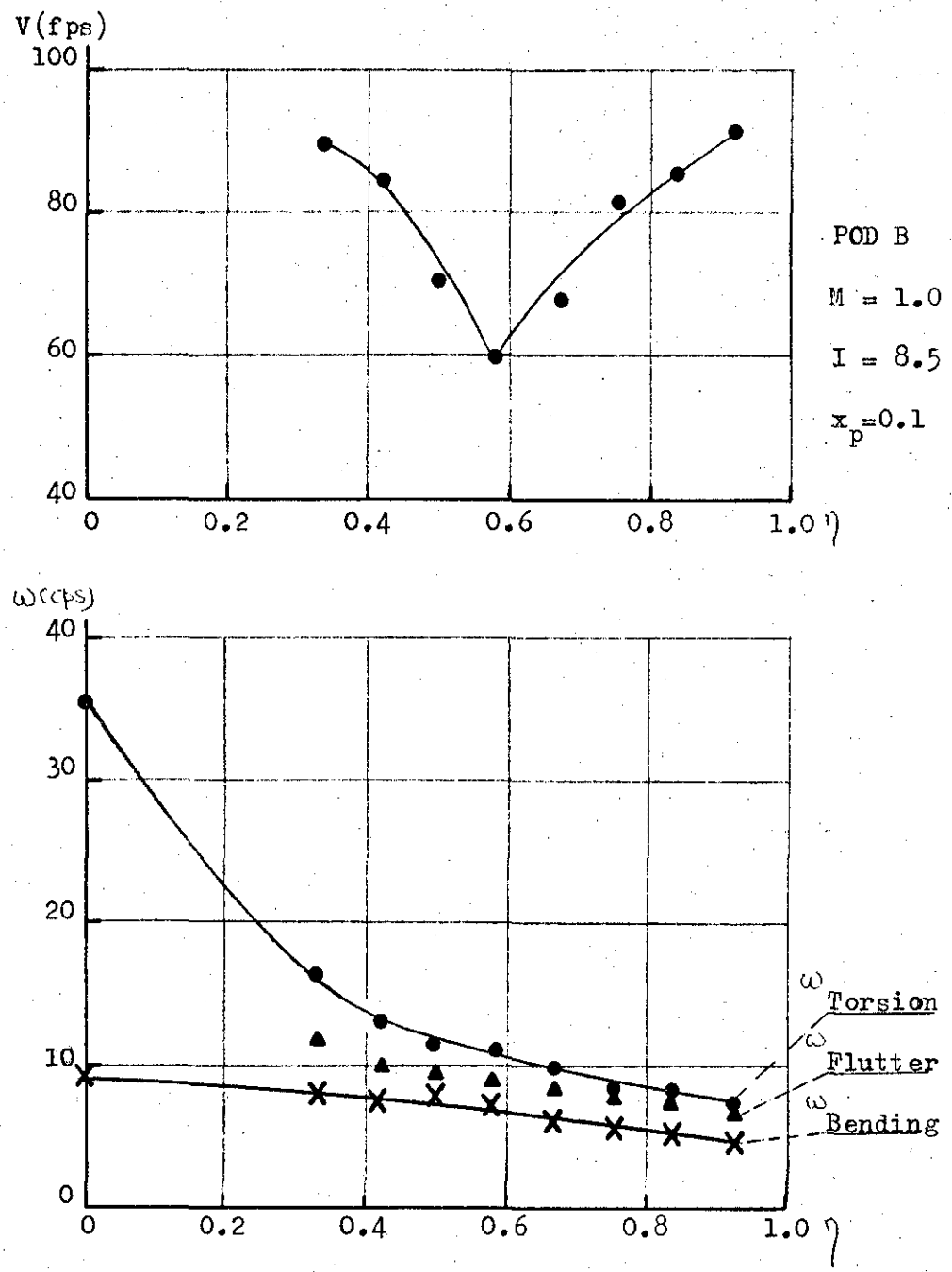

FIG. 7.14 Results of Wind Tunnel Tests: Wing A2

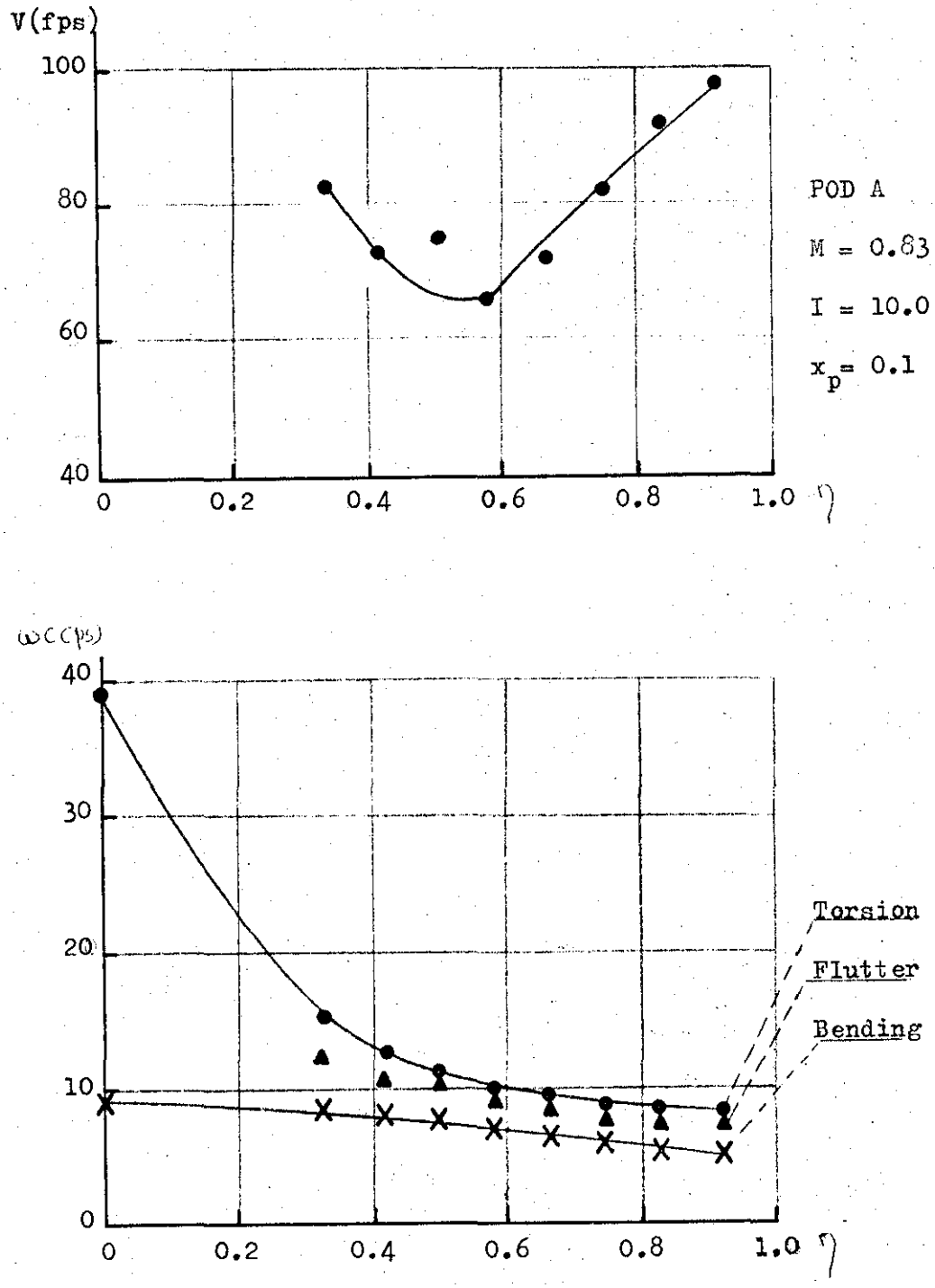

FIG. 7.15 Results of Wind Tunnel Tests: Wing A3

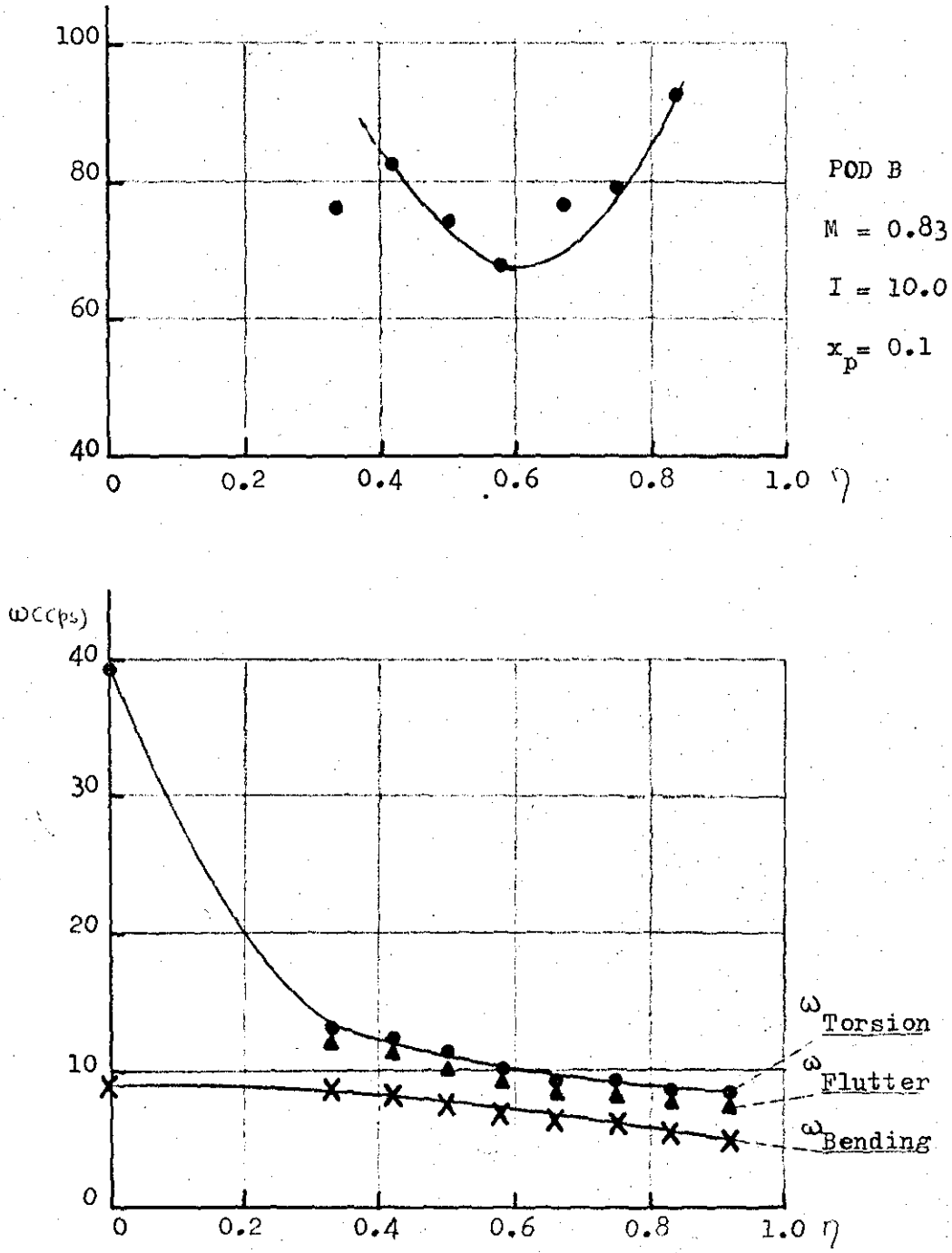

FIG. 7.16 Results of Wind Tunnel Tests: Wing A3

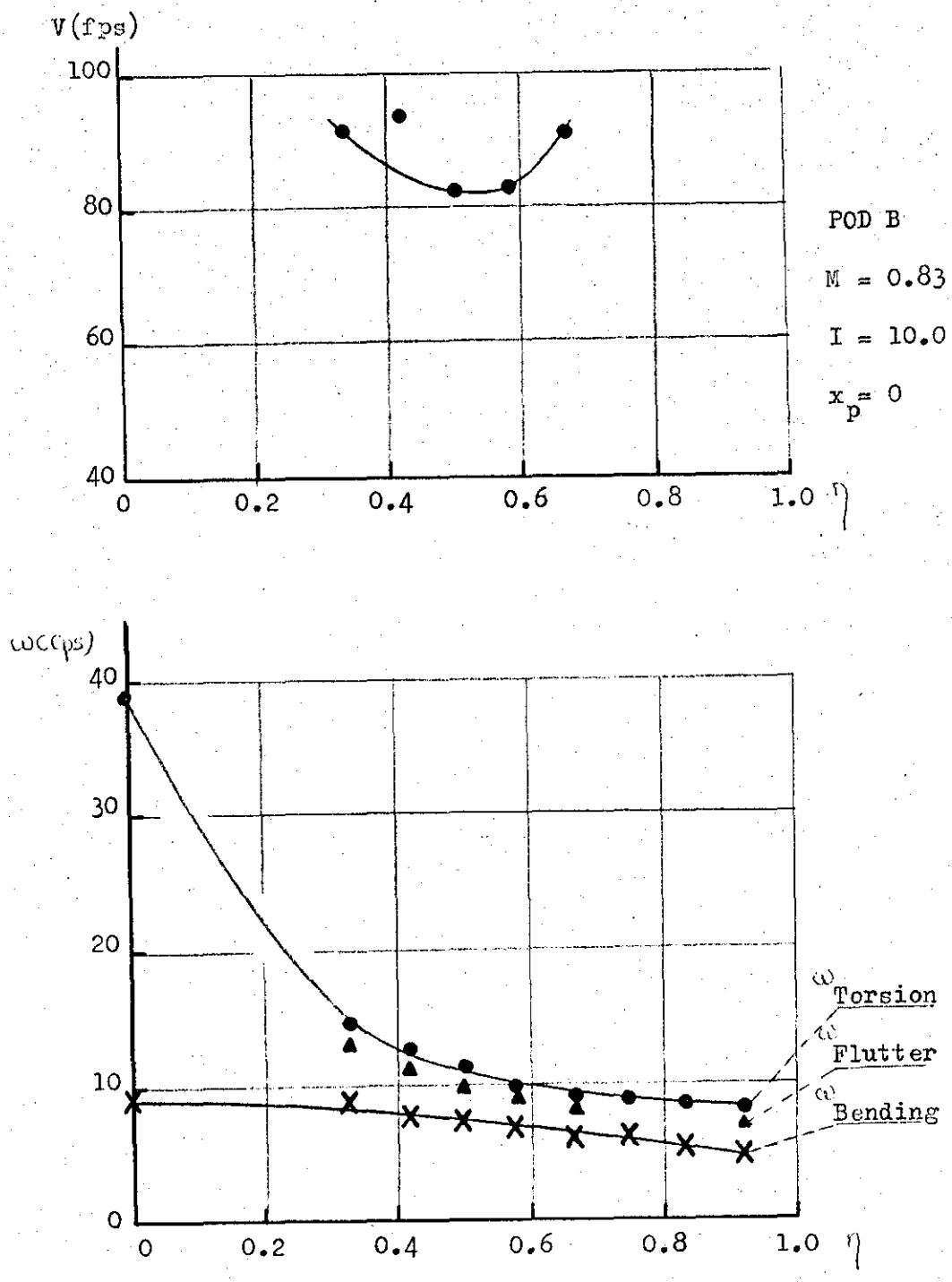

FIG. 7.17 Results of Wind Tunnel Tests: Wing A3

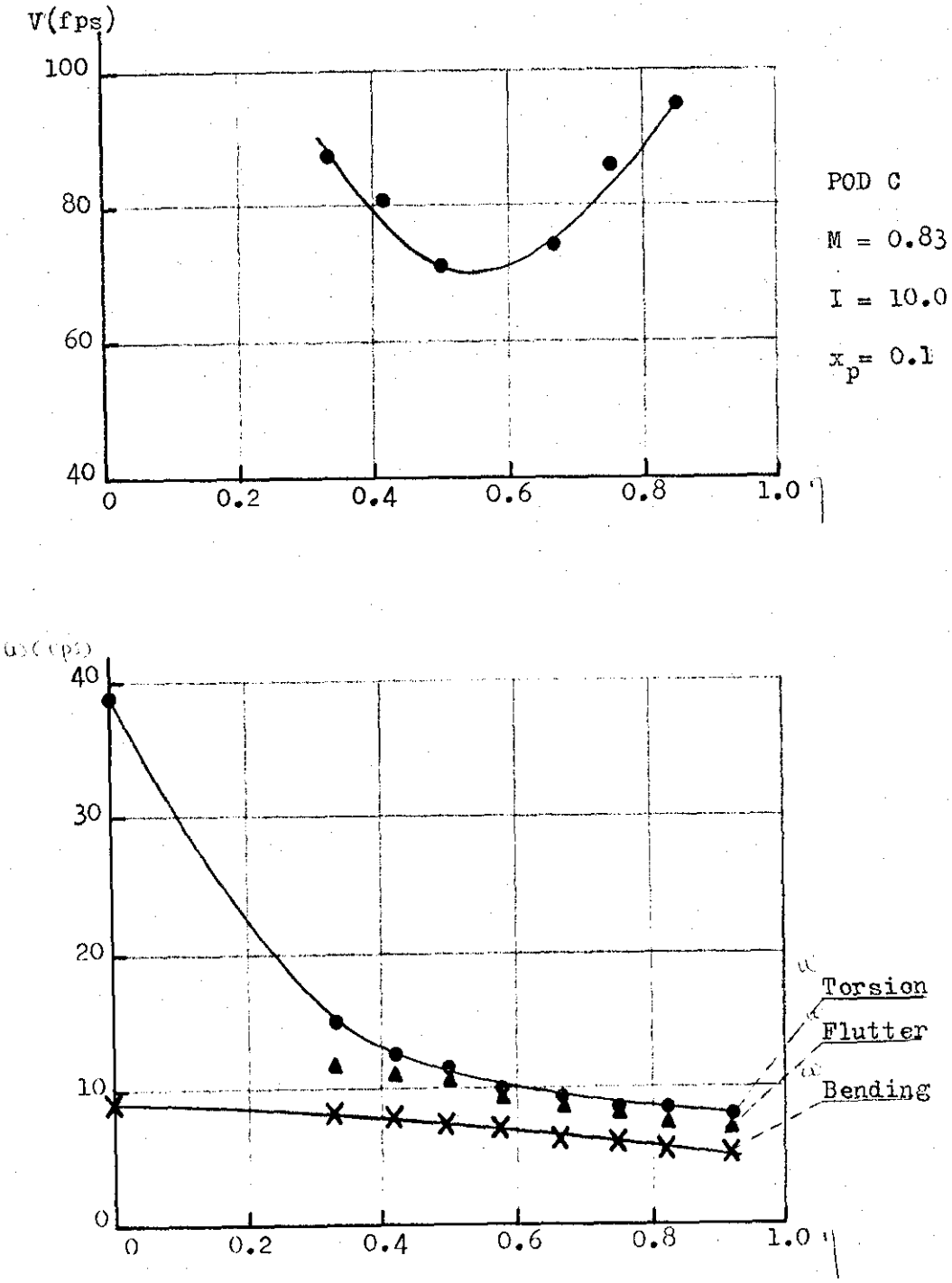

FIG. 7.18 Results of Wind Tunnel Tests: Wing A3

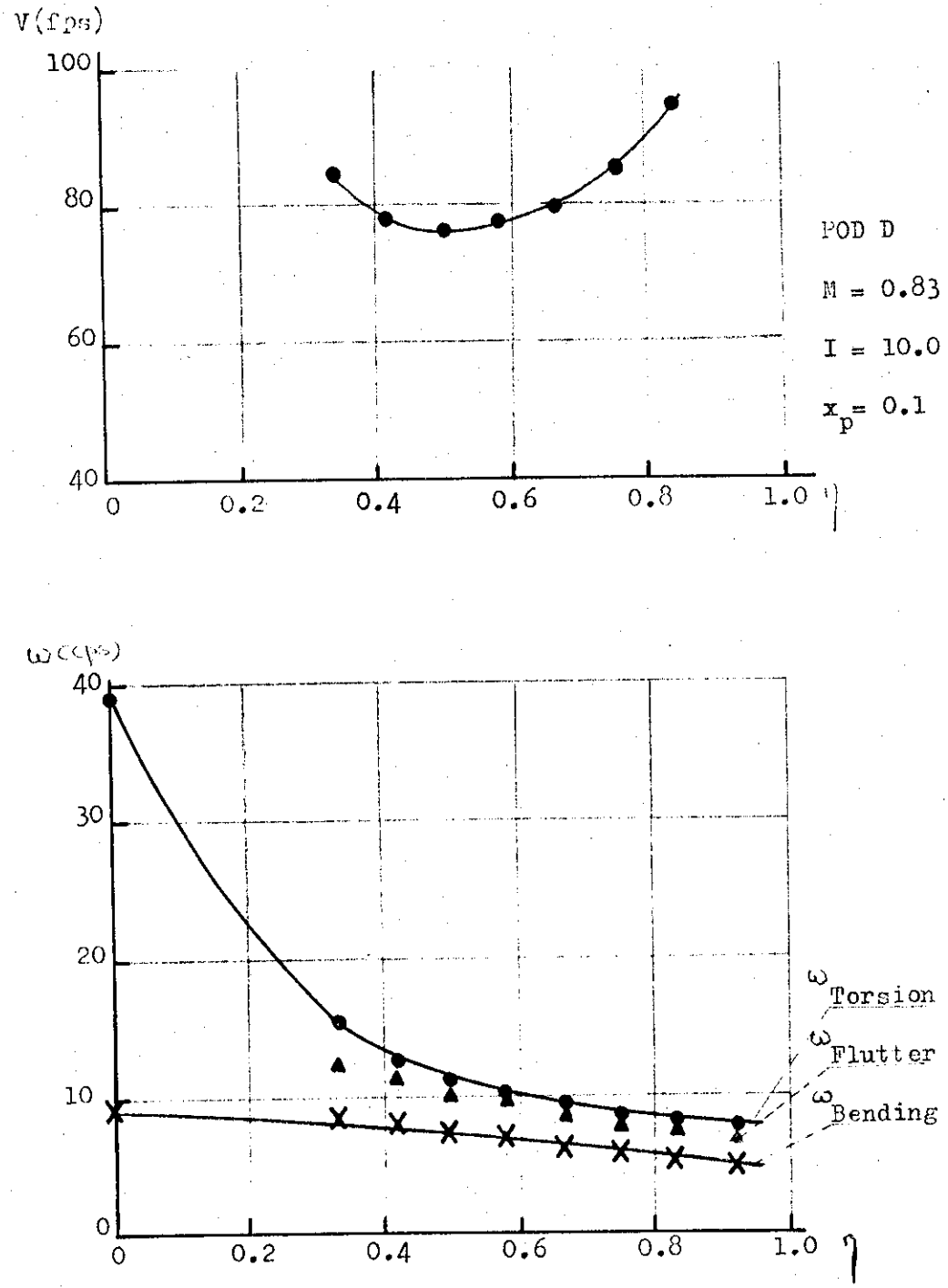

FIG. 7.19 Results of Wind Tunnel Tests: Wing A3

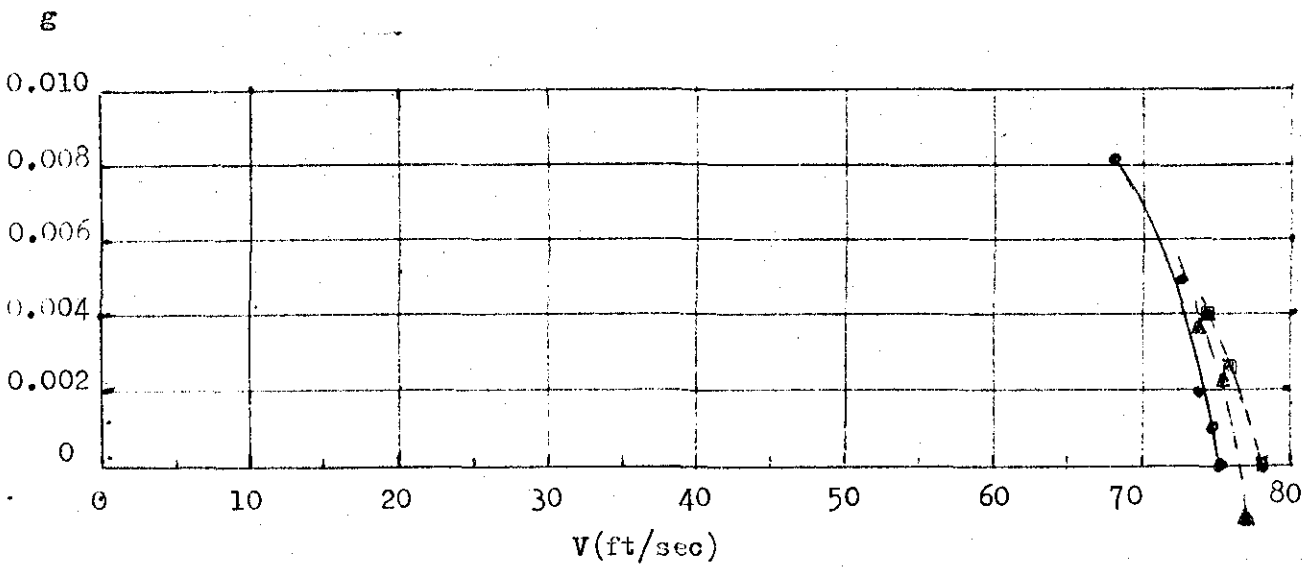

- Pod A (No Fins)
- Fin at the Pod Trailing Edge a = 1" b= 0.5"
- Fin at the Pod Trailing Edge a = 3" b = 0.5"

FIG. 7.20 V-g Curve for Two Fins on Pod A

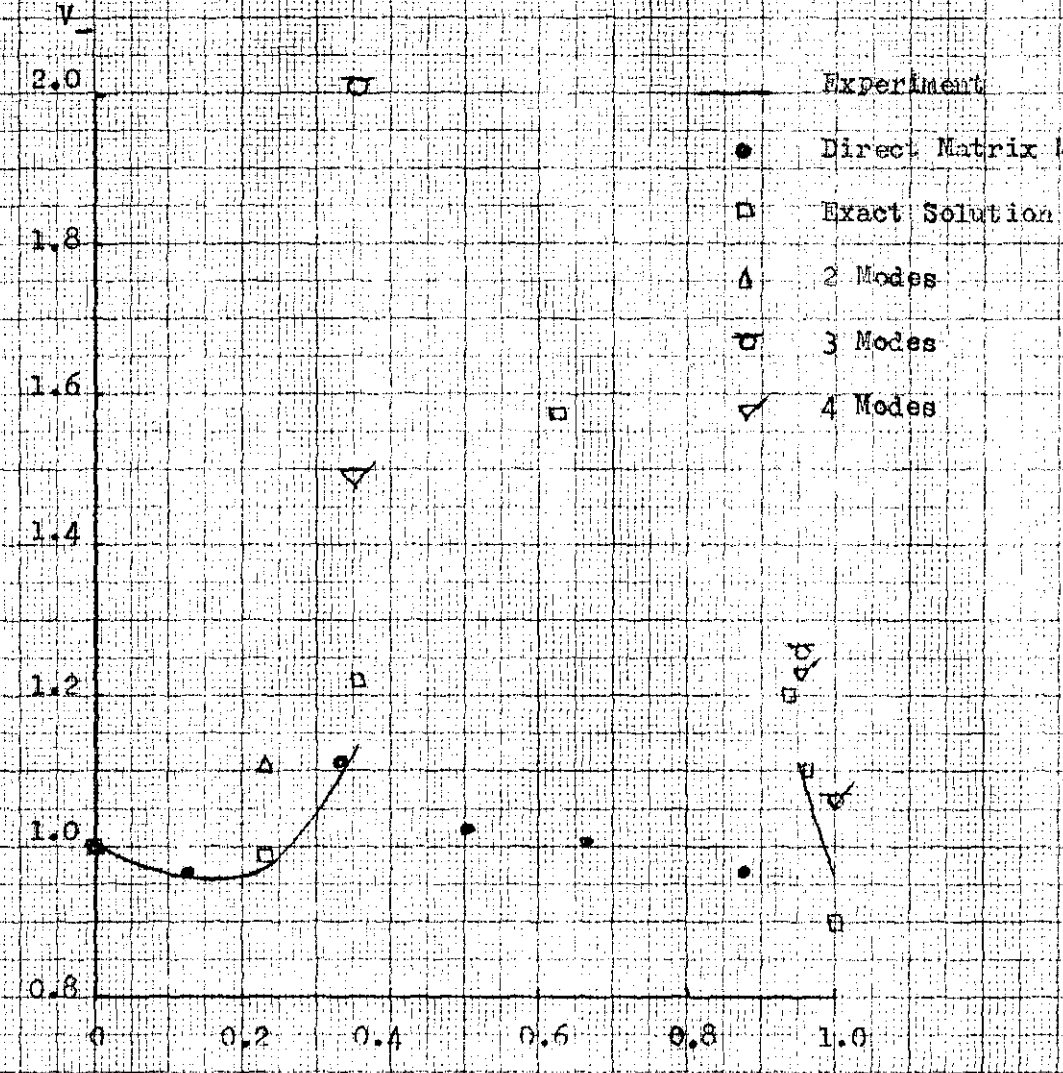

FIG. 8.2 Results of the Direct Matrix Analysis On the Wing of Ref(38): Weight 7a

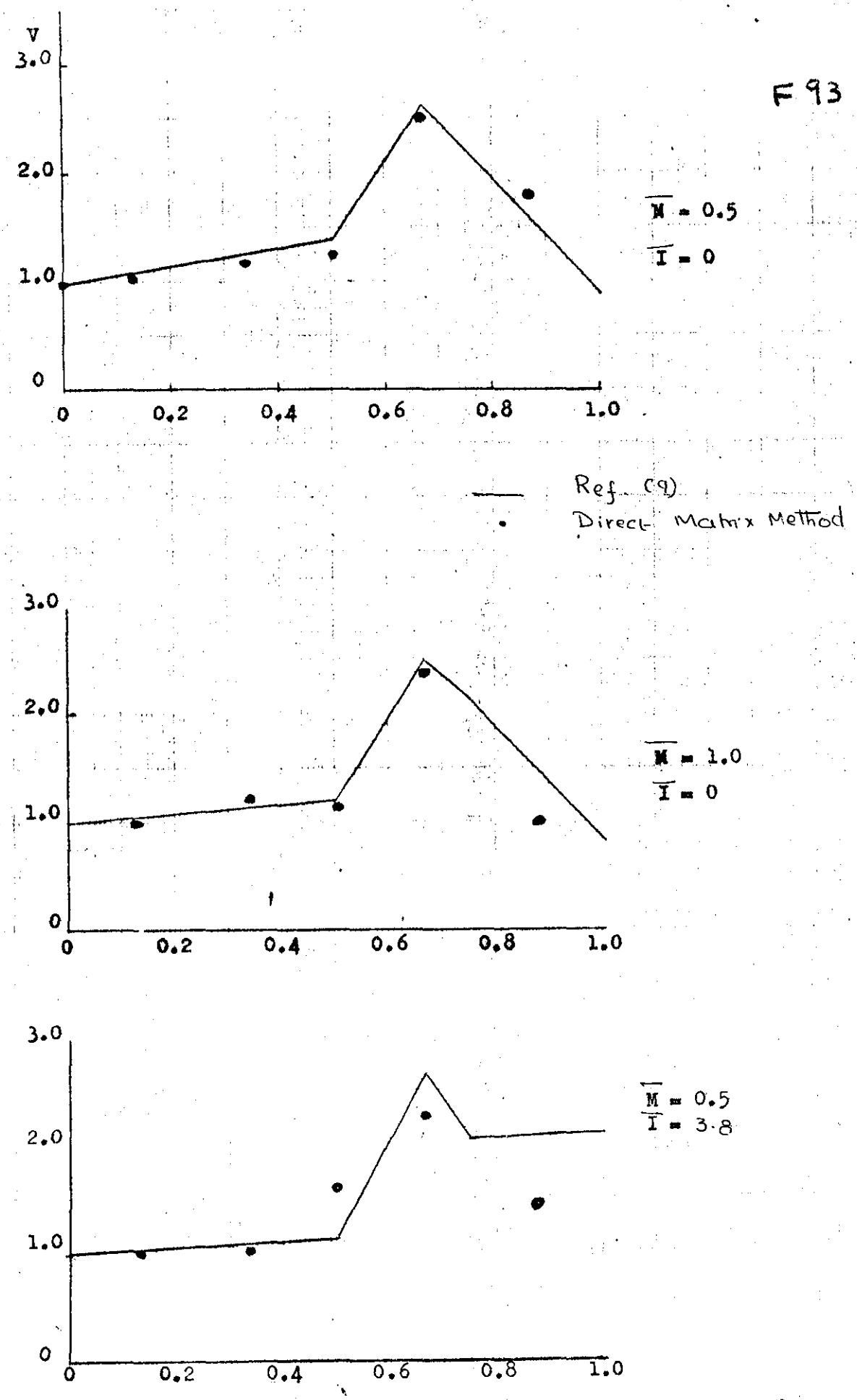

FIG 8.1 Results of Direct Matrix Analysis on the Wing of Ref(9)

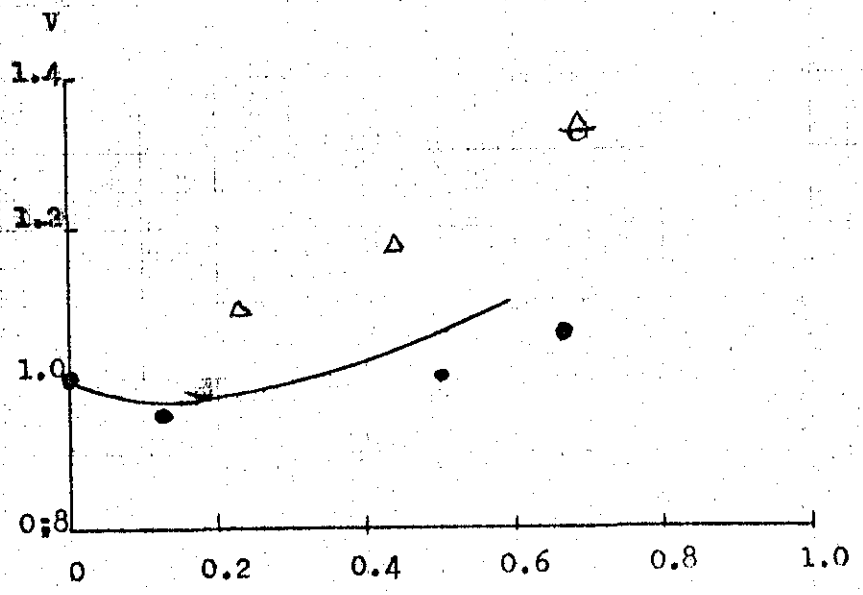

a) WEIGHT 7c

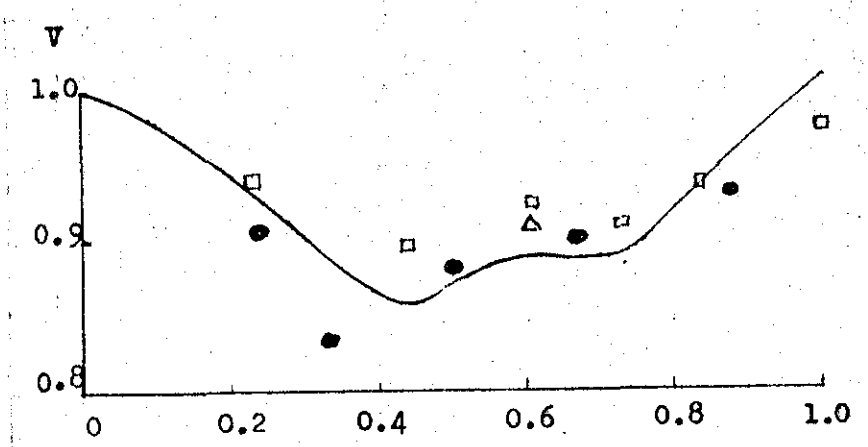

b) WEIGHT 7f

Experimental

Direct Matrix Method

2 Modes

3 Modes

FIG. 8.3 Results of the Direct Matrix Analysis on The Wing of Ref(9): Weights 7c and 7e.

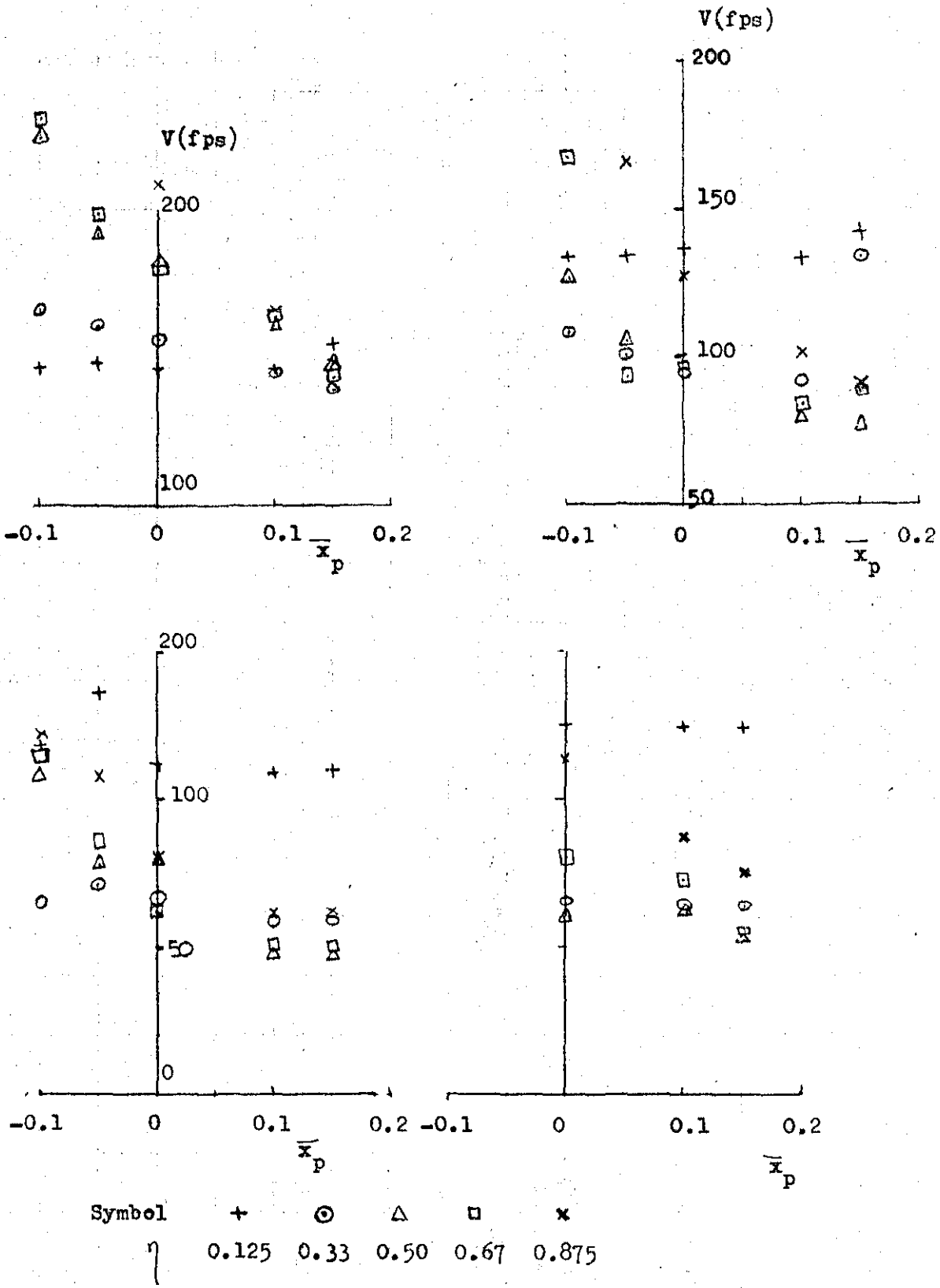

FIG 9.1 Influence of the Chordwise Position of C.G.

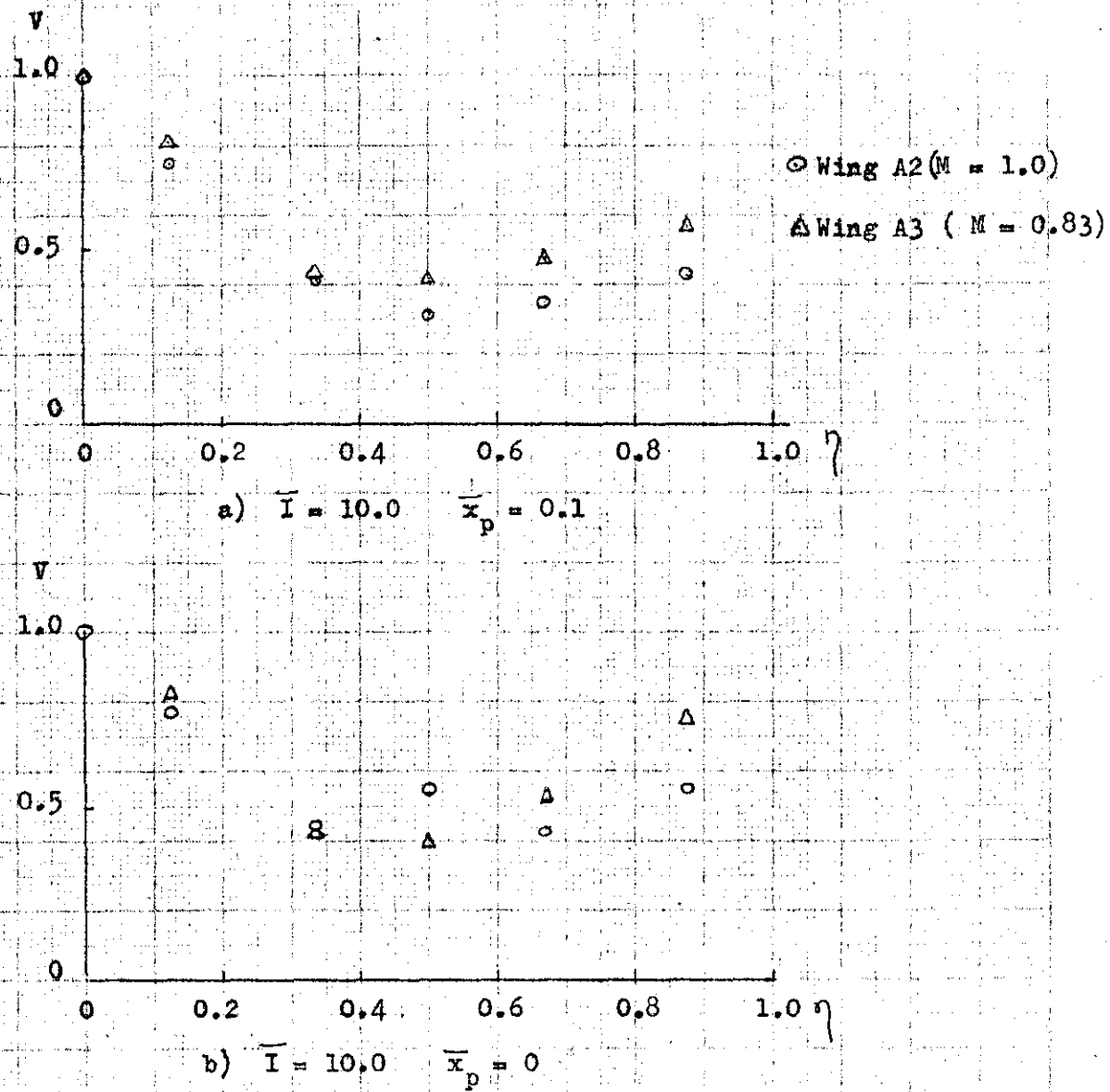

FIG 9.2 Influence of Mass Ratio on the Flutter Speed

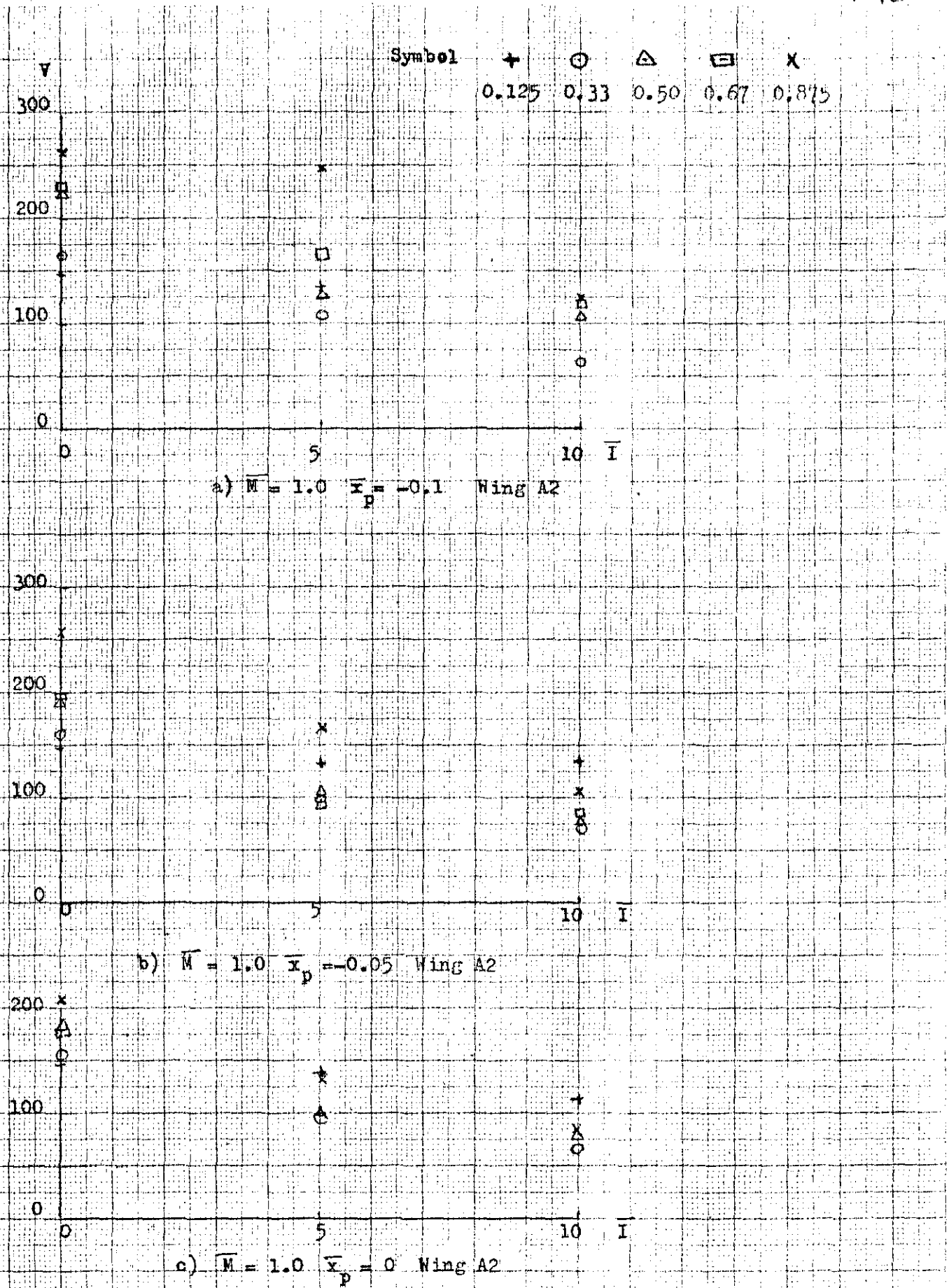

a) $\overline{M} = 1.0$ $\overline{x}_p = -0.1$ Wing A2

b) $\overline{M} = 1.0$ $\overline{x}_p = -0.05$ Wing A2

c) $\overline{M} = 1.0$ $\overline{x}_p = 0$ Wing A2

FIG 9.3 Influence of Inertia Ratio on the Flutter Speed

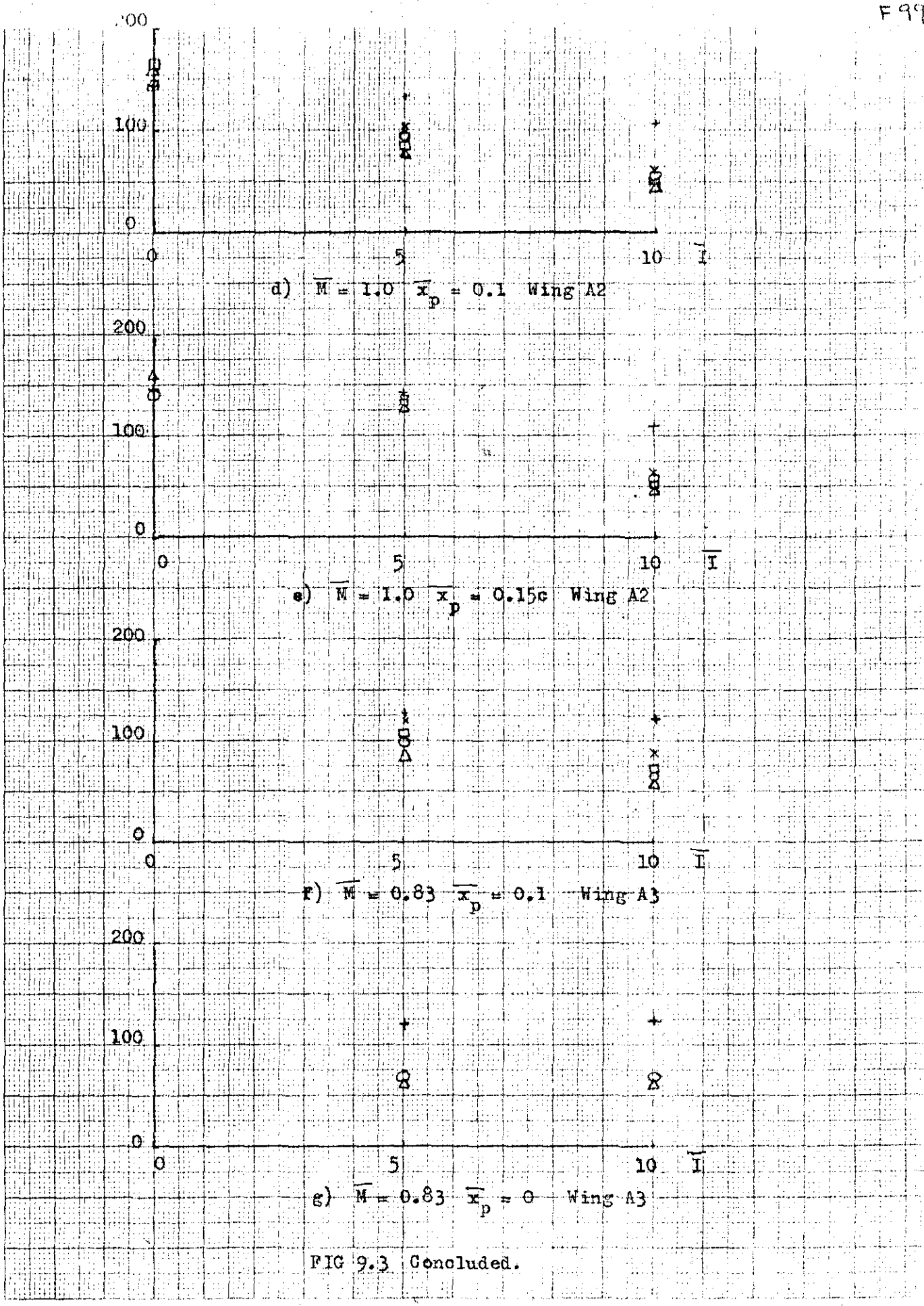

d) $\overline{M} = 1.0$ $\overline{x}_p = 0.1$ Wing A2

e) $\overline{M} = 1.0$ $\overline{x}_p = 0.15c$ Wing A2

f) $\overline{M} = 0.83$ $\overline{x}_p = 0.1$ Wing A3

g) $\overline{M} = 0.83$ $\overline{x}_p = 0$ Wing A3

FIG 9.3 Concluded.

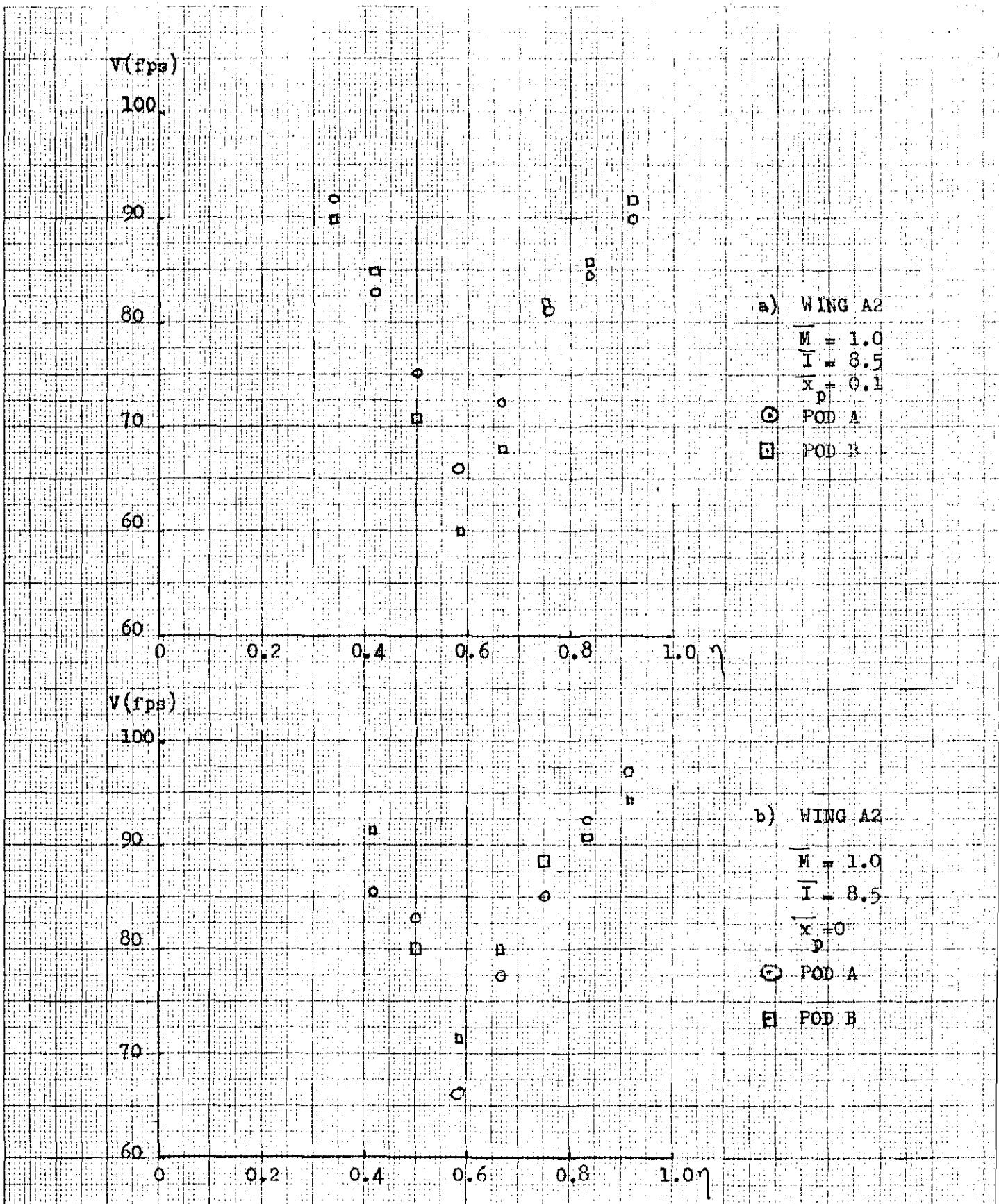

FIG 9.4 Influence of Pod Aerodynamics (Experimental Results)

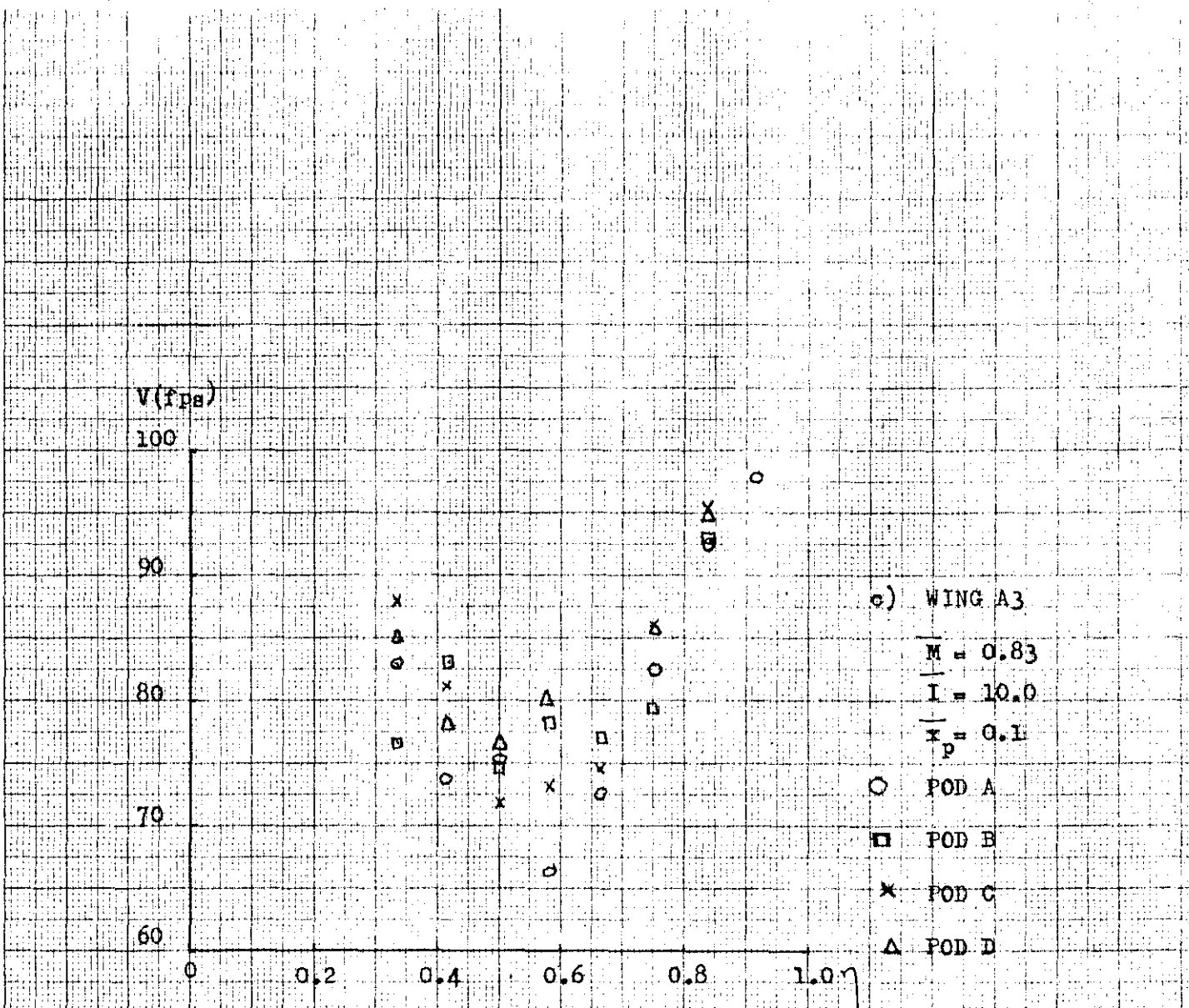

FIG 9.4 Concluded.

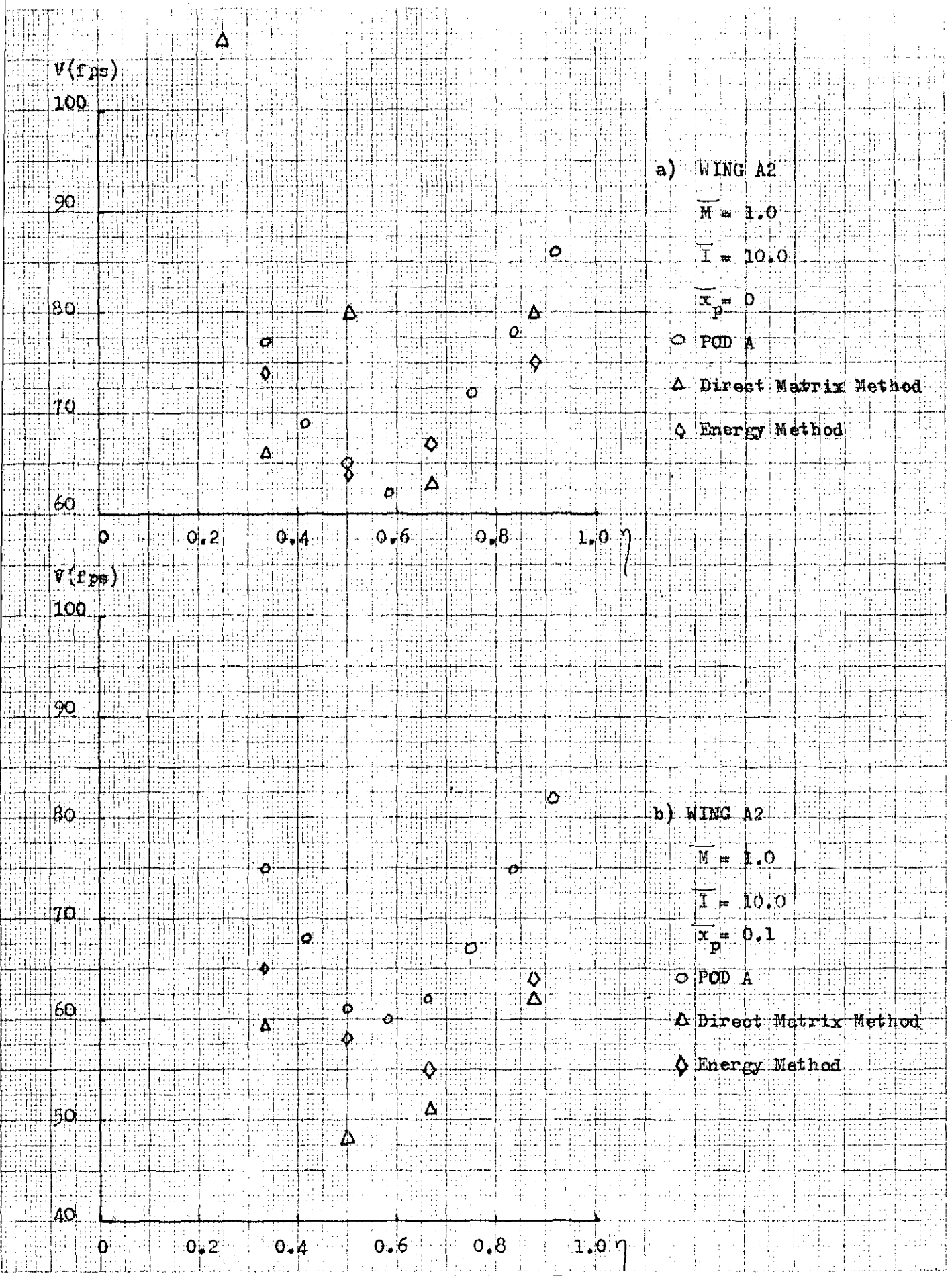

FIG 9.5 Comparison Between Theory and Experiment

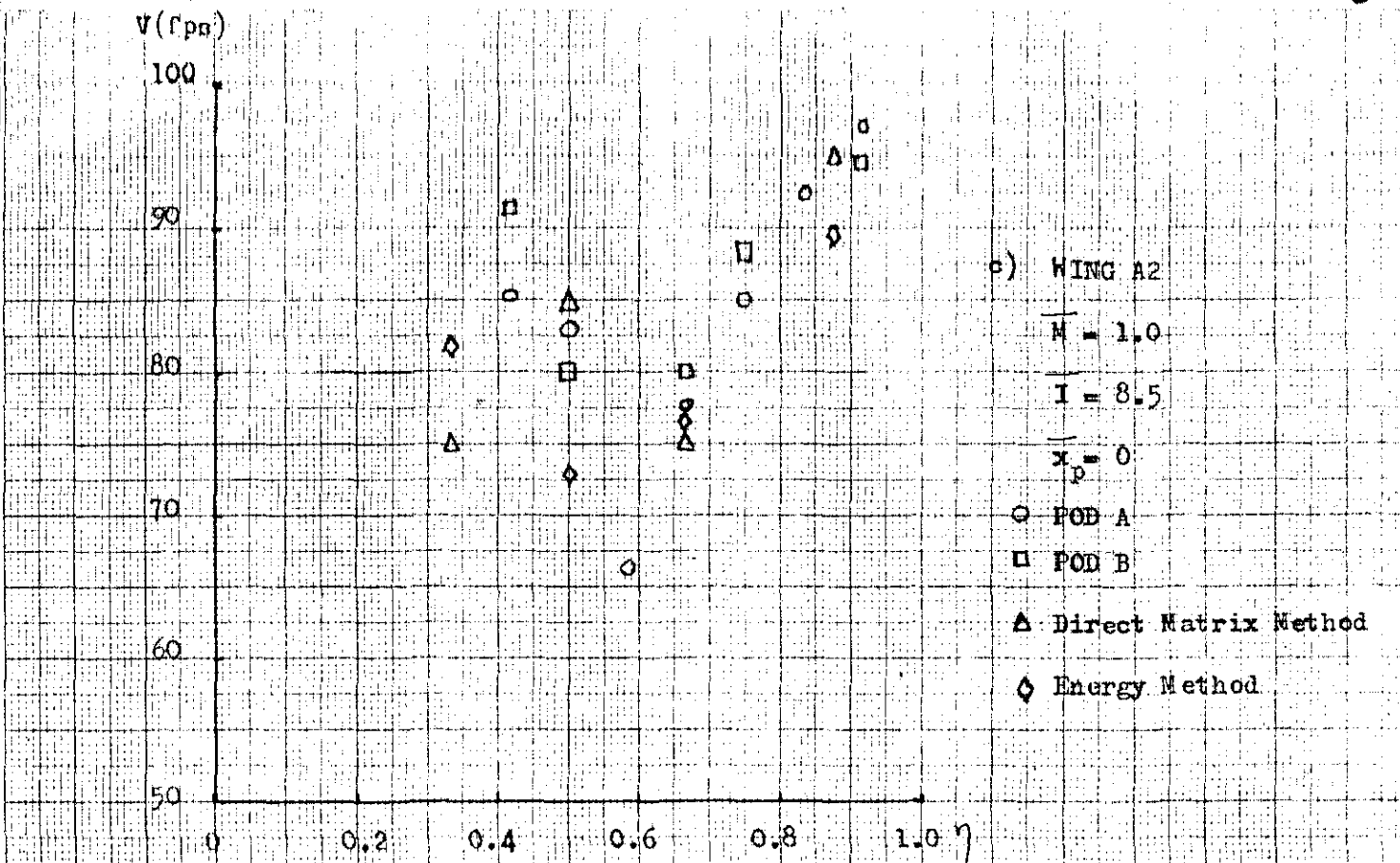

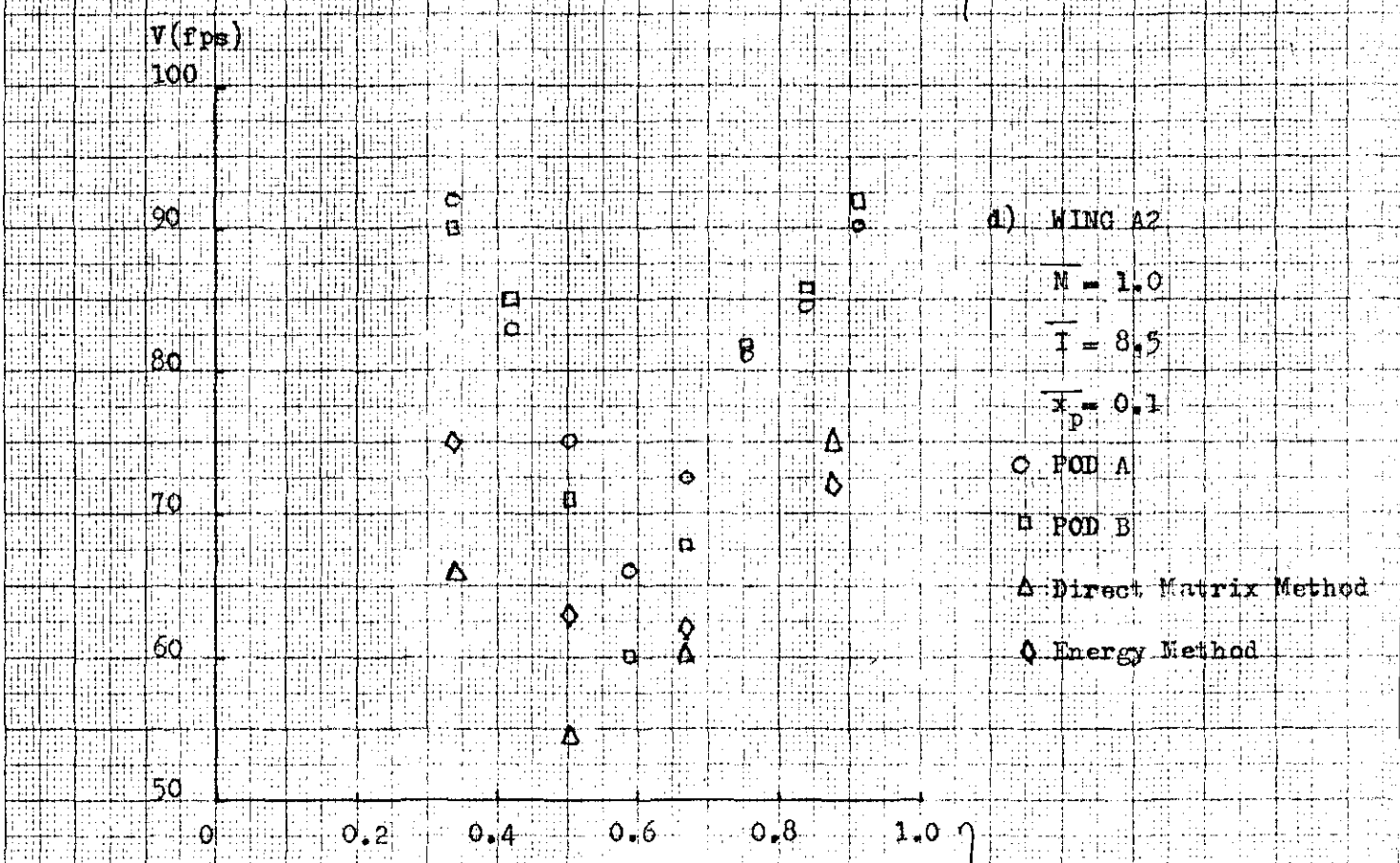

FIG 9.5 Concluded

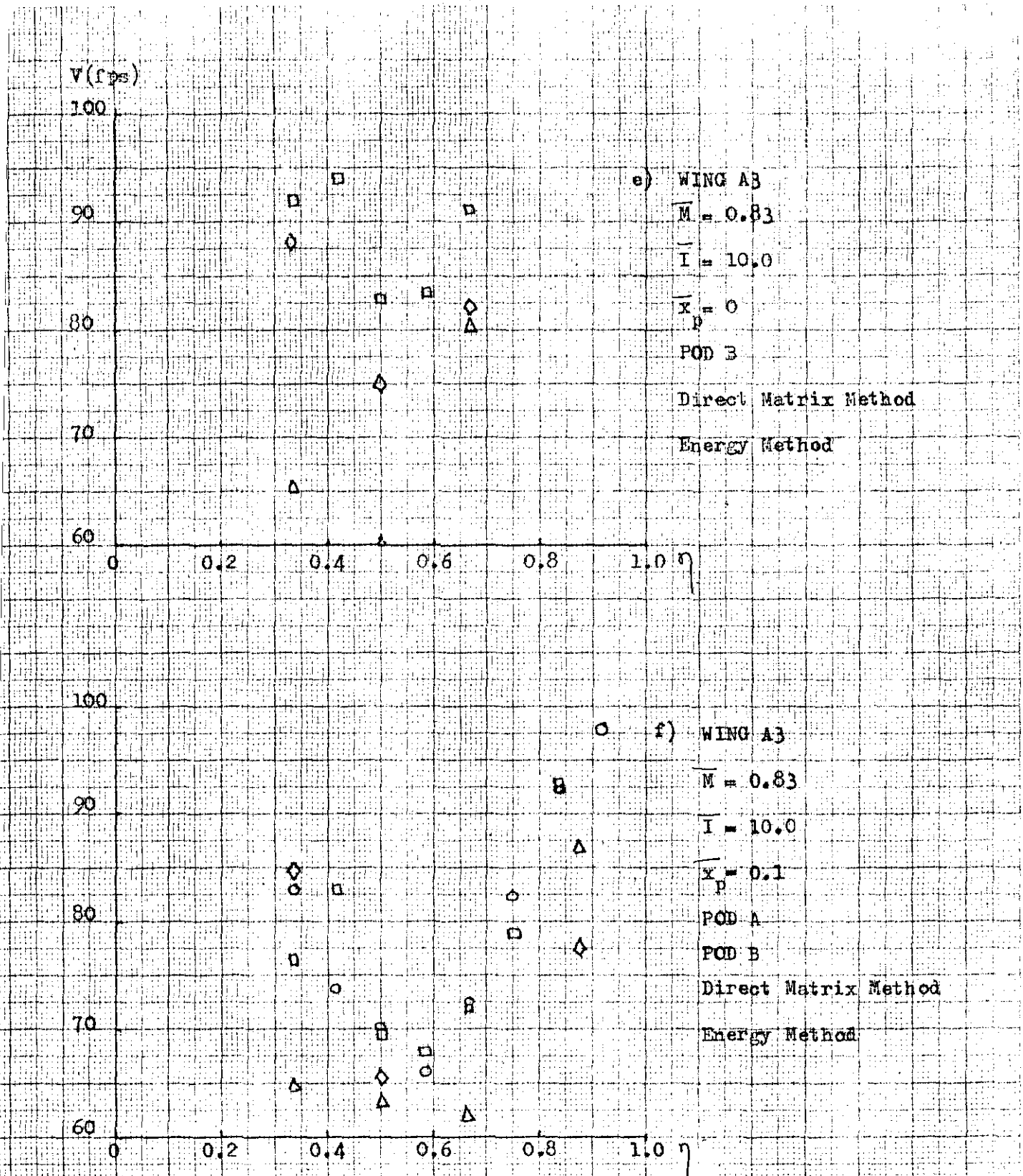

FIG 9.5 Concluded